BIOMARKERS IN PULMONARY DISEASES

EDITED BY: Bassam Mahboub, Rifat Hamoudi, Mahmood Yaseen Hachim and Hauke Busch

PUBLISHED IN: Frontiers in Medicine

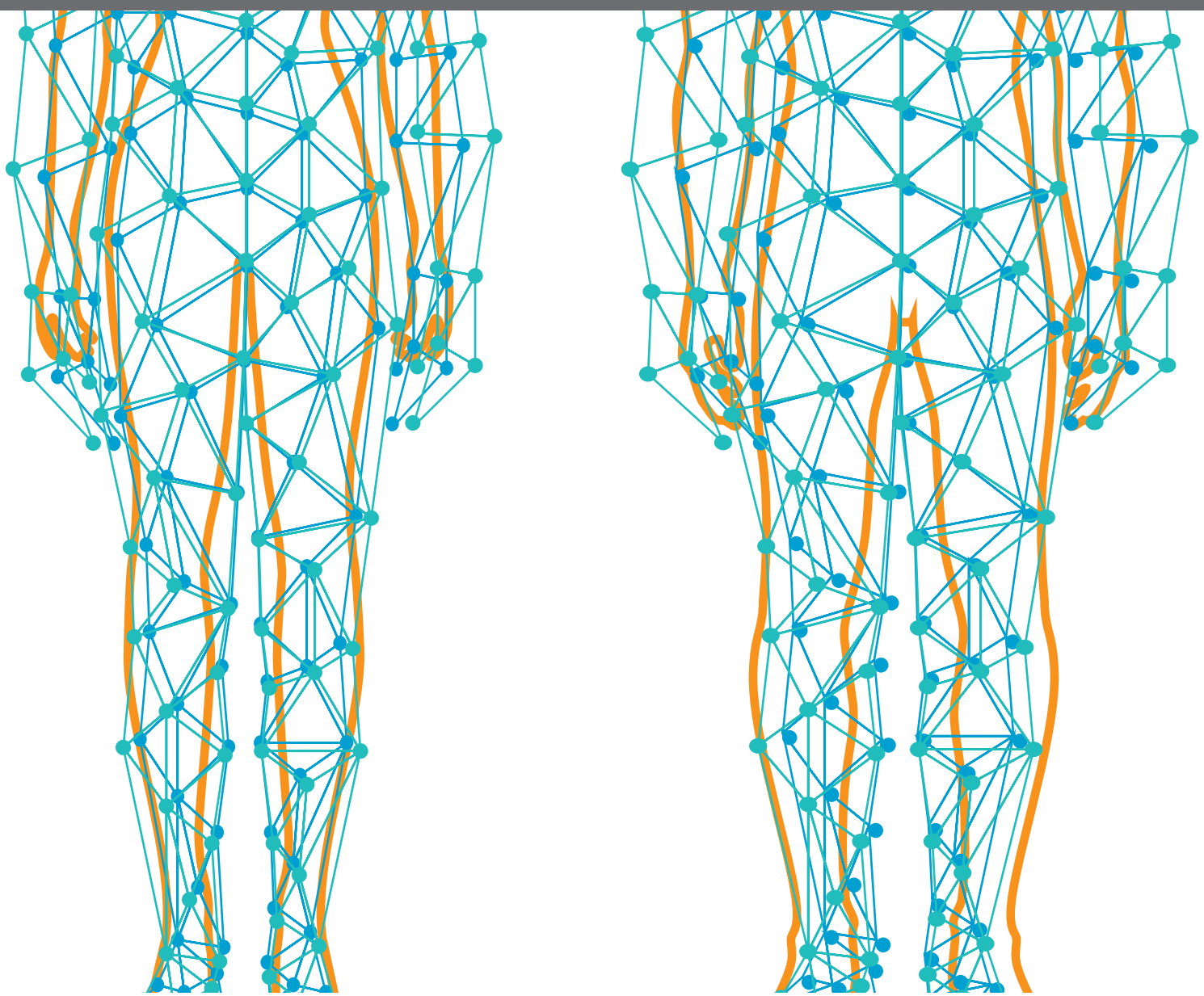

frontiers Research Topics

Frontiers eBook Copyright Statement

The copyright in the text of individual articles in this eBook is the property of their respective authors or their respective institutions or funders. The copyright in graphics and images within each article may be subject to copyright of other parties. In both cases this is subject to a license granted to Frontiers.

The compilation of articles constituting this eBook is the property of Frontiers.

Each article within this eBook, and the eBook itself, are published under the most recent version of the Creative Commons CC-BY licence. The version current at the date of publication of this eBook is CC-BY 4.0. If the CC-BY licence is updated, the licence granted by Frontiers is automatically updated to the new version.

When exercising any right under the CC-BY licence, Frontiers must be attributed as the original publisher of the article or eBook, as applicable.

Authors have the responsibility of ensuring that any graphics or other materials which are the property of others may be included in the CC-BY licence, but this should be checked before relying on the CC-BY licence to reproduce those materials. Any copyright notices relating to those materials must be complied with.

Copyright and source acknowledgement notices may not be removed and must be displayed in any copy, derivative work or partial copy which includes the elements in question.

All copyright, and all rights therein, are protected by national and international copyright laws. The above represents a summary only. For further information please read Frontiers' Conditions for Website Use and Copyright Statement, and the applicable CC-BY licence.

ISSN 1664-8714
ISBN 978-2-88974-867-9
DOI 10.3389/978-2-88974-867-9

About Frontiers

Frontiers is more than just an open-access publisher of scholarly articles: it is a pioneering approach to the world of academia, radically improving the way scholarly research is managed. The grand vision of Frontiers is a world where all people have an equal opportunity to seek, share and generate knowledge. Frontiers provides immediate and permanent online open access to all its publications, but this alone is not enough to realize our grand goals.

Frontiers Journal Series

The Frontiers Journal Series is a multi-tier and interdisciplinary set of open-access, online journals, promising a paradigm shift from the current review, selection and dissemination processes in academic publishing. All Frontiers journals are driven by researchers for researchers; therefore, they constitute a service to the scholarly community. At the same time, the Frontiers Journal Series operates on a revolutionary invention, the tiered publishing system, initially addressing specific communities of scholars, and gradually climbing up to broader public understanding, thus serving the interests of the lay society, too.

Dedication to Quality

Each Frontiers article is a landmark of the highest quality, thanks to genuinely collaborative interactions between authors and review editors, who include some of the world's best academicians. Research must be certified by peers before entering a stream of knowledge that may eventually reach the public - and shape society; therefore, Frontiers only applies the most rigorous and unbiased reviews.
Frontiers revolutionizes research publishing by freely delivering the most outstanding research, evaluated with no bias from both the academic and social point of view. By applying the most advanced information technologies, Frontiers is catapulting scholarly publishing into a new generation.

What are Frontiers Research Topics?

Frontiers Research Topics are very popular trademarks of the Frontiers Journals Series: they are collections of at least ten articles, all centered on a particular subject. With their unique mix of varied contributions from Original Research to Review Articles, Frontiers Research Topics unify the most influential researchers, the latest key findings and historical advances in a hot research area! Find out more on how to host your own Frontiers Research Topic or contribute to one as an author by contacting the Frontiers Editorial Office: frontiersin.org/about/contact

BIOMARKERS IN PULMONARY DISEASES

Topic Editors:
Bassam Mahboub, Rashid Hospital, United Arab Emirates
Rifat Hamoudi, University of Sharjah, United Arab Emirates
Mahmood Yaseen Hachim, Mohammed Bin Rashid University of Medicine and Health Sciences, United Arab Emirates
Hauke Busch, University of Lübeck, Germany

Citation: Mahboub, B., Hamoudi, R., Hachim, M. Y., Busch, H., eds. (2022). Biomarkers in Pulmonary Diseases. Lausanne: Frontiers Media SA.
doi: 10.3389/978-2-88974-867-9

Table of Contents

frontiers in Medicine

EDITORIAL
published: 11 March 2022
doi: 10.3389/fmed.2022.790475

Editorial: Biomarkers in Pulmonary Diseases

Bassam Mahboub[1]*, *Rifat Hamoudi*[2,3], *Mahmood Yaseen Hachim*[4] and *Hauke Busch*[5]

[1] Rashid Hospital, Dubai, United Arab Emirates, [2] College of Medicine, Sharjah Institute for Medical Research, University of Sharjah, Sharjah, United Arab Emirates, [3] Division of Surgery and Interventional Science, University College London, London, United Kingdom, [4] Mohammed Bin Rashid University of Medicine and Health Sciences, Dubai, United Arab Emirates, [5] University of Lübeck, Lübeck, Germany

Keywords: artificial intelligence, pulmonary, biomarker, genes, clinical

Editorial on the Research Topic

Biomarkers in Pulmonary Diseases

The incidence of pulmonary diseases such as asthma, chronic obstructive pulmonary disease (COPD), and different types of lung cancer are on the rise worldwide and will most likely continue to do so with ubiquitous air pollution and climate change, including extreme weather conditions. According to the World Health Organization, pulmonary diseases like COPD are among the leading causes of death. Lower respiratory infections are the third and fourth leading causes of death, especially in low-income countries. These diseases present themselves as highly complex and heterogeneous concerning diagnosis, treatment, or even prevention. Therefore, elucidating the disease etiology is essential to identify biomarkers for early detection, treatment, relapse, and a personalized approach to disease management.

This Research Topic gathers different contributions highlighting novel ways of clinical stratification of patients, gathering molecular markers for disease based on molecular diagnostics, novel omics, imaging, and screening technology. These approaches allow us to shed light on clinical outcomes and putative treatment schemes in the future.

Novel molecular markers for asthma, respiratory syndromes, and lung cancer have been proposed through cohort studies. Two case reports suggest novel molecular markers for rare types of lung cancer, which might be ideal proxies for more extensive cohort studies. In five cases of pulmonary sclerosing pneumocytoma, Aramini et al. found elevated levels of ALDH and SOX-2 and provided the first hint at their usefulness as a biomarker. The authors further present two cases of primary angiosarcoma of the lung in which they report on ALDH as a marker for poor outcome as well, which should be confirmed in a larger study.

In a retrospective study of 308 patients, Lu et al. proposed the albumin to globulin ratio as a prognostic factor for non-small cell lung cancer, while Yu et al. correlated PD-L1 expression based on tumor location and TTF-1 expression with poor outcome and potential for immunotherapy.

Molecular markers for respiratory diseases from larger cohort studies were proposed by Zhang R. et al. who present the analysis of a study of 133 pulmonary arterial hypertension (IPAH) patients, in which they found a significantly lower extracellular SOD in patients with BMPR2 mutations and propose this to be a vital antioxidant enzyme in the pathogenesis of IPAH.

Zhang W. et al. confirmed the neutrophil to lymphocyte ratio in a cohort of more than 1100 patients as a predictor for short-term survival in acute respiratory distress syndrome (ARDS).

Using seven clinical variables, Liu et al. developed a survival predictor with online access to evaluate acute respiratory distress syndrome.

Several manuscripts used omics approaches to identify novel markers, as such Kim et al. investigated metabolic fingerprinting for tuberculosis and smoking-induced COPD. In a transcriptome analysis of 60 blood samples from 30 asthmatics vs. healthy controls, Elena-Pérez et al. identified IL5RA as a pharmacogenetic biomarker in asthma. Hachim et al. measured

OPEN ACCESS

Edited and reviewed by:
Laurent Pierre Nicod, University of Lausanne, Switzerland

***Correspondence:**
Bassam Mahboub
drbassam_mahboub@yahoo.com

Specialty section:
This article was submitted to Pulmonary Medicine, a section of the journal Frontiers in Medicine

Received: *06 October 2021*
Accepted: *24 January 2022*
Published: *11 March 2022*

Citation:
Mahboub B, Hamoudi R, Hachim MY and Busch H (2022) Editorial: Biomarkers in Pulmonary Diseases. Front. Med. 9:790475. doi: 10.3389/fmed.2022.790475

Amphiregulin mRNA and protein in the blood, saliva, and bronchial biopsies samples from asthmatic patients and found its expression to be highly correlated with the disease.

Two papers demonstrate the usefulness of genetic association studies in the detection of novel genes and mechanisms. Raita et al. used genotype data from two large population studies, the INTERVAL and the UK Biobank, comprising more than 500,000 people, and the recent Mendelian randomization approach to confirm a causal effect with a significantly higher risk of asthma with soluble IL6 receptors. Gandhi et al. found a complex genetic association with mutations in surfactant proteins with hypersensitivity pneumonitis in the Mexican population.

With the recent worldwide SARS-CoV-2 pandemic, several papers developed novel diagnostic tools for COVID-19 based on either molecular or imaging data. For example, Chen et al. suggested carcinoembryonic antigen (CEA) in evaluating the severity and prognosis of COVID-19 in a cohort of 46 death and 68 discharged cases from the hospital. Yoo et al. developed a classifier for COVID-19 diagnosis from chest X-ray imaging, while Carvalho et al. derived radiological imaging patterns to quantify the extent of pulmonary involvement in COVID-19.

Imaging has also proven helpful for the diagnosis of the lung and respiratory organs in a clinical context. For this Ye et al. proposed a novel speckle-tracking algorithm for right diaphragm deformation analysis to detect abnormalities in respiratory movement.

Beyond genetic and transcriptomic information, also exosomes, membrane-bound extracellular vehicles (EVs) have moved into the focus of research as putative modulators of respiratory disease. Wang et al. reviewed the potential roles of exosomes in COPD as intercellular communication devices, which will probably gain more attention soon. Zhang R. et al. commented on the role of circulating serum exosomes and their role in inducing pulmonary inflammation during acute lung inflammation.

CONCLUSION THOUGHTS

Over the past 5 years, health sciences and medicine have progressed rapidly and swiftly by the wealth of information coming from understanding mechanisms of diseases.

Most of the advances happened because disease presentations rely on omics, which understand that the genetic makeup of the human being will transform into the transcription of specific messages carried by mRNA to be finally present as protein.

Proteins usually show themselves as a clinical phenotype in a patient with a particular disease presentation.

This wealth of big data was difficult to navigate without using the power of computing sciences and mainly machine learning with artificial intelligence.

When biology meets mathematics, great advances in understanding and progression in problem-solving will happen.

I hope readers will enjoy this unique issue, which touches the surface of what current and future medicine of pulmonary disease looks like.

AUTHOR CONTRIBUTIONS

BM, MH, and HB were responsible for the conception of the idea. All authors approved the final manuscript for publication.

Conflict of Interest: The authors declare that the research was conducted in the absence of any commercial or financial relationships that could be construed as a potential conflict of interest.

Publisher's Note: All claims expressed in this article are solely those of the authors and do not necessarily represent those of their affiliated organizations, or those of the publisher, the editors and the reviewers. Any product that may be evaluated in this article, or claim that may be made by its manufacturer, is not guaranteed or endorsed by the publisher.

Copyright © 2022 Mahboub, Hamoudi, Hachim and Busch. This is an open-access article distributed under the terms of the Creative Commons Attribution License (CC BY). The use, distribution or reproduction in other forums is permitted, provided the original author(s) and the copyright owner(s) are credited and that the original publication in this journal is cited, in accordance with accepted academic practice. No use, distribution or reproduction is permitted which does not comply with these terms.

frontiers in Medicine

ORIGINAL RESEARCH
published: 14 July 2020
doi: 10.3389/fmed.2020.00427

Deep Learning-Based Decision-Tree Classifier for COVID-19 Diagnosis From Chest X-ray Imaging

Seung Hoon Yoo[1], Hui Geng[1], Tin Lok Chiu[1], Siu Ki Yu[1], Dae Chul Cho[2], Jin Heo[2], Min Sung Choi[2], Il Hyun Choi[2], Cong Cung Van[3], Nguen Viet Nhung[3], Byung Jun Min[4] and Ho Lee[5]**

[1] Medical Physics and Research Department, Hong Kong Sanatorium & Hospital, Happy Valley, Hong Kong, [2] Artificial Intelligent Research Lab, Radisen, Seoul, South Korea, [3] Vietnam National Lung Hospital, Hanoi, Vietnam, [4] Department of Radiation Oncology, Chungbuk National University Hospital, Cheongju, South Korea, [5] Department of Radiation Oncology, Gangnam Severance Hospital, Yonsei University College of Medicine, Seoul, South Korea

The global pandemic of coronavirus disease 2019 (COVID-19) has resulted in an increased demand for testing, diagnosis, and treatment. Reverse transcription polymerase chain reaction (RT-PCR) is the definitive test for the diagnosis of COVID-19; however, chest X-ray radiography (CXR) is a fast, effective, and affordable test that identifies the possible COVID-19-related pneumonia. This study investigates the feasibility of using a deep learning-based decision-tree classifier for detecting COVID-19 from CXR images. The proposed classifier comprises three binary decision trees, each trained by a deep learning model with convolution neural network based on the PyTorch frame. The first decision tree classifies the CXR images as normal or abnormal. The second tree identifies the abnormal images that contain signs of tuberculosis, whereas the third does the same for COVID-19. The accuracies of the first and second decision trees are 98 and 80%, respectively, whereas the average accuracy of the third decision tree is 95%. The proposed deep learning-based decision-tree classifier may be used in pre-screening patients to conduct triage and fast-track decision making before RT-PCR results are available.

Keywords: chest X-ray radiography, COVID-19, deep learning, image classification, neural network, tuberculosis

OPEN ACCESS

Edited by:
Mahmood Yaseen Hachim, Mohammed Bin Rashid University of Medicine and Health Sciences, United Arab Emirates

Reviewed by:
J. Cleofe Yoon, Sheikh Khalifa Specialty Hospital, United Arab Emirates
Axel Künstner, University of Lübeck, Germany
Jeongjin Lee, Soongsil University, South Korea

****Correspondence:***
Byung Jun Min
bjmin@cbnuh.or.kr
Ho Lee
holee@yuhs.ac

Specialty section:
This article was submitted to Pulmonary Medicine, a section of the journal Frontiers in Medicine

Received: *12 June 2020*
Accepted: *02 July 2020*
Published: *14 July 2020*

Citation:
Yoo SH, Geng H, Chiu TL, Yu SK, Cho DC, Heo J, Choi MS, Choi IH, Cung Van C, Nhung NV, Min BJ and Lee H (2020) Deep Learning-Based Decision-Tree Classifier for COVID-19 Diagnosis From Chest X-ray Imaging. Front. Med. 7:427. doi: 10.3389/fmed.2020.00427

INTRODUCTION

Coronavirus disease 2019 (COVID-19) caused by severe acute respiratory syndrome coronavirus 2 (SARS-CoV-2) has spread from Wuhan to the rest of China and to several other countries since December 2019. More than 2 million cases were confirmed by April 18, 2020. Worldwide, more than 150,000 deaths due to COVID-19 have been reported[1].

COVID-19 is typically confirmed by reverse transcription polymerase chain reaction (RT-PCR). However, the sensitivity of RT-PCR may not be high enough for early detection, complicating the treatment of presumptive patients (1, 2).

Chest radiography imaging such as X-ray or computed tomography (CT), which is a routine technique for diagnosing pneumonia, can be easily performed, and it provides a quick, highly sensitive diagnosis of COVID-19 (1). Chest X-ray (CXR) images show visual indexes associated with COVID-19 (3), and several studies have shown the feasibility of radiography as a detection tool for COVID-19 (4–8).

[1]https://www.worldometers.info/coronavirus/

To date, there have been no detailed studies on the potential of artificial intelligence (AI) to detect COVID-19 automatically from X-ray or chest CT images due to the lack of availability of public images from COVID-19 patients. Recently, some researchers have collected a small dataset of COVID-19 CXR images to train AI models for automatic COVID-19 diagnosis[2] (9). These images were taken from academic publications reporting the results of COVID-19 X-ray and CT imaging. Minaee et al. published a study on COVID-19 prediction in CXR imaging using transfer learning (10). They compared predictions of four popular deep convolutional neural networks (CNN), which are ResNet18, ResNet50, SqueezeNet, and DenseNet-161. They trained the models using COVID-19 and non-COVID datasets, including 14 subclasses containing normal images from the ChexPert dataset (11). The models showed an average specificity rate of ∼90% with a sensitivity range of 97.5%. This strongly encourages the hope that COVID-19 can be distinguished from other diseases and normal lung conditions by CXR imaging.

Tuberculosis (TB) is the fifth leading cause of death worldwide, with ∼10 million new cases and 1.5 million deaths every year (12). Since TB caused by the bacteria that most often affect the lungs can be cured and prevented, the World Health Organization recommends systematic and broad screening to eliminate the disease. Despite its low specificity and interpretational difficulty, posteroanterior (PA) chest radiography is one of the preferred TB screening methods. TB is primarily a disease of poor countries; therefore, clinical officers trained to interpret these CXRs are often lacking (13, 14).

Several computer-aided diagnosis (CAD) researches dealing with CXR abnormalities do not focus on other specific diseases (non-TB). Most CAD systems specializing in TB detection have been reported (15–20).

TB and non-TB images are mixed in actual examination of lung disease. For diagnostic purposes, images should be classified as normal, TB, or non-TB. Several studies have been conducted on the automatic detection of various kinds of lung disease, which are not restricted to TB (21–25). In particular, the detection of anomalies, including non-TB ones, has been investigated with a multi-CNN model (26). Using an algorithm that only learns TB and normal data can result in lower accuracy when applied to examinations involving non-TB images.

In this study, we propose a deep learning-based decision-tree classifier comprising three levels. Each decision tree is trained by a deep learning model with a PyTorch frame-based convolution neural network. Using the proposed classifier, we investigate whether the detection of COVID-19 is feasible in CXR images. Furthermore, we quantify the accuracy of detection rates for normal, TB, COVID-19, and other non-TB diseases to see if the proposed classifier is a good candidate for clinical purposes.

METHOD

Workflow

In this study, we suggest a three-level decision-tree classifier for dividing CXR from the hospital or examination bus into four clinical states (normal, TB, non-TB, and COVID-19). Each step involves a binary classification, as shown in **Figure 1**. The image quality of each CXR is checked by the radiographer when it is taken, before the CAD model makes any predictions. In our suggested workflow, there are four automated X-ray imaging radiography systems (AXIRs). AXIR1 and AXIR2 are for the classification of images into abnormal/normal and TB/non-TB, respectively. If a good quality CXR is taken by AXIR1 and classified as an image of the normal state, no further action is taken. However, if the image is classified as abnormal, the next step (using AXIR2) is to determine whether it is TB or non-TB. AXIR3 and AXIR4 are used in the third step of the process, where the image is classified as COVID-19 or non-COVID-19, with or without TB. Finally, a medical doctor reviews the images and their classifications before making decisions about further investigation for clinical assessment.

In each step, the prediction model is trained with a data group optimized for its intended purpose. AXIR1 is trained with a combination of normal and abnormal data, the latter including both TB and non-TB data. The NIH ChestX-ray14 dataset was used in this study. AXIR2 is trained on TB and non-TB cases taken from the ChestX-ray14 dataset. In AXIR3, COVID-19 data, and non-COVID TB data are used for training, whereas in AXIR4, COVID-19, and non-COVID non-TB data are used. Each of the classifiers in the three-step system is designed for binary classification.

Patient Data and Augmentation

In an effort to provide sufficient training data for the research community, allowing benchmark tests, the U.S. National Library of Medicine has made two datasets of posteroanterior (PA) chest radiographs available: the MC set and the Shenzhen set, Both datasets contain normal and abnormal chest X-rays with manifestations of TB and include associated radiologist readings. The categorization of TB is based on the final pathological diagnosis. The Shenzhen set was used in this study for TB dataset. The open-source Shenzen data comprise 326 TB and 226 normal cases (https://lhncbc.nlm.nih.gov/publication/pub9931). The average image size for Shenzen data is 3000 × 3000.

Also, the NIH (National Institutes of Health, US) Clinical Center recently released over 100,000 anonymized chest x-ray images and their corresponding data to the scientific community. The database from NIH is available online at https://nihcc.app.box.com/v/ChestXray-NIHCC/folder/36938765345. The size of each image is 1024 × 1024. This dataset is categorized into 14-lung disease sub-patterns which are based on pathological diagnosis. However, this dataset does not show TB or non-TB classification with pathological confirmation.

In addition to above open dataset, we used Eastern Asia Hospital dataset (which is based on cooperation with Radisen) for TB and non-TB disease. This dataset is based on pathological diagnosis. In the case of the non-TB data, NIH 14 based categorization was applied with pathological diagnosis. The images were taken by a Vicomed system and viewed with a Radisen Detector (17" × 17"). The average image size is 2484 × 3012. The image acquisition conditions were as follows: voltage = 105 kVp, current = 125 mA, charge = 10 mAs, time = 80 ms, source-to-image distance = 130–150 cm. For the

[2]https://github.com/ieee8023/covid-chestxray-dataset

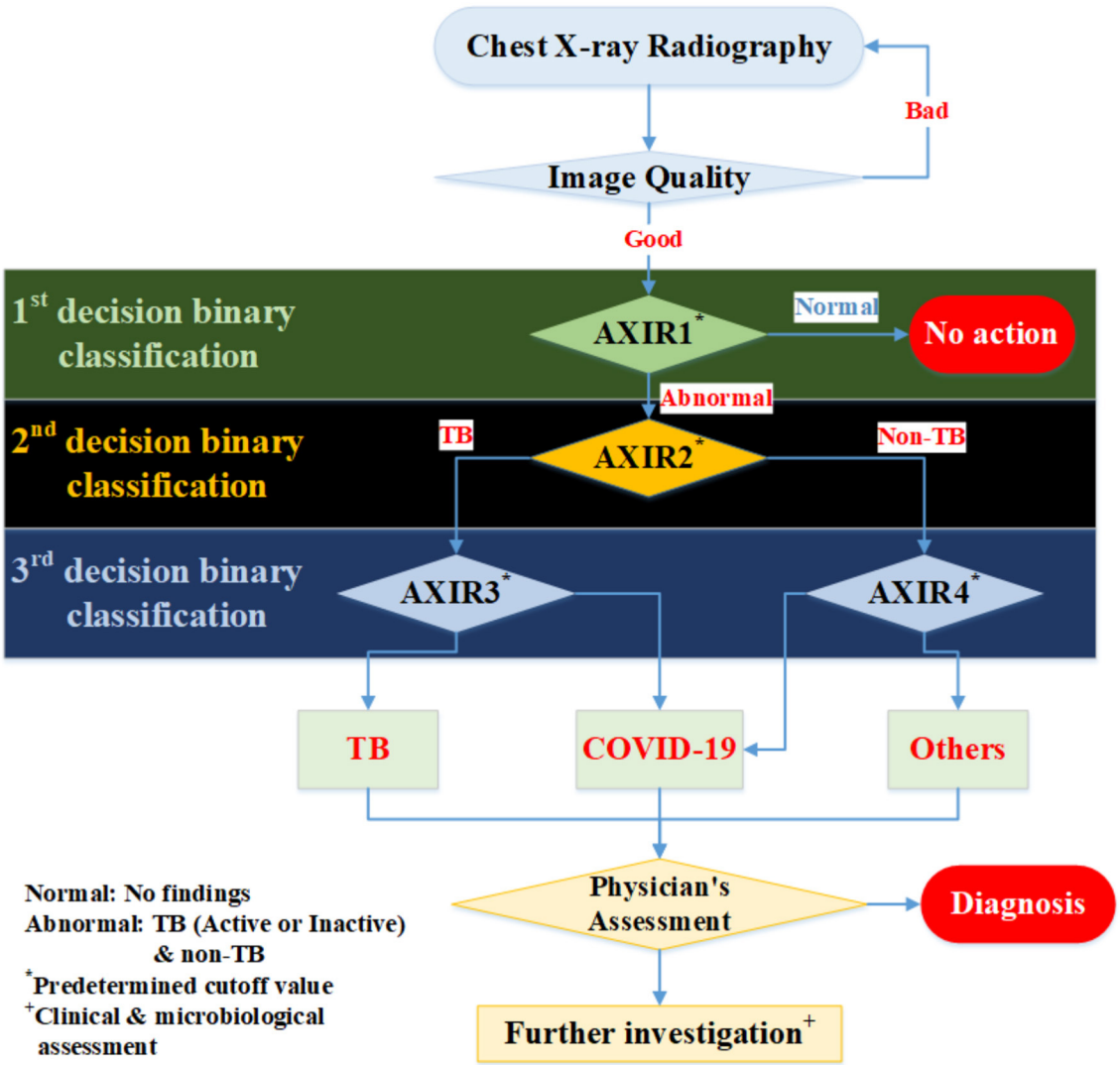

FIGURE 1 | Workflow for determining whether chest X-ray image shows a normal, tubercular (TB), or COVID-19 infected lung. AXIR (Automated X-ray Imaging Radiography system).

correct collection of the data, two radiologists review dataset and only data which is agreed by two radiologists were used in this study.

Finally, we used the recently published COVID-Chest Xray-Dataset, which contains a set of images from publications on COVID-19 topics (7, 8). We used 162 images of COVID-19 infected lungs and transferred them all to image size 1,024 × 1,024 before training and testing. The original COVID-19 image sizes are various (not the same), because the images were taken from multiple institutions. Therefore, the different image sizes were normalized to 1,024 × 1,024, which is the smallest image size of the obtained images, to avoid image size effect on the performance. Moreover, COVID-19 dataset is based on pathological diagnosis (7–9)[2].

In the case of the AXIR1, among the 1,170 patients' CXRs in the total dataset (**Table 1**), 85 normal and 85 abnormal CXR (total 170) scans were randomly selected from the data.

TABLE 1 | Data structure for AXIR1.

Normal/ abnormal	Data group	Number of images	Sub total
Abnormal	NIH data (TB + non-TB)[a]	442	585 (Train 500, Test 85) (Train with augmentation 1500)
	East Asian Hospital data (TB + non-TB)[b]	143	
Normal (NIH data + East Asian Hospital data)			585 (Train 500, Test 85) (Train with augmentation 1500)

[a] *TB and non-TB are not classified with pathological diagnosis.*
[b] *TB and non-TB are classified with pathological diagnosis.*

The remaining 1,000 CXRs were split in a 50:50% ratio to make abnormal (500 patients) and normal (500 patients) cases for training. Among the 585 abnormal cases, 442 were from

TABLE 2 | Data structure for AXIR2.

TB/non-TB	Data group	Number of images	Sub total
TB	TB (East Asian Hospital data)	372	492 (Train 410, Test 82)
	TB (Sehnzen data)	120	(Train with augmentation 1500)
Non-TB (East Asian Hospital data)		492 (Train 410, Test 82) (Train with augmentation 1500)	

TABLE 3 | Data structure for AXIR3.

Deep learning algorithm	COVID-19/TB	Training (Augmentation)	Test
PyTorch, Resnet18 model, epoc = 50, 256*256 image size	COVID-19 (GitHub)	120 (608)	42
	TB (Shenzen data)	120 (608)	42

TABLE 4 | Data structure for AXIR4.

Deep learning algorithm	COVID-19/others	Training (Augmentation)	Test
PyTorch, Resnet18 model, epoc = 50, 256*256 image size	COVID-19 (GitHub)	120 (608)	42
	Non-TB (Eastern Asian Hospital)	120 (608)	42

NIH data and 143 were from East Asian hospital data. The normal data images also came from the NIH and East Asian countries' data.

In the case of the AXIR2, among the 984 patients in the total dataset (**Table 2**), 164 CXR scans (16.7%) were randomly selected for testing. Among these 164 CXR images, 82 were TB cases, and 82 were non-TB (other) cases. The remaining 820 images were split in a 50:50% ratio to make TB (410 patients) and non-TB cases (410 patients) for training. Among the 492 TB patients' images, 372 images were from East Asian data, and the remaining 120 TB cases were from Shenzhen data. All 492 non-TB lung disease images were taken from East Asian hospital data.

In the case of the AXIR3, of the 324 patients' CXRs in the total dataset (**Table 3**), 84 images (23.0%) were randomly selected for testing. Among these 84 images, 42 were COVID-19 cases and 42 were TB (non-COVID) cases. The remaining 240 scans were split in a 50:50% ratio to make COVID-19 (120 patients) and TB (non-COVID) cases (120 patients) for training.

In the case of the AXIR4, among the 324 patients' CXRs in the total dataset (**Table 4**), 84 images (23.0%) were randomly selected for testing. Of these 84 images, 42 were COVID-19 cases and 42 were non-TB (non-COVID) cases. The remaining 240 scans were split in a 50:50% ratio to make COVID-19 (120 patients) and others (non-COVID) cases (120 patients) for training.

We applied several data augmentation algorithms to improve the training and classification accuracy of the CNN model and achieved remarkable validation accuracy. For AXIR1, 1,000 images were used for the augmentation of 3,000 images (3 times). For AXIR2, 820 images were used to augment 3,000 images (3.7 times). For AXIR3 and AXIR4, 240 images were used for the augmentation of 1,216 images (5 times). We applied the augmentation method as shown in **Table 5**. During training, the images were randomly rotated by 10°, translated, and horizontally flipped. In some cases, two methods (translation and rotation) were used at the same time.

TABLE 5 | Settings for the image augmentation of training data.

Method	Setting
Rotation angle	10
Width shift	0.2
Height shift	0.2
Horizontal flip	True

Annotation and Classification

We further categorized abnormal patterns of the NIH data as TB or non-TB. TB patterns were then subcategorized into seven active TB pattern classes (consolidation, cavitation, pleural effusion, miliary, interstitial, tree in bud, and lymphadenopathy) and an additional inactive TB pattern class. These TB pattern classes are based on those used by the Centers for Disease Control and Prevention (CDC) of the USA (26, 27). Also, we subcategorized the Shenzhen TB data into sub-classes [according to the ChestX-ray14 dataset (NIH data)], which are infiltration, consolidation, pleural effusion, pneumonia, fibrosis, atelectasis, nodule, pneumothorax, pleural thickening, mass, hernia, cardiomegaly, edema, and emphysema. These additional categorizations are based on the radiological readings for the purpose of the detailed analysis for sub-patterns of false negative (FN) and false positive (FP). The resulting annotated data were reviewed by two radiologists independently. In the case of the TB data, most data are related with infiltration, consolidation, plural effusion, fibrosis, and nodule. These patterns are strongly related with TB patterns.

We also used East Asia countries' data (TB and non-TB disease) from our cooperating hospitals to diversify the trained dataset. Non-TB disease dataset for Easter Asia Hospital is categorized based on NIH-14 disease pattern related with final confirmed diagnosis. In the case of the TB data (Eastern Asian Hospital), we annotated more detailed sub-patterns according to radiological sub-TB patterns. However, these sub-TB patterns are categorized with only radiological readings.

Deep Learning Model and Training Technique

Herein, we used a two-dimensional CNN algorithm with a PyTorch frame for the training and testing for our two-step CAD process. **Figure 2** shows the overall architecture of the proposed CNN model, which is based on the pre-trained ResNet18 (28, 29), using the ImageNet dataset. ResNet, the winner of the 2015 ImageNet competition, is one of the most popular CNN architectures, which provides easy gradient flow for more efficient training. The core idea of ResNet is the introduction of an "identity shortcut" connection, which skips one or more

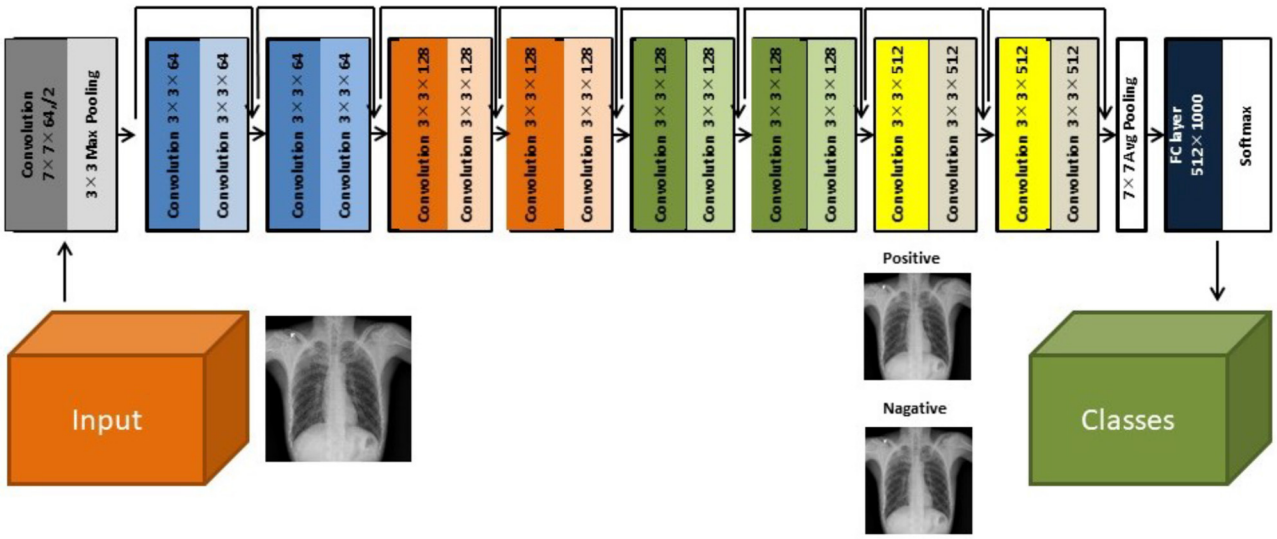

FIGURE 2 | The architecture of the ResNet18 convolutional neural network model (28).

TABLE 6 | Classification performance of AXIR1 (Normal/Abnormal) and AXIR2 (TB/non-TB).

AXIR	Accuracy	Sensitivity	Specificity	Precision	AUC
AXIR1 (Step 1)	0.98	0.99	0.97	0.97	0.98
AXIR2 (Step 2)	0.80	0.72	0.89	0.87	0.80

AUC, area under curve.

layers, thereby providing a direct path to the very early layers in the network, making the gradient updates for those layers much easier.

The verification of the model has been performed using an additional dataset. The performance of the model ResNet18 can be compared with previous work on neural nets and COVID-19 (9, 28) and verified as good matching with therein.

TABLE 7 | Sub-patterns for false positive (FP) and false negative (FN) results in AXIR2.

Prediction results	NIH classification[a]	Number of images	TB pattern in (30)[a]	Total number of images
FP (from East Asian Hospital data)	Infiltration	2	Non-TB	9
	Consolidation	1		
	Atelectasis	3		
	Plural thickening	3		
FN (from Shenzhen data and East Asian Hospital data)	Infiltration	5	Consolidation	23
	Consolidation	8	Consolidation	
	Plural effusion	2	Plural effusion	
	Fibrosis	6	Consolidation	
	Nodule	2	Milliary	

[a] *Sub-patterns are classified with only radiological readings.*

RESULTS

Accuracy of AXIR1 and AXIR2 (Identification of Normal, TB, and Non-TB Patterns)

The performances attained by AXIR1 and AXIR2 are listed in **Table 6**. The accuracies of the two decision trees were 0.98 and 0.80, respectively.

Furthermore, we investigated the classification capability of AXIR2 for normality using 100 normal test data. The normal data can be classified into TB and others with the ratio of 1:3 by AXIR2.

In addition, we analyzed detailed distribution of false negative (FN) and false positive (FP) classification errors in AXIR2. The decision tree made 9 FP and 23 FN predictions, as shown in **Table 7**. Atelectasis and plural thickening (67% of all FPs) and infiltration, consolidation, and fibrosis (NIH classification) (83% of all FNs) are the categories most likely to be involved in such errors. These three sub-patterns can be categorized as consolidation sub-pattern in CDC sub-TB classification.

Accuracy of AXIR3 and AXIR4 (Identification of COVID-19 and Non-COVID Patterns)

Table 8 shows the classification performance of AXIR3 and AXIR4. In the case of the AXIR3 (COVID-19/TB classification), all test data are classified correctly, and the accuracy is 100%. In the case of the AXIR4 (COVID-19/non-TB classification), accuracy was only 0.89 due to low specificity. Therefore, the average value of accuracy over both trees was 0.95, and the average values of sensitivity and specificity were 0.97 and 0.93, respectively.

We tested AXIR1 with 42 COVID-19 test data. Only one COVID-19 image was predicted as normal (FN) by AXIR1. Also,

TABLE 8 | Classification performance of AXIR3 (COVID-19/TB) and AXIR4 (COVID-19/non-TB).

AXIR	Accuracy	Sensitivity	Specificity	Precision	AUC
AXIR3	1.00	1.00	1.00	1.00	1.00
AXIR4	0.89	0.93	0.86	0.87	0.89
Average	0.95	0.97	0.93	0.94	0.95

AUC, area under curve.

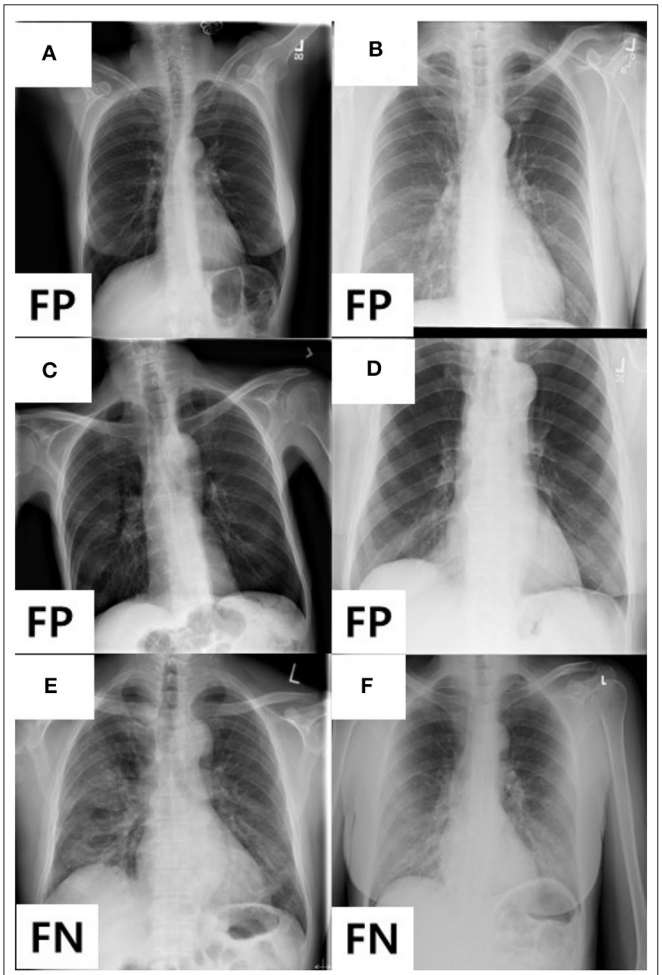

FIGURE 3 | Images showing four FPs predicted as COVID-19 and two FNs predicted as non-TB lung disease in AXIR4 results: infiltration **(A–C)**, pleural thickening **(D)**, and COVID-19 **(E, F)** symptoms.

we investigated the classification results of 42 COVID-19 test data in AXIR2. COVID-19 data were classified by AXIR2 as TB and other in the ratio 4:1.

In addition, we analyzed the detailed distribution of FN and FP results in AXIR4. There are six FPs (annotated as non-TB (non-COVID) but predicted as COVID-19) and three FNs [annotated as COVID-19 but predicted as non-TB (non-COVID)]. **Figure 3** shows the images that produced these results. Two of the three FNs were predicted as TB by AXIR2, whereas one image was predicted as non-TB.

DISCUSSION

The accuracy of AXIR1 (i.e., the binary decision-tree for classification of images as normal or abnormal) is 0.98. This prediction result shows that the ResNet18 model can be used clinically for the screening of abnormality. However, the accuracy of AXIR2 (i.e., the binary decision-tree for classification of images as showing TB or a different disease) is much lower (0.80), as shown in **Table 6**. The sensitivity and specificity for AXIR2 are 0.72 and 0.89 respectively. **Table 7** shows the detailed distribution among these classes for 9 FP and 23 FN predictions of AXIR2. Atelectasis and plural thickening show a higher portion of FP (67%) and infiltration, consolidation and fibrosis are higher potion for FN (83%). In atelectasis and plural thickening, the region can be similar to plural effusion in lower lobe in both side of lung. Thus, the algorithm's prediction results can show larger portion of FP due to atelectasis and plural thickening specifically. Clinically, plural effusion is strongly associated with TB, but atelectasis or plural thickening is not. Moreover, infiltration, consolidation and fibrosis, as defined by the NIH, are strongly associated with TB; however, some of these radiological sub-patterns can be predicted as non-TB. When these sub-patterns are annotated as TB, the position of occurrence was frequently in the upper apex region. The most of cases of FP show that the locations of occurrence are middle or lower lobe area. TB screening is not only limited to the normal/abnormal classification, but can also locate its location in CXR with abnormalities (30, 31). The clavicle region is known to be a difficult area to detect TB because it can obscure the manifestations of TB at the apex of the lung. The automatic suppression of the ribs and clavicles in the CXR could significantly improve the decision of radiologists in the detection of nodule (32, 33). Therefore, applying position-based feature filtering in the algorithm might improve the accuracy. For the analysis of sub-pattern, the data were categorized with only radiological readings. However, all training data structure for the prediction results of TB and non-TB is based on pathological diagnosis.

We analyzed the performance of the classification into COVID-19 and non-COVID through the binary decision trees AXIR3 and AXIR4. We tested AXIR1 and AXIR2 with COVID-19 images. Among the COVID-19 test images, 98% (41 images of 42) were predicted as abnormal in AXIR1. Also, 80% of the COVID-19 images were predicted as TB in AXIR2. However, we tested the AXIR3 and AXIR4 step using all the 42 COVID-19 images for each AXIR. **Table 8** shows that the accuracy of AXIR3 is 100%, although the accuracy of AXIR4 is only 89%. The average sensitivity (97%) is almost same as the 98% reported in (9), whereas the average specificity (93%) is slightly higher than 89%. We think that this is because normal images were excluded already by AXIR1. Also, if we recall that some FN images in AXIR4 (annotated as COVID-19) were categorized as

TB in AXIR2, then those images are predicted as COVID-19 in AXIR3, and the accuracy could be improved in the real process.

Both COVID-19 and TB cause respiratory symptoms (cough and shortness of breath). One of the biggest differences is the speed of onset. TB symptoms do not tend to occur immediately after infection, but gradually appear, unlike COVID-19, which can occur within a few days. In this regard, we have combined the detection of TB or COVID-19.

There are practical considerations that require further investigation. First, this study used a suitable data group as training data for each step, but training data should be confirmed with pathological data. Without the use of pathologically confirmed data, the results of the model are unreliable. Therefore, prediction of new cases requires new pathological data. Second, the proposed three-level decision tree classifier takes three times longer than a one-step process using multiple classifiers. Third, there are many data augmentation strategies for image data. We added more training data to our deep learning model using easy-to-implement methods such as horizontal flip, rotations, and shifts. Image processing techniques using stochastic region sharpening, elastic transforms, randomly erasing patches, and many more to augment data can be considered to improve the performance of the resulting model. Further studies are thus needed on advanced augmentation techniques for building better models and creating a system that does not require gathering a lot of training data to get a reliable statistical model.

CONCLUSIONS

Herein, a deep learning-based three-level decision-tree classifier for detecting TB and non-TB lung diseases, including COVID-19, has been presented and validated using patient data. For each level, a two-dimensional CNN algorithm (ResNet18 model) with PyTorch frame was used with optimized trained data. Accuracies of 98 and 80%, respectively, were achieved for AXIR1 (abnormal vs. normal data) and AXIR2 (TB vs. non-TB data). The lower accuracy of AXIR2 is due to FP atelectasis and plural thickening predictions and FN infiltration, consolidation, and infiltration. An average accuracy of 95% was achieved with AXIR3 (COVID-19 vs. TB) and AXIR4 (COVID-19 vs. other non-TB). We believe that this study will have significant clinical applications, allowing fast follow-up decision making and pre-screening in suspected COVID-19 cases prior to the availability of RT-PCR results.

DATA AVAILABILITY STATEMENT

The data analyzed in this study is subject to the following licenses/restrictions: data sets cannot be made available to the public. Requests to access these datasets should be directed to SYo, yoo7311@gmail.com.

AUTHOR CONTRIBUTIONS

Conception, design, and drafting the manuscript were performed by SYo, BM, and HL. Data collection was performed by DC, JH, MC, and IC. The statistical analysis was performed by HG, TC, and SYu. CC and NN interpreted the results. All authors read and approved the final manuscript.

FUNDING

This research was supported by the National Research Foundation of Korea (NRF) grant funded by the Korea government (MSIP) (No. NRF-2020R1A2C4001910).

REFERENCES

1. Ai T, Yang Z, Hou H, Zhan C, Chen C, Lv W, et al. Correlation of chest CT and RT-PCR testing in coronavirus disease 2019 (COVID-19) in China: a report of 1014 cases. *Radiology.* (2020) 200642. doi: 10.1148/radiol.2020200642. [Epub ahead of print].
2. Fang Y, Zhang H, Xie J, Lin M, Ying L, Pang P. Sensitivity of chest CT for COVID-19: comparison to RT-PCR. *Radiology.* (2020) 10:200432. doi: 10.1148/radiol.2020200432
3. Kanne JP, Little BP, Chung JH, Elicker BM, Ketai LH. Essentials for radiologists on COVID-19: an update—radiology scientific expert panel. *Radiological.* (2020) 200527. doi: 10.1148/radiol.2020200527. [Epub ahead of print].
4. Kong W, Agarwal PP. Chest imaging appearance of COVID-19 infection. *Radiology: Cardiothoracic Imaging.* (2020) 2:e200028. doi: 10.1148/ryct.2020200028
5. Hansell DM, Bankier AA, MacMahon H, McLoud TC, Muller NL, Remy J. Fleischner society: glossary of terms for thoracic imaging. *Radiology.* (2008) 246:697–722. doi: 10.1148/radiol.2462070712
6. Rodrigues J, Hare S, Edey A, Devaraj A, Jacob J, Johnstone A, et al. An update on COVID-19 for the radiologist-A British society of Thoracic Imaging statement. *Clin Radiol.* (2020) 75:323–5. doi: 10.1016/j.crad.2020.03.003
7. Chung M, Bernheim A, Mei X, Zhang N, Huang M, Zeng X, et al. CT imaging features of 2019 novel coronavirus (2019-nCoV). *Radiology.* (2020) 295:202–7. doi: 10.1148/radiol.2020200230
8. Huang C, Wang Y, Li X, Ren L, Zhao J, Hu Y, et al. Clinical features of patients infected with 2019 novel coronavirus in Wuhan, China. *Lancet.* (2020) 395:497–506. doi: 10.1016/S0140-6736(20)30183-5
9. Cohen JP, Morrison P, Dao L. COVID-19 image data collection. *arXiv [Preprint].* (2020). arXiv:2003.11597.
10. Minaee S, Kafieh R, Sonka M, Yazdani S, Soufi GJ. Deep-COVID: predicting COVID-19 from chest x-ray images using deep transfer learning. *arXiv [Preprint].* (2020). arXiv:2004.09363.
11. Irvin J, Rajpurkar P, Ko M, Yu Y, Ciurea-Ilcus S, Chute C, et al. (editors). Chexpert: A large chest radiograph dataset with uncertainty labels and expert comparison. IN: *Proceedings of the AAAI Conference on Artificial Intelligence.* (2019). doi: 10.1609/aaai.v33i01.3301590
12. Anderson L, Dean A, Falzon D, Floyd K, Baena I, Gilpin C, et al. *Global Tuberculosis Report 2015.* World Health Organization. (2015).
13. Van't Hoog A, Meme H, Van Deutekom H, Mithika A, Olunga C, Onyino F, et al. High sensitivity of chest radiograph reading by clinical officers in a tuberculosis prevalence survey. *Int J Tuberculosis Lung Dis.* (2011) 15:1308–14. doi: 10.5588/ijtld.11.0004
14. Melendez J, Sánchez CI, Philipsen RH, Maduskar P, Dawson R, Theron G, et al. An automated tuberculosis screening strategy combining X-ray-based computer-aided detection and clinical information. *Sci Rep.* (2016) 6:25265. doi: 10.1038/srep25265
15. Van Ginneken B, Katsuragawa S, ter Haar Romeny BM, Doi K, Viergever MA. Automatic detection of abnormalities in chest radiographs using local texture analysis. *IEEE Trans Med Imaging.* (2002) 21:139–49. doi: 10.1109/42.993132

16. Hogeweg L, Mol C, de Jong PA, Dawson R, Ayles H, van Ginneken B (editors). Fusion of local and global detection systems to detect tuberculosis in chest radiographs. IN: *International Conference on Medical Image Computing and Computer-Assisted Intervention*. Beijing: Springer (2010). doi: 10.1007/978-3-642-15711-0_81
17. Shen R, Cheng I, Basu A. A hybrid knowledge-guided detection technique for screening of infectious pulmonary tuberculosis from chest radiographs. *IEEE Trans Biomed Eng.* (2010) 57:2646–56. doi: 10.1109/TBME.2010.2057509
18. Xu T, Cheng I, Mandal M (editors). Automated cavity detection of infectious pulmonary tuberculosis in chest radiographs. IN: *2011 Annual International Conference of the IEEE Engineering in Medicine and Biology Society*. Boston, NY: IEEE (2011).
19. Pawar CC, Ganorkar S. Tuberculosis screening using digital image processing techniques. *Int Res J Eng Technol.* (2016) 3:623–7.
20. Qin ZZ, Sander MS, Rai B, Titahong CN, Sudrungrot S, Laah SN, et al. Using artificial intelligence to read chest radiographs for tuberculosis detection: a multi-site evaluation of the diagnostic accuracy of three deep learning systems. *Sci Rep.* (2019) 9:1–10. doi: 10.1038/s41598-019-51503-3
21. Antani S, Candemir S. *Automated Detection of Lung Diseases in Chest X-rays*. US National Library of Medicine. (2015).
22. Tang Y-X, Tang Y-B, Han M, Xiao J, Summers RM (editors). Abnormal chest X-ray identification with generative adversarial one-class classifier. IN: *2019 IEEE 16th International Symposium on Biomedical Imaging (ISBI 2019)*. Venice: IEEE (2019). doi: 10.1109/ISBI.2019.8759442
23. Baltruschat IM, Nickisch H, Grass M, Knopp T, Saalbach A. Comparison of deep learning approaches for multi-label chest X-ray classification. *Sci Rep.* (2019) 9:1–10. doi: 10.1038/s41598-019-42294-8
24. Wang X, Peng Y, Lu L, Lu Z, BagheriM, Summers RM (editors). Chestx-ray8: Hospital-scale chest x-ray database and benchmarks on weakly-supervised classification and localization of common thorax diseases. In: *Proceedings of the IEEE Conference on Computer Vision and Pattern Recognition*. Honolulu, HI (2017). doi: 10.1109/CVPR.2017.369
25. Elkins A, Freitas FF, Sanz V. Developing an App to interpret Chest X-rays to support the diagnosis of respiratory pathology with Artificial Intelligence. *arXiv [Preprint].* (2019). doi: 10.21037/jmai.2019.12.01
26. Kieu PN, Tran HS, Le TH, Le T, Nguyen TT (editors). Applying multi-CNNs model for detecting abnormal problem on chest x-ray images. IN: *2018 10th International Conference on Knowledge and Systems Engineering (KSE)*. Ho Chi Minh: IEEE (2018). doi: 10.1109/KSE.2018.8573404
27. Nachiappan AC, Rahbar K, Shi X, Guy ES, Mortani Barbosa Jr EJ, Shroff GS, et al. Pulmonary tuberculosis: role of radiology in diagnosis and management. *Radiographics.* (2017) 37:52–72. doi: 10.1148/rg.2017160032
28. He K, Zhang X, Ren S, Sun J, editors. Deep residual learning for image recognition. IN: *Proceedings of the IEEE Conference on Computer Vision and Pattern Recognition* (Las Vegas, NV) (2016). doi: 10.1109/CVPR.2016.90
29. Yoon HJ, Jeong YJ, Kang H, Jeong JE, Kang D-Y. Medical image analysis using artificial intelligence. *Prog Med Phys.* (2019) 30:49–58. doi: 10.14316/pmp.2019.30.2.49
30. Van Ginneken B, ter Haar Romeny BM. Automatic segmentation of lung fields in chest radiographs. *Med Phys.* (2000) 27:2445–55. doi: 10.1118/1.1312192
31. Hogeweg L, Sánchez CI, de Jong PA, Maduskar P, van Ginneken B. Clavicle segmentation in chest radiographs. *Med Image Anal.* (2012) 16:1490–502. doi: 10.1016/j.media.2012.06.009
32. Freedman MT, Lo S-CB, Seibel JC, Bromley CM. Lung nodules: improved detection with software that suppresses the rib and clavicle on chest radiographs. *Radiology.* (2011) 260:265–73. doi: 10.1148/radiol.11100153
33. Jaeger S, Karargyris A, Candemir S, Siegelman J, Folio L, Antani S, et al. Automatic screening for tuberculosis in chest radiographs: a survey. *Quant Imaging Med Surg.* (2013) 3:89. doi: 10.3978/j.issn.2223-4292.2013.04.03

Conflict of Interest: The authors declare that the research was conducted in the absence of any commercial or financial relationships that could be construed as a potential conflict of interest.

Copyright © 2020 Yoo, Geng, Chiu, Yu, Cho, Heo, Choi, Choi, Cung Van, Nhung, Min and Lee. This is an open-access article distributed under the terms of the Creative Commons Attribution License (CC BY). The use, distribution or reproduction in other forums is permitted, provided the original author(s) and the copyright owner(s) are credited and that the original publication in this journal is cited, in accordance with accepted academic practice. No use, distribution or reproduction is permitted which does not comply with these terms.

frontiers in Medicine

BRIEF RESEARCH REPORT
published: 02 September 2020
doi: 10.3389/fmed.2020.00497

Expression of ALDH and SOX-2 in Pulmonary Sclerosing Pnemocytoma (PSP) of the Lung: Is There a Meaning Behind?

Beatrice Aramini[1], Valentina Masciale[1], Beatrice Manfredini[1], Daniel Bianchi[1], Federico Banchelli[2], Roberto D'Amico[2], Federica Bertolini[3], Massimo Dominici[3], Uliano Morandi[1] and Antonino Maiorana[4]*

[1] Division of Thoracic Surgery, Department of Medical and Surgical Sciences, University of Modena and Reggio Emilia, Modena, Italy, [2] Department of Medical and Surgical Sciences, Center of Statistic, University of Modena and Reggio Emilia, Modena, Italy, [3] Division of Oncology, Department of Medical and Surgical Sciences, University of Modena and Reggio Emilia, Modena, Italy, [4] Department of Medical and Surgical Sciences, Institute of Pathology, University of Modena and Reggio Emilia, Modena, Italy

OPEN ACCESS

Edited by:
Rifat Hamoudi, University of Sharjah, United Arab Emirates

Reviewed by:
Sheng-Ming Wu, Taipei Medical University, Taiwan
Pai-Chien Chou, Taipei Medical University Hospital, Taiwan

***Correspondence:**
Beatrice Aramini
beatrice.aramini@unimore.it

Specialty section:
This article was submitted to Pulmonary Medicine, a section of the journal Frontiers in Medicine

Received: *05 May 2020*
Accepted: *20 July 2020*
Published: *02 September 2020*

Citation:
Aramini B, Masciale V, Manfredini B, Bianchi D, Banchelli F, D'Amico R, Bertolini F, Dominici M, Morandi U and Maiorana A (2020) Expression of ALDH and SOX-2 in Pulmonary Sclerosing Pnemocytoma (PSP) of the Lung: Is There a Meaning Behind? Front. Med. 7:497. doi: 10.3389/fmed.2020.00497

Background: Pulmonary sclerosing pneumocytoma (PSP) is a rare benign pulmonary tumor that derives from primitive respiratory epithelium of the pulmonary alveolus. The etiology and pathogenesis are still unclear. Histopathological diagnosis focuses on cells that are positive for TTF1, EMA, cytokeratin-7, and CAM 5.2. The aim of our study is to highlight the elevated expression of ALDH and the presence of SOX-2 in pulmonary sclerosing pneumocytoma.

Methods: We report five cases of pulmonary sclerosing pneumocytoma undergone surgery at our Division of Thoracic Surgery, during a period between 1994 and 2011. ALDH and SOX-2 markers were also tested for positivity in all the patients.

Results: Patients showed elevated expression of ALDH during immunohistochemistry and mild expression of SOX-2, although in two cases in which SOX-2 was highly expressed. Among these two patients, one presented with lymph node recurrence while the other had no recurrence with a PET-positive nodule. In particular, the patient who had developed recurrence had an ALDH score of 4 and a SOX-2 score of 3, whereas the patient with the PET-positive nodule showed an ALDH score of 4 with a mild SOX-2 expression of score 1.

Conclusions: This is the first attempt demonstrating the elevated expression of ALDH in this disease. SOX-2 expression was noted in both the patient who developed recurrence and the patient with a PET-positive nodule. We believe that further investigation may be highly useful to better characterize these two markers as well as understand their function.

Keywords: pulmonary slerosing pneumocytoma, benign disease, lung rare disease, ALDH, SOX-2

INTRODUCTION

Pulmonary sclerosing pneumocytoma (PSP) is a rare benign tumor in the lung (1). This disease was firstly described by Liebow and Hubell1 as sclerosing hemangioma of the lung owing to prominent sclerotization and vascularization of the tissue. Pathologically, sclerosing hemangioma (SH) is typically composed of solid, papillary, sclerotic, or hemangiomatous components (2). The term "sclerosing hemangioma" was recently changed in 2015 by the WHO Classification of Lung Tumors as "pulmonary sclerosing pneumocytoma" (3). PSP was thought to be a vascular tumor but greater knowledge of this disease has led scientists to reconsider PSP as derived from primitive respiratory epithelium of the pulmonary alveolus, principally in type II alveolar cells (4). However, vascularization of this tumor is one of the main characteristics (4). PSP is difficult to recognize due to the lack of significant clinical or imaging features and at first glance appears to be a benign nodule such as hamartoma, tuberculoma, bronchial cysts, or certain lung cancer nodules (5). Although the etiology and pathogenesis of PSP are still unclear, recently it has been clarified that PSP is derived from the epithelial part of the lung, which gives rise to the name sclerosing pneumocytoma of the lung (6). PSPs are composed of four major histologic patterns, which are hemangiomatous, papillary, sclerotic, and solid, as well as different radiological characteristics made apparent by computed tomography (CT) findings according to their composition (6–14). It has been described that PSP typically presents as a well-defined, juxta-pleural nodule with strong and homogeneous enhancement (14–16) on CT, while several studies have analyzed CT findings of PSP and its pathologic correlation (14, 15). However, there is a limitation due to the small number of patients and the preoperative imaging modalities used in clinical practice to diagnosis PSP (16–18). In addition, a few studies investigated PSP using 18F-fluorodeoxyglucose positron emission tomography (FDG PET) (19, 20). The interval between the PET and CT study was a mean of 3.2 months (5–10); however, the hypermetabolism in pneumocytoma has not yet been defined or correlated with the possibility of developing into a malignant disease.

Patients are usually asymptomatic in which the PSP is detected coincidentally. Moreover, a cough, chest pain, and haemoptysis may also occur (6). PSP is often a solitary, well-defined, round or oval, homogeneous nodule, or mass (14–16); however, there are also cases of metastases to the lymph nodes, pleura, and bones (14, 17, 18). Patients may present with a mass lesion of up to 7 cm although 73% of lesions measure under 3 cm (8, 10). Marginal pseudocapsules (50%), overlying vessels (26.3%), air gap (2.6%), and halo sign (17.1%) are among thoracic CT findings (12). Occasionally, pleural-based, polypoid lesions may mimic a solitary fibrous tumor. Often the tumor consists of superficial cuboidal and round interstitial cells with a combination of four patterns. In the case of a biopsy with a predominance of papillary components of the sclerosing pneumocytoma, diagnosis may be difficult. In addition, both superficial cuboidal cells and round interstitial cells are positively immunoreactive for TTF1 and EMA (10, 19). TTF1 is used in the diagnosis of lung adenocarcinoma and may be misleading for diagnosing PSP. Napsin A, a human aspartic proteinase, shows immunohistochemical reactivity in type II pneumocytes with a granular and cytoplasmic staining pattern (18). It has been widely used in the panel for diagnosis of lung adenocarcinoma along with TTF-1 (17). Recently it has been demonstrated that Napsin A preferentially stains cuboidal surface cells, rather than stromal round cells, in sclerosing pneumocytoma (20, 21). Round cells are generally uniformly negative for pan-cytokeratin and positive for cytokeratin-7 and CAM 5.2 in few cases (10). However, markers related to possible malignancy transformation have not yet been identified.

The idea to test ALDH and SOX2 markers derives from the consideration of the pathological characteristics of this tumor constituted by an abundant vascularized component, and for the roles that ALDH and SOX2 may have in the process of endothelial vascular tumor progression. In particular, it has been shown that ALDH is able to detect endothelial stem-like cells in tumor with a role into the angiogenetic process (22), although SOX2 is involved into the endothelial differentiation process since this transcription factor have been shown to be essential mediators in vascular development (23, 24).

For these considerations, the aim of our study is to highlight the elevated expression of ALDH in the pneumocytoma of the lung as described, as well as the presence of SOX-2 markers in patients with a lymph node recurrence, and in one with a PET-positive nodule. However, we are conscious of the limitation of our study for the low number of patients. If the presence of these two markers will be confirmed in a larger cohort, it would be helpful for the setting of future target therapies, which may avoid the patient from lung resection for a benign disease.

MATERIALS AND METHODS

We describe five patients (all female with a mean age of 54 years) who underwent surgery in our department between 1994 and 2011 for a pulmonary sclerosing pneumocytoma of the lung. All patients were subjected to major lung resection. The diagnosis of pneumocytoma has been carried out by morphological evaluation and immunostaining of transcription termination factor 1 (TTF-1), pan-citocheratine (MNF116), and epithelial membrane antigen (EMA) (3). No postoperative complications were noted. Patients have been checked by the oncologist for the definition of signs or symptoms for the disease and for the follow-up. Data analysis was carried out by reporting descriptive statistics of the study sample.

Immunohistochemistry and Microscopic Evaluation

Immunohistochemical stains were performed on formalin-fixed, paraffin-embedded 5 μm sections. The sections were first deparaffinized in xylene and further heated for 15 min in a 95°C water bath with a 10 mM sodium citrate buffer, then washed in PBS until the buffer had cooled. Incubation in 3% H_2O_2 at room temperature for 10 min was performed. Slides were then blocked with 10% goat serum in TBS for 15 min in order to reduce non-specific background. Sectional

incubation with rabbit monoclonal mouse anti-ALDH (1:100) (ab−134188; Abcam, Cambridge, MA, USA) and mouse monoclonal anti-SOX-2 (1:200) (MA1-014 Thermo Fisher Scientific, Meridian Road Rockford, IL, USA) was performed overnight at 4°C. Specimens were washed in PBS and incubated with a biotinylated secondary antibody (PK-4001; Vector Labs, USA) for 30 min at room temperature and then stained with 3,3'-Diaminobenzidine tetrahydrochloride (DAB) after which tissue sections were counterstained with Mayer's Hematoxylin. A secondary antibody-only staining sample was used as a background control to evaluate positivity for ALDH and SOX-2, respectively. Images were collected and positivity was evaluated by a Zeiss AxioCam ICc 3 High-Resolution through an Axioskop microscope camera. For the assessment, section samples were investigated employing a semi-quantitative method using a score value for the positivity of the markers. Shown here are the score classes: 0 (<5% positive), 1 (5–25% positive), 2 (>25–50% positive), 3 (>50–75% positive), and 4 (>75% positive) (25). Sections were scored by two trained investigators who were blinded to the outcome of the patient and other clinical findings.

RESULTS

Clinical Results

All patients were free from the disease after surgery and received a follow-up by chest and abdomen CT after 3, 6, 12, 18, 24, 36, 48, and 52 months. No recurrence was noted in four patients, although one patient had local lymph node recurrence at station 9, 11, and 12 and therefore underwent chemotherapy. PET-CT FDG was positive in only one patient (SUV max 2.3) for the lung nodule.

Identification of Tumor Endothelial Cells With High Aldehyde Dehydrogenase Activity

To evaluate ALDH and SOX-2 positivity in these five cases of pneumocytoma, immunohistochemistry was performed and a score value was then assigned, as previously described (25). Tissue sections were examined at 10, 20, and 40x magnification to assign the appropriate values. ALDH-positive cells from tissue slides, represented by brown cytoplasm, and SOX-2 positive cells by brown nuclei, were both analyzed at 10, 20, and 40x magnification (**Figures 1**, **2**). Three of the five cases of pneumocytoma showed an ALDH score value of 4, while the other two cases had a score value of 3. On the other hand, for three of the five cases of pneumocytoma, SOX-2 score value was 0, despite one case having a score value of 3 while the last case had a score value of 1.

To analyze whether ALDH is expressed in human pneumocytoma, an immunohystochemical staining was performed on the paraffin-embedded sections of the tumor patient. Tissue sections were examined at 10, 20, and 40x magnification to assign the appropriate values. ALDH staining was strongly positive in three of the five patient cases, which had

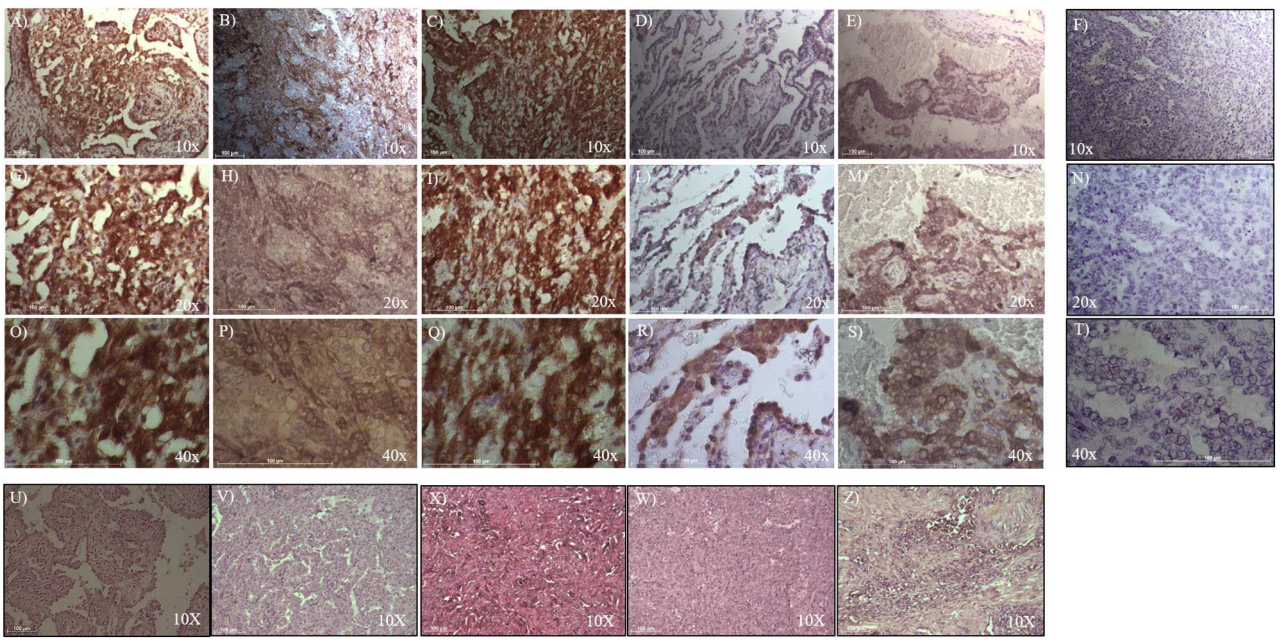

FIGURE 1 | Immunohistochemical analysis of ALDH positive cells in five cases of pneumocytoma of the lung. Tissue sections were stained with anti-ALDH antibody to detect the positivity in these five different cases of pneumocytoma of the lung. **(A–O)** Case 1, **(B–P)** Case 2, **(C–Q)** Case 3, **(D–R)** Case 4, **(E–S)** Case 5. Semi-quantitative method was used to assess the ALDH positivity of the tumor cells: 0 (<5% positive), 1 (5–25% positive), 2 (>25–50% positive), 3 (>50–75% positive), and 4 (>75% positive). Representative images of the five cases, stained for ALDH, are shown at 10, 20, and 40x magnification. Representative images corresponding to each tumor samples stained with hematoxylin and eosin **(U, V, X, W, Z)** are shown at 10x magnification. Isotype control for ALDH antibody was shown **(F, N, T)**. Scale bar = 100 μm.

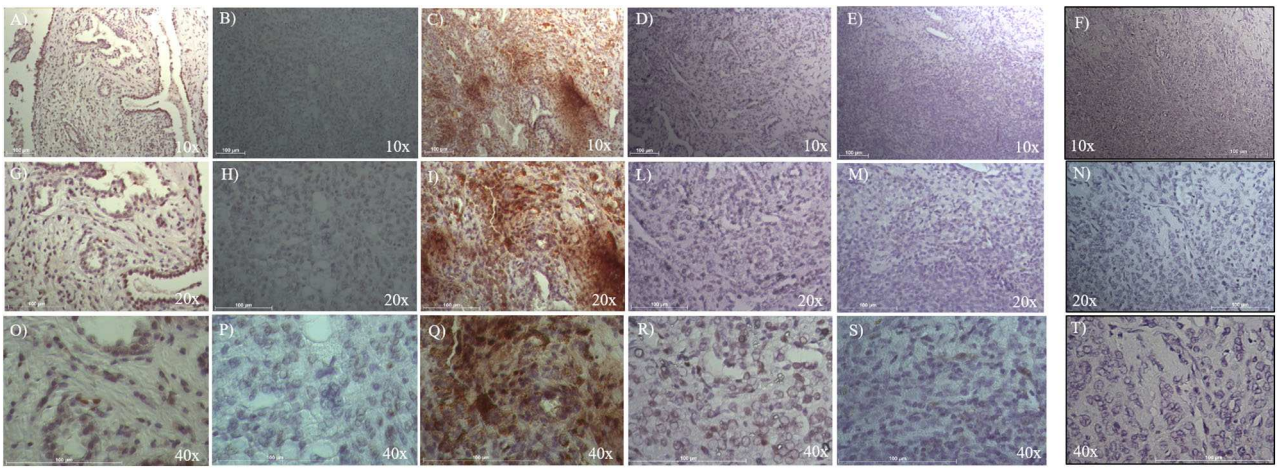

FIGURE 2 | Immunohistochemical analysis of SOX-2 positive cells in five cases of pneumocytoma of the lung. Tissue sections were stained with anti-SOX-2 antibody to detect the positivity in these five different cases of pneumocytoma of the lung. **(A–O)** Case 1, **(B–P)** Case 2, **(C–Q)** Case 3, **(D–R)** Case 4, **(E–S)** Case 5. Semi-quantitative method was used to assess the SOX-2 positivity of the tumor cells: 0 (<5% positive), 1 (5–25% positive), 2 (>25–50% positive), 3 (>50–75% positive), and 4 (>75% positive). Representative images of the five cases are shown at 10, 20, and 40x magnification. Isotype control for SOX-2 antibody was shown **(F, N, T)**. Scale bar = 100 μm.

TABLE 1 | Patients characteristics.

Patient	Tumor hystotype and characteristic	ALDH expression	SOX-2 expression
Pt#1	Pneumocytoma	3	0
Pt#2	Pneumocytoma	4	1
Pt#3	Pneumocytoma	4	3
Pt#4	Pneumocytoma	4	0
Pt#5	Pneumocytoma with lymphonodes local recurrence	3	0

This table represents the five patients case of pneumocytoma analyzed for the immunohystochemical expression of ALDH and SOX-2. A score value for ALDH and SOX-2 was assigned using the following score classes: 0 (<5% positive), 1 (5–25% positive), 2 (>25–50% positive), 3 (>50–75% positive), and 4 (>75% positive).

a score value of 4 (**Figures 1B–R**, **Table 1**). Regarding the other two patients, ALDH was strongly positive, with a score value of 3 (**Figures 1A–O,S**, **Table 1**).

Identification of Cells Expressing Stem Cell Factor SOX-2

To evaluate SOX-2 positivity in these five cases of pneumocytoma, immunohistochemistry was performed, and a score value was assigned as previously described (25). Tissue sections were examined at 10, 20, and 40x magnification to assign the appropriate values. SOX-2 positive cells were represented by brown nuclei and were analyzed at 10, 20, and 40x magnification (**Figure 2**). Three of the five patient cases of pneumocytoma had a SOX-2 score value equal to 0 (**Figures 2A-S**, **Table 1**), while the remaining two patients had a score value of 3 (**Figures 2C–Q**) and a score value of 1 (**Figures 2B–P**, **Table 1**).

DISCUSSION

Pulmonary sclerosing pneumocytoma (PSP) is a rare benign tumor typically occurring in women with a favorable prognosis. Recurrence for this disease is infrequent, although not impossible to find. The nomenclature for this benign disease (8–10) has recently been renamed "pulmonary sclerosing pneumocytoma" (6).

It is extremely difficult to obtain an accurate diagnosis for PSP due to its low incidence and the impossibility of establishing a clinical and radiological differential diagnosis from other diseases. This is well-documented in the scientific literature where surgery is the gold standard treatment and the most common immunohistochemistry markers are used for diagnosis (**Table 2**) (15). Moreover, due to the frequent expression in females, estrogen receptors have been studied using immunohistochemistry, which has revealed an overexpression of ERbeta in 91.9% of patients affected by the disease (19, 20). The frequent markers used for diagnosis indicate positivity for EMA (epithelial membrane antigen), TTF-1 (transcription termination factor 1), and CK-7 (cytokeratin-7) staining (**Table 2**) (18, 26–35). However, currently no specific markers in this type of benign tumor have been identified.

Our study is the first attempt to show the presence of ALDH and SOX-2 in pulmonary sclerosing pneumocytoma of the lung. In particular, we decided to test ALDH and SOX2 in our PSP samples for the well-known vascular aspect of this tumor which may be associated with the role that these two markers have into the tumor vascularization process. Recently, it has been revealed that tumor endothelial cells were different from normal

TABLE 2 | Review of the literature regarding PSP of the lung.

Author/year	Patients enrolled (n)	Gender (M/F)	Age (Mean)	Type of treatment	IHC marker	Methastatic lymphonodes	Recurrence
Hu et al. (26)	46	5 M 41 F	51.4	45/46 Surgery −21 enucleation −9 wedge resections −15 lobectomies	/	/	No
Devouassoux-Shisheboran et al. (18)	100	17 M 83 F	46	54/100 Surgery: 5 wedge resections 37 lobectomies 2 bilobectomies 1 pneumonectomy - 9 procedures not specified specificata	-pancytokeratin+; CAM 5.2+, CK7 +, EMA + calretinin –; CK5/6 – TTF1 +; Sp A e B + chromogranin –; synaptophysin –; Leu 7 – - S100 -	Yes, 1 case	No
Shin et al. (27)	76	9 M 67 F	50	45/76 Surgery: 33 segmentectomies 11 lobectomies - 1 bilobectomies	TTF1+, cytokeratin +, EMA+; - ki-67–	/	/
Yang et al. (28)	59	2 M 57 F	49.85	Wedge resection (58 wedge resections)	Surface cell AE1/AE3+ e CK7+; Stromal cell AE1/AE3- e CK7+; - TTF1+ e EMA+	No	No
Lei et al. (29)	28	3 M 25 F	46.1	13 enucleation 7 wedge resection 8 lobectomies	/	No	Yes
Park et al. (30)	32	1 M 31 F	47.8	19 lobectomies 5 wedge resections 1 segmentectomy 7 wedge resections	/	Yes, 1 case	No
Cho et al. (31)	11	1 M 10 F	48.6	Surgery	MMP-9 + Tubulinα + IGF1 +	/	/
Schmidt (32)	6	/	/	/	TTF1 + Napsin A +	/	/
Wu et al. (33)	18	2 M 16 F	44.6	/	P40 + TTF1+, SHL+, EMA+, Vimentin+	No	No
Lovrenski et al. (34)	6	1 M 5 F	/	Surgery	TTF1+ e panCK +	No	No

This Table shows treatments and immunohistochemical characteristics. ALDH and SOX-2 have been never considered.

endothelial cells in various aspects such as gene expression profiles and for the activities of the ALDH, enzyme that plays a key role in the metabolism of aldehydes. Several studies showed that different type of stem cell types including hematopoietic stem cells and neural stem cells possess high ALDH activities. Thus, ALDH is used extensively as a stem cell marker, also for endothelial stem-like cells (22). Scientific advantages have shown that ALDH is upregulated in human endothelial cells *in vivo* and may be involved in tumor angiogenesis in cancer patients (36). There is likely an important role for ALDH in the formation of this tumor, which derives from vascular endothelial cells. On this marked trail, our results show a very high expression of ALDH (score of 4) in three patients and a high expression (score of 3) in the other two patients. Additionally, we found that the positivity of ALDH was sparsely distributed within the tumor, which may support endothelial cell heterogeneity. This concept may be attributed to the fact that ALDH expression levels are linked to the tumor microenvironment or tumor malignancy, which may affect ALDH expression in the endothelial cells themselves (37). Furthermore, the evaluation of SOX-2 in our patients' tumors derived from the knowledge that SOX-2 is known to play an important role in vascular development and disease, since its transcription factors have been shown to be essential mediators in vascular development, and in the developing endothelium (23). The involvement of SOX-2 may be crucial also for the angiogenesis in this type of tumor, synergistically participating with ALDH positive cells in the vascular impairment of pneumocytoma (22). Interestingly, SOX-2 was found to be highly expressed (score of 3) in only one patient: the same patient showing an ALDH score of 4 and lymph node recurrence, which is highly uncommon for this disease (24).

Although we are conscious of the fact that our study focuses on a small number of patients, due to the rarity of this benign disease of the lung, we strongly believe that the presence of

ALDH and SOX-2 in pneumocytoma of the lung requires deeper analysis, especially in patients who show recurrence. This will be helpful for understanding the molecular mechanisms behind the phenomenon, and for developing future targeted therapies, which may be more effective than surgery in removing or controlling the disease.

DATA AVAILABILITY STATEMENT

The raw data supporting the conclusions of this article will be made available by the authors, without undue reservation.

ETHICS STATEMENT

This Study has been approved by the Ethics Committee at University Hospital of Modena, MODENA, Italy, on 4 June 2019, Prot. N. 395/2019/OSS/AOUMO. The patients/participants provided their consent to participate in this study.

AUTHOR CONTRIBUTIONS

The idea for the manuscript was conceived in February 2019 by BA and was further developed by VM, DB, BM, FBa, RD'A, FBe, MD, UM, and AM was involved in histopathological diagnosis. BA and VM wrote the first draft of the manuscript. BA and UM have been involved in surgery and tissue collection. VM performed laboratory experiments. BA, VM, FBa, MD, FBe, RD'A, AM, and UM all reviewed the manuscript and were involved in its critical revision before submission. All authors read and approved the final manuscript.

FUNDING

This Project has been supported by funds from the Division of Thoracic Surgery of the University Hospital of Modena and from the Institute of Pathology, Department of Medical and Surgical Sciences, University of Modena and Reggio Emilia, Modena, Italy. These funds were used to buy Laboratory Equipment and to support the project and people involved.

REFERENCES

1. Yalcin B, Bekci TT, Kozacioglu S, Bolukbas O. Pulmonary sclerosing pneumocytoma, a rare tumor of the lung. *Respir Med Case Rep*. (2019) 26:285–7. doi: 10.1016/j.rmcr.2019.02.002
2. Liebow AA, Hubbell DS. Sclerosing hemangioma (histiocytoma, xanthoma) of the lung. *Cancer*. (1956) 9:53e75.
3. Hishida T, Yoshida J, Nishimura M, Ishii G, Nishiwaki Y, Nagai K. Multiple sclerosing hemangiomas with a 10-year history. *Jpn J Clin Oncol*. (2005) 35:37e9. doi: 10.1002/1097-0142(195601/02)9:1<53::AID-CNCR2820090104>3.0.CO;2-U
4. Travis WD, Brambilla E, Nicholson AG, Yatabe Y, Austin JHM, Beasley MB, et al. The 2015 World Health Organization of lung tumors. *J Thorac Oncol*. (2015) 10:1243–60. doi: 10.1097/JTO.0000000000000630
5. Cheung YC, Ng SH, Chang JWC, Tan CF, Huang SF, Yu CT. Histopathological and CT features of pulmonary sclerosing haemangiomas. *Clin Radiol*. (2003) 58:630e5. doi: 10.1016/S0009-9260(03)00177-6
6. Cardemil G, Fernández E, Riffo P, Reyes D, Ledezma R, Mira M, et al. Sclerosing hemangioma presenting as a solitary lung nodule. report of one case. *Rev Med Chile*. (2004) 132:853–6. doi: 10.4067/S0034-98872004000700010
7. Keylock CPTJB, Galvin JR, Franks TJ. Sclerosing hemangioma of the lung. *Arch Pathol Lab Med*. (2009) 133:820–5. doi: 10.1043/1543-2165-133.5.820
8. Danciu M, Lunguleac T, Grigorescu C. Incidental finding of a sclerosing hemangioma in a Caucasian woman. *Rom J Morphol Embryol*. (2015) 56:545–8.
9. Haimoto H, Tsutsumi Y, Nagura H, Nakashima N, Watanabe K. Immunohistochemical study of so-called sclerosing haemangioma of the lung. *Vichows Arch A Pathol Anat*. (1985) 407:419–30. doi: 10.1007/BF00709988
10. Nakanishi K, Kohzaki S, Fujimoto S, Horita Y, Hayashi K. Pulmonary sclerosing hemangioma: report of a case with emphasis on dynamic MR imaging findings. *Radiat Med*. (1997) 15:117–9.
11. Iyoda A, Hiroshima K, Shiba M, Haga Y, Moriya Y, Sekine Y, et al. Clinicopathological analysis of pulmonary sclerosing hemangioma. *Ann Thorac Surg*. (2004) 78:1928–31. doi: 10.1016/j.athoracsur.2004.05.069
12. Sugio K, Yokoyama H, Kaneko S, Ishida T, Sugimachi K. Sclerosing hemangioma of the lung: radiographic and pathological study. *Ann Thorac Surg*. (1992) 53:295–300. doi: 10.1016/0003-4975(92)91336-8
13. Chung MJ, Lee KS, Han J, Sung YM, Chong S, Kwon OJ. Pulmonary sclerosing hemangioma presenting as solitary pulmonary nodule: dynamic CT findings and histopathologic comparisons. *Am J Roentgenol*. (2006) 187:430–7. doi: 10.2214/AJR.05.0460
14. Im JG, Kim WH, Han MC, Han YM, Chung JW, Ahn JM, et al. Sclerosing hemangiomas of the lung and interlobar fissures: CT findings. *J Comp Assist Tomogr*. (1994) 18:34–8. doi: 10.1097/00004728-199401000-00007
15. Xie RM, Zhou XH, Lu PX, He W. Diagnosis of pulmonary sclerosing hemangioma with incremental dynamic CT: analysis of 20 cases. *Chin J Tuberculosis Respir Dis*. (2003) 26:7–9.
16. Lin H, Yao H, Peng F. CT image morphology features of pulmonary sclerosing hemangiomas. *Chin Ger J Clin Oncol*. (2011) 10:19–23. doi: 10.1007/s10330-011-0727-5
17. Wang QB, Chen YQ, Shen JJ, Zhang C, Song B, Zhu XJ, et al. Sixteen cases of pulmonary sclerosing haemangioma: CT findings are not definitive for preoperative diagnosis. *Clin Radiol*. (2011) 66:708–14. doi: 10.1016/j.crad.2011.03.002
18. Devouassoux-Shisheboran M, Hayashi T, Linnoila RI, Koss MN, Travis WD. A clinicopathologic study of 100 cases of pulmonary sclerosing hemangioma with immunohistochemical studies: TTF-1 is expressed in both round and surface cells, suggesting an origin from primitive respiratory epithelium. *Am J Surg Pathol*. (2000) 24:906–16. doi: 10.1097/00000478-200007000-00002
19. Liu W, Tian XY, Li Y, Zhao Y, Li B, Li Z. Coexistence of pulmonary sclerosing hemangioma and primary adenocarcinoma in the same nodule of lung. *Diagn Pathol*. (2011) 6:41–6. doi: 10.1186/1746-1596-6-41
20. Hara M, Iida A, Tohyama J, Miura N, Shiraki N, Itoh M, et al. FDG-PET findings in sclerosing hemangioma of the lung: a case report. *Rad Med*. (2001) 19:215–8. Available online at: https://europepmc.org/article/med/11550723
21. Timpone V, Danielson D, Woods A, Clark B. FDG–PET imaging findings of a pulmonary sclerosing hemangioma. *Eur J Radiol Extra*. (2011) 79:e65–7. doi: 10.1016/j.ejrex.2011.05.003
22. Ohmura-Kakutani H, Akiyama K, Maishi N, Ohga N, Hida Y, Kawamoto T, et al. Identification of tumor endothelial cells with high aldehyde dehydrogenase activity and a highly angiogenic phenotype. *PLoS ONE*. (2014) 9:e113910. doi: 10.1371/journal.pone.0113910
23. Yao Y, Yao J, Boström KI, Martin KA. SOX Transcription Factors in Endothelial Differentiation and Transitions. *Front Cardiovasc Med*. (2019) 6:30. doi: 10.3389/fcvm.2019.00030
24. Horiguchi K, Fujiwara K, Yoshida S, Tsukada T, Hasegawa R, Takigami S, et al. CX3CL1/CX3CR1-signalling in the CD9/S100β/SOX2-positive adult pituitary stem/progenitor cells modulates differentiation into endothelial cells. *Histochem Cell Biol*. (2020) 153:385–96. doi: 10.1007/s00418-020-01862-0
25. Kahlert C, Bergmann F, Beck J, Welsch T, Mogler C, Herpel E, et al. Low expression of aldehyde dehydrogenase 1A1 (ALDH1A1) is a prognostic

marker for poor survival in pancreatic cancer. *BMC Cancer*. (2011) 11:275. doi: 10.1186/1471-2407-11-275
26. Hu AM, Zhao D, Zheng H, Wang QH, Lyu Y, Li BL. Preoperative diagnosis in 46 cases of pulmonary sclerosing hemangioma. *Chin Med J*. (2016) 129:1377–8. doi: 10.4103/0366-6999.182839
27. Shin SY, Kim MY, Oh SY, Lee HJ. Pulmonary sclerosing pneumocytoma of the lung : CT characteristics in a large series of a tertiary referral center. *Medicine*. (2015) 94:e498. doi: 10.1097/MD.0000000000000498
28. Yang C, Lee L. Pulmonary sclerosing pneumocytoma remains a diagnostic challenge using frozen sections : a clinicopathological analysis of 59 cases. *Histopathology*. (2018) 72:500–8. doi: 10.1111/his.13391
29. Lei Y, Yong D, Jun-zhong R, Zhi Y, Zi-tong W. Treatment of 28 patients with sclerosing hemangioma (SH) of the lung. *J Cardiothorac Surg*. (2012)7:34. doi: 10.1186/1749-8090-7-34
30. Park JS, Kim K, Shin S, Shim H, Kim HK. Surgery for pulmonary sclerosing hemangioma : lobectomy versus limited resection. *Korean J Thorac Cardiovasc Surg*. (2011)44:39–43. doi: 10.5090/kjtcs.2011.44.1.39
31. Cho SJ, Lian JJ, Kim, B-Y, Cho S-J, Jung WY, Han J-H, et al. Increased expression of matrix metalloproteinase 9 and tubulin- α in pulmonary sclerosing hemangioma. *Oncol Rep*. (2007) 18:1139–44. doi: 10.3892/or.18.5.1139
32. Schmidt LA, Myers JL, Mchugh JB. Napsin a is differentially expressed in sclerosing hemangiomas of the lung. *Arch Pathol Lab Med*. (2012) 136:1580–4. doi: 10.5858/arpa.2011-0486-OA
33. Wu J, Zhang C, Qiao H. The significance of p40 expression in in sclerosing hemangioma of lung. *Sci Rep*. (2014) 4:6102. doi: 10.1038/srep 06102
34. Lovrenski A, Vasilijević M, Panjković M, Tegeltija D, Vučković D, Baroš I, et al. Sclerosing pneumocytoma: a ten-year experience at a western balkan university hospital. *Medicina*. (2019) 55:27. doi: 10.3390/medicina55020027
35. Jungraithmayr W, Eggeling S, Ludwig C, Kayser G, Passlick B. Sclerosing hemangioma of the lung: a benign tumour with potential for malignancy? *Ann Thorac Cardiovasc Surg*. (2006) 12:352–4. Available online at: http://www.atcs.jp/pdf/2006_12_5/352.pdf
36. Corti S, Locatelli F, Papadimitriou D, Donadoni C, Salani S, Del Bo R, et al. Identification of a primitive brain-derived neural stem cell population based on aldehyde dehydrogenase activity. *Stem Cells*. (2006) 24:975–85. doi: 10.1634/stemcells.2005-0217
37. Hida K, Maishi N, Akiyama K, Ohmura-kakutani H, Torii C, Ohga N, et al. Dehydrogenase activity show drug resistance. *Cancer Sci*. (2017) 108:2195–203. doi: 10.1111/cas.13388

Conflict of Interest: The authors declare that the research was conducted in the absence of any commercial or financial relationships that could be construed as a potential conflict of interest.

Copyright © 2020 Aramini, Masciale, Manfredini, Bianchi, Banchelli, D'Amico, Bertolini, Dominici, Morandi and Maiorana. This is an open-access article distributed under the terms of the Creative Commons Attribution License (CC BY). The use, distribution or reproduction in other forums is permitted, provided the original author(s) and the copyright owner(s) are credited and that the original publication in this journal is cited, in accordance with accepted academic practice. No use, distribution or reproduction is permitted which does not comply with these terms.

frontiers in Medicine

GENERAL COMMENTARY
published: 03 September 2020
doi: 10.3389/fmed.2020.00507

Commentary: Peripheral Circulating Exosome-Mediated Delivery of miR-155 as a Novel Mechanism for Acute Lung Inflammation

*Lin Zhang, Heng Meng and Qing Geng**

Department of Thoracic Surgery, Renmin Hospital of Wuhan University, Wuhan, China

Keywords: exosomes, acute lung injury, macrophages, intercellular communication, miRNAs

A Commentary on

Peripheral Circulating Exosome-Mediated Delivery of miR-155 as a Novel Mechanism for Acute Lung Inflammation

by Jiang, K., Yang, J., Guo, S., Zhao, G., Wu, H., and Deng, G. (2019) Mol. Ther. 27, 1758–1771. doi: 10.1016/j.ymthe.2019.07.003

OPEN ACCESS

Edited by:
Mahmood Yaseen Hachim, Mohammed Bin Rashid University of Medicine and Health Sciences, United Arab Emirates

Reviewed by:
Noha Mousaad Elemam, University of Sharjah, United Arab Emirates
Saba Al Heialy, Mohammed Bin Rashid University of Medicine and Health Sciences, United Arab Emirates

****Correspondence:***
Qing Geng
gengqingwhu@whu.edu.cn

Specialty section:
This article was submitted to Pulmonary Medicine, a section of the journal Frontiers in Medicine

Received: *28 June 2020*
Accepted: *23 July 2020*
Published: *03 September 2020*

Citation:
Zhang L, Meng H and Geng Q (2020) Commentary: Peripheral Circulating Exosome-Mediated Delivery of miR-155 as a Novel Mechanism for Acute Lung Inflammation. Front. Med. 7:507. doi: 10.3389/fmed.2020.00507

Acute lung injury (ALI) is a devastating respiratory disorder characterized by clinically significant hypoxemia, diffuse bilateral pulmonary infiltration, pulmonary edema, decrease in pulmonary compliance, and decrease in functional residual capacity (1). Macrophages, the cells that play a central role in the inflammatory microenvironment of ALI, have been shown to contribute significantly to the inflammatory process of this disease (1). Although the interactions between macrophages and other cells in the inflammatory responses of lung have been well-described previously, the function of exosomes as a mediator of signal transmission in ALI has not been fully elucidated. In a previous issue of *Molecular Therapy*, Jiang et al. described the serum exosomes derived from ALI mice serum that delivered miR-155 to naive mice or naive macrophages to induce inflammation (2). The communicational role of exosomes to carry proinflammatory signals and mediate inflammation was demonstrated by using the adoptively transfer method that involves transferring of immunoreactive molecules from donor to recipient, as was applied in previous research (3).

Exosomes are one kind of extracellular vesicles (EVs) with a diameter of 30–100 nm. Although the regulatory role of microRNAs (miRNAs) in ALI has been corroborated in plenty of studies, their tendency of being degraded in body fluids has been an obstacle to their long-distance delivery. Luckily, exosomes could provide a shelter for these degradable molecules and increase their biological stability. With pleiotropic biological functions, exosomes are natural carriers of protein and nucleic acids, including messenger RNAs (mRNAs) as well as miRNAs. They could be released by various types of cells and are significant mediators in intercellular communications. These vesicles have also been reported to play important roles in pulmonary diseases, including ALI and acute respiratory distress syndrome (4).

Previous research has demonstrated that exosomal miRNAs could promote M1 macrophage polarization and trigger pro-inflammatory effects in ALI (4). Previous studies have also reported that miR-155 could promote lipopolysaccharide (LPS)-induced ALI through the down-regulation of SOCS-1 (5). The findings of Jiang et al. have added to the understanding of the roles of exosomes and exosomal miRNAs in ALI. In their study, exosomal miR-155 played an important regulatory role in the pathogenesis of ALI. Through a series of experiments, including the co-incubation of macrophages with exosomes and a dual luciferase reporter gene assay, they discovered that

exosomal miR-155 could mediate cell proliferation *via* targeting SHIP1. Furthermore, their research revealed that exosomal miR-155 could mediate inflammation through suppressing the expression of SOCS1. The proinflammatory effect of the exosomes was also confirmed by *in vivo* experiments in mice. The conclusion was convincing. However, the origin of these regulatory exosomes and their exact recipient cells had not been further clarified.

In humans, ALI could be developed when an individual is exposed to infectious pathogens or to non-infectious noxious stimuli. Thus, it could be divided into an infectious type and a sterile type according to the etiology (3). While non-infectious or sterile ALI is modeled experimentally by hypoxia, acid inhalation, and ventilator-induced baro-trauma, infection-induced ALI could be induced by bacteria, viruses, or various components of these agents, such as LPS or lipoteichoic acid (3). In sterile ALI, the major derivation of exosomes is the epithelial cells. These epithelial cell-derived exosomes could promote macrophage recruitment and lung inflammatory responses *via* their containing miRNAs (3). In contrast, in LPS or gram-negative bacteria-induced infectious ALI, exosomes are mainly secreted by macrophages (6). A further study by Lee et al. showed that, after a bacterial infection, macrophage-derived EVs were dominant in amount (7). Although epithelial cell-derived EVs constituted only a small proportion of the total EVs, they contained rich miRNAs; they could be delivered to alveolar macrophages (AMs) to play important regulatory roles and promote innate immune responses in bacterial lung infections (7). Since exosomes are important mediators of intracellular communication, addressing the question on what the origins of these exosomes are will help to further understand their regulatory mechanisms in ALI. The origin of exosomes could be determined by detection of their surface proteins because exosomes possess the same surface markers as their parent cells do. This approach has been taken in plenty of similar research such as that by Ye et al. (8).

In addition, macrophages are heterogeneous immune cells. There are various subtypes of macrophages in the lungs, with different distributions. The macrophages with the widest distribution are AMs. They are generally located on the luminal surface of the alveolar space and express MerTK, CD64, CD68, CD206, CD11c, MARCO, SiglecF, and F4/80 on the membrane surface. AMs could be easily separated from the bronchoalveolar lavage fluid and constitute the first line of the innate immune system. They are important bactericidal and antigen-presenting cells secreting IL-6 to regulate the immune response (9). In comparison, interstitial macrophages (IMs) are less populous and reside mainly in lung parenchyma or in the vicinity of the bronchi. They have different surface markers, such as MerTK, CD64, CD11b, CD86, CX3CR1, and CD169 and secret IL-1, IL-6, TNF-α, and IL-10, in their steady state (9). IMs could respond to LPS and thus might also be activated in the research by Jiang et al. They could possibly be one of the origins of EVs in the peripheral blood. Previous research has reported that the counts of IMs had been significantly increased in the injured lungs and that IMs were the major subsets of cells in the lung of mice with LPS-induced ALI (10). Thus, it is also interesting to know whether it is IMs or AMs that are the exact target cells of these peripheral blood exosomes.

In summary, the study by Jiang et al. provided further evidence for the concept that exosomes are mediators of intercellular signal transduction, with their cargo miRNAs targeting various pathways (2). The demonstration that ALI mice serum-derived exosomes could target pulmonary macrophages is consistent with the fact that macrophages play a central role in the pathogenesis of ALI. While the origin of these exosomes and the exact subtype of their recipient cells remain unknown, which is partly acknowledged in the study, there is little doubt that circulating serum exosomes play an important part in the induction of pulmonary inflammation during ALI. Overall, the authors have provided enough experimental evidence to support their conclusions.

AUTHOR CONTRIBUTIONS

LZ and HM conceived and designed this manuscript. QG was responsible for the revision. All authors contributed to the article and approved the submitted version.

FUNDING

This work was supported by National Natural Science Foundation of China to QG (81770095).

REFERENCES

1. Huang X, Xiu H, Zhang S, Zhang G. The role of macrophages in the pathogenesis of ALI/ARDS. *Mediat Inflamm.* (2018) 2018:1–8. doi: 10.1155/2018/1264913
2. Jiang K, Yang J, Guo S, Zhao G, Wu H, Deng G. Peripheral circulating exosome-mediated delivery of miR-155 as a novel mechanism for acute lung inflammation. *Mol Ther.* (2019) 27:1758–71. doi: 10.1016/j.ymthe.2019.07.003
3. Lee H, Zhang D, Laskin DL, Jin Y. Functional evidence of pulmonary extracellular vesicles in infectious and noninfectious lung inflammation. *J Immunol.* (2018) 201:1500–9. doi: 10.4049/jimmunol.1800264
4. Lanyu Z, Feilong H. Emerging role of extracellular vesicles in lung injury and inflammation. *Biomed Pharmacother.* (2019) 113:108748. doi: 10.1016/j.biopha.2019.108748
5. Wang W, Liu Z, Su J, Chen WS, Wang XW, Bai SX, et al. Macrophage micro-RNA-155 promotes lipopolysaccharide-induced acute lung injury in mice and rats. *Am J Physiol Lung Cell Mol Physiol.* (2016) 311:L494–506. doi: 10.1152/ajplung.00001.2016
6. Soni S, Wilson MR, O'Dea KP, Yoshida M, Katbeh U, Woods SJ, et al. Alveolar macrophage-derived microvesicles mediate acute lung injury. *Thorax.* (2016) 71:1020–9. doi: 10.1136/thoraxjnl-2015-208032
7. Lee H, Groot M, Pinilla-Vera M, Fredenburgh LE, Jin Y. Identification of miRNA-rich vesicles in bronchoalveolar lavage fluid: insights into the function and heterogeneity of extracellular vesicles. *J Control Release.* (2019) 294:43–52. doi: 10.1016/j.jconrel.2018.12.008

8. Ye C, Li H, Bao M, Zhuo R, Jiang G, Wang W. Alveolar macrophage - derived exosomes modulate severity and outcome of acute lung injury. *Aging*. (2020) 12:6120–8. doi: 10.18632/aging.103010
9. Mukaida N, Nosaka T, Nakamoto Y, Baba T. Lung macrophages: multifunctional regulator cells for metastatic cells. *Int J Mol Sci*. (2019) 20:116. doi: 10.3390/ijms20010116
10. Chen J, Wang S, Fu R, Zhou M, Zhang T, Pan W, et al. RIP3 dependent NLRP3 inflammasome activation is implicated in acute lung injury in mice. *J Transl Med*. (2018) 16:233. doi: 10.1186/s12967-018-1606-4

Conflict of Interest: The authors declare that the research was conducted in the absence of any commercial or financial relationships that could be construed as a potential conflict of interest.

Copyright © 2020 Zhang, Meng and Geng. This is an open-access article distributed under the terms of the Creative Commons Attribution License (CC BY). The use, distribution or reproduction in other forums is permitted, provided the original author(s) and the copyright owner(s) are credited and that the original publication in this journal is cited, in accordance with accepted academic practice. No use, distribution or reproduction is permitted which does not comply with these terms.

frontiers in Medicine

ORIGINAL RESEARCH
published: 06 October 2020
doi: 10.3389/fmed.2020.579543

Carcinoembryonic Antigen: A Potential Biomarker to Evaluate the Severity and Prognosis of COVID-19

Qianqian Chen[1†], Hui Kong[1†], Xu Qi[1], Wenqiu Ding[1], Ningfei Ji[1], Chaojie Wu[1], Chaolin Huang[2], Wenjuan Wu[2], Mao Huang[1], Weiping Xie[1*], Yun Liu[3*] and Jinhai Tang[4*]*

[1] Department of Respiratory and Critical Care Medicine, The First Affiliated Hospital of Nanjing Medical University, Nanjing, China, [2] Division of Intensive Care Unit, Wuhan Jin Yin-tan Hospital, Wuhan, China, [3] Department of Medical Informatics, School of Biomedical Engineering and Informatics, Nanjing Medical University, Nanjing, China, [4] Department of General Surgery, The First Affiliated Hospital of Nanjing Medical University, Nanjing, China

OPEN ACCESS

Edited by:
Mahmood Yaseen Hachim, Mohammed Bin Rashid University of Medicine and Health Sciences, United Arab Emirates

Reviewed by:
Rabih Halwani, University of Sharjah, United Arab Emirates
Michael Adam O'Reilly, University of Rochester, United States

***Correspondence:**
Mao Huang
hm6114@126.com
Weiping Xie
wpxie@njmu.edu.cn
Yun Liu
liuyun@njmu.edu.cn
Jinhai Tang
jhtang@njmu.edu.cn

[†] These authors have contributed equally to this work

Specialty section:
This article was submitted to Pulmonary Medicine, a section of the journal Frontiers in Medicine

Received: 02 July 2020
Accepted: 07 September 2020
Published: 06 October 2020

Citation:
Chen Q, Kong H, Qi X, Ding W, Ji N, Wu C, Huang C, Wu W, Huang M, Xie W, Liu Y and Tang J (2020) Carcinoembryonic Antigen: A Potential Biomarker to Evaluate the Severity and Prognosis of COVID-19. Front. Med. 7:579543. doi: 10.3389/fmed.2020.579543

Background and Objectives: Corona Virus Disease 2019 (COVID-19) has become a serious pandemic disease worldwide. Identification of biomarkers to predict severity and prognosis is urgently needed for early medical intervention due to high mortality of critical cases with COVID-19. This retrospective study aimed to indicate the values of carcinoembryonic antigen (CEA) in evaluating the severity and prognosis of COVID-19.

Methods: We included 46 death cases from intensive care unit and 68 discharged cases from ordinary units with confirmed COVID-19 of Wuhan Jin Yin-tan Hospital from January 1 to March 22, 2020. Laboratory and radiologic data were analyzed retrospectively. All patients were followed up until April 10, 2020.

Results: COVID-19 patients in the death group had significantly higher CEA levels (ng/ml) than discharged group (14.80 ± 14.20 vs. 3.80 ± 2.43, $P < 0.001$). The risk of COVID-19 death increased 1.317 times for each additional 1 ng/ml CEA level (OR = 1.317, 95% CI: 1.099–1.579). The standardized and weighted receiver operating characteristic curve (ROC) analysis adjusted to age, sex, and ferritin levels suggested that the area under the curve (AUC) of the serum CEA levels was 0.808 in discrimination between death cases and discharged cases with COVID-19 ($P < 0.001$). We found mortality of COVID-19 is associated with elevated CEA levels increased (HR = 1.023, 95% CI: 1.005–1.042), as well as age (HR = 1.050, 95% CI: 1.016–1.086) and ferritin levels (HR = 1.001, 95% CI: 1.001–1.002) by survival analysis of Cox regression model. Among discharged patients, CEA levels were significant lower in moderate cases compared to the severe and critical cases ($P = 0.005$; OR = 0.488, 95% CI: 0.294–0.808) from binary logistic regression analysis. The AUC of CEA levels was 0.79 in distinguishing moderate cases from discharged COVID-19 patients by standardized and weighted ROC analysis ($P < 0.001$). A positive correlation between CEA levels and CT scores existed in discharged patients (Correlation Coefficient: 0.687; $P < 0.001$).

Conclusions: Elevated CEA levels increased the risk of death from COVID-19 and CEA levels were related to CT scores of the discharged patients positively.

Keywords: corona virus disease 2019, severe acute respiratory coronavirus 2, carcinoembryonic antigen, biomarker, prognosis

INTRODUCTION

Corona Virus Disease 2019 (COVID-19) is a disease caused by severe acute respiratory coronavirus 2 (SARS-CoV-2) (1). It has developed into a serious pandemic disease worldwide and become a burden borne by health care systems in many countries since its first outbreak in Wuhan, China in December, 2019 (2, 3). According to the latest COVID-2019 situation reports released by World Health Organization (WHO) (4), there were over 23 million patients with confirmed COVID-19 globally, along with over 806,000 death cases by August 24, 2020. It was reported that the case-fatality rates of critical cases were about 24-fold higher than those of confirmed cases with COVID-19 (49.0 vs. 2.3%) (5). In view of high mortality of critical cases, identifying specific biomarkers for estimate severity and prognosis of COVID-19 is in urgent need, especially when local health systems are overwhelmed. A few inflammatory factors, coagulation parameters or cytokines were considered as potential biomarkers of COVID-19 progression or severity (6–9). However, it is a long way to identify a simple biomarker with higher sensitivity or sensitivity for better comprehensive evaluation.

Carcinoembryonic antigen (CEA), also known as CEA-related cell adhesion molecule 5 (CEACAM5) or CD66e, is a kind of glycophosphatidylinositol-linked membrane glycoprotein anchored in a specific cell membrane microdomains (10). As a cell adhesion molecule, CEA functioned as a bridge linked to pathogens or stromal cells with other members of epithelial CEACAMs, triggers CEACAM-mediated signal communication and activated integrin signaling pathways in human endothelial cells (10–12). CEA is not only related to respiratory or digestive cancers but also some infectious diseases like gonorrhea or chronic inflammatory diseases like interstitial lung diseases (ILD) (13, 14). Immunohistochemical analysis of lung specimens from patients with pulmonary fibrosis indicated that strong expression of CEA in metaplastic bronchiolar and type II alveolar epithelia (15, 16). Formation of abnormal epithelial proliferation and renewal was seen as a possible source to elevated CEA levels in patients with pulmonary fibrosis (15). Similar to pathological changes of ILD, significant hyperplasia of type II alveolar epithelial cells and interstitial fibrosis were referred to from several reports of COVID-19 autopsies and biopsies (17, 18). To our knowledge, only one study about the serum cancer biomarkers including CEA levels of COVID-19 patients have been published (19). Whether elevated CEA levels are associated with poor prognosis or severity of COVID-19 remains unclear nevertheless.

Therefore, we conducted this study to present the serum CEA levels of COVID-19 patients and indicate the relation between serum CEA levels and prognosis or severity of COVID-19, which may be of great value for effective treatment.

MATERIALS AND METHODS

Data Sources and Extraction

A total of 46 death cases with confirmed COVID-19 were included in our study, which were admitted to an intensive care unit (ICU) for COVID-19 of Wuhan Jin Yin-tan Hospital from January 1 to March 22, 2020. Respectively, 68 discharged patients (13 from ICU, 55 from ordinary units) were included during the same period. All medical records of the patients we included were reviewed and related raw data were collected by the two authors independently. A senior investigator reviewed the raw data if there were any discrepancies. The following data of each patient we included were extracted: age, sex, smoking history, length of stay, comorbidities, white blood cell count, white blood cell count, lymphocyte count, neutrophil count, monocyte count, C-reactive protein (CRP), ferritin, interleukin 6 (IL-6), alpha fetoprotein (AFP), and CEA; radiology data including chest computed tomography (CT) or chest X-rays (for patients in ICU). Comorbidities of all patients were collected on admission. We only included the baseline data on admission if patients have the same kind of laboratory tests or radiology examination more than once. The survival time were defined as the time (days) from admission date to observation endpoint (death or April 10, 2020). Our study was approved by the Ethics Committee of Wuhan Jin Yin-tan Hospital (No. KY-2020-59.01).

Inclusion and Exclusion Criteria

All patients included met the following inclusion criteria: Confirmed COVID-19 cases was diagnosed by real-time fluorescent reverse transcription-polymerase chain reaction (RT-PCR) based on "Diagnosis and Treatment Protocol for Novel Coronavirus Pneumonia (Trial Version 7)" published by the National Health Commission of the People's Republic of China (20). Exclusion criteria were followed below: (1) Patients with a history of any cancer or any chronic disease related to elevated CEA levels like chronic kidney disease. (2) Patients infected with other viruses or bacteria.

Clinical Classification of COVID-19

The clinical classification of COVID-19 in our study was based on "Diagnosis and Treatment Protocol for Novel Coronavirus Pneumonia (Trial Version 7)" published by the National Health Commission of the People's Republic of China (20). Patients with COVID-19 are divided into four types: mild cases, moderate cases, severe cases, and critical cases (detailed descriptions on **Supplementary Material**).

Radiological Assessment by CT Scores

The CT scans of all discharged COVID-19 patients were assessed by two radiologists with more than 10 years of experience in a semi-quantitative way established by Xie et al. (21). Details of the criteria for the CT scores can be found on **Supplementary Material**. The definitions of lung lesions were specified in another study (22).

Statistical Analysis

Continuous variables were analyzed by Student's *t*-test while categorical variables were analyzed by Chi-square test. Binary logistic regression was applied for analysis of survival parameters. The variables with P-values < 0.05 in the univariate analysis were included in the binary logistic regression. The detailed descriptions of the model development and evaluation were mentioned in the previous study (23). We applied Nagelkerke

TABLE 1 | Demographic and clinical characteristics of the COVID-19 patients included.

	Total ($n = 114$)	Death group ($n = 46$)	Discharged group ($n = 68$)	*P*-values
Age (years)	61.74 ± 13.57	65.93 ± 8.49	58.60 ± 15.47	0.002
Sex				0.015
Female %	53 (46.50)	15 (32.61)	38 (55.88)	
Male %	61 (53.50)	31 (67.39)	30 (44.12)	
Smoker %	45 (39.47)	23 (50.00)	22 (32.35)	0.059
Comorbidities %	65 (57.02)	30 (65.22)	35 (51.47)	0.146
Diabetes mellitus	27 (23.68)	14 (30.43)	13 (19.12)	0.163
Cardiovascular disease	12 (10.53)	3 (6.52)	9 (13.24)	0.252
COPD	5 (4.39)	3(6.52)	2(2.94)	0.360
Hypertension	50(43.86)	23(50.00)	27(39.71)	0.277
Length of stay (days)	19.56 ± 15.91	11.48 ± 8.79	25.28 ± 17.34	<0.001
White blood cell count ($\times 10^9$/L)	7.90 ± 5.80	14.21 ± 8.18	5.87 ± 2.70	<0.001
Lymphocyte count ($\times 10^9$/L)	1.15 ± 0.57	0.77 ± 0.35	1.25 ± 0.59	<0.001
Neutrophil count ($\times 10^9$/L)	6.22 ± 5.98	13.04 ± 8.51	4.09 ± 2.66	0.001
Monocyte count ($\times 10^9$/L)	0.42 ± 0.20	0.44 ± 0.23	0.41 ± 0.19	0.766
C-reactive protein (mg/L)	44.58 ± 54.27	122.96 ± 62.13	28.44 ± 38.48	<0.001
Ferritin (ng/ml)	792.78 ± 684.73	1315.06 ± 653.17	423.81 ± 423.79	<0.001
Alpha fetoprotein (ng/ml)	2.48 ± 1.64	1.75 ± 0.85	2.98 ± 1.84	<0.001
Carcinoembryonic antigen (ng/ml)	8.23 ± 10.64	14.80 ± 14.20	3.80 ± 2.43	<0.001
Interleukin 6 (pg/ml)	22.30 ± 39.59	41.95 ± 40.11	20.10 ± 39.66	0.381

COPD, chronic obstructive pulmonary disease. Continuous variables are showed as mean ± SD.

TABLE 2 | Binary logistic regression analysis of factors related to covid-19 prognosis.

Variable		Model			
		1	2	3	4
Demographic factors	Age	1.072 (1.000–1.149)	1.062 (1.007–1.121)	1.104 (1.025–1.188)	1.057 (1.002–1.115)
	Sex	0.178 (0.029–1.113)	0.255 (0.048–1.347)	0.128 (0.018–0.918)	0.249 (0.048–1.284)
	Smoker	0.777 (0.146–4.125)	0.358 (0.070–1.838)	0.522 (0.088–3.100)	0.335 (0.066–1.706)
Inflammatory factors	CRP	1.023 (1.012–1.034)	1.024 (1.013–1.034)	-	-
	Ferritin	-	-	1.002 (1.001–1.003)	1.003 (1.002–1.004)
Tumor markers	CEA	1.311 (1.096–1.568)	-	1.317 (1.099–1.579)	-
	AFP	-	0.489 (0.272–0.879)	-	0.503 (0.281–0.899)
Model evaluation	Nagelkerke R^2	0.724	0.620	0.729	0.655
	AUC	0.936	0.914	0.940	0.924

Variables in the model are showed as OR (95% CI).

R^2 to measure overall model performance and the area under the receiver operating characteristic curve (AUC) to evaluate discriminative ability of each model (24). Hosmer–Lemeshow Test was used for Goodness of Fit Test. Only one inflammatory factor and one tumor marker were included in the same logistic model to avoid multicollinearity of interactive variables. We used standard and weighted receiver operating characteristic (ROC) curve analysis to assess the sensitivity and specificity of different parameters as biomarkers of COVID-19 prognosis or severity. The weighted ROC curve analysis was defined and performed as descriptions in a published article by the way of inverse probability weighting (25). The survival analysis was conducted by Cox regression model (proportional hazard model) and Kaplan–Meier analysis with Mantel–Cox Test. The relation between CEA levels and other factors in discharged cases was evaluated by Spearman's correlation coefficient. *P*-values < 0.05 in our study were statistically significant. We performed statistical analysis with IBM SPSS Statistics (Version 24.0).

RESULTS

Demographic and Clinical Characteristics of the Patients

According to the inclusion and exclusion criteria, we totally included 114 patients with COVID-19 (46 death cases and 68 discharged cases) in our study, with two patients with cancers, one with chronic kidney disease, and one without CEA

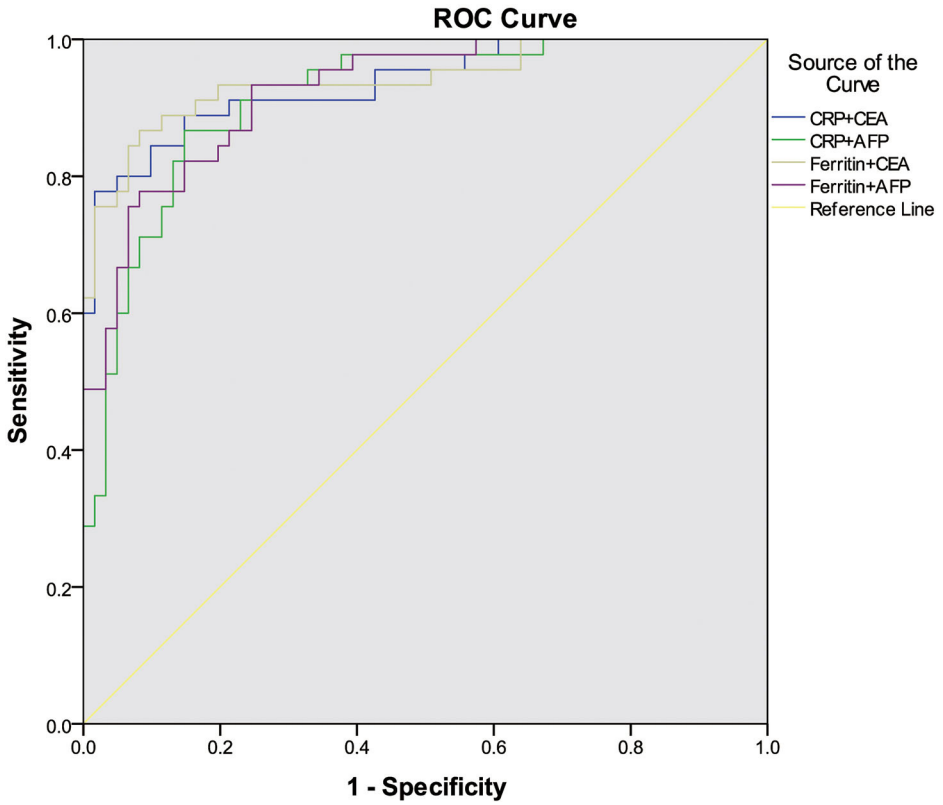

FIGURE 1 | The ROC curve analysis of different binary logistic regression models for the prediction of COVID-19 prognosis.

levels excluded. All demographic and clinical characteristics of the patients we included were demonstrated in **Table 1**. The mean age of all patients included was 61.74 ± 13.57. The patients in death group were older than those in discharged group (65.93 ± 8.49 vs. 58.60 ± 15.47, $P = 0.002$). There were 15 females in death group, which were less than those in discharged group (32.61 vs. 55.88%, $P = 0.015$). Death cases spent shorter time in hospital than discharged cases (11.48 ± 8.79 vs. 25.28 ± 17.34, $P < 0.001$). In complete blood count, white blood cell count (14.21 ± 8.18 vs. 5.87 ± 2.70, $P < 0.001$) and neutrophil count (13.04 ± 8.51 vs. 4.09 ± 2.66, $P = 0.001$) was increased significantly in death cases with COVID-19, while lymphocyte count decreased significantly (0.77 ± 0.35 vs. 1.25 ± 0.59, $P < 0.001$). We found CRP ($P < 0.001$) and ferritin levels ($P < 0.001$) were significantly higher in the death group than discharged group among inflammation indicators included in our study. No differences were found in IL-6 levels between the two groups ($P = 0.381$). Compared with the discharged group, the serum CEA levels were higher in the death group (14.80 ± 14.20 vs. 3.80 ± 2.43, $P < 0.001$).

Association Between CEA Levels and COVID-19 Prognosis

For multivariate analysis, we used binary logistic regression to build four models (**Table 2**). Variables with P-values < 0.05 in univariate analysis were included in our logistic regression models including demographic factors (sex, age, and smoking history), inflammatory factors (CRP or ferritin), and tumor markers (CEA or AFP). We found Model 3 including age, sex, smoking history, ferritin levels, and CEA levels showed the most discriminative ability among the four models we built in **Figure 1** (Nagelkerke $R^2 = 0.729$; AUC = 0.940). The Goodness of Fit Test of Model 3 was 0.408 by Hosmer–Lemeshow Test. From the binary logistic regression analysis of Model 3, age ($P = 0.009$), sex ($P = 0.041$), ferritin levels ($P < 0.001$) and CEA levels ($P = 0.003$) were significantly related to the prognosis of COVID-19. After adjustment to age, sex, and smoking history, the binary logistic regression equation (Model 3) demonstrated that the risk of COVID-19 death increased 1.002 times for each additional 1 mg/L ferritin level (OR = 1.002, 95% CI: 1.001–1.003) and 1.317 times for each additional 1 ng/ml CEA level (OR = 1.317, 95% CI: 1.099–1.579). The ROC curve analysis suggested that AUC of the serum CEA levels was 0.808 by standardized and weighted ROC curve analysis adjusted to other cofounding factors (age, sex, and ferritin levels). From survival analysis of proportional hazard model, we also found elevated CEA levels increased mortality of COVID-19 (HR = 1.023, 95% CI: 1.005–1.042), as well as age (HR = 1.050, 95% CI: 1.016–1.086) and ferritin levels (HR = 1.001, 95% CI: 1.001–1.002). The COVID-19 patients were divided into two groups (high CEA levels group

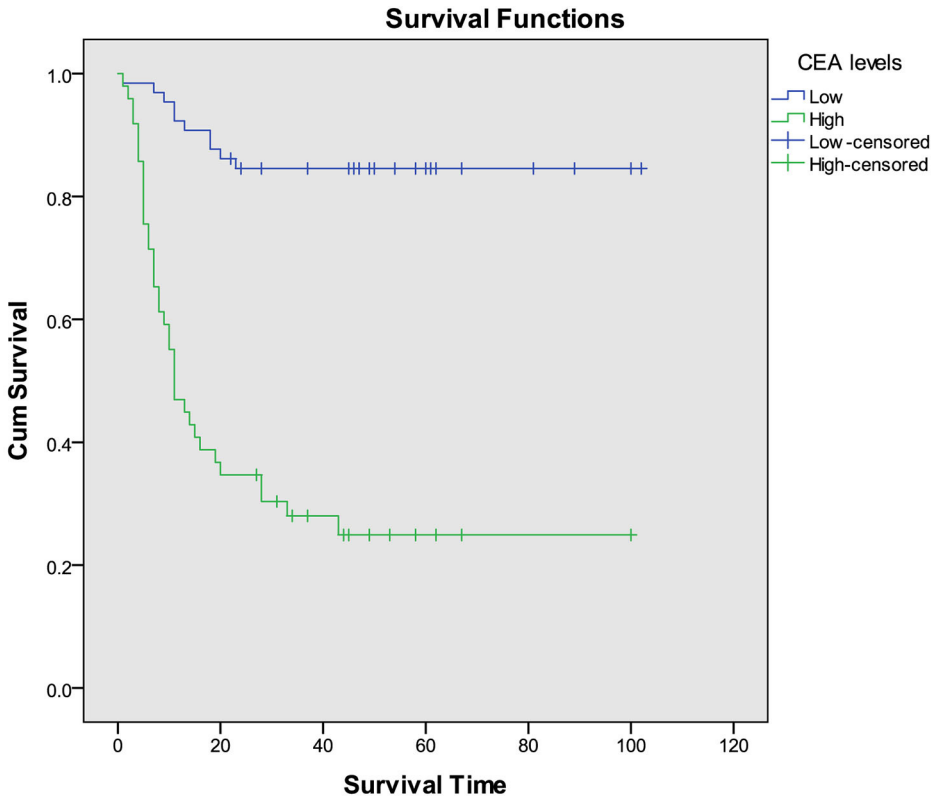

FIGURE 2 | Kaplan–Meier survival analysis of COVID-19 patients with different CEA levels.

and low CEA levels group) based on the cutoff value of CEA levels (5.2 ng/ml) calculated by time-dependent ROC curve. The COVID-19 patients with high CEA levels had higher risk of death than those with low CEA levels by Kaplan–Meier survival analysis (**Figure 2**). The Mantel–Cox Test of Kaplan–Meier survival analysis was $P < 0.001$.

Relation Between CEA Levels and COVID-19 Severity in Discharged Patients

A significant difference in CEA levels ($P < 0.001$) was found between the discharged patients with different clinical classifications, while age ($P = 0.001$) and other laboratory test including white blood cell count ($P = 0.008$), neutrophil count ($P = 0.012$), monocyte count ($P = 0.031$) and ferritin levels ($P = 0.039$) in **Table 3**. The results of binary logistic regression analysis (**Table 4**) revealed that CEA levels were lower ($P = 0.005$; OR = 0.488, 95% CI: 0.294–0.808) in moderate cases compared with the severe and critical cases after adjusted to age and the laboratory tests, which were statistic significantly in the univariate analysis. At the same time, moderate COVID-19 patients were younger than severe and critical cases from binary logistic regression analysis ($P = 0.039$; OR = 0.858, 95% CI: 0.742–0.993). **Figure 3** shows the ROC curves of CEA levels with the AUC of 0.790 ($P < 0.001$) in distinguishing moderate cases from discharged COVID-19 patients after considering age as a cofounding factor by weighted ROC analysis. The results of Spearman's correlation analyses (**Figure 4**) indicated that there was a positive correlation of CEA levels with CT scores in discharged patients (Correlation Coefficient: 0.687; $P < 0.001$). The **Figure 5** showed chest CT scans and CEA levels of three female patients in similar old age (69, 70, 71).

DISCUSSION

In our study, we found the serum CEA levels increased in non-survivors with COVID-19 compared to discharged patients statistically. Moreover, increasing levels of serum CEA were associated with more CT involvement scores in discharged COVID-19 patients. Till now, only one study reported the elevated serum CEA levels in COVID-19 patients (19). In that retrospective study, the authors found significant increases of CEA levels compared with health controls and a potential association between CEA and CRP levels. However, the role of CEA levels in clinical outcomes or CT involvements of COVID-19 patients was still unknown. This study validated the previous result that CEA levels were related to severity of COVID-19 reported by different research groups (Union Hospital of Tongji Medical College, Wuhan) (19). Furthermore,

TABLE 3 | Characteristics of 68 discharged patients with different disease severities.

	Moderate (n = 46)	Severe/critical (n = 22)	P-values
Age (years)	54.85 ± 15.78	66.95 ± 11.00	0.001
Sex			0.115
Female %	22 (47.83)	15 (68.18)	
Male %	24 (52.17)	7 (31.82)	
Smoker %	15 (32.61)	7 (31.82)	0.948
Comorbidities %	25 (54.35)	10 (45.45)	0.669
Diabetes mellitus	10 (21.74)	3 (13.64)	0.642
Cardiovascular disease	4 (8.70)	5 (22.73)	0.224
COPD	0 (0.00)	2 (9.10)	0.191
Hypertension	18 (39.13)	9 (40.91)	0.889
White blood cell count ($\times 10^9$/L)	5.31 ± 2.45	7.19 ± 2.94	0.008
Lymphocyte count ($\times 10^9$/L)	1.28 ± 0.58	1.17 ± 0.60	0.466
Neutrophil count ($\times 10^9$/L)	3.54 ± 2.27	5.80 ± 3.12	0.012
Monocyte count ($\times 10^9$/L)	0.39 ± 0.17	0.53 ± 0.27	0.031
CRP (mg/L)	27.53 ± 39.57	35.96 ± 37.14	0.424
Ferritin (ng/ml)	353.55 ± 295.24	578.94 ± 583.51	0.039
AFP (ng/ml)	2.96 ± 1.45	3.03 ± 2.51	0.895
CEA (ng/ml)	3.04 ± 1.97	5.35 ± 2.58	<0.001
IL-6 (pg/ml)	23.83 ± 44.05	10.72 ± 5.93	0.333
CT scores	12.57 ± 5.51	17.38 ± 5.53	0.002

COPD, chronic obstructive pulmonary disease. Continuous variables are showed as mean ± SD.

TABLE 4 | Binary logistic regression analysis of factors related to COVID-19 severities.

Valuable	P-value	OR	95% CI
Age	0.039	0.858	0.742–0.993
White blood cell count	0.833	1.246	0.161–9.662
Neutrophil count	0.729	0.708	0.100–5.005
Monocyte count	0.465	0.032	0.000–31.614
Ferritin	0.116	0.997	0.994–1.001
CEA	0.005	0.488	0.294–0.808
Constant	0.007	-	-

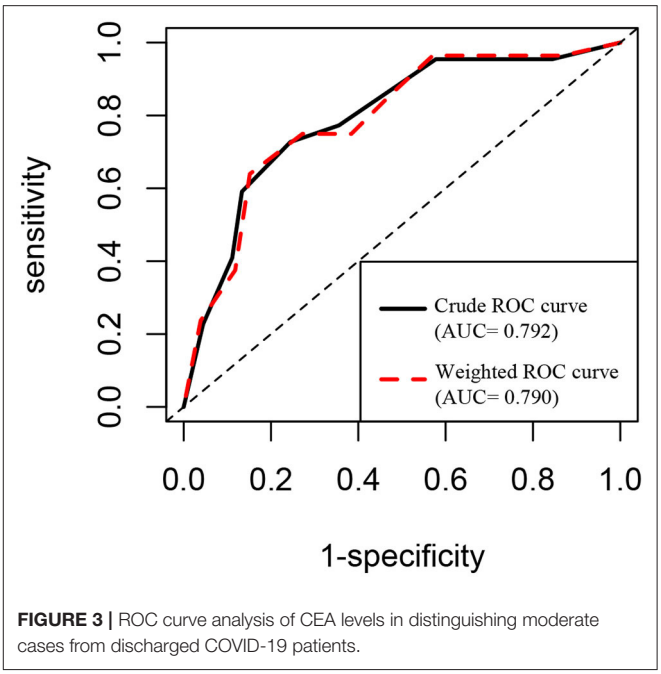

FIGURE 3 | ROC curve analysis of CEA levels in distinguishing moderate cases from discharged COVID-19 patients.

our study concentrated on different CEA levels in COVID-19 patients with different clinical outcomes (survivors or non-survivors) and potential correlations with CT involvement scores. We firstly found CEA levels are associated with prognosis and severity of COVID-19. We also calculated the value of CEA levels in evaluating the severity and prognosis of COVID-19.

Some hypotheses were formulated to explain the correlation between elevated CEA levels and poor prognosis or severity of COVID-19. Generally, CEA is considered to be a significant biomarker for adenocarcinoma in respiratory system or digestive system. Additionally, it should be noted that serum CEA levels were also significantly increased in some non-neoplastic lung diseases, especially in ILD or allergic bronchopulmonary aspergillosis (ABPA). In respiratory system, increased CEA expression of bronchiolar cells and type II pneumocytes (15) was responded to inflammation induced by mucus plug in ABPA (26) or atypical epithelial proliferation in idiopathic pulmonary fibrosis (IPF) (16). As human angiotensin-converting enzyme 2 (ACE2) is an entry receptor of SARS-CoV-2 (27, 28), bronchiolar epithelial cells and type II alveolar epithelial cells are the prime targets of SARS-CoV-2 in lung because of abundant expression on lung alveolar epithelial cells where SARS-CoV-2 particles were observed by electron microscopy (29, 30). Several autopsy studies have confirmed that bronchi were covered by mucus or mucus plug, as well as significant proliferating interstitial fibroblasts and type II pneumocyte hyperplasia (31) in COVID-19 patients. Since type II pneumocytes are considered as the stem cells or progenitors in alveoli (32), SARS-CoV-2 infection-induced massive alveolar epithelial cell death may lead to abnormal regeneration of type II pneumocytes for repair along with the production of CEA, which was similar to the uncontrolled proliferation of lung adenocarcinoma. Moreover, atypical epithelial proliferation and proliferating fibroblasts may also exacerbate obstruction of bronchioles and lung consolidation leading to refractory hypoxemia as well as worsen CT involvement scores. Therefore, it is reasonable that serum CEA levels correlate with the severity and prognosis of COVID-19.

Based on the relationship between CEA and type II pneumocyte hyperplasia and lung fibrosis, early medication focuses on atypical epithelial and fibrotic proliferation, such as Nintedanib, may be a potential therapeutic method to decrease

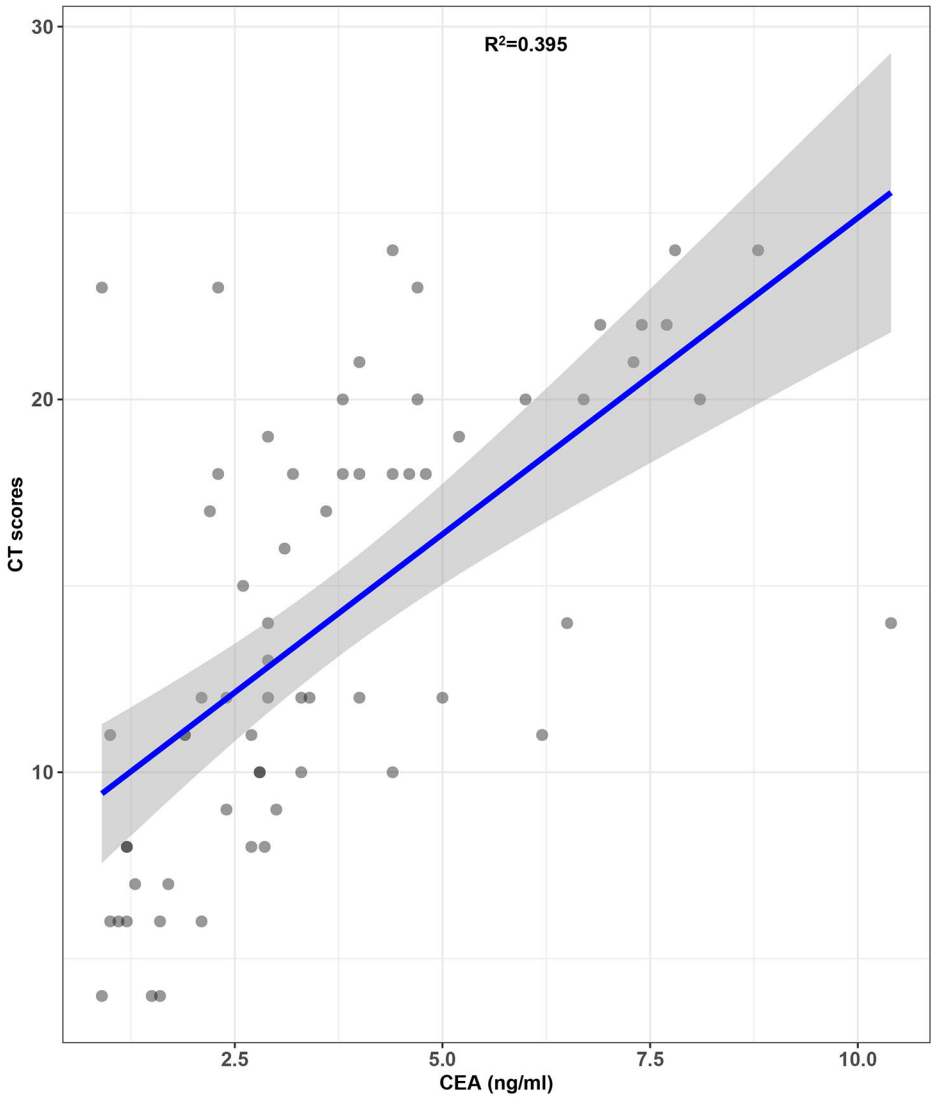

FIGURE 4 | Correlation of CEA levels with CT scores in discharged COVID-19 patients (the gray area on the figure means 95% confidence intervals).

FIGURE 5 | Chest CT scans and CEA levels of three female patients. **(A)** Four points CT scores and 0.9 ng/ml CEA levels. (70 years old). **(B)** Sixteen points CT scores and 3.1 ng/ml CEA levels (70 years old). **(C)** Twenty two points CT scores and 7.7 ng/ml CEA levels (69 years old).

the mortality of COVID-19. Nintedanib is an inhibitor of multiple tyrosine kinases including vascular endothelial growth factor (VEGF), platelet-derived growth factor (PDGF) and fibroblast growth factor (FGF) (33), which is approved for the treatment of progressive fibrosing interstitial lung diseases (PF-ILD) (34) in March, 2020. It was reported that infection of SARS-CoV-2 resulted in significant elevation of many cytokines such as IL-2, VEGF, PDGF and FGF (35, 36). Hence, some hypotheses based on the potential effects of antifibrotic drugs like Nintedanib on COVID-19 was proposed in a Personal View published in May, 2020 (37). As an antifibrotic drug, Nintedanib also proved to have antiproliferative activity in non-small-cell lung cancer (NSCLC) (38) and its efficiency combined with other anti-tumor drugs on NSCLC was confirmed in clinical trials (39). Moreover, Nintedanib was reported to inhibit transforming growth factor-β (TGF-β) signaling pathway by suppressing phosphorylation of Smad2/3 and type II TGF-β receptor in human lung fibroblasts (33) and A549 cells (alveolar epithelial-type II cells models) (40), which were considered as novel antifibrotic mechanisms of Nintedanib. Meanwhile, another study found the relation between expression of CEA (CEACAM5) gene and TGF-β pathway genes (TGFBR1, TGFBR2, and SMAD3) in colorectal adenocarcinoma cells (41). Though there were few publications about the association in alveolar epithelial cells, it is possible that similar mechanisms existed in human alveolar epithelial cells, especially when CEA on the cell membrane functioned as microbial receptors for bacteria or viruses. In fact, TGF-β pathway plays a role in the pathogenesis of SARS-CoV-2 (42). However, the detailed mechanisms of CEA or effects of Nintedanib remains unknown in SARS-CoV-2 infected alveolar epithelial cells. More in-depth studies of related molecular mechanisms need to be conducted in the future. Overall, considering significant elevated CEA levels originating from atypical epithelial proliferation in non-survivors with COVID-19 of our study, we think Nintedanib may be one of therapeutic options for antifibrotic therapy in addition to other basic treatment (oxygen therapy, antiviral therapy etc.) for COVID-19 patients especially those critical cases with elevation of CEA levels. It is possible that additional antifibrotic therapy might be an effective supplement for the present COVID-19 treatment strategy. More pilot studies can be performed to validate the effects of antifibrotic therapy on COVID-19 in the future.

A few limitations existed in our study. Firstly, the number of the participants was not very large relatively. The patients with COVID-19 were from the same hospital and selection bias of the patients may exist in our study. The association should be validated in another cohort with larger sample size. Secondly, the CT scores of death cases in ICU were missing because these patients were impossible to have CT examinations in view of their critical condition. Thus, we cannot analyze the CT scores in the death group with COVID-19. Finally, the complications of other organs besides lung cannot be analyzed in discharged patients with COVID-19 due to a lack of data.

In conclusion, our study suggested that the elevation of serum CEA levels increased the risk of death from COVID-19 and serum CEA levels were related to CT scores of the discharged patients positively. Serum CEA levels might be a potential biomarker to evaluate the severity and prognosis of COVID-19. More prospective and multicenter studies with validation cohorts are needed to be conducted in the future.

DATA AVAILABILITY STATEMENT

The raw data supporting the conclusions of this article will be made available by the authors, without undue reservation.

ETHICS STATEMENT

The studies involving human participants were reviewed and approved by Ethics Committee of Wuhan Jin Yin-tan Hospital (No. KY-2020-59.01). Written informed consent for participation was not required for this study in accordance with the national legislation and the institutional requirements.

AUTHOR CONTRIBUTIONS

JT, YL, MH, and WX contributed to funding acquisition, project administration, and supervision. QC and HK contributed to and writing original draft. XQ and WD contributed to software application and formal analysis. CH and WW contributed to data curation and investigation. NJ and CW contributed to methodology. MH and WX contributed to reviewing and editing original draft. All authors reviewed and approved the final manuscript.

FUNDING

This work was funded by grants from National Key Research & Development Plan of the Ministry of Science and Technology of the People's Republic of China (Grant Nos. 2018YFC1314900 and 2018YFC1314901), Project of Science and Technology Department of Jiangsu Province (Grant No. BE2016002-4), 2019 Provincial Special Guide Fund Project for the Development of Modern Service Industry (Grant No. 2019 [783]), 2016 Projects of Nanjing Science Bureau (Grant No. 201608003), National Health and Family Planning Commission Statistical Information Center Project, National Natural Science Foundation of China (NSFC) (Grant Nos. 81870054 and 81800011), and Key Project of National Science & Technology for Infectious Diseases of China (Grant No. 2018ZX10722301-002).

ACKNOWLEDGMENTS

The authors thank all colleagues from Division of Intensive Care Unit in Wuhan Jin Yin-tan Hospital for their support during the preparation of this manuscript.

SUPPLEMENTARY MATERIAL

The Supplementary Material for this article can be found online at: https://www.frontiersin.org/articles/10.3389/fmed.2020.579543/full#supplementary-material

REFERENCES

1. Coronaviridae Study Group of the International Committee on Taxonomy of Viruses. The species severe acute respiratory syndrome-related coronavirus: classifying 2019-nCoV and naming it SARS-CoV-2. *Nature Microbiol.* (2020) 5:536–44. doi: 10.1038/s41564-020-0695-z
2. Zhou F, Yu T, Du R, Fan G, Liu Y, Liu Z, et al. Clinical course and risk factors for mortality of adult inpatients with COVID-19 in Wuhan, China: a retrospective cohort study. *Lancet.* (2020) 395:1054–62. doi: 10.1016/S0140-6736(20)30566-3
3. Sohrabi C, Alsafi Z, O'Neill N, Khan M, Kerwan A, Al-Jabir A, et al. World Health Organization declares global emergency: a review of the 2019 novel coronavirus (COVID-19). *Int J Surg.* (2020) 76:71–6. doi: 10.1016/j.ijsu.2020.02.034
4. WHO. *Coronavirus Disease (COVID-19) Situation Reports* 2020. Available online at: https://www.who.int/emergencies/diseases/novel-coronavirus-2019/situation-reports (accessed August 24, 2020).
5. Wu Z, McGoogan JM. Characteristics of and important lessons from the coronavirus disease 2019 (COVID-19) outbreak in China: summary of a report of 72314 cases from the Chinese Center for Disease Control and Prevention. *JAMA.* (2020) 323:1239–42. doi: 10.1001/jama.2020.2648
6. Tan C, Huang Y, Shi F, Tan K, Ma Q, Chen Y, et al. C-reactive protein correlates with computed tomographic findings and predicts severe COVID-19 early. *J Med Virol.* (2020)92:856–62. doi: 10.1002/jmv.25871
7. Li H, Xiang X, Ren H, Xu L, Zhao L, Chen X, et al. Serum amyloid A is a biomarker of severe coronavirus disease and poor prognosis. *J Infect.* (2020) 80:646–55. doi: 10.1016/j.jinf.2020.03.035
8. Arachchillage DR, Laffan M. Abnormal coagulation parameters are associated with poor prognosis in patients with novel coronavirus pneumonia. *J Thromb Haemost.* (2020) 18:844–7. doi: 10.1111/jth.14768
9. Ulhaq ZS, Soraya GV. Interleukin-6 as a potential biomarker of COVID-19 progression. *Med Mal Infect.* (2020) 50:382–3. doi: 10.1016/j.medmal.2020.04.002
10. Tchoupa AK, Schuhmacher T, Hauck CR. Signaling by epithelial members of the CEACAM family—mucosal docking sites for pathogenic bacteria. *Cell Commun Signal.* (2014) 12:27. doi: 10.1186/1478-811X-12-27
11. Beauchemin N, Arabzadeh A. Carcinoembryonic antigen-related cell adhesion molecules (CEACAMs) in cancer progression and metastasis. *Cancer Metastasis Rev.* (2013) 32:643–71. doi: 10.1007/s10555-013-9444-6
12. Camacho-Leal P, Zhai AB, Stanners CP. A co-clustering model involving alpha5beta1 integrin for the biological effects of GPI-anchored human carcinoembryonic antigen (CEA). *J Cellular Physiol.* (2007) 211:791–802. doi: 10.1002/jcp.20989
13. Hao C, Zhang G, Zhang L. Serum CEA levels in 49 different types of cancer and noncancer diseases. *Prog Mol Biol Transl Sci.* (2019) 162:213–27. doi: 10.1016/bs.pmbts.2018.12.011
14. Islam EA, Anipindi VC, Francis I, Shaik-Dasthagirisaheb Y, Xu S, Leung N, et al. Specific binding to differentially expressed human carcinoembryonic antigen-related cell adhesion molecules determines the outcome of neisseria gonorrhoeae infections along the female reproductive tract. *Infect Immun.* (2018) 86:e00092. doi: 10.1128/IAI.00092-18
15. Abbona GC, Papotti M, Gugliotta P, Pecchio F, Rapellino M. Immunohistochemical detection of carcinoembryonic antigen (CEA) in non-neoplastic lung disease. *Int J Biol Markers.* (1993) 8:240–3. doi: 10.1177/172460089300800407
16. Fahim A, Crooks MG, Wilmot R, Campbell AP, Morice AH, Hart SP. Serum carcinoembryonic antigen correlates with severity of idiopathic pulmonary fibrosis. *Respirology.* (2012) 17:1247–52. doi: 10.1111/j.1440-1843.2012.02231.x
17. Liu Q, Wang RS, Qu GQ, Wang YY, Liu P, Zhu YZ, et al. Gross examination report of a COVID-19 death autopsy. *Fa yi xue za zhi.* (2020) 36:21–3. doi: 10.12116/j.issn.1004-5619.2020.01.005
18. Tian S, Xiong Y, Liu H, Niu L, Guo J, Liao M, et al. Pathological study of the 2019 novel coronavirus disease (COVID-19) through postmortem core biopsies. *Mod Pathol.* (2020) 33:1007–14. doi: 10.1038/s41379-020-0536-x
19. Wei X, Su J, Yang K, Wei J, Wan H, Cao X, et al. Elevations of serum cancer biomarkers correlate with severity of COVID-19. *J Medical Virol.* (2020) 92:2036–41. doi: 10.1002/jmv.25957
20. Zhao JY, Yan JY, Qu JM. Interpretations of "diagnosis and treatment protocol for novel coronavirus pneumonia (trial version 7)". *Chin Med J.* (2020) 133:1347–49. doi: 10.1097/CM9.0000000000000866
21. Xie X, Zhong Z, Zhao W, Zheng C, Wang F, Liu J. Chest CT for typical 2019-nCoV pneumonia: relationship to negative RT-PCR testing. *Radiology.* (2020) 296:E41–5. doi: 10.1148/radiol.2020200343
22. Ajlan AM, Ahyad RA, Jamjoom LG, Alharthy A, Madani TA. Middle East respiratory syndrome coronavirus (MERS-CoV) infection: chest CT findings. *AJR American J Roentgenol.* (2014) 203:782–7. doi: 10.2214/AJR.14.13021
23. Sharif-Askari FS, Syed Sulaiman SA, Saheb Sharif-Askari N, Al Sayed Hussain A. Development of an adverse drug reaction risk assessment score among hospitalized patients with chronic kidney disease. *PLoS ONE.* (2014) 9:e95991. doi: 10.1371/journal.pone.0095991
24. Steyerberg EW, Vickers AJ, Cook NR, Gerds T, Gonen M, Obuchowski N, et al. Assessing the performance of prediction models: a framework for traditional and novel measures. *Epidemiology.* (2010) 21:128–38. doi: 10.1097/EDE.0b013e3181c30fb2
25. Le Borgne F, Combescure C, Gillaizeau F, Giral M, Chapal M, Giraudeau B, et al. Standardized and weighted time-dependent receiver operating characteristic curves to evaluate the intrinsic prognostic capacities of a marker by taking into account confounding factors. *Stat Methods Med Res.* (2018) 27:3397–410. doi: 10.1177/0962280217702416
26. Noguchi T, Yamamoto K, Moriyama G, Saito Y, Kyoyama H, Mikami S, et al. Evaluation of serum levels of carcinoembryonic antigen in allergic bronchopulmonary aspergillosis. *J Nippon Med Sch = Nippon Ika Daigaku zasshi.* (2013) 80:404–09. doi: 10.1272/jnms.80.404
27. Zhou P, Yang XL, Wang XG, Hu B, Zhang L, Zhang W, et al. A pneumonia outbreak associated with a new coronavirus of probable bat origin. *Nature.* (2020) 579:270–3. doi: 10.1038/s41586-020-2012-7
28. Wang Q, Zhang Y, Wu L, Niu S, Song C, Zhang Z, et al. Structural and functional basis of SARS-CoV-2 entry by using human ACE2. *Cell.* (2020) 181:894–904. doi: 10.1016/j.cell.2020.03.045
29. Yao XH, Li TY, He ZC, Ping YF, Liu HW, Yu SC, et al. [A pathological report of three COVID-19 cases by minimal invasive autopsies]. *Zhonghua bing li xue za zhi = Chin J Pathol.* (2020) 49:411–7. doi: 10.3760/cma.j.cn112151-20200312-00193
30. Fox SE, Akmatbekov A, Harbert JL, Li G, Quincy Brown J, et al. Pulmonary and cardiac pathology in African American patients with COVID-19: an autopsy series from New Orleans. *Lancet Respir Med.* (2020) 8:681–6. doi: 10.1016/S2213-2600(20)30243-5
31. Tian S, Hu W, Niu L, Liu H, Xu H, Xiao SY. Pulmonary pathology of early-phase 2019 novel coronavirus (COVID-19) pneumonia in two patients with lung cancer. *J Thorac Oncol.* (2020) 15:700–4. doi: 10.1016/j.jtho.2020.02.010
32. Barkauskas CE, Cronce MJ, Rackley CR, Bowie EJ, Keene DR, Stripp BR, et al. Type 2 alveolar cells are stem cells in adult lung. *J Clin Invest.* (2013) 123:3025–36. doi: 10.1172/JCI68782
33. Rangarajan S, Kurundkar A, Kurundkar D, Bernard K, Sanders YY, Ding Q, et al. Novel mechanisms for the antifibrotic action of nintedanib. *Am J Respir Cell Mol Biol.* (2016) 54:51–9. doi: 10.1165/rcmb.2014-0445OC
34. Flaherty KR, Wells AU, Cottin V, Devaraj A, Walsh SLF, Inoue Y, et al. Nintedanib in progressive fibrosing interstitial lung diseases. *N Engl J Med.* (2019) 381:1718–27. doi: 10.1056/NEJMoa1908681
35. Nile SH, Nile A, Qiu J, Li L, Jia X, Kai G. COVID-19: pathogenesis, cytokine storm and therapeutic potential of interferons. *Cytokine Growth Factor Rev.* (2020) 53:66–70. doi: 10.1016/j.cytogfr.2020.05.002
36. Huang C, Wang Y, Li X, Ren L, Zhao J, Hu Y, et al. Clinical features of patients infected with 2019 novel coronavirus in Wuhan, China. *Lancet.* (2020) 395:497–506. doi: 10.1016/S0140-6736(20)30183-5
37. George PM, Wells AU, Jenkins RG. Pulmonary fibrosis and COVID-19: the potential role for antifibrotic therapy. *Lancet Respir Med.* (2020) 8:807–15. doi: 10.1016/S2213-2600(20)30225-3
38. Hilberg F, Tontsch-Grunt U, Baum A, Le AT, Doebele RC, Lieb S, et al. Triple angiokinase inhibitor nintedanib directly inhibits tumor cell growth and induces tumor shrinkage via blocking oncogenic receptor tyrosine kinases. *J Pharmacol Exp Ther.* (2018) 364:494–503. doi: 10.1124/jpet.117.244129
39. Capelletto E, Migliorino MR, Morabito A, Chiari R, Grossi F, Tiseo M, et al. Final results of the SENECA (SEcond line NintEdanib in non-small cell lung CAncer) trial. *Lung Cancer.* (2019) 134:210–7. doi: 10.1016/j.lungcan.2019.06.028

40. Ihara H, Mitsuishi Y, Kato M, Takahashi F, Tajima K, Hayashi T, et al. Nintedanib inhibits epithelial-mesenchymal transition in A549 alveolar epithelial cells through regulation of the TGF-β/Smad pathway. *Respir Investig.* (2020) 58:275–84. doi: 10.1016/j.resinv.2020.01.003
41. Gu S, Zaidi S, Hassan MI, Mohammad T, Malta TM, Noushmehr H, et al. Mutated CEACAMs disrupt transforming growth factor beta signaling and alter the intestinal microbiome to promote colorectal carcinogenesis. *Gastroenterology.* (2020) 158:238–52. doi: 10.1053/j.gastro.2019.09.023
42. Delpino MV, Quarleri J. SARS-CoV-2 Pathogenesis: imbalance in the renin-angiotensin system favors lung fibrosis. *Front Cell Infect Microbiol.* (2020) 10:340. doi: 10.3389/fcimb.2020.00340

Conflict of Interest: The authors declare that the research was conducted in the absence of any commercial or financial relationships that could be construed as a potential conflict of interest.

Copyright © 2020 Chen, Kong, Qi, Ding, Ji, Wu, Huang, Wu, Huang, Xie, Liu and Tang. This is an open-access article distributed under the terms of the Creative Commons Attribution License (CC BY). The use, distribution or reproduction in other forums is permitted, provided the original author(s) and the copyright owner(s) are credited and that the original publication in this journal is cited, in accordance with accepted academic practice. No use, distribution or reproduction is permitted which does not comply with these terms.

frontiers in Medicine

ORIGINAL RESEARCH
published: 29 October 2020
doi: 10.3389/fmed.2020.561866

Blood and Salivary Amphiregulin Levels as Biomarkers for Asthma

*Mahmood Yaseen Hachim[1,2], Noha Mousaad Elemam[2], Rakhee K. Ramakrishnan[2], Laila Salameh[3], Ronald Olivenstein[4], Ibrahim Yaseen Hachim[2,5], Thenmozhi Venkatachalam[2], Bassam Mahboub[3,5], Saba Al Heialy[1,4], Rabih Halwani[2,5], Qutayba Hamid[2,4,5] and Rifat Hamoudi[2,5,6]**

[1] College of Medicine, Mohammed Bin Rashid University of Medicine and Health Sciences, Dubai, United Arab Emirates, [2] Sharjah Institute for Medical Research, College of Medicine, University of Sharjah, Sharjah, United Arab Emirates, [3] Rashid Hospital, Dubai Health Authority, Dubai, United Arab Emirates, [4] Meakins-Christie Laboratories, McGill University, Montreal, QC, Canada, [5] Department of Clinical Sciences, College of Medicine, University of Sharjah, Sharjah, United Arab Emirates, [6] Division of Surgery and Interventional Science, UCL, London, United Kingdom

Background: Amphiregulin (AREG) expression in asthmatic airways and sputum was shown to increase and correlate with asthma. However, no studies were carried out to evaluate the AREG level in blood and saliva of asthmatic patients.

Objective: To measure circulating AREG mRNA and protein concentrations in blood, saliva, and bronchial biopsies samples from asthmatic patients.

Methods: Plasma and Saliva AREG protein concentrations were measured using ELISA while PBMCs, and Saliva mRNA expression was measured by RT qPCR in non-severe, and severe asthmatic patients compared to healthy controls. Primary asthmatic bronchial epithelial cells and fibroblasts were assessed for AREG mRNA expression and released soluble AREG in their conditioned media. Tissue expression of AREG was evaluated using immunohistochemistry of bronchial biopsies from asthmatic patients and healthy controls. Publicly available transcriptomic databases were explored for the global transcriptomic profile of bronchial epithelium, and PBMCs were explored for AREG expression in asthmatic vs. healthy controls.

Results: Asthmatic patients had higher AREG protein levels in blood and saliva compared to control subjects. Higher mRNA expression in saliva and primary bronchial epithelial cells plus higher AREG immunoreactivity in bronchial biopsies were also observed. Both blood and saliva AREG levels showed positive correlations with allergic rhinitis status, atopy status, eczema status, plasma periostin, neutrophilia, Montelukast sodium use, ACT score, FEV1, and FEV1/FVC. *In silico* analysis showed that severe asthmatic bronchial epithelium with high AREG gene expression is associated with higher neutrophils infiltration.

Conclusion: AREG levels measured in a minimally invasive blood sample and a non-invasive saliva sample are higher in non-allergic severe asthma.

Clinical Implications

This is the first report to show the higher level of AREG levels in blood and saliva of non-allergic severe asthma.

Keywords: asthma, biomarkers, saliva, amphiregulin (AREG), non-invasive

OPEN ACCESS

Edited by:
Hsiao-Chi Chuang,
Taipei Medical University, Taiwan

Reviewed by:
Mohib Uddin,
AstraZeneca, Sweden
Chih-Ming Weng,
Taipei Medical University, Taiwan

***Correspondence:**
Rifat Hamoudi
rhamoudi@sharjah.ac.ae

Specialty section:
This article was submitted to Pulmonary Medicine, a section of the journal Frontiers in Medicine

Received: *13 May 2020*
Accepted: *11 September 2020*
Published: *29 October 2020*

Citation:
Hachim MY, Elemam NM, Ramakrishnan RK, Salameh L, Olivenstein R, Hachim IY, Venkatachalam T, Mahboub B, Al Heialy S, Halwani R, Hamid Q and Hamoudi R (2020) Blood and Salivary Amphiregulin Levels as Biomarkers for Asthma. Front. Med. 7:561866. doi: 10.3389/fmed.2020.561866

INTRODUCTION

Asthma is characterized by chronic airway inflammation, mucus hyper-production, airway hyper-responsiveness, and variable airway obstruction (1). The prevalence of asthma has increased in the last few years, reaching alarming levels (2). Understanding the complexity of asthma will help in establishing management strategies aiming for better asthma patients stratification for personalized therapeutic options (3). Current biomarkers include eosinophil counts, a fraction of exhaled nitric oxide (Feno) values, periostin, IgE levels, and T-helper2 related cytokines (4). The identification of novel, cost-effective, reliable, and measurable non-invasive markers (5) is the goal for many research projects (6–8).

The epidermal growth factor receptor (EGFR) signaling is vital to epithelial cell physiology, and its dysregulation is involved in different pathologies (9), including pathogenesis of early stage of asthma (10). Many asthma triggers like allergens, viruses, and pollutants activate EGFR signaling, which seems to be a common pathway shared by different asthma phenotypes (11). EGFR signaling mediates airway hyper-responsiveness (AHR), tissue remodeling (12) and is implicated in lung fibrosis (10). Amphiregulin (Areg), an EGFR ligand, and a widely expressed transmembrane tyrosine kinase (13, 14), was shown to be upregulated upon inflammation, hormones, growth factors, and xenobiotics stimuli (13). Previously, high AREG expression was related to lung inflammation (15), specifically in damaged lung tissues in patients with chronic obstructive pulmonary disease (COPD) and asthma (16). AREG expression in structural cells (15) and sputum was associated with asthma severity (17), and it was shown to be increased in airways during an acute asthma attack (18).

Interestingly, hematopoietic cells that infiltrate inflamed lung tissue were shown to locally upregulate AREG expression and influence its local concentrations (15). While human monocytes were found to express AREG upon activation (19), eosinophils still represent the primary producers of AREG when compared to other types of blood cells (19) and can be reprogrammed to an inflammatory state by AREG- EGFR-mediated signaling (20). For all the above reasons, AREG was suggested to be linked to severe eosinophilic asthma with less response to asthma therapy (21). Such sensitized individual develops eosinophilic airway inflammation after the exposure to allergens through IgE antibody-mediated mast cell degranulation is labeled as allergic asthmatic. On the other hand, a non-allergic asthmatic is a non-sensitized individual who can develop eosinophilic inflammation without exposure to an allergen through the activation of ILC2 cells that do not need allergen-specific IgE (22). ILC2s and lung activated alveolar macrophages can control lung inflammation by producing AREG to promote repair of the airway epithelium, that is why depletion of these cells can result in diminished lung function after the loss of airway epithelial integrity which can be restored by adding AREG (23–26).

Non-allergic patients may have innate immunity or neutrophilic airway inflammation independent of Th2 cells (27). Triggers of asthma in non-allergic patients can vary from external triggers like viral infections, cigarette smoke, diesel particles, and ozone to patient's intrinsic factors like stress, exercise, and obesity (1). Following epithelial damage, the epidermal growth factor (EGF) can enhance the neutrophil accumulation to stimulate neutrophil defenses during acute injury (28).

Of note, T cells in peripheral blood mononuclear cells (PBMC) can also produce AREG in response to signals of tissue damage and repair (29). The association of a protective AREG with disease progression, and whether there is cell to cell variation in production and response to AREG remain unknown.

Some circulating plasma proteins originating from tissue leakage (30) and thus being detected in saliva and can reflect their upregulation in serum/plasma (31). Because saliva is easy to collect, innocuous, acceptable by patients, thus it represents a potential tool for measuring disease biomarkers (32). Therefore, measuring the expression of AREG in plasma and saliva from asthmatic patients can provide a minimally invasive approach for the assessment of AREG, which may provide a more reliable tool complementary to existing measures.

METHODS

Patient Population (Cohort 1)

From January 2017 to May 2019, individuals were recruited consecutively from the Asthma Clinic in Rashid Hospital, Pulmonary Medicine Department. Thirty-two asthmatic patients were included, 19 were non-severe asthmatic patients (mild to moderate), and 13 were severe asthmatic subjects (fulfilling the criteria for asthma as per American Thoracic Society) (**Table 1**). According to GINA and ERS/ATS Task Force on severe asthma, guidelines define asthma severity as "those who require continuous high-dose treatment, as their asthma is refractory or difficult-to-treat plus a second controller (and/or systemic corticosteroids) to prevent it from becoming uncontrolled or which remains uncontrolled despite this therapy" (33). Those patients were compared to 12 non-asthmatic volunteer subjects who had no recent infection of the respiratory tract and no histories of allergy or asthma. Participants completed the Asthma Control Test self-assessment. The Ethics Committee of Dubai Health Authority and the University of Sharjah approved the study with REC (Research Ethics Committee) approval number DSREC-11/2017_04, and each subject gave written informed consent after a thorough explanation by the treating physician and the researchers. This study was conducted in accordance with the Declaration of Helsinki. The demographic characteristics of the asthmatic patients and control subjects are shown in **Table 4**.

Abbreviations: ACT, asthma control test; ADAM, a disintegrin and metalloproteases; AHR, airway hyperresponsiveness; AREG, amphiregulin; COPD, chronic obstructive pulmonary disease; DMEM, Dulbecco's Modified Eagle's medium; EDTA, ethylenediaminetetraacetic acid; EGF, epidermal growth factor; EGFR, the epidermal growth factor receptor; ELISA, enzyme-linked immunoassay; ErbB, erythroblastic leukemia viral oncogene; FBS, fetal bovine serum; Feno, fraction of exhaled nitric oxide; GEO, Gene Expression Omnibus; HDM, house dust mite; IgE, immunoglobulin E; IL17A, Interleukin 17 A; mRNA, Messenger RNA; PBMC, peripheral blood mononuclear cells; qRT-PCR, Real-Time qRT-PCR; ROC, Receiver Operating Characteristic curve; TH2, T helper cell type 2; TNFα, TNF-alpha.

TABLE 1 | Characteristics of the cohort 1 subjects with asthma and healthy controls.

	Control	Non-severe asthma	Severe asthma	*P*-value
Number of subjects	12	19	13.00	
Age (Years)	37.00 ± 11.73	40.19 ± 15.65	48.42 ± 17.95	NS
Age of onset (adult to childhood ratio)				
Childhood asthma		11	5	
Adult asthma		5	8	
Female to male ratio	8:4	13:3	7:6	NS
BMI	24.60 ± 3.19	27.63 ± 6.40	27.03 ± 6.56	NS
ACT score	–	20.75 ± 4.31	17.55 ± 6.15	NS
Oral steroid use per day/week	–	0.6563 ± 1.06	2.083 ± 1.459	0.01
Exacerbations/year	–	1.688 ± 2.575	2.133 ± 1.482	NS
History of atopy				
Yes	0	0	4	<0.01
No	10	16	9	
History of allergic rhinitis				
Yes	1	10	9	<0.01
No	9	6	4	
Peak flow (l/min)	453.80 ± 101.00	299.30 ± 78.20	302.50 ± 139.90	<0.01
FEV1 (% predicted)	–	55.46 ± 42.42	54.06 ± 45.53	NS
FEV1/FVC	–	56.87 ± 40.30	49.13 ± 35.35	NS
Total serum IgE (IU/mL)	–	280.30 ± 358.40	1167.00 ± 1428.00	<0.01
Blood eosinophil (%)	–	4.54 ± 3.24	6.88 ± 9.57	NS
Blood neutrophil (%)	–	58.29 ± 12.34	60.04 ± 13.86	NS
Blood basophil (%)	–	0.53 ± 0.36	0.52 ± 0.24	NS
Blood lymphocytes (%)	–	28.89 ± 11.05	26.67 ± 12.15	NS
Absolute eosinophil counts (cells/μL)	–	181.6 ± 129.6	275.2 ± 382.8	NS

Patient Population (Cohort 2)

A matched cohort of severe asthmatics ($n = 17$) vs. non-severe asthmatics ($n = 21$) was recruited for fresh saliva collections and RNA extractions was performed to explore the feasibility of detecting AREG mRNA in the saliva.

Blood Collection Protocol and Plasma Isolation

Twelve milliliters of whole blood were collected from each sample in EDTA-containing blood collection tubes (3 mL each) and transferred immediately within 2 h to Sharjah Institute for Medical Research (SIMR), Sharjah for further processing to isolate PBMCs as previously described (34). Twelve milliliters of Histopaque-1077 (Sigma, #10771, Germany) were added to a 50 mL centrifuge tube and brought to room temperature (RT), then 12 mL of whole blood were carefully layered on top of the Histopaque and centrifuged at 400 × g for precisely 30 min at room temperature. After centrifugation, the plasma layer and the buffy layer interface were carefully collected with separate Pasteur pipettes and transferred to clean 15 mL conical centrifuge tubes separately, to be frozen at −80°C till future use.

Unstimulated Whole Saliva Collection Protocol

Participants were asked to fast for at least 1 h and not to brush their teeth or smoke for 30 min, accompanied by gargling and rinsing of the mouth with water 5 min before proceeding with saliva collection. One milliliter of unstimulated whole saliva via passive drool was collected in a pre-prepared 50 mL tube containing 1 mL of RNAlater (Invitrogen). Collected saliva samples were transported on ice and stored at – 80°C until analysis. Sample measurements were undertaken within 3 months of storage.

Primary Cell Lines and Bronchial Biopsies (Cohort 3)

Primary cells from healthy and asthmatic patients were isolated from bronchial biopsies in Meakins-Christie Laboratories, The Centre for Respiratory Research at McGill University and the Research Institute of McGill University Health Centre as previously described (35). In total, 17 primary cells were exploited: 7 healthy primary cells: epithelial ($n = 3$) and fibroblasts ($n = 4$), and 10 primary asthmatic cells: epithelial cells ($n = 3$), non-severe asthmatic fibroblasts ($n = 4$), and severe asthmatic fibroblasts ($n = 3$). Twelve bronchial biopsies were taken from control ($n = 3$) and asthmatic ($n = 9$, 3 in each clinical stage: mild, moderate, and severe) were used for immunohistochemical assessment. Epithelial cells were revived and maintained using epithelial growth medium PneumaCult™-Ex Medium (Stem Cell Technology, Canada), supplemented with 100 units/mL penicillin/streptomycin (Gibco, USA). Primary fibroblasts were maintained in complete Dulbecco's

Modified Eagle's medium (DMEM) (Sigma-Aldrich, Germany) with 10% fetal bovine serum (FBS) (Sigma-Aldrich, Germany) supplemented with 100 units/mL penicillin/streptomycin (Gibco, USA).

mRNA Gene Expression Using qRT-PCR

RNA was extracted using RNAeasy mini kit (Qiagen, Germany) as per the manufacturer instructions. The purified RNA was reverse transcribed into cDNA using High Capacity cDNA Reverse Transcription (Applied Biosystems, USA) as per the manufacturer instructions. 5X Hot FIREPol EvaGreen qPCR Supermix (Solis BioDyne, Estonia) was used to quantify mRNA of the selected genes using QuantStudio3 (Applied Biosystems, USA). Details of used primers are in **Table 2**.

Enzyme-Linked Immunoassay (ELISA) Quantification

Human amphiregulin was measured in plasma and saliva of healthy controls and asthmatic patients as well as the conditioned media of primary bronchial cells using the Human Amphiregulin Quantikine and Duoset ELISA Kits (R&D Systems, USA) according to the manufacturer's instructions. Periostin (POSTN) and IL-17A were assessed in plasma using human Periostin/OSF-2 and human IL-17A DuoSet ELISA Kits (R&D Systems, USA),respectively, according to the manufacturer's instructions.

Soluble Receptors Array

To assess any difference in the shedding of AREG in the conditioned media of the asthmatics vs. healthy primary fibroblasts, Non-Hematopoietic Array and the Common Analytes Array (R&D Systems, Catalog # ARY011) was used as per the manufacturer instructions. The conditioned media of healthy bronchial fibroblasts and non-severe asthmatic fibroblasts were collected, centrifuged and 1.5 mL of each were added to the array wells separately and incubated overnight on a rocking shaker. On the next day, the membranes were washed to remove any unbound material and incubated with the specific cocktail of biotinylated detection antibodies. Streptavidin-horseradish peroxidase and chemiluminescent detection reagents were added, and a chemiluminescent signal was produced in proportion to the amount of receptor-bound. Dot blots were registered with ChemiDoc Imaging System (BioRad, USA). The average pixel density of duplicate spots on the membrane was determined using ImageJ software (36). After background subtraction, the relative amounts of individual proteins were calculated as previously reported (37).

Immunohistochemical Assessment of Bronchial Biopsies

Immunohistochemical evaluation of bronchial biopsies from healthy and asthmatic patients was done on a 3 µm section of the tissue block mounted on positively charged slides. After routine deparaffination and rehydration, antigen retrieval using Tris EDTA buffer (pH 9.0) in a microwave oven at 95°C for 15 min was done. Horse radish peroxidase (HRP) kit (760-700, Optiview DAB IHC Detection kit, Ventana) was used as per the manufacturer instructions, along with neutralizing antibody for AREG (15 µg/mL) (R&D Systems, USA) for AREG detection.

In silico Validation in Lung and Blood Transcriptomic Datasets

Twenty-five publicly available transcriptomics datasets (n = 2,666) of Bronchial Epithelium, Bronchial Fibroblasts, Whole Lung, Bronchial Biopsy, Induced Sputum, Nasal, Bronchioalveolar lavage, Blood, Whole Blood, PBMCs, and CD4 cells from asthmatic patients vs. healthy subjects in different settings were downloaded from Gene Expression Omnibus (https://www.ncbi.nlm.nih.gov/geo). The raw data was extracted according to Hachim et al. (38) and the normalized gene expression of the AREG was compared between patients with different asthma severities as shown in **Table 3**.

In silico Prediction of the Percentage and Status of Immune Cells

We used the transcriptomic data to predict the percentage and status of immune cells in the bronchial epithelium or blood of severe asthmatics patients compared to the healthy controls using CIBERSORT computational method (https://cibersort.stanford.edu/) to quantify cell fractions from samples gene expression profiles as previously described (39).

Statistical Methods

GraphPad Prism version 8.00 for Windows (GraphPad Software, La Jolla, CA, USA) was used for statistical analysis. First, the D'Agostino-Pearson normality test was used to determine whether to perform parametric or non-parametric tests. One-way ANOVA test was performed to determine whether there are any statistically significant differences between the mean values of the controls and different asthma groups for the gene expression and protein levels. The same software was used to examine the correlations between the different parameters using Pearson correlation test in GraphPad Prism. Student t-test was used to look for the difference between two groups under a given experiment or treatment. A $p < 0.05$ is considered to be statistically significant.

RESULTS

Severe Asthmatic Patients PBMCs Express Less AREG mRNA but Higher Protein Compared to Non-severe Asthmatics

PBMCs AREG mRNA was lower in severe asthmatics compared to non-severe asthmatics ($p = 0.05$), (**Figure 1A**). PBMCs AREG mRNA correlated positively with IL17A plasma level (0.43, $p < 0.05$). Also, the expression correlated negatively with age (−0.38, $p < 0.05$), the use of oral corticosteroids (−0.58, $p < 0.05$), the number of exacerbations per year (−0.39, $p < 0.05$), and atopic status (−0.40, $p < 0.05$).

TABLE 2 | List of forward and reverse primers for each of the genes assessed by qRT-PCR.

Gene	NCBI reference sequence	Primer	Sequence (5′-3′)	Amplicon size (bp)
Areg	NM_001657.4	Forward primer	GAGCACCTGGAAGCAGTAAC	151
		Reverse primer	GGATCACAGCAGACATAAAGGC	
18S rRNA	NR_145820.1	Forward primer	TGACTCAACACGGGAAACC	114
		Reverse primer	TGCCTCCACCAACTAAGAAC	

TABLE 3 | List of datasets extracted from GEO omnibus for the in silico analysis.

Dataset ID	Tissue/sample	Study title	Samples
GSE4302	Bronchial epithelium	Genome-Wide Profiling of Airway Epithelial Cells in Asthmatics, Smokers and Healthy Controls	70
GSE18965	Bronchial epithelium	Decreased Fibronectin Production Significantly Contributes to Dysregulated Repair of Asthmatic Epithelium	16
GSE43696	Bronchial epithelium	Asthma	108
GSE51392	Bronchial epithelium	Expression Data From Airway Epithelial Cells Stimulated With Poly(I:C) From Patients With Asthma, Rhinitis, and Healthy Controls	12
GSE67472	Bronchial epithelium	Airway Epithelial Gene Expression in Asthma Versus Healthy Controls	105
GSE64913	Bronchial epithelium	Altered Epithelial Gene Expression in Peripheral Airways of Severe Asthma	36
GSE76227	Bronchial epithelium	Expression Data of Bronchial Biopsies and Epithelial Brushing From Unbiased Biomarkers in Prediction of Respiratory Disease Outcomes (U-BIOPRED) Project	190
GSE13785	Bronchial epithelium	Novel Mediators of Eicosanoid and Epithelial Nitric Oxide Production in Asthma	22
GSE30063	Bronchial epithelium	Epithelial Expression of Toll-like Receptor 5 is Modulated in Healthy Smokers and Smokers With Chronic Obstructive Lung Disease	63
GSE27335	Bronchial fibroblasts	Genomic Differences Distinguish the Myofibroblast Phenotype of the Distal Lung From Airway Fibroblasts	24
GSE21369	Whole lung	Gene Expression Profiles of Interstitial Lung Disease (ILD) Patients	6
GSE41649	Bronchial biopsy	Comparison of Two Sets of Microarray Experiments to Define Allergic Asthma Expression Pattern	8
GSE56396	Induced sputum	Non-invasive Analysis of the Airway Transcriptome Discriminates Clinical Phenotypes of Asthma	112
GSE41863	Induced sputum	Sputum Gene Expression Profiling in Asthmatics	56
GSE41861	Nasal	Upper Airway Gene Expression Is an Effective Surrogate Biomarker for Th2-Driven Inflammation in the Lower Airway	84
GSE41862	Nasal	Nasal Scrape Gene Expression Profiling in Asthmatics	116
GSE67940	Bronchioalveolar lavage	Asthma III	104
GSE115823	Blood	A Network of Transcriptome Modules Demonstrates Mechanistic Pathways of Both Virus-Induced and Non-viral Asthma Exacerbations in Children [Blood]	208
GSE69683	Blood	Expression Profiling in Blood From Subjects With Severe Asthma, Moderate Asthma, and Non-asthmatics Collected in the U-BIOPRED Study	498
GSE35571	Blood	Gene Expression Data From 131 Human Subjects in Detroit, Michigan	131
GSE137394	Whole blood	Genome-Wide Profiling of Allergic Asthma Peripheral Blood	309
GSE123750	Whole blood	U-BIOPRED Blood Transcriptomics From children With Asthma or Wheeze	216
GSE31773	PBMC	Comparison of mRNA Expression in Circulating T-Cells From Patients With Severe Asthma	40
GSE16032	PBMC	Gene Expression Data From Severe Asthmatic Children: PBMC Profiles During Acute Exacerbation Versus Convalescence	10
GSE73482	CD4	Gene Expression Patterns in Allergen-Driven CD4 T Cell Responses From Human Atopics With or Without Asthma	144
Total	2,666		

AREG Was Higher in Well-Controlled Asthma

Asthma Control Test (ACT) is a patient self-administered tool for identifying those with poorly controlled asthma. The scores range from 5 (poor control of asthma) to 25 (complete control of asthma), with higher scores reflecting greater asthma control. An ACT score > 20 indicates well-controlled asthma. When we divided our patients accordingly, AREG mRNA expression in PBMC correlated positively with higher ACT scores, as shown in **Figure 1B**.

AREG mRNA Was Higher in the Saliva of Severe Asthmatics Compared to Non-severe Asthmatics

A matched cohort of severe asthmatics ($n = 17$) vs. non-severe asthmatics ($n = 21$) was recruited for fresh saliva collections and RNA was extracted to detect AREG mRNA in the saliva. AREG showed significant upregulation in severe asthmatics compared to non-severe asthmatics, as shown in **Figure 1C**.

Asthmatic Patients' Plasma and Saliva AREG Protein Level Is Higher Than Healthy Controls

Plasma AREG level, as measured by ELISA, was higher in non-severe and severe asthmatic patients (333.24 ± 133.14 pg/mL, $p < 0.01$) compared to healthy controls (265.05 ± 29.49 pg/mL) as shown in **Figure 2A**. Interestingly, the saliva AREG level was also higher in severe asthmatic patients (247.35 ± 271.4 pg/mL, $p = 0.02$), as shown in **Figure 2B**. Indeed, plasma AREG correlated positively to saliva AREG level ($r = 0.3671$, $p = 0.02$), indicating the feasibility of using saliva to reflect the plasma level of AREG. AREG plasma level correlated negatively with PBMC AREG mRNA expression ($r = -0.37$, $p < 0.05$).

Blood and Saliva AREG Protein Levels Correlate With Patient's Atopy Status and Allergic Rhinitis

Plasma AREG levels had a positive correlation with ACT ($r = 0.32$, $p < 0.05$), allergic rhinitis status ($r = 0.35$, $p =$

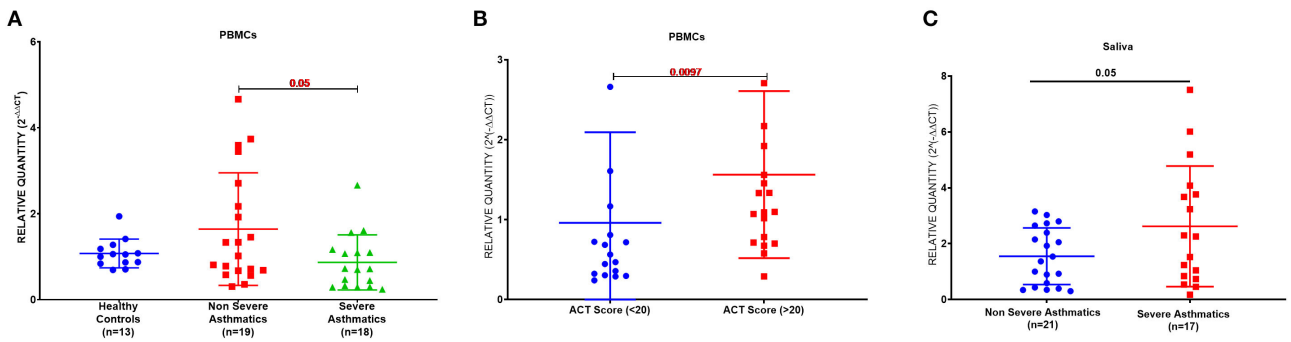

FIGURE 1 | AREG mRNA expression as measured by RT qPCR in PBMCs and saliva of cohort of asthmatic vs. healthy control. **(A)** AREG mRNA level in PBMCs of the locally recruited cohort (cohort 1), healthy controls ($n = 13$), non-severe asthmatics ($n = 20$), and severe asthmatic ($n = 18$). **(B)** AREG mRNA gene expression in PBMC of a locally recruited cohort divided according to the ACT score into two groups: a well-controlled group (ACT > 20) and those with poor control (ACT < 20). **(C)** AREG mRNA gene expression in the saliva of independent validation locally recruited cohort (cohort 2), which includes non-severe asthmatics ($n = 21$) and severe asthmatic who are not on biological treatment ($n = 17$).

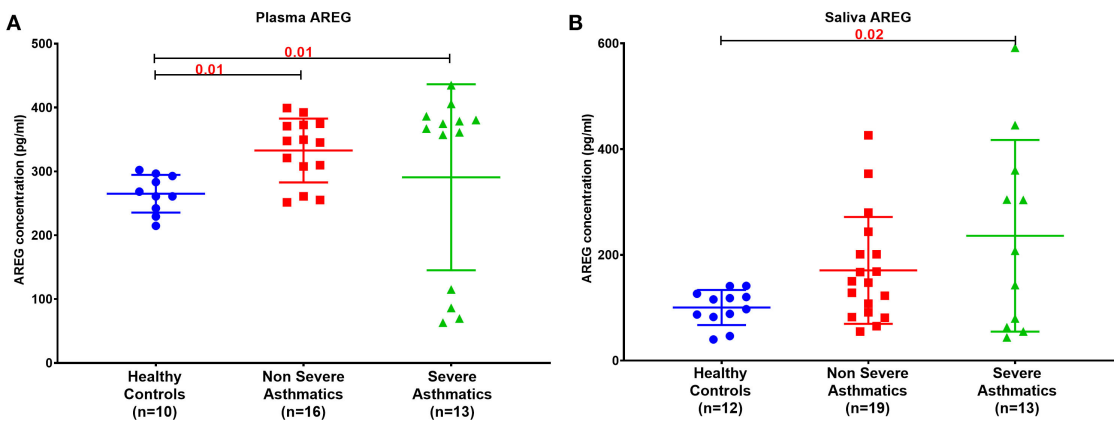

FIGURE 2 | AREG protein level in **(A)** plasma and **(B)** saliva of the locally recruited cohort (cohort 1), including healthy controls, non-severe and severe asthmatic patients.

0.03, **Figure 3A**), atopy status ($r = 0.35$, $p = 0.03$), neutrophil percentage in patients' blood ($r = 0.45$, $p = 0.01$), and the use of Montelukast sodium (Singulair) ($r = 0.39$, $p = 0.04$, **Figure 3B**). Interestingly, plasma AREG levels correlated positively with plasma POSTN levels ($r = 0.34$, $p = 0.03$). Correlation between Plasma AREG concentrations, and the cohort demographics and laboratory tests are listed in **Table 4**.

On the other hand, saliva AREG levels correlated significantly with key clinical indicators for asthma assessment compared to plasma AREG, as listed in **Table 5**. Beside allergic rhinitis ($r = 0.42$, $p = 0.02$) and atopy status ($r = 0.37$, $p = 0.02$), saliva AREG level correlated positively with ACT score ($r = 0.38$, $p = 0.04$), FEV1 (% predicted) ($r = 0.47$, $p = 0.001$), FEV1/FVC ($r = 0.48$, $p = 0.02$) and eczema status ($r = 0.35$, $p = 0.03$). Interestingly, saliva AREG level correlated positively with the age of onset as adult asthmatics showed higher levels ($r = 0.31$, $p < 0.05$).

AREG Protein Expression Was Higher in Bronchial Epithelial Cells of Mild Asthmatics Compared to Those of Moderate and Severe Patients as Well as Healthy Controls

AREG expression in lung tissue and its cellular localization were investigated using bronchial biopsies from asthmatic patients ($n = 13$) and healthy controls ($n = 4$), as shown in **Figure 4**. The asthmatic samples were from mild ($n = 5$), moderate ($n = 4$), and severe ($n = 4$) patients. Immunohistochemical expression of AREG was high in bronchial epithelial pseudostratified cells, while lower expression was observed in fibroblasts and other cells, including infiltrating immune cells. Interestingly, AREG expression in a healthy epithelium was nuclear while it was cytoplasmic in asthmatic samples. As expected, AREG expression was positive (6 out of 13, 46.15%) in asthmatic patient's samples compared to only 1 out of 4 samples in the control group (25%). Interestingly, AREG expression was positive in 4 out of the five mild asthmatic samples (80%) compared to only 1 case out of the four moderate (25%) and severe asthmatic samples (25%), $p = 0.0495$.

AREG mRNA Level Was Higher in Non-severe Asthmatic Bronchial Epithelial Cells Compared to Healthy Controls and Severe Asthmatic

AREG mRNA and protein levels were measured in primary bronchial epithelial cells and fibroblasts from asthmatic patients and healthy controls. AREG mRNA expression was upregulated in non-severe asthmatic bronchial epithelial cells compared to healthy controls ($p = 0.05$), and severe asthmatics ($p = 0.04$), **Figure 5A**. Using ELISA, secreted AREG levels detected in the conditioned media of bronchial epithelium using ELISA showed no significant difference between asthmatics and healthy controls, as shown in **Figure 5B**. Nevertheless, asthmatic bronchial epithelial cells secrete higher amounts (more than five times) of soluble AREG in their conditioned media compared to their asthma severity matching fibroblasts, indicating that

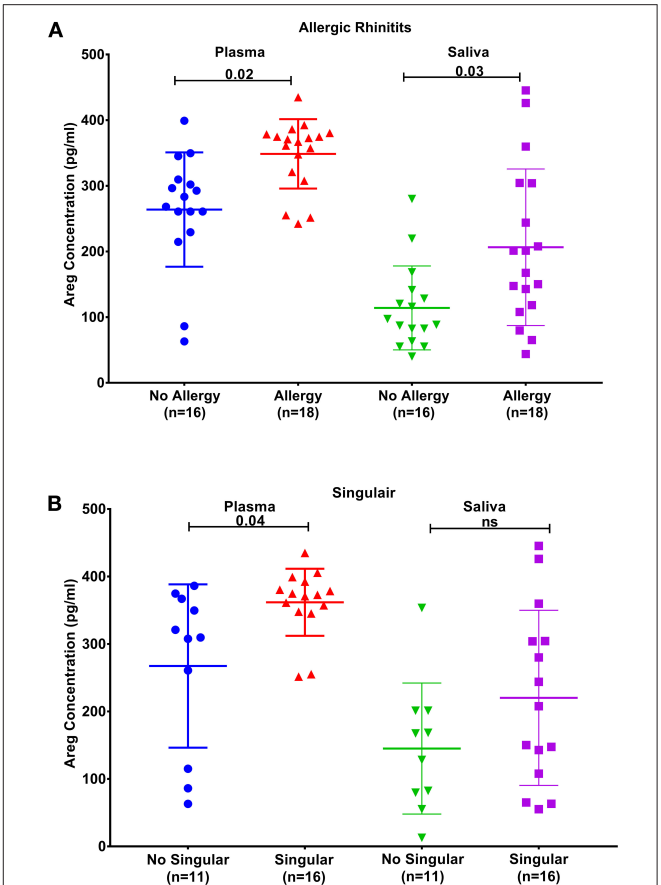

FIGURE 3 | AREG protein levels in plasma and saliva. **(A)** in asthmatic with allergic rhinitits compared to those who are not and **(B)** in asthmatics currently on Montelukast sodium (Singulair) compared to those who are not on Singulair.

epithelial cells are the primary source of pulmonary AREG in asthma. Moreover, bronchial fibroblasts of severe asthmatics ($n = 3$) showed lower expression of AREG mRNA compared to healthy fibroblasts ($n = 4$) ($p = 0.04$), which goes in line with the ELISA results ($p = 0.01$), **Figures 5C,D**.

Asthmatic Fibroblasts Secrete More AREG Ectoderm Shedders ADAM8, ADAM9, ADAM10 Compared to Healthy Fibroblasts

As the secreted levels of AREG matched its mRNA expression in severe asthmatic fibroblasts, we investigated the reason behind the low secreted levels of AREG in non-severe asthmatic fibroblasts despite of its high mRNA expression levels (**Figure 6**). We profiled the shredded proteins in their conditioned media and found that asthmatic fibroblasts secrete higher AREG ectoderm shedders ADAM8 ($p = 0.01$), ADAM9 ($p = 0.001$), ADAM10 ($p < 0.0001$) and ADAM17 ($p < 0.0001$) compared to healthy fibroblasts (**Figure 6A**). Another interesting finding is that non-severe asthmatic fibroblasts shed less ErbB1 ($p = 0.003$) and ErbB3 ($p = 0.003$) receptors compared to healthy fibroblasts (**Figure 6B**).

TABLE 4 | Correlation between plasma AREG concentrations, and the cohort demographics and laboratory tests.

AREG plasma (pg/mL)	vs. AREG saliva (pg/mL)	vs. Atopy status	vs. Allergic rhinitis status	vs. Blood neutrophil (%)	vs. POSTN plasma (pg/mL)
Pearson correlation test *r*	0.3671	0.3547	0.351	0.4494	0.3436
95% confidence interval	0.04391–0.6207	0.02475–0.615	0.02544–0.6092	0.07192–0.7143	0.01704–0.6039
P (two-tailed)	0.0234	0.0312	0.0307	0.0187	0.0347
Number of XY pairs	38	37	38	27	38

TABLE 5 | Correlation between saliva AREG concentrations, and the cohort demographics and laboratory tests.

AREG saliva (pg/mL)	vs. ACT score	vs. Atopy status	vs. Allergic rhinitis status	vs. Eczema status	vs. FEV1 (% predicted)	vs. FEV1/FVC
Pearson correlation test *r*	0.3895	0.3744	0.4216	0.3554	0.6458	0.487
95% confidence interval	−0.009556–0.6815	0.04223–0.632	0.1032–0.6616	0.02557–0.6155	0.2959–0.8429	0.06913–0.7595
P (two-tailed)	0.0492	0.0245	0.0094	0.0309	0.0012	0.0215
Number of XY pairs	26	36	37	37	22	22

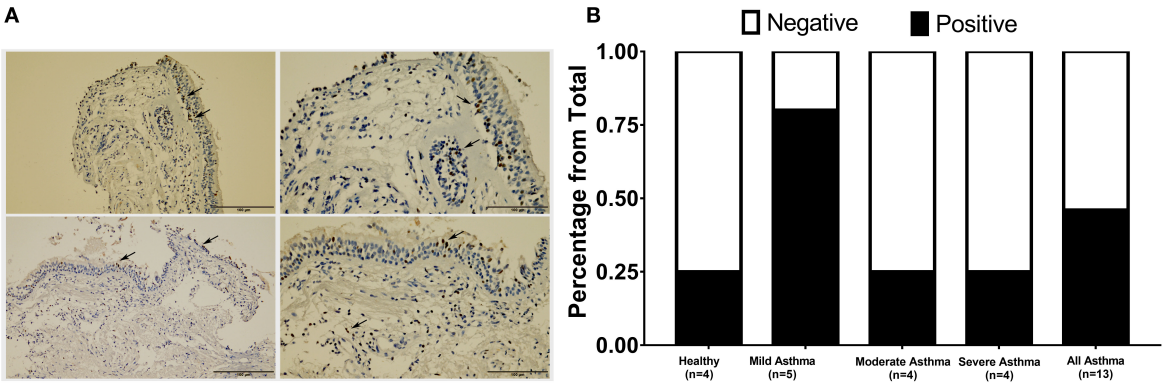

FIGURE 4 | Immunohistochemical staining of AREG in bronchial biopsies of healthy, non-severe (mild and moderate) and severe asthmatic patients. **(A)** Arrows showing positively stained epithelial cells, **(B)** percentage of positive AREG IHC staining sample among all samples examined in each group.

IN SILICO VALIDATION

AREG mRNA Expression Was Significantly Different in Asthmatic Bronchial Epithelium, Fibroblasts Using Biopsy or Brush

AREG showed consistent differential expression in asthmatic lung epithelium and fibroblasts using biopsy or brush in publicly available bronchial epithelium datasets and confirmed *in vitro* (**Table 6**).

AREG mRNA Expression Was Significantly Different in Severe Asthmatic Compared to Severe Wheezing Children Only

In order to explore the correlation of AREG mRNA in wheezing in asthmatic vs. non-asthmatic children, (GSE123750) gene set was explored. AREG mRNA expression in whole blood of children with non-severe and severe wheezes was compared to non-severe and severe asthmatics. As shown in **Figure 7A**, AREG mRNA expression was only significantly higher in severe asthmatic compared to severe wheezing children ($p = 0.03$). However, there was no significant difference in the gene expression of AREG between non-severe and severe asthmatic, indicating it is asthma specific markers.

AREG mRNA Expression in Whole Blood of Eosinophilic Asthma Was Significantly Lower Compared to Non-eosinophilic

In order to explore the correlation of AREG mRNA to the eosinophilic phenotype of asthma, (GSE137394) gene set was, as shown in **Figure 7B**. AREG was significantly lower in eosinophilic asthmatics ($p = 0.004$). This indicates that AREG can identify a non-eosinophilic subtype of a severe asthma phenotype.

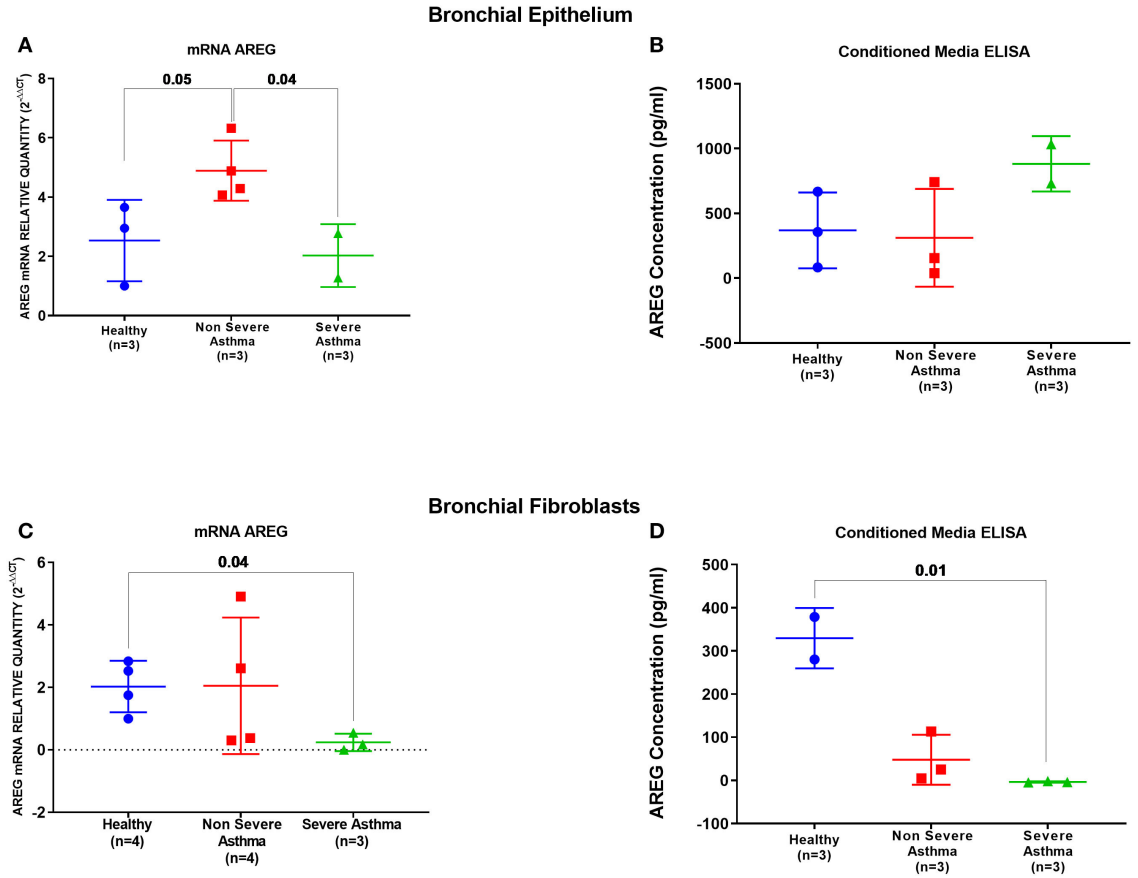

FIGURE 5 | AREG mRNA and secreted protein in bronchial epithelium cells and fibroblasts of healthy, non-severe, and severe asthmatic individuals. Assessment of AREG in asthmatic bronchial epithelium compared to the healthy epithelium on the **(A)** mRNA level measured by qRT-PCR, **(B)** secreted AREG protein levels by ELISA. Similarly, AREG was assessed in asthmatic fibroblasts compared to the healthy fibroblasts for the **(C)** AREG mRNA levels by qRT-PCR and **(D)** secreted AREG protein levels by ELISA.

PBMCs of Asthmatic Patients During Exacerbation Phase Express Higher AREG Compared to Convalescent Phase

GSE16032 dataset was chosen to identify the differential expression of the selected genes in PBMCs taken from asthmatic patients during the acute/exacerbation phase and the convalescent phase, as shown in **Figure 7C**. Interestingly, AREG was upregulated in the acute/exacerbation phase of asthma and returned back to the basal level when the attack subsides. This highlights the possible use of AREG as a marker for this specific disease phase.

SUMMARY IN BLOOD

Since, PBMCs mRNA expression was associated with asthma control score and AREG saliva mRNA was upregulated in severe asthma compared to non-severe asthmatics, we decided to explore its dynamics to understand its role in initiating and progression of the disease. AREG mRNA in the blood of drug naïve asthmatics compared to healthy, can differentiate severe asthmatic wheezes from others, can differentiate eosinophilic from non-eosinophilic, can differentiate acute attacks from convalescent-phase, and its expression was not affected by viruses (**Table 7**).

AREG Has Never been Linked to SNPs in Asthma

Genome-wide association studies (GWASs) of asthma have identified many risk alleles and loci that can be a potential source for diagnostic biomarkers. NHGRI-EBI GWAS Catalog was explored to identify 1,174 SNPs with the strongest Asthma-related SNP-risk allele. Interestingly, none of these SNPs were reported in AREG.

Severe Asthmatics Epithelium and Blood That Showed Higher AREG Expression Showed Different Immune Cells Populations Than Healthy Controls

We investigated if immune cell populations are different between asthmatic and healthy controls using the transcriptomic expression of the bronchial epithelium to predict the cell type and their state of activation. CIBERSORT tool, a digital cytometry

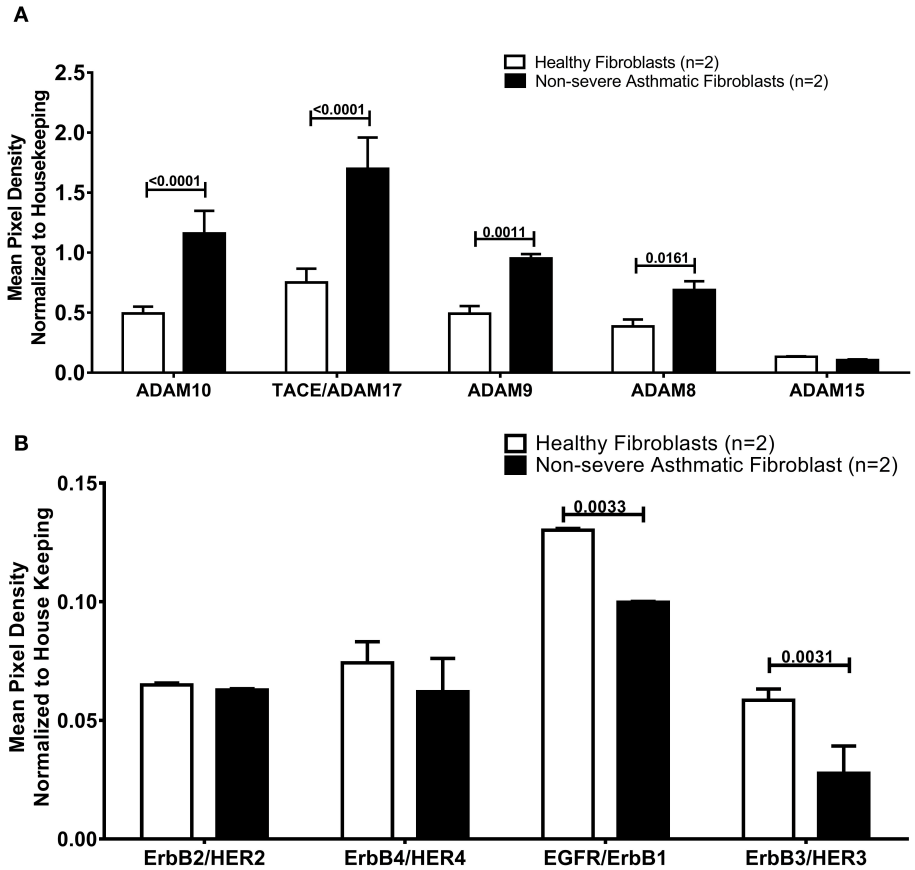

FIGURE 6 | Levels of soluble receptors shed in the conditioned media of healthy and non-severe asthmatic fibroblasts using non-hematopoietic and the common analytes array. **(A)** Protein expression of AREG shredders: ADAM 8, 9, 10, 15, and 17 in non-severe asthmatic fibroblasts compared to healthy fibroblasts. **(B)** Protein expression of shed ErbBl-4/HER1-4 in non-severe asthmatic fibroblasts compared to healthy fibroblasts.

TABLE 6 | Summary of *in silico* and *in vitro* analysis of AREG mRNA expression in different settings of asthma.

Genes	Bronchial epithelium		Bronchial fibroblasts		Biopsy vs. brush		OS = Oral Steroids	Th2 high	Th2 low
	In silico	*In vitro*	*In silico*	*In vitro*	Healthy	Asthma			
AREG	UP	UP	UP (the dataset available was with no details on severity)	Down in severe asthma	Both	-	-	-	-

that can determine cell type abundance and expression from bulk tissues (40), was used for that purpose. We used CIBERSORT tool on Bronchial epithelium transcriptomic data of (GSE64913 and GSE67472) datasets and blood transcriptomic dataset (GSE69683) of a well-characterized and a large cohort of patients with different asthma severity compared to healthy controls to estimate the percentage of the immune cells (**Figure 8**).

Bronchial Epithelium of Severe Asthmatic With Higher AREG mRNA Expression Showed a Lower Percentage of Gamma Delta (γδ) T and T Regulatory Cells but Higher Percentage of Neutrophils

In severe asthmatic bronchial epithelium with higher AREG mRNA expression, the percentage of infiltrating Gamma Delta (γδ) T and Regulatory T cells was lower than healthy controls, while there was an increase in the percentage of neutrophils (**Figure 8**).

Peripheral Blood of Severe Asthmatics Showed a Higher Percentage of Eosinophils, Neutrophils and Activated NK Cells Compared to Healthy Controls

Estimating the immune cells population in the blood of a large cohort of asthmatic patients with different severities compared to healthy controls using the transcriptomics data from (GSE69683) dataset revealed a similar trend of cells abundance of that in bronchial epithelium in terms of neutrophils and macrophages. As shown in **Figure 9**, eosinophilia was more evident in severe asthmatic blood than in local bronchial epithelium. Severe

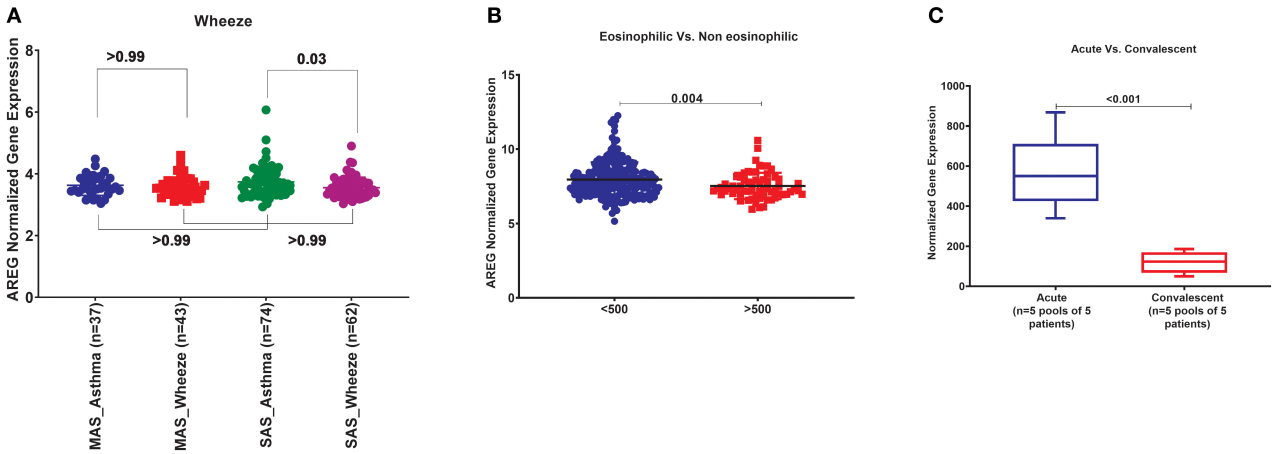

FIGURE 7 | (A) AREG normalized gene expression in whole blood of children with non-severe and severe wheezes were compared to non-severe and severe asthmatics extracted from the expression profile of publically available datasets (GSE123750), where non-severe asthmatic (MAS_Asthma) and severe asthmatic (SAS_Asthma) patients were compared to patients presented with non-severe wheezes (MAS_Wheeze) and severe wheezes (SAS_Wheeze). **(B)** Normalized gene expression of genes identified in whole blood of eosinophilic asthma (>500 cells) compared to non-eosinophilic (eosinophils count less than 500) extracted from the expression profile of publicly available datasets (GSE137394). **(C)** Normalized Gene Expression of Genes Identified in PBMC5 taken from asthmatic patients during the acute/exacerbation phase and the convalescent phase extracted from the expression profile of publicly available datasets(6SE16032).

TABLE 7 | Summary of *in silico* analysis of the AREG genes in blood of asthmatic patients in different settings compared to healthy controls.

Genes	Whole blood				
	Asthma	**Asthma wheezes**	**Eosinophilic**	**Acute**	**Viral**
AREG	–	UP	Down	UP	–

AREG expression in whole blood of asthmatics in different phenotypes, in asthmatic with wheezes vs. non-asthmatics wheezers, in eosinophilic asthmatic vs. non-eosinophilic, in acute vs. convalescent (acute) and during viral infection.

asthmatic patients showed a higher percentage of eosinophils in their blood than healthy controls ($p = 0.02$). However, the percentages of monocytes and macrophages percentages were not statistically different between the groups. Surprisingly, memory B cells showed a significant difference in severe asthmatics compared to non-severe asthmatics ($p = 0.04$) and healthy controls ($p < 0.01$).

Interestingly, peripheral neutrophilia and activated NK was consistent with airway findings. Blood neutrophils and activated NK percentages were higher in severe asthmatics compared to non-severe asthmatics and healthy controls ($p < 0.05$).

DISCUSSION

To our knowledge, no studies used saliva, while very few studies used blood levels to discover markers related to asthma pathogenesis. This is the first study to investigate AREG blood and saliva expression levels and associate them to asthma. Other studies focused on AREG expression in sputum (17), damaged bronchial epithelium (41), fibroblasts (42), smooth muscle cells (43, 44) from bronchial biopsies and hematopoietic cells such as eosinophils (19), and basophils (45) in asthma and allergic conditions.

As illustrated in **Figures 1**, **2**, our results showed that AREG plasma and saliva levels were higher in asthmatic patients compared to healthy controls. AREG plasma level was significantly different between healthy and non-severe asthmatic ($p < 0.0001$).

Currently, in asthma research, there is a growing interest in replacing the available invasive bronchoscopy sampling and sputum induction with less invasive options like blood, urine, and exhaled gas biomarkers (4). These biomarkers can aid in a personalized and targeted approach to manage asthmatic patients, especially those with severe refractory asthma (46).

Our results confirmed that AREG level in plasma and saliva are simple, minimally invasive tools that can be used as biomarkers to assess asthma pathogenesis. Salivary marker measurements of various diseases is a new concept and currently is carried out mostly in head and neck cancers (47) and oral diseases (48). However, these assays are mostly DNA based. More recently, a predictive genetic assay measuring salivary mRNA was used to predict the onset of esophageal cancer (patent no: WO2017137427A1). As saliva sampling is non-invasive and is easy to collect, it represents an attractive tool for measuring asthma biomarkers (25).

This promising discriminating power of our results can be an additional bedside marker to help the managing physician in

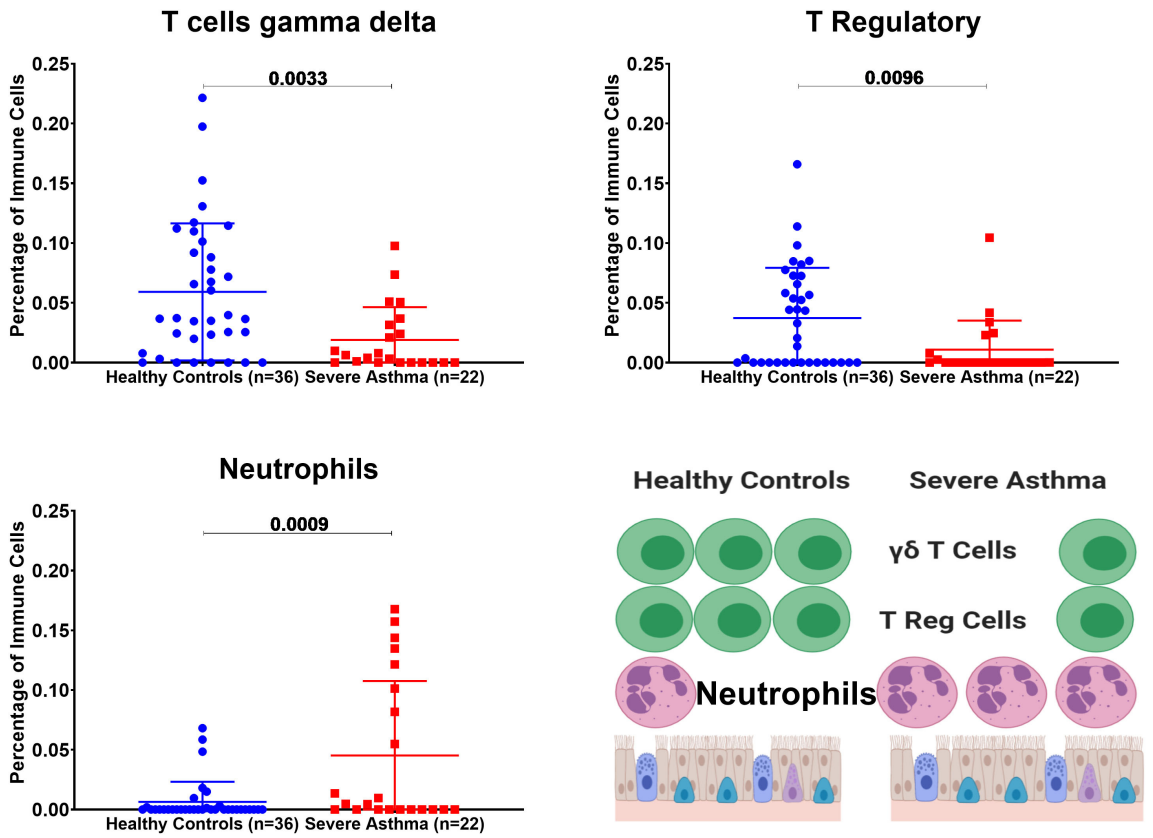

FIGURE 8 | Estimating immune cells populations in the bronchial epithelium of (c3SE64913) dataset in healthy controls ($n = 36$) compared to severe asthmatics ($n = 22$). Bronchial epithelium genes expression was loaded to CIBERSORT *in silico* flow cytometry.

diagnosing early stages of asthma with borderline clinical criteria. As for plasma, AREG saliva level was not able to differentiate between different asthma severity indicating its association with asthma as a disease; this might be explained by the limitation of the sample size and the effect of aggressive asthma medication on AREG levels in severe asthmatics.

Determining the presence of eosinophilic inflammation, or high Th2 cytokines phenotype is essential for patient stratification for targeted asthma therapy (49). Currently, peripheral blood eosinophil count is considered as a surrogate marker for eosinophilic inflammation of the airways (50); hence, finding a new reliable biomarker to predict eosinophilic asthma is needed (4). Therefore, correlating AREG expression with other pathological parameters, specifically those related to eosinophilic inflammation or high Th2 cytokines phenotype is essential.

Our results showed that AREG protein level in asthmatic patients' plasma and saliva correlate with clinical allergic phenotypes such as allergic rhinitis and atopy. Patients with a history of allergic rhinitis showed specifically a higher plasma AREG level compared to those with no history of allergic rhinitis. Allergic rhinitis is a common comorbidity of asthma and contributes to asthma severity (51) and poor asthma control (52). Asthma and allergic rhinitis share similar local and systemic eosinophil inflammation (53). AREG was shown to be secreted by eosinophils to participate in some physiological and pathological conditions *in vivo* (19). Asthma specific memory Th2 cells were shown to induce AREG to reprogram eosinophils to produce osteopontin leading to enhanced airway fibrosis (20).

On the other hand, AREG protein level in plasma correlates with the level of periostin, a known marker for Th2 high asthma phenotype (54), which can predict airway eosinophilia in patients with severe asthma (55). Periostin was found to be involved in atopic conditions such as dermatitis, rhinitis/rhinosinusitis, allergic skin inflammations; and its upregulation was shown to induce extracellular matrix (ECM) tissue remodeling (56). Beside eosinophils and mast cells, increased levels of periostin have also been detected in relation to neutrophils (56). On the other hand, periostin, was shown to play a vital role in chemokines induction to recruit neutrophils and macrophages that participate in pulmonary fibrosis in mouse model (57). Positive correlation between AREG and periostin might augment the role of neutrophils in non-eosinophilic severe asthma.

Of note, plasma AREG levels correlated positively with neutrophil levels in patients' blood. It is known that neutrophilia correlates with asthma that is refractory to the mainstay of asthma treatment (corticosteroids) (58). It was shown that during epithelial damage and repair, neutrophils enhance AREG production by epithelial cells to promote tissue repair (59). It can be suggested that patients with high circulating AREG might

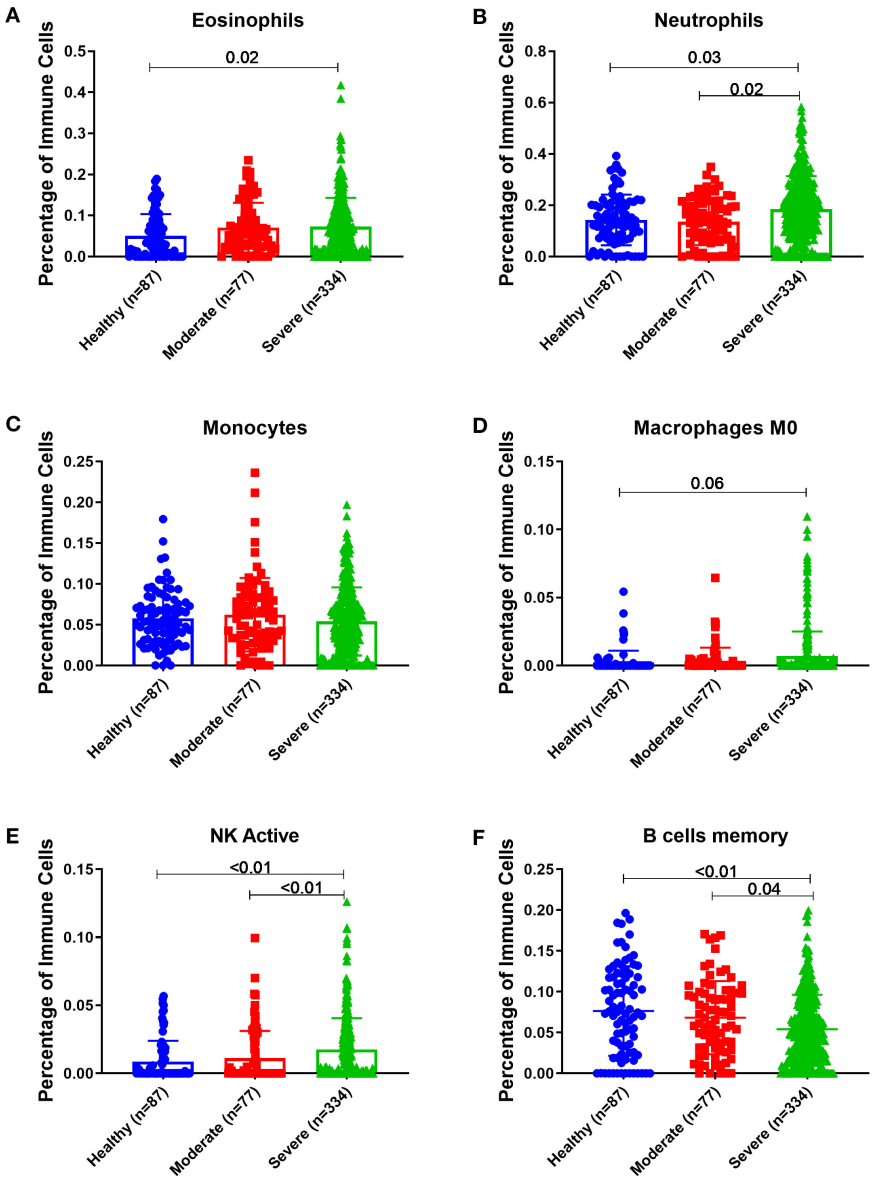

FIGURE 9 | Estimating immune cells populations in blood of (GSE69683) dataset to compare healthy controls ($n = 87$), non-severe asthma ($n = 77$), and severe asthmatics ($n = 334$). Blood genes expression was loaded to CIBERSORT *in silico* flow cytometry and immune cells which showed significant differences between the groups are shown. **(A)** Eosinophils, **(B)** Neutrophils, **(C)** Monocytes, **(D)** Macrophages M0, **(E)** NK active, and **(F)** B cells memory.

be in need of that level to be used for the massive tissue repair process ongoing during asthma.

A non-allergic asthmatic is a non-sensitized individual who can develop eosinophilic inflammation without exposure to an allergen through the activation of ILC2 cells that do not need allergen-specific IgE (22). Non-allergic patients may have innate immunity or neutrophilic airway inflammation independent of Th2 cells (27). Triggers of asthma in non-allergic patients can vary from external triggers like viral infections, cigarette smoke, diesel particles, and ozone to patient's intrinsic factors like stress, exercise, and obesity (1).

The type and quantity of inflammatory cells in the airway of asthma is an attractive research area now as it can guide the selection of biological treatment (60). Differentiating neutrophilic asthma (usually characterized by acute severe asthma exacerbations and steroid-resistant) from the eosinophilic phenotype is very important as the later phenotype can respond to corticosteroids and targeted therapies (61).

During acute lung injury, AREG was shown to suppress ICAM-1 expression and neutrophil accumulation (62). However, if neutrophils infiltration occurs, their elastase can promote myofibroblast differentiation that ends up with lung fibrosis; thus, AREG can limit fibrosis by limiting neutrophil arrival

earlier in inflammation (63). This model is opposite to the skin model of psoriasis, where AREG enhanced the transmigration of human neutrophils through epithelial cell monolayers (64).

Our results showed that in severe asthmatic bronchial epithelium, the percentage of infiltrating Gamma Delta (γδ) T and Regulatory T cells was lower than in those of healthy controls. The high content of neutrophils in severe asthmatic bronchial epithelium compared to healthy controls matches the decrease in γδ T and Tregs as it might indicate more inflammatory consequences of lack of the primary tolerogenic and regulators of an immune response.

Estimating the immune cells population in the blood of a large cohort of asthmatic patients with different severities compared to healthy controls revealed a similar trend of cells abundance of that in bronchial epithelium in terms of neutrophils and macrophages. Eosinophilia was more evident in severe asthmatic blood than in local bronchial epithelium.

Interestingly, peripheral neutrophilia was consistent with airway neutrophilia. Increased local airway neutrophils count in asthma in neutrophilic asthma is associated with steroid resistance, suggesting that the neutrophil plays a role in asthma pathophysiology (65). Increased airway neutrophils in severe asthma and Th2 low phenotype might indicate specific endotype of asthma that share neutrophilia and eosinophilia but not Th2-high phenotype. In response to allergens, activation of LPS receptor TLR4 on lung epithelial cells can stimulate CXCL8 chemokine secretion to recruit neutrophil to the lung in association with increased eosinophilic inflammation, IgE, Th2 cytokines and mucus secretion (66). TLR signaling activation during the sensitization phase recruit neutrophils and inflammatory monocytes, to attenuate allergic symptoms by promoting the Th1-associated cytokines (67).

High levels of IL17 are linked to both eosinophils and neutrophils infiltrates in the airways of severe asthmatics (68). In neutrophilic asthma, Th17 cells released interleukins can recruit macrophages, and lymphocytes alongside neutrophils (69). Despite being glucocorticoid sensitive in some autoimmune diseases, Th17 cells are glucocorticoid resistant in asthma (70).

During allergen exposure, the first immune cells arriving the airways are the neutrophils that usually have a short life before it undergoes apoptosis, except in severe asthmatics who showed defective neutrophil apoptosis and/or clearance (71).

Another interesting finding was the correlation between plasma AREG level and the use of Montelukast sodium (Singulair); a selective and orally active leukotriene receptor antagonist that inhibits the cysteinyl leukotriene CysLT1 receptor (72). Our results showed that asthmatic patients who are on regular Singulair treatment have a higher level of AREG in their plasma compared to those who are not using Singulair. CysLTs as a potent contractile agonist of airways smooth muscles can stimulate their amphiregulin release and enhance their proliferation (73). Moreover, cysteinyl leukotriene was recently found to activate human ILC2s to secrete amphiregulin (72). This can have an important translational impact on patients' stratifications and appropriate drug selection.

Immunohistochemistry staining of bronchial biopsies showed that AREG staining intensity was higher in non-severe mild asthmatic epithelium when compared to healthy controls (**Figure 4**). These findings confirm the role of AREG in the sequence of events in asthma pathogenesis involving both bronchial epithelial cells and fibroblasts. Our results agree with previous studies where AREG level in sputum was associated with asthma severity (17) and was found to be increased in airways during an acute asthma attack (18).

Our results confirmed that AREG is locally upregulated in the asthmatic lung. AREG is constitutively expressed during development and physiologic processes but rapidly upregulated in damaged epithelium to restore tissue integrity (15). Asthmatic bronchial epithelial cells had higher AREG mRNA expression and protein levels than healthy ones but no significant difference in the secreted levels. However, AREG secretion in conditioned media was higher in bronchial epithelial cells compared to their asthma severity matching bronchial fibroblasts confirming that epithelial cells are the primary source of local lung cells in asthma (**Figure 5**). The insignificant difference between AREG secreted levels of healthy and asthmatic epithelial cells despite the overexpression of its mRNA levels can be explained by the complex regulatory network controlling AREG synthesis and secretion.

AREG was reported to show the ability to restore tissue integrity (15), through the mechanism of shedding to bind to autocrine or paracrine EGF receptor family. AREG ectodomain shedding is mediated by ADAM17 (74) and under some conditions ADAM8 and ADAM15 that are called sheddases (75). Most of these enzymes are secreted proteins (76). This processing adds another layer of regulation of AREG (77). Our results showed that asthmatic fibroblasts showed higher shedding of AREG ectoderm shedders (ADAM8, 9, 10, and 17). This goes with previous reports that in asthmatics airways, ADAMs, and ADAMTSs and their inhibitors are involved in asthma development (76).

As illustrated in **Figure 6A**, asthmatic fibroblasts showed higher shedding of AREG ectoderm shedders (ADAM8, 9, 10, and 17). The loss of the shedders can decrease the amount of the shed protein in the conditioned media. These shedders can still act on the adjacent cells to shed more AREG and increase its soluble forms. ADAM8 plays a proinflammatory role in asthma airway inflammation, and ADAM8-deficient mice failed to develop an experimental model of asthma (78). Nevertheless, there is a controversy about its function in asthma, ADAM8 can induce or inhibit the transmigration of leukocytes in airway inflammation of asthma (79). Also, ADAM8 was shown to mediate the infiltration of eosinophils and Th2 lymphocytes to airways of asthmatic patients (80). On the other hand, some reports showed that ADAM8 facilitates neutrophil migration to the airways in severe asthma and COPD (81).

Moreover, as illustrated in **Figure 6B**, our results revealed that non-severe asthmatic fibroblasts shed less ErbB1 and ErbB3 EGFR receptors compared to healthy ones. The indispensability of ErbB1/EGFR for AREG-mediated responses was previously reported in lung structural cells, and it was suggested that ErbB1-ErbB3 and/or ErbB2-ErbB3 heterodimers are involved in the AREG-mediated responses (82). AREG soluble form can act in an autocrine fashion to increase the stability and accumulation of its

active EGFR (83). Alternatively, it was recently documented that in stressed cells (like the case of asthma), mRNA concentrations can transiently escalate in pulse-like pattern and return to basal level, while protein concentrations establish a new steady-state (84). It was reported that upon stimulation, cells would release soluble ADAM17 in exosomes to reach more distant substrates or cells (85).

AREG can activate intracellular signaling network that controls cell survival, proliferation, and motility (13). AREG binding to EGFR induced EGFR homodimerization or heterodimerization with ErbB2, ErbB3, and ErbB4 to trigger intracellular signals (13). The membrane proteoglycan, CD44, is a cofactor for the interaction of AREG with EGFR (86).

In contrast to most of EGFR ligands, AREG did not generate nuclear translocation of EGFR but showed markedly different patterns of EGFR internalization and trafficking (87). The ubiquitination of pro-AREG accelerated its half-life on the cell surface with the subsequent trafficking to intracellular organelles (88). The remaining cytoplasmic carboxy-terminal domain of AREG plays a vital role in regulating autocrine growth through the EGFR (77). The released AREG can circulate in a recently discovered type of extracellular nanoparticle called exomeres can modulate EGFR trafficking and prolong EGFR downstream signaling in recipient cells (89). Cells lacking AREG showed growth arrest that is restored by proAREG and AREG-CTD (90). AREG has "geographically" specific and unique intracellular signaling pathways that can determine whether cells grow or differentiate (77).

Helminth-induced type 2 inflammation enhance EGFR expression and AREG production under the effect of IL33 cytokine; later, AREG-EGFR activation will stimulate IL13 secretion needed for host resistance (15, 91). The upregulated AREG can reprogram infiltrating eosinophils to an inflammatory phenotype that produces an excess of profibrotic immunomodulatory protein osteopontin (20). IL5 stimulated eosinophils can contribute to the progression of airway remodeling, through the production of AREG (19).

There is translational evidence indicating upregulated expression of EGFR appears in the airways of asthmatics and activity of this signaling pathway is enhanced in relation to asthma severity (92). Specifically mucus hypersecretion is induced by EGFR activation to promote goblet-cell metaplasia in severe asthma (12). EGFR signaling of the asthmatic epithelium has been reported to be increased in relation to disease severity through the capacity of driving neutrophil fate and function through elaboration of neutrophil-specific factors in relation to disease severity (28). Others have reported a strong correlation between EGFR expression and neutrophilic-specific chemokines in the epithelium of patients with severe asthma (93, 94).

The high AREG expression in blood and saliva of asthmatic patients can be linked to the local increase in AREG expression secreted by structural cells into the extracellular spaces. AREG will then enter the systemic circulation due to the increased microvascular permeability during tissue inflammation (95, 96). The increased AREG blood levels will most likely diffuse into saliva and hence used as a reflective marker for upregulated plasma levels (31).

One limitation of our study is the small size of the participants, although we tried to include all patients who fulfill the criteria, many of the patients refused to participate in the study. Since asthma is a heterogeneous disease, having larger cohort can be more informative about the applicability of the new biomarkers. The number of females in each group was higher than males, previous reports showed that mice males differentially produce and utilize AREG in their lungs in response to viral infections, with greater EGFR internalization and was linked to the combinational effect of testosterone and AREG, that can improve the repair and recovery of damaged tissue in males compared with females (97). On the other hand circulating AREG was undetectable with no significant variation during the menstrual cycle (98). On the other hand, AREG mRNA expression was peaked in the pregnant females and correlated positively with number of good-quality embryos under the induction by diverse luteinizing hormones (99).

In conclusion, our findings suggest circulating AREG expression level can be a reliable, non-invasive, and cost-effective biomarker that can provide additional discriminating power to the available clinical and laboratory tests of asthma.

DATA AVAILABILITY STATEMENT

All datasets generated for this study are included in the article/Supplementary Material.

ETHICS STATEMENT

The studies involving human participants were reviewed and approved by the Ethics Committee of Dubai Health Authority and the University of Sharjah approved the study with REC (Research Ethics Committee) approval number DSREC-11/2017_04, and each subject gave written informed consent after a thorough explanation by the treating physician and the researchers. The patients/participants provided their written informed consent to participate in this study.

AUTHOR CONTRIBUTIONS

MH, RHam, and QH: conception and design of the study, data and sample collection, analysis and interpretation of data, and writing the manuscript. BM and RHam: conception and design of the study, clinical samples selections, and collections. MH and IH: *in silico* validation and analysis. SA, IH, and RHal: reviewing the manuscript. RO: primary lung cell lines and bronchial biopsies provision. NE, MH, and RHam: data collection and interpretation of ELISA and reviewing the manuscript. RR and MH: sample collections and cell lines maintenance. TV and LS: samples and data collections. All authors contributed to the article and approved the submitted version.

FUNDING

This work was funded by Sharjah Research Academy (Grant No: MED001) and University of Sharjah (Grant No: 1901090254).

REFERENCES

1. Kim HY, DeKruyff RH, Umetsu DT. The many paths to asthma: phenotype shaped by innate and adaptive immunity. *Nat Immunol*. (2010) 11:577–84. doi: 10.1038/ni.1892
2. Thomsen SF. Genetics of asthma: an introduction for the clinician. *Eur Clin Respir J*. (2015) 2. doi: 10.3402/ecrj.v2.24643
3. Thomas M. Why aren't we doing better in asthma: time for personalised medicine? *NPJ Prim Care Respir Med*. (2015) 25:15004. doi: 10.1038/npjpcrm.2015.4
4. Wan XC, Woodruff PG. Biomarkers in severe asthma. *Immunol Allergy Clin North Am*. (2016) 36:547–57. doi: 10.1016/j.iac.2016.03.004
5. Byrnes SA, Weigl BH. Selecting analytical biomarkers for diagnostic applications: a first principles approach. *Expert Rev Mol Diagn*. (2018) 18:19–26. doi: 10.1080/14737159.2018.1412258
6. Chiappori A, De Ferrari L, Folli C, Mauri P, Riccio AM, Canonica GW. Biomarkers and severe asthma: a critical appraisal. *Clin Mol Allergy*. (2015) 13:20. doi: 10.1186/s12948-015-0027-7
7. Dawson SJ, Tsui DW, Murtaza M, Biggs H, Rueda OM, Chin SF, et al. Analysis of circulating tumor DNA to monitor metastatic breast cancer. *N Engl J Med*. (2013) 368:1199–209. doi: 10.1056/NEJMoa1213261
8. Yoshizawa JM, Schafer CA, Schafer JJ, Farrell JJ, Paster BJ, Wong DTW. Salivary biomarkers: toward future clinical and diagnostic utilities. *Clin Microbiol Rev*. (2013) 26:781–91. doi: 10.1128/CMR.00021-13
9. Wee P, Wang Z. Epidermal growth factor receptor cell proliferation signaling pathways. *Cancers*. (2017) 9:52. doi: 10.3390/cancers9050052
10. Vallath S, Hynds RE, Succony L, Janes SM, Giangreco A. Targeting EGFR signalling in chronic lung disease: therapeutic challenges and opportunities. *Eur Respir J*. (2014) 44:513–22. doi: 10.1183/09031936.00146413
11. Acciani TH, Suzuki T, Trapnell BC, Le Cras TD. Epidermal growth factor receptor signalling regulates granulocyte-macrophage colony-stimulating factor production by airway epithelial cells and established allergic airway disease. *Clin Exp Allergy*. (2016) 46:317–28. doi: 10.1111/cea.12612
12. Le Cras TD, Acciani TH, Mushaben EM, Kramer EL, Pastura PA, Hardie WD, et al. Epithelial EGF receptor signaling mediates airway hyperreactivity and remodeling in a mouse model of chronic asthma. *Am J Physiol Lung Cell Mol Physiol*. (2011) 300:L414–21. doi: 10.1152/ajplung.00346.2010
13. Berasain C, Avila MA. Amphiregulin. *Semin Cell Dev Biol*. (2014) 28:31–41. doi: 10.1016/j.semcdb.2014.01.005
14. Amin K, Yaqoob U, Schultz B, Vaughn BP, Khoruts A, Howard JR, et al. Amphiregulin in intestinal acute graft-versus-host disease: a possible diagnostic and prognostic aid. *Mod Pathol*. (2019) 32:560–7. doi: 10.1038/s41379-018-0170-z
15. Zaiss DMW, Gause WC, Osborne LC, Artis D. Emerging functions of amphiregulin in orchestrating immunity, inflammation, and tissue repair. *Immunity*. (2015) 42:216–26. doi: 10.1016/j.immuni.2015.01.020
16. Manzo ND, Foster WM, Stripp BR. Amphiregulin-dependent mucous cell metaplasia in a model of nonallergic lung injury. *Am J Respir Cell Mol Biol*. (2012) 47:349–57. doi: 10.1165/rcmb.2011-0257OC
17. Kim KW, Jee HM, Park YH, Choi BS, Sohn MH, Kim KE. Relationship between amphiregulin and airway inflammation in children with asthma and eosinophilic bronchitis. *Chest*. (2009) 136:805–10. doi: 10.1378/chest.08-2972
18. Takamasu T, Enomoto Y, Orihara K, Matsuda A, Gon Y, Saito H, et al. An acute asthma attack induces tissue remodeling by hypersecretion of epidermal growth factor (egf) and amphiregulin (areg) in the airway. *J Allergy Clin Immunol*. (2011) 127:AB59. doi: 10.1016/j.jaci.2010.12.245
19. Matsumoto K, Fukuda S, Nakamura Y, Saito H. Amphiregulin production by human eosinophils. *Int Arch Allergy Immunol*. (2009) 149(Suppl. 1):39–44. doi: 10.1159/000210652
20. Morimoto Y, Hirahara K, Kiuchi M, Wada T, Ichikawa T, Kanno T, et al. Amphiregulin-producing pathogenic memory T helper 2 cells instruct eosinophils to secrete osteopontin and facilitate airway fibrosis. *Immunity*. (2018) 49:134–50.e6. doi: 10.1016/j.immuni.2018.04.023
21. Buhl R, Humbert M, Bjermer L, Chanez P, Heaney Liam G, Pavord I, et al. Severe eosinophilic asthma: a roadmap to consensus. *Eur Respir J*. (2017) 49:1700634. doi: 10.1183/13993003.00634-2017
22. Yamauchi K, Ogasawara M. The role of histamine in the pathophysiology of asthma and the clinical efficacy of antihistamines in asthma therapy. *Int J Mol Sci*. (2019) 20:1733. doi: 10.3390/ijms20071733
23. Kim HY, Umetsu DT, Dekruyff RH. Innate lymphoid cells in asthma: will they take your breath away? *Eur J Immunol*. (2016) 46:795–806. doi: 10.1002/eji.201444557
24. Monticelli LA, Sonnenberg GF, Abt MC, Alenghat T, Ziegler CG, Doering TA, et al. Innate lymphoid cells promote lung-tissue homeostasis after infection with influenza virus. *Nat Immunol*. (2011) 12:1045–54. doi: 10.1038/ni.2131
25. Minutti CM, Modak RV, Macdonald F, Li F, Smyth DJ, Dorward DA, et al. A macrophage-pericyte axis directs tissue restoration via amphiregulin-induced transforming growth factor beta activation. *Immunity*. (2019) 50:645–54e6. doi: 10.1016/j.immuni.2019.01.008
26. Xu Y, Meng C, Liu G, Yang D, Fu L, Zhang M, et al. Classically activated macrophages protect against lipopolysaccharide-induced acute lung injury by expressing amphiregulin in mice. *Anesthesiology*. (2016) 124:1086–99. doi: 10.1097/ALN.0000000000001026
27. Pasha MA, Patel G, Hopp R, Yang Q. Role of innate lymphoid cells in allergic diseases. *Allergy Asthma Proc*. (2019) 40:138–45. doi: 10.2500/aap.2019.40.4217
28. Uddin M, Lau LC, Seumois G, Vijayanand P, Staples KJ, Bagmane D, et al. EGF-induced bronchial epithelial cells drive neutrophil chemotactic and anti-apoptotic activity in asthma. *PLoS ONE*. (2013) 8:e72502. doi: 10.1371/journal.pone.0072502
29. Lourenço O, Fonseca AM, Taborda-Barata L. Human $CD8^+$ T cells in asthma: possible pathways and roles for NK-like subtypes. *Front Immunol*. (2016) 7:638. doi: 10.3389/fimmu.2016.00638
30. Geyer PE, Holdt LM, Teupser D, Mann M. Revisiting biomarker discovery by plasma proteomics. *Mol Syst Biol*. (2017) 13:942. doi: 10.15252/msb.20156297
31. Castagnola M, Scarano E, Passali GC, Messana I, Cabras T, Iavarone F, et al. Salivary biomarkers and proteomics: future diagnostic and clinical utilities. *Acta Otorhinolaryngol It*. (2017) 37:94–101. doi: 10.14639/0392-100X-1598
32. Koh GC-H, Pei-Chi Shek L, Kee J, Wee A, Ng V, Koh D. Saliva and serum eosinophil cationic protein in asthmatic children and adolescents with and without allergic sensitization. *J Asthma*. (2010) 47:61–5. doi: 10.3109/02770900903350499
33. Chung KF, Wenzel SE, Brozek JL, Bush A, Castro M, Sterk PJ, et al. International ERS/ATS guidelines on definition, evaluation and treatment of severe asthma. *Eur Respir J*. (2014) 43:343–73. doi: 10.1183/09031936.00202013
34. Dagur PK, McCoy JP Jr. Collection, storage, and preparation of human blood cells. *Curr Protoc Cytom*. (2015) 73:5.1.1–16. doi: 10.1002/0471142956.cy0501s73
35. Wang SW, Oh CK, Cho SH, Hu G, Martin R, Demissie-Sanders S, et al. Amphiregulin expression in human mast cells and its effect on the primary human lung fibroblasts. *J Allergy Clin Immunol*. (2005) 115:287–94. doi: 10.1016/j.jaci.2004.11.037
36. Schneider CA, Rasband WS, Eliceiri KW. NIH Image to ImageJ: 25 years of image analysis. *Nat Methods*. (2012) 9:671. doi: 10.1038/nmeth.2089
37. Szatmári T, Mundt F, Heidari-Hamedani G, Zong F, Ferolla E, Alexeyenko A, et al. Novel genes and pathways modulated by syndecan-1: implications for the proliferation and cell-cycle regulation of malignant mesothelioma cells. *PLoS ONE*. (2012) 7:e48091. doi: 10.1371/journal.pone.0048091
38. Hachim MY, Mahboub B, Hamid Q, Hamoudi R, editors. Identifying Asthma genetic signature patterns by mining Gene Expression BIG Datasets using Image Filtering Algorithms. In: *2019 IEEE International Conference on Imaging Systems and Techniques (IST)*. Abu Dhabi (2019).
39. Chen B, Khodadoust MS, Liu CL, Newman AM, Alizadeh AA. Profiling tumor infiltrating immune cells with CIBERSORT. *Methods Mol Biol*. (2018) 1711:243–59. doi: 10.1007/978-1-4939-7493-1_12
40. Newman AM, Steen CB, Liu CL, Gentles AJ, Chaudhuri AA, Scherer F, et al. Determining cell type abundance and expression from bulk tissues with digital cytometry. *Nat Biotechnol*. (2019) 37:773–82. doi: 10.1038/s41587-019-0114-2
41. Lambrecht BN, Hammad H. The airway epithelium in asthma. *Nat Med*. (2012) 18:684. doi: 10.1038/nm.2737
42. Vermeer PD, Panko L, Karp P, Lee JH, Zabner J. Differentiation of human airway epithelia is dependent on erbB2. *Am J Physiol Lung Cell Mol Physiol*. (2006) 291:L175–80. doi: 10.1152/ajplung.00547.2005

43. Deacon K, Knox AJ. Human airway smooth muscle cells secrete amphiregulin via bradykinin/COX-2/PGE2, inducing COX-2, CXCL8, and VEGF expression in airway epithelial cells. *Am J Physiol Lung Cell Mol Physiol*. (2015) 309:L237–49. doi: 10.1152/ajplung.00390.2014
44. Hirota N, Risse P-A, Novali M, McGovern T, Al-Alwan L, McCuaig S, et al. Histamine may induce airway remodeling through release of epidermal growth factor receptor ligands from bronchial epithelial cells. *FASEB J*. (2012) 26:1704–16. doi: 10.1096/fj.11-197061
45. Qi Y, Operario DJ, Oberholzer CM, Kobie JJ, Looney RJ, Georas SN, et al. Human basophils express amphiregulin in response to T cell-derived IL-3. *J Allergy Clin Immunol*. (2010) 126:1260-6.e4. doi: 10.1016/j.jaci.2010.08.040
46. Kim H, Ellis AK, Fischer D, Noseworthy M, Olivenstein R, Chapman KR, et al. Asthma biomarkers in the age of biologics. *Allergy Asthma Clin Immunol*. (2017) 13:48. doi: 10.1186/s13223-017-0219-4
47. Nonaka T, Wong DTW. Liquid biopsy in head and neck cancer: promises and challenges. *J Dent Res*. (2018) 97:701–8. doi: 10.1177/0022034518762071
48. Roi A, Rusu LC, Roi CI, Luca RE, Boia S, Munteanu RI. A new approach for the diagnosis of systemic and oral diseases based on salivary biomolecules. *Dis Markers*. (2019) 2019:8761860. doi: 10.1155/2019/8761860
49. Bhakta NR, Woodruff PG. Human asthma phenotypes: from the clinic, to cytokines, and back again. *Immunol Rev*. (2011) 242:220–32. doi: 10.1111/j.1600-065X.2011.01032.x
50. Kostikas K, Brindicci C, Patalano F. Blood eosinophils as biomarkers to drive treatment choices in asthma and COPD. *Curr Drug Targets*. (2018) 19:1882–96. doi: 10.2174/1389450119666180212120012
51. Egan M, Bunyavanich S. Allergic rhinitis: the "Ghost Diagnosis" in patients with asthma. *Asthma Res Pract*. (2015) 1:8. doi: 10.1186/s40733-015-0008-0
52. de Groot EP, Nijkamp A, Duiverman EJ, Brand PLP. Allergic rhinitis is associated with poor asthma control in children with asthma. *Thorax*. (2012) 67:582–7. doi: 10.1136/thoraxjnl-2011-201168
53. Kämpe M, Stolt I, Lampinen M, Janson C, Stålenheim G, Carlson M. Patients with allergic rhinitis and allergic asthma share the same pattern of eosinophil and neutrophil degranulation after allergen challenge. *Clin Mol Allergy*. (2011) 9:3. doi: 10.1186/1476-7961-9-3
54. Jia G, Erickson RW, Choy DF, Mosesova S, Wu LC, Solberg OD, et al. Periostin is a systemic biomarker of eosinophilic airway inflammation in asthmatic patients. *J Allergy Clin Immunol*. (2012) 130:647–54e10. doi: 10.1016/j.jaci.2012.06.025
55. Noguchi T, Nakagome K, Kobayashi T, Uchida Y, Soma T, Nakamoto H, et al. Periostin upregulates the effector functions of eosinophils. *J Allergy Clin Immunol*. (2016) 138:1449–52e5. doi: 10.1016/j.jaci.2016.05.020
56. Li W, Gao P, Zhi Y, Xu W, Wu Y, Yin J, et al. Periostin: its role in asthma and its potential as a diagnostic or therapeutic target. *Respir Res*. (2015) 16:57. doi: 10.1186/s12931-015-0218-2
57. Uchida M, Shiraishi H, Ohta S, Arima K, Taniguchi K, Suzuki S, et al. Periostin, a matricellular protein, plays a role in the induction of chemokines in pulmonary fibrosis. *Am J Respir Cell Mol Biol*. (2012) 46:677–86. doi: 10.1165/rcmb.2011-0115OC
58. Ray A, Kolls JK. Neutrophilic inflammation in asthma and association with disease severity. *Trends Immunol*. (2017) 38:942–54. doi: 10.1016/j.it.2017.07.003
59. Chen F, Yang W, Huang X, Cao AT, Bilotta AJ, Xiao Y, et al. Neutrophils promote amphiregulin production in intestinal epithelial cells through TGF-beta and contribute to intestinal homeostasis. *J Immunol*. (2018) 201:2492–501. doi: 10.4049/jimmunol.1800003
60. Nishio T, Wakahara K, Suzuki Y, Nishio N, Majima S, Nakamura S, et al. Mixed cell type in airway inflammation is the dominant phenotype in asthma patients with severe chronic rhinosinusitis. *Allergol Int*. (2019) 68:515–20. doi: 10.1016/j.alit.2019.05.004
61. Pillai RA, Calhoun WJ. Introduction to asthma and phenotyping. In: Brasier AR, editor. *Heterogeneity in Asthma*. Boston, MA: Springer US (2014). p. 5–15.
62. Ogata-Suetsugu S, Yanagihara T, Hamada N, Ikeda-Harada C, Yokoyama T, Suzuki K, et al. Amphiregulin suppresses epithelial cell apoptosis in lipopolysaccharide-induced lung injury in mice. *Biochem Biophys Res Commun*. (2017) 484:422–8. doi: 10.1016/j.bbrc.2017.01.142
63. Gregory AD, Kliment CR, Metz HE, Kim KH, Kargl J, Agostini BA, et al. Neutrophil elastase promotes myofibroblast differentiation in lung fibrosis. *J Leukoc Biol*. (2015) 98:143–52. doi: 10.1189/jlb.3HI1014-493R
64. Chung E, Cook PW, Parkos CA, Park YK, Pittelkow MR, Coffey RJ. Amphiregulin causes functional downregulation of adherens junctions in psoriasis. *J Invest Dermatol*. (2005) 124:1134–40. doi: 10.1111/j.0022-202X.2005.23762.x
65. Jasper AE, McIver WJ, Sapey E, Walton GM. Understanding the role of neutrophils in chronic inflammatory airway disease. *F1000Res*. (2019) 8:F1000 Faculty Rev-557. doi: 10.12688/f1000research.18411.1
66. Radermecker C, Louis R, Bureau F, Marichal T. Role of neutrophils in allergic asthma. *Curr Opin Immunol*. (2018) 54:28–34. doi: 10.1016/j.coi.2018.05.006
67. Huang C, Wang J, Zheng X, Chen Y, Wei H, Sun R, et al. Activation of TLR signaling in sensitization-recruited inflammatory monocytes attenuates OVA-induced allergic asthma. *Front Immunol*. (2018) 9:2591. doi: 10.3389/fimmu.2018.02591
68. Morishima Y, Ano S, Ishii Y, Ohtsuka S, Matsuyama M, Kawaguchi M, et al. Th17-associated cytokines as a therapeutic target for steroid-insensitive asthma. *Clin Dev Immunol*. (2013) 2013:609395. doi: 10.1155/2013/609395
69. Wu X, Tian J, Wang S. Insight into non-pathogenic Th17 cells in autoimmune diseases. *Front Immunol*. (2018) 9:1112. doi: 10.3389/fimmu.2018.01112
70. Banuelos J, Cao Y, Shin SC, Lu NZ. Immunopathology alters Th17 cell glucocorticoid sensitivity. *Allergy*. (2017) 72:331–41. doi: 10.1111/all.13051
71. Uddin M, Nong G, Ward J, Seumois G, Prince LR, Wilson SJ, et al. Prosurvival activity for airway neutrophils in severe asthma. *Thorax*. (2010) 65:684–9. doi: 10.1136/thx.2009.120741
72. Salimi M, Stöger L, Liu W, Go S, Pavord I, Klenerman P, et al. Cysteinyl leukotriene E4 activates human group 2 innate lymphoid cells and enhances the effect of prostaglandin D2 and epithelial cytokines. *J Allergy Clin Immunol*. (2017) 140:1090–100.e11. doi: 10.1016/j.jaci.2016.12.958
73. Holgate ST, Peters-Golden M, Panettieri RA, Henderson WR Jr. Roles of cysteinyl leukotrienes in airway inflammation, smooth muscle function, and remodeling. *J Allergy Clin Immunol*. (2003) 111(1 Suppl.):S18–34; discussion S-6. doi: 10.1067/mai.2003.25
74. Kasina S, Scherle PA, Hall CL, Macoska JA. ADAM-mediated amphiregulin shedding and EGFR transactivation. *Cell Prolif*. (2009) 42:799–812. doi: 10.1111/j.1365-2184.2009.00645.x
75. Hosur V, Farley ML, Burzenski LM, Shultz LD, Wiles MV. ADAM17 is essential for ectodomain shedding of the EGF-receptor ligand amphiregulin. *FEBS Open Bio*. (2018) 8:702–10. doi: 10.1002/2211-5463.12407
76. Paulissen G, Rocks N, Quesada-Calvo F, Gosset P, Foidart JM, Noel A, et al. Expression of ADAMs and their inhibitors in sputum from patients with asthma. *Mol Med*. (2006) 12:171–9. doi: 10.2119/2006-00028.Paulissen
77. Seykora JT. Grabbing amphiregulin by the tail to better understand keratinocyte growth. *J Invest Dermatol*. (2010) 130:1966–8. doi: 10.1038/jid.2010.199
78. Naus S, Blanchet MR, Gossens K, Zaph C, Bartsch JW, McNagny KM, et al. The metalloprotease-disintegrin ADAM8 is essential for the development of experimental asthma. *Am J Respir Crit Care Med*. (2010) 181:1318–28. doi: 10.1164/rccm.200909-1396OC
79. Chen J, Jiang X, Duan Y, Long J, Bartsch JW, Deng L. ADAM8 in asthma. Friend or foe to airway inflammation? *Am J Respir Cell Mol Biol*. (2013) 49:875–84. doi: 10.1165/rcmb.2013-0168TR
80. Chen J, Deng L, Dreymuller D, Jiang X, Long J, Duan Y, et al. A novel peptide ADAM8 inhibitor attenuates bronchial hyperresponsiveness and Th2 cytokine mediated inflammation of murine asthmatic models. *Sci Rep*. (2016) 6:30451. doi: 10.1038/srep30451
81. Oreo KM, Gibson PG, Simpson JL, Wood LG, McDonald VM, Baines KJ. Sputum ADAM8 expression is increased in severe asthma and COPD. *Clin Exp Allergy*. (2014) 44:342–52. doi: 10.1111/cea.12223
82. Enomoto Y, Orihara K, Takamasu T, Matsuda A, Gon Y, Saito H, et al. Tissue remodeling induced by hypersecreted epidermal growth factor and amphiregulin in the airway after an acute asthma attack. *J Allergy Clin Immunol*. (2009) 124:913–20.e7. doi: 10.1016/j.jaci.2009.08.044
83. Kappler CS, Guest ST, Irish JC, Garrett-Mayer E, Kratche Z, Wilson RC, et al. Oncogenic signaling in amphiregulin and EGFR-expressing PTEN-null human breast cancer. *Mol Oncol*. (2015) 9:527–43. doi: 10.1016/j.molonc.2014.10.006

84. Cheng Z, Teo G, Krueger S, Rock TM, Koh HW, Choi H, et al. Differential dynamics of the mammalian mRNA and protein expression response to misfolding stress. *Mol Syst Biol*. (2016) 12:855. doi: 10.15252/msb.20156423
85. Groth E, Pruessmeyer J, Babendreyer A, Schumacher J, Pasqualon T, Dreymueller D, et al. Stimulated release and functional activity of surface expressed metalloproteinase ADAM17 in exosomes. *Biochim Biophy Acta*. (2016) 1863:2795–808. doi: 10.1016/j.bbamcr.2016.09.002
86. Nylander N, Smith LT, Underwood RA, Piepkorn M. Topography of amphiregulin expression in cultured human keratinocytes: colocalization with the epidermal growth factor receptor and CD44. *In Vitro Cell Dev Biol Anim*. (1998) 34:182–8. doi: 10.1007/s11626-998-0103-0
87. Faria J, de Andrade C, Goes AM, Rodrigues MA, Gomes DA. Effects of different ligands on epidermal growth factor receptor (EGFR) nuclear translocation. *Biochem Biophys Res Commun*. (2016) 478:39–45. doi: 10.1016/j.bbrc.2016.07.097
88. Fukuda S, Nishida-Fukuda H, Nakayama H, Inoue H, Higashiyama S. Monoubiquitination of pro-amphiregulin regulates its endocytosis and ectodomain shedding. *Biochem Biophys Res Commun*. (2012) 420:315–20. doi: 10.1016/j.bbrc.2012.02.156
89. Zhang Q, Higginbotham JN, Jeppesen DK, Yang YP, Li W, McKinley ET, et al. Transfer of functional cargo in exomeres. *Cell Rep*. (2019) 27:940–54e6. doi: 10.1016/j.celrep.2019.01.009
90. Stoll SW, Stuart PE, Lambert S, Gandarillas A, Rittié L, Johnston A, et al. Membrane-tethered intracellular domain of amphiregulin promotes keratinocyte proliferation. *J Invest Dermatol*. (2016) 136:444–52. doi: 10.1016/j.jid.2015.10.061
91. Minutti CM, Drube S, Blair N, Schwartz C, McCrae JC, McKenzie AN, et al. Epidermal growth factor receptor expression licenses type-2 helper T cells to function in a T cell receptor-independent Fashion. *Immunity*. (2017) 47:710-22e6. doi: 10.1016/j.immuni.2017.09.013
92. El-Hashim AZ, Khajah MA, Renno WM, Babyson RS, Uddin M, Benter IF, et al. Src-dependent EGFR transactivation regulates lung inflammation via downstream signaling involving ERK1/2, PI3Kδ/Akt and NFκB induction in a murine asthma model. *Sci Rep*. (2017) 7:9919. doi: 10.1038/s41598-017-09349-0
93. Burgel PR, Nadel JA. Epidermal growth factor receptor-mediated innate immune responses and their roles in airway diseases. *Eur Respir J*. (2008) 32:1068–81. doi: 10.1183/09031936.00172007
94. Hamilton LM, Torres-Lozano C, Puddicombe SM, Richter A, Kimber I, Dearman RJ, et al. The role of the epidermal growth factor receptor in sustaining neutrophil inflammation in severe asthma. *Clin Exp Allergy*. (2003) 33:233–40. doi: 10.1046/j.1365-2222.2003.01593.x
95. Chung K, Rogers D, Barnes P, Evans T. The role of increased airway microvascular permeability and plasma exudation in asthma. *Eur Respir J*. (1990) 3:329–37.
96. Zanini A, Chetta A, Imperatori AS, Spanevello A, Olivieri D. The role of the bronchial microvasculature in the airway remodelling in asthma and COPD. *Respir Res*. (2010) 11:132. doi: 10.1186/1465-9921-11-132
97. Vermillion MS, Ursin RL, Kuok DIT, Vom Steeg LG, Wohlgemuth N, Hall OJ, et al. Production of amphiregulin and recovery from influenza is greater in males than females. *Biol Sex Differ*. (2018) 9:24. doi: 10.1186/s13293-018-0184-8
98. Peterson EA, Shabbeer S, Kenny PA. Normal range of serum Amphiregulin in healthy adult human females. *Clin Biochem*. (2012) 45:460–3. doi: 10.1016/j.clinbiochem.2011.12.029
99. Huang Y, Zhao Y, Yu Y, Li R, Lin S, Zhang C, et al. Altered amphiregulin expression induced by diverse luteinizing hormone receptor reactivity in granulosa cells affects IVF outcomes. *Reprod Biomed Online*. (2015) 30:593–601. doi: 10.1016/j.rbmo.2015.03.001

Conflict of Interest: The authors declare that the research was conducted in the absence of any commercial or financial relationships that could be construed as a potential conflict of interest.

Copyright © 2020 Hachim, Elemam, Ramakrishnan, Salameh, Olivenstein, Hachim, Venkatachalam, Mahboub, Al Heialy, Halwani, Hamid and Hamoudi. This is an open-access article distributed under the terms of the Creative Commons Attribution License (CC BY). The use, distribution or reproduction in other forums is permitted, provided the original author(s) and the copyright owner(s) are credited and that the original publication in this journal is cited, in accordance with accepted academic practice. No use, distribution or reproduction is permitted which does not comply with these terms.

frontiers in Medicine

CASE REPORT
published: 30 October 2020
doi: 10.3389/fmed.2020.544158

ALDH Expression in Angiosarcoma of the Lung: A Potential Marker of Aggressiveness?

Beatrice Aramini[1], Valentina Masciale[1], Daniel Bianchi[1], Beatrice Manfredini[1], Federico Banchelli[2], Roberto D'Amico[2], Federica Bertolini[3], Massimo Dominici[3], Uliano Morandi[1] and Antonino Maiorana[4]*

[1] Division of Thoracic Surgery, Department of Medical and Surgical Sciences, University of Modena and Reggio Emilia, Modena, Italy, [2] Department of Medical and Surgical Sciences, Center of Statistic, University of Modena and Reggio Emilia, Modena, Italy, [3] Division of Oncology, Department of Medical and Surgical Sciences, University of Modena and Reggio Emilia, Modena, Italy, [4] Department of Medical and Surgical Sciences, Institute of Pathology, University of Modena and Reggio Emilia, Modena, Italy

Background: Primary angiosarcoma of the lung is a very aggressive rare malignant disease resulting in a severe prognosis (1). This type of cancer represents about 2% of all soft tissue sarcomas and has a high rate of metastasis through the hematogenous route. For the rarity of this malignant vascular tumor it is still challenging to set a diagnosis (1). The diagnostic features that have thus far been considered include primarily clinical and radiological findings. In some cases, immunohistochemical characteristics based on the most common markers used in pathology have been described. The aim of this report is to present two cases of angiosarcoma of the lung in which the aldehyde dehydrogenase (ALDH) marker was analyzed by immunohistochemistry.

Methods: We report two cases of angiosarcoma of the lung in patients underwent lung surgery at our Unit. In addition to the standard histopathological analysis for this disease, immunohistochemistry using an ALDH1A1 antibody was performed in both of the cases. For ALDH quantification, a semi-quantitative method based on the positivity of the tumor cells was used: 0 (<5%), 1 (5–25%), 2 (>25–50%), 3 (>50–75%), 4 (>75%).

Results: One patient with recurrent lung disease survived, achieving complete remission after chemo- and radiotherapy. The second patient died of recurrent disease within 5 years of diagnosis. ALDH1A1 was evaluated in both of these cases using an immunohistochemistry scoring system based on the positivity for this marker. The scores were consistent with the patients' clinical outcomes, as the lower (score 1) was observed in the patient with the better clinical outcome, while the higher (score 3) was seen in the patient with the worse outcome.

Conclusion: Our data suggest that ALDH may be an important clinical marker in angiosarcoma of the lung. Although further studies need to be performed in a larger cohort of patients, we believe that, if the results will be confirmed, ALDH1A1 may be used to stratify patients in terms of prognosis and for targeted therapy.

Keywords: target therapy, aldehyde dehydrogenase (ALDH), malignant rare lung tumor, rare tumor, angiosarcoma, marker, angiogenetic process, malignant vascular tumors

OPEN ACCESS

Edited by:
Hauke Busch,
University of Lübeck, Germany

Reviewed by:
Sheng-Ming Wu,
Taipei Medical University, Taiwan
Ralph Pries,
University of Lübeck, Germany

****Correspondence:***
Beatrice Aramini
beatrice.aramini@unimore.it

Specialty section:
This article was submitted to Pulmonary Medicine, a section of the journal Frontiers in Medicine

Received: *05 June 2020*
Accepted: *09 October 2020*
Published: *30 October 2020*

Citation:
Aramini B, Masciale V, Bianchi D, Manfredini B, Banchelli F, D'Amico R, Bertolini F, Dominici M, Morandi U and Maiorana A (2020) ALDH Expression in Angiosarcoma of the Lung: A Potential Marker of Aggressiveness? Front. Med. 7:544158. doi: 10.3389/fmed.2020.544158

BACKGROUND

Angiosarcoma is a rare form of malignant vascular tumor occurring for the 2% of soft tissue sarcoma (1–3). Clinical symptoms are similar to those observed in other pulmonary tumors (2). The radiological presentation is highly variable, ranging from a solitary nodule to multiple bilateral lesions. In addition, due to its clinicopathological similarity to metastatic angiosarcoma of the lung, a diagnosis of primary disease requires a complete clinical and radiological examination of the body in order to ensure that there are no primary lesions outside of the chest. Therefore, immunohistochemistry is the gold standard technique to make a diagnosis of angiosarcoma of the lung; in particular, the most used markers are Factor VIII, CD31, CD34, and Fli-1 (4). There is not yet a standardized therapy for this disease; however, therapy usually consists of surgical treatment, chemotherapy, and radiotherapy, depending on the clinical presentation and the number of lesions.

However, aldehyde dehydrogenase (ALDH) which is an enzyme able to detect normal and malignant stem/progenitor cells (5) is now used as marker in tumor initiating cells (TICs) especially for the two ALDH isoforms, ALDH1A1 and ALDH1A3 (6–8). In particular, ALDH1A1 has been considered the most effective markers in consideration of poor prognosis for lung cancer and it is considered a marker of stemness, promoting angiogenesis, which is one of the main characteristics in high vascularised tumor as the angiosarcoma (9–11). Moreover, ALDH1A3, which is another ALDH isoform, is mainly enrolled in the regulation of matricellular proteins promoting the vascular smooth muscle cell proliferation (12).

ALDH has also the capacity to regulate the most important cells functions as self-renewal, expansion, differentiation and drug resistance (13). A deeper knowledge of the ALDH molecular pathways will be useful in many specialties, as regenerative medicine and oncology. In particular, a current clinical trial demonstrates the importance of comparing the effects of the ALDH inhibitor dimethyl ampal thiolester (DIMATE) on normal and malignant hematopoietic cells and stem cells (9, 13). In particular, it has been shown that DIMATE could potentially be used to selectively eliminate cancer cells (9). Although these results were obtained in hematological disease, they demonstrated the importance of ALDH in oncology and suggested that ALDH may be considered not only a marker, but also a target.

In this report, we present our experience with two cases of primary angiosarcoma of the lung that had completely different clinical presentations and, therefore, completely different treatments. In particular, we found that, while both of the angiosarcomas showed ALDH expression, high and low ALDH scores were associated with worse and better prognosis, respectively. Further studies on the presence of this marker in angiosarcomas of the lung may highlight the importance of ALDH as a prognostic factor and as a potential biomarker for targeted therapies.

Abbreviations: ALDH, aldehyde dehydrogenase; CT, computed tomography; DAB, 3,3-diaminobenzidine; DIMATE, dimethyl ampal thiolester; PBS, phosphate buffered saline; VATS, video-assisted thoracic surgery; ^{18}F-FDG PET/CT, 18-fluorodeoxyglucose integrated with computed tomography.

METHODS

Case 1

A 27-year-old man arrived at our Department in June 2016 after multiple episodes of hemoptysis followed by intense chest pain. He referred only previous episodes of inflammatory bowel disease (IBD). Chest X-rays showed multiple bilateral lesions in the lungs that were confirmed by the computed tomography (CT) scan in which multiple pseudonodular features surrounded by a ground glass halo were identified in both lungs (**Figure 1A**). The abdomen and brain CT scan were negative for atypical lesions. A PET scan was performed, revealing evidence of multiple active sites in the lungs (**Figure 1B**). In June 2016, transbronchial biopsies were non-diagnostic and the patient underwent surgical left lung biopsies performed using a video-assisted thoracic surgery (VATS) approach. The pathological exam revealed spindle cells of endothelial origin that stained positive for CD31 and partially positive for cytokeratin AE3/AE4. Staining for CD34, TTF1, and CD30 were found to be negative. An angiosarcoma of the lung was diagnosed.

The patient was sent to the oncologist. A new chest CT performed in July 2016 showed a recurrence at the level of the thoraco-abdominal passage at the cardiophrenic angle and caudally to the right lower lobar pulmonary vein; after positioning of a port-a-cath (PORT device), patient started first-line chemotherapy with epirubicin and ifosfamide. The revaluation after three cycles revealed an excellent response in the parenchymal lung lesions, a net reduction of bilateral pleural effusion, and a reduction in the lesion at the level of the D5 soma in net volumetric evolution. On October 2016, radiosurgery (18 Gy in single dose) on the D5 lesion was performed. Another three cycles with the same scheme followed. In January 2017, due to lung progression, the patient was started on second-line chemotherapy with docetaxel plus gemcitabine associated with radiotherapy until April 2017 (four total cycles given); starting in April, the therapy continued with only gemcitabine. After these treatments, in May 2017, the patient showed additional hemoptysis episodes, which drew attention to a recurrence at the level of the left lower lobe. In August 2017, he started weekly paclitaxel and achieved a complete remission of the disease, which has been confirmed in the subsequent follow-up examinations. The most recent chest CT (performed in January 2020) showed a complete remission of angiosarcoma (**Figure 2**).

Case 2

A 61-year-old woman came to our hospital for persistent cough in the last 2 years, initially treated as an allergic bronchiolitis without any improvement. Her medical history was notable only for a prior isterectomy due to fibromatosis. She denied smoking habit.

In August 2005, a chest X-ray showed a small single lesion in the left lung. At the same time, a CT scan of the chest

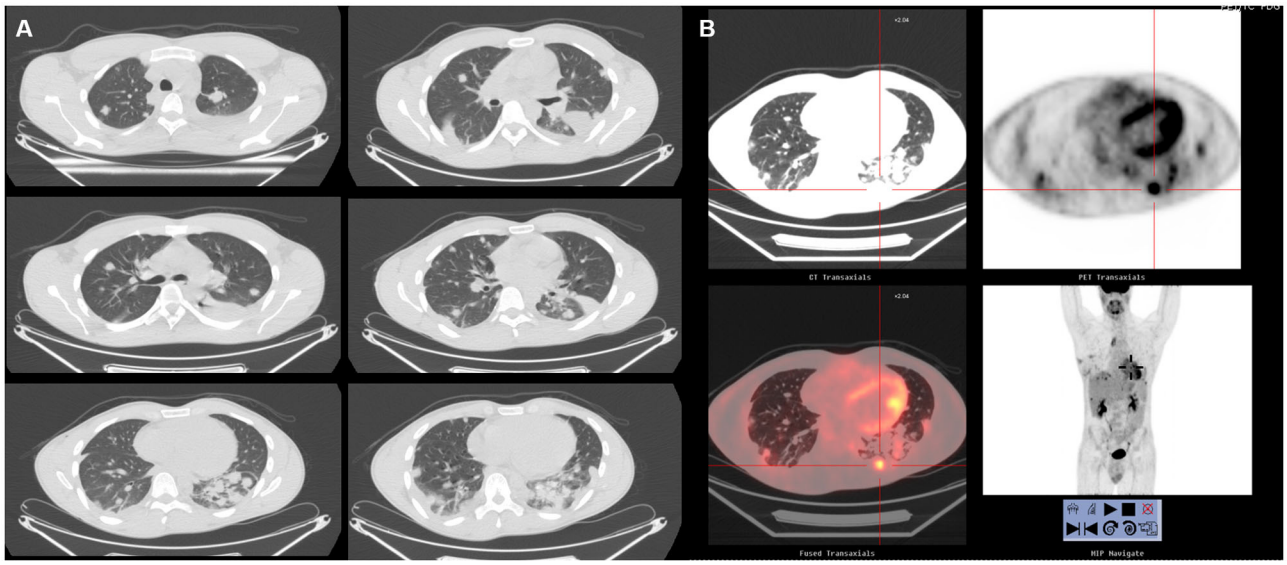

FIGURE 1 | (A) Chest CT in case 1 before treatment. The lungs showed bilateral nodules. **(B)** Total body ^{18}F-FDG PET. No hypermetabolic lesions other than the lesions in the lungs.

showed evidence of hyper-dense tissue of ∼2 cm around the lower left bronchus.

In September 2005, we performed a bronchoscopy with transbronchial biopsy, leading to the diagnosis of angiosarcoma. To ensure that it was not a metastatic lesion, we performed a magnetic resonance imaging (MRI) of the abdomen followed by an 18-fluorodeoxyglucose integrated with computed tomography (^{18}F-FDG PET/CT). Neither showed evidence of any other atypical lesion. Primary angiosarcoma of the lung was diagnosed.

In October 2005, a left lower lobectomy was performed by thoracotomy, without any major complications after the surgical procedure.

The histological examination confirmed the initial diagnosis of angiosarcoma, with immunohistochemistry positive for myocyte nuclear factor (MNF116) and CD34 and partially positive for Factor VIII and CD31. A hilar lymph node was found positive for local invasion.

After 1 month from surgery, she was undergone chemotherapy with docetaxel plus gemcitabine (four total cycles given), associated with radiotherapy on the mediastinum (∼50 Gy in 25 fractions). Patient performed 3 years follow up by chest and abdomen CT with contrast enhancement until 2008, which showed normal radiological findings, free from the tumor lung disease.

In 2009, the patient was admitted to our Unit for left thoracic pain and suspicious for rib fractures. She underwent to a chest CT with contrast enhancement showing a neoformation of 3.5 × 2 × 1.5 cm at the level of the left intercostal space, between the tenth and the eleventh rib. Due to the previous history of angiosarcoma of the lung, patient underwent surgery in general anesthesia to remove the mass and make a diagnosis. An excision was performed at the level of the chest neoformation with partial removal of the ninth and tenth left rib and a plastic reconstruction of the left thoracic wall. Patient stayed clinically stable and she was discharged from hospital after 6 days without complications. The oncologic team evaluated the patient after few weeks from surgery and a chemotherapy plan was set with only gemcitabine for other 4 months, with no complete remission. The patient died in early 2010 due to insufficient respiratory function caused by lung recurrence.

Immunohistochemistry

Paraffin was firstly removed from tissue section with the use of xylene, and subsequently a descending scale of ethyl alcohol (100, 90, 80, and 70°) was used to rehydrate the slices before the washing procedure with phosphate-buffered saline (PBS). The antigen retrieval was performed with a 10 mM sodium citrate buffer ad a high temperature water bath (95°C). After 15 min the slices were washed with PBS for 30 min. To suppress the interference of endogenous peroxidase a solution of 3% H_2O_2 was used to dip samples. Therefore, serum was necessary for blocking non-specific signal. At the end of this procedure primary antibodies were added for hours to tissue slices (ab-134188, Abcam, Cambridge, MA, USA), anti-CD34 (Ventana Medical Systems, Arizona, USA), and anti-CD31 (Cell Marque, California, USA). Furthermore, sections were incubated for 30 min with a secondary antibody (PK-4001; Vector Labs, USA) before three times washing with PBS. Samples were subsequently incubated with ABC-HRP (PK-4001; Vector Labs, USA), washed in PBS in order to remove the excess antibody, and stained with 3,3-diaminobenzidine (DAB). Finally, a secondary stain with Mayer's hematoxylin was applied to provide contrast in the section. At the end slices were dehydrated with an ascendant alcohol grade scale (70, 80, 90, and 100°), and then subsequently mounting media was added. Tissue sections were analyzed using a Zeiss Axioskop microscope, with a Zeiss AxioCam

FIGURE 2 | Chest CT in case 1 after chemo- and radiotherapy treatment. After 1 year of treatment, the patient showed a complete remission of the disease.

ICc 3 High-Resolution Microscope Camera, at 10× and at 20× magnification. Blinded a and independent evaluation of the sample were performed to assign the right score for the evaluation of positive cells, in accordance to a previous score (6–8). Immunoreactivity for ALDH marker was assess by a semi-quantitative method based on this range of positivity for the tumor cells: 0 (<5% positive), 1 (5–25%), 2 (>25–50%), 3 (>50–75%), and 4 (>75%) (7).

RESULTS

Clinical Results

Case 1

After 1 year of chemotherapy and radiotherapy cycles, the patient showed a complete remission of the disease. The last chest CT performed in January 2020 showed complete remission.

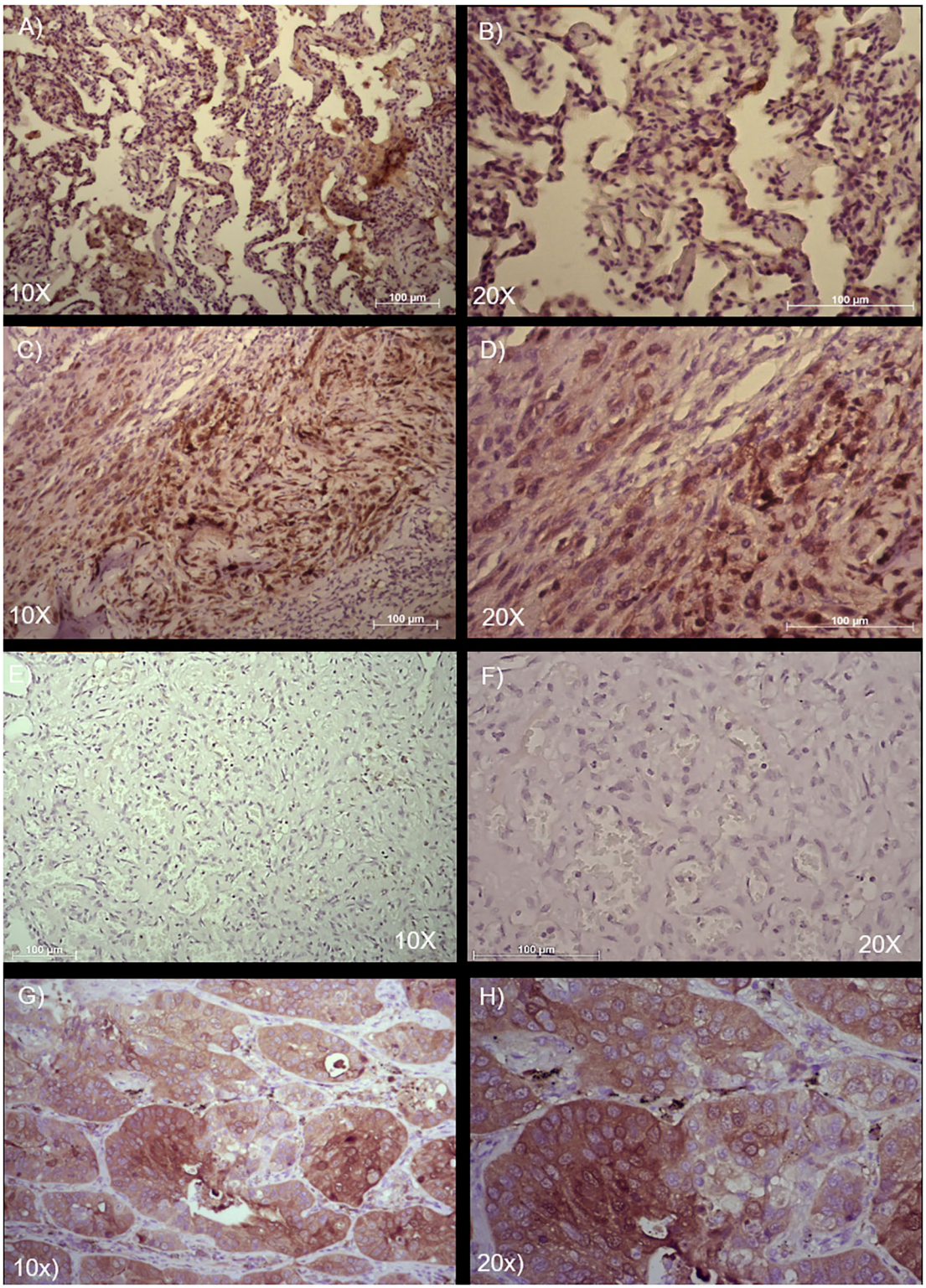

FIGURE 3 | Immunohistochemical analysis and quantification of ALDH-positive cells in two cases of angiosarcoma of the lung. Paraffin-embedded tissues were stained with an ALDH antibody to detect positive cells in these two different cases of angiosarcoma of the lung. **(A,B)** Case 1 and **(C,D)** Case 2. **(E,F)** Isotype control of anti-ALDH antibody. **(G,H)** Adenocarcinoma of the lung used as positive control of anti-ALDH antibody. Semi-quantitative method to measure ALDH based on the positivity of the tumor cells: 0 (<5% positive), 1 (5–25% positive), 2 (>25–50% positive), 3 (>50–75% positive), and 4 (>75% positive). Representative images are shown, with 10× and 20× magnification. Scale bar = 100 µm.

TABLE 1 | Angiosarcoma of the lung.

References	Patients enrolled (n)	Gender (M/F)	Age	Type of treatment (surgery and/or medical treatment)	Type of resection	Type of treatment	Immunohistochemistry (IHC) markers
Aramini et al. (19)	2	1 M 1 F	27 61	Diagnostic surgery + chemotherapy and radiotherapy 2. Surgery + chemotherapy	Surgical left lung biopsies 2. Left lower lobectomy	First line (epirubicin and ifosfamide + radiotherapy); second line (docetaxel plus gemcitabine) and then only gemcitabine 2. Four cycles gemcitabine	CD31 + CD 34 +
Carillo et al. (20)	1	M	56	Chemotherapy	Not resectable for advanced disease.	Adriamicin, II line ifosfamide	AE1/AE3 + CD31 + EMA + Vimentin + + + CD34 + + + (CEA, TTF-1, calretinin, trombomodulin, S100, HMB45, melan-A, Bcl-2, actin, desmin, CD117-)
Chen et al. (21)	2	1 F 1 M	41 50	Surgery + chemotherapy 2. Surgery + chemotherapy	Wedge resection middle lobe 2. Left lower lobectomy and lingula segmentectomy	Sorafenib 2. Four cycles Docetaxel + cisplatin	CD31 + CD 34 + Factor VIII + (CK, EMA, SMA, HMB-45, desmin, S100, ALK-)
Maglaras et al. (22)	1	M	46	Diagnostic surgery + chemotherapy	Right surgical biospy	Adriamicin + ifosfamide	Vimentin + CD31 + (EMA, CEA, S-100, pancytocheratin, cheratin, Leu-M, CD34, Factor VIII, desmin, NSE-)
Modrzewska et al. (23)	1	F	65	Diagnostic surgery	Lung surgical biopsy	/	CD31 + CD34 + (AE1/AE3, calretinin-)
Ozcelik et al. (24)	1	M	62	Surgery	Right upper lobectomy	/	CD31 + CD34 + Factor VIII + CAM 5.2 +
Palvio et al. (25)	1	M	59	Surgery	Right pneumonectomy	/	Factor VIII + Vimentin + (chetarin, desmin, EMA-)
Pandit et al. (26)	1	F	79	Surgery + chemotherapy	Wedge resection Left lower lobe	/	Factor VIII + Vimentin + CD34 +
Ng et al. (14)	1	M	60	Surgery	Left upper lobectomy	/	ERG + CD31 + (CD34, TTF-1-)
Yang et al. (27)	1	M	41	Surgery	Wedge resection left upper lobe	/	Vimentin + CD34 + CD31 + (CK7, CK5, CK20, CK8, S-100, AE1/AE3, TTF-1, Napsin-A, HMB-45, sinaptofisin, CD68, EMA, LCA, actin, desmin-)
Tanaka et al. (28)	1	M	48	Surgery + chemotherapy	Left pneumonectomy	/	ERG + CD31 + Factor VIII + FLI-1 + P53 + (CD34, C2-40, CK7, CK20, EMA, TTF-1, HMB-45, CD10)

(Continued)

TABLE 1 | Continued

References	Patients enrolled (n)	Gender (M/F)	Age	Type of treatment (surgery and/or medical treatment)	Type of resection	Type of treatment	Immunohistochemistry (IHC) markers
Shirey et al. (29)	1	M	65	Surgery + chemotherapy	Wedge resection Right upper lobe	Gemcitabin and Docetaxel	CD31 + + + Vimentin + + + AE1/AE3 + Pancytocheratin + CK7 + EMA + (CAM5.2, CK5/6, p63, S-100, desmin, SMA, Factor VIII, TTF-1, napsin-A, CD34, D2-40, CD21-)
Sheppard et al. (30)	1	M	65	Diagnostic surgery	Lung biopsy	/	CD31 + Factor VIII + CD34 + CAM 5.2 +
Zhang et al. (31)	1	M	72	Surgery for age	Left lower lobectomy	/	CD34 + CD31 + FLI-1 + Vimentin +

Review of the literature on the surgical and medical approaches in the past and at the present time. The table shows also the markers used in each study to highlight the diagnosis.

Case 2

After 5 years of treatments, the patient died in 2010 due to respiratory insufficiency caused by this malignant lung disease.

Immunohistochemical Evaluation of the ALDH Stem Cell Marker in Two Cases of Angiosarcoma of the Lung

The positivity to the ALDH marker was assessed for these pulmonary angiosarcoma cases, using a previous score system (10–12, 14). Samples were examined at 10× and at 20× magnification to assign the appropriate score value. In accordance with the literature, in the normal bronchial epithelium ALDH1A1 expression was assed (8). These two patient samples had a different expression of ALDH1A1 staining in the tumor fraction: for case 1, the score was 1 (<5–25% positive tumor cells), while in case 2 the score was 3 (>50–75% positive tumor cells) (**Figure 3**). The scores seem to be consistent with the clinical outcome of these two patients, as the lower score was observed in the patient with the better clinical outcome, while the higher score was measured in the patient with the worse clinical outcome.

DISCUSSION

Angiosarcoma of the lung is an extremely rare tumor described in only a few case reports because of its low prevalence in the population. However, it is very interesting to study because of the aggressiveness of this disease which tends to be spread in different part of the body. The rate of recurrence is very high for the intrinsic properties of this tumor with a 5-year survival rate around 20–35% (15–17), which is in contrast to the 5-year survival for all types of soft tissue sarcomas, around 65% (18).

The approaches to treat this malignancy are primarily surgery (in operable patients) and chemoradiotherapy for advanced disease. **Table 1** shows an updated information from the recent literature (10–12, 14–18, 20–29), highlighting the clinical and surgical approaches, as well as also the most frequently used markers for this disease.

It has been recently showed that ALDH identifies tumor cells with increased affinity for primary tumors, as well as a high capacity to disseminate in many organs (30–32). The scientists have recently found a correlation between ALDH and the capacity to calibrate the tumor cells dissemination into the body (30–33). In particular, different ALDH isoforms seem to be able to regulate the cells diffusion into several solid tumors (30–33). In an interesting study published in 2014 by Nicholas Greco et al. it has been demonstrated a significant correlation of aldehyde dehydrogenase (ALDH) activity and the presence/absence of distant metastases in ten consecutive cases of human bone sarcomas (34). Although angiosarcoma is more difficult to investigate for the rarity of this tumor into the population, it is important to understand the possible role that ALDH may have in this tumor for the possibility to set new target treatment against this aggressive malignant disease. Another interesting aspect recently described which needs to be considered regards the central role of ALDH into the angiogenetic process, detected into the endothelial stem-like cells in vascularized tumors (35, 36). This aspect may strongly confirm the possible presence of ALDH even in a vascularized tumor as the angiosarcoma of the lung.

In our report, we showed two cases of angiosarcoma of the lung with different scores of ALDH protein expression. In particular, in case 1, we noted a low ALDH expression

(score 1). This patient had a very good outcome: he had recurrence, but achieved remission of the disease after chemo- and radiotherapeutic treatments. In case 2, the patient showed a higher ALDH expression (score 3), and the patient died due to disease recurrence. This may indicate that the severity of the ALDH score could link with the worst prognosis and viceversa. This is the first report showing the presence of the ALDH marker in angiosarcoma of the lung. Notably, this is a report of only two cases; however, although the publications in this field are limited, we believe that the current data on this marker in this disease support future studies in a larger cohort of patients to test the presence of this marker and, possibly, determine whether prognosis is correlated with the expression of this protein. If the results from this report will be confirmed in a larger population, it will be interesting to consider new targeted treatment based on ALDH, which is currently being tested in a clinical trial for hematological malignancies (9).

Limitations

Our study is the first report showing the presence of ALDH1A1 in lung angiosarcoma. We are conscious that this is a brief report of only two clinical cases, probably due to the rarity of this disease. Further multicentric studies will need to be set to confirm our data. However, we believe that our report is important to amplify the knowledge regarding possible markers which have been already studied in non-small cell lung cancer showing a high impact of this marker on the prognosis, as well as also in responses to cancer treatments (9, 10, 13, 33, 34).

In conclusion, although not confirmed in a larger cohort of patients for lung angiosarcoma, ALDH targeted therapy may be an effective treatment perspective for this malignancy, which usually appears at a high grade with an aggressive prognosis.

DATA AVAILABILITY STATEMENT

The raw data supporting the conclusions of this article will be made available by the authors, without undue reservation.

ETHICS STATEMENT

The studies involving human participants were reviewed and approved by Ethics committee at University Hospital of Modena, MODENA, Italy, on 4 June 2019, Prot. N. 395/2019/OSS/AOUMO. Consent for publication of data has been obtained from study participants.

AUTHOR CONTRIBUTIONS

The idea for the manuscript was conceived in February 2019 by BA and was further developed by VM, DB, BM, FB, RD'A, FB, MD, UM, and AM was involved in histopathological diagnosis. BA and VM wrote the first draft of the manuscript. BA and UM had been involved in surgery and tissue collection. VM performed laboratory experiments. BA, VM, FB, MD, RD'A, AM, and UM all reviewed the manuscript and were involved in its critical revision before submission. All authors read and approved the final manuscript.

FUNDING

The Project had been supported by funds from the Division of Thoracic Surgery of the University Hospital of Modena and from the Institute of Pathology, Department of Medical and Surgical Sciences, University of Modena and Reggio Emilia, Modena, Italy. These funds were used to buy laboratory equipment and to support the project and people involved.

SUPPLEMENTARY MATERIAL

The Supplementary Material for this article can be found online at: https://www.frontiersin.org/articles/10.3389/fmed.2020.544158/full#supplementary-material

Supplementary Figure 1 | Immunohistochemical analysis of anti CD34 and CD31 in angiosarcoma of the lung. Paraffin-embedded tissues were stained with anti-CD34 and anti-CD31 antibodies used for the diagnosis of the angiosarcoma of the lung. **(A–C)** Representative immunohistochemical staining of anti-CD34. **(D–F)** Representative immunohistochemical staining of anti-CD31. Representative images are shown, with 10× and 20× magnification. Scale bar = 100 μm.

REFERENCES

1. Ren Y, Zhu M, Liu Y, Diao X, Zhang Y. Primary pulmonary angiosarcoma: three case reports and literature review: primary pulmonary angiosarcoma. *Thorac Cancer*. (2016) 7:607–13. doi: 10.1111/1759-7714.12376
2. Cao J, Wang J, He C, Fang M. Angiosarcoma: a review of diagnosis and current treatment. *Am J Cancer Res.* (2019) 9:2303–13.
3. Grafino M, Alves P, Mendes de Almeida M, Garrido P, Hasmucrai D, Teixeira E, et al. Angiosarcoma of the lung. *J Bras Pneumol.* (2016) 42:68–70. doi: 10.1590/S1806-37562016000000193
4. Hart J, Mandavilli S. Epithelioid angiosarcoma: a brief diagnostic review and differential diagnosis. *Arch Pathol Lab Med*. (2011) 135:268–72. doi: 10.1043/1543-2165-135.2.268
5. Vassalli G. Aldehyde dehydrogenases: not just markers, but functional regulators of stem cells. *Stem Cells Int*. (2019) 2019:3904645. doi: 10.1155/2019/3904645
6. Masciale V, Grisendi G, Banchelli F, D'Amico R, Maiorana A, Sighinolfi P, et al. Isolation and identification of cancer stem-like cells in adenocarcinoma and squamous cell carcinoma of the lung: a pilot study. *Front Oncol.* (2019) 9:1394. doi: 10.3389/fonc.2019.01394
7. Masciale V, Grisendi G, Banchelli F, D'Amico R, Maiorana A, Sighinolfi P, et al. Correlating tumor-infiltrating lymphocytes and lung cancer stem cells: a cross-sectional study. *Ann Transl Med*. (2019) 7:619. doi: 10.21037/atm.2019.11.27
8. Masciale V, Grisendi G, Banchelli F, D'Amico R, Maiorana A, Morandi U, et al. Cancer stem-neuroendocrine cells in an atypical carcinoid case report. *Transl Lung Cancer Res.* (2019) 8:1157–62. doi: 10.21037/tlcr.2019.12.07
9. Liu WT, Liu WB, Gao M, Zhang YY, Gu KS. Expression of ALDH1A1 and CD133 is associated with the prognosis and effect of different chemotherapeutic regimens in gastric cancer. *Oncol Lett.* (2019) 18:4573–82. doi: 10.3892/ol.2019.10798
10. Kahlert C, Bergmann F, Beck J, Welsch T, Mogler C, Herpel E, et al. Low expression of aldehyde dehydrogenase 1A1 (ALDH1A1) is a prognostic marker for poor survival in pancreatic cancer. *BMC Cancer.* (2011) 11:275. doi: 10.1186/1471-2407-11-275

11. Jiang F, Qiu Q, Khanna A, Todd NW, Deepak J, Xing L, et al. Aldehyde dehydrogenase 1 is a tumor stem cell-associated marker in lung cancer. *Mol Cancer Res*. (2009) 7:330–8. doi: 10.1158/1541-7786.MCR-08-0393
12. Xie X, Urabe G, Marcho L, Stratton M, Guo L-W, Kent CK. ALDH1A3 regulations of matricellular proteinspromote vascular smooth muscle cell proliferation. *iScience*. (2019) 19:872–82. doi: 10.1016/j.isci.2019.08.044
13. Rossi A, Voigtlaender M, Klose H, Schlüter H, Schön G, Logesl S, et al. High aldehyde dehydrogenase levels are detectable in the serum of patients with lung cancer and may be exploited as screening biomarkers. *J Oncol*. (2019) 2019:8970645. doi: 10.1155/2019/8970645
14. Ng FH, Yu SM, Wai OKH, Chan JCS. Primary epithelioid angiosarcoma of lung: radiologic and clinicopathologic correlation. *J. Clin Imaging Sci*. (2017) 7:33. doi: 10.4103/jcis.JCIS_71_16
15. Buehler D, Rice SR, Moody JS, Rush P, Hafez GR, Attia S, et al. Angiosarcoma outcomes and prognostic factors: a 25-year single institution experience. *Am J Clin Oncol*. (2014) 37:473–9. doi: 10.1097/COC.0b013e31827e4e7b
16. Singla S, Papavasiliou P, Powers B, Gaughan J, von Mehren M, Watson JC, et al. Challenges in the treatment of angiosarcoma: a single institution experience. *Am J Surg*. (2014) 208:254–9. doi: 10.1016/j.amjsurg.2014.01.007
17. Mark RJ, Poen JC, Tran LM, Fu YS, Juillard GF. Angiosarcoma. A report of 67 patients and a review of the literature. *Cancer*. (1996) 77:2400–6. doi: 10.1002/(SICI)1097-0142(19960601)77:11<2400::AID-CNCR32>3.0.CO;2-Z
18. Schottenfeld D, Fraumeni J, editors. *Cancer. Epidemiology and Prevention*. 3rd ed. New York, NY: Oxford University Press (2006).
19. Aramini B, Masciale V, Manfredini B, Bianchi D, Banchelli F, D'Amico R, et al. Expression of ALDH and SOX-2 in pulmonary sclerosing pneumocytoma (PSP) of the lung: is there a meaning behind? *Front Med*. (2020) 7:497. doi: 10.3389/fmed.2020.00497
20. Carillo GA, Carretero MA, Vazquez JE, Fontan EG, Ramos MB, Ventura JA, et al. Epithelioid angiosarcoma of the lung with pleural metastases: a rare cause of haemoptysis clinicopathological conference. *Heart Lung Circ*. (2010) 19:624–8. doi: 10.1016/j.hlc.2010.05.007
21. Chen Y-B, Guo L-C, Yang L, Feng W, Zhang X-Q, Ling C-H, et al. Angiosarcoma of the lung: 2 cases report and literature reviewed. *Lung Cancer*. (2010) 70:352–6. doi: 10.1016/j.lungcan.2010.09.002
22. Maglaras GC, Katsenos S, Kakadelis J, Katsanos C, Metafratzi Z, Stefanou DG, et al. Primary angiosarcoma of the lung and pleura. *Monaldi Arch Chest Dis*. (2004) 61:234–6. doi: 10.4081/monaldi.2004.687
23. Modrzewska K, Radzikowska E, Szołkowska M, Oniszh K, Szczesna M, Roszkowski-Sliz K. Diffuse pulmonary haemorrhage accompanied by haemothorax as a rare presentation of primary lung angiosarcoma. *Kardiochir Torakochirurgia Pol*. (2015) 12:367–71. doi: 10.5114/kitp.2015.56792
24. Ozcelik C, Onat S, Yaldiz M, Ozcelik Z. Primary epithelioid angiosarcoma of the lung presenting as pulmonary hemorrhage. *Asian Cardiovasc Thorac Ann*. (2006) 14:69–71. doi: 10.1177/021849230601400118
25. Palvio DHB, Paulsen SM, Henneberg EW. Primary angiosarcoma of the lung presenting as intractable hemoptysis. *Thorac Cardiovasc Surg*. (1987) 35:105–7. doi: 10.1055/s-2007-1020207
26. Pandit SA, Fiedler PN, Westcott JL. Primary angiosarcoma of the lung. *Ann Diagn Pathol*. (2005) 9:302–4. doi: 10.1016/j.anndiagpath.2005.04.001
27. Yang CF, Chen TW, Tseng GC, Chiang I-P. Primary pulmonary epithelioid angiosarcoma presenting as a solitary pulmonary nodule on image. *Pathol Int*. (2012) 62:424–8. doi: 10.1111/j.1440-1827.2012.02809.x
28. Tanaka H, Yorita K, Takahashi N, Usuma Y, Nakamura K, Kataoka H. Primary pulmonary angiosarcoma: a case report. *Pathol Int*. (2015) 65:554–7. doi: 10.1111/pin.12341
29. Shirey L, Coombs D, Talwar A, Mickus T. Pulmonary epithelioid angiosarcoma responsive to chemotherapy: a case report. *Radiol Case Rep*. (2018) 13:479–84. doi: 10.1016/j.radcr.2018.02.002
30. Sheppard MN, Hansell DM, Du Bois RM, Nicholson AG. Primary epithelioid angiosarcoma of the lung presenting as pulmonary haemorrhage. *Hum Pathol*. (1997) 28:383–5. doi: 10.1016/S0046-8177(97)90140-4
31. Zhang Y, Huang X, Peng C, Wang Y, Wu Q, Wu Z, et al. Primary pulmonary epithelioid angiosarcoma: a case report and literature review. *J Cancer Res Ther*. (2018) 14:533–5. doi: 10.4103/0973-1482.176419
32. Sullivan JP, Spinola M, Dodge M, Raso MG, Behrens C, Gao B, et al. Aldehyde dehydrogenase activity selects for lung adenocarcinoma stem cells dependent on Notch signaling. *Cancer Res*. (2010) 70:9937–48. doi: 10.1158/0008-5472.CAN-10-0881
33. Lohberger B, Rinner B, Stuendl N, Absenger M, Liegl-Atzwanger B, Walzer SM, et al. Aldehyde dehydrogenase 1, a potential marker for cancer stem cells in human sarcoma. *PLoS ONE*. (2012) 7:e43664. doi: 10.1371/journal.pone.0043664
34. Lei HM, Zhang KR, Wang CH, Wang Y, Zhuang GL, Lu LM, et al. Aldehyde dehydrogenase 1A1 confers erlotinib resistance via facilitating the reactive oxygen species-reactive carbonyl species metabolic pathway in lung adenocarcinomas. *Theranostics*. (2019) 9:7122–39. doi: 10.7150/thno.35729
35. Greco N, Schott T, Mu X, Rothenberg A, Voigt C, McGough RL, III, et al. ALDH activity correlates with metastatic potential in primary sarcomas of bone. *J Cancer Ther*. (2014) 5:331–8. doi: 10.4236/jct.2014.54040
36. Ohmura-Kakutani H, Akiyama K, Maishi N, Ohga N, Hida Y, Kawamoto T, et al. Identification of tumor endothelial cells with high aldehyde dehydrogenase activity and a highly angiogenic phenotype. *PLoS ONE*. (2014) 9:e113910. doi: 10.1371/journal.pone.0113910

Conflict of Interest: The authors declare that the research was conducted in the absence of any commercial or financial relationships that could be construed as a potential conflict of interest.

Copyright © 2020 Aramini, Masciale, Bianchi, Manfredini, Banchelli, D'Amico, Bertolini, Dominici, Morandi and Maiorana. This is an open-access article distributed under the terms of the Creative Commons Attribution License (CC BY). The use, distribution or reproduction in other forums is permitted, provided the original author(s) and the copyright owner(s) are credited and that the original publication in this journal is cited, in accordance with accepted academic practice. No use, distribution or reproduction is permitted which does not comply with these terms.

frontiers in Medicine

ORIGINAL RESEARCH
published: 17 November 2020
doi: 10.3389/fmed.2020.00509

Alteration of Extracellular Superoxide Dismutase in Idiopathic Pulmonary Arterial Hypertension

Rui Zhang[1†], *Lan Wang*[1†], *Qin-Hua Zhao*[1], *Rong Jiang*[1], *Su-Gang Gong*[1], *Xin Jiang*[2], *Xi-Qi Xu*[2], *Yang-Yang He*[2], *Yuan Li*[1] *and Zhi-Cheng Jing*[1,2*]

[1] *Department of Cardio-Pulmonary Circulation, Shanghai Pulmonary Hospital, Tongji University School of Medicine, Shanghai, China,* [2] *Department of Cardiology, Peking Union Medical College Hospital, Chinese Academy of Medical Sciences & Peking Union Medical College, Beijing, China*

Background: Superoxide dismutases (SODs) are an important family of antioxidant enzymes that modulate reactive oxygen species levels. It is largely unknown which SOD isoform(s) change *in vivo* in idiopathic pulmonary arterial hypertension (IPAH) patients.

Methods: A total of 133 consecutive adult IPAH patients who underwent bone morphogenetic protein receptor type 2 (*BMPR2)* genetic counseling were enrolled in this prospective study. The plasma activities of three subtypes of SOD [copper–zinc (Cu/Zn-SOD), manganese (Mn-SOD), and extracellular SOD (Ec-SOD)] were examined.

Results: The activities of SODs were significantly lower in IPAH patients than in healthy subjects. However, only Ec-SOD activity in *BMPR2* mutation patients was significantly decreased compared to those in patients without a mutation. The reduced Ec-SOD activity was markedly associated with mean pulmonary arterial pressure, pulmonary vascular resistance (PVR), and 6-min walking distance (6MWD). The reduction of Mn-SOD activity was only associated with 6MWD. There was no association between Cu/Zn-SOD and hemodynamics. Patients with a lower Ec-SOD level had a worse survival compared to those with a higher baseline. The reduced Ec-SOD activity and the raised PVR increased the mortality risk.

Conclusions: Ec-SOD was correlated with *BMPR2* mutation, hemodynamic dysfunction, and poor outcomes. Circulating Ec-SOD could be a potentially vital antioxidant enzyme in the pathogenesis of IPAH.

Keywords: idiopathic pulmonary arterial hypertension, superoxide dismutases, extracellular SOD, biomarkers, prognosis

OPEN ACCESS

Edited by:
Mahmood Yaseen Hachim, Mohammed Bin Rashid University of Medicine and Health Sciences, United Arab Emirates

Reviewed by:
Mohamed A. Saleh, University of Sharjah, United Arab Emirates
Claudia Mickael, University of Colorado Denver, United States
Viviane De Maertelaer, Université Libre de Bruxelles, Belgium

***Correspondence:**
Zhi-Cheng Jing
jingzhicheng@vip.163.com

[†] *These authors have contributed equally to this work*

Specialty section:
This article was submitted to Pulmonary Medicine, a section of the journal Frontiers in Medicine

Received: *08 May 2020*
Accepted: *23 July 2020*
Published: *17 November 2020*

Citation:
Zhang R, Wang L, Zhao Q-H, Jiang R, Gong S-G, Jiang X, Xu X-Q, He Y-Y, Li Y and Jing Z-C (2020) Alteration of Extracellular Superoxide Dismutase in Idiopathic Pulmonary Arterial Hypertension. Front. Med. 7:509. doi: 10.3389/fmed.2020.00509

INTRODUCTION

The enhanced production of superoxide anions and other reactive oxygen species (ROS) contributes to the pathogenesis of pulmonary arterial hypertension (PAH) (1). The superoxide or ROS inactivates endothelium-derived nitric oxide (NO) and promotes the progression of endothelial dysfunction. Accordingly, steady-state levels of superoxide are dependent on both its rate of production and the activity of various antioxidant enzymes (2, 3). Superoxide dismutases (SODs) are one family of important antioxidant enzymes that defend against superoxide radicals in vascular protection.

The expression and the activity of SODs presumably have a profound effect on the responses of vascular cells to both acute and chronic oxidative stress (4).

Blood vessels express three isoforms of SODs: copper–zinc SOD (Cu/Zn-SOD, SOD 1), which locates in the cytosol, manganese SOD (Mn-SOD, SOD 2), which locates in the mitochondrial matrix, and an extracellular form of Cu/Zn-SOD (Ec-SOD, SOD 3) (4, 5). In mammals, different SOD isoforms are encoded by distinct genes but catalyze the same reaction. A reduction of SOD activity has been implicated in patients with PAH and in animal models of PAH (1, 6–12). For example, Cu/Zn-SOD knockout mice spontaneously displayed signs of elevated right ventricular systolic pressure and pulmonary arterial remodeling under normoxia (6). Mn-SOD deficiency was likewise evident in pulmonary arteries and plexiform lesions. Tissue-specific, epigenetic Mn-SOD deficiency initiated and sustained a heritable form of PAH by impairing redox signaling and resulting in proliferation and apoptosis resistance of pulmonary arterial smooth muscle cells (PASMC) (7). In a recent phase I and open-label clinical study in IPAH patients, the plasma Mn-SOD level change was used as a potential marker of drug effect (8). Remarkably, both Ec-SOD mRNA expression and activity were decreased in the lung tissue of idiopathic PAH (IPAH) (9). The loss of function or selective depletion of Ec-SOD exacerbated PAH (10, 11). The intratracheal delivery of adenoviruses overexpressing Ec-SOD could suppress monocrotaline-induced PAH in rats (12). Taken together, these data suggested that SODs are important antioxidant enzymes in the pathogenesis of PAH.

Identifying the link between defective SOD activity and clinical characteristics in IPAH patients is important, which, in turn, can be used as an epigenetic biomarker for a new and improved therapeutic strategy. Approximately 20% of patients with IPAH carried mutations in bone morphogenetic protein receptor type 2 (*BMPR2*), where a loss of *BMPR2* function may compromise the integrity of the endothelial barrier and contribute to endothelial dysfunction by mediating endothelium-derived nitric oxide bioactivity (2, 13, 14). To date, there is limited information on plasma SOD alteration in IPAH patients with or without *BMPR2* mutation. Thus, the objective of the present study was to prospectively determine whether (a) the abnormalities of SOD levels were related to hemodynamic dysfunction and clinical characteristics, (b) patients with *BMPR2* mutation had a more severe reduction of SOD levels, and (c) plasma SOD level could be a predictor for prognosis and clinical outcome.

Abbreviations: BMI, body mass index; *BMPR2*, bone morphogenetic protein receptor type 2; BNP, brain natriuretic peptide; CI, cardiac index; 95% CI, 95% confidence interval; CO, cardiac output; Cu/Zn-SOD, copper–zinc superoxide dismutase; Ec-SOD, extracellular form of Cu/Zn superoxide dismutase; IPAH, idiopathic pulmonary arterial hypertension; Mn-SOD, manganese superoxide dismutase; mPAP, mean pulmonary arterial pressure; mRAP, mean right atrial pressure; 6MWD, 6-min walk distance; PAWP, pulmonary artery wedge pressure; PVR, pulmonary vascular resistance; ROC, receiver operation characteristic; SOD, superoxide dismutase; SvO_2, mixed venous oxygen saturation.

MATERIALS AND METHODS

Study Subjects

One hundred thirty-three consecutive adult IPAH patients (≥18 years of age at diagnosis) who underwent *BMPR2* genetic counseling at the time of their first right heart catheterization were prospectively enrolled in this study between January 2010 and July 2013. One hundred thirty control subjects were selected from a cohort of healthy volunteers. The median age of the control subjects was 40 (20–57) years, and the ratio of women to men was 3:1. IPAH was diagnosed according to standard criteria: mean pulmonary artery pressure (mPAP) ≥25 mmHg and pulmonary vascular resistance (PVR) at rest >3 Wood units, in the presence of a normal pulmonary artery wedge pressure (PAWP ≤15 mmHg) (15). Patients were excluded if they have definite causes for PAH, such as connective tissue disease and congenital heart disease, and also those with portopulmonary hypertension, chronic pulmonary thromboembolism, pulmonary hypertension due to left heart diseases, and lung diseases and/or hypoxemia. Other exclusion criteria for the study included potential confounding factors associated with plasma antioxidant enzyme production: cigarette smoking and excessive alcohol consumption, hypertension, and type 2 diabetes mellitus (16, 17). We also excluded the participants who completed an acute exercise and were with vitamin C and E supplementation (18). We prospectively followed up these patients for a mean of 26 ± 9 months after enrollment, and no patient received lung or heart–lung transplantation. The major endpoint was defined as all-cause mortality.

The study was conducted according to the principles of the Declaration of Helsinki and was approved by the Shanghai Pulmonary Hospital Ethics Committee (number K16-055). Written informed consent was obtained from all the participants.

Blood Sampling and Plasma SOD Assay

Venous blood was collected from all subjects after fasting overnight (>12 h) to minimize the influence of foods and beverages on the plasma SOD concentrations. All the samples were collected directly into specially prepared sodium ethylene diamine tetra-acetic acid tubes containing a preservative to retard auto-oxidation. After centrifuging at 3,000 rpm at 4 for 15 min, the supernatant was separated for SOD activity immediate determinations. The whole procedure was completed within 20 min. For the oxidant test, the presence of 0.005% butylated hydroxytoluene (without glutathione) in plasma was allowed for anti-*ex vivo* oxidation and improving the stability, routinely. Each sample was measured within a month of collection, and at least two different dilutions of the same sample were tested. To minimize the inter- and the intra-assay coefficients of variation, each analyte was duplicated on three different days within 1 month. The plasma Cu/Zn-SOD and Mn-SOD activities were determined by an SOD assay kit (Cayman Chemical Company, item no. 706002) using a tetrazolium salt reaction (9). The method utilized tetrazolium salt for the detection of superoxide radicals generated by xanthine oxidase and hypoxanthine. Detection of only Mn-SOD activity needs

the addition of potassium cyanide to inhibit both Cu/Zn-SOD and Ec-SOD. The samples can be assayed in the absence of xanthine oxidase to generate a sample background. This sample background absorbance (at 440–460 nm) was subtracted from the sample absorbance generated in the presence of xanthine oxidase, thus correcting for non-SOD-generated absorbance.

The plasma activity of Ec-SOD was performed based on the competitive ELISA assay kit (Lifespan Biosciences, NBP1-90377) according to the manufacturer's instructions (19). Each well of the supplied microtiter plate has been pre-coated with a target-specific capture antibody. Standards or samples are added to the wells as well as a fixed quantity of biotin-conjugated target antigen. The antigens in the standards or samples compete with the biotin-conjugated antigen to bind to the capture antibody. An avidin–horseradish peroxidase (HRP) conjugate is then added, which binds to the biotin. A 3,3′,5,5′-tetramethylbenzidine substrate was used for testing for Ec-SOD, and the optical density of the well is measured at a wavelength of 450 ± 2 nm.

Statistical Analysis

Results were expressed as numbers, percentages, means with corresponding standard deviations, or medians with corresponding 25th and 75th percentiles [interquartile range (IQR)]. Continuous variables were compared with baseline characteristics, hemodynamic parameters, and SOD levels using Student's *t*-test or Mann–Whitney *U*-test according to normality. The proportions were compared with Pearson chi-square test or Fisher's exact test, as appropriate. Continuous variables were assessed for linearity of their relationship with the outcome variable. Spearman's ρ was investigated for correlations, with a Bonferroni correction for each variable. If these variables were not found to be linearly related to the outcome, they were grouped into quartiles and modeled to avoid violating model assumptions. A univariate analysis of covariance adjusted for age and sex was carried out to compare the means among the three groups (control subjects, *BMPR2* mutation carrier group, and BMPR2 wild-type group). Bonferroni method was applied to correct the *p*-value for multiple comparisons in *post hoc* tests.

For comparison of the prognostic values of SODs and selected hemodynamic parameters, receiver operating characteristic curves (ROC) were generated and the areas under the curves were calculated. The optimal thresholds for baseline Ec-SOD for death prediction was determined using Youden index (sensitivity + specificity−1). The value of Ec-SOD corresponding to the maximum value of Youden's index was considered as the optimal cutoff point for Ec-SOD. Survival analyses were performed using Kaplan–Meier method and were compared by means of log-rank test. Two steps were performed to analyze the survival. First, a univariable Cox proportional regression was used for time-to-event analysis to estimate hazard ratios (HR) and 95% confidence intervals (CI) for all-cause mortality according to the stratified covariates (SODs, hemodynamic parameters, 6MWD, WHO FC, female gender, and age). All variables with a $p < 0.05$ were then tested in a stepwise forward Cox regression analyses; the variables were entered at a $p < 0.05$. In the second step of the survival analysis, a multivariable stepwise forward Cox regression model was used to estimate the HR and the 95% CI for association in different SOD groups and outcomes adjusted for age and sex. For all analyses, $p < 0.05$ were considered as statistically significant. All calculations were performed using the SPSS 14.0 statistical software package (Statistical Package for Social Science, Chicago, IL, USA) or StatView 5.0.1 (SAS Institute, Cary, NC, USA).

RESULTS

SOD Levels and Characteristics of the Study Population

Among the 133 IPAH patients recruited, 28 (21%) were *BMPR2* mutation carriers (*BMPR2* mut); the other 105 patients were *BMPR2* wild-type (*BMPR2* wt). The clinical characteristics are summarized in **Table 1**. The patients with *BMPR2* mut had a younger median age at diagnosis (28 years; IQR, 22–34 years) than those of with *BMPR2* wt (39 years; IQR, 29–53 years; $p < 0.001$). The sex ratio of females to males was 2.4:1 ($n = 94/39$) in the total population. In *BMPR2* wt patients, the female/male ratio was 3.0:1 ($n = 79/26$), whereas in the *BMPR2* mut group, the female/male ratio was 1.2:1 ($n = 15/13$, $p < 0.001$). In patients with IPAH, plasma Cu/Zn-SOD (148 U/ml; 95% CI, 114–213), Mn-SOD (40 U/ml; 95% CI, 34–115), and Ec-SOD (85 U/L, 95% CI, 79–119) activities were significantly lower compared to those in the 130 control subjects (212 U/ml, 95% CI: 153–266; 144 U/ml, 95% CI: 114–157; and 175 U/L, 95% CI: 143–193, respectively; $p < 0.01$ or $p < 0.001$). Among the three comparison groups (control subjects, *BMPR2* mut group, and *BMPR2* wt group), plasma Ec-SOD activity was still lowest in the *BMPR2* mut group, adjusted for female gender ($F = 6.679$, $p = 0.010$) and age ($F = 1.420$, $p = 0.002$). There was no difference of Cu/Zn-SOD and Mn-SOD in the multiple-comparison tests. Only Ec-SOD activity in patients with *BMPR2* mut group was statistically decreased compared to those in the *BMPR2* wt group (*BMPR2* wt, $p = 0.02$, **Figure 1**). However, there was no significant difference regarding WHO functional class severity in both *BMPR2* mut and *BMPR2* wt groups as well as total patients.

Correlation of SOD Activity With Hemodynamic Variables

The *BMPR2* mut patients had a more severe hemodynamic compromise, with a significantly higher mPAP and PVR in comparison with the *BMPR2* wt patients (**Table 1**). The baseline plasma Ec-SOD activities were negatively correlated with mPAP ($r = -0.22$; $p = 0.04$) and PVR ($r = -0.21$; $p = 0.02$). The Ec-SOD and the Mn-SOD activities were correlated positively with 6MWD ($r = 0.26$; $p = 0.003$, $r = 0.19$; $p = 0.04$, respectively, **Figure 2**). The other baseline SOD activities did not correlate with age, mRAP, and mixed venous oxygen saturation (S_VO_2) (**Supplementary Figures S1–S8**).

SOD Activities in Relation to Other Markers of Adverse Outcomes

A univariate analysis identified several factors related to mortality. An elevated mRAP, an increased PVR, and a reduced Ec-SOD were all significantly associated with an increased risk of death. By a stepwise multivariate Cox regression analysis, only

TABLE 1 | Baseline characteristics and SOD levels in patients with IPAH.

	Total (n = 133)	*BMPR2* mut (n = 28)	*BMPR2* wt (n = 105)	*P*-value[a]
Age, years	36 (27, 51)	28 (22, 34)	39 (29, 53)	<0.001
Female gender, *n* (%)	94 (71)	15 (54)	79 (75)	<0.001
BMI, kg/m^2	22 (20, 24)	21 (20, 23)	22 (20, 24)	0.163
WHO FC, *n* (%)				0.191
Class II	45 (34)	9 (32)	36 (34)	
Class III	71 (53)	17 (61)	54 (51)	
Class IV	17 (13)	2 (7)	15 (14)	
Onset to diagnosis, months	24 (7, 48)	18 (5, 43)	24 (8, 48)	0.293
6MWD, meters[b]	367 (311, 439)	407 (330, 248)	360 (308, 440)	0.376
BNP, pg/ml	355 (144, 515)	307 (143, 533)	391 (157, 475)	0.812
Cu/Zn-SOD, U/ml	148 (114, 213)	147 (125, 215)	142 (110, 213)	0.608
Mn-SOD, U/ml	40 (34, 65)	40 (34, 80)	40 (34, 163)	0.863
Ec-SOD, U/l	85 (79, 91)	82 (77, 86)	86 (81, 93)	0.010
Hemodynamic variables				
HR, bpm	84 (75, 94)	86 (76, 92)	84 (74, 98)	0.787
mRAP, mmHg	7 (5, 12)	5 (7, 12)	7 (5, 12)	0.862
mPAP, mmHg	62 (51, 69)	68 (57, 82)	59 (50, 66)	0.003
PAWP, mmHg	9 (7, 11)	9 (7, 11)	9 (7, 11)	0.959
CO, L/min	3.6 (3.0, 4.7)	3.4 (2.8, 4.7)	3.6 (3.0, 4.7)	0.561
CI, L/min/m^2	2.2 (1.8, 32.8)	2.0 (1.7, 2,7)	1.9 (1.6, 2.5)	0.362
PVR, Wood units	15 (10, 19)	16 (13, 23)	14 (9, 19)	0.039
S_VO_2, %	59 (54, 67)	58 (55, 67)	59 (54, 67)	0.654
PAH-specific therapies, *n* (%)[c]				0.848
Bosentan (oral)	16 (12)	4 (14)	12 (11)	
Iloprost (inhaled)	3 (2)	0 (0)	3 (3)	
Sildenafil (oral)	59 (44)	14 (50)	45 (43)	
Vardenafil (oral)	30 (23)	5 (18)	25 (24)	
Combination therapy	15 (11)	2 (7)	13 (12)	

Values are expressed as medians (interquartile range), except for female gender and WHO functional class, which are numbers of patients (%).
[a]Comparison between groups with BMPR2 mut and BMPR2 wt.
[b]6MWD could be successfully measured in 124 patients.
[c]Seven patients (5%) were enrolled in PATENT-1 (Riociguat) study.
BMI, body mass index; BMPR 2, bone morphogenetic protein receptor type 2; BNP, brain natriuretic peptide; CI, cardiac index; CO, cardiac output; Cu/Zn-SOD, copper–zinc superoxide dismutase; Ec-SOD, extracellular form of Cu/Zn superoxide dismutase; HR, heart rate; Mn-SOD, manganese superoxide dismutase; mPAP, mean pulmonary arterial pressure; mRAP, mean right atrial pressure; mut, mutation; 6MWD, 6-min walking distance; PAWP, pulmonary artery wedge pressure; PVR, pulmonary vascular resistance; SvO_2, mixed venous oxygen saturation; WHO FC, World Health Organization functional class; wt, wild-type.

the lower Ec-SOD and the higher PVR remained as significant predictors of adverse outcomes (**Figure 3**).

The ROC curve analyses further illustrated that Ec-SOD was a strong indicator of adverse outcomes in IPAH. The best Ec-SOD cutoff level for predicting outcome was 83 U/L, giving a sensitivity rate of 69% and a specificity rate of 71%. The c-statistic for Ec-SOD level was 0.72 (95% CI, 0.64–0.85), which was similar to PVR (0.73; 0.60–0.86) but numerically superior to 6MWD (0.66; 0.55–0.76), mPAP (0.58; 0.44–0.71), Mn-SOD (0.54; 0.41–0.67), and Cu/Zn-SOD (0.47; 0.32–00.61, **Figure 4A**).

Survival Analysis

The observed cardiopulmonary mortality was 26% (35 patients) in the current cohort of IPAH patients. Twenty-five of the deaths were directly related to right ventricular failure; six had a sudden death, and the cause of death was not able to be ascertained in four cases. The total patients with IPAH were divided into two groups based on the cutoff levels for Ec-SOD calculated by ROC analysis to detect mortality.

In the group of 59 patients with Ec-SOD activity ≤83 U/L, 24 (41%) died, but only 11 of 74 (15%) patients were in the group with Ec-SOD activity >83 U/L ($p < 0.001$). The patients with Ec-SOD activity >83 U/L had a significantly lower mPAP and PVR than those with Ec-SOD activity ≤83 U/L. Moreover, the proportion of female gender and the severity of WHO functional class in the group with Ec-SOD ≤83U/L were higher than those with Ec-SOD >83 U/L (**Table 2**). Survival was significantly better in patients with Ec-SOD activity >83 U/L (**Figure 4B**). The 1- and 3- year survival estimates were 84 and 63%, respectively, in patients with Ec-SOD activity ≤83 U/L and 95 and 86%,

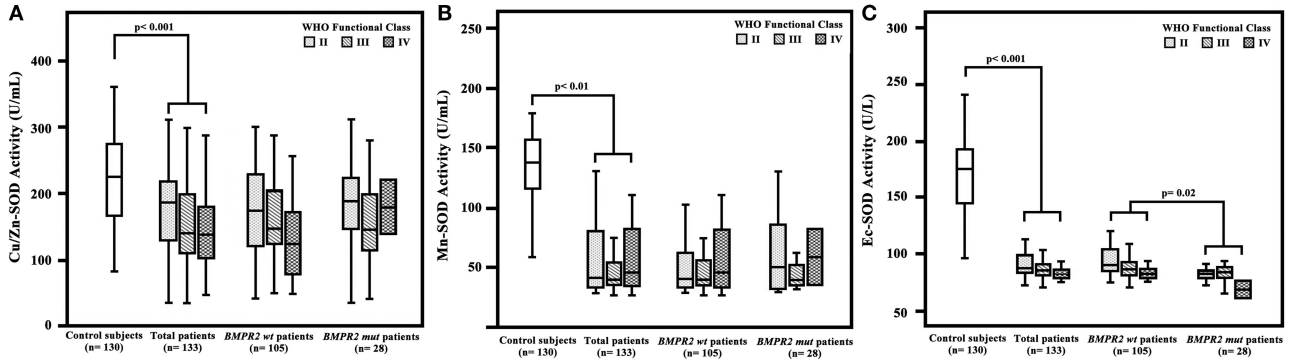

FIGURE 1 | Plasma superoxide dismutase (SOD) activity in patients with idiopathic pulmonary arterial hypertension (IPAH), control subjects, patients with *BMPR2* mutation (*BMPR2* mut), and those with wild-type *BMPR2* (*BMPR2* wt), associated with WHO functional class. **(A)** The plasma Cu/Zn level was significantly decreased in patients with IPAH compared to that in the control subjects. **(B)** The Mn-SOD activity was significantly lower in patients with IPAH compared to that in the control subjects. **(C)** The Ec-SOD activities in patients with IPAH were significantly lower compared to those in the control subjects. The Ec-SOD activity in patients of the *BMPR2* mut group was statistically decreased compared to that in patients of the *BMPR2* wt group. The line through the center of the boxes represents the median. *BMPR 2*, bone morphogenetic protein receptor type 2; Cu/Zn-SOD, copper–zinc superoxide dismutase; Mn-SOD, manganese superoxide dismutase; Ec-SOD, extracellular form of Cu/Zn superoxide dismutase.

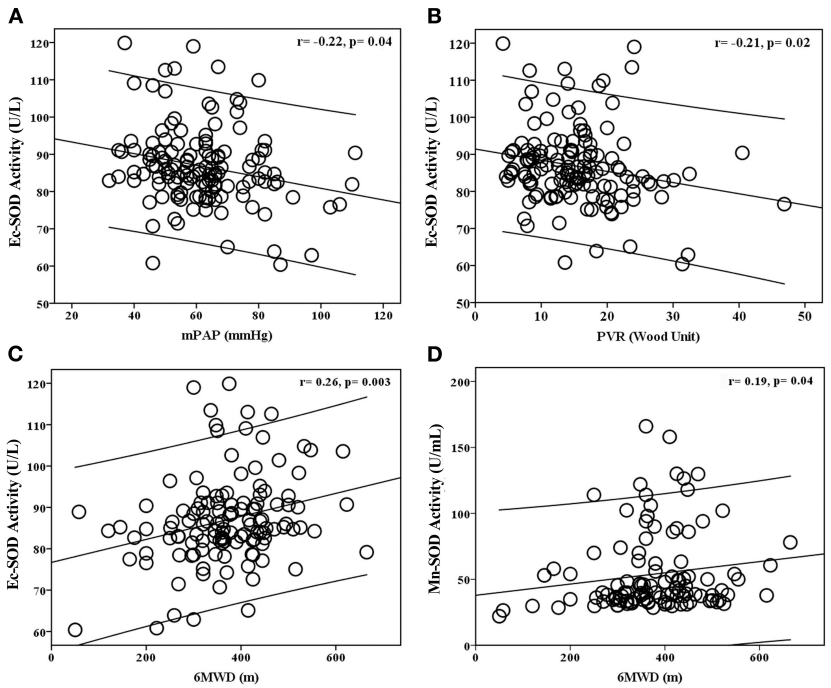

FIGURE 2 | Relationship between baseline plasma Ec-SOD activity with **(A)** mean pulmonary arterial pressure (mPAP), **(B)** pulmonary vascular resistance (PVR), **(C)** 6-min walking distance (6MWD), and **(D)** plasma Mn-SOD activity with 6MWD in patients with idiopathic pulmonary arterial hypertension (IPAH). The baseline plasma Ec-SOD activities were negatively correlated with mPAP and PVR. The Ec-SOD and Mn-SOD activities were correlated positively with 6MWD.

respectively, in patients with Ec-SOD activity >83U/L (p = 0.004), adjusted by age and female gender.

DISCUSSION

Antioxidant enzymes play prominent roles against oxidative damage and provide protective signals in pathological remodeling of the pulmonary vasculature during the development of PAH. Understanding the SOD pathway will greatly help in the clinical development of medications for PAH therapy. However, it is unclear whether an abnormality of SOD activity is associated with hemodynamic dysfunction and poor outcomes in patients with IPAH. Our results demonstrate that (a) the plasma SOD activity was markedly reduced in

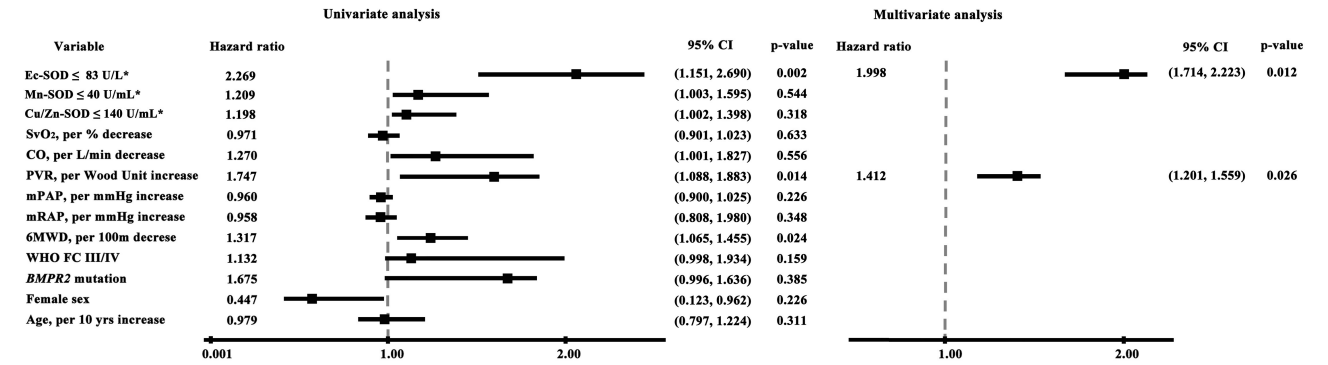

FIGURE 3 | Cox proportional hazards model of factors associated with survival in idiopathic pulmonary arterial hypertension (univariate and multivariate analyses). The lower Ec-SOD and the higher PVR remained as significant predictors of adverse outcomes. The asterisk indicates identification by the receiver operating characteristic analysis curve-derived cutoff value. *BMPR 2*, bone morphogenetic protein receptor type 2; CO, cardiac output; Cu/Zn-SOD, copper–zinc superoxide dismutase; Ec-SOD, extracellular form of Cu/Zn superoxide dismutase; Mn-SOD, manganese superoxide dismutase; mPAP, mean pulmonary arterial pressure; mRAP, mean right atrial pressure; 6MWD, 6-min walking distance; PVR, pulmonary vascular resistance; SvO_2, mixed venous oxygen saturation.

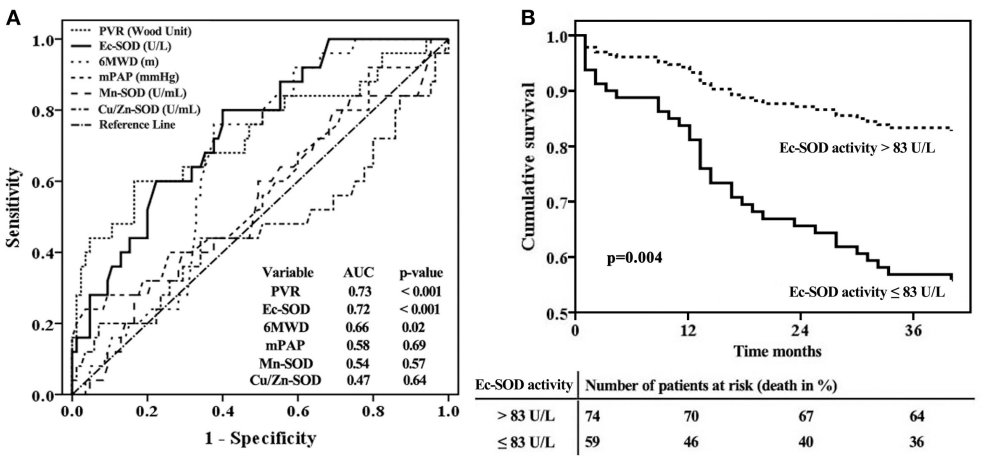

FIGURE 4 | Extracellular form of Cu/Zn superoxide dismutase (Ec-SOD) activity in relation to other markers for an adverse prognosis according to **(A)** receiver operation characteristic analyses and **(B)** survival curves for the baseline cutoff plasma Ec-SOD activity in patients with idiopathic pulmonary arterial hypertension, adjusted by age and female gender. The best Ec-SOD cutoff level for predicting outcome was 83 U/L. Survival was significantly better in patients with Ec-SOD activity >83 U/L.

patients with IPAH compared to that in healthy subjects, (b) patients with *BMPR2* mutation had a lower Ec-SOD level than the no-mutation subjects, (c) only Ec-SOD activity was correlated with hemodynamic abnormalities and survival, and (d) a decreased Ec-SOD activity was associated with an increased mortality risk, suggesting that the use of Ec-SOD may be superior to Cu/Zn-SOD or Mn-SOD for supplemental treatment if possible.

Oxidative stress in PAH is rather inescapable with the increased lipid peroxidation and reduced antioxidant defenses (20). The expression and the activity of SODs presumably have profound effects on the responses of vascular cells to oxidative stress (4). It is noteworthy that the plasma activity of all SODs' isoforms is statistically decreased in patients with IPAH compared with that in the healthy subjects in our study, especially for Ec-SOD activity. The decreases in Ec-SOD activities might not be attributed solely to superoxide or ROS level; the mechanisms of post-translation modification, genetic polymorphisms, and epigenetic regulation are included (21–23). For example, exogenous hydrogen peroxide (H_2O_2) inactivates Ec-SOD in persistent pulmonary hypertension of newborn lambs. Through oxidation of histidine residues in copper-containing catalytic sites, H_2O_2 has been shown to inhibit Ec-SOD activity (21). Moreover, Nozik-Grayck et al. have reported that histone deacetylation contributed to low Ec-SOD expression in PASMC from IPAH patients, specifically *via* class I histone deacetylase 3 (9, 23). There is also evidence that miR21 could inhibit Ec-SOD expression in lung epithelial cells in PAH (23). Collectively, Ec-SOD activity may be regulated by comprehensive processes in pulmonary hypertension; substantial

TABLE 2 | Baseline characteristics in relation to Ec-SOD activity.

	Ec-SOD ≤ 83 U/L (*n* = 59)	Ec-SOD > 83 U/L (*n* = 74)	*P*-value[a]
Age, years	31 (25, 48)	39 (29, 52)	0.022
Female gender, ***n*** (%)	45 (76)	49 (66)	< 0.001
BMI, kg/m^2	22 (19, 23)	22 (21, 24)	0.500
BMPR2 mutation	17 (29)	11 (15)	0.521
WHO FC, ***n*** (%)			< 0.001
Class II	14 (24)	31 (42)	
Class III	35 (59)	36 (49)	
Class IV	10 (17)	7 (9)	
Onset to diagnosis, months	18 (6, 33)	34 (7, 60)	0.033
6MWD, meters[b]	360 (276, 415)	390 (329, 452)	0.008
BNP, pg/ml	387 (158, 529)	319 (147, 488)	0.857
Cu/Zn-SOD, U/ml	146 (110, 213)	148 (120, 213)	0.911
Mn-SOD, U/ml	46 (34, 90)	39 (29, 52)	0.082
Hemodynamic variables			
HR, bpm	82 (73, 94)	86 (76, 97)	0.409
mRAP, mmHg	8 (5, 13)	7 (5, 11)	0.631
mPAP, mmHg	63 (54, 77)	59 (50, 67)	0.048
PAWP, mmHg	9 (6, 11)	9 (7, 12)	0.453
CO, L/min	3.5 (3.0, 4.5)	3.6 (2.9, 5.0)	0.410
CI, L/min/m^2	2.3 (1.8, 2.8)	2.2 (1.8, 2.8)	0.792
PVR, Wood units	16 (12, 22)	14 (9, 17)	0.040
S_VO_2, %	58 (53, 62)	61 (54, 68)	0.192

Values are expressed as medians (interquartile range), except for female gender and WHO functional class, which are numbers of patients (%).

[a] *Comparison between groups with Ec-SOD ≤ 83 U/L and Ec-SOD > 83 U/L.*

[b] *6MWD could be successfully measured in 124 patients.*

BMI, body mass index; BMPR 2, bone morphogenetic protein receptor type 2; BNP, brain natriuretic peptide; CI, cardiac index; CO, cardiac output; Cu/Zn-SOD, copper–zinc superoxide dismutase; Ec-SOD, extracellular form of Cu/Zn superoxide dismutase; HR, heart rate; Mn-SOD, manganese superoxide dismutase; mPAP, mean pulmonary arterial pressure; mRAP, mean right atrial pressure; 6MWD, 6-min walking distance; PAWP, pulmonary artery wedge pressure; PVR, pulmonary vascular resistance; SvO_2, mixed venous oxygen saturation; WHO FC, World Health Organization functional class.

work is geared on how to use Ec-SOD to evaluate the oxidative stress system.

Despite important advances in understanding the genetics of PAH (such as mutation in *BMPR2* in familial PAH) and the recognition of somatic chromosomal abnormalities in sporadic PAH, the cause of most cases of PAH remains yet unclear (24, 25). It has been reported that patients with *BMPR2* mutations exhibited a reduced level of NO production (26). Despite finding 21% of IPAH patients to have *BMPR2* mutations, not all patients with a mutation in the present cohort had a corresponding lower activity of SODs. It has been shown that Ec-SOD is the only extracellular isoform and occurs in bodily fluids such as plasma, lymph, and synovial and cerebrospinal fluid in the human organism (27). Ec-SOD can bind to the surface of endothelial cells by a high abundance of heparin sulfate. Consequently, it is highly expressed in lung tissue (28). Notably, Ec-SOD is the predominant isoform responsible for up to 70% of all SOD activity in the cardiovascular system (29, 30). Xu et al. reported that Ec-SOD gene mutation (SOD 3^{E124D}) in rats or SOD 3 knockout in mice aggravated the development of PAH under stress conditions (10). In addition, Ec-SOD preserves NO levels as it diffuses from the endothelium to its major target (soluble guanylate cyclase) in the vascular muscle (4, 31). The activity of Ec-SOD was markedly lower in *BMPR2* mutation patients in our present study, possibly due to the decreased bioavailability of NO and/or decreased responsiveness to NO in PAH.

We found that the reduced Ec-SOD activity was closely associated with the severity of hemodynamic impairment in the study population as a whole, implying that antioxidant enzyme deficiency might partly reflect pulmonary vascular resistance under oxidative stress status. ROS could stimulate vasoconstriction or proliferation of PASMC through NO reduction, leading to the pathogenesis of PAH (12). Ec-SOD might halt the ROS cascade by disproportioning superoxide anion and maintaining NO bioavailability in pulmonary arteries (12). Our group has reported that patients with IPAH who carry the *BMPR2* mutation had further reduced NO metabolites and worse hemodynamics (27). Sustained Ec-SOD expression in the pulmonary artery might exert a central role in extracellular antioxidative properties (32). Hence, the low NO availability perhaps disturbs the balance and the distribution of SODs.

The role of SODs in pulmonary vasculature has not been fully understood. In a competing reaction, superoxide reacts six times faster with NO than with any isoform of the SODs (33, 34). The endogenous Ec-SOD does not participate in the development of PAH under basal conditions but plays a role of protecting the lung from the development of PAH under stress conditions (9). Reports of the association of genes encoding the SOD enzymes in cardiovascular complications are scarce (35). One study found a rare functional variant rs1799895 (Arg213Gly) in the heparin-binding domain of Ec-SOD. The Gly allele was associated with reduced Ec-SOD affinity for heparin and decreased tissue binding (36). Accordingly, the associations of the Gly allele with cardiovascular risk factors, morbidity, or mortality have been reported (35, 37, 38). Although we did not design and detect the genetic variant of Ec-SOD in patients with IPAH, it is an important finding that Ec-SOD, but not Cu/Zn-SOD or Mn-SOD levels, could predict long-term outcomes in our study as the strength of risk prediction for Ec-SOD activity was robust. The vascular wall contains large amounts of Ec-SOD, implicating that reduced Ec-SOD activity might contribute to endothelial dysfunction and NO degradation. Thus, SODs, which are responsible for preventing oxidative damage, might be beneficial for the supplemental treatment for IPAH.

Several limitations of the present study must be noted while interpreting the results. First, since plasma SOD levels were only measured at baseline, it was difficult for us to evaluate the variability and the prognosis of level changes over time or the impact of different therapies. Second, blood samples for measuring the plasma SOD levels were collected after an overnight (>12 h) fast in all patients and subjects; the best time to collect samples for prediction remains unclear. However, there are studies reporting that

SOD activities were stable in samples initially kept frozen, whose activities were not subject to protein alteration as a result of the freezing procedure (39). The difference between inter-batch and inter-operator variability was reasonable. Furthermore, another potential limitation is lack of race; the findings may be applicable to the Chinese Han population. It remains to be explained whether the results of this study are exclusive to the selected population. Finally, we had better to perform the sensitivity analyses in order to assess the validity and the robustness of the analyses based on the cutoff value.

CONCLUSION

In summary, we demonstrated that the baseline plasma SOD activities were significantly lower in patients with IPAH than in healthy control subjects. Only the Ec-SOD level was associated with the hemodynamic measures of disease severity and *BMPR2* mutation. Patients with reduced Ec-SOD activity had increased risks for mortality independent of clinical characteristics and other risk factors. Decreased circulating Ec-SOD could potentially be used as a biomarker in the prognosis of IPAH patients.

WHAT IS ALREADY KNOWN ON THIS SUBJECT?

► Antioxidant enzymes play prominent roles against oxidative damage and protective signals in pathological remodeling of the pulmonary vasculature during the development of idiopathic pulmonary arterial hypertension (IPAH). Superoxide dismutases (SODs) are an important family of antioxidant enzymes that modulate reactive oxygen species levels.

WHAT MIGHT THIS STUDY ADD?

► This study adds to the present knowledge that plasma SOD activities were significantly lower in patients with IPAH than in healthy control subjects. Only Ec-SOD level was associated with the hemodynamic measures of disease severity and BMPR2 mutation. Patients with reduced Ec-SOD activity had increased risks for mortality, independent of clinical characteristics and other risk factors. Ec-SOD is a vital antioxidant enzyme and superior to the other two isoforms in PAH pathogenesis.

HOW MIGHT THIS IMPACT ON CLINICAL PRACTICE?

► Understanding the SOD pathway will greatly help in the clinical development of medications for PAH therapy. This study demonstrated that the use of Ec-SOD may be superior to the other two SOD isoforms for supplemental treatment.

DATA AVAILABILITY STATEMENT

All datasets presented in this study are included in the article/**Supplementary Material**.

ETHICS STATEMENT

The studies involving human participants were reviewed and approved by Shanghai Pulmonary Hospital Ethics Committee. The patients/participants provided their written informed consent to participate in this study.

AUTHOR CONTRIBUTIONS

All authors participated in the design of this study and/or patient enrolment and met the criteria for authorship. Z-CJ contributed to the study design, conduct of the study, data analysis, scientific overview, and editing of the manuscript and was directly involved in the recruitment and care of the participants. RZ contributed to the data analysis, scientific interpretation, and drafting and editing of the manuscript. LW, Q-HZ, RJ, S-GG, XJ, X-QX, Y-YH, and YL were directly involved in the recruitment and care of the participants and in data collection. All the authors had full access to all data of this study and had final responsibility for the decision to submit for publication. All the authors have reviewed the manuscript and approved the final version for submission.

FUNDING

This study was supported in part by Shanghai Pujiang Program 18PJD043 and the International Cooperation Project of Science and Technology Commission Shanghai Municipality 19410741000 (RZ), the Program of Natural Science Foundation of Shanghai 18ZR1431500 (LW), the Cohort Study of Orphan Diseases, Major Program of the National Natural Science Foundation of China, Precision Medicine, the 13th 5-Year Plan 2016YFC0901500, the Key Program of National Natural Science Foundation of China 81630003, and CAMS Innovation Fund for Medical Sciences 2016-I2M-1-002, 2017-I2M-B&R-02 (Z-CJ). The sponsors had no involvement in the study design, data analysis, data interpretation, and writing or revision of the manuscript.

ACKNOWLEDGMENTS

The authors acknowledge the contribution of all investigators who participated in this study. We also thank the patients who participated in this study.

SUPPLEMENTARY MATERIAL

The Supplementary Material for this article can be found online at: https://www.frontiersin.org/articles/10.3389/fmed.2020.00509/full#supplementary-material

REFERENCES

1. Bowers R, Cool C, Murphy RC, Tuder RM, Hopken MW, Flores SC, et al. Oxidative stress in severe pulmonary hypertension. *Am J Respir Crit Care Med.* (2004) 169:764–9. doi: 10.1164/rccm.200301-147OC
2. Thomas SR, Witting PK, Drummond GR. Redox control of endothelial function and dysfunction: molecular mechanisms and therapeutic opportunities. *Antioxid Redox Signal.* (2008) 10:1713–65. doi: 10.1089/ars.2008.2027
3. Wei EP, Kontos HA, Christman CW, DeWitt DS, Povlishock JT. Superoxide generation and reversal of acetylcholine-induced cerebral arteriolar dilation after acute hypertension. *Circ Res.* (1985) 57:781–7. doi: 10.1161/01.RES.57.5.781
4. Faraci FM, Didion SP. Vascular protection: superoxide dismutase isoforms in the vessel wall. *Arterioscler Thromb Vasc Biol.* (2004) 24:1367–73. doi: 10.1161/01.ATV.0000133604.20182.cf
5. Fukai T, Ushio-Fukai M. Superoxide dismutases: role in redox signaling, vascular function, and diseases. *Antioxid Redox Signal.* (2011) 15:1583–606. doi: 10.1089/ars.2011.3999
6. Ramiro-Diaz JM, Nitta CH, Maston LD, Codianni S, Giermakowska W, Resta TC, et al. Nfat is required for spontaneous pulmonary hypertension in superoxide dismutase 1 knockout mice. *Am J Physiol Lung Cell Mol Physiol.* (2013) 304:L613–25. doi: 10.1152/ajplung.00408.2012
7. Archer SL, Marsboom G, Kim GH, Zhang HJ, Toth PT, Svensson EC, et al. Epigenetic attenuation of mitochondrial superoxide dismutase 2 in pulmonary arterial hypertension: a basis for excessive cell proliferation and a new therapeutic target. *Circulation.* (2010) 121:2661–71. doi: 10.1161/CIRCULATIONAHA.109.916098
8. Hemnes AR, Rathinasabapathy A, Austin EA, Brittain EL, Carrier EJ, ChenX, et al. A potential therapeutic role for angiotensin-converting enzyme 2 in human pulmonary arterial hypertension. *Eur Respir J.* (2018) 51:1702638. doi: 10.1183/13993003.02638-2017
9. Nozik-Grayck E, Woods C, Stearman RS, Venkataraman S, Ferguson BS, Swain K, et al. Histone deacetylation contributes to low extracellular superoxide dismutase expression in human idiopathic pulmonary arterial hypertension. *Am J Physiol Lung Cell Mol Physiol.* (2016) 311:L124–34. doi: 10.1152/ajplung.00263.2015
10. Xu D, Guo H, Xu X, Lu Z, Fassett J, Hu X, et al. Exacerbated pulmonary arterial hypertension and right ventricular hypertrophy in animals with loss of function of extracellular superoxide dismutase. *Hypertension.* (2011) 58:303–9. doi: 10.1161/HYPERTENSIONAHA.110.166819
11. Nozik-Grayck E, Woods C, Taylor JM, Benninger RK, Johnson RD, Villegas LR, et al. Selective depletion of vascular ec-sod augments chronic hypoxic pulmonary hypertension. *Am J Physiol Lung Cell Mol Physiol.* (2014) 307:L868–76. doi: 10.1152/ajplung.00096.2014
12. Kamezaki F, Tasaki H, Yamashita K, Tsutsui M, Koide S, Nakata S, et al. Gene transfer of extracellular superoxide dismutase ameliorates pulmonary hypertension in rats. *Am J Respir Crit Care Med.* (2008) 177:219–26. doi: 10.1164/rccm.200702-264OC
13. Machado RD, Eickelberg O, Elliott CG, Geraci MW, Hanaoka M, Loyd JE, et al. Genetics and genomics of pulmonary arterial hypertension. *J Am Coll Cardiol.* (2009) 54:S32–42. doi: 10.1016/j.jacc.2009.04.015
14. Gangopahyay A, Oran M, Bauer EM, Wertz JW, Comhair SA, Erzurum SC, et al. Bone morphogenetic protein receptor ii is a novel mediator of endothelial nitric-oxide synthase activation. *J Biol Chem.* (2011) 286:33134–40. doi: 10.1074/jbc.M111.274100
15. Galiè N, Humbert M, Vachiery JL, Bibbs S, Lang I, Torbicki A, et al. 2015 ESC/ERS Guidelines for the diagnosis and treatment of pulmonary hypertension: the joint task force for the diagnosis and treatment of pulmonary hypertension of the european society of cardiology (ESC) and the european respiratory society (ERS): endorsed by: association for european paediatric and congenital cardiology (AEPC), international society for heart and lung transplantation (ISHLT). *Eur Repir J.* (2015) 46:903–75. doi: 10.1183/13993003.01032-2015
16. Bandeira Sde M, Guedes Gda S, da Fonseca LJ, Pires AS, Gelain DP, Moreira JC, et al. Characterization of blood oxidative stress in type 2 diabetes mellitus patients: increase in lipid peroxidation and sod activity. *Oxid Med Cell Longev.* (2012) 2012:819310. doi: 10.1155/2012/819310
17. Dong X, Li D, Liu H, Zhao Y. Sod3 and enos genotypes are associated with sod activity and nox. *Exp Ther Med.* (2014) 8:328–34. doi: 10.3892/etm.2014.1720
18. Morrison D, Hughes J, Della Gatta PA, Mason S, Lamon S, Russell AP, et al. Vitamin C and E supplementation prevents some of the cellular adaptations to endurance-training in humans. *Free Radic Biol Med.* (2015) 89:852–62. doi: 10.1016/j.freeradbiomed.2015.10.412
19. Lu Z, Xu X, Hu X, Zhang P, vanDell ED, French JP, et al. Extracellular superoxide dismutase deficiency exacerbates pressure overload-induced left ventricular hypertrophy and dysfunction. *Hypertension.* (2008) 51:19–25. doi: 10.1161/HYPERTENSIONAHA.107.098186
20. Anwar A, Ruffenach G, Mahajan A, eEghbali M, Umar S. Novel biomarkers for pulmonary arterial hypertension. *Respir Res.* (2016) 17:88. doi: 10.1186/s12931-016-0396-6
21. Wedgwood S, Lakshminrusimha S, Fukai T, Russell JA, Schumacker PT, Steinhorn RH. Hydrogen peroxide regulates extracellular superoxide dismutase activity and expression in neonatal pulmonary hypertension. *Antioxid Redox Signal.* (2011) 15:1497–506. doi: 10.1089/ars.2010.3630
22. Zelko IN, Folz RJ. Regulation of oxidative stress in pulmonary artery endothelium. modulation of extracellular superoxide dismutase and NOX4 expression using histone deacetylase class I inhibitors. *Am J Respir Cell Mol Biol.* (2015) 53:513–24. doi: 10.1165/rcmb.2014-0260OC
23. Boucherat O, Potus F, Bonnet S. microRNA and pulmonary hypertension. *Adv Exp Med Biol.* (2015) 888:237–52. doi: 10.1007/978-3-319-22671-2_12
24. Archer SL. Acquired mitochondrial abnormalities, including epigenetic inhibition of superoxide dismutase 2, in pulmonary hypertension and cancer: therapeutic implications. *Adv Exp Med Biology.* (2016) 903:29–53. doi: 10.1007/978-1-4899-7678-9_3
25. Aldred MA, Comhair SA, Varella-Garcia M, Asosingh K, Xu W, Noon GP, et al. Somatic chromosome abnormalities in the lungs of patients with pulmonary arterial hypertension. *Am J Respir Crit Care Med.* (2010) 182:1153–60. doi: 10.1164/rccm.201003-0491OC
26. Zhang R, Wang XJ, Zhang HD, Sun XQ, Zhao QH, Wang L, et al. Profiling nitric oxide metabolites in patients with idiopathic pulmonary arterial hypertension. *Eur Respir J.* (2016) 48:1386–95. doi: 10.1183/13993003.00245-2016
27. Pinto A, Immohr MB, Jahn A, Jenke A, Boeken U, Lichtenberg A, et al. The extracellular isoform of superoxide dismutase has a significant impact on cardiovascular ischaemia and reperfusion injury during cardiopulmonary bypass. *Eur J Cardiothorac Surg.* (2016) 50:1035–44. doi: 10.1093/ejcts/ezw216
28. Nozik-Grayck E, Suliman HB, Majka S, Albietz J, Van-Rheen Z, Roush K, et al. Lung ec-sod overexpression attenuates hypoxic induction of egr-1 and chronic hypoxic pulmonary vascular remodeling. *Am J Physiol Lung Cell Mol Physiol.* (2008) 295:L422–30. doi: 10.1152/ajplung.90293.2008
29. Fattman CL, Schaefer LM, Oury TD. Extracellular superoxide dismutase in biology and medicine. *Free Radic Biol Med.* (2003) 35:236–56. doi: 10.1016/S0891-5849(03)00275-2
30. Stralin P, Karlsson K, Johansson BO, Marklund SL. The interstitium of the human arterial wall contains very large amounts of extracellular superoxide dismutase. *Arterioscler Thromb Vasc Biol.* (1995) 15:2032–6. doi: 10.1161/01.ATV.15.11.2032
31. Wolin MS. Interactions of oxidants with vascular signaling systems. *Arterioscler Thromb Vascu Biol.* (2000) 20:1430–42. doi: 10.1161/01.ATV.20.6.1430
32. Lakshminrusimha S, Russell JA, Wedgwood S, Gugino SF, Kazzaz JA, Davis JM, et al. Superoxide dismutase improves oxygenation and reduces oxidation in neonatal pulmonary hypertension. *Am J Respir Crit Care Med.* (2006) 174:1370–7. doi: 10.1164/rccm.200605-676OC
33. Brown DI, Griendling KK. Regulation of signal transduction by reactive oxygen species in the cardiovascular system. *Cir Res.* (2015) 116:531–49. doi: 10.1161/CIRCRESAHA.116.303584
34. Gheddouchi S, Mokhtari-Soulimane N, Merzouk H, Bekhti F, Soulimane F, Guermouche B, et al. Low sod activity is associated with overproduction of peroxynitrite and nitric oxide in patients with acute coronary syndrome. *Nitric Oxide.* (2015) 49:40–6. doi: 10.1016/j.niox.2015.05.007
35. Mohammedi K, Bellili-Munoz N, Marklund SL, Driss F, Le-Nagard H, Patente TA, et al. Plasma extracellular superoxide dismutase concentration, allelic variations in the sod3 gene and risk of myocardial infarction and all-cause

mortality in people with type 1 and type 2 diabetes. *Cardiovasc Diabetol.* (2015) 14:845. doi: 10.1186/s12933-014-0163-2
36. Chu Y, Alwahdani A, Iida S, Lund DD, Faraci FM, Heistad DD. Vascular effects of the human extracellular superoxide dismutase R213g variant. *Circulation.* (2005) 112:1047–53. doi: 10.1161/CIRCULATIONAHA.104.531251
37. Juul K, Tybjaerg-Hansen A, Marklund S, Heegaard NH, Steffensen R, Sillesen H, et al. Genetically reduced antioxidative protection and increased ischemic heart disease risk: the copenhagen city heart study. *Circulation*. (2004) 109:59–65. doi: 10.1161/01.CIR.0000105720.28086.6C
38. Marklund SL, Nilsson P, Israelsson K, Schampi I, Peltonen M, Asplund K. Two variants of extracellular-superoxide dismutase: Relationship to cardiovascular risk factors in an unselected middle-aged population. *J Intern Med.* (1997) 242:5–14. doi: 10.1046/j.1365-2796.1997.00160.x
39. Ito Y, Nakachi K, Imai K, Hashimoto S, Watanabe Y, Inaba Y, et al. Stability of frozen serum levels of insulin-like growth factor-i, insulin-like growth factor-ii, insulin-like growth factor binding protein-3, transforming growth factor beta, soluble fas, and superoxide dismutase activity for the jacc study. *J Epidemiol.* (2005) 15 (Suppl. 1): S67–73. doi: 10.2188/jea.15.S67

Conflict of Interest: The authors declare that the research was conducted in the absence of any commercial or financial relationships that could be construed as a potential conflict of interest.

Copyright © 2020 Zhang, Wang, Zhao, Jiang, Gong, Jiang, Xu, He, Li and Jing. This is an open-access article distributed under the terms of the Creative Commons Attribution License (CC BY). The use, distribution or reproduction in other forums is permitted, provided the original author(s) and the copyright owner(s) are credited and that the original publication in this journal is cited, in accordance with accepted academic practice. No use, distribution or reproduction is permitted which does not comply with these terms.

frontiers in Medicine

ORIGINAL RESEARCH
published: 04 December 2020
doi: 10.3389/fmed.2020.577609

COVID-19 Chest Computed Tomography to Stratify Severity and Disease Extension by Artificial Neural Network Computer-Aided Diagnosis

Alysson Roncally S. Carvalho[1,2,3], Alan Guimarães[2], Gabriel Madeira Werberich[4], Stephane Nery de Castro[5,6], Joana Sofia F. Pinto[7], Willian Rebouças Schmitt[7], Manuela França[7,8], Fernando Augusto Bozza[6,9], Bruno Leonardo da Silva Guimarães[10], Walter Araujo Zin[3] and Rosana Souza Rodrigues[4,9]*

[1] UnIC, Faculty of Medicine, Cardiovascular R&D Center, Centro Hospitalar Universitário Do Porto (CHUP), Porto University, Porto, Portugal, [2] Laboratory of Pulmonary Engineering, Biomedical Engineering Program, Alberto Luiz Coimbra Institute of Post-Graduation and Research in Engineering, Universidade Federal do Rio de Janeiro, Rio de Janeiro, Brazil, [3] Laboratory of Respiration Physiology, Carlos Chagas Filho Institute of Biophysics, Universidade Federal do Rio de Janeiro, Rio de Janeiro, Brazil, [4] Department of Radiology, Universidade Federal do Rio de Janeiro, Rio de Janeiro, Brazil, [5] Hospital Barra D'Or, Rio de Janeiro, Brazil, [6] National Institute of Infectious Disease, Oswaldo Cruz Foundation (INI/Fiocruz), Rio de Janeiro, Brazil, [7] Radiology Department, Centro Hospitalar Complexo Universitário Do Porto (CHUP), Porto, Portugal, [8] Instituto de Ciências Biomédicas Abel Salazar (ICBAS), Porto University, Porto, Portugal, [9] IDOR - D'Or Institute for Research and Education, Rio de Janeiro, Brazil, [10] Hospital Niterói D'Or, Rio de Janeiro, Brazil

OPEN ACCESS

Edited by:
Rifat Hamoudi, University of Sharjah, United Arab Emirates

Reviewed by:
Don Sin, University of British Columbia, Canada
Rafael López-González, University of Valencia, Spain

***Correspondence:**
Alysson Roncally S. Carvalho
roncally.carvalho@gmail.com

Specialty section:
This article was submitted to Pulmonary Medicine, a section of the journal Frontiers in Medicine

Received: *29 June 2020*
Accepted: *30 October 2020*
Published: *04 December 2020*

Citation:
Carvalho ARS, Guimarães A, Werberich GM, de Castro SN, Pinto JSF, Schmitt WR, França M, Bozza FA, Guimarães BLdS, Zin WA and Rodrigues RS (2020) COVID-19 Chest Computed Tomography to Stratify Severity and Disease Extension by Artificial Neural Network Computer-Aided Diagnosis. Front. Med. 7:577609. doi: 10.3389/fmed.2020.577609

Purpose: This work aims to develop a computer-aided diagnosis (CAD) to quantify the extent of pulmonary involvement (PI) in COVID-19 as well as the radiological patterns referred to as lung opacities in chest computer tomography (CT).

Methods: One hundred thirty subjects with COVID-19 pneumonia who underwent chest CT at hospital admission were retrospectively studied (141 sets of CT scan images). Eighty-eight healthy individuals without radiological evidence of acute lung disease served as controls. Two radiologists selected up to four regions of interest (ROI) per patient (totaling 1,475 ROIs) visually regarded as well-aerated regions (472), ground-glass opacity (GGO, 413), crazy paving and linear opacities (CP/LO, 340), and consolidation (250). After balancing with 250 ROIs for each class, the density quantiles (2.5, 25, 50, 75, and 97.5%) of 1,000 ROIs were used to train (700), validate (150), and test (150 ROIs) an artificial neural network (ANN) classifier (60 neurons in a single-hidden-layer architecture). Pulmonary involvement was defined as the sum of GGO, CP/LO, and consolidation volumes divided by total lung volume (TLV), and the cutoff of normality between controls and COVID-19 patients was determined with a receiver operator characteristic (ROC) curve. The severity of pulmonary involvement in COVID-19 patients was also assessed by calculating Z scores relative to the average volume of parenchymal opacities in controls. Thus, COVID-19 cases were classified as mild (<cutoff of normality), moderate (cutoff of normality $\leq$ pulmonary involvement $<$ Z score 3), and severe pulmonary involvement (Z score $\geq$3).

Results: Cohen's kappa agreement between CAD and radiologist classification was 81% (79–84%, 95% CI). The ROC curve of PI by the ANN presented a threshold of 21.5%, sensitivity of 0.80, specificity of 0.86, AUC of 0.90, accuracy of 0.82, *F* score of 0.85, and 0.65 Matthews' correlation coefficient. Accordingly, 77 patients were classified as having severe pulmonary involvement reaching 55 ± 13% of the TLV (*Z* score related to controls ≥3) and presented significantly higher lung weight, serum C-reactive protein concentration, proportion of hospitalization in intensive care units, instances of mechanical ventilation, and case fatality.

Conclusion: The proposed CAD aided in detecting and quantifying the extent of pulmonary involvement, helping to phenotype patients with COVID-19 pneumonia.

Keywords: COVID-19 pneumonia, radiomics, computer-aided diagnosis, deep learning, quantitative chest CT-analysis

INTRODUCTION

Chest computed tomography (CT) has been widely used to assess COVID-19 pneumonia and is a key tool for the detection of lung abnormalities and for evaluating the extension and severity of pulmonary involvement (PI) (1, 2).

Patients with COVID-19 usually exhibit radiological patterns classified as ground-glass opacity (GGO), crazy paving (CP), linear opacities (LO), and consolidation (1, 2). Reticular opacities (RO), characterized by coarse linear, curvilinear opacities, fibrotic streaks, and subpleural lines, may be seen in late phases, often associated with GGO and parenchymal distortion (1, 3, 4).

Some attempts have been made to achieve an automatic quantification of PI in chest CT, most of them based on texture analysis techniques. Classic statistical methods may include the parameters of first-, second-, and third-order statistics and other composite or custom-made texture parameters (5–7). Their disadvantages include the extensive training required before automated or semiautomated segmentation, evaluation of the potential usefulness of a particular parameter only after implementation, and cumbersome and time-consuming adaptation to new segmentation tasks.

In the present study, we propose a method for objective and automated quantification and classification of COVID-19-related pneumonia from chest CT using a simple computer-aided diagnosis (CAD) system, considering the different radiological CT lung patterns commonly used in clinical practice. Determining the quantity, type, and distribution of abnormalities by an automated tool should prove helpful in clinical practice by aiding in noninvasive diagnostic determination, detecting change in disease over symptom onset, and stratifying the risk of hospitalization in the intensive care unit (ICU), the necessity of mechanical ventilation, or case fatality.

MATERIALS AND METHODS

Study Design and Patients

One hundred thirty consecutive patients with COVID-19, confirmed with reverse-transcription polymerase chain reaction (RT-PCR) for COVID-19 in nasal-pharyngeal swab, admitted to three hospitals between April to June 2020, who underwent chest CT scans and presented with pneumonia, were retrospectively studied. Ten patients underwent more than one CT scan, totaling to 141 scans. The chest CTs of 88 healthy subjects served as controls. Scans with severe motion artifacts and contrast-enhanced scans were excluded. **Figure 1** shows the patient enrollment and CT scan selection flow chart.

The Research Ethics Committee approved the study that complied with the current national and international standards.

Clinical and Laboratory Data, Definitions, and Outcomes

The clinical and laboratory findings of each patient were recorded at admission. CT was performed within 12 h after the clinical evaluation and laboratory findings.

Serum C-reactive protein concentration collected at the admission was used as a marker of systemic inflammation. ICU admission, invasive ventilation, and in-hospital case fatality were considered as our clinical outcomes.

Chest Computed Tomography Acquisition

CT scans were performed on a 64-channel multislice (Brilliance 40 scanner, Philips Medical Systems, Cleveland, OH, USA, and General Electrics Lightspeed VCT, Chicago, IL, USA), a 128-channel multislice dual-source CT system (Somatom Definition Flash, Siemens, Forchheim, Germany), or a 16-channel multislice (Emotion 16 CT, Siemens, Erlangen, Germany). The acquisitions were gathered with the patients in supine position with 120 kV and 120–300 mA, slice thickness ranging from 1 to 2 mm with 50% superposition, and 512 × 512, 768 × 768, or 1,024 × 1,024 voxels matrix.

Reconstruction algorithms were B50f (49 subjects), B60f (1), B70s (17), C (1), FC13 (5), FC86 (2), I50f2 (1), L (80), LUNG (69), and SOFT (4), depending on the CT manufacture.

Lung and Airway Segmentation

The lung parenchyma and the airways were segmented from chest CT scans using the Region Growing algorithm using

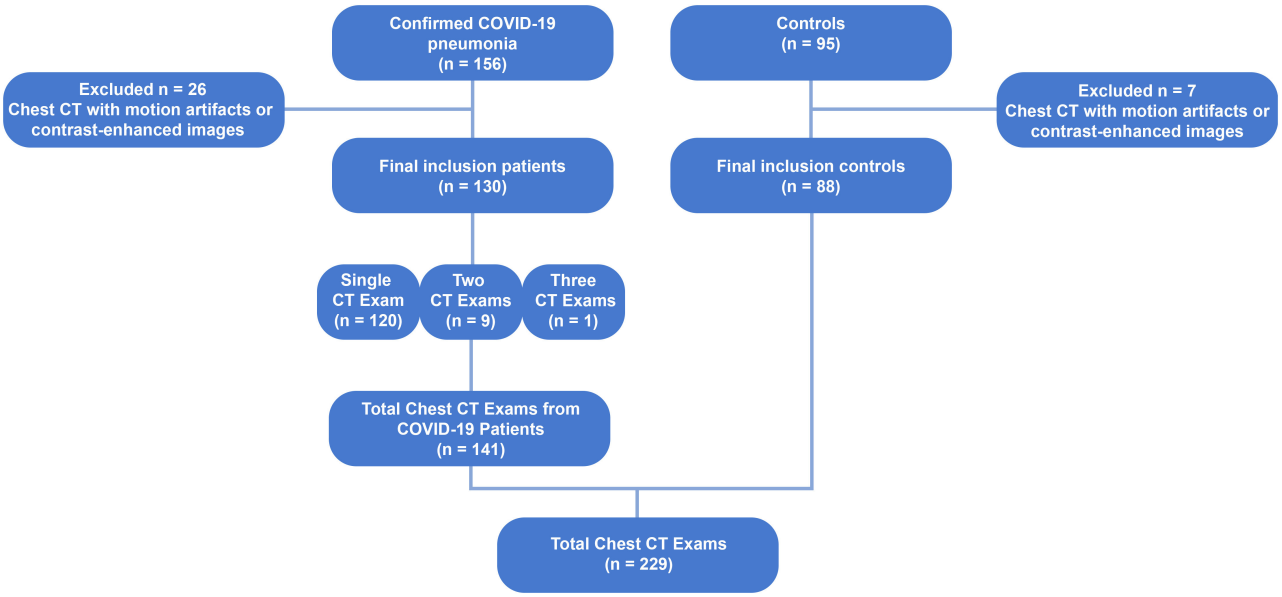

FIGURE 1 | Flow chart diagram showing the patient enrollment and computed tomography selection process. CT, computed tomography; COVID-19, corona virus disease-19; RT-PCR, reverse-transcription polymerase chain reaction.

the module Chest Imaging Platform (3D Slicer version 4.8.1). Then, the region of interest (ROI) selected by the algorithm was edited by visual inspection (8). Thereafter, all images were exported to an in-house-developed software (Quantitative Lung Image, QUALI) written in MATLAB® (MathWorks®, Natick, MA, USA), and airways were subtracted from the lung ROI.

Image Rescaling

After segmentation, CT images were rescaled so that images from different CT scans could be comparable. For that purpose, a circular ROI was positioned outside the body of the individuals (HU_{Air}) and another, with the same shape and area, was positioned in the descending aorta (HU_{Aorta}).

Then, the average density value present within both ROIs was calculated, and a linear regression was performed, using the least squares method, using the mean HU_{Air} and HU_{Aorta} values as dependent variables and −1,000 and +50 HU, respectively, as independent variables. Scaling was performed by multiplying all voxels present in the lung parenchyma by the angular coefficient together with the addition of the intercept (9, 10). Both the selection of the ROIs and the scaling of the voxels were carried out using QUALI Software.

Visual Classification of Radiological Patterns in COVID-19 CT Scans

Two chest radiologists blinded to patient identification, clinical data, and outcomes independently selected up to four ROI per COVID-19 patient visually classified as well-aerated regions, GGO, CP/LO, and consolidation. The ROI consisted of a circle with a fixed radius of 4 mm, with a spanning area of about 30 voxels in each CT section.

Development of the Supervised Neural Network Architecture

From all ROIs belonging to the same radiological pattern class, a density histogram was calculated, and the respective quantiles (2.5, 25, 50, 75, and 97.5%) were used to train a supervised artificial neural network (ANN). Initially, the number of ROIs consensually assigned to well-aerated regions (472 ROIs), GGO (413 ROIs), CP/LO (340 ROIs), and consolidation (250 ROIs), totaling 1,475 ROIs, were balanced by the lowest number of ROIs (250 ROIs). Thus, 1,000 ROIs were used for ANN training (700 ROIs), validation (150 ROIs), and test (150 ROIs). In order to keep the same ROIs for ANN architecture assessment, ROIs were drawn to undergo training, validation, and test only once since the same groups were used in each training, validation, and test session. No feature scale was necessary since all data are expressed in the same scale in Hounsfield units and the training algorithm used the scaled conjugate gradient backpropagation (11). The training stopped when the validation error increased for six iterations, and the best validation performance was obtained based on the minimization of the cross-entropy.

Several architectures were tested with a single hidden layer with 20 up to 100 neurons. The overall and intraclass agreement of the balanced test confusion matrix between each respective ROI quantile consensually classified by radiologists and by the ANN classifier was assessed and used to define the best ANN architecture.

To evaluate the ANN classifier's final performance, the confusion matrix, the receiver operator characteristic (ROC)

curve for each class, and the relationship between cross-entropy and ANN epochs in training, validation, and test sets were assessed.

Having established the qualitative equivalence of ANN classifier and expert groupings, all results were verified with expert visual validation (**Figure 2**). Additionally, a grid of regular hexagons with radii of 2, 3, and 4 mm, accounting for 12 up to 42 voxels, was created. In the overlapping region of each radiologist ROI and hexagons (**Figure 2C**), the local histogram quantiles were computed from the voxels contained in the hexagon and served as an impute to ANN classifier. The best hexagon dimension was computed with the unweighted Cohen's kappa test between the ANN classification and their respective ROI classification attributed by the radiologist. In the assessment of the overlapped regions by radiologist's ROI, if there were hexagons belonging to different classes into a given ROI, the most prevalent classification would be used as the final classification of the voxels for comparison purposes (**Figure 2D**).

CT Scan Quantitative Analysis and CAD Report

The previously defined regular hexagon grid was used to group voxels in the whole-lung CT scan. The number of voxels belonging to each of the parenchymal classes was calculated across the whole lungs. The voxels identified as vessels were included as normal to account for the total lung volume.

Total lung volume (TLV), i.e., the sum of air plus tissue volume, was calculated as:

$$\begin{aligned} \text{TLV(ml)} &= (\text{pixel size})^2 \times \text{slice thickness} \\ &\times \text{total number of pixels of the whole lung} \end{aligned} \quad (1)$$

Lung weight, in grams, was calculated as:

$$\begin{aligned} \text{Lung weight (g)} &= [(\text{HU} - \text{HU}_{\text{Air}})/(\text{HU}_{\text{Aorta}} - \text{HU}_{\text{Air}})] \\ &\times \text{voxel volume} \times 1.04\ \text{g/ml} \end{aligned} \quad (2)$$

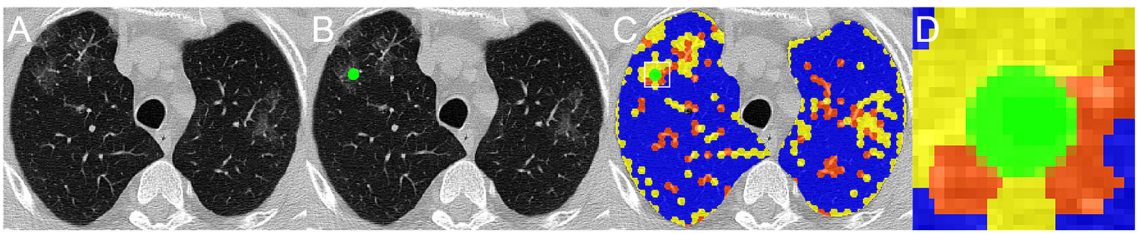

FIGURE 2 | A representative CT scan axial image of a COVID-19 patient **(A)**, the region of interest (ROI), in green, classified by one radiologist as ground glass opacities (GGO) **(B)**, and the overlapping of radiologist's ROI and the grid of regular hexagons with radii of 4 mm **(C)**, with each grid already classified as well-aerated regions (blue), GGO (yellow), and CP/LO (orange) areas. **(D)** Amplification of the overlapped region marked with the white square in **(C)**. Note that, within ROI, there are voxels of two different classes, GGO in yellow and CP/LO in orange. For comparison purposes, the ROI region is classified as the most prevalent voxel class, in this case as GGO class.

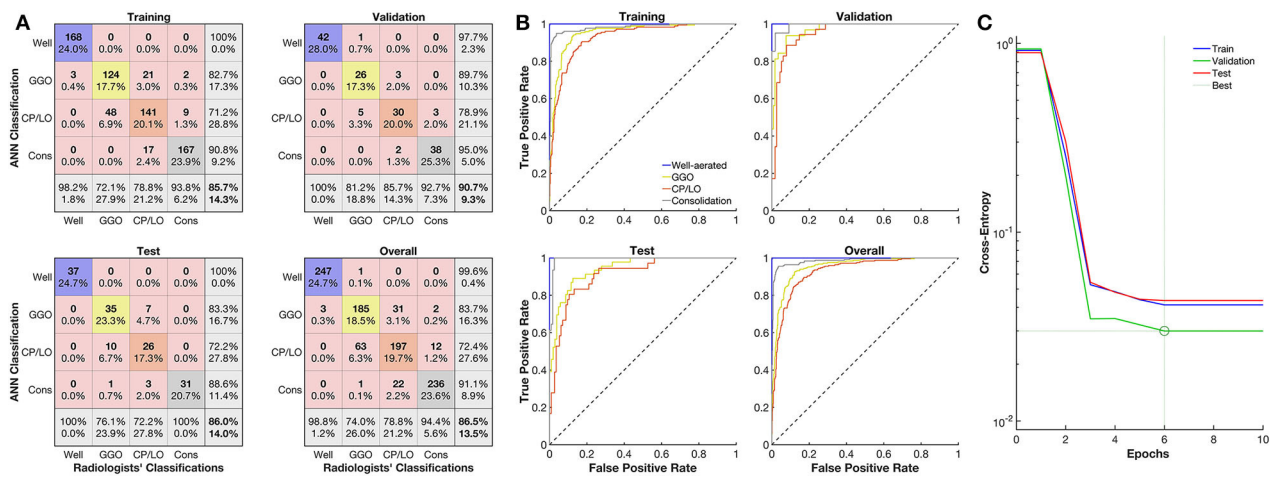

FIGURE 3 | Evaluation of the artificial neural network (ANN) classifier performance. **(A)** Confusion matrix from the comparison between the ANN and radiologists' classification of well-aerated (blue line), ground glass opacities (GGO, yellow line), CP/LO (orange), and consolidation (gray) in training (first row and column), validation (first row, second column), test (second row, first column), and overall (second row, second column) sets. **(B)** Each respective receiver operator characteristic curve for well-aerated regions (blue line), GGO (yellow line), CP/LO (orange) and consolidation (gray) ANN classification in training (first row and column), validation (first row, second column), test (second row, first column), and overall (second row, second column) sets. **(C)** Cross-entropy at each epoch in training (blue line), validation (green line), and test (red line) sets. Dotted lines represent the best validation performance determined based on the minimization of the cross-entropy at epoch 6.

where 1.04 mg/ml means lung tissue density, and HU is voxel density in HU scale (9).

Determination of PI

After CAD classification of parenchymal opacities, the extent of PI was calculated as the cumulative volumetric sum of GGO, CP/LO, and consolidation adjusted to TLV.

The threshold of parenchymal opacities between controls and COVID-19 was determined with a ROC curve from the histogram of parenchymal opacities in the control group and COVID-19 patients. The area under the ROC curve (AUC) was calculated, and the threshold sensibility, specificity, accuracy, positive and negative predictive values, *F* score (a measure of ANN's precision and recall balance), and Matthews correlation coefficient were also computed.

To evaluate the severity of PI in COVID-19, we used the *Z* score in relation to the average volume of lung parenchyma opacities in the control group. Thus, the *Z* score was used to describe the position of the calculated volume of pneumonia in COVID-19 patients in terms of its distance from the mean calculated volume of GGO plus CP/LO and consolidation in the control group. This distance is expressed in terms of standard deviation units. Accordingly, the *Z* score of COVID-19 patients is positive if the value lies above the mean volume of GGO, CP/LO, and consolidation in the control group and negative if it lies below it.

Thereafter, patients with COVID-19 were classified as having mild (PI $<$ ROC threshold), moderate (ROC threshold $\leq$ PI $<$ 3 *Z* score), or severe (PI $\geq$ 3 *Z* score) PI.

Statistical Analysis

The normality of the data (Kolmogorov–Smirnov test with Lilliefors' correction) and the homogeneity of variances (Levene median test) were tested. Since both conditions were always satisfied, all data are presented as mean and standard deviation.

A one-way ANOVA test followed by Bonferroni's *post hoc* test assessed the statistical differences among patients with mild, moderate, and severe COVID-19 pneumonia. A p-value < 0.05 was defined as statistically significant. All statistical analyses were performed using Matlab® software (MathWorks®, Natick, MA, USA).

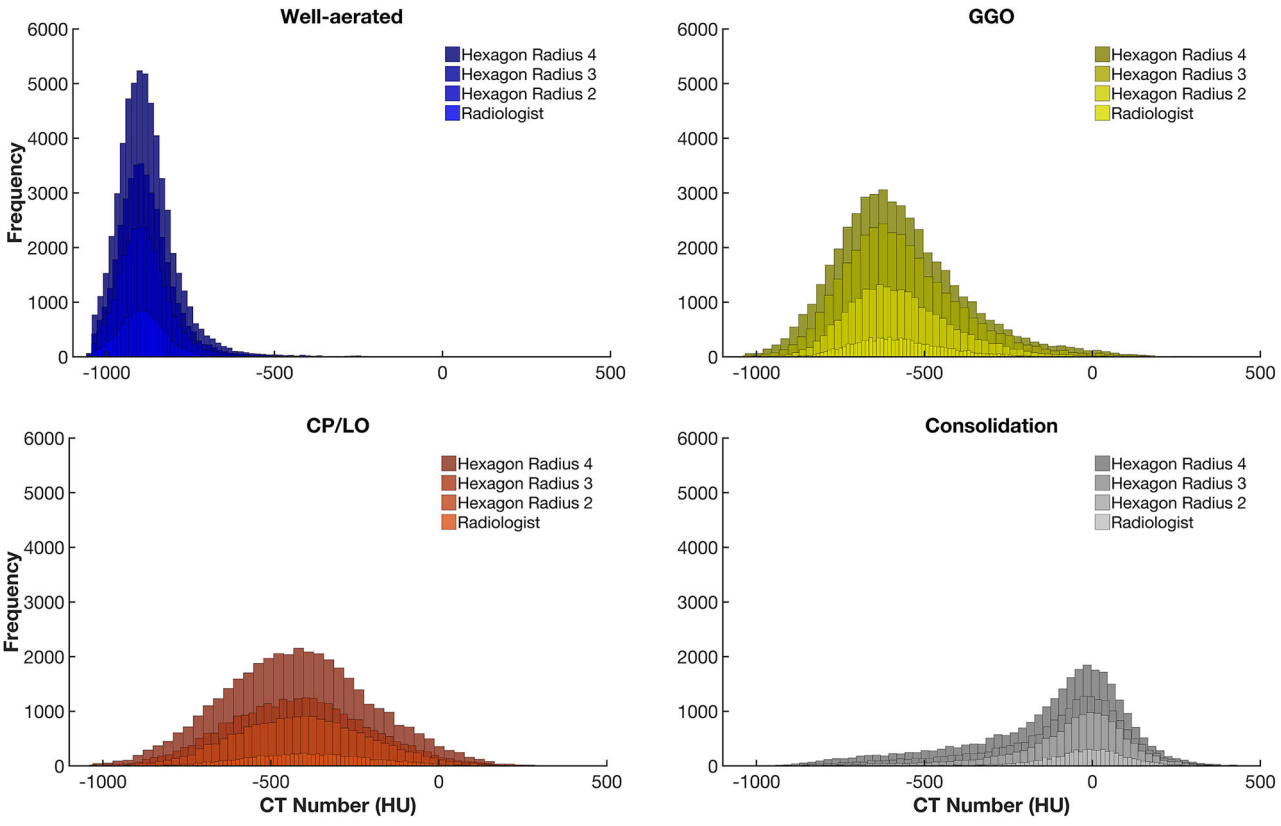

FIGURE 4 | Frequency histograms of the densities expressed in Hounsfield units from all regions of interest visually assigned as well-aerated regions (colored in blue), ground glass opacities (GGO, yellow), crazy paving and linear opacities (CP/LO, orange), and consolidation (light gray). Note that, with the increase in the radius of the regular hexagon, there is an increase in the number of voxels and that, although there is no significant change in the average density values, there is an important increase in the dispersion of voxel densities. This appears to contribute to a reduction in the artificial neural network classifier performance.

RESULTS

The ANN architecture with a single hidden layer of 60 neurons showed the best agreement in the confusion test matrix among the other architectures tested, with an overall agreement of 86% being 100% for well-aerated regions, 76% for GGO, 72% for CP/LO, and 100% for consolidation (**Figure 3A**). The architecture with 40 and 100 neurons presented overall agreements of 66 and 74%, respectively. Despite that the architecture with 20 and 80 neurons presented a similar overall agreement, a reduction in the agreement of well-aerated regions (from 100 to 98 and 95%) and consolidation (from 100 to 95 and 94%) was observed in 60-, 80-, and 20-neuron architectures, respectively. No improvement in the performance of the ANN classifier was observed with the addition of a second neuron layer.

TABLE 1 | Agreement between all (1,475) consensual radiologists' regions of interest (columns) and the supervised neural network (ANN) classifier with the regular hexagon grid of radii 2 (rows) for the 1,000 ROIs used to train, test, and validate Quantitative Lung Image Deep Learning software.

		Consensual radiologists' classification			
		Well aerated	**GGO**	**CP/LO**	**Consolidation**
ANN classifier	Well aerated	**464 (98%)**	1	0	0
	GGO	7	**335 (81%)**	68	2
	CP/LO	1	76	**239 (70%)**	16
	Consolidation	0	1	33	**232 (93%)**

The overall strength of agreement as evaluated by Cohen's kappa test was 81% (79–84%, 95% CI). Data between parentheses are the agreement for each radiological pattern. Bold values represent concordance between consensus radiology and ANN classifier.

The ROC curve from each radiological pattern is presented in **Figure 3B**. The classifier performance was much better for well-aerated regions and consolidation, with an AUC of 1.00 and 0.99, respectively. The performance for GGO and CP/LO, despite being lower, was quite acceptable with an AUC of 0.94 and 0.91, respectively. The best validation performance occurred at epoch 6 (**Figure 3C**).

The CT density histogram of ROIs visually assigned as well-aerated regions, GGO, CP/LO, and consolidation in COVID-19 patients is depicted in **Figure 4**. Additionally, the histograms from overlapped regions with regular hexagons with radii of 2, 3, and 4 mm are also presented. The best overall agreement between the neural network and the radiologists' ROIs occurred with the 2-mm-radius hexagon with an unweighted Cohen's kappa of 81% (79–84%, 95% CI) when compared to the hexagons of 3-mm radius (76%, 79–84%, 95% CI) and 4-mm radius (72%, 79–84%, 95% CI). Thus, the 2-mm-radius hexagon presented an agreement of 98% for well-aerated regions, 81% for GGO, 70% for CP/LO, and 93% for consolidation (**Table 1**).

Figure 5A presents the histogram of parenchymal opacities in controls and COVID-19 patients. Accordingly, the ROC curve determined an optimal threshold of 21.5%, with sensitivity of 0.80, specificity of 0.86, AUC of 0.90, accuracy of 0.82, *F* score of 0.85, and Matthews' correlation coefficient of 0.65 (**Figure 5B**).

In controls, the volume related to all parenchymal opacities was 16 ± 6%, with being 12 ± 6% classified as GGO, 3 ± 1% as CP/LO, and 1 ± 0.3% as consolidation that represent small bronchi and peribronchial vessels and possible partial volume effects of pleural or diaphragm interfaces as can be seen in **Figure 6** (uppermost panels).

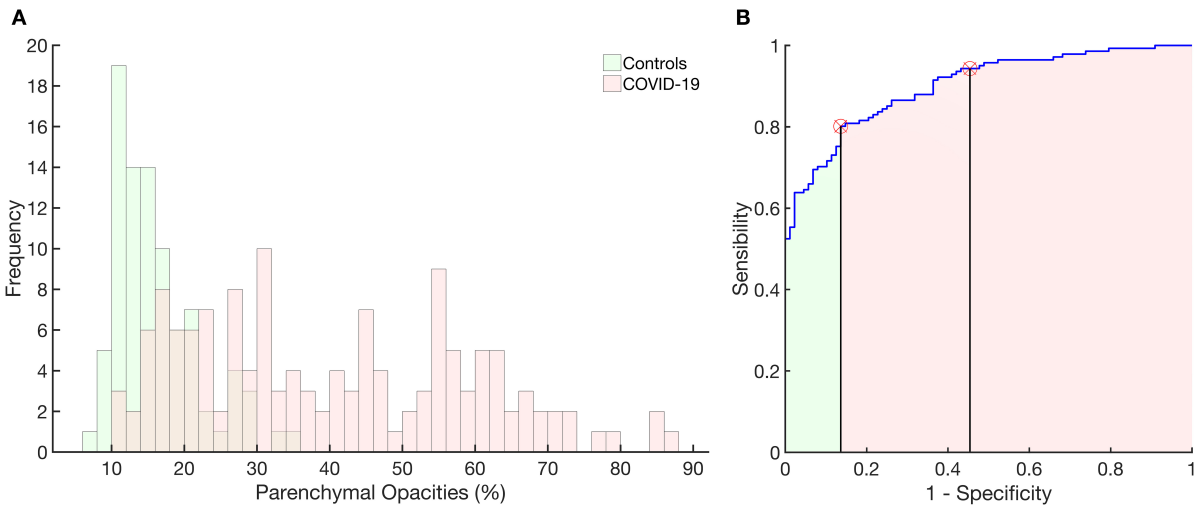

FIGURE 5 | Histograms of the frequency of occurrence of parenchymal opacities in the control group (light green) and in patients with COVID-19 (pink). Right panel: receiver operator characteristic curve with the area under the curve (AUC) hatched in light green and pink. The vertical lines mark the normality cutoff (equivalent to 21% of total lung volume represented by pulmonary opacities) and the Z score = 3 (equivalent to 33% of the total lung volume and used to classify SSc patients as with severe pulmonary involvement). Between the normality cutoff up to Z score < 3, COVID-19 patients were classified as with moderate pulmonary involvement. The use of parenchymal opacities as an indicator of pulmonary involvement presented 0.80 sensitivity, 0.86 specificity, with an AUC of 0.90, accuracy of 0.82, 0.90 positive predictive value and 0.73 negative predictive value, *F* score of 0.85, and Matthews correlation coefficient of 0.65.

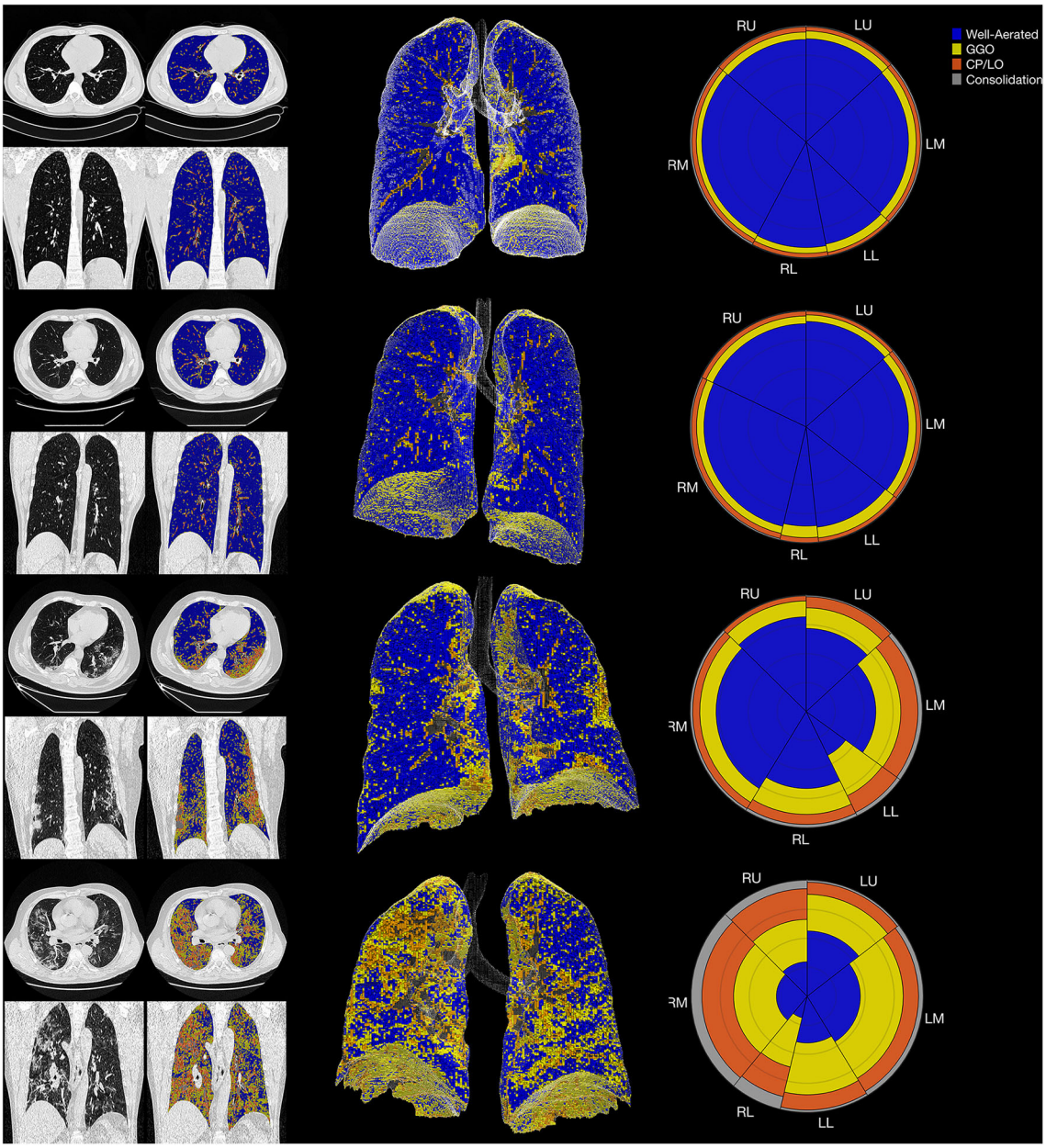

FIGURE 6 | The summary glyph (right column) to the underlying 3D scan data (middle column) and CT images in axial and coronal slices (left column) in a representative case from the control group (row A) and COVID-19 with mild (row B), moderate (row C), and severe (row D) pneumonia involvement. In the glyph (right column), the first letter (R/L) indicates the right and left lung, the second letter (U/M/L) denotes, respectively, the upper, middle, and lower lung zones.

The final CAD reports from four representative subjects (control, mild, moderate, and severe COVID-19 PI) are presented in **Figure 6**.

Seventy-seven chest CT images of COVID-19 patients were classified as presenting severe PI (55 ± 13% of the TLV with GGO + CP/LO + consolidation), while 36 (25%) and 28 (20%) were classified as just moderate (27 ± 4%) or mild (17 ± 3%) (**Table 2**). In patients with severe PI, pneumonia was mainly characterized by GGO (35 ± 10%) and CP/LO (14 ± 7%) with just 5 ± 4% of the TLV being assigned as consolidation. Furthermore, the degree of PI was fairly different from that observed in patients with moderate or mild PI ($p < 0.001$) (**Table 2**).

COVID-19 patients classified as having a severe PI were older than those with mild PI (65 ± 16 vs. 54 ± 17 years, respectively) and presented a significant reduction in TLV (3,639 ± 931 vs. 4,890 ± 704 in moderate and 5,247 ± 1,067 ml in mild COVID-19 pneumonia), significant increase in lung weight (1,037 ± 251 vs. 935 ± 143 and 799 ± 159 g, respectively), and higher serum

TABLE 2 | COVID-19 and controls demographic and computer-aided diagnosis (CAD) quantitative data, laboratory parameters and clinical outcomes.

	COVID-19 *N* = 130			Controls *N* = 88	*P* value
	Severe *N* = 71	Moderate *N* = 32	Mild *N* = 27		
Demographic data					
Sex (male/female)	51/20	20/12	16/11	24/64	
Age (years)	65 ± 16	58 ± 15	54 ± 17	59 ± 21	0.006[b]
BMI (kg/m^2)	28 ± 5	29 ± 5	27 ± 5	26 ± 4	
CAD data*	N = 77	N = 36	N = 28		
Total lung volume (ml)	3,639 ± 931	4,905 ± 782	5,266 ± 1,030	4,411 ± 1,035	<0.001[a,b]
Lung weight (g)	1,037 ± 251	928 ± 151	795 ± 152	628 ± 166	<0.001[b] 0.03[a,c]
Pulmonary involvement (%)	55 ± 13	27 ± 4	17 ± 3	16 ± 6	<0.001[a,b,c]
Well aerated (%)	45 ± 13	73 ± 4	83 ± 3	84 ± 6	<0.001[a,b,c]
GGO (%)	35 ± 10	20 ± 3	11 ± 3	12 ± 6	<0.001[a,b,c]
CP/LO (%)	14 ± 7	6 ± 2	4 ± 1	3 ± 1	<0.001[a,b]
Consolidation (%)	5.0 ± 4	1.5 ± 0.5	1.0 ± 0.2	1.0 ± 0.3	<0.001[a,b]
Laboratory data	N = 71	N = 32	N = 27		
White blood count (×10^3/μl)	6.4 ± 3.0	4.4 ± 1.9	5.6 ± 1.5	–	0.002[a]
Lymphocytes count (×10^3/μl)	1.2 ± 1.1	1.0 ± 0.7	1.3 ± 0.6	–	
Lactate dehydrogenase (U/L)	334 ± 161	260 ± 159	266 ± 112	–	
CRP (mg/L)	64 ± 80	23 ± 74	4 ± 5	–	0.03[a] <0.001[b]
GOT (U/L)	44 ± 30	34 ± 22	33 ± 21	–	
GPT (U/L)	41 ± 33	37 ± 33	31 ± 28	–	
Creatinine (mg/dl)	1.0 ± 0.4	1.2 ± 1.6	1.0 ± 0.3	–	
Clinical outcome	N = 71	N = 32	N = 27		
Symptom onset (days)	7.7 ± 4.6	5.1 ± 3.4	6.0 ± 4.4		0.015[a]
ICU (%)	27%	19%	22%	–	
i-MV (%)	14%	9%	15%	–	
Case fatality (%)	11%	6%	0%		

[a]*Severe vs. moderate.*
[b]*Severe vs. mild.*
[c]*Moderate vs. mild.*
Data are shown as mean ± one standard deviation. Significant p-values (<0.05) are shown in italics.
CRP, C-reactive protein; GOT, glutamic oxaloacetic transaminase; GPT, glutamic pyruvic transaminase; TLV, total lung volume (in ml); lung weight, whole lung tissue fraction (in g); GGO, volume related to ground glass opacities adjusted to TLV; CP/LO, volume related to crazy paving and linear opacities adjusted to TLV; consolidation, volume related to consolidation adjusted to TLV; CRP, serum C-reactive protein concentration; ICU, intensive care unit; i-MV, invasive mechanical ventilation.
**Data from COVID-19 refer to 141 CT scan series.*

C-reactive protein concentrations at admission (62 ± 79 in severe vs. 23 ± 73 in moderate and 4 ± 5 mg/dl in mild COVID-19 pneumonia). Moreover, a higher prevalence of hospitalization in ICU (31 vs. 20 and 21%), necessity of mechanical ventilation (18 vs. 9 and 14%), and case fatality (11 vs. 6 and 0%) was observed when compared to moderate and mild PI, respectively (**Table 2**).

Figure 7 shows a glyph mosaic of 88 CT scans from the control group and 141 from the 130 COVID-19 patients. The regional distribution of well-aerated regions, GGO, CP/LO, and consolidation can be easily determined in each glyph. The division into the different classes of evolution since the onset of symptoms follows a previous report (4).

DISCUSSION

We developed a CAD to quantify the extent of PI and to identify the most frequent radiological patterns in COVID-19 pneumonia. For that, a classifier based on a supervised ANN was trained, validated, and tested to classify radiological patterns previously selected and consensually classified by two specialized chest radiologists.

Different ANN architectures were tested using the degree of agreement between the ANN and the radiologists. The best validation performance was determined based on the minimization of the cross-entropy, and the performance of the ANN classifier was evaluated with the confusion matrix of the test set as well as from the ROC curve of each radiological pattern between the ANN and the radiologists' classification (**Figure 3**).

After establishing the best ANN architecture and characterizing the classifier performance, a CAD was constructed to quantify different radiological opacity patterns in a group of voxels clustered into a regular hexagon grid. Thus, we tested the effect of hexagon dimensions on the performance of the classifier since increasing the dimension would represent more noise due to an expected increase in the dispersion of voxel densities and therefore of the quantiles used as input for the ANN classifier (**Figure 4**). In fact, such effect was demonstrated, and the hexagon with a radius of 2 mm seemed to be the best dimension for grouping voxels maintaining a good performance of the classifier, although there was a slight reduction in agreement both in overall and within classes (**Table 1**) when compared to ANN performance in the confusion matrix. However, there is still a very significant and promising agreement and, even with the simplicity of the neural network architecture, the performance of the proposed classifier was quite similar to other more complex classifiers already presented in the literature (5, 6, 12).

The extent of PI has been used to phenotype patients with COVID-19 in profiles with greater involvement, "H" profile, that in general presents with greater elastance and intrapulmonary shunt. These patients also have a higher lung weight and tend to require more aggressive clinical management (13–15).

Our CAD was able to determine the extent of the PI and separate controls from COVID-19 patients with great sensitivity and specificity based on the ROC curve (**Figure 5**). The most severe cases of COVID-19 patients were more prevalent in the later stages of the disease (symptom onset > 9 days; **Figure 7**), required care in an ICU and mechanical ventilation, and showed

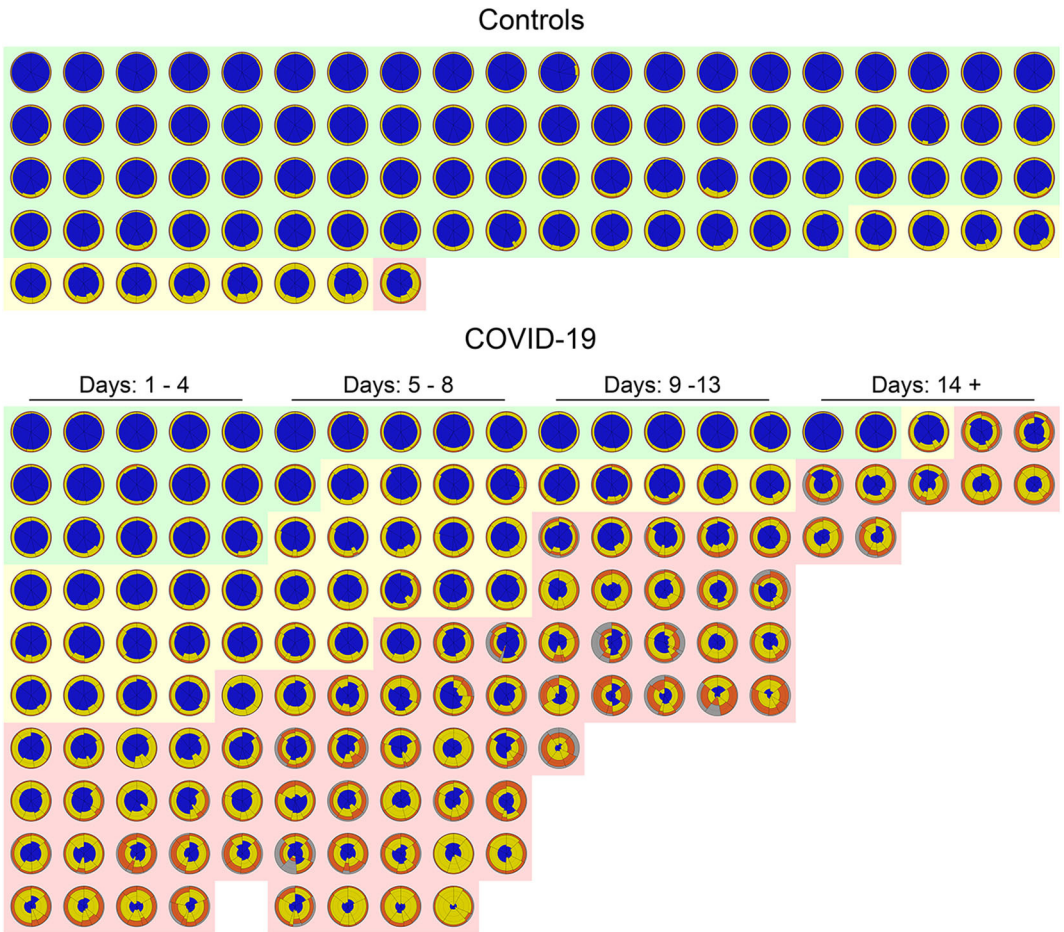

FIGURE 7 | Glyphs of all CT scans of 88 controls (upper panel) and 141 COVID-19 CT scans (lower panel). In the control group, glyphs were sorted by the extent of parenchymal opacities related to ground glass opacities (GGO), CP/LO, and consolidation. Note that just 11 (12%) subjects presented some parenchymal opacities, whereas in just one subject (1%) such opacities presented a Z score higher than 3. Also note that there is a clear predominance of GGO in controls. In COVID-19, glyphs were sorted by days of symptom onset and by the extent of pulmonary involvement with the three classified groups: severe (light red cluster), moderate (light yellow cluster), and mild (light green cluster). Patients' glyphs clearly demonstrate the spectrum of parenchymal abnormalities showing a variety of GGO, CP/LO, and consolidation. Note the predominance of yellow and orange (GGO and CP/LO, respectively) in patients classified as presenting severe pulmonary involvement and with longer time since symptom onset. There are few "normal" subjects (22%) in the COVID-19 database, and therefore only a minority of glyphs are predominantly blue all over the lung.

greater case fatality (**Table 2**). Lung weight was also greater in the most severe COVID-19 pneumonia (**Table 2**), with GGO, CP/LO, and consolidation representing, altogether, 76 ± 10% of the total lung weight.

The worst performance of our CAD was related to the differentiation between GGO and CP/LO, with the highest misclassification, when the 2-mm-radius hexagon was used, occurring between these two classes. Accordingly, 68 CP/LO cases were misclassified by the CAD as GGO and 76 GGO as CP/LO (**Table 1**). The overlapping zone between GGO and CP/LO and the important dispersion of voxel densities (**Figure 4**) are probably related to the presence of GGO in the background of CP/LO (3), contributing to reduced ANN performance between these classes. In addition, it is possible that the separation between GGO and CP/LO depends on the scale used for sampling purposes. In fact, a hexagon with a larger radius, therefore grouping a greater number of voxels, tended to reduce the agreement for GGO (from 81 to 61% for hexagons with 2-mm and 4-mm radii, respectively), whereas it increased the concordance for CP/LO (from 70 to 80% for hexagons of 2-mm and 4-mm radii, respectively).

However, it is important to stress that the classification errors between GGO and CP/LO do not seem to significantly influence the computation of the extent of PI. Thus, it is possible that only more complex methods that use the texture pattern of ROIs, such as convolutional neural networks, can precisely distinguish between GGO and CP/LO (16, 17). Since we opted for a simple and computationally less demanding method, we suggest that the neural network proposed herein may be sufficient to quantitate the extent of COVID-19 pneumonia. In addition, a 70%

agreement level is considered to be reasonable in the classification of different radiological standards (5) and was achieved in all radiological patterns examined in our study (18–20).

The mosaic of the glyphs from 88 CT scans from the control group and 141 from the COVID-19 patients summarizes information from 35 gigabytes of CT scan data and clearly demonstrates the difference between these two groups in terms of pulmonary aeration and even severity of PI (**Figure 7**). Even at this resolution, the glyphs provide a succinct overview of the entire database of subjects and highlight the easiness of pinpointing the intra- and intersubject disease distribution.

Some characteristics of our CAD should be highlighted. The ANN classifier was trained with information extracted from the same database of the image to be processed. This likely mitigated possible bias related to reconstruction algorithms or even artifacts attributed to CT acquisition parameters, such as voltage, amperage, and field of view. In spite of that, the inclusion of more heterogeneous pulmonary opacification patterns in the database should be considered in future studies in order to improve the ANN classifier capacity.

Although the proposed ANN was not tested in the clinical practice scenario, the CT scan images used to train and test the ANN algorithm were quite heterogeneous, using several acquisition protocols and about eight kernels belonging to three different manufacturers. However, further studies evaluating the usefulness of the proposed ANN in radiological practice, as well as studies including non-COVID-19 pneumonia patients, are still necessary for the final assessment of the clinical viability of a CAD platform in the routine of radiology services. In fact, future studies using a similar ANN architecture could be performed to identify highly suspicious COVID-19 chest CT images. Certainly, samples from non-COVID-19 must be included in the database for new ANN training, validation, and test sets.

Furthermore, in the face of the high capacity for information synthesis and easy interpretation of quantitative results, the computational time required for processing a whole-lung CT image is quite low (no more than 60 s). Much of the time expense is still in the lung segmentation stage (2 min in most cases, but reaching more than 10 min in cases where there is consolidation in the subpleural regions). Accordingly, the proposed CAD still needs some improvements in imaging pre-processing to simplify the whole pipeline process and become feasible at the clinical scenario.

Finally, the CAD proposed in the present study seems to be able to identify and quantify the extent of pulmonary involvement, helping to phenotype patients with COVID-19 pneumonia. However, further studies are necessary to investigate the association between the extent of pulmonary involvement and the clinical outcomes or even inflammatory markers.

TAKE-HOME MESSAGE

- The proposed deep learning CAD seems to be able to identify and quantify the extent of pulmonary involvement, helping to phenotype patients with COVID-19 pneumonia.
- Patients with severe COVID-19 pulmonary involvement, as determined by the proposed CAD, presented higher lung weight and C-reactive protein at admission and more frequently required invasive ventilation and intensive care unit hospitalization with higher case fatality.

CODE AVAILABILITY

CAD will be available upon request to the corresponding author.

DATA AVAILABILITY STATEMENT

All datasets generated for this study are included in the article.

ETHICS STATEMENT

The studies involving human participants were reviewed and approved by The study was conducted in one-hundred thirty patients with COVID-19, confirmed by RT-PCR, admitted at Hospital Copa Star and Hospital Barra D'Or, Rio de Janeiro, Brazil and at Centro Hospitalar Universitário do Porto (CHUP), Porto, Portugal, and underwent chest CT scans. Eighty-eight healthy subjects who underwent chest CT for clinical purposes and who images were considered nonpathological by radiologists served as controls. Each respective Research Ethics Committee approved the present study (075-DEFI/ 076-CE from CHUP and CAAE – 29496920.8.0000.5262, Institute D'Or), that complied with the current national and international standards. The ethics committee waived the requirement of written informed consent for participation. Written informed consent was not obtained from the individual(s) for the publication of any potentially identifiable images or data included in this article.

CONSENT TO PARTICIPATE

As this is a retrospective study without intervention in patients with infectious disease still in hospital or isolation, the consent form was waived by the respective ethics committees.

CONSENT FOR PUBLICATION

All authors involved in the present work have read the text and agree to its publication.

AUTHOR CONTRIBUTIONS

AC contributed to image processing and analysis of results, statistical evaluation, theoretical development of the neural network, and the computation method of voxel-to-voxel analysis as well as writing of the text and submission of the article. AG contributed to image processing and segmentation, statistical evaluation, and neural network implementation. GW contributed to the determination of image regions of interest, capture and organization of clinical data and draft review. SC and MF contributed to capturing and organization of clinical data and draft review. JP and BG contributed to capturing and organization of clinical data. WS contributed to the determination of image regions of interest and draft review. FB contributed to the results, discussion, and draft review.

WZ contributed to draft review. RR contributed to capturing and organization of clinical data, results discussion, and draft review. All authors contributed to the article and approved the submitted version.

FUNDING

This research was supported by the Brazilian Council for Scientific and Technological Development (Conselho Nacional de Desenvolvimento Científico e Tecnológico—CNPq, Grant No. 302839/2017-8) and the Rio de Janeiro State Research Supporting Foundation (Fundação de Amparo à Pesquisa do Estado do Rio de Janeiro—FAPERJ, Grant No. E-26/203.001/2018).

ACKNOWLEDGMENTS

We would like to thank Dr. Alessandro Beda for his technical comments on the design and testing of the artificial neural network used in the present study.

REFERENCES

1. Hope MD, Raptis CA, Shah A, Hammer MM, Henry TS, Six Signatories A role for CT in COVID-19? What data really tell us so far. *Lancet.* (2020) 395:1189–90. doi: 10.1016/S0140-6736(20)30728-5
2. Simpson S, Kay FU, Abbara S, Bhalla S, Chung JH, Chung M, et al. Radiological Society of North America expert consensus statement on reporting chest CT findings related to COVID-19. Endorsed by the Society of Thoracic Radiology, the American College of Radiology, and RSNA. *Radiol Cardiothorac Imaging.* (2020) 2:e200152. doi: 10.1148/ryct.2020200152
3. Hansell DM, Bankier AA, MacMahon H, McLoud TC, Müller NL, Remy J. Fleischner society: glossary of terms for thoracic imaging. *Radiology.* (2008) 246:697–722. doi: 10.1148/radiol.2462070712
4. Pan F, Ye T, Sun P, Gui S, Liang B, Li L, et al. Time course of lung changes on chest CT during recovery from 2019 novel coronavirus (COVID-19) pneumonia. *Radiology.* (2020) 295:200370. doi: 10.1148/radiol.2020200370
5. Bartholmai BJ, Raghunath S, Karwoski RA, Moua T, Rajagopalan S, Maldonado F, et al. Quantitative computed tomography imaging of interstitial lung diseases. *J Thorac Imaging.* (2013) 28:298–307. doi: 10.1097/RTI.0b013e3182a21969
6. Maldonado F, Moua T, Rajagopalan S, Karwoski RA, Raghunath S, Decker PA, et al. Automated quantification of radiological patterns predicts survival in idiopathic pulmonary fibrosis. *Eur Respir J.* (2014) 43:204–12. doi: 10.1183/09031936.00071812
7. Occhipinti M, Bosello S, Sisti LG, Cicchetti G, de Waure C, Pirronti T, et al. Quantitative and semi-quantitative computed tomography analysis of interstitial lung disease associated with systemic sclerosis: a longitudinal evaluation of pulmonary parenchyma and vessels. *PLoS ONE.* (2019) 14:e0213444. doi: 10.1371/journal.pone.0213444
8. Fedorov A, Beichel R, Kalpathy-Cramer J, Finet J, Fillion-Robin J-C, Pujol S, et al. 3D slicer as an image computing platform for the quantitative imaging network. *Magn Reson Imaging.* (2012) 30:1323–41. doi: 10.1016/j.mri.2012.05.001
9. Staring M, Bakker ME, Stolk J, Shamonin DP, Reiber JHC, Stoel BC. Towards local progression estimation of pulmonary emphysema using CT. *Med Phys.* (2014) 41:021905. doi: 10.1118/1.4851535
10. Stoel BC, Vrooman H, Stolk J, Reiber J. Sources of error in lung densitometry with CT. *Invest Radiol.* (1999) 303–9. doi: 10.1097/00004424-199904000-00008
11. Møller MF. A scaled conjugate gradient algorithm for fast supervised learning. *Neural Netw.* (1993) 6:525–33. doi: 10.1016/S0893-6080(05)80056-5
12. Christe A, Peters AA, Drakopoulos D, Heverhagen JT, Geiser T, Stathopoulou T, et al. Computer-aided diagnosis of pulmonary fibrosis using deep learning and CT images. *Invest Radiol.* (2019) 54:627–32. doi: 10.1097/RLI.0000000000000574
13. Gattinoni L, Chiumello D, Caironi P, Busana M, Romitti F, Brazzi L, et al. COVID-19 pneumonia: different respiratory treatments for different phenotypes? *Intens Care Med.* (2020) 382:724–7. doi: 10.1007/s00134-020-06033-2
14. Gattinoni L, Coppola S, Cressoni M, Busana M, Rossi S, Chiumello D. Covid-19 does not lead to a "typical" acute respiratory distress syndrome. *Am J Respir Crit Care Med.* (2020) 201:1299–300 doi: 10.1164/rccm.202003-0817LE
15. Rello J, Storti E, Belliato M, Serrano R. Clinical phenotypes of SARS-CoV-2: implications for clinicians and researchers. *Eur Respir J.* (2020) 12:2001028. doi: 10.1183/13993003.01028-2020
16. Huang S, Lee F, Miao R, Si Q, Lu C, Chen Q. A deep convolutional neural network architecture for interstitial lung disease pattern classification. *Med Biol Eng Comput.* (2020) 58:725–37. doi: 10.1007/s11517-019-02111-w
17. Yang S, Jiang L, Cao Z, Wang L, Cao J, Feng R, et al. Deep learning for detecting corona virus disease 2019 (COVID-19) on high-resolution computed tomography: a pilot study. *Ann Transl Med.* (2020) 8:450. doi: 10.21037/atm.2020.03.132
18. Zhang H, Zhou P, Wei Y, Yue H, Wang Y, Hu M, et al. Histopathologic changes and SARS-CoV-2 immunostaining in the lung of a patient with COVID-19. *Ann Intern Med.* (2020). doi: 10.7326/L20-0895
19. Rossi SE, Erasmus JJ, Volpacchio M, Franquet T, Castiglioni T, McAdams HP. "Crazy-paving" pattern at thin-section CT of the lungs: radiologic-pathologic overview. *Radiographics.* (2003) 23:1509–19. doi: 10.1148/rg.236035101
20. Kauczor HU, Heitmann K, Heussel CP, Marwede D, Uthmann T, Thelen M. Automatic detection and quantification of ground-glass opacities on high-resolution CT using multiple neural networks: comparison with a density mask. *AJR Am J Roentgenol.* (2000) 175:1329–34. doi: 10.2214/ajr.175.5.1751329

Conflict of Interest: The authors declare that the research was conducted in the absence of any commercial or financial relationships that could be construed as a potential conflict of interest.

Copyright © 2020 Carvalho, Guimarães, Werberich, de Castro, Pinto, Schmitt, França, Bozza, Guimarães, Zin and Rodrigues. This is an open-access article distributed under the terms of the Creative Commons Attribution License (CC BY). The use, distribution or reproduction in other forums is permitted, provided the original author(s) and the copyright owner(s) are credited and that the original publication in this journal is cited, in accordance with accepted academic practice. No use, distribution or reproduction is permitted which does not comply with these terms.

frontiers in Medicine

ORIGINAL RESEARCH
published: 05 January 2021
doi: 10.3389/fmed.2020.588404

SNP and Haplotype Interaction Models Reveal Association of Surfactant Protein Gene Polymorphisms With Hypersensitivity Pneumonitis of Mexican Population

*Chintan K. Gandhi[1], Chixiang Chen[2], Shaili Amatya[1], Lili Yang[3], Chenqi Fu[2], Shouhao Zhou[2], Rongling Wu[2], Ivette Buendía-Roldan[4], Moisés Selman[4], Annie Pardo[5] and Joanna Floros[1,6]**

[1] Center for Host Defense, Inflammation, and Lung Disease (CHILD) Research, Department of Pediatrics, Pennsylvania State University College of Medicine, Hershey, PA, United States, [2] Department of Public Health Science, Pennsylvania State University College of Medicine, Hershey, PA, United States, [3] School of First Clinical Medicine, Nanjing University of Chinese Medicine, Nanjing, China, [4] Unidad de Investigación, Instituto Nacional de Enfermedades Respiratorias "Ismael Cosio Villegas", Mexico City, Mexico, [5] Universidad Nacional Autonoma de Mexico, Mexico City, Mexico, [6] Department of Obstetrics & Gynecology, Pennsylvania State University College of Medicine, Hershey, PA, United States

OPEN ACCESS

Edited by:
Bassam Mahboub,
Rashid Hospital, United Arab Emirates

Reviewed by:
Haruhiko Furusawa,
University of Colorado, United States
Yasunari Miyazaki,
Tokyo Medical and Dental University, Japan

***Correspondence:**
Joanna Floros
jfloros@pennstatehealth.psu.edu

Specialty section:
This article was submitted to Pulmonary Medicine, a section of the journal Frontiers in Medicine

Received: 28 July 2020
Accepted: 07 December 2020
Published: 05 January 2021

Citation:
Gandhi CK, Chen C, Amatya S, Yang L, Fu C, Zhou S, Wu R, Buendía-Roldan I, Selman M, Pardo A and Floros J (2021) SNP and Haplotype Interaction Models Reveal Association of Surfactant Protein Gene Polymorphisms With Hypersensitivity Pneumonitis of Mexican Population. Front. Med. 7:588404. doi: 10.3389/fmed.2020.588404

Background: Hypersensitivity pneumonitis (HP) is an interstitial lung disease caused by inhalation of common environmental organic particles. Surfactant proteins (SPs) play a role in innate immunity and surfactant function. We hypothesized that single nucleotide polymorphisms (SNPs) or haplotypes of the SP genes associate with HP.

Methods: Seventy-five HP patients caused by avian antigen and 258 controls, asymptomatic antigen exposed and non-exposed were enrolled. SNP association was performed using logistic regression analysis and SNP-SNP interaction models.

Results: Based on odds ratio, regression analyses showed association of (a) rs7316_G, 1A^3 (protective) compared to antigen exposed; (b) male sex, smoking, rs721917_T and rs1130866_T (protective) compared to non-exposed controls with HP; (c) compared to antigen exposed, 25 interactions associated with HP in a three-SNP model; (d) compared to non-exposed, (i) rs1136451 associated with increased, whereas rs1136450 and rs1130866 associated with lower HP risk, (ii) 97 interactions associated with HP in a three-SNP model. The majority of SNP-SNP interactions associated with increased HP risk involved SNPs of the hydrophilic SPs, whereas, the majority of interactions associated with lower HP risk involved SNPs of both hydrophilic and hydrophobic SPs; (e) haplotypes of SP genes associated with HP risk.

Conclusions: The complexity of SNPs interactions of the *SFTP* genes observed indicate that the lung inflammatory response to avian antigens is modulated by a complex gene interplay rather than by single SNPs.

Keywords: SNP-SNP interaction, surfactant protein gene polymorphism, *SFTPA1*, *SFTPA2*, *SFTPB*, *SFTPC*, *SFTPD*, genetic susceptibility

INTRODUCTION

Hypersensitivity pneumonitis (HP) is an interstitial lung disease caused by an abnormal immune response to a wide variety of inhaled environmental antigens, mainly small organic particles ($<5\,\mu m$) that reach the alveoli (1). These antigens provoke an exaggerated immune response in susceptible individuals (1, 2). HP is seen worldwide, and the most common implicated antigens are actinomyces species, fungi, and bird proteins (1). The pigeon breeder's disease caused by proteins from avian serum, feces, and feathers is the most common form of HP in Mexico (3). Given the universal and wide distribution of the offending antigens, it is unclear why only few individuals develop the disease, indicating the complex interaction between environment and genetic factors. Nonetheless, the host genetic factors that may play a role in HP susceptibility are understudied (1, 2).

Although pulmonary surfactant or its components have the potential to be contributors to the pathogenesis of HP, very little to no work has been done in this regard. Pulmonary surfactant is a complex mixture of 90% lipids and 10% proteins. The surfactant specific proteins are SP-A1, SP-A2, SP-B, and SP-C. Though SP-D is not part of the functional surfactant complex, it is grouped with the other surfactant proteins because it coisolates with them. SP-B and SP-C are hydrophobic proteins and play a role primarily in lowering the surface tension and stabilizing alveoli (4), whereas, SP-A and SP-D are hydrophilic proteins and play a role in innate immunity and host defense (5, 6), although SP-A also contributes to surfactant-related function (6). The human SP-A locus includes two functional genes, *SFTPA1* and *SFTPA2*, in opposite transcriptional orientation (7), encoding SP-A1 and SP-A2, respectively. Several genetic polymorphisms for each *SFTPA* gene are found frequently in the general population (8). SP-B, SP-C, and SP-D are each encoded by a single gene, *SFTPB, SFTPC*, and *SFTPD*, respectively (9), and several polymorphisms have been described for each (10–12).

Single nucleotide polymorphisms (SNPs) of the SP genes have been shown to associate with various acute and chronic pulmonary diseases, such as idiopathic pulmonary fibrosis (IPF) (13), chronic obstructive pulmonary disease (COPD) (14, 15), acute respiratory distress syndrome (10), cystic fibrosis (16), and neonatal respiratory distress syndrome (RDS) (17–20). More importantly, we have shown an association of SP gene polymorphisms with IPF (13), COPD (14), and tuberculosis (21) in the Mexican population. Furthermore, some of the common SP-A variants have been shown to differentially affect function (22, 23) and regulation (24–27) of alveolar macrophages in an animal model, as well as SP-A variants have been associated with differential lung function mechanics and survival of mice (28–30). For the current study, we selected from physiologically and biologically relevant genes, 17 well-characterized SP SNPs that have been shown to associate with various acute and chronic pulmonary diseases (12, 31). Previous studies have shown increased SP-A in bronchoalveolar lavage (BAL) and alveolar macrophages, and elevated serum SP-A and SP-D concentration in HP patients compared to controls (32–34). Though the exact mechanisms are unknown, HP pathogenesis may include alveolar epithelial injury by altered immune response and increased leakage of SP-A and SP-D from the alveolar to the vascular compartment. Moreover, previous research showed altered concentration of SP-A, SP-B, and phospholipids in IPF, HP, and sarcoidosis patients (34, 35). Taken together, it is likely that SPs play a critical role in HP.

HP is characterized by an abnormal immune response leading to chronic inflammation and abnormal lung function and is probably the result of complex interactions of genetic and environmental factors. Due to the importance of SPs in normal lung function, innate immunity and host defense of the lung, we hypothesized that natural genetic variants of SPs and their interactions are associated with HP in Mexican population.

Abbreviations: HP, Hypersensitivity Pneumonitis; *SFTPA1,* gene encoding SP-A1; *SFTPA2*, gene encoding SP-A2; *SFTPB,* gene encoding SP-B; *SFTPC,* gene encoding SP-C; *SFTPD,* gene encoding SP-D; SNPs, Single nucleotide polymorphisms; IPF, Interstitial pulmonary fibrosis; COPD, Chronic obstructive pulmonary disease; RDS, Respiratory distress syndrome; OR, Odds ratio.

SUBJECTS AND METHODS

Study Population

The study was conducted at the National Institute of Respiratory Diseases (INER) in Mexico City and the protocol was approved by the Ethics Committee. INER is a tertiary referral and one of the National Institutes of Health centers in Mexico. The study cohort compromised 3 groups (age > 18 years) and at least 3 generations of study participants were born in Mexico.

Group 1 (Cases) was composed of 75 consecutive unrelated patients 18 years of age or older with a diagnosis of HP (**Table 1**). HP was diagnosed as previously described using clinical characteristics, history of antecedent antigen exposure and specific antibodies against avian proteins, pulmonary function tests, high-resolution computed tomography, BAL findings (all 75 patients), and/or surgical biopsy when available (23 out of 75 patients) (1, 36). Attending clinicians systematically recorded the relevant data in every patient before making the final diagnosis and was confirmed by a multidisciplinary team. As per recently published official clinical practice guidelines from American Thoracic Society, all enrolled patients in the current study were classified to have a fibrotic HP (mixed inflammatory plus fibrosis) (37). Patients with other known interstitial lung diseases were excluded.

Group 2 (Exposed controls) was composed of 64 healthy individuals with a history of avian antigen exposure but remained symptom-free. Some of these individuals were relatives of HP patients.

Group 3 (Non-exposed controls) was composed of 194 healthy individuals without a history of antigen exposure. Out of 194, 91 subjects were recruited randomly from the Smoking Cessation program with more than 5 years of smoking history and normal pulmonary function tests (smoker controls), and the other 103 unrelated healthy blood donors (non-smoker controls) were recruited randomly from the INER, as noted previously (13).

We collected blood samples of study participants after obtaining informed consent from subjects.

TABLE 1 | Demographic and clinical characteristics of the study group.

Characteristic	Hypersensitivity pneumonitis ($n = 75$)	Avian antigen exposed controls ($n = 64$)	*p*-value	Non-exposed controls ($n = 194$)	*p*-value
Sex, male/female (%)	5/70 (8/92)	45/19 (70/30)	3.4E-16	124/70(64/36)	3.5E-17
Age (years)	44 ± 13.2	35 ± 8.8	NS	41 ± 14.5	NS
Non-smokers/smokers (%)	61/14 (81/19)	57/7 (90/10)	NS	103/91(53/47)	0.00002
FVC % predicted	56.6 ± 21.6	ND		106.5 ± 11.3*	
FEV1 % predicted	59.6 ± 21.7	ND		99.7 ± 12.8*	
FEV1/FVC%	90.7 ± 8.5	ND		79.3 ± 5.5*	
DL_{CO} ($n = 43$)	53.7 ± 21.4	ND		ND	
Oxygen saturation at rest (%)	85.4 ± 8.4b	ND		ND	

*ND, Not done; NS, Not significant; *Performed in 122 healthy non-exposed controls.*
Paired t-test was done between HP vs. Avian antigen exposed controls and HP vs. Non-exposed controls.

Genotype Analysis

Genomic DNA was extracted from blood samples as described previously (8) and used as a template for polymerase chain reaction (PCR). A total of 17 targeted SNPs of surfactant protein genes, *SFTPA1*, *SFTPA2*, *SFTPB*, *SFTPC*, and *SFTPD*, were selected for the current study. The 17 SNPs include 5 SNPs from *SFTPA1*: rs1059047, rs1136450, rs1136451, rs1059057, and rs4253527; 4 SNPs from *SFTPA2*: rs1059046, rs17886395, rs1965707, and 1965708; 4 SNPs from *SFTPB*: rs2077079, rs3024798, rs1130866, and rs7316; 2 SNPs from *SFTPC*: rs4715 and rs1124; and 2 SNPs from *SFTPD*: rs721917 and rs2243639. The PCR-restriction fragment length polymorphism method was used to genotype the *SFTPA1*, *SFTPA2*, *SFTPD* (8, 10), *SFTPB* (10, 38), and *SFTPC* (13) gene polymorphisms, as described elsewhere in detail (8, 16). The PCR primer sequences used are reported in **Supplementary Table 1**. To avoid genotyping bias, each sample was given a sequential laboratory number without identifiers in the order they were received and all samples were genotyped together in a blinded fashion with those assigning genotype unaware of the group of subjects.

Statistical Analysis

To determine the frequency of each SNP, we used the Chi-squared test, or Fisher's exact test when the expected frequency was too small (<5) and compared the allele distribution between the case and two control groups (avian antigen exposed and non-exposed). Dummy variables for each allele or SP-A genotype were created and applied for univariate logistic regression analysis, assuming no dose-effect for the alleles (13, 21). The selected markers, which were significantly associated with HP in unadjusted univariate analysis (p-value < 0.1), were passed to the multivariate logistic regression analysis after adjusting for smoking status and sex. Variable selection was performed using the backward elimination method with staying significance level less than 0.05.

To detect the effects of SNP-SNP interactions, we used Wang et al.'s case-control approach to study associations of SP genes polymorphisms with HP in cases vs. exposed controls and cases vs. non-exposed controls (39). Compared to traditional logistic methods, this approach is more efficient (40) in the detection of different genetic effects. It decomposes the overall genetic effect of each SNP into different components: the additive (a), recessive (r), and dominant (d) effect in a single SNP model. For two- and three-SNP models, this approach can also detect pairwise and triad-wise (high-order) epistasis, as described previously (41). If a statistically significant difference between the groups was observed, the p-value was corrected for variables such as sex and smoking status. The false discovery rate was controlled at 5% to account for multiple comparisons using the Benjamini-Hochberg method (42, 43). We used the Cochran's and Mantel–Haenszel test to adjust for variables (sex and smoking status) and calculated odds ratios (OR) with 95% of confidence interval (95% CI) (44). All possible SNP-SNP interactions were tested for single-, two-, and three-SNP interaction model and those with p-value < 0.05 are reported.

SP-A1 and SP-A2 haplotypes were assigned as described (8) and the frequency analysis was done similar to that of SNP frequencies. For haplotype estimation, we used the two-SNP haplotype estimation model to study association of haplotypes with HP patients (45). The effect of haplotype was studied in a similar way to that of the SNP-SNP interaction model in a case-control setting.

RESULTS

Clinical Characteristics of HP Study Group

Table 1 shows the baseline characteristics of the HP patients, and exposed and non-exposed controls. Out of seventy-five HP patients, 92% ($n = 70$) were females compared to 30% ($n = 19$) of 64 exposed controls, and 36% ($n = 70$) of the 194 non-exposed controls ($p < 0.00001$). Only 19% ($n = 14$) of HP patients and 10% ($n = 10$) of exposed controls ($p =$ NS) were current or former smokers compared to 47% ($n = 91$) of non-exposed controls ($p = 0.00002$). All HP patients demonstrated a significant reduction in FVC% and FEV1% on pulmonary function tests and hypoxemia at rest (**Table 1**).

Association of SP SNP Allele With HP in Univariate and Multivariate Analysis

The observed frequency distribution of the majority of SNPs did not deviate from Hardy-Weinberg equilibrium (data not shown). The univariate and multivariate logistic regression analysis was

TABLE 2 | Hypersensitivity Pneumonitis (HP) vs. avian antigen exposed controls (univariate analysis).

Gene	Allele	HP		Avian antigen control		w/o adjusting for sex and smoking status		After adjusting for sex and smoking status	
		n	MAF (%)	*n*	MAF (%)	OR (95% CI)	*p*-value	OR (95% CI)	*p*-value
SFTPA2	rs1965707_T	72	0.22	51	0.39	0.5 (0.2–1)	0.05	0.6 (0.2–1.9)	0.41
SFTPA2	rs1965708_A	72	0.19	52	0.33	0.5 (0.2–1.1)	0.1	0.8 (0.3–2.71)	0.76
SFTPB	rs7316_G	75	0.39	64	0.19	2.7 (1.2–6.0)	0.01	8.1 (2.3–39.3)	<0.01
SFTPC	rs1124_A	74	0.51	63	0.37	1.8 (0.9–3.7)	0.08	1.6 (0.6–4.1)	0.31

Percentage of n with at least one copy of the given allele. OR, odds ratio; CI, confidence interval; MAF, minor allele frequency.

TABLE 3 | Hypersensitivity Pneumonitis (HP) vs. non-exposed controls (univariate analysis).

Gene	Allele	HP		Healthy control		w/o adjusting for sex and smoking status		After adjusting for sex and smoking status	
		n	MAF (%)	*n*	MAF (%)	OR (95% CI)	*p*-value	OR (95% CI)	*p*-value
SFTPA1	rs1059047_C	72	0.49	192	0.4	1.4 (0.8–2.4)	0.21	1.8 (0.9–3.8)	0.1
SFTPA1	rs1136450_G	72	0.65	192	0.71	0.8 (0.4–1.4)	0.38	0.5 (0.2–1.0)	0.06
SFTPA1	rs1136451_G	72	0.58	192	0.52	1.3 (0.7–2.2)	0.37	2.0 (1.0–4.1)	0.07
SFTPA1	rs1059057_G	72	0.49	192	0.4	1.4 (0.8–2.5)	0.19	2.0 (1.0–4.2)	0.06
SFTPA2	rs1059046_C	72	0.78	193	0.71	1.5 (0.8–2.8)	0.24	2.1 (0.9–4.7)	0.07
SFTPA2	rs17886395_C	72	0.5	193	0.46	1.2 (0.7–2.0)	0.57	1.9 (0.9–4.0)	0.08
SFTPB	rs1130866_T	75	0.49	194	0.68	0.5 (0.3–0.8)	0.01	0.3 (0.2–0.7)	<0.01
SFTPD	rs721917_T	75	0.73	192	0.83	0.6 (0.3–1.1)	0.08	0.3 (0.1–0.6)	<0.01
SFTPD	rs2243639_A	75	0.61	191	0.71	0.6 (0.4–1.1)	0.12	0.4 (0.2–0.9)	0.02

OR, odds ratio; CI, confidence interval; MAF, minor allele frequency.

TABLE 4 | Hypersensitivity Pneumonitis (HP) vs. non-exposed controls (multivariate analysis).

Gene	Variable	OR (95% CI)	*p*-value
SFTPB	rs1130866_T	0.4 (0.2–0.9)	<0.01
SFTPD	rs721917_T	0.3 (0.1–0.7)	0.01
	Smoker	0.1 (0.05–0.3)	<0.01
	Male	0.02 (0.01–0.1)	<0.01

OR, odds ratio; CI, confidence interval.

performed to study difference in frequencies of marker allele in HP patients compared to two control groups.

HP Group (n = 75) vs. Avian Antigen Exposed Controls (n = 64)

Marker allele that showed significant differences ($p < 0.1$) in the univariate analysis (**Table 2**) were included in the multivariate analysis. After multiple logistic regression analysis, the marker allele rs7316_G of the *SFTPB* is associated with increased risk for HP, $p = 0.03$, OR (95% CI) = 4.6 (1.3–22.0), whereas, male sex appears to be associated with decreased risk for HP, $p < 0.01$, OR = 0.02 (0.01–0.08).

HP Group (n = 75) vs. Non-exposed Controls (n = 194)

Similarly, marker alleles that showed significant differences ($p < 0.1$) in the univariate analysis (**Table 3**) were included in the multivariate analysis. Based on the OR, marker allele (rs1130866_T of the *SFTPB* and rs721917_T of the *SFTPD*), as well as male sex and smoking appear to be associated with decreased risk of HP (**Table 4**).

Association of SNP-SNP Interactions With HP

A particular SNP can have an additive (denoted as "a"), dominant (denoted as "d") or recessive (not observed in our study) effect on the disease and the number that follows "a" or "d" indicates the position of the corresponding SNP. For example, a notation d1 x a2 x d3 means that SNPs in position 1 and 3 have dominant effect and SNP in position 2 has an additive effect on that particular interaction. These interactions could be intragenic, i.e., among SNPs of the same gene (shown in bold in the Tables), or intergenic, i.e., among SNPs of different genes. In general, each SNP exhibited either additive and/or dominant effect on HP in the single-, two-, and three-SNP model.

HP Group (n = 75) vs. Avian Antigen Exposed Controls (n = 64)

Since there was a statistically significant sex difference between the study groups, we adjusted for sex in the SNP analysis models. In the single- or two-SNP model, we did not observe significant association of SP genes SNPs with HP compared to exposed controls. **Table 5** shows a total of 25 significant interactions associated with HP in the three-SNP model. Out of these 25 interactions, 16 were associated with increased risk for HP,

TABLE 5 | Association of SP gene SNP interactions with HP compared to avian antigen exposed controls.

	SNP # 1	Gene	SNP # 2	Gene	SNP # 3	Gene	Interaction	FDR	*p*-value	OR (95% CI)
1*	**rs1059046**	***SFTPA2***	**rs1059047**	***SFTPA1***	**rs2243639**	***SFTPD***	d1 x a2 x d3	**0.05**	**<0.01**	**5.4 (1.7–20.1)**
2*	rs1059046	*SFTPA2*	rs1130866	*SFTPB*	rs4715	*SFTPC*		0.05	<0.01	5.8 (1.8–22.4)
3*	rs1059046	*SFTPA2*	rs1130866	*SFTPB*	rs1124	*SFTPC*		0.05	<0.01	5.8 (1.8–22.4)
4*	**rs1059046**	***SFTPA2***	**rs721917**	***SFTPD***	**rs2243639**	***SFTPD***		**0.05**	**<0.01**	**5.0 (1.7–17.1)**
5	rs1059047	*SFTPA1*	rs1136450	*SFTPA1*	rs2077079	*SFTPB*		0.05	<0.01	0.1 (0.0–0.5)
6*	rs1059047	*SFTPA1*	rs1136451	*SFTPA1*	rs2077079	*SFTPB*		0.02	<0.01	14.5 (2.7–148.6)
7	rs2077079	*SFTPB*	rs1130866	*SFTPB*	rs721917	*SFTPD*		0.00	<0.01	0.1 (0.0–0.4)
8	rs1059046	*SFTPA2*	rs2077079	*SFTPB*	rs4715	*SFTPC*	d1 x d2 x a3	0.02	<0.01	0.1 (0.0–0.5)
9	rs1059046	*SFTPA2*	rs2077079	*SFTPB*	rs1124	*SFTPC*		0.02	<0.01	0.2 (0.0–0.5)
10*	**rs1059046**	***SFTPA2***	**rs17886395**	***SFTPA2***	**rs721917**	***SFTPD***	d1 x d2 x d3	**0.04**	**<0.01**	**2.6 (1.4–4.9)**
11*	**rs1059046**	***SFTPA2***	**rs17886395**	***SFTPA2***	**rs2243639**	***SFTPD***		**0.00**	**<0.01**	**3.2 (1.7–6.2)**
12*	**rs1059046**	***SFTPA2***	**rs1059047**	***SFTPA1***	**rs2243639**	***SFTPD***		**0.02**	**<0.01**	**2.9 (1.5–5.8)**
13*	rs1059046	*SFTPA2*	rs1136450	*SFTPA1*	rs2077079	*SFTPB*		0.00	<0.01	5.3 (2.3–13.1)
14*	rs1059046	*SFTPA2*	rs2077079	*SFTPB*	rs1130866	*SFTPB*		0.02	<0.01	2.6 (1.4–5.0)
15*	rs1059046	*SFTPA2*	rs3024798	*SFTPB*	rs1130866	*SFTPB*		0.02	<0.01	2.8 (1.5–5.8)
16	rs1059046	*SFTPA2*	rs3024798	*SFTPB*	rs721917	*SFTPD*		0.00	<0.01	0.3 (0.1–0.5)
17*	rs17886395	*SFTPA2*	rs1059047	*SFTPA1*	rs2077079	*SFTPB*		0.00	<0.01	5.7 (2.3–16.3)
18	rs17886395	*SFTPA2*	rs1136451	*SFTPA1*	rs1130866	*SFTPB*		0.00	<0.01	0.3 (0.1–0.5)
19*	**rs1059047**	***SFTPA1***	**rs1136451**	***SFTPA1***	**rs2243639**	***SFTPD***		**0.05**	**<0.01**	**2.6 (1.3–5.5)**
20*	rs1136450	*SFTPA1*	rs1136451	*SFTPA1*	rs2077079	*SFTPB*		0.05	<0.01	2.8 (1.4–6.0)
21*	**rs1136450**	***SFTPA1***	**rs1136451**	***SFTPA1***	**rs721917**	***SFTPD***		**0.02**	**<0.01**	**3.1 (1.5–6.7)**
22	rs1136450	*SFTPA1*	rs3024798	*SFTPB*	rs721917	*SFTPD*		0.04	<0.01	0.4 (0.2–0.7)
23*	rs2077079	*SFTPB*	rs3024798	*SFTPB*	rs2243639	*SFTPD*		0.01	<0.01	3.1 (1.6–6.4)
24	rs2077079	*SFTPB*	rs1130866	*SFTPB*	rs2243639	*SFTPD*		0.00	<0.01	0.3 (0.1–0.5)
25	rs3024798	*SFTPB*	rs1130866	*SFTPB*	rs2243639	*SFTPD*		0.02	<0.01	0.4 (0.2–0.7)

Sign "" shows interactions that increased HP risk.*
Interactions among the hydrophilic SPs alone are shown in bold.
FDR, False discovery rate.

p = 0.001–0.05, OR = 2.6–14.5, whereas 9 interactions were associated with lower risk for HP, p = 0.002–0.05, OR = 0.1–0.4. Out of those 25 interactions, 16 were with three dominant effects and 9 were with two dominant effects [d1 x a2 x d3 (n = 7), d1 x d2 x a3 (n = 2)]. We did not observe any significant interaction with additive effects only.

Out of the 16 interactions associated with increased HP risk, 7 were among SNPs of the hydrophilic SPs (*SFTPA1, SFTPA2,* and *SFTPD*) alone, the rest (n = 9) were among SNPs of both the hydrophilic and hydrophobic (*SFTPB* and *SFTPC*) SPs. There were no interactions among SNPs of the hydrophobic SP genes alone. Of note, all but one interaction had SNPs of either the *SFTPA1* or *SFTPA2* gene. The exception was the interaction among two SNPs of *SFTPB* (rs2077079 x rs3024798) and the rs2243639 of *SFTPD*, p = 0.01, OR (95% CI) = 3.1(1.6–6.4).

All interactions (n = 9) associated with lower risk of HP were among SNPs of both hydrophilic and hydrophobic SPs. Moreover, SNPs of the *SFTPB* constituted the majority (∼45%) of the SNPs in the significant interactions associated with lower risk of HP, whereas fewer than ∼30% of the combined *SFTPA1* and *SFTPA2* SNPs in the interactions were associated with lower risk of HP.

HP Group (n = 75) vs. Non-exposed Controls (n = 194)

We observed a statistically significant difference of sex and smoking status between the groups, therefore for SNP analysis, we adjusted for both of these covariates. In the single SNP model, we observed that rs1136451 of the *SFTPA1* was associated with increased HP risk, p = 0.02, OR = 11.4 (2.3–57.9), whereas rs1136450 of *SFTPA1* and rs1130866 of *SFTPB* were associated with lower risk of HP, p = 0.02, OR = 0.2 (0.0–0.6) compared to non-exposed controls. Each of these SNPs exhibited an additive effect on HP risk, e.g., in rs1136451 (A/G), risk allele "G" exhibited an additive (GG>GA>AA) effect on increased HP risk rather than the recessive (GG>GA=AA) or dominant (GG=GA>AA) effect. We did not observe any significant interactions associated with HP in the two-SNP model. We observed a total of 97 interactions associated with HP in the three-SNP model. Out of the 97 interactions, 29 were associated with increased HP risk, p = 0.00009–0.05, OR = 1.9–13.3 (1.2–128.8), and the remaining 68 were associated with lower risk for HP, p = 0.0001–0.05, OR = 0.1–0.6 (0.0–0.9). Of the 97 interactions, (a) 3 interactions with additive effects (a1 x a2 x a3, no dominant effect of any SNP), (b) 8 interactions had one dominant effect (a1 x a2 x d3), (c) 51

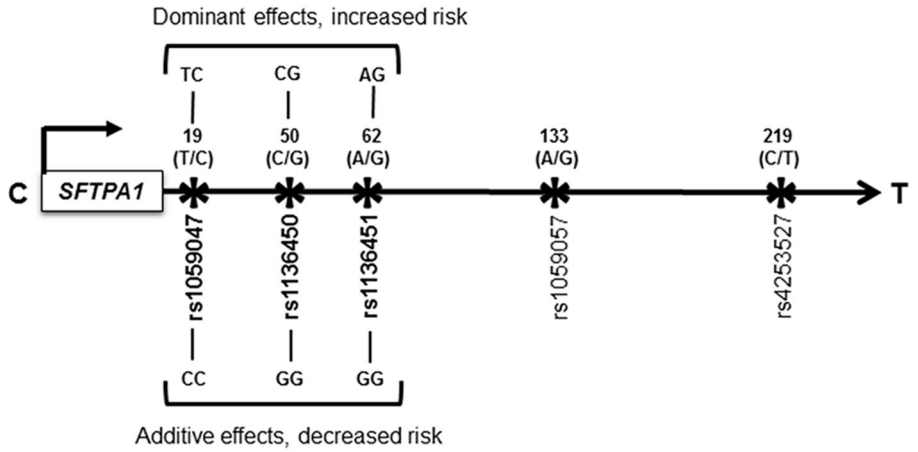

FIGURE 1 | Schematic representation of the *SFTPA1* single nucleotide polymorphisms (SNPs). All the studied SNPs of the *SFTPA1* are shown. The relative location of the gene is shown from centromere (C) to telomere (T) and the arrow indicates transcriptional orientation. The number above the black arrow indicates the amino acid (AA) number of the precursor molecule and the corresponding nucleotide change shown in parenthesis. The SNP id is shown below the black arrow. The SNPs (rs1059047 x rs1136450 x rs1136451) of the *SFTPA1* involved in an intragenic interaction in the three-SNP model are shown in bold font and are associated with HP risk compared to non-exposed controls. The change for AA at the codon 19 is Val/Ala corresponding to the T/C alleles, respectively; for AA50 is Val/Leu corresponding to C/G alleles. The SNP at the codon 62 does not change the encoded amino acid. Of note, the physical location of the SNPs in this interaction is very close to each other as shown in Figure. On the basis of odds ratio, the interaction (rs1059047 x rs1136450 x rs1136451) exhibiting a dominant effect is associated with increased risk of HP (d x d x d). The dominant genotype for each SNP is shown above the black arrow. On the other hand, the same interaction is associated with decreased risk of HP when each SNP exhibited an additive effect (a x a x a). The additive genotype for each SNP is shown below the black arrow.

interactions had two dominant effects [a1 x d2 x d3 ($n = 9$), d1 x a2 x d3 ($n = 12$), d1x d2 x a3 ($n = 30$)], and (d) 35 interactions had three dominant effects (d1 x d2 x d3) as shown in **Supplementary Tables 2, 3**.

Of the 29 interactions associated with increased HP risk, we observed (a) one intragenic interaction among SNPs of the *SFTPA1* (rs1059047 x rs1136450 x rs1136451), where each SNP exhibited a dominant effect, $p = 0.03$, OR = 1.9 (1.2–3) (shown in **Figure 1**), and the remaining 28 interactions were intergenic. (b) out of the 28 intergenic interactions, seven were among SNPs of the hydrophilic SPs (*SFTPA1, SFTPA2*, and *SFTPD*) alone, and the rest were among SNPs of both hydrophobic and hydrophilic SPs. (c) all but four of the significant intergenic interactions had SNPs of either *SFTPA1* or *SFTPA2*.

Of the 68 interactions associated with lower risk of HP, we observed (a) two intragenic interactions: (i) among SNPs (rs1059047 x rs1136450 x rs1136451) of the *SFTPA1*, which were the same as the ones with increased HP risk. However, in this case, each SNP exhibited an additive effect, $p = 0.05$, OR = 0.1 (0–0.5) whereas when this interaction was associated with increased risk, each SNP exhibited a dominant effect (shown in **Figure 1**), and (ii) among SNPs of the *SFTPB* (rs2077079 x rs3024798 x rs1130866 exhibiting dominant x dominant x additive effect, respectively), $p = 0.001$, OR = 0.2 (0.1–0.5). (b) the remaining 66 intergenic interactions included; (i) 12 interactions among SNPs of the hydrophilic SPs alone, (ii) 3 interactions among SNPs of the hydrophobic SPs alone, and (iii) the rest ($n = 51$) were among SNPs of both hydrophobic and hydrophilic SPs.

Interactions That Are Common With HP in the Three-SNP Model

We observed seven interactions associated with HP that were found to be in common in two separate comparisons, where cases were compared to either antigen exposed or to non-exposed controls (**Figure 2**). Out of the seven interactions: (a) five interactions were associated with lower risk of HP compared to antigen exposed and non-exposed controls (Panel A) and these interactions were among SNPs of both hydrophilic and hydrophobic SPs, $p = 0.002$–0.04, OR = 0.4–0.5 (0.3–0.8); (b) one was associated with increased risk of HP (Panel B – black dotted arrows) and this interaction was among SNPs of the hydrophilic SPs (rs1059046 x rs1059047 x rs2243639, *SFTPA2* x *SFTPA1* x *SFTPD*, d1 x a2 x d3), $p = 0.009$–0.05, OR = 3.5–5.4 (1.7–20.1); (c) In Panel B, one (red arrows) interaction (rs2077079 x rs3024798 x rs2243639, *SFTPB* x *SFTPB* x *SFTPD*, d1 x d2 x d3) was associated with increased risk of HP [$p = 0.008$, OR = 3.1 (1.6–6.4)] compared to antigen exposed controls, however, the same interaction was associated with lower risk of HP [$p = 0.002$, OR = 0.4 (0.3–0.7)] when compared to non-exposed controls.

Association of Haplotypes With HP

The univariate analysis (**Supplementary Table 4**) showed that the frequency of several haplotypes of the *SFTPA1* and *SFTPA2* differed between HP patients vs. each of the two control groups ($p < 0.1$). In the multivariate analysis, the $1A^3$ of the *SFTPA2* and male sex were associated with decreased risk of HP compared to avian antigen control, $p < 0.05$, OR = 0.1 ($1A^3$) and OR = 0.03 (male), whereas smoking and male sex, but none of the

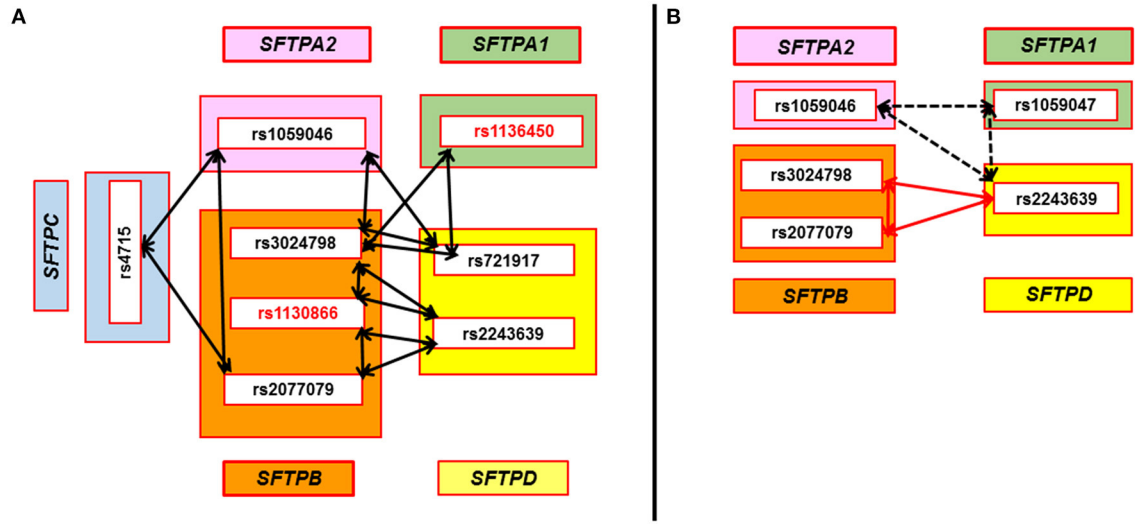

FIGURE 2 | SNP-SNP interactions associated with HP compared to avian antigen exposed and non-exposed controls in the three-SNP model. Double head arrows represent common SNP-SNP interactions associated with HP and found to be significant in two sets of comparisons (HP vs. avian antigen exposed controls and HP vs. non-antigen exposed controls) in the three-SNP model. The SNPs of surfactant protein genes *SFTPA1, SFTPA2, SFTPB, SFTPC,* and *SFTPD* encoding SP-A1, SP-A2, SP-B, SP-C, and SP-D, respectively, are depicted within the green, pink, orange, blue, and yellow rectangles, respectively. **(A)** shows five significant interactions that were associated with lower risk of HP compared to antigen exposed and non-exposed controls. All these interactions were among SNPs of both hydrophobic and hydrophilic SPs and involve at least one SNP of *SFTPB* ($n = 5$) that interacts with SNPs of *SFTPD* ($n = 4$), *SFTPA1* ($n = 1$), *SFTPA2* ($n = 2$), and *SFTPC* ($n = 1$), $p = 0.002$–0.04, OR = 0.4–0.5 (0.3–0.8). Two cases of the three-SNP model involved two *SFTPB* SNPs interacting (rs3024798 and rs1130866, or rs1130866 and rs2077079) with the same *SFTPD* SNP (rs2243639). SNPs associated with lower risk of HP compared to non-exposed controls in the single-SNP model are shown in red bold font (rs1130866 of *SFTPB* and rs1136450 of *SFTPA1*). **(B)** shows two significant interactions associated with increased risk of HP compared to antigen exposed controls. One of the interactions, shown by the black dash double head arrow, is among SNPs of the hydrophilic SPs alone and was associated with increased risk of HP compared to antigen exposed and non-exposed controls, $p = 0.009$–0.05, OR = 3.5–5.4 (1.7–20.1). However, the other interaction, shown by red double head arrow among SNPs of the *SFTPB* and *SFTPD,* was associated with increased risk of HP compared to antigen exposed controls [$p = 0.008$, OR = 3.1 (1.6–6.4)]. Of interest, the same interaction was associated with lower risk of HP compared to non-exposed controls [$p = 0.002$, OR = 0.4 (0.3–0.7)].

SFTPA1 and *SFTPA2* haplotypes, appeared to decrease risk of HP compared to non-exposed healthy control, $p < 0.01$, OR = 0.13 (smoking) and OR = 0.03 (male).

Using the two-SNP haplotype model, **Figure 3** shows associations of haplotypes with HP compared to avian antigen exposed and non-exposed controls. Compared to avian antigen exposed controls, six haplotypes of the *SFTPA1*, *SFTPA2*, and *SFTPB* were associated with HP. Of the six haplotypes, four were associated with decreased risk of HP (OR = 0.02–0.3) and the remaining were associated with increased risk of HP (OR = 4.26–13.19), **Supplementary Table 5**. As shown in **Figure 3**, the haplotype "CC" of the *SFTPB* (rs2077079 (A/C) x rs3024798 (C/A)) is associated with decreased risk of HP and exhibited an additive, OR = 0.02 (0.002–0.2) as well as a dominant effect, OR = 0.12 (0.07–0.39). In this example, each parent can transmit the risk haplotype in four forms: AC, AA, CC, and CA. The additive effect of the risk haplotype "CC" means that the presence of two copies of "CC/CC" decreases the risk of HP compared to the combination of two copies of any non-risk haplotypes (AC/AC, AA/AA, and CA/CA). Whereas the dominant effect of the same haplotype "CC" means that the presence of the risk haplotype "CC" in combination with any other haplotype (AC, AA, and CA) decreases the risk of HP compared to the presence of two copies of CC or any other combination of the non-risk haplotypes (AC/AC, AC/AA, AC/CA, AA/AA, AA/CA, and CA/CA). The dominant effect of a risk haplotype may have a non-linear interaction effect in which the combination of the risk haplotype "CC" with other non-risk haplotype (AC, AA, and CA) may produce a larger effect on the disease risk than the sum of two copies of the risk haplotype "CC." This complexity (non-linear) of interactions is our challenge for the study of human disease. Unexpected and not readily understood phenomena may occur, and this finding is one of the examples of this phenomenon. In other words, 1 + 1 > 2 in this risk haplotype. The haplotypes "CC" of the *SFTPA2* (rs1059046 x rs17886395), OR = 0.07 (0.02–0.26) and "AA" of the *SFTPA1* (rs1136451 x rs1059057), OR = 0.30 (0.12–0.78), exhibited a dominant effect on decreased HP risk. The haplotypes "AC" of the *SFTPA1* (rs1059057 x rs4253527), OR = 13.19 (4.44–39.17) and "CA" of the *SFTPB* (rs1130866 x rs7316), OR = 13.19 (4.44–39.17), exhibited a dominant effect on increased HP risk (**Figure 3**, red arrows).

Compared to non-exposed controls, all four significant susceptibility haplotypes of the *SFTPA1*, *SFTPB*, and *SFTPD* were associated with decreased risk of HP, OR = 0.15–0.35, **Supplementary Table 6** and **Figure 3** (black arrows). The haplotypes "TG" and "GA" of the *SFTPA1,* rs1059047 x rs1136450 and rs1136450 x rs1136451, respectively, exhibited an additive

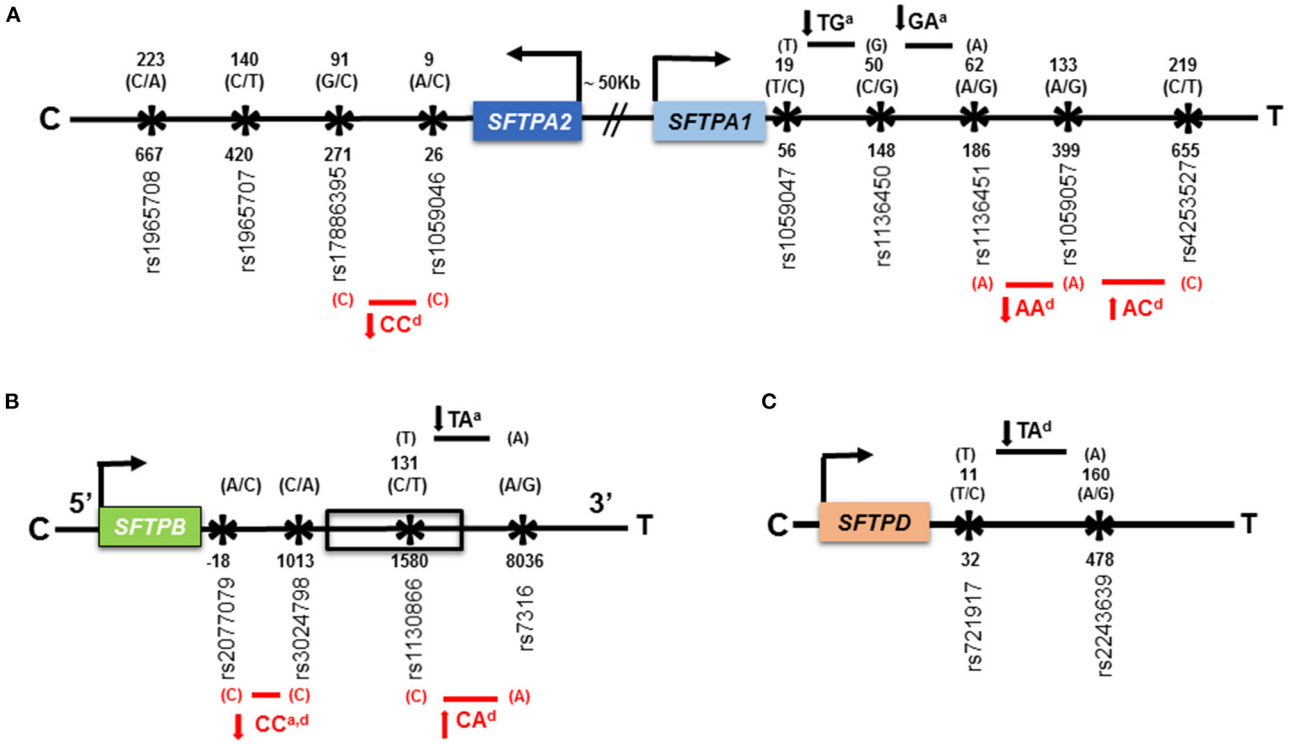

FIGURE 3 | Association of haplotypes of the *SFTPA1, SFTPA2, SFTPB, and SFTPD* genes with HP compared to avian antigen exposed and non-exposed controls in the two-SNP haplotype estimation model. **(A)** is a schematic representation of SNPs of the *SFTPA1* and *SFTPA2* genes. The distance between the genes is ~50 kb shown with sign "//." The studied SNPs are located within exons. **(B)** is a schematic representation of the *SFTPB* gene shown in 5' to 3' UTR direction. Only rs1130866 of the *SFTPB* shown in box, is located within an exon and the corresponding amino acid (AA) is shown above that. The *SFTPB* (1) rs2077079 is located 10 nucleotides downstream of TATAA box, in the 5′ regulatory region; (2) rs3024798 is located in the intron; and (3) rs7316 is located in the 3′UTR. Thus, no AA is shown for these SNPs. **(C)** is a schematic representation of SNPs of the *SFTPD* gene. The studied SNPs are located within exons. The gene direction is shown from centromere (C) to telomere (T) and the arrow above the color box indicates transcriptional orientation. The number above the black arrow indicates the AA number and the corresponding nucleotide change for that particular SNP is shown in parenthesis. The numbering of AAs in *SFTPA2, SFTPA1*, and *SFTPB* is based on the sequence of the precursor molecule, whereas, it is based on the mature protein (i.e., minus the signal peptide) in *SFTPD*. The numbers below the black arrow indicate the nucleotide number and the corresponding SNP ids. The transmitted haplotypes and nucleotide changes are shown in bold. The haplotypes associated with HP risk compared to avian antigen exposed and non-exposed controls are shown in red font with red line and black font with black line, respectively. The direction of the solid arrows besides haplotypes indicates increased or decreased HP risk compared to control groups. The superscript "a" and "d" after a given haplotype indicates additive and dominant effect, respectively, of that particular haplotype.

effect, OR = 0.15 (0.04–0.54). The haplotype "TA" of the *SFTPB* (rs1130866 x rs7316) exhibited an additive effect, OR = 0.17 (0.05–0.64), whereas, the haplotype "TA" of the *SFTPD* (rs721917 x rs2243639) exhibited a dominant effect, OR = 0.35 (0.18–0.66) on decreasing the risk of HP.

DISCUSSION

Hypersensitivity Pneumonitis is an interstitial lung disease caused by an abnormal immune response to antigen exposure and most likely due to complex interactions between environmental and genetic factors (1, 2). Surfactant proteins play an important role in normal lung function as well as innate immunity and host defense (6, 46), and alterations in their function is central to several pulmonary diseases. Several genetic variants have been identified for *SFTPA1, SFTPA2, SFTPB, SFTPC*, and *SFTPD* that are associated with pulmonary diseases (12, 47). Taking advantage of the homogeneity of the Mexican population, in the current study, we tested the hypothesis that SP genetic variants are associated with susceptibility of HP. Our results showed that (a) in the multivariate analysis, the rs7316_G of the *SFTPB* and male sex were associated with increased and decreased risk of HP, respectively, compared to antigen exposed controls, whereas the rs1130866_T of the *SFTPB*, rs721917_T of the *SFTPD*, male sex, and smoking were associated with decreased risk of HP compared to non-exposed controls; (b) in the single-SNP model, the rs1136451 of *SFTPA1* was associated with increased HP risk whereas the rs1136450 of the *SFTPA1* and the rs1130866 of the *SFTPB,* each associated with lower risk and exhibited an additive effect on HP compared to non-exposed controls; (c) in the three-SNP model, when HP patients were compared to antigen exposed and non-exposed controls, the majority of SNP-SNP interactions associated with increased risk of HP involved SNPs of the hydrophilic SPs alone, whereas, the majority of the interactions with hydrophobic SPs were

associated with lower risk of HP; (d) based on OR, the $1A^3$ and "CC" haplotypes of the *SFTPA2,* each associated with decreased risk and certain haplotypes of the *SFTPA1* and *SFTPB* were associated with increased or decreased risk to HP compared to antigen exposed controls, whereas, certain haplotypes of *SFTPA1*, *SFTPB,* and *SFTPD,* each associated with decreased risk of HP compared to non-exposed controls. Thus, the SP genetic marker alleles, SNPs and haplotypes, either alone and/or via their interactions may contribute to the development of HP. These results also indicate that the use of multiple markers may better predict the risk of disease and be used as diagnostic and/or prognostic markers of HP.

For the current study, we used two statistical approaches: (1) a traditional logistic regression analysis, and (2) a newer SNP-SNP interaction models in case-control settings. Moreover, to avoid overestimation of an association of SNP and SNP-SNP interactions for HP patients and also to account for the heterogeneity secondary to genetic differences and environmental factors that could affect the case-control study, we used two distinct controls: (1) asymptomatic antigen exposed and (2) non-exposed healthy controls. The antigen exposed controls who did not develop disease can be classified as a resistant population and non-exposed controls represent the general population where the history of exposure is not known. Of note, 30–40% of confirmed HP patients do not have a history of antigen exposure (1) making this study clinically useful.

The regression analysis revealed a protective association of male sex and smoking with HP, although the duration and/or amount of smoking was unknown. Previous human and animal studies have shown a protective role of smoking in HP under similar antigen risk exposure (48, 49). Smoking has a paradoxical role in HP in the sense that HP develops more frequently in non-smokers than in smokers but when HP occurs in smokers, the outcome is poor (50). Similar to our study, a higher incidence of HP has been reported in females in a recent epidemiological study (49). Thus, modifiable and non-modifiable environmental factors may change the susceptibility of complex diseases. Adjusting for these significant variables and the use of two different statistical approaches could provide confidence in the observations made.

The rs7316_G of the *SFTPB* is shown to associate with increase HP risk compared to antigen exposed controls only in the multivariate regression analysis. Although the rs7316 is located in the 3′ untranslated region that frequently acts as a regulatory region affecting mRNA stability, the functional significance of this variant is unclear (51). In the single-SNP model and the univariate analysis, we found three SNPS, two of the *SFTPA1* and one of the *SFTPB*, each associated with HP compared to non-exposed controls. The rs1136451_G of the *SFTPA1* associated with increased risk of HP. This SNP at codon 62 of SP-A1 does not result in an amino acid change (proline). Moreover, the C allele of this SNP is previously shown to associate with increased risk of COPD (14) and decreased risk of TB (21) in Mexicans. Of note, the G allele of the same SNP was found to associate with decreased risk of COPD in a Chinese population (52). Though the biological effect of the variant is not known, collectively these data indicate that this variant is differentially associated with pulmonary diseases in various ethnic groups. Moreover, we observed that the rs1136450_G allele of the *SFTPA1* is associated with decreased risk of HP compared to general controls. This SNP is known to change the encoded amino acid Leucine to Valine at codon 50, but its effect on structure, function and/or stability of the SP-A is not known. Though there are some similarities in the pathogenesis of the two types of interstitial lung diseases (IPF and HP), the C allele of rs1136450 is shown to associate with six-times higher odds of developing IPF in the Mexican population compared to general controls (13), but the same allele is associated with a decreased risk of HP. Whether this along with other markers could be used to differentiate between interstitial lung diseases in Mexicans remains to be determined. A previous study has shown a 3-fold increase in SP-A in BAL of HP patients (34), however, the question remains whether increased SP-A causes or contributes to HP or it is the result of the disease process. The level of SP-A1 and SP-A2 differs among individual as a function of age and lung health status (e.g., heathy vs. cystic fibrosis, culture positive vs. culture negative), as shown by differences in the protein ration of SP-A1 to total SP-A in human BAL samples (53). In addition, several studies have shown that SPs levels are influence by age, health, smoking status, lung health disease as well as by genetic factors (54–56), however, very few studies have correlated genetic polymorphisms with serum levels (57). For the current study, we did not measure the level of SPs in BAL; therefore, the effect of SP SNPs on surfactant protein concentration is unknown in healthy and/or in HP subjects. The N-terminal segment, the collagen-like region and the neck domain but not the carbohydrate recognition domain participate in SP-A oligomerization (6). Of interest, all the significant SNPs of the *SFTPA1* and *SFTPA2* associated with HP are located within regions that participate in oligomerization, whereas SNPs (rs1965707, rs1965708, and rs4253527) located in the carbohydrate recognition domain are not associated with HP. Currently it is unknown if and how any of the significant SNPs alone or in combination contribute to SP-A oligomerization.

The rs1130866_T allele of the *SFTPB* was also associated with lower risk of HP. This SNP is a missense mutation that changes the encoded amino acid Threonine to Isoleucine and eliminates an N-linked glycosylation site (58). The T allele of rs1130866 is protective against neonatal RDS (20) and systemic sclerosis associated interstitial lung disease in a Japanese population (59). On the other hand, the C allele that has the N-linked glycosylation site is associated with increased risk of COPD (15), acute respiratory distress syndrome (10), and IPF in Mexicans (13). The presence of N-linked glycosylation may interfere with SP-B processing and protein folding in disease conditions, hence the T allele, without the N-linked glycosylation somehow protects against HP. This has been shown in a transgenic mouse model of pneumonia and sepsis, where the C allele of rs1130866 of human SP-B resulted in a decreased number of lamellar bodies, SP-B concentration, and increase surface tension compared to the T allele of rs1130866 and compared to the wild type mice (60).

In summary, the fact that the marker alleles (rs1130866_T, rs1136450_G, and rs1136451_G) identified by logistic regression analysis and SNPs identified (see below) by the single-SNP model (i.e., the additive effect of the T, G, and G alleles of the rs1130866,

rs1136450, and rs1136451, respectively) are identical, based on the calculated OR (regardless of the statistical approaches used), associate with HP provide confidence that these associations are true rather than spurious.

It is known that a genetic variant in the presence of another variant can alter the susceptibility of an individual to certain diseases (61). By studying SNP-SNP interactions, we can better understand the role of genetics in complex diseases such as HP. It is possible that networks of additive and/or epistatic interactions among surfactant protein genetic variants may alter functional capabilities of certain SPs, more importantly, alveolar integrity and/or host defense at the cellular, molecular or tissue level (61). In the three-SNP model, we observed 96 interactions (HP vs. non-exposed) compared to 25 interactions (HP vs. avian antigen exposed), with only 7 interactions being in common between them. The observed difference in the number of interactions could be due to the difference in the patient population, statistical approach and/or sample size. For the current study, we enrolled HP patients, exposed and non-exposed controls from a homogeneous Mexican population and used similar statistical approach to compare HP patients with two different control groups. Therefore, the observed difference in the number of interactions is likely due to the sample size difference.

We observed 44 interactions associated with avian-antigen controls compared to non-exposed controls in a three-SNP model after adjusting for smoking status (data not shown). This indicates that although the demographics of the two control groups (antigen-exposed and non-exposed) appear identical except for the smoking status (**Table 1**), genetically the two control groups differ. This difference between the two control groups may be in part due to the fact that 25% of the antigen exposed controls were relatives to the cases or other. However, despite genetic differences between the two control groups, we observed seven interactions associated with HP that were found to be in common in the two separate comparisons, where HP cases were compared to either antigen exposed or to non-exposed controls (**Figure 2**). The association of these interactions with HP is likely robust given the two different controls and considering the baseline genetic differences between the two control groups and should be investigated further in the future.

The complex three SNP model identified various significant interactions among the hydrophilic and hydrophobic SPs associated with HP after adjusting for sex and smoking status of study participants. Interestingly, we noted that one of the common interactions, involving the *SFTPB* (rs3024798 and rs2077079) and the rs2243639 of the *SFTPD*, was associated with increased risk of HP compared to the homogeneous antigen exposed control group, however, the same interaction was associated with decreased risk of HP compared to the heterogeneous non-exposed control group, in which the history of exposure and living conditions were unknown. Heterogeneity due to differences in genetic background and/or environmental conditions is probably one of the sources of apparent discrepancies in case-control study results. Therefore, the differences indicate that caution should be exercised in the definition of cases and control groups and that findings should be interpreted within the context of experimental design.

The intragenic interaction (rs1059047 x rs1136450 x rs1136451) of the *SFTPA1* is associated with increased or decreased risk of HP depending on dominant or additive effects of each SNP, respectively, in the three-SNP model compared to non-exposed controls (**Figure 1**). Although the study population remained the same, the susceptibility to disease changes based on the effect the particular SNP exhibits in a particular interaction. It is possible that either too much or too little of a gene product and their interactions could lead to either over or under function, of genes in a disease state (62). Of note, the concentration and biochemical properties of surfactant proteins are altered in HP patients compared to controls (32–34). This may explain the change in HP risk based on the effect of a particular SNP in that interaction. Moreover, the majority of previous associations studies have assumed only additive effects of SNPs, without considering non-additive effects (63). By studying non-additive effects (i.e., dominant or recessive) of SNPs and their interactions in the present study, we identified associations that could change the disease risk as shown in this *SFTPA1* intragenic SNP interaction. Conversely, the same *SFTPA1* intragenic SNP interaction (rs1059047 x rs1136450 x rs1136451) with dominant effects of each SNP was associated with decreased risk of pediatric acute respiratory failure (41). The clinical outcome of a quantitative or qualitative imbalance of a given gene product in a given microenvironment, may differ among individuals. The fact that enrolled subjects in that study (41) were predominantly white children aged less than 2 years and admitted with viral infections, the contrasting effect of the same interaction on disease risk is not surprising.

Interactions of the *SFTPB* and *SFTPD* SNPs had a variable susceptibility to HP (**Figure 2**). For example, the rs1130866 of the *SFTPB* is associated with lower risk of HP in the single-SNP model. Interactions of that particular SNP with other *SFTPB* SNPs (rs3024798 and rs2077079); and with the rs2243639 of the *SFTPD* associated with a decreased risk of HP. These findings likely highlight the protective role of rs1130866 of the *SFTPB* in HP. However, the interaction of two other SNPs of the *SFTPB* (rs3024798 and rs2077079) with the rs2243639 of the *SFTPD* was associated with increased risk of HP. In addition, the rs1136451 of the *SFTPA1* is associated with increased risk of HP in the single-SNP model but interactions of the same SNP with other hydrophobic SPs (*SFTPB* and *SFTPC*) SNPs were associated with decreased risk of HP in the three-SNP model. As shown in the current study, a given SNP could change the susceptibility of a disease depending on its interactions with other SNPs, and this highlights the importance of studying SNP-SNP interactions rather than a single SNP association to fully understand the role of genetics in complex diseases such as HP.

In general, the majority of interactions associated with increased HP risk involved SNPs of either the *SFTPA1* and/or *SFTPA2*, whereas their interactions with the hydrophobic SPs (*SFTPB* and *SFTPC*) were associated with a decreased risk of HP. The significance for the *SFTPAs* association may be due to the differential effect of *SFTPA* gene variants in lung function parameters (29), which, in the case of HP, is also altered due to antigen-induced lung inflammation. Based on

these, we speculate that the presence of the hydrophilic SP genetic variants, particularly of *SFTPA1* and *SFTPA2,* in a susceptible population contribute to a dysfunction/poor functioning of the innate immune response to avian antigen exposure, alters lung function and this in turn may contribute to the pathogenesis of HP. However, interactions of these SNPs with the hydrophobic SP gene variants, particularly with *SFTPB*, may confer protection against HP. SP-B profoundly influences intracellular processing, secretion, and the pool size of surfactant (46). SP-A and SP-B have an interactive role in maintaining surface activity *in vitro*, and both are essential components of tubular myelin, an extracellular form of surfactant (64, 65). Together, these interactions among SNPs of *SFTPA* and *SFTPB* may alter the level and/or properties of SPs in HP patients that may provide protection against dysregulated inflammation. Moreover, interactions of the *SFTPA* with *SFTPB* have been previously shown to change susceptibility to neonatal RDS based on ethnic background, where certain variants increased risk of RDS in white neonates compared to black neonates (20). Nonetheless, the impact of these actual gene-gene interactions on levels and biophysical/biochemical properties of SPs need to be studied in biological experiments.

The study of haplotypes (SNPs that are inherited together) is shown to be a powerful tool to identify associations in complex diseases such as HP (66). The $1A^3$ and "CC" haplotypes of the *SFTPA2* were associated with decreased risk of HP compared to avian antigen controls. Moreover, the $1A^3$ haplotype is shown to associate with increased risk of TB in a Mexican population compared to healthy controls. Of note, the $1A^3$ differs from most other SP-A2 haplotypes at amino acid 223 (Lys instead of Gly) located within carbohydrate recognition domain that is responsible for recognizing, binding and clearing foreign materials entering into the lungs (9). Previous studies of SP-A1 and SP-A2 variants using the transgenic mouse model showed that the $1A^3$ of the *SFTPA2* was associated with better survival (28) and exhibited significantly higher lung function compared to other SP-A1 variants (29). Thus, findings of the current study, although it is an association study, are consistent with our previous animal data where a functional outcome was measured. How this haplotype alters the functional capabilities of SP-A remains to be determined, particularly in response to a potentially dysregulated inflammation and infection. It would be interesting, guided by the SNP-SNP interaction data, to generate additional SP-A cDNAs to use them to either generate stably transfected cell lines or transgenic mice for functional and regulatory studies as done with some of the common SP-A variants (65, 67). Similar to the SNP-SNP interaction model, a haplotype estimation model showed increased or decreased risk of HP based on the effect (i.e., dominant and recessive) of that particular haplotype. It is important to note that the significant haplotypes associated with HP are located very close to each other on the gene as shown in **Figure 3** and biologically have a higher chance of transmitted together.

The strengths of the study includes, (1) some of the susceptibility SNPs and SNP-SNP interactions associated with HP were the same by two different statistical approaches as well as by multiple comparisons adjusting for variables; (2) use of physiologically and biologically relevant SP SNPs, which is prerequisite for the SNP-SNP interaction model to study complex diseases (39). The limitations of the present study are the moderate sample size and the homogeneous patient population. A previous simulation study of SNP-SNP interaction indicated that a sample size of at least 100 in both case and control groups is needed to detect all the possible interactions. The moderate sample size of the current study may have resulted in under-reporting of causative SNP-SNP interactions and haplotypes, since the power to detect small differences is limited by the sample size, particularly for comparison of HP patients ($n = 75$) with antigen-exposed controls ($n = 64$). Furthermore, the findings of the present study may not be generalized in heterogeneous non-Hispanic patients. These associations should be strengthened and validated by increasing the sample size and replicating the findings in other groups of heterogeneous non-Hispanic HP patients. In addition, we did not measure SP expression/level in BAL of HP patients, therefore, the impact of these SNPs on SP expression, and in turn, on HP is unknown.

In summary, this is the first study showing association of SP SNPs and haplotypes with HP using two different statistical approaches in a Mexican population. The rs1136451 of the *SFTPA1* is associated with increased risk, whereas, the rs1136450 and the rs1130866 of the *SFTPA1* and *SFTPB*, respectively, are associated with decreased risk of HP compared to non-exposed controls using logistic regression analysis and a single-SNP model. Moreover, SNPs that are significantly associated with HP in the multivariate analysis also remained significant in the three-SNP interaction model after adjusting for smoking and sex. The rs1965707, rs1965708, and rs4253527 located within the carbohydrate recognition domain of the *SFTPA1* and *SFTPA2* were not associated with HP. SNPs of the *SFTPA1* and *SFTPA2* were overrepresented in interactions associated with increased HP risk, and their interactions with SNPs of the hydrophobic SPs for the most part associated with decreased HP risk. These observations indicate that specific SP genetic variants play role in the susceptibility of Mexicans to HP. This study focuses on complex and unique interactions of the SP SNPs with HP and gives valuable information of possible functional role of surfactant proteins in innate immunity against antigens as well as in the pathogenesis of HP. This knowledge may be useful in specific marker development for diagnosis of HP.

DATA AVAILABILITY STATEMENT

The data that support the findings of this study are available from the corresponding author, Chintan K. Gandhi, upon reasonable request.

ETHICS STATEMENT

The studies involving human participants were reviewed and approved by National Institute of Respiratory Diseases (INER). The patients/participants provided their written informed consent to participate in this study.

AUTHOR CONTRIBUTIONS

CG: data curation. LY, CC, CF, SZ, RW, and CG: formal analysis. JF: funding acquisition. MS, IB-R, AP, and JF: resources. RW, MS, AP, and JF: supervision and writing – review & editing. CG, SA, and JF: writing – original draft. All authors read and approved the final manuscript.

FUNDING

This work was supported by NIH HL34788 to JF.

ACKNOWLEDGMENTS

The authors thank the study participants. We thank Susan DiAngelo for her technical assistance in genotyping samples.

SUPPLEMENTARY MATERIAL

The Supplementary Material for this article can be found online at: https://www.frontiersin.org/articles/10.3389/fmed.2020.588404/full#supplementary-material

REFERENCES

1. Selman M, Pardo A, Talmadge E, King J. Hypersensitivity Pneumonitis. *Am J Respir Crit Care Med.* (2012) 186:314–24. doi: 10.1164/rccm.201203-0513CI
2. Vasakova M, Selman M, Morell F, Sterclova M, Molina-Molina M, Raghu G. Hypersensitivity pneumonitis: current concepts of pathogenesis and potential targets for treatment. *Am J Respir Crit Care Med.* (2019) 200:301–8. doi: 10.1164/rccm.201903-0541PP
3. Selman M, Lacasse Y, Pardo A, Cormier Y. Hypersensitivity pneumonitis caused by fungi. *Proc Am Thorac Soc.* (2010) 7:229–36. doi: 10.1513/pats.200906-041AL
4. Serrano AG, Perez-Gil J. Protein-lipid interactions and surface activity in the pulmonary surfactant system. *Chem Phys Lipids.* (2006) 141:105–18. doi: 10.1016/j.chemphyslip.2006.02.017
5. Wright JR. Immunoregulatory functions of surfactant proteins. *Nat Rev Immunol.* (2005) 5:58–68. doi: 10.1038/nri1528
6. Kishore U, Greenhough TJ, Waters P, Shrive AK, Ghai R, Kamran MF, et al. Surfactant proteins SP-A and SP-D: structure, function and receptors. *Mol Immunol.* (2006) 43:1293–315. doi: 10.1016/j.molimm.2005.08.004
7. Hoover RR, Floros J. Organization of the human SP-A and SP-D loci at 10q22-q23. Physical and radiation hybrid mapping reveal gene order and orientation. *Am J Respir Cell Mol Biol.* (1998) 18:353–62. doi: 10.1165/ajrcmb.18.3.3035
8. DiAngelo S, Lin Z, Wang G, Phillips S, Ramet M, Luo J, et al. Novel, non-radioactive, simple and multiplex PCR-cRFLP methods for genotyping human SP-A and SP-D marker alleles. *Dis Markers.* (1999) 15:269–81.
9. Floros J, Phelps D. Pulmonary surfactant. In: Yaksh TL, Lynch III C, Zapol WM, Maze M, Biebuyck JF, Saidman LJ, editors. *Anesthesia: Biologic Foundations.* Philadelphia, PA: Lippincott-Raven (1997). p. 1259–79.
10. Lin Z, Pearson C, Chinchilli V, Pietschmann SM, Luo J, Pison U, et al. Polymorphisms of human SP-A, SP-B, and SP-D genes: association of SP-B Thr131Ile with ARDS. *Clin Genet.* (2000) 58:181–91. doi: 10.1034/j.1399-0004.2000.580305.x
11. Wert SE, Whitsett JA, Nogee LM. Genetic disorders of surfactant dysfunction. *Pediatr Dev Pathol.* (2009) 12:253–74. doi: 10.2350/09-01-0586.1
12. Silveyra P, Floros J. Genetic variant associations of human SP-A and SP-D with acute and chronic lung injury. *Front Biosci.*(2012) 17:407–29. doi: 10.2741/3935
13. Selman M, Lin HM, Montano M, Jenkins AL, Estrada A, Lin Z, et al. Surfactant protein A and B genetic variants predispose to idiopathic pulmonary fibrosis. *Hum Genet.* (2003) 113:542–50. doi: 10.1007/s00439-003-1015-4
14. Guo X, Lin HM, Lin Z, Montano M, Sansores R, Wang G, et al. Surfactant protein gene A, B, and D marker alleles in chronic obstructive pulmonary disease of a Mexican population. *Eur Respir J.* (2001) 18:482–90. doi: 10.1183/09031936.01.00043401
15. Seifart C, Plagens A, Brodje D, Muller B, von Wichert P, Floros J. Surfactant protein B intron 4 variation in German patients with COPD and acute respiratory failure. *Dis Markers.* (2002) 18:129–36. doi: 10.1155/2002/194075
16. Lin Z, Thorenoor N, Wu R, DiAngelo SL, Ye M, Thomas NJ, et al. Genetic association of pulmonary surfactant protein genes, SFTPA1, SFTPA2, SFTPB, SFTPC, and SFTPD with cystic fibrosis. *Front Immunol.* (2018) 9:2256. doi: 10.3389/fimmu.2018.02256
17. Kala P, Ten Have T, Nielsen H, Dunn M, Floros J. Association of pulmonary surfactant protein A (SP-A) gene and respiratory distress syndrome: interaction with SP-B. *Pediatr Res.* (1998) 43:169–77. doi: 10.1203/00006450-199804001-01004
18. Nogee LM, Wert SE, Proffit SA, Hull WM, Whitsett JA. Allelic heterogeneity in hereditary surfactant protein B (SP-B) deficiency. *Am J Respir Crit Care Med.* (2000) 161(3 Pt 1):973–81. doi: 10.1164/ajrccm.161.3.9903153
19. Ramet M, Haataja R, Marttila R, Floros J, Hallman M. Association between the surfactant protein A (SP-A) gene locus and respiratory-distress syndrome in the Finnish population. *Am J Hum Genet.* (2000) 66:1569–79. doi: 10.1086/302906
20. Floros J, Fan R, Diangelo S, Guo X, Wert J, Luo J. Surfactant protein (SP) B associations and interactions with SP-A in white and black subjects with respiratory distress syndrome. *Pediatr Int.* (2001) 43:567–76. doi: 10.1046/j.1442-200x.2001.01474.x
21. Floros J, Lin HM, Garcia A, Salazar MA, Guo X, DiAngelo S, et al. Surfactant protein genetic marker alleles identify a subgroup of tuberculosis in a Mexican population. *J Infect Dis.* (2000) 182:1473–8. doi: 10.1086/315866
22. Mikerov AN, Umstead TM, Huang W, Liu W, Phelps DS, Floros J. SP-A1 and SP-A2 variants differentially enhance association of *Pseudomonas aeruginosa* with rat alveolar macrophages. *Am J Physiol Lung Cell Mol Physiol.* (2005) 288:L150–8. doi: 10.1152/ajplung.00135.2004
23. Mikerov AN, Wang G, Umstead TM, Zacharatos M, Thomas NJ, Phelps DS, et al. Surfactant protein A2 (SP-A2) variants expressed in CHO cells stimulate phagocytosis of *Pseudomonas aeruginosa* more than do SP-A1 variants. *Infect Immun.* (2007) 75:1403–12. doi: 10.1128/iai.01341-06
24. Phelps DS, Umstead TM, Floros J. Sex differences in the acute *in vivo* effects of different human SP-A variants on the mouse alveolar macrophage proteome. *J Proteomics.* (2014) 108:427–44. doi: 10.1016/j.jprot.2014.06.007
25. Thorenoor N, Kawasawa YI, Gandhi CK, Zhang X, Floros J. Differential impact of co-expressed SP-A1/SP-A2 protein on AM miRNome; sex differences. *Front Immunol.* (2019) 10:1960. doi: 10.3389/fimmu.2019.01960
26. Phelps DS, Chinchilli VM, Weisz J, Yang L, Shearer D, Zhang X, et al. Differences in the alveolar macrophage toponome in humanized SP-A1 and SP-A2 transgenic mice. *JCI Insight.* (2020) 3:141410. doi: 10.1172/jci.insight.141410. [Epub ahead of print].
27. Thorenoor N, Kawasawa YI, Gandhi CK, Floros J. Sex-specific regulation of gene expression networks by surfactant protein A (SP-A) variants in alveolar macrophages in response to *Klebsiella pneumoniae*. *Front Immuno.* (2020) 11:1290. doi: 10.3389/fimmu.2020.01290
28. Thorenoor N, Umstead TM, Zhang X, Phelps DS, Floros J. Survival of surfactant protein-A1 and SP-A2 transgenic mice after *Klebsiella pneumoniae* infection, exhibits sex-, gene-, and variant specific differences; treatment with surfactant protein improves survival. *Front Immunol.* (2018) 9:2404. doi: 10.3389/fimmu.2018.02404
29. Thorenoor N, Zhang X, Umstead TM, Scott Halstead E, Phelps DS, Floros J. Differential effects of innate immune variants of surfactant protein-A1 (SFTPA1) and SP-A2 (SFTPA2) in airway function after

Klebsiella pneumoniae infection and sex differences. *Respir Res.* (2018) 19:23. doi: 10.1186/s12931-018-0723-1
30. Thorenoor NS, Phelps D, Kala P, Ravi R, Floros Phelps A, Umstead T, et al. Impact of surfactant protein-A variants on survival in aged mice in response to *Klebsiella pneumoniae* infection and ozone: serendipity in action. *Microorganisms.* (2020) 8:1276. doi: 10.3390/microorganisms8091276
31. Floros J, Thomas N. Genetic variations of surfactant proteins and lung injury. In: Nakos G, Papathanasiou A, editors. *Surfactant Pathogenesis and Treatment of Lung Diasease* (2009). pp. 25–48.
32. Guzman J, Wang YM, Kalaycioglu O, Schoenfeld B, Hamm H, Bartsch W, et al. Increased surfactant protein A content in human alveolar macrophages in hypersensitivity pneumonitis. *Acta Cytol.* (1992) 36:668–73.
33. Hamm H, Lührs J, Rotaeche JG, Costabel U, Fabel H, Bartsch W. Elevated surfactant protein A in bronchoalveolar lavage fluids from sarcoidosis and hypersensitivity pneumonitis patients. *Chest.* (1994) 106:1766–70. doi: 10.1378/chest.106.6.1766
34. Phelps DS, Umstead TM, Mejia M, Carrillo G, Pardo A, Selman M. Increased surfactant protein-A levels in patients with newly diagnosed idiopathic pulmonary fibrosis. *Chest.* (2004) 125:617–25. doi: 10.1378/chest.125.2.617
35. Gunther A, Schmidt R, Nix F, Yabut-Perez M, Guth C, Rosseau S, et al. Surfactant abnormalities in idiopathic pulmonary fibrosis, hypersensitivity pneumonitis and sarcoidosis. *Eur Respir J.* (1999) 14:565.
36. Buendía-Roldán I, Santiago-Ruiz L, Pérez-Rubio G, Mejía M, Rojas-Serrano J, Ambrocio-Ortiz E, et al. A major genetic determinant of autoimmune diseases is associated with the presence of autoantibodies in Hypersensitivity Pneumonitis. *Eur Respir J.* (2020) 56:1901380. doi: 10.1183/13993003.01380-2019
37. Raghu G, Remy-Jardin M, Ryerson CJ, Myers JL, Kreuter M, Vasakova M, et al. Diagnosis of hypersensitivity pneumonitis in adults. *Am J Respir Crit Care Med.* (2020) 202:e36–69. doi: 10.1164/rccm.202005-2032ST
38. Lin Z, deMello DE, Batanian JR, Khammash HM, DiAngelo S, Luo J, et al. Aberrant SP-B mRNA in lung tissue of patients with congenital alveolar proteinosis (CAP). *Clin Genet.* (2000) 57:359–69. doi: 10.1034/j.1399-0004.2000.570506.x
39. Wang Z, Liu T, Lin Z, Hegarty J, Koltun WA, Wu R. A general model for multilocus epistatic interactions in case-control studies. *PLoS ONE.* (2010) 5:e11384. doi: 10.1371/journal.pone.0011384
40. Liu T, Thalamuthu A, Liu JJ, Chen C, Wang Z, Wu R. Asymptotic distribution for epistatic tests in case-control studies. *Genomics.* (2011) 98:145–51. doi: 10.1016/j.ygeno.2011.05.001
41. Gandhi CK, Chen C, Wu R, Yang L, Thorenoor N, Thomas NJ, et al. Association of SNP–SNP interactions of surfactant protein genes with pediatric acute respiratory failure. *J Clin Med.* (2020) 9:1183. doi: 10.3390/jcm9041183
42. Hope ACA. A simplified Monte Carlo significance test procedure. *J R Stat Soc Ser B.* (1968) 30:582–98. doi: 10.1111/j.2517-6161.1968.tb00759.x
43. Hochberg YBY. Controlling the false discovery rate: a practical and powerful approach to multiple testing. *J R Stat Soc. Ser B.* (1995) 57:289–300.
44. Day NE, Byar DP. Testing hypotheses in case-control studies-equivalence of mantel-haenszel statistics and logit score tests. *Biometrics.* (1979) 35:623–30. doi: 10.2307/2530253
45. Zhang L, Liu R, Wang Z, Culver D, Wu R. Modeling haplotype-haplotype interactions in case-control genetic association studies. *Front Genet.* (2012) 3:2. doi: 10.3389/fgene.2012.00002
46. Cañadas O, Olmeda B, Alonso A, Pérez-Gil J. Lipid–protein and protein–protein interactions in the pulmonary surfactant system and their role in lung homeostasis. *Int J Mol Sci.* (2020) 21:3708. doi: 10.3390/ijms21103708
47. Floros J, Thomas NJ. Surfactant protein genetics in community-acquired pneumonia: balancing the host inflammatory state. *Crit Care.* (2011) 15:156. doi: 10.1186/cc10115
48. Blanchet M-R, Israël-Assayag E, Cormier Y. Inhibitory effect of nicotine on experimental hypersensitivity pneumonitis in *vivo* and *in vitro*. *Am J Respir Crit Care Med.* (2004) 169:903–9. doi: 10.1164/rccm.200210-1154OC
49. Pérez ERF, Kong AM, Raimundo K, Koelsch TL, Kulkarni R, Cole AL. Epidemiology of hypersensitivity pneumonitis among an insured population in the United States: a claims-based cohort analysis. *Ann Am Thorac Soc.* (2018) 15:460–9. doi: 10.1513/AnnalsATS.201704-288OC
50. Ohtsuka Y, Munakata M, Tanimura K, Ukita H, Kusaka H, Masaki Y, et al. Smoking promotes insidious and chronic farmer's lung disease, and deteriorates the clinical outcome. *Intern Med.* (1995) 34:966–71. doi: 10.2169/internalmedicine.34.966
51. Fatahi N, Niknafs N, Kalani M, Dalili H, Shariat M, Amini E, et al. Association of SP-B gene 9306 A/G polymorphism (rs7316) and risk of RDS. *J Matern Fetal Neonat Med.* (2018) 31:2965–70. doi: 10.1080/14767058.2017.1359829
52. Guan J, Liu X, Xie J, Xu X, Luo S, Wang R, et al. Surfactant protein a polymorphism is associated with susceptibility to chronic obstructive pulmonary disease in Chinese Uighur population. *J Huazhong Univ Sci Technol.* (2012) 32:186–9. doi: 10.1007/s11596-012-0033-7
53. Tagaram HR, Wang G, Umstead TM, Mikerov AN, Thomas NJ, Graff GR, et al. Characterization of a human surfactant protein A1 (SP-A1) gene-specific antibody; SP-A1 content variation among individuals of varying age and pulmonary health. *Am J Physiol Lung Cell Mol Physiol.* (2007) 292:L1052–1063. doi: 10.1152/ajplung.00249.2006
54. Betsuyaku T, Kuroki Y, Nagai K, Nasuhara Y, Nishimura M. Effects of ageing and smoking on SP-A and SP-D levels in bronchoalveolar lavage fluid. *Eur. Respir J.* (2004) 24:964. doi: 10.1183/09031936.04.00064004
55. Sørensen GL, Hjelmborg JB, Kyvik KO, Fenger M, Høj A, Bendixen C, et al. Genetic and environmental influences of surfactant protein D serum levels. *Am J Physiol Lung Cell Mol Physiol.* (2006) 290:L1010–7. doi: 10.1152/ajplung.00487.2005
56. Sorensen GL, Husby S, Holmskov U. Surfactant protein A and surfactant protein D variation in pulmonary disease. *Immunobiology.* (2007) 212:381–416. doi: 10.1016/j.imbio.2007.01.003
57. Heidinger K, König IR, Bohnert A, Kleinsteiber A, Hilgendorff A, Gortner L, et al. Polymorphisms in the human surfactant protein-D (SFTPD) gene: strong evidence that serum levels of surfactant protein-D (SP-D) are genetically influenced. *Immunogenetics.* (2005) 57:1–7. doi: 10.1007/s00251-005-0775-5
58. Wang G, Christensen ND, Wigdahl B, Guttentag SH, Floros J. Differences in N-linked glycosylation between human surfactant protein-B variants of the C or T allele at the single-nucleotide polymorphism at position 1580: implications for disease. *Biochem J.* (2003) 369(Pt 1):179–84. doi: 10.1042/bj20021376
59. Sumita Y, Sugiura T, Kawaguchi Y, Baba S, Soejima M, Murakawa Y, et al. Genetic polymorphisms in the surfactant proteins in systemic sclerosis in Japanese: T/T genotype at 1580 C/T (Thr131Ile) in the SP-B gene reduces the risk of interstitial lung disease. *Rheumatology.* (2008) 47:289–91. doi: 10.1093/rheumatology/kem355
60. Yang F, Zhang J, Yang Y, Ruan F, Chen X, Guo J, et al. Regulatory roles of human surfactant protein B variants on genetic susceptibility to *Pseudomonas aeruginosa* Pneumonia-Induced sepsis. *Shock.* 54:507–19. (2019). doi: 10.1097/shk.0000000000001494
61. Cordell HJ. Detecting gene-gene interactions that underlie human diseases. *Nat Rev Genet.* (2009) 10:392–404. doi: 10.1038/nrg2579
62. Floros J, Wang G. A point of view: quantitative and qualitative imbalance in disease pathogenesis; pulmonary surfactant protein A genetic variants as a model. *Comp Biochem Physiol A Mol Integr Physiol.* (2001) 129:295–303. doi: 10.1016/s1095-6433(01)00325-7
63. Sabourin J, Nobel AB, Valdar W. Fine-mapping additive and dominant SNP effects using group-LASSO and fractional resample model averaging. *Genet Epidemiol.* (2015) 39:77–88. doi: 10.1002/gepi.21869
64. Poulain FR, Nir S, Hawgood S. Kinetics of phospholipid membrane fusion induced by surfactant apoproteins A and B. *Biochim Biophys Acta.* (1996) 1278:169–75. doi: 10.1016/0005-2736(95)00212-X
65. Wang G, Guo X, Diangelo S, Thomas NJ, Floros J. Humanized SFTPA1 and SFTPA2 transgenic mice reveal functional divergence of SP-A1 and SP-A2: formation of tubular myelin *in vivo* requires both gene products. *J Biol Chem.* (2010) 285:11998–2010. doi: 10.1074/jbc.M109.046243
66. Stram DO. Multi-SNP haplotype analysis methods for association analysis. In: Elston RC, editor. *Statistical Human Genetics: Methods and Protocols.* New York, NY: Springer (2017). p. 485–504.
67. Wang G, Umstead TM, Phelps DS, Al-Mondhiry H, Floros J. The effect of ozone exposure on the ability of human

surfactant protein a variants to stimulate cytokine production. *Environ Health Perspect.* (2002) 110:79–84. doi: 10.1289/ehp.02 11079

Conflict of Interest: The authors declare that the research was conducted in the absence of any commercial or financial relationships that could be construed as a potential conflict of interest.

Copyright © 2021 Gandhi, Chen, Amatya, Yang, Fu, Zhou, Wu, Buendía-Roldan, Selman, Pardo and Floros. This is an open-access article distributed under the terms of the Creative Commons Attribution License (CC BY). The use, distribution or reproduction in other forums is permitted, provided the original author(s) and the copyright owner(s) are credited and that the original publication in this journal is cited, in accordance with accepted academic practice. No use, distribution or reproduction is permitted which does not comply with these terms.

frontiers in Medicine

REVIEW
published: 14 January 2021
doi: 10.3389/fmed.2020.618506

The Potential Roles of Exosomes in Chronic Obstructive Pulmonary Disease

Nan Wang[1†], Qin Wang[2†], Tiantian Du[3], Abakundana Nsenga Ariston Gabriel[3], Xue Wang[4], Li Sun[1], Xiaomeng Li[1], Kanghong Xu[1], Xinquan Jiang[1] and Yi Zhang[5*]*

[1] School of Public Health, Shandong First Medical University and Shandong Academy of Medical Sciences, Taian, China, [2] Department of Anesthesiology, Qilu Hospital, Shandong University, Jinan, China, [3] Department of Clinical Laboratory, Cheeloo College of Medicine, The Second Hospital, Shandong University, Jinan, China, [4] Department of Pharmacy, Binzhou Medical University Hospital, Binzhou, China, [5] Respiratory and Critical Care Medicine Department, Qilu Hospital, Shandong University, Jinan, China

OPEN ACCESS

Edited by:
Mahmood Yaseen Hachim, Mohammed Bin Rashid University of Medicine and Health Sciences, United Arab Emirates

Reviewed by:
Sarina Mueller, University of Erlangen Nuremberg, Germany
Iman Mamdouh Talaat, University of Sharjah, United Arab Emirates

***Correspondence:**
Xinquan Jiang
taianjxq@163.com
Yi Zhang
cnzhang1@126.com

[†] These authors have contributed equally to this work

Specialty section:
This article was submitted to Pulmonary Medicine, a section of the journal Frontiers in Medicine

Received: 17 October 2020
Accepted: 17 December 2020
Published: 14 January 2021

Citation:
Wang N, Wang Q, Du T, Gabriel ANA, Wang X, Sun L, Li X, Xu K, Jiang X and Zhang Y (2021) The Potential Roles of Exosomes in Chronic Obstructive Pulmonary Disease. Front. Med. 7:618506. doi: 10.3389/fmed.2020.618506

Currently, chronic obstructive pulmonary disease (COPD) is one of the most common chronic lung diseases. Chronic obstructive pulmonary disease is characterized by progressive loss of lung function due to chronic inflammatory responses in the lungs caused by repeated exposure to harmful environmental stimuli. Chronic obstructive pulmonary disease is a persistent disease, with an estimated 384 million people worldwide living with COPD. It is listed as the third leading cause of death. Exosomes contain various components, such as lipids, microRNAs (miRNAs), long non-coding RNAs(lncRNAs), and proteins. They are essential mediators of intercellular communication and can regulate the biological properties of target cells. With the deepening of exosome research, it is found that exosomes are strictly related to the occurrence and development of COPD. Therefore, this review aims to highlight the unique role of immune-cell-derived exosomes in disease through complex interactions and their potentials as potential biomarkers new types of COPD.

Keywords: exosomes, COPD, immune cell, biomarker, treatment

INTRODUCTION

Chronic obstructive pulmonary disease (COPD) is a common chronic airway disease, characterized by irreversible, progressive airflow limitation, and repeated airway inflammation, which seriously affects the patient's breathing and interferes with the patient's life and work (1, 2). There are several viewpoints in COPD's pathogenesis, such as oxidative stress, epigenetics, cell aging, apoptosis, chronic inflammation, protease/antiprotease, and linear green body function (3). Environmental factors and genetic mutations play a role in it. Exposure to cigarette smoking(CS), whether active smoking or second-hand smoke, is the leading risk factor to get COPD (4, 5). Environmental pollution and occupational chemical exposure in some developing countries, are essential factors causing COPD (6). Exposure to indoor air pollution can affect unborn babies and is a risk factor for chronic obstructive pulmonary disease. According to the World Health Organization (WHO), COPD is the third leading cause of death globally. Statistical projections state that by 2040, the annual death toll will reach 4.4 million, and 90% of chronic obstructive pulmonary disease deaths will be more in both low-income and middle-income countries (7, 8). The airway epithelium CS events such as the first contact, long-term exposure to CS can induce epithelial cells to produce pro-inflammatory medium, senescence-associated secretory phenotype (MCP-1, IL-1, IL-6, IL-8),

damage-associated molecular patterns (receptor for advanced glycation end-products, heat shock proteins, S100 proteins, high-mobility group box), the media which is released into the pulmonary and systemic circulation (9, 10), can stimulate the damage to the lung parenchyma, alveolar damage, and promote the development of COPD (11). Current treatment methods for COPD can only slow down the loss of lung function and cannot reverse the deterioration of lung structure and function. Therefore, it is essential to understand the molecular mechanism of COPD's occurrence and development and optimize the clinical treatment strategy. Various studies support the fact that exosomes containing miRNA, lncRNA, and proteins that are involved in the pathogenesis of COPD (12, 13), many exosomes, including miR-101, miR-223, miR-144, and miR-1274a act by influencing the molecular pathways associated with the pathogenesis of COPD which includes Kras, Notch, Smad, and TGF-β (14). Besides, these molecules are potential candidates for the early diagnosis and treatment of COPD. There are much-emerging shreds of evidence reporting that increased or decreased exosomes' expressions are a common feature of various lung diseases, including COPD (15). Takahashi et al. reported that changes in exosome numbers could predict a patient's physiological outcomes. For example, exosomes derived from bronchial endothelial cells were increased significantly in stable COPD (SCOPD), which were also increased in acute exacerbation COPD (AECOPD) (16).

Exosomes can maintain the stability of the intracellular environment (17). However, they can also get involved in different functions of the recipient cells (18). Direct exposure to a harmful stimulus (e.g., CS, air pollutants, and infection) may affect the nucleic acid load of lung-derived exosomes and participate in the progress of lung diseases (19). It was also found that exosomes may cause COPD pathological disturbances, that include chronic inflammation, oxidative stress, multiple organ dysfunction, epigenetic changes, cell apoptosis, aging, and diseases related to linear green body dysfunction (20, 21), and this proves that exosomes may act as a promising biomarker for the diagnosis of COPD (14). This is because, during the progression of COPD disease, COPD patients will produce a large number of exosomes, and can be isolated from sputum (22), plasma (23, 24), bronchial lavage fluid (BALF) (25), which suggests that exosomes considered as potential non-invasive diagnostic tools for COPD. This review first introduces the biological characteristics and functions of exosomes, introduces the role of exosomes in mediating intercellular communication and regulating immune cells in COPD, and finally clarifies the recent progress of exosomes in auxiliary clinical diagnosis and treatment of COPD.

Abbreviations: AECOPD, acute exacerbation chronic obstructive pulmonary disease; A1AT, alpha one anti-trypsin; Alix, ALG-2 interacting protein X; AM, alveolar macrophages; BALF, bronchial lavage fluid; CAMP, cyclic adenosine monophosphate; CCN1, protein cysteine-rich angiogenic protein 61; CCR10, chemokine receptor 10; COPD, chronic obstructive pulmonary disease; COX2, cyclooxygenase-2; CS, cigarette smoking; CSE, cigarette smoke extract; DC, dendritic cells; ECM, extracellular matrix; EMT, epithelial-mesenchymal transition; FAIM, Fas apoptosis inhibitory molecule Hsp70: heat shock 70 kDa protein 4; FEV1, forced expiratory volume in 1 s; FEV1/FVC, forced expiratory volume in 1 s/forced vital capacity; FFMI, fat-free body mass index; HBECs, human bronchial epithelial cells; HPMECs, human pulmonary microvascular endothelial cells; HRV, human rhinovirus; ICSs, Inhalation corticosteroids; lncRNA, long non-coding RNA; MAP3K, mitogen-activated protein kinase kinase kinase; MC, mast cells; miRNA, microRNA; MMP, matrix metalloproteinase protein; MVB, multivesicular bodies; Mϕ, macrophages; NE, neutrophilic elastase; NK:17, natural killer cells; NTHI, non-typeable Hemophilus influenza; NOR, neuron-derived orphan receptor; PASMCs, pulmonary artery smooth muscle cells; SCOPD, stable chronic obstructive pulmonary disease; SOCS, suppressor of cytokine signaling; siRNA, Small interfering RNA; STAT, signal transducer and activator of transcription; TGF-β, transforming growth factor β; TNFR2, tumor necrosis factor receptor 2; Trop, Trophoblast cells surface antigen; Tsg101, tumor susceptibility gene 101; TUG1, taurine-upregulated gene 1; UCHL1, ubiquitin C-terminal hydrolase; WHO, World Health Organization.

MAIN COMPONENTS OF EXOSOMES

Biological Characteristics of Exosomes

Exosomes are membrane vesicles with a bilayer lipid of about 30–150 nm in diameter, produced by early and late endosomes, and eventually, form multivesicular bodies (MVB) (26). A variety of cells releases these vesicles, such as structure cells (epithelial cells, endothelial cells, and alveolar I and II, alveolar macrophages, fibroblasts), and immune cells (B and T lymphocytes, macrophages, dendritic cells) (3). CD9, CD63, CD81, and CD82 proteins from the peripheral membrane are fused during release into the extracellular space. These proteins are considered markers of exosomes (27). Besides, endosome markers also include heat shock 70 kDa protein 4 (Hsp70), MHC classes I and II, ALG-2 interacting protein X (Alix), and tumor susceptibility gene 101 (Tsg101) (28, 29).

The Genetic Material in Exosomes

The main components of exosomes are protein and lipid, genetic material including DNA, mRNA, miRNA, lncRNA, and metabolites (30, 31). Among them, miRNA is a highly studied regulatory molecule. It has found that a small non-coding RNA between 19 and 25 nucleotides in length together with silencing the 3′-untranslated region (3′UTR) of the target mRNA, negatively regulates its expression at the transcriptional and post-transcriptional levels, which in return affects various cellular functions such as proliferation, apoptosis, differentiation, and emergency resistance. The events mentioned above also affect biological processes that include autophagy, inflammatory response, cellular senescence, tissue remodeling, immune regulation, and angiogenesis (32, 33). These processes usually involve the level of multiple genes. Besides, the length of the lncRNA is over 200 nucleotides, and located in the nucleus, transcripted by RNA polymerase II, but cannot make reaction with proteins; lncRNA has been shown to participate in mRNA splicing after transcription and protein translation process, usually expresses the tissue specificity and cell specificity, and in the maintenance of steady-state (34). More information about these two types of RNA is summarized in **Table 1**.

Biological Functions of Exosomes

Exosomes can transmit information to target cells in three ways: (1) Interact with the cell surface through receptors; (2) Endocytosis; (3) The direct fusion of outer cell membrane and

plasma membrane as it is shown in **Figure 1**. Briefly, exosomes' primary function is to transport essential substances and mediate communication between cells (35). This biological effect unit regulates the properties of target cells (36, 37). More evidence shows that exosomes are involved in different respiratory diseases, including COPD (38). In airway physiology, exosomes from alveolar macrophages, epithelial cells, and endothelial cells affect the disease's progress in controlling the stability of the intracellular environment and changing the function of receptor cells (39). Under normal circumstances, exosomes are highly stable in biological fluids due to the bilayer protection of lipids. High-throughput sequencing technology can detect highly sensitive and highly specific exosomes. A large amount of exosome secretion can be detected in various biological fluids, such as sputum, blood, BALF, urine, pleural effusion, ascites, synovial fluid, and breast milk (40). This makes exosomes potentially valuable for the diagnosis, prognosis, and treatment of respiratory diseases.

TABLE 1 | miRNA vs. lncRNA.

	miRNA	lncRNA
Source	Pri-miRNA	Multiple sources
Length	19–25 nt	>200 nt
Protein coding	no	no
Regulatory target	mRNA 3′UTR	Proteins, RNAs, and DNAs
Effect	Up-regulate or downregulate mRNA	Up-regulate or downregulate target
Mechanisms	Inhibits gene expression at the transcriptional and post-transcriptional levels	Maintain the dynamic balance of cells and tissues and regulate inflammation

miRNA, microRNA; lncRNA, long non-coding RNAs.

THE CLINICALLY RELEVANT ROLES OF EXOSOMES IN COPD

Chronic obstructive pulmonary disease is a chronic inflammatory respiratory disease characterized by irreversible airflow limitations caused by prolonged exposure to cigarette smoke or harmful irritants. Multiple studies have demonstrated that exosomes play an essential role in the occurrence and progression of COPD, including inflammation of the lung parenchyma and surrounding small airways (chronic bronchitis), degeneration of lung tissue (emphysema), and remodeling of small airways, leading to decreased lung function (41). The related exosomes miRNAs and lncRNAs involved in COPD's development and progression are summarized in **Figure 2**.

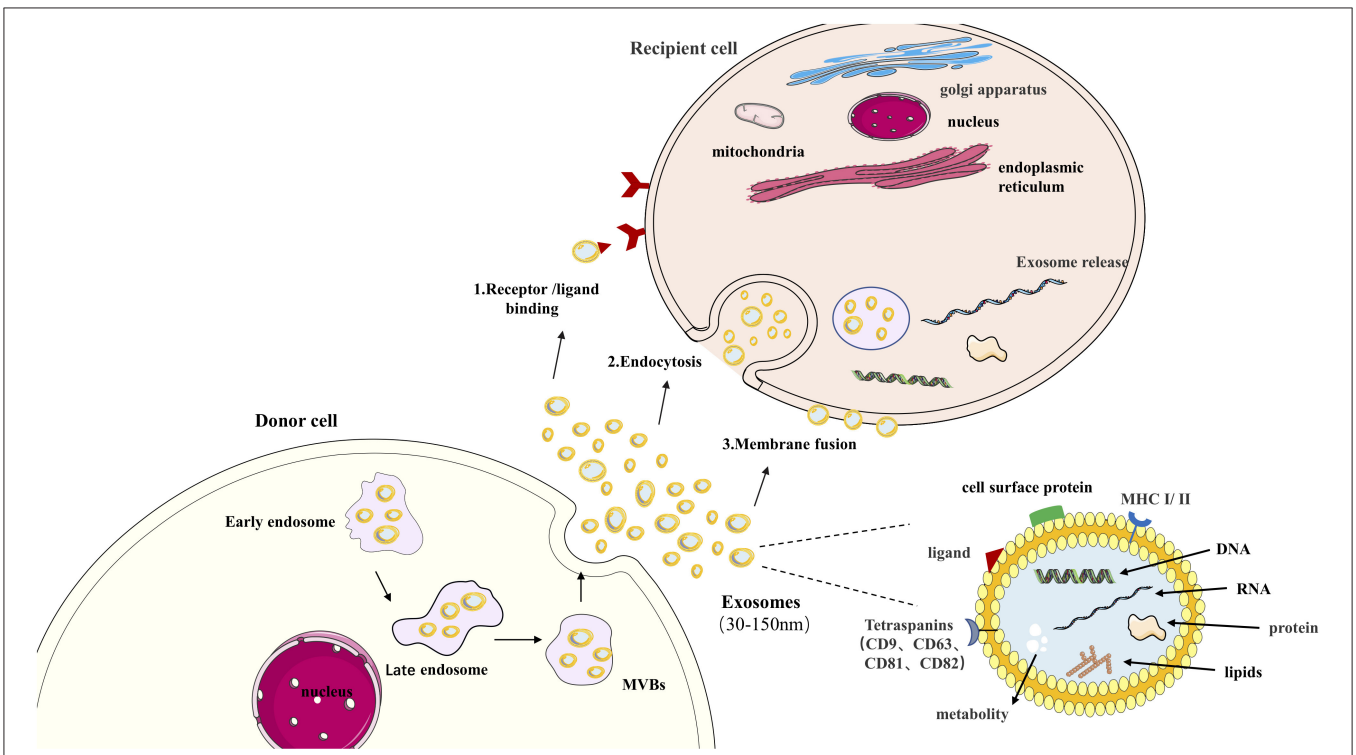

FIGURE 1 | Exosome in cell communication. Exosomes are nanovesicles (30–150 nm) that originate formed by early endosomes, late endosomes, and ultimately multivesicular bodies (MVB). Exosomes contain a variety of proteins, lipids, DNA, RNA, and metabolites. The cell body's surface includes major histocompatibility complex (MHC I/II), Tetraspanins (CD9, CD63, CD81, CD82), cell surface proteins ligand. This confers them with functional features. Exosomes can transmit information to target cells by: (1) binding to the cell surface by ligand, (2) endocytosis, (3) direct fusion of extracellular with plasma membranes.

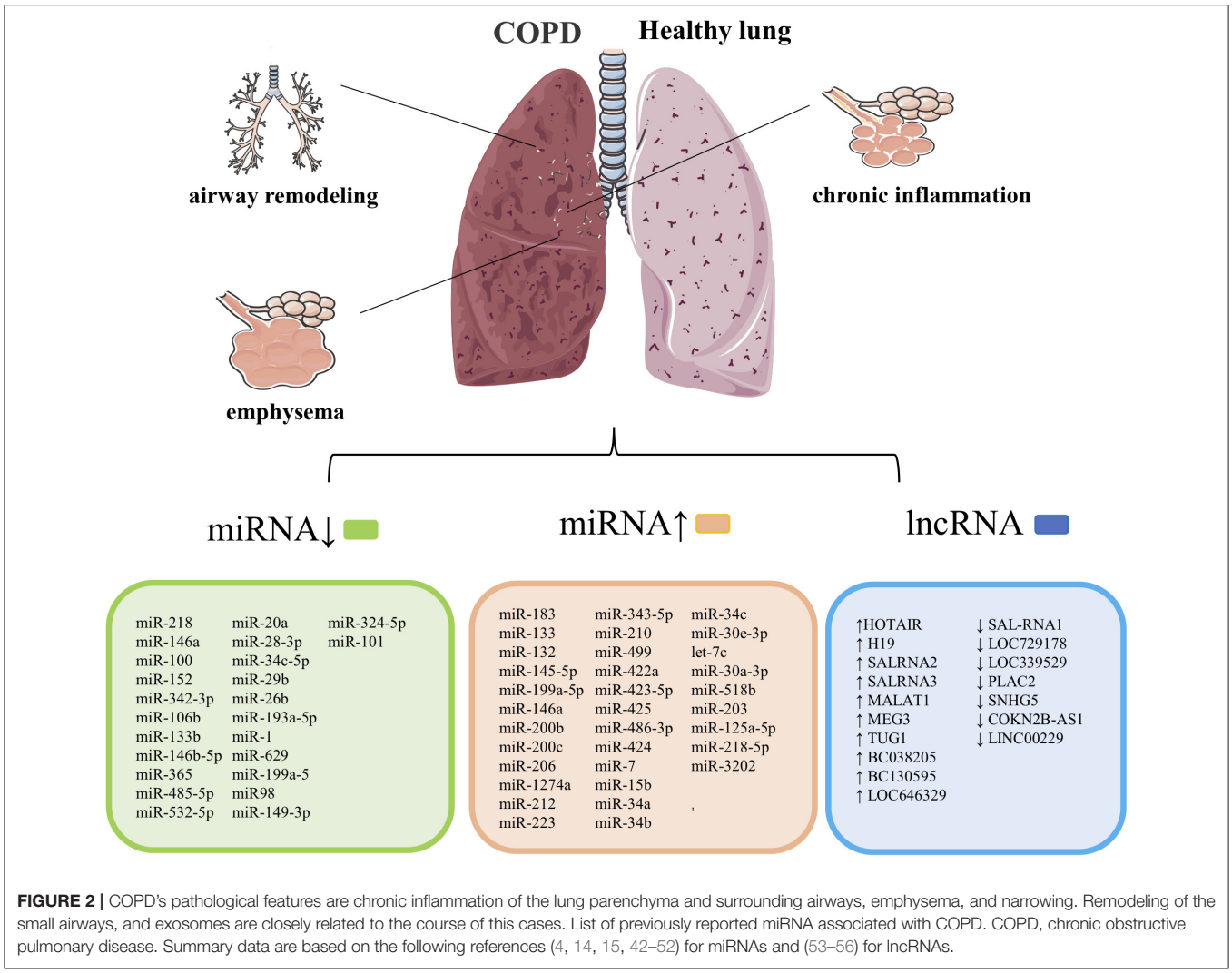

FIGURE 2 | COPD's pathological features are chronic inflammation of the lung parenchyma and surrounding airways, emphysema, and narrowing. Remodeling of the small airways, and exosomes are closely related to the course of this cases. List of previously reported miRNA associated with COPD. COPD, chronic obstructive pulmonary disease. Summary data are based on the following references (4, 14, 15, 42–52) for miRNAs and (53–56) for lncRNAs.

The Role of Exosomes in the Pathogenesis of COPD

Exosomes and Chronic Airway Inflammation

Cordazzo et al. reported that cigarette smoke extract (CSE) could induce exosomes to be released from mononuclear cells, induce bronchial epithelial cells to produce IL8, monocyte chemoattractant protein-1, and up-regulate CD542, thereby promoting inflammation (57). Also, Tan et al. believe that inflammation and exosomes increase in patients with COPD Relevant, they used Exo ELISA kits to compare the levels of $CD9^{+}$ exosomes in COPD patients and healthy controls, and found that the levels of COPD patients were significantly higher (58). Moon et al. believe that exosomes rich in COPD-related protein cysteine-rich angiogenic protein 61 (CCN1) can be cleaved after CS exposure. CCN1 allows inflammatory signaling to the far end of the lung. Interaction with integrin 7 in pulmonary epithelial cells activates the secretion of matrix metalloproteinase protein (MMP-1) in pulmonary epithelial cells, thereby promoting the release of vascular endothelial growth factor and IL-8.Il-8 promotes neutrophil infiltration into the lung parenchyma and causes inflammation (59). Besides, after CSE treatment, MEG3 up-regulated in 16HBE cells of COPD patients can release the expressions of inflammatory factors IL1, IL6, and TNF by regulating HSA-Mir-218, thus inducing inflammation and cell apoptosis.

Exosomes and Emphysema

Emphysema is characterized by decreased airway elasticity, hyperinflation, and swelling of the terminal bronchioles (60). Ezzie et al. believe that transforming growth factor β (TGF-β) suggested changes in miRNA expression, such as miR-223 and miR-15b. After knocking out the transforming growth factor TGF R-II in mouse lung epithelial cells, they showed emphysema signs (14). Van Pottelberge et al. analyzed miRNA expression in sputum samples from 32 subjects using qPCR. The results showed that the expression of miR-125b and let-7C in PATIENTS with COPD was lower than that in healthy non-smokers. Low let-7C expression was negatively correlated with the concentration of tumor necrosis factor receptor 2(TNFR2) (42).

TABLE 2 | List of miRNAs potentially associated with COPD pathogenesis.

miRNA	Expression	Target	Function/pathogenesis	References
miR-210	↑	ATG7	Promoted myofibroblast differentiation in primary lung fibroblasts control autophagy	(63)
miR-144	↑	CFTR, IRF7	Regulate inflammatory and antiviral responses in COPD	(43)
miR-101	↑	CFTR, MKP1		
miR-223	↑	TGF-β	TGF-β signal activation is associated with emphysema	(14)
miR-15b	↑	SMAD7	TGF-β inhibitory primary intracellular signal smad2/3/4	(14)
miR-218	↓	NF-κB	Up-regulates the expression of several pro-inflammatory cytokines by AEC, including IL-6 and CXCL8.	(65)
miR-128-5p	↓	apoptotic processes	Participate in the epithelial damage and remodeling in COPD	(44)
miR-181d	↑	and growth factor pathways		(43)
miR-1274a	↑	FOXO4	Probably related to oxidative stress or cellular aging in COPD	(14)
miR-1	↓	AKT	COPD-associated skeletal muscle dysfunction	(66)
miR-542-5p	↑	–		(45)
miR-542-3p				

↑*Upregulation;* ↓*downregulation.*

Furthermore, Stockley and Turne reported that glycoproteins alpha one anti-trypsin (A1AT) works by inhibiting the process of preventing excessive inflammation neutrophils and eosinophil enzymes work, and A1AT deficiency will lead to the development of emphysema (61). It was also found that in the evaluation of miRNA expression in lung tissue of patients with COPD patients with mild and moderate emphysema, moderate five miRNAs in lung samples of emphysema patients were significantly down-regulated, namely miR-34c, miR34b, miR-149, miR-133a, and miR-133b. Among them, the expression of miR-34c was significantly down-regulated (62).

Exosomes and Airway Remodeling

Long-term harmful stimuli lead to damage to airway epithelial cells, promote phenotypic changes of epithelial cells, and lead to fibrosis and airway remodeling. Fujita's research showed that CS-induced down-regulation of miR-210 could drive the differentiation of myofibroblasts in airway remodeling and inhibit the expression of ATG7 in LFS to control the autophagy process directly (63). This indicates that exosomes may contribute to the tracking of COPD differentiated fibers. miR-15b may be involved in airway remodeling by mediating TGF- related signaling pathways (15). Besides, it has also revealed that different microRNAs such as miR-224, miR-339-5p, and miR-382 are involved in COPD's pathogenesis (64), and particular pieces of information are presented in **Table 2**.

Gu's research shows that taurine-upregulated gene 1 (TUG1) expression is enhanced in COPD patients, and TUG1 inhibits the expression of miR-145-5pp/DUSP6 axis to promote airway remodelings such as TGF-β1, mucus hypersecretion, collagen 1 and α-SMA and inflammation such as increased IL-6 and pulmonary neutrophil infiltration (67). TUG1, combined with CDKN2B-AS1, can be used to predict acute exacerbation in COPD patients (68). It was found that the expressions of SAL-RNA2 and SAL-RNA3 (senescence-related genes) were significantly increased in COPD lung tissues, and the expressions of p53 and P21 were up-regulated. This shows that lncRNA in airway epithelial cells II type error control in the process of aging may be involved in the pathogenesis of COPD (53). In summary, exosomes influence COPD's occurrence and development by regulating inflammatory, emphysema, airway remodeling, and pulmonary fibrosis. MiRNAs and lncRNAs involved in the development of COPD are summarized in **Figure 2**.

Immune Cell-Derived Exosome Participate in COPD

Exosomes are recognized as tools for mediating intercellular communication and signal transduction and signaling to immune cells to regulate function. Various studies highlighted that exosomes are secreted by some types of cells, including immune cells, such as B lymphocytes (69), T lymphocytes (70), macrophages (Mϕ) (71), mast cells (MC) (30), dendritic cells (DC) (72), and 17 natural killer cells (NK) (73). Immune-cell-derived exosomes perform numerous physiological and pathological functions, including antigen presentation, immunosuppression, T-cell polarization toward Treg cells, and anti-inflammatory effects, to enhance or suppress immune activity (74). Infiltration of various immune cells, such as neutrophils and macrophages, into small airways, is a common phenomenon in COPD (75). For these reasons, in-depth research is needed to explore the role of immune-cell-derived exosomes in COPD.

Role of Macrophages and Exosomes in COPD

Alveolar macrophages (AM) form the first host defense line against infection/inhalation of harmful substances. They are one of the primary cells in the lung that produce exosomes (76). AM promotes inflammation of COPD. First, macrophage-derived exosomes induce differentiation of immature monocytes into macrophages by mediating miR-223 (77). Exosomes miR-17 and miR-221 then promote macrophage migration by mediating integrin β under sterility stimulation (78). Finally,

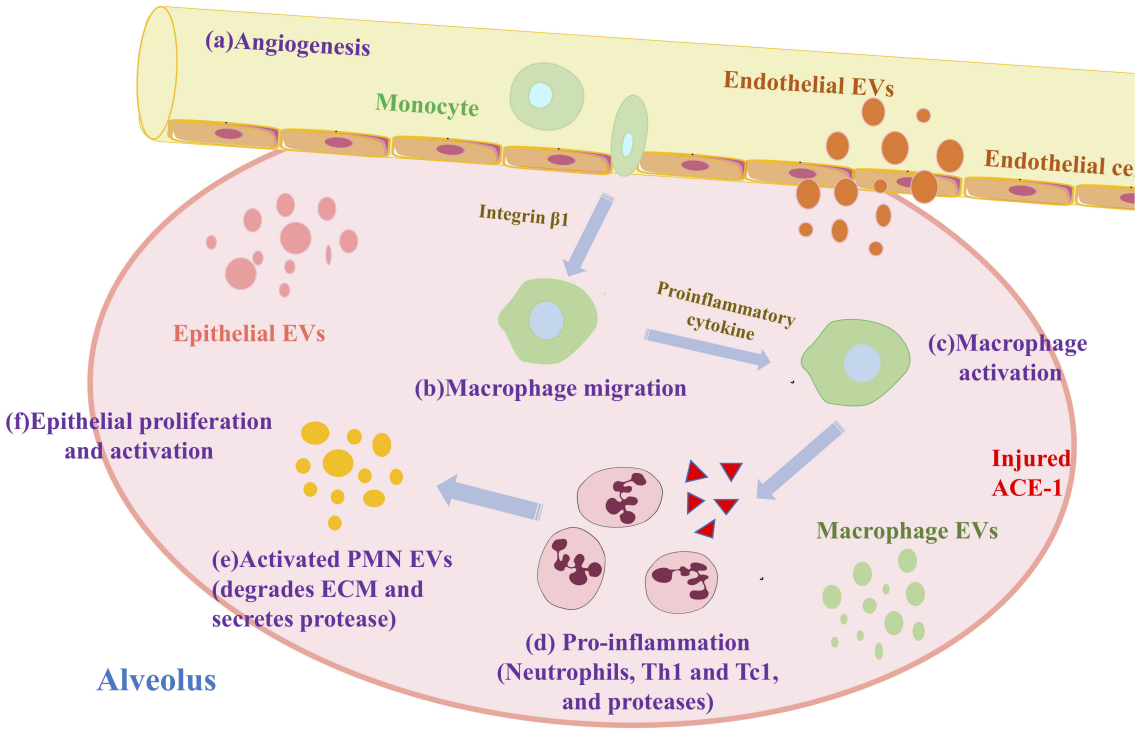

FIGURE 3 | Exosomes and macrophages promote alveolar inflammation in COPD.

exosomes miR-221 and miR-320 stimulate the secretion of pro-inflammatory cytokines, thereby activating AM (79). After a series of differentiation, migration, and activation, AM recruits neutrophils, Th1, and Tc1, to promote inflammation (32). The specific process is shown in **Figure 3**.

After CS stimulation, miRNA mediated by endothelial cells, such as miR-125a, miR-126, miR-191, were transferred to macrophages to promote apoptotic cell clearance (80). A study reported that macrophages release outside secretes body with antigen-presenting ability lower associated macrophage transfer specific immune (81). Kulshreshtha et al. found that epithelial-derived exosomes extracted from BALF of mice with COPD induced undifferentiated macrophages and proliferative effects (82). During the pathogenesis of COPD, alveolar macrophages combine with suppressor of cytokine signaling (SOCS) protein, which is taken up by alveolar epithelial cells and inhibits IFN γ-induced signal transducer and activator of transcription (STAT) (58). Also, M1 macrophages (pro-inflammatory) are the predominant cells in the peripheral blood of COPD patients, leading to pro-inflammatory factors (IL-1β, IL-12, TNF-α) and lncRNA miR-155HG are up-regulated (83). As mentioned above, the studies show that the increase of exosomes in the regulation of lung inflammation by macrophages in the lung has practical significance.

Role of Neutrophils and Exosomes in COPD

Neutrophils are a crucial component of innate immune responses in COPD, and Kristopher described a new pathogen, activated PMN (neutrophil) source of NE-rich exosomes (84). These exosomes bind and degrade the extracellular matrix (ECM) involved in COPD's pathogenesis. Mac-1 and neutrophilic elastase (NE) play essential roles in this process. NE is the surface binding protease obtained by $CD63^{+}/CD66b^{+}$ nanovesicles during PMN degranulation, and NE is resistant to A1AT. It is because of the resistance of the A1AT. The ECM targeting, the outer body of the outer body, which is more potent than the free NE biology (85), and an imbalance of the proteinase-antiprotease system are typical in COPD (86). In this system, PMN-derived NE and lung suppressor A1AT are most prominent (87). Experiments have shown that injecting enough NE into an animal's airways can cause emphysema (88). These findings show that novel exosomes derived from neutrophils participate in disease progression by breaking ECM dynamic balance through NE activity in COPD.

Role of Other Cells and Exosomes in COPD

Among mast cells, the exosomes of human mast cell line-1 overlapped with the proteins of the exosomes inhaled by the patient, suggesting that mast cells also contribute to the lung exosome pool (89). It is worth noting that exosomes from NK cells can react against NK cells and increase the cytotoxic activity and NK cells' targeting (90). Besides, exosomes released by macrophages, NK cells, and dendritic cells through a paracrine act as pro-inflammatory mediators of the innate immune system (81). Exosomes secreted by DC are associated with amplification of the immune response, and DC-based exosomes induce

specific humoral responses and activation of $CD4^+$T cells and $CD8^+$T cells (91). As mentioned above, immune cell-derived exosomes are involved in the development and progression of COPD. Exosomes derived from circulating immune cells have immunomodulatory effects. Therefore, it has been reported that immune-cell-derived exosomes can be delivered to target cells by small molecule drugs or specific molecules to stimulate the immune system in patients to recognize and destroy lesions (90). Also, exosomes derived from circulating immune cells can serve as specific biomarkers for the severity of inflammation, which has been demonstrated in liver inflammation (92, 93). The application of exosomes derived from immune cells in immunotherapy is now considered a promising tool in COPD treatment. In conclusion, there are still many questions to be answered about the relationship between immune cells and exosomes involved in lung inflammation and injury in COPD.

CLINICAL APPLICATION OF EXOSOMES IN COPD

Exosomes as Potential Biomarkers for the Clinical Diagnosis of COPD

The study results compared healthy exosomes and exosomes released by bronchial epithelial cells in COPD patients, especially in the AECOPD, and the study reported that exosomes from AECOPD were significantly increased. Moreover, they found that by detecting exosomes' content, pulmonary endothelial cell apoptosis can be analyzed. The degree of activation and the dysfunction of endothelial cells is directly related to the severity of COPD. It is usually evaluated by forced expiratory volume in 1 s (FEV1) to track the disease's advancement (16). Lacedonia and his research team reported that the number of exosomes in sputum is negatively correlated with FEV1, similar to changes in exosome levels related to inflammation. It shows that senescent cells accumulated with age in COPD may affect the release and competition of circulating exosomes (94). Moreover, Shi et al. reported that miR-203 might be a new biomarker for COPD diagnosis; it is just because miR-203 targets P13KCA to inhibit nuclear factors light chain enhancers, which activate B cell signaling pathways significantly involved in COPD (95). Another critical study showed that evidence suggests that miR-21 has potential value in the diagnosis and treatment of COPD. The level of miR-21 in the serum of smokers and patients with COPD is significantly increased. The increased level of miR-21 is associated with the percentage of forced expiratory volume in 1 s/forced vital capacity (FEV1/FVC) (18).

Besides, comparing miR-4455 and miR-4785 in smokers and non-smokers in COPD patients, there was a significant expression difference (96). This made the two exosomal microRNAs to be considered as a potential biomarker for early diagnosis of COPD. Chronic obstructive pulmonary disease, early diagnosis, and patient monitoring are other essential factors. Based on that, researchers conducted a study. They found that miR-218-5p is another essential miRNA that plays an essential role in COPD pathogenesis and promises to be a successful candidate for diagnosing and controlling COPD patients (65). Moreover, other essential study findings showed that miR-29c and miR-126 were up-regulated in Stage III COPD patients relative to stable controls. Such results indicate that all these miRNAs may be used as screening biomarkers for COPD patients (97). As mentioned above from different studies, the findings show that exosomal miRNAs can be used as potential biomarkers for the diagnosis of COPD.

Application of Exosomes in COPD Prognosis

Studies have shown that exosomes with CD144, CD31, and CD62E are more abundant in patients with AECOPD than in patients with SCOPD, suggesting that COPD patients tend to deteriorate can be used as an indicator of prognosis (16). Ge et al. detected the expression of ANRIL in SCOPD patients, AECOPD, and the whole group. They found that the expression of ANRIL in AECOPD patients was the lowest. The expression of ANRIL in SCOPD patients was not related to the GOLD stage. In contrast, the expression of ANRIL in patients with AECOPD was negatively correlated with the GOLD stage. Most importantly, ANRIL expression in patients with AECOPD and stable COPD is negatively correlated with inflammatory cytokines such as IL1B, IL17A, TNF, and LTB4 (98). They finally concluded that lncRNA ANRIL (antisense non-coding RNA at INK4 locus) is associated with chronic diseases' occurrence and prognosis.

It is well-known that skeletal muscle weakness is a severe systemic complication of COPD, which seriously affects patients' quality of life and mobility. Lewis et al. showed that exosome miR-1 plays a crucial role in skeletal muscle dysfunction in patients with COPD, associated with smoking history, function, defatted body mass index, 6-min walking distance, and percentage of quadriceps type I muscle fibers (66). Besides, compared with healthy COPD patients with fat-free body mass index (FFMI), H19 is expressed by demethylation isolation of has-miR-519a after up-regulation increases patients' susceptibility with COPD to low FFMI (99). So far, researchers have used exosomes as a potential non-invasive biomarker for COPD that has never stopped. In short, these studies are mainly used to identify the role of exosomes in the diagnosis of COPD, providing a new basis for the early clinical diagnosis of some exosomes in COPD. Through continuous efforts, new diagnostic tools and more complete treatment methods may appear.

Exosomes Are Essential in the Treatment of COPD

COPD Treatment Using Exosomal miRNA

At present, the drugs used to treat COPD are mainly bronchodilators, which are borrowed from medications used to treat asthma. Inhalation corticosteroids (ICSs) are added to LAMA/LABA combination therapy (triple therapy), and the risk of exacerbation and death in COPD patients. However, most patients are not sensitive to steroids, and the use of large doses increases the risk of pneumonia (100). Therefore, COPD patients urgently need critical target treatment. There is also a great need

for drugs to prevent the aggravation of the disease and pulmonary hypertension, plus many other COPD complications.

Sun's study reported that miR-206 expression in human pulmonary microvascular endothelial cells (HPMECs) exposed to CS was up-regulated. They also noted that both Caspase3 and HPMEC apoptosis activities were increased. There was a negative correlation between the expression levels of miR-206 and Notch3 and VEGFA mRNA levels. During their study, they concluded that miR-206 could directly target Notch3 and VEGF-A to regulate the process of COPD vascular remodeling (101). It was reported that anti-miR-27-3p could effectively reverse the inflammatory process and reduce the infiltration of neutrophils and macrophages in the lungs and the level of inflammatory cytokines in BALF. Another study aimed to determine miRNA-3202 in COPD noted that the overexpression of miR-3202 could significantly inhibit the increase of T lymphocyte IFN-γ and TNF-α levels induced by CSE while increasing the expression of Fas and FasL. The study also revealed that the high levels of miR-3202 pass target gene Fas apoptosis inhibitory molecule (FAIM) 2 to inhibit T cell apoptosis and protect human bronchial epithelial cells (HBECs). FAIM2 plays a central role in COPD's pathogenesis, inhibits T cell death, and participates in CS-induced cell apoptosis and cell wall destruction (64). Besides, it has also been found that the high levels of miR-145-5p alleviate CS-induced apoptosis and the production of pro-inflammatory cytokines by inhibiting the lytic expression of p53 and caspase339. Besides, some miR-145-5p and KLF5 inhibits CSE-induced NF-κB signal activation, thereby reducing participation in the pathogenesis of COPD (102).

Du et al. tested the expression rates of miR-181c in 34 COPD (smoking cases) patients relative to safety controls, and findings showed that miR-181c might be slightly less controlled in COPD patients than healthy control patients had never smoked. They also demonstrated that the upregulation of miR-181c might be correlated with several consequences, such as inflammatory response reduction, neutrophil invasion, reactive oxygen species formation, and inflammatory cytokine development. MiR-181c downregulation may be correlated with different consequences. They also found that miR-181c exerts its impact by attacking CCN1. The downregulation of the miR-181c could contribute to the increase in CCN1 expression in the pulmonary tissues of patients with COPD relative to stable controls. The results mentioned above show that miR-181c might be used as a therapeutic target to treat COPD patients (103). Another study also reported that the deregulation of miR-126 is correlated with ATM kinase activation, and they have also demonstrated that miR-126 levels have been decreased in the smoker and COPD endothelial blood cells relative to non-smoker subjects. These findings indicated that the reduction of miR-126 through ATM targeting might facilitate tissue aging and dysfunction in smokers and COPD subjects. This miRNA may also be seen as a new therapeutic target for treating COPD patients (104). Taken together, it is clear that exosomes play an essential role in the treatment of COPD patients.

The Treatment of COPD by Synthetic siRNA

Synthetic siRNAs' potential to treat COPD by transcriptionally down-regulating target genes' expression has been successfully

TABLE 3 | Principle, advantages and disadvantages of common exosome isolation methods.

Methods	Theory	Advantages	Disadvantages	References
Ultracentrifugation techniques (UC)	The required components are obtained according to the size and density differences of each component in the sample.	There is no need to mark the outer cut body to avoid cross contamination	High cost, Time consuming, structural failure, aggregation and lipoprotein separation are not conducive to downstream analysis	(46)
Density gradient centrifugation	Usually used in combination with the overspeed centrifuge method	Improve the purity of exosomes	The high viscosity of sucrose solution will reduce the settling velocity of exosomes and lead to long time consuming	(47)
Polymer Precipitatio	Using the method of virus extraction, exosomes is obtained by reducing the solubility of exosomes, usually using polyethylene glycol (PEG) as medium	Simple operation, short analysis time, suitable for large—dose sample treatment	Due to its low purity and recovery rate, the resulting polymer is difficult to remove and may produce false positive	(48)
Size-based isolation techniques	Based on the size differences between exosomes and other components of a biological sample	Fast, simple, low-cost and separated exosomes have complete structure and uniform size, and their biological characteristics will not be significantly affected.	Other particles of similar size are difficult to separate, resulting in reduced purity	(46)
Ultrafiltration	Ultrafiltration membranes with different molecular weight cutoffs (MWCO) were used to selectively separate the samples	The sample cost is low, the concentration efficiency is high, and the activity of the exosomes is not affected	Low purity and poor binding of the exosomes to the ultrafiltration membrane resulted in low recovery rate.	(49)
Immunoaffinity chromatography (IAC)	The specificity of antibodies and ligand is combined to separate the required exosomes from heterogeneous mixtures	The sample size required is small.It can be used for the qualitative and quantitative detection of exosomes.This method has strong specificity, high sensitivity, high purity and high yield	The preservation condition of the exosomes obtained by this method is harsh, and it is not suitable for large scale separation of the exosomes. The non-specific interference adsorption of matrix produces interfering proteins, which limits the wide application of this method.	(50)

validated in multiple animal models (105). For example, mitogen-activated protein kinase kinase kinase (MAP3K) 19 phosphorylates the nucleus of Smad2/3 Translocation and activation of NF-κB reduces lung neutrophil infiltration and BALF levels of KC (a mouse homolog of human IL-8) (106). A recent study has shown that it is caused by infection of the upper respiratory tract. Among the causes of worsening COPD, human rhinovirus (HRV) and non-typeable Hemophilus influenza (NTHI) is the most common. The combined HRV/NTHI response increased IL-17C production, and IL-17C-specific siRNA could block IL-17C and CXCL1 and neutrophil migration induced by HRV/NTHI (107). Trophoblast cells' surface antigen (Trop) 2 expressed on the basal lung compartment's multipotent progenitor cells in preventing COPD airway remodeling Surface antigen. Its specific siRNA reverses cell movement and migration of basal cell hyperplasia. Epithelial-mesenchymal transition (EMT) (108), COPD combined pulmonary hypertension is a common complication of patients, which is closely related to the high expression of the neuron-derived orphan receptor (NOR)1.NOR1 plays a role in regulating inflammation and vascular remodeling. Its specific siRNA inhibits hypoxia-induced cyclin D1 level, cell proliferation, and DNA synthesis in primary human pulmonary artery smooth muscle cells (PASMCs) (109) SI00A4, a secretory member of S100 calcium-binding protein, is highly expressed in COPD patients and mouse models and is involved in the proliferation, migration, and EMT of smooth muscle cells. HIF-1α or HIF-2α siRNA can inhibit the high expression of S100A4 (110). Based on the above facts, exosomes play a crucial role in the treatment of COPD. However, COPD is a disease caused by a variety of factors.

FUTURE DIRECTION AND THE LIMITATION

The study of exosomes vs. COPD is an emerging and rapidly evolving field where we can use exosomes to develop therapeutic tools to prevent and stop lung injury caused by COPD. However, there are still many problems to be solved, such as the lack of uniformity and standardization of exosome detection, isolation, and purification technologies. The advantages and disadvantages of exosome isolation methods are shown in **Table 3**. Secondly, the mechanism of exosome uptake by recipient cells is not fully understood. Also, collecting tissue samples from the lungs is more complicated. More in-depth studies are needed to fully understand the pathogenesis of exosomes in COPD and fully reveal the role of miRNA and lncRNA in the disease.

CONCLUSION

Chronic obstructive pulmonary disease is a heterogeneous disorder marked by airway inflammation, lung tissue damage, and airflow restriction consistent with airway remodeling. Exacerbations are a significant cause of disease development, morbidity, and death, and novel therapies and medications for COPD remain particularly crucial due to a lack of effective drugs. Exosomes are incredibly durable and practical packages of cellular material. They can transfer their bioactive loads to receiver cells across the body, influencing physiological and pathological conditions. Exosomes have considerable clinical value due to their capacity to be controlled and optimized to guide treatment. Although this review tried to highlight the latest evidence of exosomes from various cell sources as biomarkers and their potential for application in COPD treatment, in-depth researches are needed to be used in daily early diagnosis and treatment of COPD.

AUTHOR CONTRIBUTIONS

NW and QW designed and drafted the manuscript. TD, AG, XW, LS, XL, and KX discussed and revised the manuscript. All authors read and approved the final manuscript.

FUNDING

This work was supported by the Natural Science Foundation of Shandong Province, China (Grant no. ZR2020MH008).

REFERENCES

1. Putcha N, Puhan MA, Hansel NN, Drummond MB, Boyd CM. Impact of co-morbidities on self-rated health in self-reported COPD: an analysis of NHANES 2001-2008. *COPD*. (2013) 10:324–32. doi: 10.3109/15412555.2012.744963
2. Chen Y, Wang H, Luo G, Dai X. SIRT4 inhibits cigarette smoke extracts-induced mononuclear cell adhesion to human pulmonary microvascular endothelial cells *via* regulating NF-κB activity. *Toxicol Lett*. (2014) 226:320–7. doi: 10.1016/j.toxlet.2014.02.022
3. Sundar IK, Li D, Rahman I. Small RNA-sequence analysis of plasma-derived extracellular vesicle miRNAs in smokers and patients with chronic obstructive pulmonary disease as circulating biomarkers. *J Extracell Vesicles*. (2019) 8:1684816. doi: 10.1080/20013078.2019.1684816
4. Salimian J, Mirzaei H, Moridikia A, Harchegani AB, Sahebkar A, Salehi H. Chronic obstructive pulmonary disease: microRNAs and exosomes as new diagnostic and therapeutic biomarkers. *J Res Med Sci*. (2018) 23:27. doi: 10.4103/jrms.JRMS_1054_17
5. Chen Y, Luo H, Kang N, Guan C, Long Y, Cao J, et al. Beraprost sodium attenuates cigarette smoke extract-induced apoptosis in vascular endothelial cells. *Mol Biol Rep*. (2012) 39:10447–57. doi: 10.1007/s11033-012-1924-1
6. GBD 2015 Chronic Respiratory Disease Collaborators. Global, regional, and national deaths, prevalence, disability-adjusted life years, and years lived with disability for chronic obstructive pulmonary disease and asthma, 1990-2015: a systematic analysis for the Global Burden of Disease Study 2015. *Lancet Respir Med*. (2017) 5:691–706. doi: 10.1016/S2213-2600(17)30293-X
7. GBD 2017 Causes of Death Collaborators. Global, regional, and national age-sex-specific mortality for 282 causes of death in 195 countries and territories, 1980-2017: a systematic analysis for the Global Burden of Disease Study 2017. *Lancet*. (2018) 392:1736–88. doi: 10.1016/S0140-6736(18)32203-7
8. Rabe KF, Watz H. Chronic obstructive pulmonary disease. *Lancet*. (2017) 389:1931–40. doi: 10.1016/S0140-6736(17)31222-9
9. Pouwels SD, Heijink IH, ten Hacken NH, Vandenabeele P, Krysko DV, Nawijn MC, et al. DAMPs activating innate and adaptive immune responses in COPD. *Mucosal Immunol*. (2014) 7:215–26. doi: 10.1038/mi.2013.77

10. Kumar M, Seeger W, Voswinckel R. Senescence-associated secretory phenotype and its possible role in chronic obstructive pulmonary disease. *Am J Respir Cell Mol Biol*. (2014) 51:323–33. doi: 10.1165/rcmb.2013-0382PS
11. Yao H, Rahman I. Current concepts on oxidative/carbonyl stress, inflammation and epigenetics in pathogenesis of chronic obstructive pulmonary disease. *Toxicol Appl Pharmacol*. (2011) 254:72–85. doi: 10.1016/j.taap.2009.10.022
12. Gomez-Cabrero D, Menche J, Vargas C, Cano I, Maier D, Barabási AL, et al. From comorbidities of chronic obstructive pulmonary disease to identification of shared molecular mechanisms by data integration. *BMC Bioinformatics*. (2016) 17(Suppl. 15):441. doi: 10.1186/s12859-016-1291-3
13. Hobbs BD, Hersh CP. Integrative genomics of chronic obstructive pulmonary disease. *Biochem Biophys Res Commun*. (2014) 452:276–86. doi: 10.1016/j.bbrc.2014.07.086
14. Ezzie ME, Crawford M, Cho JH, Orellana R, Zhang S, Gelinas R, et al. Gene expression networks in COPD: microRNA and mRNA regulation. *Thorax*. (2012) 67:122–31. doi: 10.1136/thoraxjnl-2011-200089
15. Osei ET, Florez-Sampedro L, Timens W, Postma DS, Heijink IH, Brandsma CA. Unravelling the complexity of COPD by microRNAs: it's a small world after all. *Eur Respir J*. (2015) 46:807–18. doi: 10.1183/13993003.02139-2014
16. Takahashi T, Kobayashi S, Fujino N, Suzuki T, Ota C, He M, et al. Increased circulating endothelial microparticles in COPD patients: a potential biomarker for COPD exacerbation susceptibility. *Thorax*. (2012) 67:1067–74. doi: 10.1136/thoraxjnl-2011-201395
17. Njock MS, Cheng HS, Dang LT, Nazari-Jahantigh M, Lau AC, Boudreau E, et al. Endothelial cells suppress monocyte activation through secretion of extracellular vesicles containing antiinflammatory microRNAs. *Blood*. (2015) 125:3202–12. doi: 10.1182/blood-2014-11-611046
18. Xu H, Ling M, Xue J, Dai X, Sun Q, Chen C, et al. Exosomal microRNA-21 derived from bronchial epithelial cells is involved in aberrant epithelium-fibroblast cross-talk in COPD induced by cigarette smoking. *Theranostics*. (2018) 8:5419–33. doi: 10.7150/thno.27876
19. Maes T, Cobos FA, Schleich F, Sorbello V, Henket M, De Preter K, et al. Asthma inflammatory phenotypes show differential microRNA expression in sputum. *J Allergy Clin Immunol*. (2016) 137:1433–46. doi: 10.1016/j.jaci.2016.02.018
20. Lerner CA, Sundar IK, Rahman I. Mitochondrial redox system, dynamics, and dysfunction in lung inflammaging and COPD. *Int J Biochem Cell Biol*. (2016) 81:294–306. doi: 10.1016/j.biocel.2016.07.026
21. Sundar IK, Yao H, Rahman I. Oxidative stress and chromatin remodeling in chronic obstructive pulmonary disease and smoking-related diseases. *Antioxid Redox Signal*. (2013) 18:1956–71. doi: 10.1089/ars.2012.4863
22. Porro C, Lepore S, Trotta T, Castellani S, Ratclif L, Battaglino A, et al. Isolation and characterization of microparticles in sputum from cystic fibrosis patients. *Respir Res*. (2010) 11:94. doi: 10.1186/1465-9921-11-94
23. Caby MP, Lankar D, Vincendeau-Scherrer C, Raposo G, Bonnerot C. Exosomal-like vesicles are present in human blood plasma. *Int Immunol*. (2005) 17:879–87. doi: 10.1093/intimm/dxh267
24. Ohtani N, Hara E. Roles and mechanisms of cellular senescence in regulation of tissue homeostasis. *Cancer Sci*. (2013) 104:525–30. doi: 10.1111/cas.12118
25. Admyre C, Grunewald J, Thyberg J, Gripenbäck S, Tornling G, Eklund A, et al. Exosomes with major histocompatibility complex class II and co-stimulatory molecules are present in human BAL fluid. *Eur Respir J*. (2003) 22:578–83. doi: 10.1183/09031936.03.00041703
26. van Niel G, D'Angelo G, Raposo G. Shedding light on the cell biology of extracellular vesicles. *Nat Rev Mol Cell Biol*. (2018) 19:213–28. doi: 10.1038/nrm.2017.125
27. Cocucci E, Meldolesi J. Ectosomes and exosomes: shedding the confusion between extracellular vesicles. *Trends Cell Biol*. (2015) 25:364–72. doi: 10.1016/j.tcb.2015.01.004
28. Escola JM, Kleijmeer MJ, Stoorvogel W, Griffith JM, Yoshie O, Geuze HJ. Selective enrichment of tetraspan proteins on the internal vesicles of multivesicular endosomes and on exosomes secreted by human B-lymphocytes. *J Biol Chem*. (1998) 273:20121–7. doi: 10.1074/jbc.273.32.20121
29. Yoshioka Y, Konishi Y, Kosaka N, Katsuda T, Kato T, Ochiya T. Comparative marker analysis of extracellular vesicles in different human cancer types. *J Extracell Vesicles*. (2013) 18:2. doi: 10.3402/jev.v2i0.20424
30. Keerthikumar S, Chisanga D, Ariyaratne D, Al Saffar H, Anand S, Zhao K, et al. ExoCarta: a web-based compendium of exosomal cargo. *J Mol Biol*. (2016) 428:688–92. doi: 10.1016/j.jmb.2015.09.019
31. Pathan M, Fonseka P, Chitti SV, Kang T, Sanwlani R, Van Deun J, et al. Vesiclepedia 2019: a compendium of RNA, proteins, lipids and metabolites in extracellular vesicles. *Nucleic Acids Res*. (2019) 47:D516–9. doi: 10.1093/nar/gky1029
32. Hough KP, Chanda D, Duncan SR, Thannickal VJ, Deshane JS. Exosomes in immunoregulation of chronic lung diseases. *Allergy*. (2017) 72:534–44. doi: 10.1111/all.13086
33. Nana-Sinkam SP, Acunzo M, Croce CM, Wang K. Extracellular vesicle biology in the pathogenesis of lung disease. *Am J Respir Crit Care Med*. (2017) 196:1510–8. doi: 10.1164/rccm.201612-2457PP
34. De Smet EG, Mestdagh P, Vandesompele J, Brusselle GG, Bracke KR. Non-coding RNAs in the pathogenesis of COPD. *Thorax*. (2015) 70:782–91. doi: 10.1136/thoraxjnl-2014-206560
35. Raposo G, Stoorvogel W. Extracellular vesicles: exosomes, microvesicles, and friends. *J Cell Biol*. (2013) 200:373–83. doi: 10.1083/jcb.201211138
36. Mathieu M, Martin-Jaular L, Lavieu G, Théry C. Specificities of secretion and uptake of exosomes and other extracellular vesicles for cell-to-cell communication. *Nat Cell Biol*. (2019) 21:9–17. doi: 10.1038/s41556-018-0250-9
37. Kalluri R, LeBleu VS. The biology, function, and biomedical applications of exosomes. *Science*. (2020) 367:eaau6977. doi: 10.1126/science.aau6977
38. Kubo H. Extracellular vesicles in lung disease. *Chest*. (2018) 153:210–6. doi: 10.1016/j.chest.2017.06.026
39. Fujita Y, Kosaka N, Araya J, Kuwano K, Ochiya T. Extracellular vesicles in lung microenvironment and pathogenesis. *Trends Mol Med*. (2015) 21:533–42. doi: 10.1016/j.molmed.2015.07.004
40. Simpson RJ, Jensen SS, Lim JW. Proteomic profiling of exosomes: current perspectives. *Proteomics*. (2008) 8:4083–99. doi: 10.1002/pmic.200800109
41. Wahlund CJE, Eklund A, Grunewald J, Gabrielsson S. Pulmonary extracellular vesicles as mediators of local and systemic inflammation. *Front Cell Dev Biol*. (2017) 5:39. doi: 10.3389/fcell.2017.00039
42. Van Pottelberge GR, Mestdagh P, Bracke KR, Thas O, van Durme YM, Joos GF, et al. MicroRNA expression in induced sputum of smokers and patients with chronic obstructive pulmonary disease. *Am J Respir Crit Care Med*. (2011) 183:898–906. doi: 10.1164/rccm.201002-0304OC
43. Molina-Pinelo S, Pastor MD, Suarez R, Romero-Romero B, González De la Peña M, Salinas A, et al. MicroRNA clusters: dysregulation in lung adenocarcinoma and COPD. *Eur Respir J*. (2014) 43:1740–9. doi: 10.1183/09031936.00091513
44. Cao Z, Zhang N, Lou T, Jin Y, Wu Y, Ye Z, et al. MicroRNA-183 down-regulates the expression of BKCaβ1 protein that is related to the severity of chronic obstructive pulmonary disease. *Hippokratia*. (2014) 18:328–32.
45. Donaldson A, Natanek SA, Lewis A, Man WD, Hopkinson NS, Polkey MI, et al. Increased skeletal muscle-specific microRNA in the blood of patients with COPD. *Thorax*. (2013) 68:1140–9. doi: 10.1136/thoraxjnl-2012-203129
46. Savarimuthu Francis SM, Davidson MR, Tan ME, Wright CM, Clarke BE, Duhig EE, et al. MicroRNA-34c is associated with emphysema severity and modulates SERPINE1 expression. *BMC Genomics*. (2014) 15:88. doi: 10.1186/1471-2164-15-88
47. Gelb AF, Hogg JC, Müller NL, Schein MJ, Kuei J, Tashkin DP, et al. Contribution of emphysema and small airways in COPD. Chest. 1996;109(2):353-9. doi: 10.1378/chest.109.2.353
48. Grimson A, Farh KK, Johnston WK, Garrett-Engele P, Lim LP, Bartel DP. MicroRNA targeting specificity in mammals: determinants beyond seed pairing. *Mol Cell*. (2007) 27:91–105. doi: 10.1016/j.molcel.2007.06.017
49. Halappanavar S, Nikota J, Wu D, Williams A, Yauk CL, Stampfli M. IL-1 receptor regulates microRNA-135b expression in a negative feedback mechanism during cigarette smoke-induced inflammation. *J Immunol*. (2013) 190:3679–86. doi: 10.4049/jimmunol.1202456
50. Mizuno S, Bogaard HJ, Gomez-Arroyo J, Alhussaini A, Kraskauskas D, Cool CD, et al. MicroRNA-199a-5p is associated with hypoxia-inducible factor-1α expression in lungs from patients with COPD. *Chest*. (2012) 142:663–72. doi: 10.1378/chest.11-2746
51. Schembri F, Sridhar S, Perdomo C, Gustafson AM, Zhang X, Ergun A, et al. MicroRNAs as modulators of smoking-induced gene expression changes in

human airway epithelium. *Proc Natl Acad Sci USA*. (2009) 106:2319–24. doi: 10.1073/pnas.0806383106
52. Xie L, Wu M, Lin H, Liu C, Yang H, Zhan J, et al. An increased ratio of serum miR-21 to miR-181a levels is associated with the early pathogenic process of chronic obstructive pulmonary disease in asymptomatic heavy smokers. *Mol Biosyst*. (2014) 10:1072–81. doi: 10.1039/C3MB70564A
53. Gu C, Li Y, Liu J, Ying X, Liu Y, Yan J, et al. LncRNA-mediated SIRT1/FoxO3a and SIRT1/p53 signaling pathways regulate type II alveolar epithelial cell senescence in patients with chronic obstructive pulmonary disease. *Mol Med Rep*. (2017) 15:3129–34. doi: 10.3892/mmr.2017.6367
54. Tang W, Shen Z, Guo J, Sun S. Screening of long non-coding RNA and TUG1 inhibits proliferation with TGF-β induction in patients with COPD. *Int J Chron Obstruct Pulmon Dis*. (2016) 11:2951–64. doi: 10.2147/COPD.S109570
55. Bi H, Zhou J, Wu D, Gao W, Li L, Yu L, et al. Microarray analysis of long non-coding RNAs in COPD lung tissue. *Inflamm Res*. (2015) 64:119–26. doi: 10.1007/s00011-014-0790-9
56. Poulet C, Njock MS, Moermans C, Louis E, Louis R, Malaise M, et al. Exosomal long non-coding RNAs in lung diseases. *Int J Mol Sci*. (2020) 21:3580 doi: 10.3390/ijms21103580
57. Cordazzo C, Petrini S, Neri T, Lombardi S, Carmazzi Y, Pedrinelli R, et al. Rapid shedding of proinflammatory microparticles by human mononuclear cells exposed to cigarette smoke is dependent on Ca2+ mobilization. *Inflamm Res*. (2014) 63:539–47. doi: 10.1007/s00011-014-0723-7
58. Tan DBA, Armitage J, Teo TH, Ong NE, Shin H, Moodley YP. Elevated levels of circulating exosome in COPD patients are associated with systemic inflammation. *Respir Med*. (2017) 132:261–4. doi: 10.1016/j.rmed.2017.04.014
59. Moon HG, Kim SH, Gao J, Quan T, Qin Z, Osorio JC, et al. CCN1 secretion and cleavage regulate the lung epithelial cell functions after cigarette smoke. *Am J Physiol Lung Cell Mol Physiol*. (2014) 307:L326–37. doi: 10.1152/ajplung.00102.2014
60. Kanazawa H, Yoshikawa J. Elevated oxidative stress and reciprocal reduction of vascular endothelial growth factor levels with severity of COPD. *Chest*. (2005) 128:3191–7. doi: 10.1378/chest.128.5.3191
61. Stockley RA, Turner AM. α-1-Antitrypsin deficiency: clinical variability, assessment, and treatment. *Trends Mol Med*. (2014) 20:105–15. doi: 10.1016/j.molmed.2013.11.006
62. Disayabutr S, Kim EK, Cha SI, Green G, Naikawadi RP, Jones KD, et al. miR-34 miRNAs regulate cellular senescence in type II alveolar epithelial cells of patients with idiopathic pulmonary fibrosis. *PLoS ONE*. (2016) 11:e0158367. doi: 10.1371/journal.pone.0158367
63. Fujita Y, Araya J, Ito S, Kobayashi K, Kosaka N, Yoshioka Y, et al. Suppression of autophagy by extracellular vesicles promotes myofibroblast differentiation in COPD pathogenesis. *J Extracell Vesicles*. (2015) 4:28388. doi: 10.3402/jev.v4.28388
64. Shen W, Liu J, Fan M, Wang S, Zhang Y, Wen L, et al. MiR-3202 protects smokers from chronic obstructive pulmonary disease through inhibiting FAIM2: an *in vivo* and *in vitro* study. *Exp Cell Res*. (2018) 362:370–7. doi: 10.1016/j.yexcr.2017.11.038
65. Conickx G, Mestdagh P, Avila Cobos F, Verhamme FM, Maes T, Vanaudenaerde BM, et al. MicroRNA profiling reveals a role for microRNA-218-5p in the pathogenesis of chronic obstructive pulmonary disease. *Am J Respir Crit Care Med*. (2017) 195:43–56. doi: 10.1164/rccm.201506-1182OC
66. Lewis A, Riddoch-Contreras J, Natanek SA, Donaldson A, Man WD, Moxham J, et al. Downregulation of the serum response factor/miR-1 axis in the quadriceps of patients with COPD. *Thorax*. (2012) 67:26–34. doi: 10.1136/thoraxjnl-2011-200309
67. Gu W, Yuan Y, Wang L, Yang H, Li S, Tang Z, et al. Long non-coding RNA TUG1 promotes airway remodelling by suppressing the miR-145-5p/DUSP6 axis in cigarette smoke-induced COPD. *J Cell Mol Med*. (2019) 23:7200–9. doi: 10.1111/jcmm.14389
68. Ge J, Geng S, Jiang H. Long noncoding RNAs antisense noncoding RNA in the INK4 locus (ANRIL) correlates with lower acute exacerbation risk, decreased inflammatory cytokines, and mild GOLD stage in patients with chronic obstructive pulmonary disease. *J Clin Lab Anal*. (2019) 33:e22678. doi: 10.1002/jcla.22678
69. Buschow SI, van Balkom BW, Aalberts M, Heck AJ, Wauben M, Stoorvogel W. MHC class II-associated proteins in B-cell exosomes and potential functional implications for exosome biogenesis. *Immunol Cell Biol*. (2010) 88:851–6. doi: 10.1038/icb.2010.64
70. Barnes PJ. Immunology of asthma and chronic obstructive pulmonary disease. *Nat Rev Immunol*. (2008) 8:183–92. doi: 10.1038/nri2254
71. Mittelbrunn M, Sánchez-Madrid F. Intercellular communication: diverse structures for exchange of genetic information. *Nat Rev Mol Cell Biol*. (2012) 13:328–35. doi: 10.1038/nrm3335
72. Sobo-Vujanovic A, Munich S, Vujanovic NL. Dendritic-cell exosomes cross-present Toll-like receptor-ligands and activate bystander dendritic cells. *Cell Immunol*. (2014) 289:119–27. doi: 10.1016/j.cellimm.2014.03.016
73. Lunding L, Wegmann M. NK cells in asthma exacerbation. *Oncotarget*. (2015) 6:19932–3. doi: 10.18632/oncotarget.4841
74. Zhang B, Yin Y, Lai RC, Lim SK. Immunotherapeutic potential of extracellular vesicles. *Front Immunol*. (2014) 5:518. doi: 10.3389/fimmu.2014.00518
75. Wang Y, Xu J, Meng Y, Adcock IM, Yao X. Role of inflammatory cells in airway remodeling in COPD. *Int J Chron Obstruct Pulmon Dis*. (2018) 13:3341–8. doi: 10.2147/COPD.S176122
76. Lefkowitz DL, Lefkowitz SS. Macrophage-neutrophil interaction: a paradigm for chronic inflammation revisited. *Immunol Cell Biol*. (2001) 79:502–6. doi: 10.1046/j.1440-1711.2001.01020.x
77. Ismail N, Wang Y, Dakhlallah D, Moldovan L, Agarwal K, Batte K, et al. Macrophage microvesicles induce macrophage differentiation and miR-223 transfer. *Blood*. (2013) 121:984–95. doi: 10.1182/blood-2011-08-374793
78. Lee H, Zhang D, Wu J, Otterbein LE, Jin Y. Lung epithelial cell-derived microvesicles regulate macrophage migration *via* microRNA-17/221-induced integrin β(1) recycling. *J Immunol*. (2017) 199:1453–64. doi: 10.4049/jimmunol.1700165
79. Lee H, Zhang D, Zhu Z, Dela Cruz CS, Jin Y. Epithelial cell-derived microvesicles activate macrophages and promote inflammation via microvesicle-containing microRNAs. *Sci Rep*. (2016) 6:35250. doi: 10.1038/srep35250
80. Serban KA, Rezania S, Petrusca DN, Poirier C, Cao D, Justice MJ, et al. Structural and functional characterization of endothelial microparticles released by cigarette smoke. *Sci Rep*. (2016) 6:31596. doi: 10.1038/srep31596
81. Yáñez-Mó M, Siljander PR, Andreu Z, Zavec AB, Borràs FE, Buzas EI, et al. Biological properties of extracellular vesicles and their physiological functions. *J Extracell Vesicles*. (2015) 4:27066. doi: 10.3402/jev.v4.27066
82. Kulshreshtha A, Ahmad T, Agrawal A, Ghosh B. Proinflammatory role of epithelial cell-derived exosomes in allergic airway inflammation. *J Allergy Clin Immunol*. (2013) 131:1194–203, 203.e1–14. doi: 10.1016/j.jaci.2012.12.1565
83. Li N, Liu Y, Cai J. LncRNA MIR155HG regulates M1/M2 macrophage polarization in chronic obstructive pulmonary disease. *Biomed Pharmacother*. (2019) 117:109015. doi: 10.1016/j.biopha.2019.109015
84. Van Eeden SF, Hogg JC. Immune-modulation in chronic obstructive pulmonary disease: current concepts and future strategies. *Respiration*. (2020) 99:550–65. doi: 10.1159/000502261
85. Genschmer KR, Russell DW, Lal C, Szul T, Bratcher PE, Noerager BD, et al. Activated PMN exosomes: pathogenic entities causing matrix destruction and disease in the lung. *Cell*. (2019) 176:113–26.e15. doi: 10.1016/j.cell.2018.12.002
86. Laurell CB, Eriksson S. The electrophoretic α1-globulin pattern of serum in α1-antitrypsin deficiency. 1963. *COPD*. (2013) 10(Suppl. 1):3–8. doi: 10.3109/15412555.2013.771956
87. Sng JJ, Prazakova S, Thomas PS, Herbert C. MMP-8, MMP-9 and neutrophil elastase in peripheral blood and exhaled breath condensate in COPD. *COPD*. (2017) 14:238–44. doi: 10.1080/15412555.2016.1249790
88. Senior RM, Tegner H, Kuhn C, Ohlsson K, Starcher BC, Pierce JA. The induction of pulmonary emphysema with human leukocyte elastase. *Am Rev Respir Dis*. (1977) 116:469–75. doi: 10.1164/arrd.1977.116.3.469
89. Veerappan A, Thompson M, Savage AR, Silverman ML, Chan WS, Sung B, et al. Mast cells and exosomes in hyperoxia-induced neonatal lung disease. *Am J Physiol Lung Cell Mol Physiol*. (2016) 310:L1218–32. doi: 10.1152/ajplung.00299.2015

90. Wen C, Seeger RC, Fabbri M, Wang L, Wayne AS, Jong AY. Biological roles and potential applications of immune cell-derived extracellular vesicles. *J Extracell Vesicles*. (2017) 6:1400370. doi: 10.1080/20013078.2017.1400370
91. Qazi KR, Gehrmann U, Domange Jordö E, Karlsson MC, Gabrielsson S. Antigen-loaded exosomes alone induce Th1-type memory through a B-cell-dependent mechanism. *Blood*. (2009) 113:2673–83. doi: 10.1182/blood-2008-04-153536
92. Julich H, Willms A, Lukacs-Kornek V, Kornek M. Extracellular vesicle profiling and their use as potential disease specific biomarker. *Front Immunol*. (2014) 5:413. doi: 10.3389/fimmu.2014.00413
93. Kornek M, Lynch M, Mehta SH, Lai M, Exley M, Afdhal NH, et al. Circulating microparticles as disease-specific biomarkers of severity of inflammation in patients with hepatitis C or nonalcoholic steatohepatitis. *Gastroenterology*. (2012) 143:448–58. doi: 10.1053/j.gastro.2012.04.031
94. Lacedonia D, Carpagnano GE, Trotta T, Palladino GP, Panaro MA, Zoppo LD, et al. Microparticles in sputum of COPD patients: a potential biomarker of the disease? *Int J Chron Obstruct Pulmon Dis*. (2016) 11:527–33. doi: 10.2147/COPD.S99547
95. Shi L, Xin Q, Chai R, Liu L, Ma Z. Ectopic expressed miR-203 contributes to chronic obstructive pulmonary disease *via* targeting TAK1 and PIK3CA. *Int J Clin Exp Pathol*. (2015) 8:10662–70.
96. Wang R, Li M, Zhou S, Zeng D, Xu X, Xu R, et al. Effect of a single nucleotide polymorphism in miR-146a on COX-2 protein expression and lung function in smokers with chronic obstructive pulmonary disease. *Int J Chron Obstruct Pulmon Dis*. (2015) 10:463–73. doi: 10.2147/COPD.S74345
97. Kara M, Kirkil G, Kalemci S. Differential expression of microRNAs in chronic obstructive pulmonary disease. *Adv Clin Exp Med*. (2016) 25:21–6. doi: 10.17219/acem/28343
98. Devadoss D, Long C, Langley RJ, Manevski M, Nair M, Campos MA, et al. Long noncoding transcriptome in chronic obstructive pulmonary disease. *Am J Respir Cell Mol Biol*. (2019) 61:678–88. doi: 10.1165/rcmb.2019-0184TR
99. Lewis A, Lee JY, Donaldson AV, Natanek SA, Vaidyanathan S, Man WD, et al. Increased expression of H19/miR-675 is associated with a low fat-free mass index in patients with COPD. *J Cachexia Sarcopenia Muscle*. (2016) 7:330–44. doi: 10.1002/jcsm.12078
100. Mei D, Tan WSD, Tay Y, Mukhopadhyay A, Wong WSF. Therapeutic RNA strategies for chronic obstructive pulmonary disease. *Trends Pharmacol Sci*. (2020) 41:475–86. doi: 10.1016/j.tips.2020.04.007
101. Sun Y, An N, Li J, Xia J, Tian Y, Zhao P, et al. miRNA-206 regulates human pulmonary microvascular endothelial cell apoptosis via targeting in chronic obstructive pulmonary disease. *J Cell Biochem*. (2019) 120:6223–36. doi: 10.1002/jcb.27910
102. Sørheim IC, Johannessen A, Gulsvik A, Bakke PS, Silverman EK, DeMeo DL. Gender differences in COPD: are women more susceptible to smoking effects than men? *Thorax*. (2010) 65:480–5. doi: 10.1136/thx.2009.122002
103. Du Y, Ding Y, Chen X, Mei Z, Ding H, Wu Y, et al. MicroRNA-181c inhibits cigarette smoke-induced chronic obstructive pulmonary disease by regulating CCN1 expression. *Respir Res*. (2017) 18:155. doi: 10.1186/s12931-017-0639-1
104. Paschalaki KE, Zampetaki A, Baker JR, Birrell MA, Starke RD, Belvisi MG, et al. Downregulation of microRNA-126 augments DNA damage response in cigarette smokers and patients with chronic obstructive pulmonary disease. *Am J Respir Crit Care Med*. (2018) 197:665–8. doi: 10.1164/rccm.201706-1304LE
105. Dua K, Wadhwa R, Singhvi G, Rapalli V, Shukla SD, Shastri MD, et al. The potential of siRNA based drug delivery in respiratory disorders: recent advances and progress. *Drug Dev Res*. (2019) 80:714–30. doi: 10.1002/ddr.21571
106. Boehme SA, Franz-Bacon K, Ludka J, DiTirro DN, Ly TW, Bacon KB. MAP3K19 is overexpressed in COPD and is a central mediator of cigarette smoke-induced pulmonary inflammation and lower airway destruction. *PLoS ONE*. (2016) 11:e0167169. doi: 10.1371/journal.pone.0167169
107. Jamieson KC, Traves SL, Kooi C, Wiehler S, Dumonceaux CJ, Maciejewski BA, et al. Rhinovirus and bacteria synergistically induce IL-17C release from human airway epithelial cells to promote neutrophil recruitment. *J Immunol*. (2019) 202:160–70. doi: 10.4049/jimmunol.1800547
108. Liu Q, Li H, Wang Q, Zhang Y, Wang W, Dou S, et al. Increased expression of TROP2 in airway basal cells potentially contributes to airway remodeling in chronic obstructive pulmonary disease. *Respir Res*. (2016) 17:159. doi: 10.1186/s12931-016-0463-z
109. Wang CG, Li C, Lei W, Jiang JH, Huang JA, Zeng DX. The association of neuron-derived orphan receptor 1 with pulmonary vascular remodeling in COPD patients. *Int J Chron Obstruct Pulmon Dis*. (2018) 13:1177–86. doi: 10.2147/COPD.S151820
110. Reimann S, Fink L, Wilhelm J, Hoffmann J, Bednorz M, Seimetz M, et al. Increased S100A4 expression in the vasculature of human COPD lungs and murine model of smoke-induced emphysema. *Respir Res*. (2015) 16:127. doi: 10.1186/s12931-015-0284-5

Conflict of Interest: The authors declare that the research was conducted in the absence of any commercial or financial relationships that could be construed as a potential conflict of interest.

Copyright © 2021 Wang, Wang, Du, Gabriel, Wang, Sun, Li, Xu, Jiang and Zhang. This is an open-access article distributed under the terms of the Creative Commons Attribution License (CC BY). The use, distribution or reproduction in other forums is permitted, provided the original author(s) and the copyright owner(s) are credited and that the original publication in this journal is cited, in accordance with accepted academic practice. No use, distribution or reproduction is permitted which does not comply with these terms.

frontiers in Medicine

ORIGINAL RESEARCH
published: 25 January 2021
doi: 10.3389/fmed.2020.621838

Differential Expression of PD-L1 in Central and Peripheral and TTF1-Positive and -Negative Small-Cell Lung Cancer

Shili Yu, Meng Jia, Yuemin Li, Ping-Li Sun and Hongwen Gao**

Department of Pathology, The Second Hospital of Jilin University, Changchun, China

OPEN ACCESS

Edited by:
Mahmood Yaseen Hachim, Mohammed Bin Rashid University of Medicine and Health Sciences, United Arab Emirates

Reviewed by:
Ibrahim Y. Hachim, University of Sharjah, United Arab Emirates
Shroque Zaher, Mohammed Bin Rashid University of Medicine and Health Sciences, United Arab Emirates
Nikolaj Frost, Charité—Universitätsmedizin Berlin, Germany

***Correspondence:**
Hongwen Gao
gaohw@jlu.edu.cn
Ping-Li Sun
pinglisun@naver.com

Specialty section:
This article was submitted to Pulmonary Medicine, a section of the journal Frontiers in Medicine

Received: *27 October 2020*
Accepted: *30 December 2020*
Published: *25 January 2021*

Citation:
Yu S, Jia M, Li Y, Sun P-L and Gao H (2021) Differential Expression of PD-L1 in Central and Peripheral and TTF1-Positive and -Negative Small-Cell Lung Cancer. Front. Med. 7:621838. doi: 10.3389/fmed.2020.621838

Background: Central and peripheral location as well as thyroid transcription factor-I (TTF-1) expression was reported to be associated with different characteristics and prognosis of small-cell lung cancer (SCLC). This study aimed to investigate differential expression of PD-L1 in different SCLC subtypes, and in biopsy and resection specimens.

Methods: We retrospectively analyzed 142 SCLC tumor samples using immunohistochemistry to correlate PD-L1 (22C3) expression with clinicopathologic features and survival data.

Results: PD-L1 expression was found in 19.7% SCLCs (28/142) and was more frequent in females than in males (32%, 16/50 vs. 13%, 12/92, $p = 0.009$), in central type than in peripheral type SCLCs (26%, 26/100 vs. 4.8%, 2/42, $p = 0.003$), and in TTF-1 positive than in negative SCLCs (23.8%, 25/105 vs. 8.1%, 3/37, $p = 0.039$). PD-L1 expression was associated with vascular ($p = 0.001$) and lymphatic invasion ($p = 0.001$). There was no significant difference in PD-L1 expression between biopsy and resection specimens. On univariate analysis, patients with PD-L1 expression had significantly shorter progression-free survival (PFS; $p = 0.026$) and overall survival (OS; $p = 0.012$). Multivariate analysis revealed that PD-L1 expression was an independent prognostic factor for OS (HR, 2.317; 95% CI 1.199–4.478; $p = 0.012$) and PFS (HR, 1.636; 95% CI 0.990–2.703; $p = 0.051$) in SCLC.

Conclusions: PD-L1 expression was more frequent in central type, TTF-1 positive SCLCs, and predicted a poor clinical outcome in these patients. Therefore, tumor location and TTF-1 expression could predict expression status of PD-L1, and could potentially serve as clinical response to immunotherapy.

Keywords: small-cell lung cancer, PD-L1, central and peripheral, immunohistochemistry, clone 22C3, TTF-1

INTRODUCTION

Small-cell lung cancer (SCLC) is an aggressive malignant disease with early development of metastasis. Surgery generally benefits only about 1% of the patients (1). The first-line therapy for SCLC is platinum-based systemic chemotherapy which has a good initial response rate. However, the vast majority of patients relapse and become resistant within a year (2). Immunotherapy, especially the one based on programmed death 1/programmed death-ligand 1 (PD-1/PD-L1)

checkpoint inhibitor has generated significant breakthrough in the treatment of SCLC recently (3, 4).

The expression of PD-L1 on tumor cells has demonstrated good correlation with response in some clinical trials, but positive responses were only observed in a relatively small section of the patients with PD-L1 expression. Moreover, evidence suggests that patients with PD-L1–negative tumors may also respond to immunotherapy (2, 5, 6). This has prompted many researchers to seek out the subtype of patients who could benefit from immune treatments that has not yet been identified in SCLC.

The morphological features of small-cell carcinoma are relatively consistent between different tumors and different areas of an individual tumor. However, studies have shown inter-and intratumoral heterogeneity of SCLC, and the impact of these differences on the response to specific therapeutic agents in both patients and animal models (7–10). SCLC tumors have been grouped into distinct subgroups based on a few factors including tumor location, expression of immunohistochemical markers, and genetic profiles. Previous evidence suggest that the central and peripheral type SCLCs show different immunohistochemical phenotypes (TTF-1 and some neuroendocrine markers) and prognosis (11, 12). In a mouse model of SCLC, central and peripheral tumors showed different response to cisplatin treatment (7). TTF-1 was expressed in 81–97% of SCLCs and TTF-1–negative SCLCs exhibited decreased neuroendocrine differentiation, but the prognosis and treatment efficacy of its expression remains unclear because of the limited number of reports (8, 11, 13). These facts raise the questions as to whether PD-L1 expression differs in different types of SCLC and what may be the prognostic significance of its expression?

Although few studies have evaluated the expression of PD-L1 and its prognostic role in SCLC, the results are inconsistent (14, 15). No study has evaluated PD-L1 expression in different SCLCs based on tumor location, TTF-1 expression, and specimen types so far. Therefore, to address the above questions, we investigated the expression of PD-L1 in different types of SCLCs in terms of clinicopathologic characteristics and prognosis in this study, with the objective of finding more specific candidates for immunotherapy.

MATERIALS AND METHODS

Patients and Data Collection

In this study, a total of 2,524 SCLC patients (24%, including 71 resection cases) were selected from 10,458 lung cancer patients who were admitted at The Second Hospital of Jilin University (Jilin, China) between January, 2009 and December, 2018. A total of 142 SCLC patients with follow-up data were finally selected. Patients who had received preoperative neoadjuvant chemotherapy or radiotherapy were excluded in this study. A total of 54 resection cases with medical record were enrolled in this study. The median follow-up period was 21.3 months. The overall 3-year survival rate of the patients was 10.8%, and 5-year survival was 0%. Smoking status was obtained from the electronic medical records or through telephone surveys. Tumors involving segmental or more proximal bronchi were defined as central type, whereas tumors involving subsegmental or more distal bronchi were defined as peripheral type. A few cases were excluded from the study because of the difficulty in grouping them into the central or peripheral types. This study was approved by the Ethics Committee of The Second Hospital of Jilin University.

Definition of Central- and Peripheral-Type SCLC

Definition of central-and peripheral-type SCLC based on previous reports (8, 16, 17), primary tumors involving segmental or more proximal bronchi were defined as central-type tumors. Primary tumors involving subsegmental or more distal bronchi were defined as peripheral-type tumors.

Immunohistochemistry (IHC)

Immunohistochemistry was performed on formalin-fixed, paraffin-embedded tissue sections using the FDA (Food and Drug Administration) and NMPA (National Medical Products Administration) approved PD-L1 IHC 22C3 pharmDx kit on the Dako Autostainer Link 48 platform according to manufacturer recommendations. PD-L1 positivity was defined as membranous staining of any intensity in at least 1% of the tumor cells and inflammatory cells (tumor associated lymphocytes and macrophages) with more than 1% membrane and/or cytoplasm staining of any intensity was defined as positive. The slides were examined independently by two observers (P-LS and SY) blinded to both the clinical and pathologic data.

Statistical Analysis

All statistical analyses were performed using SPSS version 22.0 for Windows (Inc., Chicago, IL). Categorical variables were compared using Fisher's exact test or Chi-square test. Kaplan-Meier analysis was performed for survival curves, and statistical significance was assessed by the log rank test. To evaluate whether a biomarker was an independent prognostic factor of OS, multivariate analysis using the Cox proportional hazard regression model was performed. All tests were two sided, and $p < 0.05$ was considered statistically significant.

RESULTS

Patient Characteristics

The clinicopathologic features of the 142 patients are summarized in **Table 1**. The cohort consisted of 92 (64.8%) men and 50 (35.2%) women with a median age of 61.72 years (range, 41–87), and included 102 (71.8%) smokers and 40 (28.2%) non-smokers. Of the 142 tumor samples obtained, 88 were biopsy and 54 were resection samples, and among these 86 (60.6%) were limited-stage and 56 (39.4%) were extensive-stage cases. Further, 26.8% (38/142) of the patients presented with distant metastatic disease at the time of diagnosis, and the metastatic sites included supraclavicular lymph node, liver, and contralateral lungs among others. Of the 54 resected SCLCs, eight cases were available with paired preoperative bronchoscopic biopsy specimens.

Regarding the tumor location, 100 cases (70.4%) were of the central type and 42 (29.6%) cases were of the peripheral type. TTF-1 was expressed in 73.9% (105/142) of the SCLC cases.

TABLE 1 | PD-L1 status in 142 small-cell lung cancer according to clinicopathologic characteristics.

Variable	PD-L1 expression status			*P*-value
	No. (%)	Positive No. (%)	Negative No. (%)	
Total	142	28 (19.7)	114 (80.3)	
Age (year)				
<60	67 (47.2)	16 (23.9)	51 (76.1)	0.293
≥60	75 (52.8)	12 (16.0)	63 (84.0)	
Sex				
Male	92 (64.8)	12 (13.0)	80 (87.0)	**0.009**
Female	50 (35.2)	16 (32.0)	34 (68.0)	
Smoking status				
Smoker	102 (71.8)	20 (19.6)	82 (80.4)	0.958
Non-smoker	40 (28.2)	8 (20.0)	32 (80.0)	
Specimen types				
Biopsy	88 (62.0)	17 (19.3)	71 (80.7)	1.000
Resection	54 (38.0)	11 (20.4)	43 (79.6)	
Tumor locations				
Central-type	100 (70.4)	26 (26.0)	74 (74.0)	**0.003**
Peripheral-type	42 (29.6)	2 (4.8)	40 (95.2)	
Stage				
Limited-stage	86 (60.6)	17 (19.8)	69 (80.2)	0.985
Extensive-stage	56 (39.4)	11 (19.6)	45 (80.4)	
Pleural invasion				
Present	13 (24.1)	2 (15.4)	11 (84.6)	1.000
Absent	41 (75.9)	9 (22.0)	32 (78.0)	
Vascular invasion				
Present	24 (44.4)	10 (41.7)	14 (58.3)	**0.001**
Absent	30 (55.6)	1 (3.3)	29 (96.7)	
Lymphatic invasion				
Present	20 (37.0)	9 (45.0)	11 (55.0)	**0.001**
Absent	34 (63.0)	2 (5.9)	32 (94.1)	
TTF-1 expression				
Positive	105 (73.9)	25 (23.8)	80 (76.2)	**0.039**
Negative	37 (26.1)	3 (8.1)	34 (91.9)	
Chromogranin A				
Positive	115 (82.1)	26 (22.6)	89 (77.4)	0.165
Negative	25 (17.9)	2 (8.0)	23 (92.0)	
Synaptophysin				
Positive	129 (92.1)	26 (20.2)	103 (79.8)	1.000
Negative	11 (7.9)	2 (18.2)	9 (81.8)	
CD56				
Positive	129 (93.5)	26 (20.2)	103 (79.8)	
Negative	9 (6.5)	2 (22.2)	7 (77.8)	1.000

The bold values indicates significantly difference.

Moreover, 72.0% (72/100) of the central type tumors and 78.6% (33/42) of the peripheral type tumors showed positivity for TTF-1. There was no significant correlation between TTF-1 expression and tumor type. Most of the cases showed positive expression of the common neuroendocrine markers including chromogranin A (82.1%, 115/140), synaptophysin (92.1%, 129/140), and CD56 (93.5%, 129/138). The Ki-67 labeling index was high (>70%) in almost all cases (99.3%, 141/142).

Expression and Clinicopathologic Correlation of PD-L1 in Total SCLC

PD-L1 protein expression was not detected in peribronchial mucus glands and bronchial epithelium, non-neoplastic type I pneumocytes, type II pneumocytes, and mesenchymal cells. Some inflammatory cells in the lung cancer microenvironment including T cells, macrophages, and mast cells showed weak to moderate PD-L1 cytoplasmic and membrane immunoreactivity (**Figures 1A–F**). PD-L1 expression was detected in the membrane and/or cytoplasm of tumor cells (**Figures 1G–I**). Tumor cells with more than 1% membrane staining of any intensity was defined as positive and a total of 19.7% (28 of 142) of the SCLC cases were found to express PD-L1. Tumor associated lymphocytes and macrophages with more than 1% membrane and/or cytoplasm staining of any intensity was defined as positive and the total percentage is 41.5% (59/142). The intensity of staining ranged from weak to moderate and strong, and majority of the cases showed moderate staining. The stained tumor percentage of the positive cases was between 2 and 35% with a mean value of 16%.

Among the 142 patients, PD-L1 expression was more commonly observed in females than in males (32%, 16/50 vs. 13%, 12/92, $p = 0.009$), in central type than in peripheral type SCLC (26%, 26/100 vs. 4.8%, 2/42, $p = 0.003$), and in TTF-1 positive than in negative cases (23.8%, 25/105 vs. 8.1%, 3/37, $p = 0.039$). There was a significant correlation between PD-L1 expression and the presence of vascular ($p = 0.001$) and lymphatic ($p = 0.001$) invasion. No significant difference of PD-L1 expression was observed between smokers (19.6%, 20/102) and non-smokers (20.0%, 8/40), biopsy (19.3%, 17/88) and resected specimens (20.4%, 11/54), limited-stage (19.8%, 17/86), and extensive-stage cases (19.6%, 11/56). Correlation between PD-L1 expression and neuroendocrine markers was also evaluated and no correlation was found between PD-L1 expression and any of the neuroendocrine markers (**Table 1**).

PD-L1 Expression in Different Types of SCLCs

To investigate whether PD-L1 was differentially expressed in different types of SCLCs, we analyzed the association of PD-L1 expression and some clinicopathological parameters including tumor location (central and peripheral), TTF-1 expression (positive and negative), and sample types (biopsy and resection).

There was a significant correlation between PD-L1 expression and female sex ($p = 0.035$), the presence of vascular invasion ($p < 0.001$), the presence of lymphatic invasion ($p = 0.004$), and TTF-1 expression ($p = 0.001$) in central type SCLC. There were no significant correlations between PD-L1 expression and the clinicopathologic characteristics except a negative correlation with TTF-1 expression ($p = 0.042$) in the peripheral type SCLC (**Table 2**).

Significant differences in PD-L1 expression were observed between female and male sex ($p = 0.035$), and between central

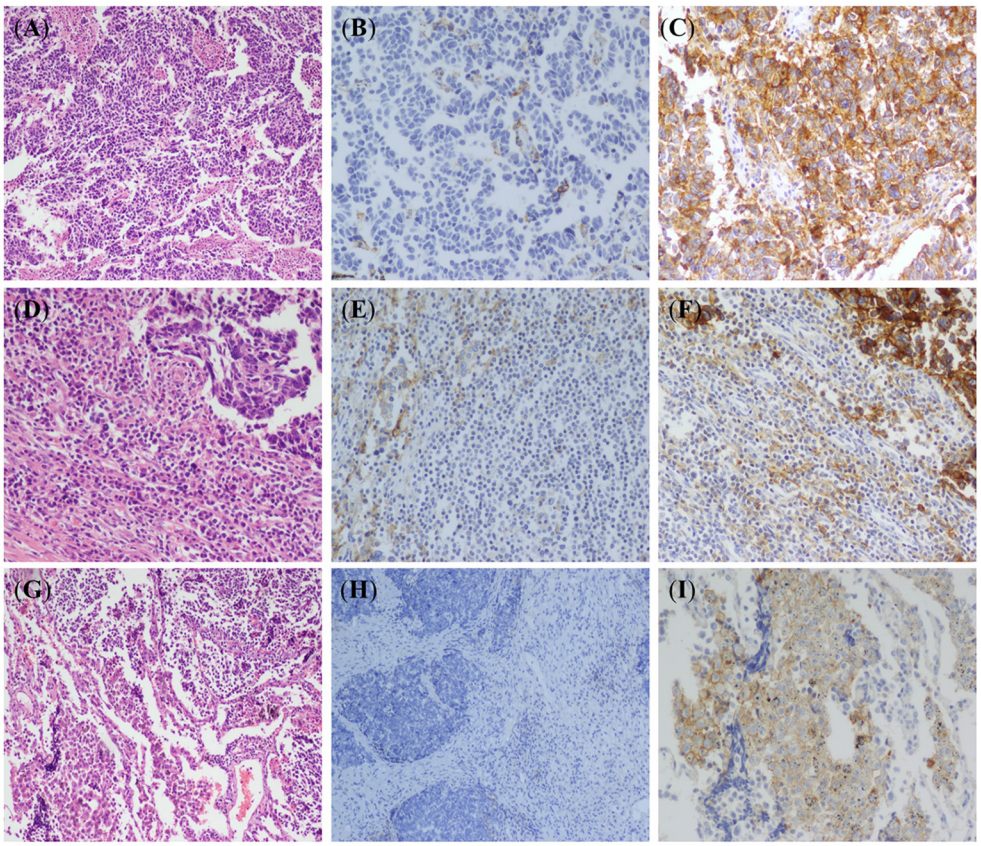

FIGURE 1 | Hematoxylin-eosin (HE) staining and PD-L1 immunohistochemical (IHC) staining in small-cell lung cancer (SCLC). **(A)** HE stained images of SCLC tumor (×100). **(B)** IHC stained images of PD-L1 negative in SCLC tumor cells (EnVision, ×100). **(C)** IHC stained images of PD-L1 expression in SCLC tumor cells (EnVision, ×200). **(D)** Lymphocyte infiltration around tumor cells (HE, ×100). **(E)** IHC stained images of PD-L1 negative in tumor infiltrating lymphocytes (EnVision, ×100). **(F)** IHC stained images of PD-L1 positive cell membranes of tumor infiltrating lymphocytes (EnVision, ×200). **(G)** Macrophages infiltration around tumor cells (HE, ×100). **(H)** IHC stained images of PD-L1 negative in tumor-associated macrophages (EnVision, ×100). **(I)** IHC stained images of PD-L1 positive cell membranes of tumor-associated macrophages (EnVision, ×200).

and peripheral SCLCs of the TTF-1 positive subtype. PD-L1 expression was positively correlated with the presence of vascular invasion ($p = 0.003$) and the presence of lymphatic invasion ($p = 0.001$) in TTF-1 positive SCLCs. Further, there were no significant correlations between PD-L1 expression and any of the clinicopathologic parameters in TTF-1 negative SCLCs (**Table 3**).

We subsequently evaluated PD-L1 expression in small biopsy and surgically resected specimens (**Table 4**). Among the 88 small biopsy specimens, PD-L1 expression significantly correlated with TTF-1 ($p = 0.023$) and chromogranin A ($p = 0.034$) expression. In the 54 resected cases, PD-L1 expression was positively correlated with female sex ($p = 0.010$) and central location of the tumor ($p = 0.002$). Of the 54 resected SCLC, eight cases were also available as biopsy specimens for the comparison of PD-L1 expression between small biopsy and surgical resected specimens from the same patients. Of the eight paired cases, PD-L1 expression was observed in one case in which the biopsy and paired resected specimen showed the identical results with the similar intensity and percentage staining of the tumor cells (weak to moderate, 10% for resection and 8% for biopsy). The overall concordance rate of PD-L1 expression between resected and their corresponding biopsy specimens was 100%.

Survival Analysis

Survival analysis was performed among the entire SCLC cohort and then among the different subtypes. In univariate analysis, PD-L1 expression was associated with a significantly poorer PFS and OS ($p = 0.026$ and $p = 0.003$, respectively) in entire SCLC cohort (**Figures 2A,B**). Multivariate Cox analysis confirmed that PD-L1 expression was an independent poor prognostic factor for OS (HR, 2.317; 95% CI 1.199–4.478; $p = 0.012$) and tended to be an independent prognostic factor for PFS (HR, 1.636; 95% CI 0.990–2.703; $p = 0.051$) (**Table 5**). In TTF-1 positive and central type SCLCs, PD-L1 expression was associated with poorer PFS ($p = 0.014$ and $p = 0.042$, respectively) and OS ($p = 0.009$ and $p = 0.019$, respectively), and in peripheral type SCLC, with poorer OS ($p = 0.005$).

TABLE 2 | Correlation between PD-L1 expression and clinicopathologic features in central-type and peripheral-type SCLC.

Variable		PD-L1 expression in central-type SCLC			PD-L1 expression in peripheral-type SCLC			
	No. (%)	Positive No. (%)	Negative No. (%)	*P*-value	No. (%)	Positive No. (%)	Negative No. (%)	*P*-value
Total	100	26 (26.0)	74 (74.0)		42	2 (4.8)	40 (95.2)	
Age (year)								
<60	51 (51.0)	15 (29.4)	36 (70.6)	0.498	16 (38.1)	1 (6.3)	15 (93.8)	
≥60	49 (49.0)	11 (22.4)	38 (77.6)		26 (61.9)	1 (3.8)	25 (96.2)	1.000
Sex								
Male	61 (61.0)	11 (18.0)	50 (82.0)	**0.035**	31 (73.8)	1 (3.2)	30 (96.8)	
Female	39 (39.0)	15 (38.5)	24 (61.5)		11 (26.2)	1 (9.1)	10 (90.9)	0.460
Smoking status								
Smoker	70 (70.0)	17 (24.3)	53 (75.7)	0.621	30 (71.4)	2 (6.7)	28 (93.3)	
Non-smoker	30 (30.0)	9 (30.0)	21 (70.0)		12 (28.6)	0 (0.0)	12 (100.0)	1.000
Stage								
Limited-stage	57 (57.0)	16 (28.1)	41 (71.9)	0.650	29 (69.0)	1 (3.4)	28 (96.6)	
Extensive-stage	43 (43.0)	10 (23.3)	33 (76.7)		13 (30.9)	1 (7.7)	12 (92.3)	0.528
Pleural invasion								
Present	8 (30.8)	2 (25.0)	6 (75.0)	0.420	5 (17.9)	0 (0.0)	5 (100.0)	
Absent	18 (69.2)	8 (44.4)	10 (55.6)		23 (82.1)	1 (4.3)	22 (95.7)	1.000
Vascular invasion								
Present	12 (46.2)	9 (75.0)	3 (25.0)	**0.001**	12 (42.9)	1 (8.3)	11 (91.7)	
Absent	14 (53.8)	1 (7.1)	13 (92.9)		16 (57.1)	0 (0.0)	16 (100.0)	0.429
Lymphatic invasion								
Present	13 (50.0)	9 (69.2)	4 (30.8)	**0.004**	7 (25.0)	0 (0.0)	7 (100.0)	
Absent	13 (50.0)	1 (7.7)	12 (92.3)		21 (75.0)	1 (4.8)	20 (95.2)	1.000
TTF-1 expression								
Positive	72 (72.0)	25 (34.7)	47 (65.3)	**0.001**	33 (78.6)	0 (0.0)	33 (100.0)	
Negative	28 (28.0)	1 (3.6)	27 (96.4)		9 (21.4)	2 (22.2)	7 (77.8)	**0.042**
Chromogranin A								
Positive	83 (84.7)	25 (30.1)	58 (69.9)	0.065	32 (76.2)	1 (3.1)	31 (96.9)	
Negative	15 (15.3)	1 (6.7)	14 (93.3)		10 (23.8)	1 (10.0)	9 (90.0)	0.424
Synaptophysin								
Positive	90 (91.8)	25 (27.8)	65 (72.2)	0.677	39 (92.9)	1 (2.6)	38 (97.4)	
Negative	8 (8.2)	1 (12.5)	7 (87.5)		3 (7.1)	1 (33.3)	2 (66.7)	0.139
CD56								
Positive	89 (92.7)	25 (28.1)	64 (71.9)	0.670	40 (95.2)	1 (2.5)	39 (97.5)	
Negative	7 (7.3)	1 (14.3)	6 (85.7)		2 (4.8)	1 (50.0)	1 (50.0)	0.094

SCLC, small-cell lung cancer. The bold values indicates significantly difference.

DISCUSSION

To the best of our knowledge, this is the first study to investigate the correlation among tumor location, TTF-1 expression, and sample type and PD-L1 expression in SCLCs. In this study, the clinicopathologic and prognostic significance of PD-L1 expression were assessed in 142 cases of SCLC and different SCLC subsets. We demonstrated that PD-L1 expression was more frequent in females than males, in central type than peripheral type SCLCs, and in TTF-1 positive than negative SCLCs. PD-L1 expression was positively associated with vascular and lymphatic invasion, which have been implicated in unfavorable prognosis. PD-L1 expression was associated with a significantly poorer PFS and OS in all SCLCs as well as in TTF-1 positive and central type SCLCs. Multivariate analysis revealed that PD-L1 expression in SCLC was an independent prognostic factor for OS and tended to be an independent prognostic factor for PFS.

So far, there is no study on the relationship between the expression of PD-L1 and gender by using 22C3 antibody in patients with small cell lung cancer. There are some studies on the relationship between the expression of PD-L1 and gender in non-small-cell lung cancer (NSCLC). One of the result showed that there is no significant correlation between gender and the expression of PD-L1 (18). However, the other literature results showed that the expression rate of PD-L1 is higher in male patients (19). Some animal studies and emerging clinical evidence suggested a role for estrogens in upregulation of PD-1 and PD-L1 expression, this may be a factor in the high expression level of

TABLE 3 | Correlation between PD-L1 expression and clinicopathologic features in TTF-1-positive and TTF-1-negative SCLC.

	PD-L1 expression in TTF-1-positive SCLC				PD-L1 expression in TTF-1-negative SCLC			
Variable	**No. (%)**	**Positive No. (%)**	**Negative No. (%)**	***P*-value**	**No. (%)**	**Positive No. (%)**	**Negative No. (%)**	***P*-value**
Total	105	25 (23.8)	80 (76.2)		37	3 (8.1)	34 (91.9)	
Age (year)								
<60	50 (47.6)	15 (30.0)	35 (70.0)	0.175	17 (45.9)	1 (5.9)	16 (94.1)	
≥60	55 (52.4)	10 (18.2)	45 (81.8)		20 (54.1)	2 (10.0)	18 (90.0)	1.000
Sex								
Male	68 (64.8)	10 (14.7)	58 (85.3)	**0.004**	24 (64.9)	2 (8.3)	22 (91.7)	
Female	37 (35.2)	15 (40.5)	22 (59.5)		13 (35.1)	1 (7.7)	12 (92.3)	1.000
Smoking status								
Smoker	69 (65.7)	17 (24.6)	52 (75.4)	1.000	33 (89.2)	3 (9.1)	30 (90.9)	
Non-smoker	36 (34.3)	8 (22.2)	28 (77.8)		4 (10.8)	0 (0.0)	4 (100.0)	1.000
Tumor locations								
Central-type	72 (68.6)	25 (34.7)	47 (65.3)	**0.000**	28 (75.7)	1 (3.6)	27 (96.4)	
Peripheral-type	33 (31.4)	0 (0.0)	33 (100.0)		9 (24.3)	2 (22.2)	7 (77.8)	0.141
Stage								
Limited-stage	67 (63.8)	15 (22.4)	52 (77.6)	0.643	19 (51.4)	2 (10.5)	17 (89.5)	
Extensive-stage	38 (36.2)	10 (26.3)	28 (73.7)		18 (48.6)	1 (5.6)	17 (94.4)	1.000
Pleural invasion								
Present	13 (26.0)	2 (15.4)	11 (84.6)	0.688	33 (89.2)	2 (6.0)	31 (94.0)	
Absent	37 (74.0)	8 (21.6)	29 (78.4)		4 (10.8)	1 (25.0)	3 (75.0)	0.298
Vascular invasion								
Present	23 (46.0)	9 (39.1)	14 (60.9)	**0.003**	1 (25.0)	1 (100.0)	0 (0.0)	
Absent	27 (54.0)	1 (3.7)	26 (96.3)		3 (75.0)	0 (0.0)	3 (100.0)	0.250
Lymphatic invasion								
Present	20 (40.0)	9 (45.0)	11 (55.0)	**0.001**	33 (89.2)	2 (6.0)	31 (94.0)	
Absent	30 (60.0)	1 (3.3)	29 (96.7)		4 (10.8)	1 (25.0)	3 (75.0)	0.298
Chromogranin A								
Positive	94 (91.3)	25 (26.6)	69 (73.4)	0.109	21 (56.8)	1 (4.8)	20 (95.2)	
Negative	9 (8.7)	0 (0.0)	9 (100.0)		16 (43.2)	2 (12.5)	14 (87.5)	0.568
Synaptophysin								
Positive	102 (99.0)	25 (24.5)	77 (75.5)	1.000	27 (73.0)	1 (3.7)	26 (96.3)	
Negative	1 (1.0)	0 (0.0)	1 (100.0)		10 (27.0)	2 (20.0)	8 (80.0)	0.172
CD56								
Positive	97 (94.2)	24 (24.7)	73 (75.3)	1.000	32 (91.4)	2 (6.3)	30 (93.8)	
Negative	6 (5.8)	1 (16.7)	5 (83.3)		3 (8.6)	1 (33.3)	2 (66.7)	0.242

SCLC, small-cell lung cancer. The bold values indicates significantly difference.

PD-L1 in women, but further research is needed to confirm the above results (20, 21).

Multiple clinical trials have defined PD-L1 as a biomarker for PD-1/PD-L1 checkpoint inhibitor treatment in NSCLC, and PD-L1 is expressed in ∼50–70% of NSCLC as reported in the previous studie (22–25). However, the immunotherapeutic efficacy of PD-L1 in SCLC is far lower than that in NSCLC, and PD-L1 expression is relatively low in SCLC compared to NSCLC. Limited number of studies have evaluated PD-L1 expression in SCLC. PD-L1 expression was found in 19.7% of SCLCs in our study, and this result is consistent with two previous studies in which the expression rates were 18 and 25%, respectively (26, 27). Two other studies showed relatively lower rates of PD-L1 expression in SCLCs (2.5 and 10%), but the sample sizes in those studies were small (39 and 30, respectively) (28, 29). The reason of the variable expression in PD-L1 positivity in our study compared to the other studies may be the use of different types of antibodies as well as the variable definitions of PD-L1 positivity. However, Yasuda et al. (29) used the same antibody and same scoring criteria, they found positivity of only 2.5%. Except for the sample size, the heterogeneity of the study population and interpretation criteria may be responsible for the differences in PD-L1 expression levels. First of all, according to the interpretation criteria, PD-L1 protein expression is determined by using Tumor Proportion Score (TPS), which is the percentage of tumor cells showing partial or complete membrane staining with any extent (1+ - 3+). Specimens with a 1+ result in routine immunohistochemical staining are

TABLE 4 | Correlation between PD-L1 expression and clinicopathologic features in biopsy specimen and resection specimen of small-cell lung cancer.

	PD-L1 expression in biopsy specimen				PD-L1 expression in resection specimen			
Variable	**n (%)**	**Positive n (%)**	**Negative n (%)**	***P*-values**	**n (%)**	**Positiven n (%)**	**Negative n (%)**	***P*-values**
Total	88	17 (19.3)	71 (80.7)		54	11 (20.4)	43 (79.6)	
Age (year)								
<60	36 (40.9)	7 (19.4)	29 (80.6)	1.000	31 (57.4)	9 (29.0)	22 (71.0)	0.092
≥60	52 (59.1)	10 (19.2)	42 (80.8)		23 (42.6)	2 (8.7)	21 (91.3)	
Sex								
Male	57 (64.8)	9 (15.8)	48 (84.2)	0.272	35 (64.8)	3 (8.6)	32 (91.4)	0.010
Female	31 (35.2)	8 (25.8)	23 (74.2)		19 (35.2)	8 (42.1)	11 (57.9)	
Smoking status								
Smoker	66 (75.0)	14 (21.2)	52 (78.8)	0.545	34 (63.0)	5 (14.7)	29 (85.3)	0.294
Non-smoker	22 (25.0)	3 (13.6)	19 (86.4)		20 (37.0)	6 (30.0)	14 (70.0)	
Tumor locations								
Peripheral-type	74 (84.1)	16 (21.6)	58 (78.4)	0.288	26 (48.1)	10 (38.5)	16 (61.5)	0.002
Central-type	14 (15.9)	1 (7.1)	13 (92.9)		28 (51.9)	1 (3.6)	27 (96.4)	
Stage								
Limited-stage	38 (43.2)	7 (18.4)	31 (81.6)	1.000	50 (92.6)	11 (22.0)	39 (78.0)	0.571
Extensive-stage	50 (56.8)	10 (20.0)	40 (80.0)		4 (7.4)	0 (0.0)	4 (100.0)	
TTF-1 expression								
Positive	55 (62.5)	15 (27.3)	40 (72.7)	0.023	50 (92.6)	10 (20.0)	40 (80.0)	1.000
Negative	33 (37.5)	2 (6.1)	31 (93.9)		4 (7.4)	1 (25.0)	3 (75.0)	
Chromogranin A								
Positive	70 (81.4)	23 (32.9)	47 (67.1)	0.034	45 (83.3)	32 (71.1)	13 (28.9)	0.053
Negative	16 (18.6)	1 (6.3)	15 (93.8)		9 (16.7)	3 (33.3)	6 (66.7)	
Synaptophysin								
Positive	76 (88.4)	16 (21.1)	60 (78.9)	0.679	53 (98.1)	10 (18.9)	43 (81.1)	0.204
Negative	10 (11.6)	1 (10.0)	9 (90.0)		1 (1.9)	1 (100.0)	0 (0.0)	
CD56								
Positive	77 (91.7)	16 (20.8)	61 (79.2)	1.000	52 (96.3)	10 (19.2)	42 (80.8)	0.369
Negative	7 (8.3)	1 (14.3)	6 (85.7)		2 (3.7)	1 (50.0)	1 (50.0)	

sometimes judged negative, but in the latest criteria, as long as there is a positive cell membrane, it should be judged as positive. All the samples we selected were not treated with chemotherapy, which can avoid the effect of chemotherapy on the expression level of PD-L1, which may also be a reason. Further large-scale investigations or multicenter studies are warranted to determine the actual rate of expression of PD-L1 in SCLCs. PD-L1 was identified as a poor prognostic factor in the current study. The prognostic role of PD-L1 in SCLC is still unclear due to the relatively small number of reports available and the different antibody clones used in the reports (14, 15, 30). Besides tumor cells, lymphocytes, and macrophages in the stroma were also included in the evaluation in several studies (26) which showed PD-L1 expression rates ranging between 31.7 and 45.7%, which were similar to the results from our study (41.5%, 59/142) (28, 31). In our study, PD-L1 expression on the inflammatory cells was also analyzed in terms of clinicopathological parameters and prognosis, but no positive correlations were noted.

Although the implementation of anti-PD-1/PD-L1 therapy in SCLC has improved the clinical outcome for a small percentage of patients, the majority of patients show little to no response to the treatment even in cases with high PD-L1 expression. Conversely, clinical benefit from immunotherapeutic agents has also been observed in patients with PD-L1-negative tumors (5, 31). These data support the notion that PD-L1 expression cannot be considered as a unique criterion to predict which population will benefit from anti-PD-1 antibodies. Therefore, identification of additional predictors is imperative to improve the response to immune checkpoint inhibitors. Association analysis between the expression of PD-L1 and clinicopathological factors demonstrated high frequency of PD-L1 expression in both central type and TTF-1 expressed SCLC. Primary tumor location has been reported to predict prognosis of SCLC (12, 32). A previous study using a mouse model of SCLC reported that centrally located tumors showed better response to cisplatin than peripheral lesions (7). Based on the differential expression of PD-L1, we speculate that peripheral and central SCLCs may show different therapeutic reactivity to immunotherapy. TTF-1 is a master regulator of lung morphogenesis and an important marker for SCLC. TTF-1 expression in SCLC has been reported to be associated with neuroendocrine differentiation and aggressive biology (8, 13). However, TTF-1 is not a marker

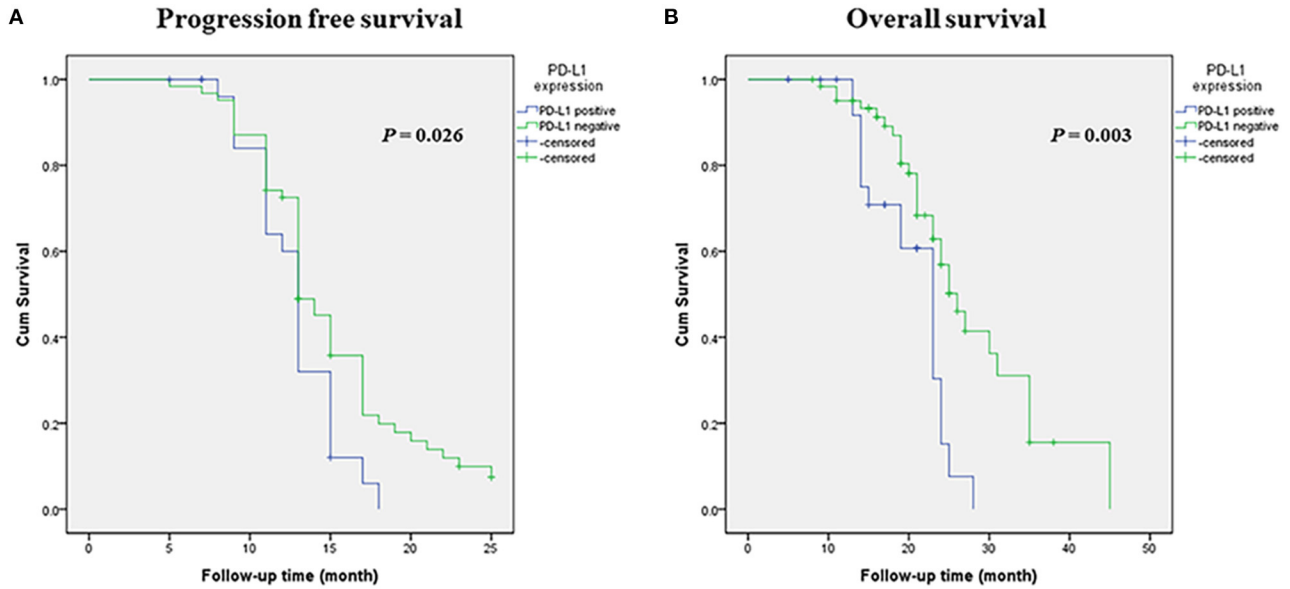

FIGURE 2 | Kaplan-Meier survival estimates of progression-free survival (PFS) and overall survival (OS) based on the expression of PD-L1. **(A)** Kaplan-Meier plot showing PFS. **(B)** Kaplan-Meier plot showing OS.

TABLE 5 | Univariate and multivariate analyses of factors associated with PFS and OS in small cell lung cancer patients.

Factor	Category	PFS					OS				
		Mean	Univariate		Multivariate		Mean	Univariate		Multivariate	
			p	HR (95% CI)	*p*	HR (95% CI)		*p*	HR (95% CI)	*p*	HR (95% CI)
TTF1 expression	Positive vs. Negative	17.82 ± 0.54 19.96 ± 0.65	0.311	1.259 (0.764–2.075)			29.35 ± 1.12 32.81 ± 2.94	0.423	1.300 (0.662–2.552)		
Tumor types	Central vs. Peripheral	19.25 ± 0.056 19.51 ± 0.97	0.6	0.600 (0.376–0.956)			29.43 ± 1.19 31.93 ± 2.46	0.501	0.783 (0.430–1.425)		
Vascular invasion	Present vs. Absent	20.07 ± 0.81 20.53 ± 0.91	0.808	1.066 (0.596–1.908)			30.96 ± 1.80 32.49 ± 2.93	0.976	1.011 (1.464–2.204)		
Lymphatic invasion	Present vs. Absent	19.55 ± 0.74 21.45 ± 0.98	0.188	1.430 (0.782–2.613)			29.88 ± 1.81 33.40 ± 3.03	0.377	1.392 (0.636–3.045)		
Pleural invasion	Present vs. Absent	19.23 ± 1.16 20.58 ± 0.74	0.343	1.344 (0.674–2.681)			28.15 ± 2.56 31.92 ± 2.11	0.202	1.635 (0.715–3.741)		
PD-L1 expression	Positive vs. Negative	17.82 ± 0.54 19.96 ± 0.65	0.026	1.640 (0.994–2.707)	0.055	1.636 (0.990–2.703)	25.61 ± 1.04 32.87 ± 1.70	0.003	2.514 (1.325–4.771)	0.012	2.317 (1.199–4.478)
Stage	Extensive vs. Limited	18.08 ± 0.91 19.85 ± 0.58	0.051	1.745 (1.060–2.875)	0.087	1.566 (0.937–2.616)	27.04 ± 1.96 31.77 ± 1.50	0.072	1.020 (0.447–2.329)	0.265	1.450 (0.754–2.786)

specific for SCLCs, a significant proportion of extrapulmonary SCLCs are positive for TTF-1. In other studies, TTF-1 has been proposed to be a candidate lineage lung oncogene, knockdown of it reduced growth, and cell viability of lung cancer containing the TTF-1 amplicon (24). A study by Takahashi et al. also demonstrated that TTF-1 stimulated the AKT pathway by directly regulating the expression of a tyrosine kinase-like receptor (22), and AKT pathway has been reported to regulate the expression of PD-L1 in lung cancer (31). The high expression of PD-L1 in TTF-1 positive cases may due to activated oncogenic pathway which was mediated by TTF-1. The positive association between PD-L1 and TTF-1 expression has been reported in pulmonary sarcomatoid carcinomas (33). Furthermore, TTF-1 expression was shown to predict the response to immune checkpoint inhibitors in NSCLC (34). So it can be speculated that high TTF-1 expression could be a predictive marker for anti-PD-1/PD-L1 therapy in SCLC. Further studies are needed to elucidate this possibility and the underlying mechanisms.

Discordances between surgically resected and biopsy specimens have been reported in several studies in NSCLC (35, 36). However, there is no relevant research in SCLC at present, and this may be because most SCLC cases are unresectable, and only a small number of patients receive surgery owing to the lack of preoperative biopsy results. To investigate whether expressional heterogeneity of PD-L1 exists between biopsy and resection specimens, our study evaluated the PD-L1 expression in the two types of samples and revealed no heterogeneity of PD-L1 expression between the two type of samples. This may due to the relatively lower intratumoral (within a tumor) heterogeneity of SCLCs compared to NSCLCs.

The above findings provide the first evidence of an association between PD-L1 expression, central location, and TTF-1 expression in SCLC. Nevertheless, this study has a few limitations. Firstly, we only included those resected cases that had follow-up data and sufficient specimen, which may have introduced a bias into the analysis. Secondly, the data were collected retrospectively, including some of the information on smoking history which was obtained by telephonic enquiry. It is plausible that some of the patient families may not have provided particularly accurate information, which may explain why there were relatively more non-smokers in our cohort. Another possible reason is that indoor air pollution or secondhand smoking at home or at work may have contributed to the increased risk of developing lung cancer.

In conclusion, our results revealed a significant association of PD-L1 expression with female sex, central tumor location, TTF-1 expression, and prognosis of the patients with SCLC. Our study provides compelling evidences which can help guide future research and clinical trials in SCLC. However, further studies are needed before drawing definitive conclusions and implementing them clinically.

SYNOPSIS

This study retrospectively analyzed the effect of PD-L1 expression in different types of small-cell lung cancers (SCLCs), in terms of the clinicopathologic features and survival, with the objective of identifying more specific candidates for immunotherapy.

DATA AVAILABILITY STATEMENT

The original contributions presented in the study are included in the article/supplementary material, further inquiries can be directed to the corresponding author/s.

AUTHOR CONTRIBUTIONS

P-LS designed the review. SY collected the data and prepared the draft. YL and MJ participated in data interpretation. P-LS and HG provided research fund. All authors read and approved the final manuscript.

FUNDING

This work was supported by Science and Technology of Jilin Province, Jilin Province Key Laboratory (3D517K363429), The Role and Molecular Mechanism of EMT in the Resistance of ROS1-positive Lung Cancer (20180101014JC/3D518PS23429), Jilin Province Department of Finance Project (3D5197398429, 3D5197464429), and Youth Program of National Natural Science Foundation of China (3A4197642429).

ACKNOWLEDGMENTS

We would like to thank Xianliang Sha for technical support.

REFERENCES

1. Waqar SN, Morgensztern D. Treatment advances in small cell lung cancer (SCLC). *Pharmacol Ther Dec.* (2017) 180:16–23. doi: 10.1016/j.pharmthera.2017.06.002
2. Gazdar AF, Bunn PA, Minna JD. Small-cell lung cancer: what we know, what we need to know and the path forward. *Nat Rev Cancer. Dec.* (2017) 17:725–37. doi: 10.1038/nrc.2017.87
3. Ott PA, Elez E, Hiret S, Kim DW, Morosky A, Saraf S, et al. Pembrolizumab in patients with extensive-stage small-cell lung cancer: results from the phase Ib KEYNOTE-028 study. *J Clin Oncol.* (2017) 35:3823–9. doi: 10.1200/JCO.2017.72.5069
4. Horn L, Mansfield AS, Szczesna A, Havel L, Krzakowski M, Hochmair MJ, et al. First-Line atezolizumab plus chemotherapy in extensive-stage small-cell lung cancer. *N Engl J Med.* (2018) 379:2220–9. doi: 10.1056/NEJMoa1809064
5. Armstrong SA, Liu SV. Immune checkpoint inhibitors in small cell lung cancer: a partially realized potential. *Adv Ther.* (2019) 36:1826–32. doi: 10.1007/s12325-019-01008-2
6. Gelsomino F, Lamberti G, Parisi C, Casolari L, Melotti B, Sperandi F, et al. The evolving landscape of immunotherapy in small-cell lung cancer: a focus on predictive biomarkers. *Cancer Treat Rev.* (2019) 79:101887. doi: 10.1016/j.ctrv.2019.08.003
7. Böttger F, Semenova EA, Song JY, Ferone G, van der Vliet J, Cozijnsen M, et al. Tumor heterogeneity underlies differential cisplatin sensitivity in mouse models of small-cell lung cancer. *Cell Rep.* (2019) 27:3345–58.e4. doi: 10.1016/j.celrep.2019.05.057
8. Miyauchi E, Motoi N, Ono H, Ninomiya H, Ohyanagi F, Nishio M, et al. Distinct characteristics of small cell lung cancer correlate with central or peripheral origin: subtyping based on location and expression of transcription factor TTF-1. *Medicine.* (2015) 94:e2324. doi: 10.1097/MD.0000000000002324
9. Park HS, Harder EM, Mancini BR, Decker RH. Central versus peripheral tumor location: influence on survival, local control, and toxicity following stereotactic body radiotherapy for primary non-small-cell lung cancer. *J Thorac Oncol.* (2015) 10:832–7. doi: 10.1097/JTO.0000000000000484
10. Shue YT, Lim JS, Sage J. Tumor heterogeneity in small cell lung cancer defined and investigated in pre-clinical mouse models. *Transl Lung Cancer Res.* (2018) 7:21–31. doi: 10.21037/tlcr.2018.01.15
11. Ito M, Yamashita Y, Miyata Y, Ohara M, Tsutani Y, Ikeda T, et al. Prognostic impact of the primary tumor location based on the hilar structures in non-small cell lung cancer with mediastinal lymph node metastasis. *Lung Cancer.* (2012) 76:93–7. doi: 10.1016/j.lungcan.2011.07.015
12. Kanaji N, Sakai K, Ueda Y, Miyawaki H, Ishii T, Watanabe N, et al. Peripheral-type small cell lung cancer is associated with better survival and higher frequency of interstitial lung disease. *Lung Cancer.* (2017) 108:126–33. doi: 10.1016/j.lungcan.2017.03.013
13. Iida Y, Masuda S, Nakanishi Y, Shimizu T, Nishimaki H, Takahashi M, et al. Clinicopathological characteristics of thyroid transcription

factor 1-negative small cell lung cancers. *Hum Pathol.* (2018) 79:127–34. doi: 10.1016/j.humpath.2018.05.009
14. Inamura K, Yokouchi Y, Kobayashi M, Ninomiya H, Sakakibara R, Nishio M, et al. Relationship of tumor PD-L1 (CD274) expression with lower mortality in lung high-grade neuroendocrine tumor. *Cancer Med.* (2017) 6:2347–56. doi: 10.1002/cam4.1172
15. Chang YL, Yang CY, Huang YL, Wu CT, Yang PC. High PD-L1 expression is associated with stage IV disease and poorer overall survival in 186 cases of small cell lung cancers. *Oncotarget*. (2017) 8:18021–30. doi: 10.18632/oncotarget.14935
16. Bandoh S, Fujita J, Ueda Y, Fukunaga Y, Dohmoto K, Hojo S, et al. Expression of carcinoembryonic antigen in peripheral- or central-located small cell lung cancer: its clinical significance. *Jpn J Clin Oncol.* (2001) 31:305–10. doi: 10.1093/jjco/hye067
17. Nobashi T, Koyasu S, Nakamoto Y, Kubo T, Ishimori T, Kim YH, et al. Prognostic value of fluorine-18 fludeoxyglucose positron emission tomography parameters differs according to primary tumour location in small-cell lung cancer. *Br J Radiol.* (2016) 89:20150618. doi: 10.1259/bjr.20150618
18. Pan ZK, Ye F, Wu X, An HX, Wu JX. Clinicopathological and prognostic significance of programmed cell death ligand1 (PD-L1) expression in patients with non-small cell lung cancer: a meta-analysis. *J Thorac Dis.* (2015) 7:462–70. doi: 10.3978/j.issn.2072-1439.2015.02.13
19. Zhang M, Li G, Wang Y, Wang Y, Zhao S, Haihong P, et al. PD-L1 expression in lung cancer and its correlation with driver mutations: a meta-analysis. *Sci Rep.* (2017) 7:10255. doi: 10.1038/s41598-017-10925-7
20. Polanczyk MJ, Hopke C, Vandenbark AA, Offner H. Estrogen-mediated immunomodulation involves reduced activation of effector T cells, potentiation of Treg cells, and enhanced expression of the PD-1 costimulatory pathway. *J Neurosci Res.* (2006) 84:370–8. doi: 10.1002/jnr.20881
21. Wang C, Dehghani B, Li Y, Kaler LJ, Vandenbark AA, Offner H. Oestrogen modulates experimental autoimmune encephalomyelitis and interleukin-17 production via programmed death 1. *Immunology*. (2009) 126:329–35. doi: 10.1111/j.1365-2567.2008.03051.x
22. Yamaguchi T, Yanagisawa K, Sugiyama R, Hosono Y, Shimada Y, Arima C, et al. NKX2-1/TITF1/TTF-1-Induced ROR1 is required to sustain EGFR survival signaling in lung adenocarcinoma. *Cancer Cell.* (2012) 21:348–61. doi: 10.1016/j.ccr.2012.02.008
23. Gandhi L, Rodríguez-Abreu D, Gadgeel S, Esteban E, Felip E, De Angelis F, et al. Pembrolizumab plus chemotherapy in metastatic non-small-cell lung cancer. *N Engl J Med.* (2018) 378:2078–92. doi: 10.1056/NEJMoa1801005
24. Kwei KA, Kim YH, Girard L, Kao J, Pacyna-Gengelbach M, Salari K, et al. Genomic profiling identifies TITF1 as a lineage-specific oncogene amplified in lung cancer. *Oncogene.* (2008) 27:3635–40. doi: 10.1038/sj.onc.1211012
25. Paz-Ares L, Luft A, Vicente D, Tafreshi A, Gümüş M, Mazières J, et al. Pembrolizumab plus chemotherapy for squamous non-small-cell lung cancer. *N Engl J Med.* (2018) 379:2040–51. doi: 10.1056/NEJMoa1810865
26. Bonanno L, Pavan A, Dieci MV, Di Liso E, Schiavon M, Comacchio G, et al. The role of immune microenvironment in small-cell lung cancer: distribution of PD-L1 expression and prognostic role of FOXP3-positive tumour infiltrating lymphocytes. *Eur J Cancer.* (2018) 101:191–200. doi: 10.1016/j.ejca.2018.06.023
27. Yoshimura A, Yamada T, Miyagawa-Hayashino A, Sonobe Y, Imabayashi T, Yamada T, et al. Comparing three different anti-PD-L1 antibodies for immunohistochemical evaluation of small cell lung cancer. *Lung Cancer.* (2019) 137:108–12. doi: 10.1016/j.lungcan.2019.09.012
28. Gadgeel SM, Pennell NA, Fidler MJ, Halmos B, Bonomi P, Stevenson J, et al. Phase II study of maintenance pembrolizumab in patients with extensive-stage small cell lung cancer (SCLC). *J Thorac Oncol.* (2018) 13:1393–9. doi: 10.1016/j.jtho.2018.05.002
29. Yasuda Y, Ozasa H, Kim YH. PD-L1 expression in small cell lung cancer. *J Thorac Oncol.* (2018) 13:e40–1. doi: 10.1016/j.jtho.2017.10.013
30. Xu Y, Cui G, Jiang Z, Li N, Zhang X. Survival analysis with regard to PD-L1 and CD155 expression in human small cell lung cancer and a comparison with associated receptors. *Oncol Lett.* (2019) 17:2960–8. doi: 10.3892/ol.2019.9910
31. Han Y, Liu D, Li L. PD-1/PD-L1 pathway: current researches in cancer. *Am J Cancer Res.* (2020) 10:727–42.
32. Liu S, Zhang G, Li C, Chen X, Wang S, Wang M, et al. Prognostic factors and survival of patients with small cell lung cancer in a northeastern Chinese population. *Thorac Cancer.* (2013) 4:143–52. doi: 10.1111/j.1759-7714.2012.00149.x
33. Vieira T, Antoine M, Hamard C, Fallet V, Duruisseaux M, Rabbe N, et al. Sarcomatoid lung carcinomas show high levels of programmed death ligand-1 (PD-L1) and strong immune-cell infiltration by TCD3 cells and macrophages. *Lung Cancer.* (2016) 98:51–8. doi: 10.1016/j.lungcan.2016.05.013
34. Baraibar I, Roman M, Castañón E, García MÁ, Rolfo C, López-Picazo JM, et al. Lymphocytes and neutrophils count after two cycles and TTF1 expression as early outcome predictors during immunotherapy (IT) in stage IV non-small cell lung cancer (NSCLC) patients. *J Clin Oncol.* (2017) 35:e20553. doi: 10.1200/JCO.2017.35.15_suppl.e20553
35. Ilie M, Long-Mira E, Bence C, Butori C, Lassalle S, Bouhlel L, et al. Comparative study of the PD-L1 status between surgically resected specimens and matched biopsies of NSCLC patients reveal major discordances: a potential issue for anti-PD-L1 therapeutic strategies. *Ann Oncol.* (2016) 27:147–53. doi: 10.1093/annonc/mdv489
36. Jin Y, Shen X, Pan Y, Zheng Q, Chen H, Hu H, et al. Correlation between PD-L1 expressionand clinicopathological characteristics of non-small cell lung cancer: a real-world study of a large Chinese cohort. *J Thorac Dis.* (2019) 11:4591–601. doi: 10.21037/jtd.2019.10.80

Conflict of Interest: The authors declare that the research was conducted in the absence of any commercial or financial relationships that could be construed as a potential conflict of interest.

Copyright © 2021 Yu, Jia, Li, Sun and Gao. This is an open-access article distributed under the terms of the Creative Commons Attribution License (CC BY). The use, distribution or reproduction in other forums is permitted, provided the original author(s) and the copyright owner(s) are credited and that the original publication in this journal is cited, in accordance with accepted academic practice. No use, distribution or reproduction is permitted which does not comply with these terms.

frontiers in Medicine

ORIGINAL RESEARCH
published: 11 February 2021
doi: 10.3389/fmed.2020.624576

Molecular Analysis of IL-5 Receptor Subunit Alpha as a Possible Pharmacogenetic Biomarker in Asthma

Sandra Elena-Pérez[1], David Hansoe Heredero-Jung[1], Asunción García-Sánchez[2,3,4], Miguel Estravís[2,3,4], Maria J. Martin[2,4], Jacinto Ramos-González[5], Juan Carlos Triviño[6], María Isidoro-García[1,2,4,7], Catalina Sanz[2,4,8] and Ignacio Dávila[2,3,4,9]*

[1] Department of Clinical Biochemistry, University Hospital of Salamanca, Salamanca, Spain, [2] Allergic Disease Research Group IIMD-01, Institute for Biomedical Research of Salamanca, Salamanca, Spain, [3] Department of Biomedical Sciences and Diagnostics, University of Salamanca, Salamanca, Spain, [4] Network for Cooperative Research in Health - RETICS ARADyAL, Carlos III Health Institute, Madrid, Spain, [5] Department of Pneumology, University Hospital of Salamanca, Salamanca, Spain, [6] Sistemas Genómicos, Paterna, Spain, [7] Department of Medicine, University of Salamanca, Salamanca, Spain, [8] Department of Microbiology and Genetics, University of Salamanca, Salamanca, Spain, [9] Department of Allergy, University Hospital of Salamanca, Salamanca, Spain*

OPEN ACCESS

Edited by:
Bassam Mahboub, Rashid Hospital, United Arab Emirates

Reviewed by:
Ubaldo Martin, AstraZeneca, United States
Jose Antonio Cañas, Health Research Institute Foundation Jimenez Diaz (IIS-FJD), Spain

***Correspondence:**
Catalina Sanz
catsof@usal.es

Specialty section:
This article was submitted to Pulmonary Medicine, a section of the journal Frontiers in Medicine

Received: *31 October 2020*
Accepted: *30 December 2020*
Published: *11 February 2021*

Citation:
Elena-Pérez S, Heredero-Jung DH, García-Sánchez A, Estravís M, Martin MJ, Ramos-González J, Triviño JC, Isidoro-García M, Sanz C and Dávila I (2021) Molecular Analysis of IL-5 Receptor Subunit Alpha as a Possible Pharmacogenetic Biomarker in Asthma. Front. Med. 7:624576. doi: 10.3389/fmed.2020.624576

Background: Asthma is a heterogeneous syndrome with a broad clinical spectrum and high drug response variability. The inflammatory response in asthma involves multiple effector cells and mediator molecules. Based on asthma immunopathogenesis, precision medicine can be a promising strategy for identifying biomarkers. Biologic therapies acting on the IL-5/IL-5 receptor axis have been developed. IL-5 promotes proliferation, differentiation and activation of eosinophils by binding to the IL-5 receptor, located on the surface of eosinophils and basophils. This study aimed to investigate the expression of *IL5RA* in patients with several types of asthma and its expression after treatment with benralizumab, a biologic directed against IL-5 receptor subunit alpha.

Methods: Sixty peripheral blood samples, 30 from healthy controls and 30 from asthmatic patients, were selected for a transcriptomic RNAseq study. Differential expression analysis was performed by statistical assessment of fold changes and *P*-values. A validation study of *IL5RA* expression was developed using qPCR in 100 controls and 187 asthmatic patients. The effect of benralizumab on *IL5RA* expression was evaluated in five patients by comparing expression levels between pretreatment and after 3 months of treatment. The *IL5RA* mRNA levels were normalized to *GAPDH* and *TBP* expression values for each sample. Calculations were made by the comparative $\Delta\Delta$Ct method. All procedures followed the MIQE guidelines.

Results: *IL5RA* was one of the most differentially overexpressed coding transcripts in the peripheral blood of asthmatic patients ($P = 8.63E\text{-}08$ and fold change of 2.22). In the qPCR validation study, *IL5RA* expression levels were significantly higher in asthmatic patients than in controls ($P < 0.001$). Significant expression differences were present in different asthmatic types. In the biological drug study, patients treated with benralizumab showed a significant decrease in *IL5RA* expression and blood eosinophil counts. A notable improvement in ACT and lung function was also observed in these patients.

Conclusions: These results indicate that *IL5RA* is overexpressed in patients with different types of asthma. It could help identify which asthmatic patients will respond more efficiently to benralizumab, moving toward a more personalized asthma management. Although further studies are required, *IL5RA* could play a role as a biomarker and pharmacogenetic factor in asthma.

Keywords: asthma, pharmacogenetic biomarker, transcriptomic, *IL5RA*, benralizumab, precision medicine

INTRODUCTION

Asthma is a chronic inflammatory disease of the airways affecting more than 300 million people worldwide, and its prevalence is increasing, becoming a health and economic problem (1). It is defined by variable expiratory airflow limitation and respiratory symptoms such as wheeze, cough and shortness of breath, which vary in frequency and intensity (2). Asthma is recognized as a heterogeneous syndrome with different underlying disease processes, determined by complex interactions between genetic and environmental factors. This variety of interactions results in different clinical presentations, phenotypes and response to treatment (3).

Despite the broad clinical spectrum of asthma, the presence of inflammation of the airway is a common pathologic feature and the primary treatment target. Nevertheless, the relationship between the intensity of inflammation and the severity of asthma has not been consistently established (4). The characteristic inflammatory pattern in most asthmatic patients includes an increase in type 2 helper T (Th2) lymphocytes, eosinophils, basophils, mast cells and type 2 innate lymphoid cells (ILC2). These effector cells release numerous mediating molecules that cause disease symptoms (5). Type 2 inflammation is characterized by an increase in type 2 cytokines, particularly IL-4, IL-5, IL-9, and IL-13, involved in eosinophil activation and immunoglobulin E production (6).

Asthma comprises different phenotypes with similar clinical manifestations but probably involving different underlying mechanisms (7). These phenotypes have been characterized based on the age of onset of disease, clinical presentation, severity and presence of other disorders such as atopy and eosinophilia (8–10). Eosinophilic asthma is the best-studied inflammatory phenotype and is characterized by elevated eosinophils in peripheral blood and sputum. Patients in whom eosinophilic inflammation persists despite treatment with high doses of corticosteroids are often associated with more severe asthma and a higher risk of exacerbations (11, 12). Therefore, phenotype characterization in patients with severe uncontrolled or poorly controlled asthma could help in guiding specific treatments (13).

Asthma management aims to achieve and maintain control of the disease and reduce the risk of exacerbations. Understanding the underlying pathophysiologic mechanisms is necessary for stratifying patients toward individualized therapy. The implementation of precision medicine requires identifying specific biomarkers easily measurable in biological fluids, which can help in evaluating treatment effectiveness (14, 15). In this context, new biologic therapies are being developed targeting cytokines and their receptors. IL-5 plays a crucial role in eosinophilic asthma pathophysiology and has been proposed as a novel therapeutic target. This cytokine is involved in the proliferation, differentiation, survival and activation of eosinophils by binding to the IL-5 receptor, located on the surface of eosinophils and basophils (16, 17). The IL-5 receptor is a heterodimer comprising one alpha subunit (IL-5RA) and one beta subunit, also found in both IL-3 and GM-CSF receptors (18).

In recent years, new drugs based on monoclonal antibodies have been developed against the action of IL-5 in eosinophilic-mediated inflammation. Benralizumab is a humanized IgG1κ monoclonal antibody that binds to IL-5RA via its Fab domain with high affinity and specificity, blocking IL-5 signaling (19). Besides, this antibody can bind through its afucosylated Fc domain to the Fcγ receptor IIIa, expressed on the surface of natural killer cells, macrophages and neutrophils, thus inducing antibody-directed cell-mediated cytotoxicity of eosinophils and basophils. As a result, the administration of benralizumab results in a dramatic depletion of eosinophils counts in blood, sputum, airway mucosa and bone marrow (20). In this context, benralizumab has proved effectivity in treating patients with severe eosinophilic asthma, improving lung function and asthma control and reducing the rate of exacerbations (21).

The present study aims to investigate the expression of *IL5RA* in patients with different types of asthma and its role as a possible biomarker of response to treatment with benralizumab.

MATERIALS AND METHODS

Study Population

The study involved 347 unrelated Caucasian individuals, 130 controls and 217 asthmatic patients, from the Allergy Department of the University Hospital of Salamanca. The study was approved by the Clinical Research Ethics Committee of the Institute for Biomedical Research of Salamanca (IBSAL) (PI 2020-02-433) and all participants signed a written informed consent. Controls had to fulfill the following criteria: (i) no symptoms or history of asthma, rhinitis or other pulmonary diseases; (ii) no symptoms or history of allergic diseases; (iii) negative skin prick tests with a battery of locally adapted common aeroallergens; (iv) absence of family history of asthma, rhinitis or atopy; and (v) age >16 years old. Asthmatic patients were recruited if they met all the following criteria: (i) at least two symptoms consistent with asthma (cough, wheeze and dyspnea); (ii) either a positive bronchodilator or methacholine test; and (iii) absence of other pulmonary disorders; and (iv) age >16 years old.

Lung function was measured by spirometry according to the American Thoracic Society (ATS) criteria (22). Asthma severity was established following the Spanish Guide for the Management of Asthma (GEMA) guidelines (7) and severe asthma was diagnosed according to the ERS/ATS criteria (23). Skin prick tests were performed with a battery of common aeroallergens (24), according to The European Academy of Allergy and Clinical Immunology (EAACI) recommendations (25). Skin tests were considered positive if there was at least one wheal reaction of >3 mm of diameter. Patients were considered atopic if they had a positive skin prick test to at least one allergen. Patients were considered monosensitized if they had a positive skin prick test result to only one group of aeroallergens (pollens, mites, molds or animal dander) and polysensitized if they had positive skin tests for two or more groups. Early-onset asthma was defined as the presence of asthma symptoms that appeared before 18 years, and late-onset asthma was defined as the presence after the age of 18 years (26). Asthmatic patients were classified into two subgroups, eosinophilic and non-eosinophilic asthma, according to the number of eosinophils (cut-off point of 150 cells per μl) (2). Blood cell counts were determined on the XN-1000 hematology analyzer (Sysmex Corporation, Kobe, Japan) and total serum IgE levels were measured using a fluoroenzyme immunoassay (Thermo Fisher Scientific, Waltham, MA, USA).

Transcriptomic RNAseq Study

A total of 60 peripheral blood samples, 30 from healthy controls and 30 from patients with pollen allergic asthma, were selected for a transcriptomic RNAseq study. Total RNA extraction was performed using the Ambion RiboPure^{TM}-Blood kit (Thermo Fisher Scientific, Waltham, MA, USA). After Ambion DNAse I treatment (Thermo Fisher Scientific, Waltham, MA, USA), RNA was purified and concentrated with the RNeasy MinElute Cleanup Kit (Qiagen, Hilden, Germany). All purification protocols were performed with the modifications indicated by the manufacturers. RNA was quantified by Nanodrop 1000 spectrophotometer (Thermo Fisher Scientific, Waltham, MA, USA). The RNA integrity number (RIN) algorithm was used to determine RNA quality on the Agilent 2100 Bioanalyzer using the Eukaryote Total RNA Nano kit (Agilent Technologies, Waldbronn, Germany). RNA samples with a RIN value above 8 were used. Globin transcripts and ribosomal RNA were removed, and RNA was cleaved to prepare RNA strand-specific libraries. Finally, the generated libraries were sequenced on the Illumina HiSeq 2500 platform (Illumina, San Diego, CA, USA).

Bioinformatic Analysis

In the bioinformatic analysis of the transcriptomic data, the FastQC software (27) was used to analyze the quality of raw reads. Sequencing reads were mapped on the human reference genome (GRCh38) using the TopHat2 software (28). The low-quality readings were removed with Picard Tools (29) and the unmapped and non-properly paired reads were re-mapped using the BWA-MEM algorithm (30). Gene and isoform prediction were estimated using the Cufflinks method (31). The HTSeq software (v.0.6.0) (32) was used to calculate gene expression levels. Differential expression analysis was performed by DESeq2 package (33) and only the transcripts with a fold change value ≥ 1.5 or ≤ -1.5 and a FDR-adjusted P-value <0.05 were considered as differentially expressed genes. Potential interactions between selected proteins were examined by cluster analysis using the STRING software (34), a database which include functional and physical associations between known and predicted proteins.

qPCR Validation Assays

For the validation of the transcriptomic gene expression data, 287 peripheral blood samples were selected including 100 samples from controls and 187 from asthmatic patients. Total RNA was isolated using the RiboPure-Blood kit (Ambion, Thermo Fisher Scientific, Waltham, MA, USA). DNAse treatment was performed using Ambion DNAse I (Thermo Fisher Scientific, Waltham, MA, USA). Concentrations and RNA quality ratios were determined in a Nanodrop 1000 spectrophotometer (Thermo Fisher Scientific, Waltham, MA, USA). cDNA was generated from 500 ng of total RNA using Superscript III First-Strand Synthesis System for RT-PCR (Invitrogen, Thermo Fisher Scientific, Waltham, MA, USA), in a final volume of 20 μl. Conditions for PCR included a single cycle and incubation periods of 65°C for 5 min, 25°C for 10 min, 50°C for 50 min, 85°C for 5 min, and 37°C for 20 min.

qPCR reactions were performed in a LightCycler480 system (Roche Applied Science, Indianapolis, IN, USA). *IL5RA* primers were designed using Primer 3.0 (35) and the Beacon Designer (36) software. *GAPDH* and *TBP* reference gene primers were chosen from The Real Time ready Human Reference GenePanel (Roche Applied Science, Indianapolis, IN, USA). The sequence of the primers used are shown in **Table 1**. Primers efficacies were analyzed by amplifying serial dilutions of cDNA sample of known concentration and according to the following equation: $E = (10^{-1/\text{slope}} - 1) \times 100$. All efficiencies ranged from 90 to 110%. The reaction mixture in each well-contained a final volume of 15 μl based on 7.5 μl of Master Mix SYBR Green I (Roche Applied Science, Indianapolis, IN, USA), 10 μM of each primers and 20 ng of cDNA. All reactions were performed in triplicate. In each experiment, non-template controls and calibrator were included. The PCR conditions included 10 min at 95°C followed by 45 cycles of 10 s at 95°C for denaturation, 10 s at 60°C for annealing and 10 s at 72°C for polymerization. Finally, melting curve analyses were carried out to verify the specificity of the qPCR products. *IL5RA* mRNA levels were normalized to *GAPDH* and *TBP* expression levels

TABLE 1 | Sequences of primers used in the qPCR assay.

	Primer	Sequence 5′ → 3′
IL5RA	Forward	TGAAAGAGTGAAGAACCGCC
	Reverse	CCTGGCCTGAGAAATGCG
GAPDH	Forward	CTCTGCTCCTCCTGTTCGAC
	Reverse	ACGACCAAATCCGTTGACTC
TBP	Forward	GAACATCATGGATCAGAACAACA
	Reverse	ATAGGGATTCCGGGAGTCAT

TABLE 2 | Characteristics of the study population in the RNAseq study and the validation analyses.

	N	Sex (% Female)	Age (Mean ± SD)	FeNO, ppb (Mean ± SD)	IgE, kU/l (Median ± IQR)
RNAseq study					
Controls	30	46.7	57 ± 17	-	46.7 ± 87.8
Asthmatic patients	30	56.7	30 ± 13	-	179.0 ± 239.0
Validation analysis					
Controls	100	66.0	57 ± 17	-	28.8 ± 57.7
Asthmatic patients	187	55.1	45 ± 19	44.8 ± 48.3	174.0 ± 398.2
Non-allergic asthma (NAA)	76	60.5	58 ± 15	38.1 ± 40.6	77.0 ± 118.8
NAA without NP	33	72.7	56 ± 16	24.8 ± 19.3	37.9 ± 103.5
NAA with NP	43	51.2	61 ± 14	52.2 ± 51.7	83.0 ± 258.7
Allergic asthma (AA)	111	51.4	35 ± 16	49.8 ± 53.0	312.5 ± 472.3
AA without NP	82	57.3	31 ± 14	39.8 ± 29.5	312.5 ± 445.5
AA with NP	29	34.5	46 ± 17	79.6 ± 88.7	307.0 ± 747.0
Early-onset asthma	76	61.8	31 ± 17	42.5 ± 43.1	271.0 ± 402.1
Late-onset asthma	111	50.5	54 ± 16	46.5 ± 51.9	126.0 ± 406.5
Non-eosinophilic asthma	32[a]	59.4	44 ± 17	26.4 ± 18.2	109.0 ± 260.5
Eosinophilic asthma	120[a]	53.3	46 ± 20	49.7 ± 54.5	196.0 ± 405.4

SD, standard deviation; IQR, interquartile range.

[a]*Blood eosinophil counts were not available for all non-eosinophilic and eosinophilic asthma patients.*

using the formula $2^{-\Delta\Delta Ct}$ by the comparative ΔΔCt method (37). All procedures followed the Minimum Information for Publication of Quantitative Real-Time PCR Experiment (MIQE) guidelines (38).

Pharmacogenetic Study

A proof-of-concept study of the *IL5RA* expression in peripheral blood before and after 3 months of treatment with benralizumab was performed in five severe eosinophilic asthmatic patients. Benralizumab was administered at a dose of 30 mg by subcutaneous injection once every 4 weeks. Asthma control test (ACT), fractional exhaled nitric oxide (FeNO) and lung function parameters were performed before and after 3 months of treatment. Patients were considered responders in the ACT score if they achieved a score of 25 or an increase of 3 or more points after 3 months of treatment. Also, they were considered FEV1 responders if they achieved a FEV1.0 $\geq$ 200 ml or FEV1.0 $\geq$ 12% after 3 months of treatment. As only three doses were evaluated, exacerbations were not considered. Blood samples were collected and lung function tests were performed at each time point. All patients provided their informed consent to receive benralizumab therapy.

Statistical Analysis

Descriptive analysis was carried out using central (mean and median) and dispersion tendency (standard deviation and interquartile range) measurements, followed by bivariate and multivariate analysis. The normality distribution was assessed by Kolmogorov-Smirnov test and the homoscedasticity was also tested before applying statistical tests. Continuous variables were evaluated using either ANOVA or Kruskal-Wallis test. Statistical significance was assessed by Wilcoxon's test for changes before

TABLE 3 | The 26 protein-coding transcripts most differentially expressed ($P < 0.025$) between the group of controls and patients with allergic asthma, listed by their fold change value.

Ensemble ID	External ID gene	Fold change	*P*-value
Up-regulated expression			
ENSG00000161905	*ALOX15*	2.45	3.91E-05
ENSG00000091181	*IL5RA*	2.22	8.63E-08
ENSG00000103056	*SMPD3*	2.16	1.44E-07
ENSG00000105205	*CLC*	2.04	4.63E-06
ENSG00000183134	*PTGDR2*	1.99	2.64E-06
ENSG00000134489	*HRH4*	1.93	7.21E-07
ENSG00000152207	*CYSLTR2*	1.84	1.15E-09
ENSG00000171659	*GPR34*	1.83	1.27E-08
ENSG00000143297	*FCRL5*	1.75	3.18E-05
ENSG00000255587	*RAB44*	1.74	8.10E-06
ENSG00000132465	*JCHAIN*	1.70	0.007
ENSG00000276231	*PIK3R6*	1.67	9.12E-06
ENSG00000131203	*IDO1*	1.67	0.014
Down-regulated expression			
ENSG00000118113	*MMP8*	−2.75	3.17E-04
ENSG00000012223	*LTF*	−2.35	4.79E-04
ENSG00000124469	*CEACAM8*	−2.19	2.47E-03
ENSG00000123689	*G0S2*	−2.02	4.95E-03
ENSG00000118520	*ARG1*	−2.00	4.51E-05
ENSG00000168209	*DDIT4*	−1.91	4.11E-04
ENSG00000179094	*PER1*	−1.86	6.80E-04
ENSG00000096006	*CRISP3*	−1.78	0.002
ENSG00000005961	*ITGA2B*	−1.75	6.90E-04
ENSG00000179869	*ABCA13*	−1.73	0.001
ENSG00000100985	*MMP9*	−1.69	0.001
ENSG00000124102	*PI3*	−1.65	7.32E-04
ENSG00000122025	*FLT3*	−1.64	3.66E-05

and after treatment. A *P*-value <0.05 was considered statistically significant. All statistical analyses were performed using SPSS Statistics version 21 (IBM, Armonk, NY, USA). Graphs were plot using GraphPad Prism version 6 (San Diego, CA, USA).

RESULTS

Study Population

The phenotypic characteristics of the studied subjects of the RNAseq study and the validation analysis are shown in **Table 2**. In both assays, control individuals were older to permit a more extended period for asthma to have appeared. Thus, age was significantly higher in the control group than in patients ($P < 0.001$), except in the case of non-allergic and late-onset asthma groups, in which the disease had begun at older ages. According to the inclusion criteria, total IgE levels were significantly higher in all patient groups than in controls ($P \leq 0.001$). Moderate persistent asthma was the most common type in both the RNAseq study and the validation analysis (43.3 and 45.7%, respectively), followed by intermittent asthma (33.3 and 26.3%, respectively). The most common aeroallergen sensitization in the validation analysis patients was pollen, followed by animal dander. No patient was receiving oral corticosteroids.

Transcriptomic RNAseq Study

Significant differences between control and asthmatic patients were observed in the transcriptomic assay ($P < 0.05$). **Table 3** shows the top 26 most differentially expressed transcripts between controls and patients with allergic asthma, according to *P*-value and fold change. The main biological roles of these

TABLE 4 | Gene Ontology term enrichment analysis of the more differentially expressed genes.

Term ID	Biological process	FDR	Genes
Immune system			
GO:0002376	Immune system process	1.74E-07	*ABCA13, ARG1, CEACAM8, CRISP3, CYSLTR2, DDIT4, FLT3, IDO1, IL5RA, LTF, MMP8, MMP9, PI3, PTGDR2, RAB44, SMPD3.*
GO:0006955	Immune response	5.94E-06	*ABCA13, ARG1, CEACAM8, CRISP3, CYSLTR2, IL5RA, LTF, MMP8, MMP9, PI3, PTGDR2, RAB44.*
GO:0043312	Neutrophil degranulation	7.28E-05	*ABCA13, ARG1, CEACAM8, CRISP3, LTF, MMP8, MMP9, RAB44.*
Cellular process			
GO:0001775	Cell activation	1.32E-06	*ABCA13, ARG1, CEACAM8, CRISP3, FLT3, ITGA2B, LTF, MMP8, MMP9, PIK3R6, RAB44.*
GO:0019221	Cytokine-mediated signaling pathway	8.10E-03	*ALOX15, FLT3, IL5RA, MMP9.*
GO:0007166	Cell surface receptor signaling pathway	0.017	*ALOX15, DDIT4, FLT3, G0S2, GPR34, IL5RA, MMP9.*
GO:0007165	Signal transduction	0.012	*ALOX15, CYSLTR2, DDIT4, FLT3, G0S2, GPR34, HRH4, IL5RA, MMP9, PIK3R6, PTGDR2.*
Cellular response			
GO:0050896	Response to stimulus	2.52E-06	*ABCA13, ALOX15, ARG1, CEACAM8, CRISP3, CYSLTR2, DDIT4, FLT3, G0S2, GPR34, HRH4, IDO1, IL5RA, ITGA2B, LTF, MMP8, MMP9, PER1, PI3, PIK3R6, PTGDR2, RAB44.*
GO:0006952	Defense response	9.28E-05	*ALOX15, ARG1, CRISP3, DDIT4, HRH4, IDO1, IL5RA, LTF.*
GO:0006950	Response to stress	3.00E-04	*ALOX15, ARG1, CRISP3, DDIT4, HRH4, IDO1, IL5RA, ITGA2B, LTF, MMP9, PIK3R6.*
GO:0006954	Inflammatory response	2.50E-03	*ALOX15, HRH4, IDO1, IL5RA.*
GO:0071345	Cellular response to cytokine stimulus	9.30E-03	*ALOX15, ARG1, FLT3, IL5RA, MMP9.*
Biological regulation			
GO:0048583	Regulation of response to stimulus	6.84E-05	*ALOX15, ARG1, CLC, CYSLTR2, DDIT4, FLT3, G0S2, HRH4, IDO1, LTF, MMP9, PER1, PIK3R6, PTGDR2.*
GO:0009966	Regulation of signal transduction	6.84E-05	*ALOX15, ARG1, CYSLTR2, DDIT4, FLT3, G0S2, HRH4, LTF, MMP9, PER1, PIK3R6 PTGDR2.*
GO:0051239	Regulation of multicellular organismal process	2.30E-04	*ARG1, CLC, CYSLTR2, IDO1, IL5RA, ITGA2B, LTF, MMP9, PER1, PIK3R6, PTGDR2.*
GO:0001817	Regulation of cytokine production	6.20E-03	*ARG1, CLC, IDO1, IL5RA, LTF, PER1.*
GO:0050794	Regulation of cellular process	0.018	*ALOX15, ARG1, CLC, CRY2, CYSLTR2, DDIT4, FLT3, G0S2, GPR34, HRH4, IDO1, IL5RA, ITGA2B, LTF, MMP9, PER1, PI3, PIK3R6, PTGDR2, SMPD3.*

FDR, false discovery rate.

genes are described in **Table 4**, which highlights the biological processes related to the immune system. Among these genes, *IL5RA* attracted our attention as a putative asthma biomarker because it was the best positioned when considering both fold change and *P*-value data, and because of its role in different immune processes.

A protein-protein interaction network analysis was performed with the selected transcripts to analyze the interactions among them. Four main clusters were obtained, referred to as clusters A, B, C, and D (**Figure 1**). *IL5RA* was found in cluster A, which included seven genes: *IL5RA*, *IL5*, *FLT3* (receptor-type tyrosine-protein kinase), *PTGDR2* (prostaglandin D2 receptor 2), *HRH4* (histamine H4 receptor), *TIMP1* (metalloproteinase inhibitor 1) and *IDO1* (indoleamine 2,3-dioxygenase 1). Regarding the role of *IL5RA* in biological processes, the most significant terms were "immune system process" (FDR 1.74E-07) and "response to stimulus" (FDR 2.52E-06) (**Table 4**), as well as in Reactome pathways, such as "signaling by interleukins" and "RAF/MAP kinase cascade."

qPCR Validation Assays

A validation qPCR analysis was performed to confirm the differences observed in the RNAseq study. Patients were classified according to the presence of atopy and nasal polyposis (NP), the severity of asthma and the age of onset of asthma. As summarized in **Table 5**, asthmatic patients had significantly higher levels of peripheral blood eosinophil counts and *IL5RA* expression than controls ($P < 0.001$). That also occurred in all subgroups except for non-eosinophilic asthma ($P = 0.707$). Interestingly, the lower increase in *IL5RA* expression levels was observed in patients with non-allergic asthma (NAA) without NP (10.3 ± 11.2; $P = 0.037$). Significant differences were observed when comparing these patients with the subgroup of patients who had NAA with NP ($P = 0.047$). These significant differences were not observed among the other subgroups, although *IL5RA* expression levels were significantly higher in eosinophilic asthma than in non-eosinophilic asthma ($P < 0.001$). Also, *IL5RA* expression levels were slightly higher in monosensitized patients to pollens.

In general, there was an association between asthma severity and increased levels of *IL5RA* expression (**Table 5**). Patients with intermittent asthma had the lowest expression levels of *IL5RA* (12.0 ± 13.7), while patients with severe asthma had the highest levels (19.9 ± 20.3; $P = 0.056$). In addition, there was a statistically significant association between asthma severity and the number of eosinophils ($P = 0.015$).

To discard a possible influence of anti-inflammatory treatments on the expression of *IL5RA*, patients receiving inhaled corticosteroids or allergen immunotherapy were compared with patients not receiving these treatments. One hundred thirty-nine patients were receiving therapy with inhaled corticosteroids; 54 patients were receiving allergen immunotherapy. No statistically significant differences in the *IL5RA* expression levels were observed between patients receiving corticosteroid treatment or allergen immunotherapy and patients not receiving these treatments.

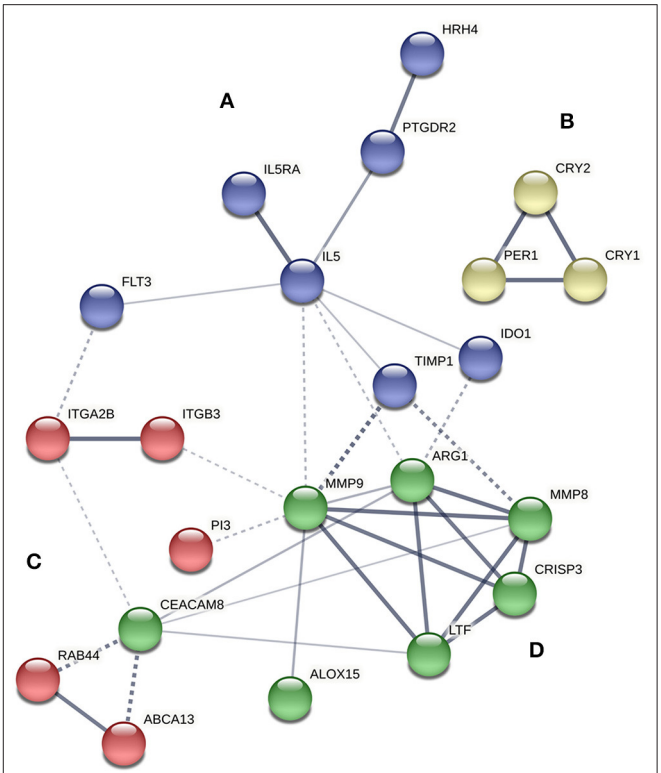

FIGURE 1 | Protein interaction network of proteins encoded by differentially expressed genes between controls and asthmatic patients using STRING software. The strength of data support is indicated by line thickness. The four main clusters are shown in blue **(A)**, yellow **(B)**, red **(C)**, and green **(D)**.

The relationship between *IL5RA* expression levels and peripheral blood eosinophil counts was also analyzed, observing some correlation with a Pearson's correlation coefficient of 0.520 ($P < 0.001$). Remarkably, as shown in **Figure 2A**, there were patients with the same eosinophil counts and very different expression levels of *IL5RA*. In addition, an eosinophil count-dependent increase in both *IL5RA* expression levels and dispersion was observed when the eosinophil counts were divided into quartiles (**Figure 2B**). This fact was also observed according to asthma severity. The more severe the asthma was, the greater the *IL5RA* levels were (**Figure 3**).

Pharmacogenetic Study

The clinical parameters of the patients included in the proof-of-concept study are shown in **Table 6**. Three of the patients had NP, and three were sensitized to pollens, without present clinical relevance. All patients were in treatment with high dose inhaled corticosteroids and tiotropium bromide at entry, although no patient was treated with oral corticosteroids. Before treatment with benralizumab, *IL5RA* expression levels and eosinophil counts were high in two patients, intermediate in two, and lower in another one. After 3 months of treatment, a dramatic reduction (90–100%) of peripheral eosinophil count was observed in all patients ($P = 0.042$) (**Figure 4A**). *IL5RA*

TABLE 5 | Blood eosinophil counts and *IL5RA* expression levels according to asthma diagnosis, sensitization and severity.

	N	Eosinophils/μl[a] (Mean ± SD)	*IL5RA*, relative expression (Mean ± SD)	*P*-value[b]	*P*-value[c]
Controls	100	127.8 ± 89.4	7.1 ± 6.3		
Asthmatic patients	187	380.4 ± 331.0	15.5 ± 15.4	<0.001	
Non-allergic asthma (NAA)	76	373.4 ± 367.1	13.9 ± 13.7	<0.001	
NAA without NP	33	223.7 ± 169.4	10.3 ± 11.2	0.037	0.047
NAA with NP	43	510.0 ± 441.6	16.6 ± 14.9	<0.001	
Allergic asthma (AA)	111	385.6 ± 303.3	16.6 ± 16.4	<0.001	
AA without NP	82	308.4 ± 222.9	16.5 ± 17.0	<0.001	0.982
AA with NP	29	577.1 ± 386.9	16.6 ± 15.0	<0.001	
Monosensitized to pollens	22	478.7 ± 301.6	20.2 ± 17.3	<0.001	
Monosensitized to animal dander	6	300.0 ± 205.2	21.4 ± 29.2	0.050	
Monosensitized to mites	10	411.1 ± 513.4	14.5 ± 14.5	0.064	
Polysensitized	73	358.8 ± 266.4	15.2 ± 14.7	<0.001	
Intermittent asthma	49	290.8 ± 199.3	12.0 ± 13.7	0.003	0.056
Mild persistent asthma	29	337.4 ± 192.7	17.7 ± 18.4	<0.001	
Moderate persistent asthma	85	380.5 ± 340.9	15.4 ± 13.4	<0.001	
Severe persistent asthma	23	574.0 ± 494.3	19.9 ± 20.3	<0.001	
Early-onset asthma	76	364.0 ± 307.4	14.5 ± 14.4	<0.001	
Late-onset asthma	111	391.1 ± 346.7	16.1 ± 16.0	<0.001	
Non-eosinophilic asthma	32	98.5 ± 66.1	6.6 ± 5.8	0.707	<0.001
Eosinophilic asthma	120	455.6 ± 332.9	18.2 ± 15.4	<0.001	

SD, standard deviation.

[a] *All P-value results for blood eosinophil counts were significant ($P < 0.05$) among each patient group vs. controls, except for non-eosinophilic asthma ($P = 0.082$).*

[b] *P-value obtained for the comparison of IL5RA expression levels from each patient group vs. controls.*

[c] *P-value obtained for comparison of IL5RA expression levels from NAA without NP vs. NAA with NP; AA without NP vs. AA with NP; intermittent asthma vs. severe persistent asthma; and non-eosinophilic asthma vs. eosinophilic asthma, respectively.*

expression levels were reduced between 70–96% after treatment ($P = 0.043$) (**Figure 4B**). A strong correlation was found between *IL5RA* levels and peripheral blood eosinophil counts at pretreatment (**Figure 4C**) with a Pearson's correlation coefficient of 0.940 ($P = 0.017$). In addition, all patients achieved an ACT score >20 and a mean increase of 30% in FEV1, except patient 4. This patient had the highest pretreatment levels of *IL5RA* expression, and the improvement of FEV1 reached 50% (**Figure 5**).

DISCUSSION

Novel biological therapies have increased clinical treatment options for asthma. The necessity of identifying biomarkers to achieve a proper selection of these expensive compounds has led to the application of transcriptomic methods as a starting point for discovering new genes involved in the disease. In a previous transcriptomic study, increased expression of interleukin-4 receptor (IL-4R) on B cells was observed in allergic asthma patients (39). In the present study, we have focused on another type 2 cytokine, IL-5, which is also involved in asthma pathophysiology. Thus, IL-5RA has been analyzed due to its implication with eosinophilic-mediated immunity.

In the RNAseq study, significant gene expression differences were observed between the peripheral blood samples of controls and allergic asthmatic patients, with a top 26 differentially expressed genes, as shown in **Table 3**. Interestingly, most of these genes are involved in biological processes related to the immune system, suggesting their potential implication in the pathophysiology of asthma. *IL5RA* turned out to be one of the genes with the highest differential expression, which is also supported by its relevant role in asthma (16, 17) and its interactions with other immune response effector molecules that were detected in the protein-protein interaction network analysis. All proteins of the *IL5RA* cluster had already been reported to participate in functions related to inflammatory response, signal transduction and eosinophil mediated immunity, such as eosinophil chemotaxis, regulation of type 2 cytokine production or cell differentiation and proliferation (40–44). These functions are consistent with the biological processes obtained in our transcriptomic study, described in **Table 4**. Furthermore, differential *IL5RA* expression levels have also been described in the literature, both between asthmatic patients and controls (45, 46) and pre and post-benralizumab treatment samples (47).

Following the results obtained in the RNAseq study, we decided to carry out a qPCR validation study to evaluate

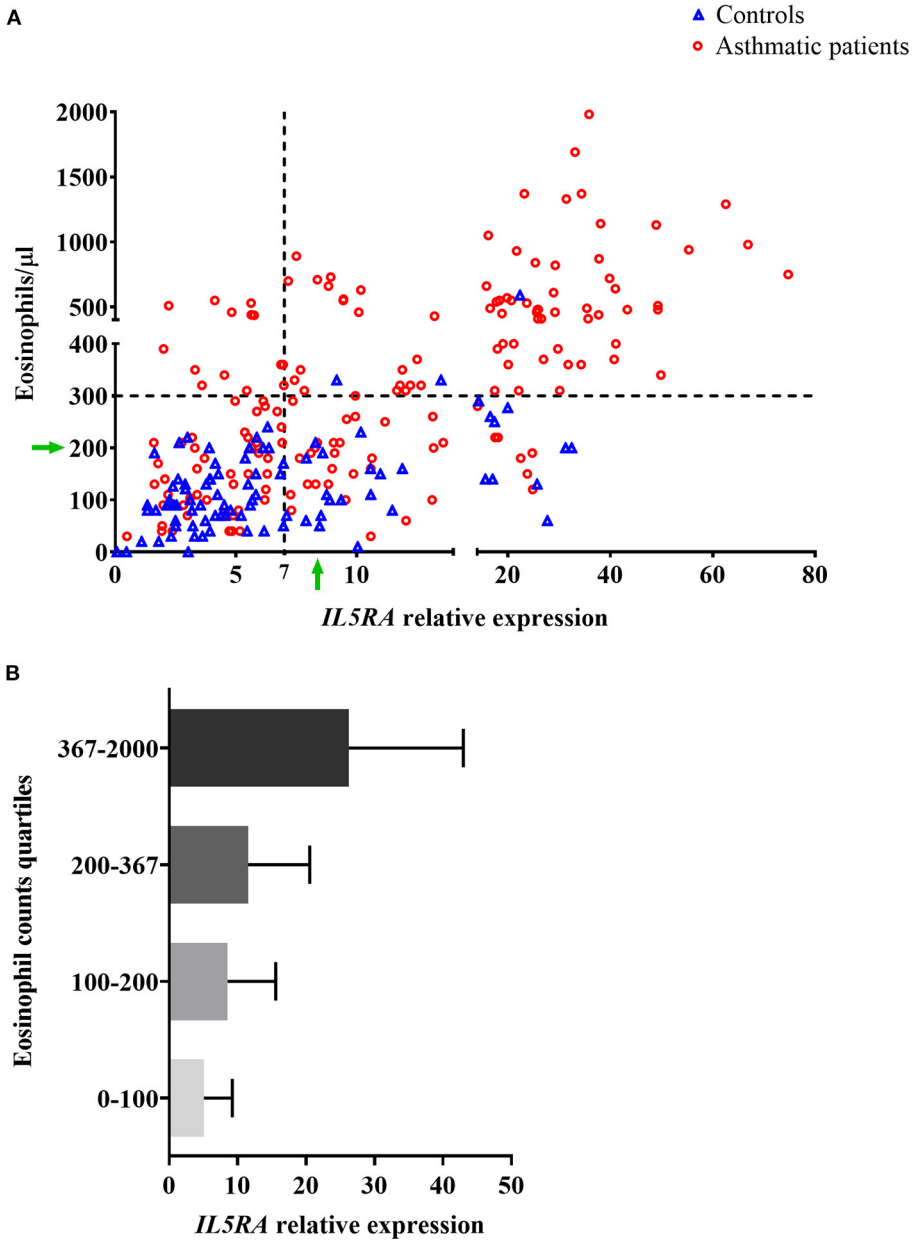

FIGURE 2 | (A) Correlation between *IL5RA* expression levels and peripheral blood eosinophil counts of controls and asthmatic patients from the validation analysis. Four quadrants were obtained by dividing according to the normality values for eosinophil counts (300/µl) and *IL5RA* expression (7-fold). The green arrows indicate a constant value of eosinophils at which a wide range of expressed *IL5RA* values is observed, and vice versa. **(B)** *IL5RA* expression levels (mean ± SD) in eosinophil count quartiles.

the performance of the peripheral blood *IL5RA* expression levels in the diagnosis of asthma. Levels were significantly higher in asthmatic patients than in controls, independently of the type of asthma (**Table 5**). This result suggests that it could be a potential marker in the diagnosis of asthma. One main limitation is its correlation with eosinophil counts, as a moderate correlation was observed ($r = 0.520$). Nevertheless, as shown by green arrows in **Figure 2A**, there was a notable dispersion of values, and some patients had high *IL5RA* expression levels compared to their eosinophil counts and vice versa. Also, we found that patients with the same eosinophil counts can show very different *IL5RA* expression levels. For example, *IL5RA* expression values ranging from 4 to 32 were observed for counts of 200 eosinophils/µl. This distribution was also found in controls, as variability in *IL5RA* expression levels was observed at low eosinophil counts. However, the dispersion was considerably more significant in patients with high eosinophil counts. This dispersion was also observed

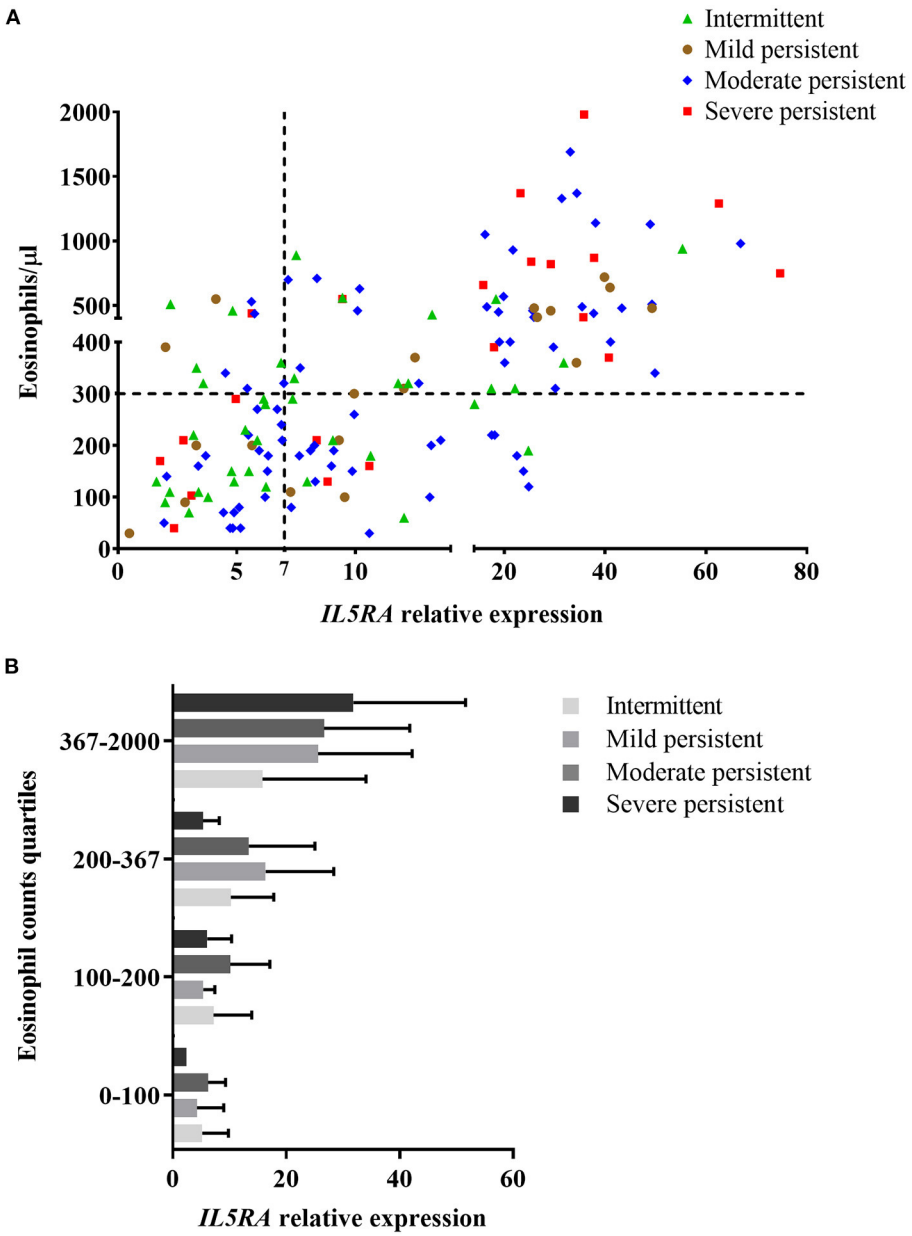

FIGURE 3 | (A) Correlation between *IL5RA* expression levels and peripheral blood eosinophil counts according to asthma severity of patients from the validation analysis. Four quadrants were obtained by dividing according to the normality values for eosinophil counts (300/μl) and *IL5RA* expression (7-fold). **(B)** *IL5RA* expression levels (mean ± SD) in eosinophil count quartiles according to asthma severity.

in all subgroups according to asthma severity. It can be speculated that differences could be due to different levels of expression of the *IL5RA* by eosinophils, caused by unknown elements, such as genetic or environmental factors driving the expression of the receptor. Besides, differences could reflect the expression by other cell types, such as basophils (20). In this sense, basophils have been involved in the immunology of eosinophilic asthma (48). Furthermore, this differential expression of *IL5RA* could be related to the different responses observed to biologics directed against *IL5RA*. In fact, in the proof-of-concept study, the patient with the highest levels of *IL5RA* expression was the best responder in terms of ACT and FEV1 (see below).

Concerning the different types of asthma, *IL5RA* expression levels were elevated in both allergic and non-allergic asthma. This finding is in agreement with the fact that responses to benralizumab are not influenced by the atopy status (49). In addition, we observed a progressive increase in the expression of *IL5RA* levels from intermittent to severe asthma, which could be related to the number of eosinophils to a great extent.

TABLE 6 | *IL5RA* expression levels and clinical parameters in pretreatment and after 3 months of benralizumab treatment.

	Eosinophils/μl	*IL5RA*, relative expression	FEV1, ml	FeNO, ppb	ACT
Patient 1					
Pretreatment	630	1.8	1,897	43	13
3 months	10	0.6	2,462	68	22
Patient 2					
Pretreatment	820	29.2	1,960	-	8
3 months	10	1.2	2,520	-	24
Patient 3[a]					
Pretreatment	437	10.9	2,310	154	12
3 months	0	1.0	3,100	113	22
Patient 4					
Pretreatment	1,290	62.5	1,890	66	19
3 months	0	4.7	2,840	198	25
Patient 5[a]					
Pretreatment	630	12.6	2,060	65	12
3 months	10	0.8	2,630	64	21

[a] *Patients previously treated with other biological drugs, but no improvement was observed.*

One streaking feature was that *IL5RA* expression levels were significantly higher in non-allergic asthma patients with NP respect to non-allergic asthma patients without NP. In this sense, it has been described that *IL5RA* expression is increased in patients with NP, particularly those with Aspirin-Exacerbated Respiratory Disease (50). Whether this could be related to response to the treatment with biologics in patients with chronic rhinosinusitis with NP remains speculative.

In the proof-of-concept pharmacogenetic study, we selected peripheral blood because it is easily accessible, a crucial characteristic of an ideal biomarker (51). In addition, as we were trying to check the *IL5RA* expression as a biomarker, we selected benralizumab treatment as it is directed against *IL5RA* (21). All patients were good responders, as demonstrated by the increase of ACT and FEV1. It is known that anti-IL-5 and anti-IL-5RA treatments do not significantly modify FeNO levels (52), as it happened in most of our patients. The increase observed in some of them could be due to acute exposure to allergens (53) because adherence to inhaled corticosteroids seemed to be appropriated. Due to the short follow-up period, exacerbations were not considered, although no patient had an exacerbation after treatment with benralizumab; even more, they almost did not require rescue bronchodilators. All patients showed a dramatic decrease in peripheral blood eosinophil counts with values between 0 and 10 eosinophils/μl, as observed in the phase III studies (21). The pretreatment levels of *IL5RA* were highly variable in patients, ranging from 1.8 to 62.5, and were strongly correlated with pretreatment peripheral blood eosinophil counts ($r = 0.940$). Thus, we believe that *IL5RA* expression level could add value to peripheral blood eosinophil counts. Accordingly, the patient with the highest *IL5RA* expression levels showed the best lung function response and reached an ACT of 25. In a very recent study, Nakajima et al. (54) described a group of super responder to benralizumab patients that had higher expression of genes related to eosinophils in peripheral blood, together with significant reductions in the expressions of genes associated with eosinophilic inflammatory responses after treatment with benralizumab, with *IL5RA* among them. So, the expression of *IL5RA* could be a useful biomarker of response, as it seems to be more discriminant than eosinophil counts.

This study is not without limitations since it is a unicentric study, and the number of patients is low. Nevertheless, this fact gives uniformity to the study. Additionally, we have mainly focused on *IL5RA*, and other genes may also be relevant in response to treatment. Nevertheless, we selected *IL5RA* by its crucial implication in the immunology of T2-asthma and because benralizumab is directed against this molecule. Finally, the proof-of-concept study has a limited number of patients and a short period of follow-up.

CONCLUSION

There is an urgent need for biomarkers of response to biologics in asthma. In this study, we have explored the peripheral blood *IL5RA* expression levels as a possible useful biomarker for several reasons. First, *IL5RA* is a plausible etiopathogenic target and a biologic target for the treatment of asthma. Second, peripheral blood is easily accessible. Third, its expression is easily measurable and reproducible. Fourth, it varies in different types of asthma. And, finally, although it has a moderate correlation with eosinophils, *IL5RA* expression levels probably do not reflect the same, as these levels vary for a particular count of peripheral blood eosinophils. Further studies are required for confirming the findings of the present study.

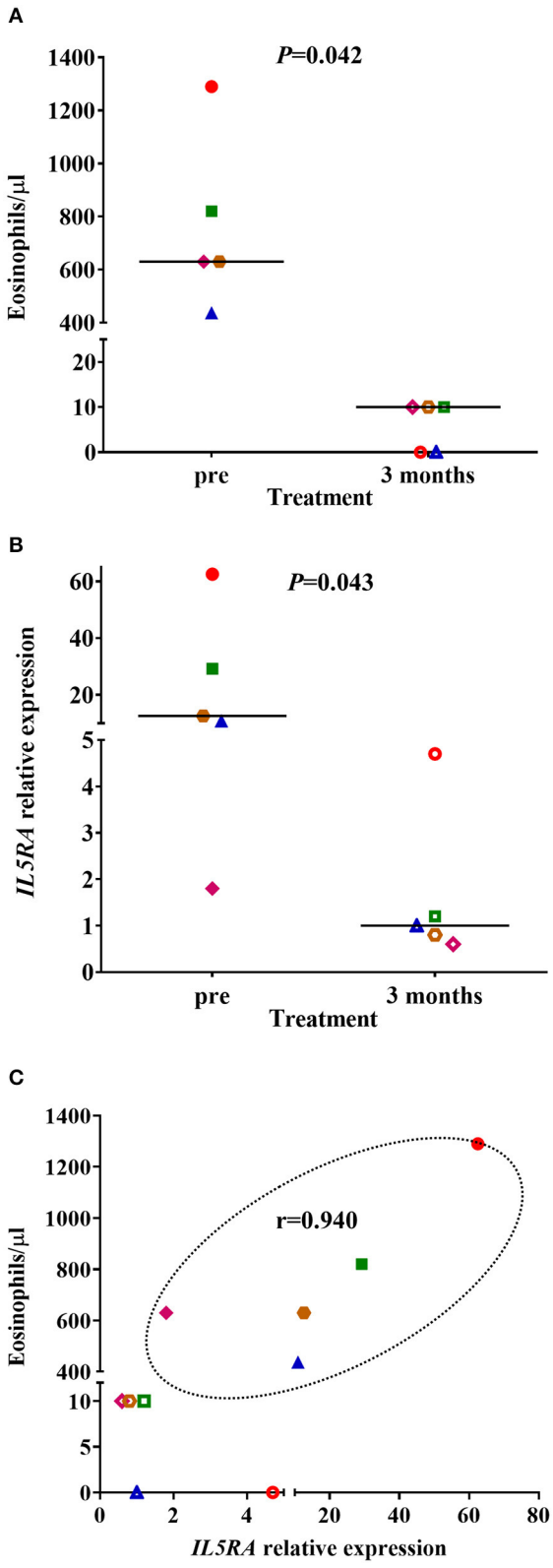

FIGURE 4 | (A) Peripheral blood eosinophil counts and **(B)** *IL5RA* expression levels in pretreatment and after 3 months of benralizumab treatment. The *(Continued)*

FIGURE 4 | median of each group is also shown. **(C)** Correlation between *IL5RA* expression levels and peripheral blood eosinophil counts at pretreatment and after 3 months of benralizumab treatment. Pearson's correlation coefficient in the pretreatment is also shown. Each symbol represents a patient (◆ Patient 1; ■ Patient 2; ▲ Patient 3; ● Patient 4; ⬢ Patient 5). The filled symbols correspond to the pretreatment and the empty symbols to after 3 months of benralizumab treatment.

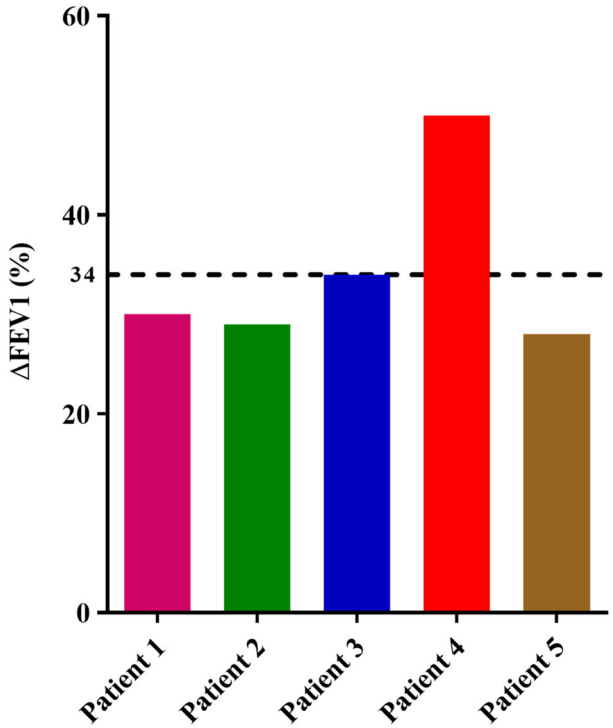

FIGURE 5 | Percentage of FEV1 value variation in each patient between pretreatment and after 3 months of treatment with benralizumab. The dotted line shows the mean of all patients.

DATA AVAILABILITY STATEMENT

The required data is now publicly accessible in the NCBI repository with the code PRJNA686899.

ETHICS STATEMENT

The studies involving human participants were reviewed and approved by The Clinical Research Ethics Committee of the Institute for Biomedical Research of Salamanca (IBSAL) (PI 2020-02-433). The patients/participants provided their written informed consent to participate in this study.

AUTHOR CONTRIBUTIONS

SE-P, DH-J, AG-S, ME, MM, JR-G, JT, MI-G, CS, and ID have contributed in designing research studies, conducting experiments, acquiring data, analyzing data, and writing the manuscript. All authors read and approved the final manuscript.

FUNDING

This work was supported by the Instituto de Salud Carlos III and the European Regional Development Fund (Grant Nos. PI17/00818 and PI20/00268), by a grant of the Junta de Castilla y León and the European Regional Development Fund (IES161P20) and by a grant of the Instituto de Salud Carlos III to the Red temática de investigación en salud Asma, Reacciones Adversas y Alérgicas (ARADYAL) RD16/0006/0019.

REFERENCES

1. Vos T, Abajobir AA, Abbafati C, Abbas KM, Abate KH, Abd-Allah F, et al. Global, regional, and national incidence, prevalence, and years lived with disability for 328 diseases and injuries for 195 countries, 1990-2016: a systematic analysis for the global burden of disease study 2016. *Lancet*. (2017) 390:1211–59. doi: 10.1016/S0140-6736(17)32154-2
2. Global Initiative for Asthma. *Global Strategy for Asthma Management and Prevention*. (2020). Available online at: https://www.ginasthma.org/ (accessed April 25, 2020).
3. Wenzel SE. Asthma phenotypes: the evolution from clinical to molecular approaches. *Nat. Med*. (2012) 18:716–25. doi: 10.1038/nm.2678
4. Levine SJ, Wenzel SE. Narrative review: The role of Th2 immune pathway modulation in the treatment of severe asthma and its phenotypes. *Ann. Intern. Med*. (2010) 152:232–7. doi: 10.7326/0003-4819-152-4-201002160-00008
5. Lambrecht BN, Hammad H. The immunology of asthma. *Nat. Immunol*. (2015) 16:45–56. doi: 10.1038/ni.3049
6. Caminati M, Le Pham D, Bagnasco D, Canonica GW. Type 2 immunity in asthma. *World Allergy Organ. J*. (2018) 11:13. doi: 10.1186/s40413-018-0192-5
7. GEMA 4.4. *Guía española para el manejo del asma*. (2020). Available online at: https://www.gemasma.com/ (accessed May 1, 2020).
8. Kaur R, Chupp G. Phenotypes and endotypes of adult asthma: moving toward precision medicine. *J. Allergy Clin. Immunol*. (2019) 144:1–12. doi: 10.1016/j.jaci.2019.05.031
9. Moore WC, Meyers DA, Wenzel SE, Teague WG, Li H, Li X, et al. Identification of asthma phenotypes using cluster analysis in the severe asthma research program. *Am. J. Respir. Crit. Care Med*. (2010) 181:315–23. doi: 10.1164/rccm.200906-0896OC
10. Haldar P, Pavord ID, Shaw DE, Berry MA, Thomas M, Brightling CE, et al. Cluster analysis and clinical asthma phenotypes. *Am. J. Respir. Crit. Care Med*. (2008) 178:218–24. doi: 10.1164/rccm.200711-1754OC
11. Coumou H, Bel EH. Improving the diagnosis of eosinophilic asthma. *Expert Rev. Respir. Med*. (2016) 10:1093–103. doi: 10.1080/17476348.2017.1236688
12. Buhl R, Humbert M, Bjermer L, Chanez P, Heaney LG, Pavord I, et al. Severe eosinophilic asthma: a roadmap to consensus. *Eur. Respir. J*. (2017) 49:1700634. doi: 10.1183/13993003.00634-2017
13. Fitzpatrick AM, Moore WC. Severe asthma phenotypes—how should they guide evaluation and treatment? *J. Allergy Clin. Immunol. Pract*. (2017) 5:901–8. doi: 10.1016/j.jaip.2017.05.015
14. Isidoro-García M, Sánchez-Martín A, García-Sánchez A, Sanz C, García-Berrocal B, Dávila I. Pharmacogenetics and the treatment of asthma. *Pharmacogenomics*. (2017) 18:1271–80. doi: 10.2217/pgs-2017-0024
15. Canonica GW, Ferrando M, Baiardini I, Puggioni F, Racca F, Passalacqua G, et al. Asthma: personalized and precision medicine. *Curr. Opin. Allergy Clin. Immunol*. (2018) 18:51–8. doi: 10.1097/ACI.0000000000000416
16. Kouro T, Takatsu K. IL-5- and eosinophil-mediated inflammation: from discovery to therapy. *Int. Immunol*. (2009) 21:1303–9. doi: 10.1093/intimm/dxp102
17. Brussino L, Heffler E, Bucca C, Nicola S, Rolla G. Eosinophils target therapy for severe asthma: critical points. *Biomed. Res. Int*. (2018) 2018:7582057. doi: 10.1155/2018/7582057
18. Tavernier J, Devos R, Cornelis S, Tuypens T, Van der Heyden J, Fiers W, et al. A human high affinity interleukin-5 receptor (IL5R) is composed of an IL5-specific α chain and a β chain shared with the receptor for GM-CSF. *Cell*. (1991) 66:1175–84. doi: 10.1016/0092-8674(91)90040-6
19. Kupczyk M, Kuna P. Benralizumab: an anti-IL-5 receptor α monoclonal antibody in the treatment of asthma. *Immunotherapy*. (2018) 10:349–59. doi: 10.2217/imt-2017-0161
20. Kolbeck R, Kozhich A, Koike M, Peng L, Andersson CK, Damschroder MM, et al. MEDI-563, a humanized anti-IL-5 receptor α mAb with enhanced antibody-dependent cell-mediated cytotoxicity function. *J. Allergy Clin. Immunol*. (2010) 125:1344–53. doi: 10.1016/j.jaci.2010.04.004
21. Dávila González I, Moreno Benítez F, Quirce S. Benralizumab: a new approach for the treatment of severe eosinophilic asthma. *J. Investig. Allergol. Clin. Immunol*. (2019) 29:84–93. doi: 10.18176/jiaci.0385
22. American Thoracic Society. Standards for the diagnosis and care of patients with chronic obstructive pulmonary disease. *Am. J. Respir. Crit. Care Med*. (1995) 152:77–121.
23. Chung KF, Wenzel SE, Brozek JL, Bush A, Castro M, Sterk PJ, et al. International ERS/ATS guidelines on definition, evaluation and treatment of severe asthma. *Eur. Respir. J*. (2014) 43:343–73. doi: 10.1183/09031936.00202013
24. Sanz C, Isidoro-García M, Dávila I, Moreno E, Laffond E, Ávila C, et al. Promoter genetic variants of prostanoid DP receptor (PTGDR) gene in patients with asthma. *Allergy*. (2006) 61:543–8. doi: 10.1111/j.1398-9995.2006.01025.x
25. Sub-Committee on Skin Tests of the European Academy of Allergology and Clinical Immunology. Skin tests used in type I allergy testing Position paper. *Allergy*. (1989) 44 Suppl 10:1–59.
26. Sendín-Hernández MP, Ávila-Zarza C, Sanz C, García-Sánchez A, Marcos-Vadillo E, Muñoz-Bellido FJ, et al. Cluster analysis identifies 3 phenotypes within allergic asthma. *J. Allergy Clin. Immunol. Pract*. (2018) 6:955–61. doi: 10.1016/j.jaip.2017.10.006
27. Babraham Bioinformatics. *FastQC A Quality Control Tool for High Throughput Sequence Data*. (2020). Available online at: http://www.bioinformatics.babraham.ac.uk/projects/fastqc/ (accessed August 17, 2020).
28. Kim D, Pertea G, Trapnell C, Pimentel H, Kelley R, Salzberg SL. TopHat2: Accurate alignment of transcriptomes in the presence of insertions, deletions and gene fusions. *Genome Biol*. (2013) 14:R36. doi: 10.1186/gb-2013-14-4-r36
29. Picard Tools. By Broad Institute (2020). Available online at: http://broadinstitute.github.io/picard/ (accessed August 28, 2020).
30. Li H. Aligning sequence reads, clone sequences and assembly contigs with BWA-MEM. (2013) *arXiv[Preprint]*. arXiv:1303.3997.
31. Trapnell C, Williams BA, Pertea G, Mortazavi A, Kwan G, Van Baren MJ, et al. Transcript assembly and quantification by RNA-Seq reveals unannotated transcripts and isoform switching during cell differentiation. *Nat. Biotechnol*. (2010) 28:511–5. doi: 10.1038/nbt.1621
32. Anders S, Pyl PT, Huber W. HTSeq-A Python framework to work with high-throughput sequencing data. *Bioinformatics*. (2015) 31:166–9. doi: 10.1093/bioinformatics/btu638
33. Love MI, Huber W, Anders S. Moderated estimation of fold change and dispersion for RNA-seq data with DESeq2. *Genome Biol*. (2014) 15:550. doi: 10.1186/s13059-014-0550-8
34. STRING. *Functional Protein Association Networks*. (2020). Available online at: https://string-db.org/ (accessed October 13, 2020).
35. Primer3.0. (2018). Available online at: http://bioinfo.ut.ee/primer3-0.4.0/ (accessed March 6, 2018).
36. Beacon Designer (2020). Available online at: http://www.premierbiosoft.com/qOligo/Oligo.jsp?PID=1 (accessed March 6, 2018).
37. Livak KJ, Schmittgen TD. Analysis of relative gene expression data using real-time quantitative PCR and the 2-ΔΔCT method. *Methods*. (2001) 25:402–8. doi: 10.1006/meth.2001.1262
38. Bustin SA, Benes V, Garson JA, Hellemans J, Huggett J, Kubista M, et al. The MIQE guidelines: minimum information for publication of quantitative real-time PCR experiments. *Clin. Chem*. (2009) 55:611–22. doi: 10.1373/clinchem.2008.112797

39. Pascual M, Roa S, García-Sánchez A, Sanz C, Hernandez-Hernandez L, Greally JM, et al. Genome-wide expression profiling of B lymphocytes reveals IL4R increase in allergic asthma. *J. Allergy Clin. Immunol*. (2014) 134:972–5. doi: 10.1016/j.jaci.2014.05.015
40. Agrawal DK, Hopfenspirger MT, Chavez J, Talmadge JE. Flt3 ligand: a novel cytokine prevents allergic asthma in a mouse model. *Int. Immunopharmacol*. (2001) 1:2081–9. doi: 10.1016/S1567-5769(01)00122-9
41. Domingo C, Palomares O, Sandham DA, Erpenbeck VJ, Altman P. The prostaglandin D2 receptor 2 pathway in asthma: a key player in airway inflammation 11 medical and health sciences 1107 immunology 11 medical and health sciences 1102 Cardiorespiratory Medicine and Haematology. *Respir. Res*. (2018) 19:189. doi: 10.1186/s12931-018-0893-x
42. Ling P, Ngo K, Nguyen S, Thurmond RL, Edwards JP, Karlsson L, et al. Histamine H4 receptor mediates eosinophil chemotaxis with cell shape change and adhesion molecule upregulation. *Br. J. Pharmacol*. (2004) 142:161–71. doi: 10.1038/sj.bjp.0705729
43. Hassan N, Mohamed-Hussein A, Mohamed E, Mohamed O, Mohamed H, Tammam M. Matrix metalloproteinase- 9 (MMP-9) and tissue inhibitor of metalloproteinase-1(TIMP-1) as non-invasive biomarkers of remodelling in asthma. *Eur. Respir. J*. (2015) 46(Suppl. 59):OA1467. doi: 10.1183/13993003.congress-2015.OA1467
44. Hayashi T, Beck L, Rossetto C, Gong X, Takikawa O, Takabayashi K, et al. Inhibition of experimental asthma by indoleamine 2,3-dioxygenase. *J. Clin. Invest*. (2004) 114:270–9. doi: 10.1172/JCI21275
45. Bigler J, Boedigheimer M, Schofield JPR, Skipp PJ, Corfield J, Rowe A, et al. A severe asthma disease signature from gene expression profiling of peripheral blood from U-BIOPRED cohorts. *Am. J. Respir. Crit. Care Med*. (2017) 195:1311–20. doi: 10.1164/rccm.201604-0866OC
46. Virkud Y V., Kelly RS, Croteau-Chonka DC, Celedón JC, Dahlin A, Avila L, et al. Novel eosinophilic gene expression networks associated with IgE in two distinct asthma populations. *Clin. Exp. Allergy*. (2018) 48:1654–64. doi: 10.1111/cea.13249
47. Sridhar S, Liu H, Pham TH, Damera G, Newbold P. Modulation of blood inflammatory markers by benralizumab in patients with eosinophilic airway diseases. *Respir. Res*. (2019) 20:14. doi: 10.1186/s12931-018-0968-8
48. Suzuki Y, Wakahara K, Nishio T, Ito S, Hasegawa Y. Airway basophils are increased and activated in eosinophilic asthma. *Allergy Eur. J. Allergy Clin. Immunol*. (2017) 72:1532–9. doi: 10.1111/all.13197
49. Chipps BE, Newbold P, Hirsch I, Trudo F, Goldman M. Benralizumab efficacy by atopy status and serum immunoglobulin E for patients with severe, uncontrolled asthma. *Ann. Allergy Asthma Immunol*. (2018) 120:504–11. doi: 10.1016/j.anai.2018.01.030
50. Buchheit KM, Dwyer DF, Ordovas-Montanes J, Katz HR, Lewis E, Vukovic M, et al. IL-5Rα marks nasal polyp IgG4- and IgE-expressing cells in aspirin-exacerbated respiratory disease. *J. Allergy Clin. Immunol*. (2020) 145:1574–84. doi: 10.1016/j.jaci.2020.02.035
51. Medrek SK, Parulekar AD, Hanania NA. Predictive biomarkers for asthma therapy. *Curr. Allergy Asthma Rep*. (2017) 17:69. doi: 10.1007/s11882-017-0739-5
52. Hoyte FCL, Gross LM, Katial RK. Exhaled nitric oxide: an update. *Immunol. Allergy Clin. North Am*. (2018) 38:573–85. doi: 10.1016/j.iac.2018.06.001
53. Sordillo JE, Webb T, Kwan D, Kamel J, Hoffman E, Milton DK, et al. Allergen exposure modifies the relation of sensitization to fraction of exhaled nitric oxide levels in children at risk for allergy and asthma. *J. Allergy Clin. Immunol*. (2011) 127:1165–72.e5. doi: 10.1016/j.jaci.2011.01.066
54. Nakajima M, Matsuyama M, Arai N, Yamada H, Hyodo K, Nonaka M, et al. Identification of whole blood gene expressions correlated with responsiveness to benralizumab. *J. Allergy Clin. Immunol*. (2020) S0091-6749:31110–6. doi: 10.1016/j.jaci.2020.08.004

Conflict of Interest: ID declares having received honoraria for participation in speakers' bureaus or advisory boards from Astra-Zeneca, GSK, and Sanofi.

The remaining authors declare that the research was conducted in the absence of any commercial or financial relationships that could be construed as a potential conflict of interest.

Copyright © 2021 Elena-Pérez, Heredero-Jung, García-Sánchez, Estravís, Martin, Ramos-González, Triviño, Isidoro-García, Sanz and Dávila. This is an open-access article distributed under the terms of the Creative Commons Attribution License (CC BY). The use, distribution or reproduction in other forums is permitted, provided the original author(s) and the copyright owner(s) are credited and that the original publication in this journal is cited, in accordance with accepted academic practice. No use, distribution or reproduction is permitted which does not comply with these terms.

frontiers in Medicine

ORIGINAL RESEARCH
published: 16 February 2021
doi: 10.3389/fmed.2021.604694

A Simple-to-Use Web-Based Calculator for Survival Prediction in Acute Respiratory Distress Syndrome

Yong Liu[†], *Jian Liu*[†] *and Liang Huang*[*]

Department of Emergency, The First Affiliated Hospital of Nanchang University, Nanchang, China

Background: The aim of this study was to construct and validate a simple-to-use model to predict the survival of patients with acute respiratory distress syndrome.

Methods: A total of 197 patients with acute respiratory distress syndrome were selected from the Dryad Digital Repository. All eligible individuals were randomly stratified into the training set (n=133) and the validation set (n=64) as 2: 1 ratio. LASSO regression analysis was used to select the optimal predictors, and receiver operating characteristic and calibration curves were used to evaluate accuracy and discrimination of the model. Clinical usefulness of the model was also assessed using decision curve analysis and Kaplan-Meier analysis.

Results: Age, albumin, platelet count, PaO_2/FiO_2, lactate dehydrogenase, high-resolution computed tomography score, and etiology were identified as independent prognostic factors based on LASSO regression analysis; these factors were integrated for the construction of the nomogram. Results of calibration plots, decision curve analysis, and receiver operating characteristic analysis showed that this model has good predictive ability of patient survival in acute respiratory distress syndrome. Moreover, a significant difference in the 28-day survival was shown between the patients stratified into different risk groups ($P < 0.001$). For convenient application, we also established a web-based calculator (https://huangl.shinyapps.io/ARDSprognosis/).

Conclusions: We satisfactorily constructed a simple-to-use model based on seven relevant factors to predict survival and prognosis of patients with acute respiratory distress syndrome. This model can aid personalized treatment and clinical decision-making.

Keywords: acute respiratory distress syndrome, LASSO regression, nomogram, model, survival

OPEN ACCESS

Edited by:
Rifat Hamoudi,
University of Sharjah, United Arab Emirates

Reviewed by:
Rui-Qing Zhai,
Harbin Medical University, China
Tingfan Wu,
GE Healthcare (China), China
Nao Yan,
Wuhan University, China

***Correspondence:**
Liang Huang
huangliang6312@sina.com

[†]*These authors have contributed equally to this work*

Specialty section:
This article was submitted to Pulmonary Medicine, a section of the journal Frontiers in Medicine

Received: *10 September 2020*
Accepted: *29 January 2021*
Published: *16 February 2021*

Citation:
Liu Y, Liu J and Huang L (2021) A Simple-to-Use Web-Based Calculator for Survival Prediction in Acute Respiratory Distress Syndrome. Front. Med. 8:604694. doi: 10.3389/fmed.2021.604694

INTRODUCTION

Acute respiratory distress syndrome (ARDS) is a clinically and pathophysiologically complex syndrome characterized by rapid progression and devastating hypoxemic respiratory failure (1). Many risk factors, such as sepsis, pneumonia, pancreatitis, and major trauma, are associated with the development of ARDS (2). Although there has been some progress in ARDS treatment in the last several decades, the prognosis of patients with ARDS are still not satisfactory. The in-hospital mortality rate of ARDS patients remains between 34 and 60% (3). At present, the treatment of ARDS predominantly includes mechanical ventilation therapy (4). Therefore, identification of

TABLE 1 | Baseline characteristics of included patients in training and validation sets.

Characteristic	Entire cohort (n = 197)	Training set (n = 133)	Validation set (n = 64)	P-value
Age, years	73.94 ± 11.92	74.41 ± 11.95	72.97 ± 11.90	0.427
Sex				0.647
Female	74(37.6%)	48(36.1%)	26(40.6%)	
Male	123(62.4%)	85(63.9%)	38(59.4%)	
Alb, g/Dl	2.84 ± 0.58	2.81 ± 0.58	2.90 ± 0.59	0.317
PLT, per mm^3	19.23 ± 10.56	19.18 ± 10.50	19.32 ± 10.75	0.927
WBC, per mm^3	11010.66 ± 7255.91	10600.75 ± 7076.02	11862.50 ± 7602.22	0.254
CRP, mg/dl	17.42 ± 10.66	16.77 ± 10.83	18.77 ± 10.26	0.219
SOFA score	7.71 ± 3.47	8.09 ± 3.63	6.91 ± 2.98	0.024
McCabe score				0.474
1	174 (88.3%)	115 (86.5%)	59 (92.2%)	
2	11 (5.6%)	9 (6.8%)	2 (3.1%)	
3	12 (6.1%)	9 (6.8%)	3 (4.7%)	
PaO2/FiO2	116.11 ± 50.96	117.66 ± 50.57	112.89 ± 52.01	0.540
LDH, IU/L	390.57 ± 231.73	386.68 ± 199.63	398.64 ± 288.90	0.735
HRCT score	236.69 ± 66.70	233.46 ± 64.94	243.41 ± 70.27	0.328
PEEP, cmH_2O	10.40 ± 5.23	10.14 ± 5.22	10.92 ± 5.25	0.329
ARDS etiology				0.036
DARDS	170(86.3%)	120(90.2%)	50(78.1%)	
Non-DARDS	27(13.7%)	13(9.8%)	14(21.9%)	
Vital status				0.212
Living	128(65.0%)	82(61.7%)	46(71.9%)	
Deceased	69(35.0%)	51(38.3%)	18(28.1%)	

Alb, albumin; PLT, platelet count; WBC, white cell count; CRP, C reactive protein; SOFA, sequential organ failure assessment; LDH, lactate dehydrogenase; HRCT, high-resolution computed tomography; DARDS, drug-associated ARDS.

novel and effective treatment strategies is crucial for patients with ARDS. Moreover, a simple-to-use clinical prediction model is also required to provide adequate care to patients with ARDS.

The severity of ARDS is often assessed using the PaO_2/FiO_2 ratio, although this variable has a low-to-moderate prognostic value (5). Recently, several biomarkers including inflammation cytokines, epithelial or endothelial damage, and coagulation have been established to evaluated prognosis and therapeutic response of patients with ARDS. For example, a meta-analysis reported that elevated plasma levels of angiopoietin-2 strongly correlate with diagnosis and mortality in populations at high risk of ARDS (6). Moreover, various clinical biomarkers including lung inflammatory mediators (soluble suppression of tumorigenicity-2 and interleukin-6) (7) and products of epithelial and endothelial injury (the soluble form of the receptor for advanced glycation end products) (8, 9) were developed to monitor pathophysiologic changes and outcomes of ARDS. Unfortunately, although several lung-specific biomarkers have been validated to assess ARDS; however, none of them have been applied into clinical practice. Currently, there is no favorable prognosis prediction model for ARDS.

Nomograms (visualized graphs of a predictive model) are widely applied for prognosis and prediction of various diseases (10, 11). To date, no nomogram and corresponding web-based calculator has been developed to predict the prognosis of ARDS patients. Therefore, a refined model is needed to predict the prognosis of ARDS and guide clinical treatment. In this study, we aimed to construct a web-based calculator to predict the 28-day survival of patients with ARDS using several clinical parameters that are routinely used and readily available. This simple-to-use calculator might serve as an early warning and prediction system for patients with ARDS.

METHODS

Patients

A total of 197 patients with ARDS were extracted from the Dryad Digital Repository (http://www.datadryad.org/), which was shared by Anan et al. (12). All ARDS patients were diagnosed according to the Berlin definition (5). Patients with chronic interstitial lung disease (idiopathic pulmonary fibrosis), vasculitis or alveolar hemorrhage, hypersensitivity pneumonitis were excluded. All eligible patients were randomly stratified into two groups in a 2:1 ratio (training set and validation set, respectively). The extracted clinical data included age, gender, white cell count (WBC), C-reactive protein (CRP), lactate dehydrogenase (LDH), albumin (Alb), platelet count (PLT), PEEP, SOFA score, high-resolution computed tomography (HRCT) score, McCabe score, PaO2/FiO2, ARDS etiology, survival time, and survival status. Institutional ethical approval was not necessary because all the data were obtained from an online database.

Development of the Nomogram

To obtain the subset of predictors, the LASSO regression analysis was used to select the optimal predictors from the risk factors in the training cohort. The "glmnet" package was used to perform the LASSO regression analysis (13, 14). Finally, using the selected predictors from the LASSO regression, a nomogram was developed using the "rms," "survival," "foreign," and "openxlsx" R packages (15–18). A dynamic web-based calculator was constructed using "DynNom" package (19).

Validation of the Nomogram

To validate the constructed nomogram, the corresponding calibration map and receiver operating characteristic (ROC) analysis were performed in the training and validation sets to assess the prognostic accuracy of the nomogram by using the "rms," "survival," "foreign," and "timeROC" R packages (20).

Abbreviations: Alb, albumin; PLT, platelet count; WBC, white cell count; CRP, C reactive protein; SOFA, sequential organ failure assessment; APACHE, acute physiology and chronic health evaluation; LDH, lactate dehydrogenase; HRCT, high-resolution computed tomography; DARDS, drug-associated ARDS.

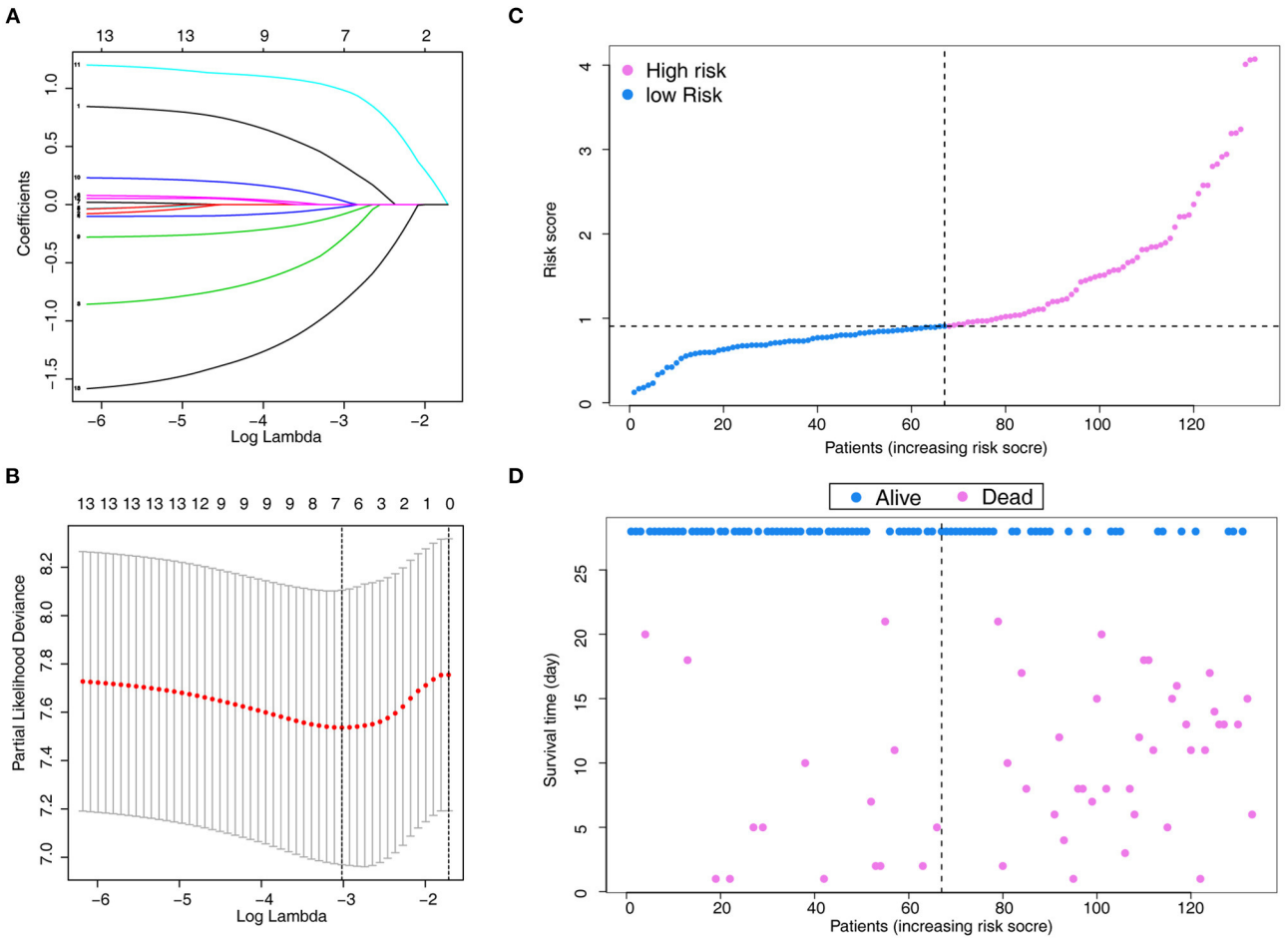

FIGURE 1 | Parameter selection using LASSO regression. **(A)** LASSO coefficient profiles of the 13 features. A coefficient profile plot is produced against the log(λ) sequence. **(B)** Variables selected through LASSO with 10-fold cross-validation. **(C)** Distribution of the risk score. **(D)** Relationships between survival status and survival times of ARDS patients ranked by risk score. The black dotted line represents the optimum cut-off point dividing patients into low- and high-risk groups. LASSO, least absolute shrinkage and selection operator.

In addition, decision curve analysis (DCA) was performed to quantify the clinical applicability of the nomogram.

Statistical Analysis

The raw data were expressed as mean ± standard deviation when normally distributed, while expressed as median (interquartile range) when non-normally distributed. Differences between two groups were analyzed using chi-square tests for categorical variables and t-tests for continuous variables. The Kaplan–Meier method and the log-rank test were used to estimate survival. All statistical analyses were performed using R software (Version 3.6.2; http://www.Rproject.org). A two-sided P-value < 0.05 was considered to indicate statistical significance.

RESULTS

Baseline Characteristics

In total, 197 eligible ARDS patients with integrated information were randomly stratified into two independent cohorts (training set, $n = 133$; validation set, $n = 64$). Patients' baseline clinical characteristics are shown in **Table 1**. A total of 123 male patients and 74 female patients were enrolled in this study. The average age of the patients was 73.94 ± 11.92 years. After 28 days of follow-up, 69 (35.0%) patients died during the entire study population.

Construction of the Model

A total of 13 parameters were used for LASSO regression, and seven parameters were selected as the optimal predictors by LASSO (**Figures 1A,B**). The seven retained variables were then used to construct the predictive model. The risk-score for each individual was calculated based on the model coefficients combined with the corresponding value of the identified seven clinical parameters. Thereafter, the patients were classified into low- and high-risk groups in both cohorts according to the median risk-score. **Figures 1C,D** show the risk-score distribution and the survival status of individual in the high- and low-risk cluster. The variables including Age, Alb, PLT, PaO_2/FiO_2,

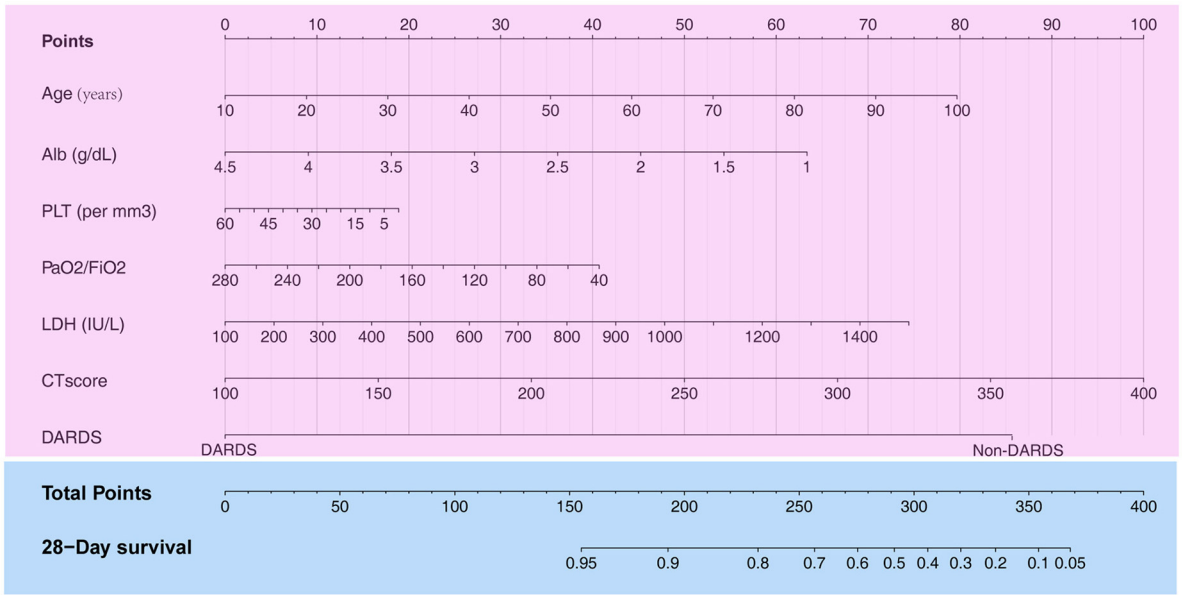

FIGURE 2 | Construction of a nomogram with clinical indices to predict ARDS-related survival (based on the training set). The score for each value is assigned by drawing a line upward to the points line, and the sum of the seven scores is plotted on the Total points line. ARDS, acute respiratory distress syndrome.

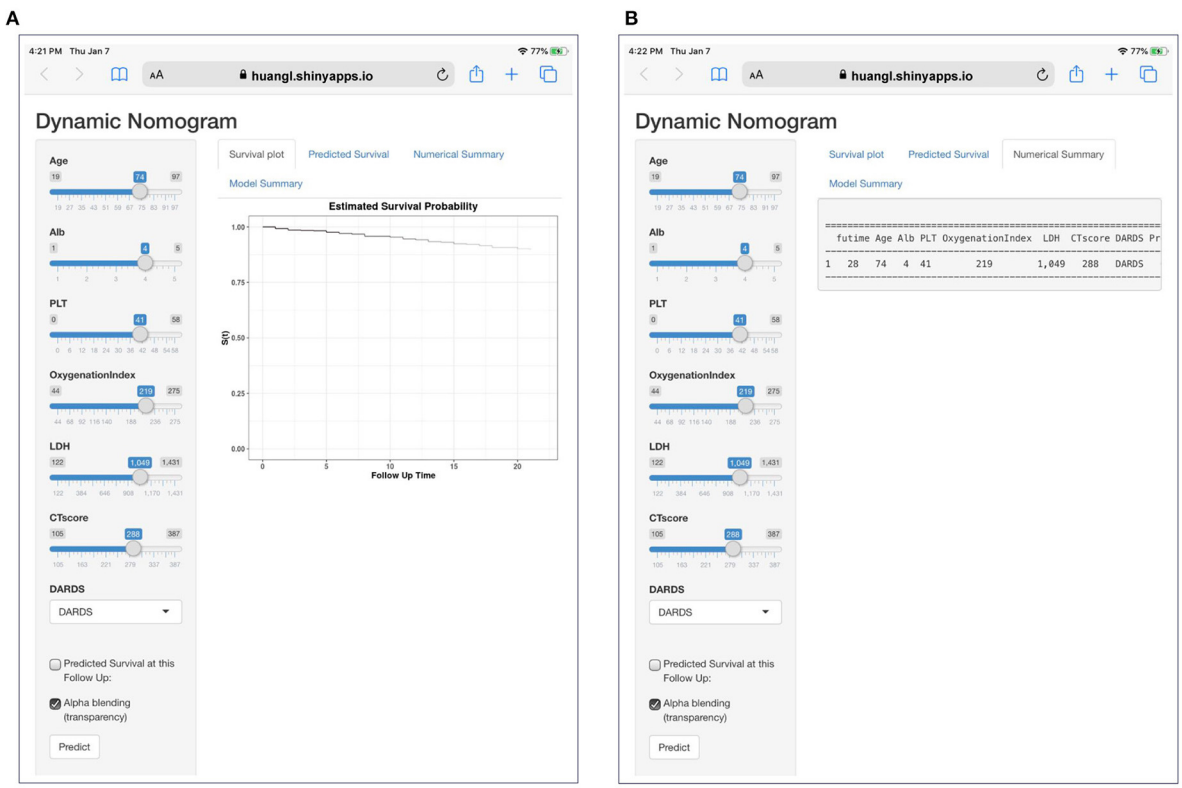

FIGURE 3 | A dynamic web-based calculator to predict ARDS-related survival (https://huangl.shinyapps.io/ARDSprognosis/). **(A)** Web survival rate calculator. **(B)** 95% confidence interval of the web survival rate calculator.

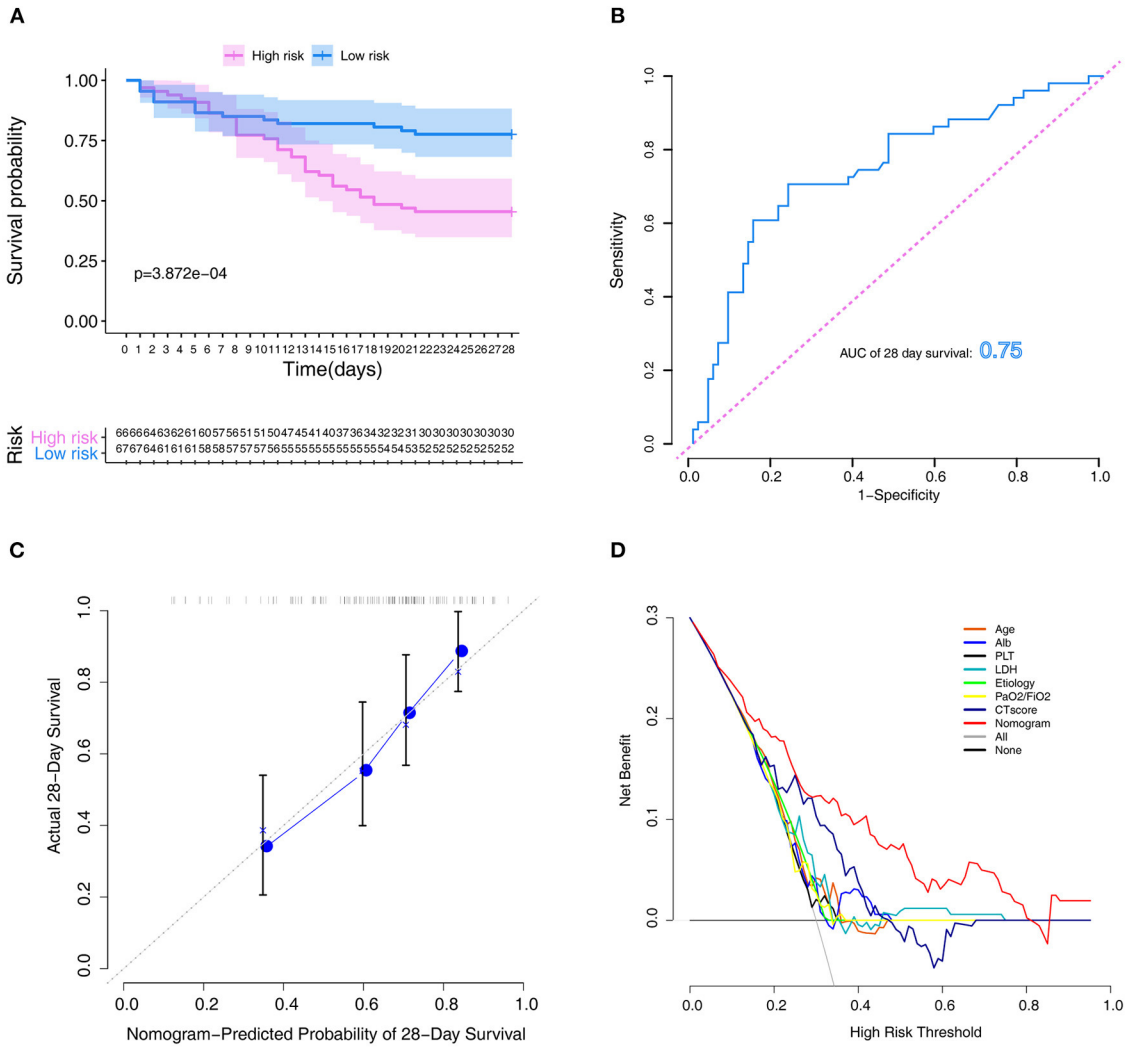

FIGURE 4 | Assessment of the model in the training set. **(A)** Kaplan–Meier survival analysis between the high- and low-risk groups. **(B)** ROC curves of predictive models at 28 days. **(C)** Calibration plot for the training set that show the predicted and observed (with 95% confidence intervals) overall survival rates at 28 days. Model performance is shown by the plot, relative to the 45-degree line, which represents perfect prediction. **(D)** Decision curve of the model. The gray line represents the treat-all-patients scheme. The dotted line represents the treat-none scheme. The red line represents prediction nomogram scheme in training dataset. The X axis represents threshold probability. The Y axis represents net benefit. ROC, receiver operator characteristic.

LDH, HRCT, and etiology were incorporated into the nomogram (**Figure 2**). To facilitate the clinical application of our findings, we developed a web-based calculator (https://huangl.shinyapps.io/ARDSprognosis/) to predict prognosis of ARDS patients according to the nomogram (**Figures 3A,B**). The estimated 28-day survival probabilities could be obtained by drawing a perpendicular line from the total point axis to the outcome axis.

Performance of the Model

The Kaplan–Meier survival curves revealed significantly poor overall survival in the high-risk group (p = 3.872e-04; **Figure 4A**). Thereafter, we performed ROC analysis to assess the discriminability of the model. The area under the ROC curve (AUC) indicative of the 28-day survival prediction was 0.75 (**Figure 4B**), which implied an efficacious performance of the model to predict prognosis. The calibration plots based on the training set showed that the model could accurately predict the 28-day survival (**Figure 4C**). The results of DCA also exhibited that the model could help clinicians to obtain maximum benefit when making clinical decisions (**Figure 4D**).

To further study the predictive value of each parameter included in the model, we performed ROC analysis for each of them (**Figures 5A–G**). The AUC values of all parameters were lower than that of the complete nomogram model. These results demonstrated that the model had superior predictive performance and clinical value than any single factor.

Performance Validation of the Model

To verify the reliability of the constructed novel model, risk-scores were calculated in the validation set with the same formula

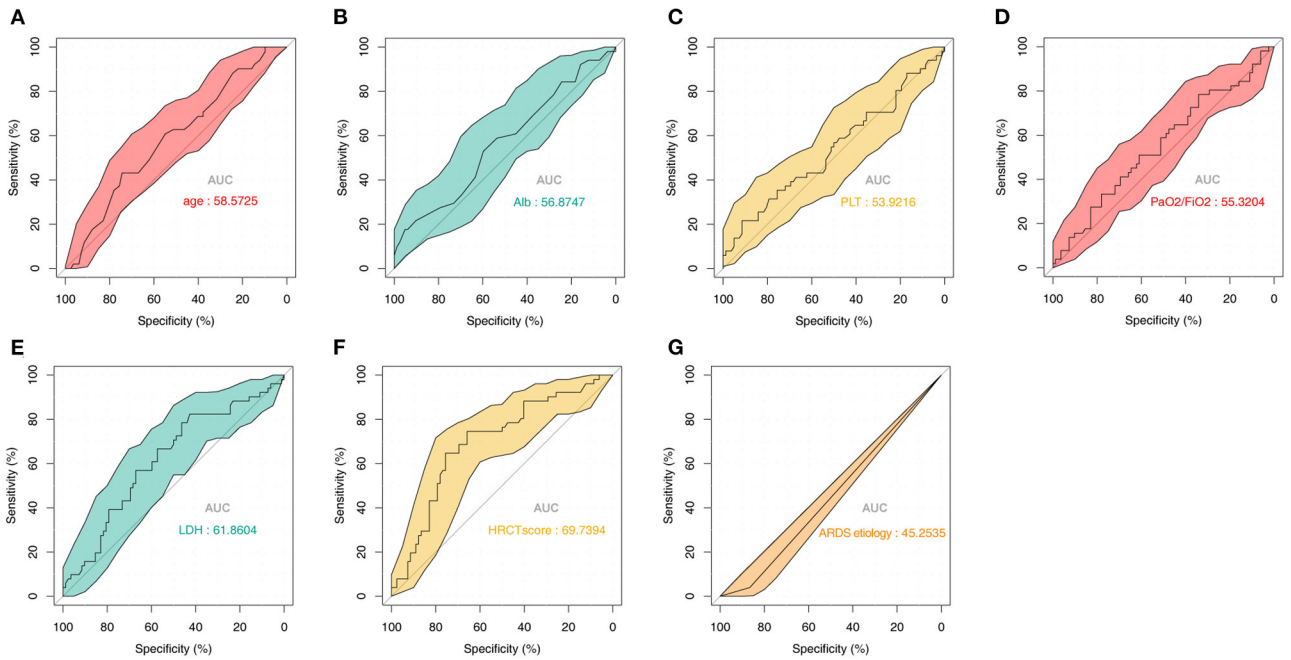

FIGURE 5 | Predictive value of the seven parameters included in the model from the training set. ROC analysis of **(A)** Age, **(B)** Alb, **(C)** PLT, **(D)** PaO_2/FiO_2, **(E)** LDH, **(F)** HRCT score, and **(G)** ARDS etiology. ROC, receiver operator characteristic; Alb, albumin; PLT, platelet; LDH, lactate dehydrogenase; HRCT, high-resolution computed tomography; ARDS, acute respiratory distress syndrome.

that was used for calculating the risk-scores of patients in the training set. In the validation set, the distribution of risk-scores and the survival status (**Figures 6A,B**) had a trend similar to that in the training set between high- and low-risk groups. Also, survival analysis indicated that low-risk patients had significantly favor prognosis than high-risk patients (**Figure 6C**). ROC curves were used to assess the prognostic value of the risk-scores; the analysis results suggested that risk-scores could accurately predict the survival rate in patients (AUC = 0.776, **Figure 6D**). The calibration plot in the validation set also showed that the model could accurately predict the 28-day survival (**Figure 6E**).

DISCUSSION

ARDS, one of the main critical diseases encountered in intensive care units, is a clinically and pathophysiologically complex syndrome of acute lung inflammation. Despite substantial progress in respiratory support strategies for critically ill patients, including the incorporation of a small tidal volume (21), high positive end-expiratory pressure (22), prone position ventilation (23), lung recruitment (24), use of neuromuscular blockers (25), high-frequency oscillatory ventilation (26, 27), and extracorporeal membrane oxygenation (28, 29), the mortality rate among patients with ARDS remains unacceptably high (30). However, to our knowledge, no study has previously developed a nomogram to predict the prognosis of patients with ARDS.

Herein, we first developed a nomogram using simple and easily available variables to evaluate the 28-day survival probabilities of ARDS patients whose information were extracted from an online database. Thereafter, we tested the performance of the nomogram in training and validation cohorts. Seven risk factors were identified in this model: age, Alb, PLT, PaO_2/FiO_2, LDH, CT score, and ARDS etiologies. Additionally, our results showed that PaO_2/FiO_2, and CT score could, albeit less accurately, predict the survival probability of ARDS patients compared to our novel model. These results suggest that the nomogram could be used as a cost-effective tool to predict the prognosis of ARDS and assist with clinical decision-making.

In 2012, the Berlin ARDS Society defined the severity of ARDS according to the oxygenation index (5). The oxygenation index (PaO_2/FiO_2) was helpful to categorize ARDS patients with different severity, and the mortality was reported to be higher in more severe stages of ARDS (mild, moderate, or severe) (5, 31). However, these severity categories have a low-to-moderate prognostic value to predict respiratory failure (32). Kamo and colleagues (33) reported that the severity stratification of the Berlin ARDS criteria may have a low capacity to differentiate between mild and moderate ARDS. In this study, the results of ROC curve analysis also indicated that the oxygenation index had low prognostic power (AUC, 55.3204%), which was consistent with previous studies.

CT or other lung imaging techniques have been used as diagnostic tools to optimize lung assessment and ventilator management in patients with ARDS; however, it is still controversial whether CT findings can predict ARDS outcomes (34–36). HRCT scores have been reported to correlate with the pathological stage of diffuse alveolar damage (37). Ichikado

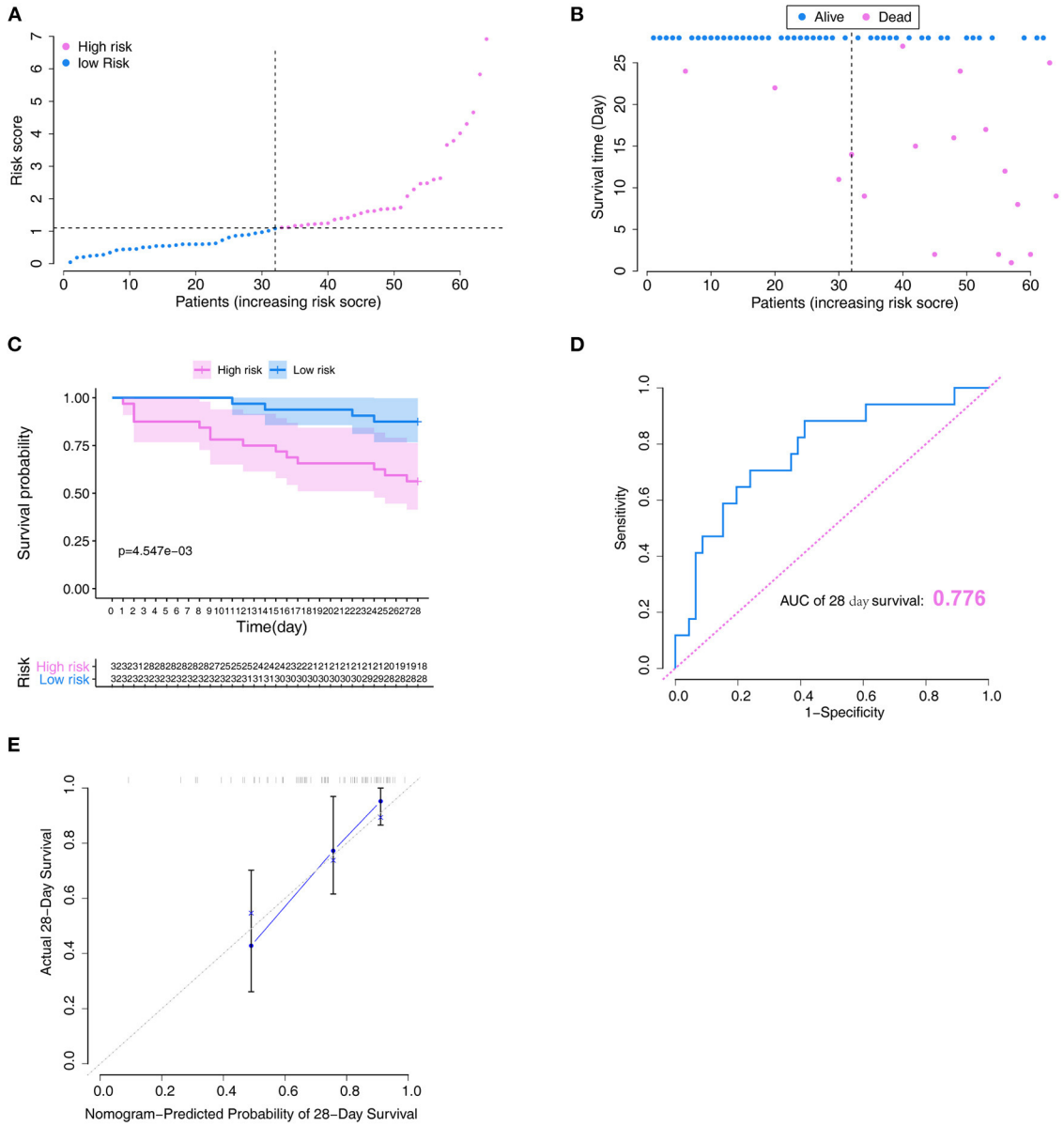

FIGURE 6 | Verification of the model in the validation set. **(A)** Distribution of the risk score. **(B)** Relationships between survival status and survival times of ARDS patients ranked by risk score. The black dotted line represents the optimum cut-off point dividing patients into low- and high-risk groups. **(C)** Kaplan–Meier survival analysis between high- and low-risk groups. **(D)** ROC curves of predictive models at 28 days. **(E)** Calibration plot for the training set that show the predicted and observed (with 95% confidence intervals) overall survival rates at 28 days. Model performance is shown by the plot, relative to the 45-degree line, which represents perfect prediction. ROC, receiver operator characteristic.

and colleagues (38) noted that HRCT score was one of the independent predictors of death and ventilator dependency in ARDS patients. Simultaneously, HRCT score was also found to be associated with multiorgan failure and ventilator-associated complications (38). In the present study, to increase model accuracy, HRCT score was incorporated into the nomogram. To evaluate the performance of HRCT score as a prognostic biomarker for the survival of ARDS patients, we performed ROC analysis. Our results showed that the model fit was significantly better than that of the one-factor HRCT model.

APACHE II score can be used as indicators to evaluate the prognosis among critically ill patients; it has been used worldwide to measure ICU performance (39). As APACHE II score included age and other factors in the calculation process, and repeated operations would be generated if the model was built again, APACHE II was not included in the LASSO regression analysis. The APACHE II score is calculated based on acute physiological

parameters and chronic health conditions, all of which have significant effects on the predictive prognosis of ICU patients (40). Hwang and colleagues (41) revealed that APACHE II score was a mortality predictor for ARDS patients, but that the accuracy was not high. Lesur and colleagues (42) reported that APACHE II score may be less predictive value when applied for ARDS patients, and that in those patients, it might be less accurate than other indicators, such as age. In the present study, it was also found that the prediction accuracy of this model was better than APACHE II score when compared to the results of precious study (AUC = 0.623) (41).

Certain drugs have also been reported to have the potential to cause ARDS. It has been proved that molecular targeted therapy, such as methotrexate and certain herbal medicines, can cause severe respiratory failure or ARDS (43–45). However, only few studies have focused on the prognostic role of different etiologies of ARDS. In the present study, our results indicated that there is a lower risk of death if ARDS is caused by drugs. However, these discrepancies may be partly related to differences in the dose and duration of drug treatments.

Our study has some limitations. Firstly, the model was developed mainly based on the seven variables. As these factors were unstable throughout the whole follow-up period, which may partly influence the precision of the model. Secondly, only 197 patients were included in this study; further studies with bigger sample sizes are needed. Thirdly, the lack of external validation may limit the extrapolation of the nomogram.

To summarize, we identified eight variables and developed a novel model to predict prognosis in patients with ARDS. These results may help to further improve clinical decision-making and individualized treatment of ARDS patients. Also, this model could distinguish patients with high-risk of ARDS, and further help to perform a careful follow-up among those patients.

DATA AVAILABILITY STATEMENT

The raw data supporting the conclusions of this article will be made available by the authors, without undue reservation.

ETHICS STATEMENT

Ethical review and approval was not required for the study on human participants in accordance with the local legislation and institutional requirements. Written informed consent for participation was not required for this study in accordance with the national legislation and the institutional requirements.

AUTHOR CONTRIBUTIONS

YL and LH designed the study. YL and JL performed the data analysis statistical analysis. YL prepared the manuscript. LH contributed funding for the project. All authors read and approved the final manuscript.

FUNDING

This study was supported by Key R & D Program of Jiangxi Province (No. 20202BBG73011).

ACKNOWLEDGMENTS

We thank the Anan et al. for-data collection and sharing.

REFERENCES

1. Urner M, Jüni P, Hansen B, Wettstein MS, Ferguson ND, Fan E. Time-varying intensity of mechanical ventilation and mortality in patients with acute respiratory failure: a registry-based, prospective cohort study. *Lancet Respir Med.* (2020) 8:905–13. doi: 10.1016/S2213-2600(20)30325-8
2. Suresh R, Kupfer Y, Tessler S. Acute respiratory distress syndrome. *N Engl J Med.* (2000) 343:660–1. doi: 10.1056/NEJM200008313430914
3. Ware LB, Matthay MA. The acute respiratory distress syndrome. *N Engl J Med.* (2000) 342:1334–49. doi: 10.1056/NEJM200005043421806
4. Kim JS, Kim YJ, Kim M, Ryoo SM, Sohn CH, Ahn S, et al. Impact of lung compliance on neurological outcome in patients with acute respiratory distress syndrome following out-of-hospital cardiac arrest. *J Clin Med.* (2020) 9:527. doi: 10.3390/jcm9020527
5. Ranieri VM, Rubenfeld GD, Thompson BT, Ferguson ND, Caldwell E, Fan E, et al. Acute respiratory distress syndrome: the Berlin Definition. *JAMA.* (2012) 307:2526–33. doi: 10.1001/jama.2012.5669
6. Terpstra ML, Aman J, van Nieuw Amerongen GP, Groeneveld AB. Plasma biomarkers for acute respiratory distress syndrome: a systematic review and meta-analysis*. *Crit Care Med.* (2014) 42:691–700. doi: 10.1097/01.ccm.0000435669.60811.24
7. Yehya N, Thomas NJ, Meyer NJ, Christie JD, Berg RA, Margulies SS. Circulating markers of endothelial and alveolar epithelial dysfunction are associated with mortality in pediatric acute respiratory distress syndrome. *Intensive Care Med.* (2016) 42:1137–45. doi: 10.1007/s00134-016-4352-1
8. Levitt JE, Gould MK, Ware LB, Matthay MA. The pathogenetic and prognostic value of biologic markers in acute lung injury. *J Intensive Care Med.* (2009) 24:151–67. doi: 10.1177/0885066609332603
9. Jones TK, Feng R, Kerchberger VE, Reilly JP, Anderson BJ, Shashaty MGS, et al. Plasma sRAGE acts as a genetically regulated causal intermediate in sepsis-associated acute respiratory distress syndrome. *Am J Respir Crit Care Med.* (2020) 201:47–56. doi: 10.1164/rccm.201810-2033OC
10. Graesslin O, Abdulkarim BS, Coutant C, Huguet F, Gabos Z, Hsu L, et al. Nomogram to predict subsequent brain metastasis in patients with metastatic breast cancer. *J Clin Oncol.* (2010) 28:2032–7. doi: 10.1200/JCO.2009.24.6314
11. Wang J, He L, Tang Y, Li D, Yang Y, Zeng Z. Development and validation of a nomogram with an epigenetic signature for predicting survival in patients with lung adenocarcinoma. *Aging.* (2020) 12:23200–16. doi: 10.18632/aging.104090
12. Anan K, Ichikado K, Kawamura K, Johkoh T, Fujimoto K, Suga M. Clinical characteristics and prognosis of drug-associated acute respiratory distress syndrome compared with non-drug-associated acute respiratory distress syndrome: a single-centre retrospective study in Japan. *BMJ Open.* (2017) 7:e015330. doi: 10.1136/bmjopen-2016-015330
13. Friedman J, Hastie T, Tibshirani R. Regularization paths for generalized linear models via coordinate descent. *J Stat Softw.* (2010) 33:1–22. doi: 10.18637/jss.v033.i01
14. Simon N, Friedman J, Hastie T, Tibshirani R. Regularization paths for cox's proportional hazards model via coordinate descent. *J Stat Softw.* (2011) 39:1–13. doi: 10.18637/jss.v039.i05

15. Frank E Harrell Jr. *RMS: Regression Modeling Strategies. R Package Version 6.0-1*. (2020).
16. Therneau T. *A Package for Survival Analysis in R. R Package Version 3.1-12*. (2020).
17. R Core Team. *Foreign: Read Data Stored by 'Minitab', 'S','SAS', 'SPSS', 'Stata', 'Systat', 'Weka', 'dBase', R Package Version 0.8-76*. R Core Team (2020).
18. Schauberger P, Walker A. *Openxlsx: Read, Write and Edit xlsx Files. R Package Version 4.1.5*. (2020).
19. Jalali A, Roshan D, Alvarez-Iglesias A, Newell J. *DynNom: Visualising Statistical Models Using Dynamic Nomograms. R Package Version 5.0.1*. (2019). doi: 10.1371/journal.pone.0225253
20. Kamarudin AN, Cox T, Kolamunnage-Dona R. Time-dependent ROC curve analysis inmedical research: current methods and applications. *BMC Med Res Methodol.* (2017) 17:53. doi: 10.1186/s12874-017-0332-6
21. Brower RG, Matthay MA, Morris A, Schoenfeld D, Thompson BT, Wheeler A. Ventilation with lower tidal volumes as compared with traditional tidal volumes for acute lung injury and the acute respiratory distress syndrome. *N Engl J Med.* (2000) 342:1301–8. doi: 10.1056/NEJM200005043421801
22. Brower RG, Lanken PN, MacIntyre N, Matthay MA, Morris A, Ancukiewicz M, et al. Higher versus lower positive end-expiratory pressures in patients with the acute respiratory distress syndrome. *N Engl J Med.* (2004) 351:327–36. doi: 10.1056/NEJMoa032193
23. Guérin C, Reignier J, Richard JC, Beuret P, Gacouin A, Boulain T, et al. Prone positioning in severe acute respiratory distress syndrome. *N Engl J Med.* (2013) 368:2159–68. doi: 10.1056/NEJMoa1214103
24. Meade MO, Cook DJ, Guyatt GH, Slutsky AS, Arabi YM, Cooper DJ, et al. Ventilation strategy using low tidal volumes, recruitment maneuvers, and high positive end-expiratory pressure for acute lung injury and acute respiratory distress syndrome: a randomized controlled trial. *JAMA.* (2008) 299:637–45. doi: 10.1001/jama.299.6.637
25. Papazian L, Forel JM, Gacouin A, Penot-Ragon C, Perrin G, Loundou A, et al. Neuromuscular blockers in early acute respiratory distress syndrome. *N Engl J Med.* (2010) 363:1107–16. doi: 10.1056/NEJMoa1005372
26. Young NH, Andrews PJ. High-frequency oscillation as a rescue strategy for brain-injured adult patients with acute lung injury and acute respiratory distress syndrome. *Neurocrit Care.* (2011) 15:623–33. doi: 10.1007/s12028-011-9550-7
27. Ferguson ND, Cook DJ, Guyatt GH, Mehta S, Hand L, Austin P, et al. High-frequency oscillation in early acute respiratory distress syndrome. *N Engl J Med.* (2013) 368:795–805. doi: 10.1056/NEJMoa1215554
28. Zampieri FG, Mendes PV, Ranzani OT, Taniguchi LU, Pontes Azevedo LC, Vieira Costa EL, et al. Extracorporeal membrane oxygenation for severe respiratory failure in adult patients: a systematic review and meta-analysis of current evidence. *J Crit Care.* (2013) 28:998–1005. doi: 10.1016/j.jcrc.2013.07.047
29. Peek GJ, Clemens F, Elbourne D, Firmin R, Hardy P, Hibbert C, et al. CESAR: conventional ventilatory support vs extracorporeal membrane oxygenation for severe adult respiratory failure. *BMC Health Serv Res.* (2006) 6:163. doi: 10.1186/1472-6963-6-163
30. Chen X, Wu S, Tang L, Ma L, Wang F, Feng H, et al. Mesenchymal stem cells overexpressing heme oxygenase-1 ameliorate lipopolysaccharide-induced acute lung injury in rats. *J Cell Physiol.* (2019) 234:7301–19. doi: 10.1002/jcp.27488
31. Ferguson ND, Fan E, Camporota L, Antonelli M, Anzueto A, Beale R, et al. The Berlin definition of ARDS: an expanded rationale, justification, and supplementary material. *Intensive Care Med.* (2012) 38:1573–82. doi: 10.1007/s00134-012-2682-1
32. Hernu R, Wallet F, Thiollière F, Martin O, Richard JC, Schmitt Z, et al. An attempt to validate the modification of the American-European consensus definition of acute lung injury/acute respiratory distress syndrome by the Berlin definition in a University hospital. *Intensive Care Med.* (2013) 39:2161–70. doi: 10.1007/s00134-013-3122-6
33. Kamo T, Tasaka S, Suzuki T, Asakura T, Suzuki S, Yagi K, et al. Prognostic values of the Berlin definition criteria, blood lactate level, and fibroproliferative changes on high-resolution computed tomography in ARDS patients. *BMC Pulm Med.* (2019) 19:37. doi: 10.1186/s12890-019-0803-0
34. Chiumello D, Taccone P, Berto V, Marino A, Migliara G, Lazzerini M, et al. Long-term outcomes in survivors of acute respiratory distress syndrome ventilated in supine or prone position. *Intensive Care Med.* (2012) 38:221–9. doi: 10.1007/s00134-011-2445-4
35. Chung JH, Kradin RL, Greene RE, Shepard JA, Digumarthy SR. CT predictors of mortality in pathology confirmed ARDS. *Eur Radiol.* (2011) 21:730–7. doi: 10.1007/s00330-010-1979-0
36. Chiumello D, Froio S, Bouhemad B, Camporota L, Coppola S. Clinical review: lung imaging in acute respiratory distress syndrome patients—an update. *Crit Care.* (2013) 17:243. doi: 10.1186/cc13114
37. Anan K, Kawamura K, Suga M, Ichikado K. Clinical differences between pulmonary and extrapulmonary acute respiratory distress syndrome: a retrospective cohort study of prospectively collected data in Japan. *J Thorac Dis.* (2018) 10:5796–803. doi: 10.21037/jtd.2018.09.73
38. Ichikado K, Muranaka H, Gushima Y, Kotani T, Nader HM, Fujimoto K, et al. Fibroproliferative changes on high-resolution CT in the acute respiratory distress syndrome predict mortality and ventilator dependency: a prospective observational cohort study. *BMJ Open.* (2012) 2:e000545. doi: 10.1136/bmjopen-2011-000545
39. Giamarellos-Bourboulis EJ, Norrby-Teglund A, Mylona V, Savva A, Tsangaris I, Dimopoulou I, et al. Risk assessment in sepsis: a new prognostication rule by APACHE II score and serum soluble urokinase plasminogen activator receptor. *Crit Care.* (2012) 16:R149. doi: 10.1186/cc11463
40. Hsu YT, He YT, Ting CK, Tsou MY, Tang GJ, Pu C. Administrative and claims data help predict patient mortality in intensive care units by logistic regression: a nationwide database study. *Biomed Res Int.* (2020) 2020:9076739. doi: 10.1155/2020/9076739
41. Hwang H, Choi SM, Lee J, Park YS, Lee CH, Yoo CG, et al. Validation of age, PaO(2)/FlO(2) and plateau pressure score in Korean patients with acute respiratory distress syndrome: a retrospective cohort study. *Respir Res.* (2020) 21:94. doi: 10.1186/s12931-020-01357-5
42. Lesur O, Langevin S, Berthiaume Y, Légaré M, Skrobik Y, Bellemare JF, et al. Outcome value of Clara cell protein in serum of patients with acute respiratory distress syndrome. *Intensive Care Med.* (2006) 32:1167–74. doi: 10.1007/s00134-006-0235-1
43. Wolkove N, Baltzan M. Amiodarone pulmonary toxicity. *Can Respir J.* (2009) 16:43–8. doi: 10.1155/2009/282540
44. Imokawa S, Colby TV, Leslie KO, Helmers RA. Methotrexate pneumonitis: review of the literature and histopathological findings in nine patients. *Eur Respir J.* (2000) 15:373–81. doi: 10.1034/j.1399-3003.2000.15b25.x
45. Enomoto YM, Nakamura YMP, Enomoto NMP, Fujisawa TMP, Inui NMP and Suda T. Japanese herbal medicine-induced pneumonitis: a review of 73 patients. *Respir Investig.* (2017) 55:138–44. doi: 10.1016/j.resinv.2016.11.007

Conflict of Interest: The authors declare that the research was conducted in the absence of any commercial or financial relationships that could be construed as a potential conflict of interest.

Copyright © 2021 Liu, Liu and Huang. This is an open-access article distributed under the terms of the Creative Commons Attribution License (CC BY). The use, distribution or reproduction in other forums is permitted, provided the original author(s) and the copyright owner(s) are credited and that the original publication in this journal is cited, in accordance with accepted academic practice. No use, distribution or reproduction is permitted which does not comply with these terms.

frontiers in Medicine

ORIGINAL RESEARCH
published: 01 March 2021
doi: 10.3389/fmed.2021.621592

A Low Albumin-to-Globulin Ratio Predicts a Poor Prognosis in Patients With Metastatic Non-small-cell Lung Cancer

Ping Lu[1], *Yifei Ma*[2], *Shaozhong Wei*[2*†] *and Xinjun Liang*[1*†]

[1] Department of Medical Oncology, Hubei Cancer Hospital, The Seventh Clinical School Affiliated of Tongji Medical College, Huazhong University of Science and Technology, Wuhan, China, [2] Department of Gastrointestinal Oncology Surgery, Hubei Cancer Hospital, The Seventh Clinical School Affiliated With Tongji Medical College, Huazhong University of Science and Technology, Wuhan, China

OPEN ACCESS

Edited by:
Mahmood Yaseen Hachim,
Mohammed Bin Rashid University of Medicine and Health Sciences, United Arab Emirates

Reviewed by:
Maha Guimei,
Alexandria University, Egypt
Ritu Lakhtakia,
Mohammed Bin Rashid University of Medicine and Health Sciences, United Arab Emirates

***Correspondence:**
Xinjun Liang
doctorlxj@163.com
Shaozhong Wei
weishaozhong@163.com

† These authors have contributed equally to this work and share senior authorship

Specialty section:
This article was submitted to Pulmonary Medicine, a section of the journal Frontiers in Medicine

Received: 26 October 2020
Accepted: 08 February 2021
Published: 01 March 2021

Citation:
Lu P, Ma Y, Wei S and Liang X (2021) A Low Albumin-to-Globulin Ratio Predicts a Poor Prognosis in Patients With Metastatic Non-small-cell Lung Cancer. Front. Med. 8:621592. doi: 10.3389/fmed.2021.621592

Objective: The serum albumin-to-globulin ratio (AGR) may be a useful prognostic factor for various cancers. This study aimed to evaluate the prognostic value of the AGR in patients with metastatic non-small-cell lung cancer (NSCLC).

Methods: A retrospective study was conducted on patients with stage IV NSCLC diagnosed in Hubei Cancer Hospital from July 2012 to December 2013. The formula for calculating the AGR was serum albumin/total protein-serum albumin. The chi-square test or Fisher's exact test was used to analyze the classified variables. The Kaplan-Meier method was used to analyze the overall survival (OS) rate, which was plotted with the R language. The impact of the AGR on OS and progression-free survival (PFS) was analyzed by a multivariate Cox proportional hazard model.

Results: A total of 308 patients were included in the study population. The optimal cutoff values for the AGR in terms of OS and PFS were 1.12 and 1.09, respectively, as determined by X-Tile software. Kaplan-Meier curve analysis showed that the difference in survival rate between patients with different AGR levels was statistically significant ($p = 0.04$). The OS of patients with a high AGR ($\geq$1.12) was longer than that of patients with a low AGR (<1.12). PFS in the high AGR group were better than those in the low AGR group (16.90 vs. 32.07months, $p = 0.008$). The univariate and multivariate models proved that the AGR was an independent prognostic factor in metastatic NSCLC patients in terms of both OS ($p = 0.009$, hazard ratio [HR] = 0.55, 95% confidence interval [95% CI] = 0.35–0.86) and PFS ($p = 0.004$, HR = 0.55, 95% CI = 0.37–0.83).

Conclusion: The AGR, which is measured in routine clinical practice, is an independent prognostic factor in terms of OS and PFS in metastatic NSCLC and can serve as a prognostic tool for metastatic NSCLC.

Keywords: serum albumin, albumin to globulin ratio, prognosis, metastatic non-small-cell lung cancer, overall survival, progression-free survival

INTRODUCTION

As a result of early screening and treatment, as well as the aging of the population, the ratio of cancer survivors to cancer cases continues to increase (1). Over the past few decades, the overall incidence of cancer among women has been basically stable. It is estimated that there will be 1,762,450 new cancer cases and 606,880 cancer-related deaths in the United States in 2019. The incidence of lung cancer has continuously declined, and the incidence of lung cancer in men is declining twice as fast as that in women (2). Data from 2008 to 2014 indicate that among all cancers, pancreatic cancer (9%), esophageal cancer (19%), liver cancer (18%) and lung cancer (19%) have the lowest 5-year relative survival rates (2).

Although a variety of markers have been shown to predict the prognosis of cancer patients, the value of these markers in clinical practice is limited because they require invasive detection methods and/or are difficult to assess before treatment. The prognostic assessment of patients is crucial for the selection of better treatment strategies. In view of this, it is necessary to find prognostic indicators that are affordable, convenient and highly clinically feasible to predict and distinguish the prognosis of tumor patients according to their clinical characteristics (3).

Albumin and globulin have attracted wide attention as non-invasive prognostic factors of tumors. Albumin can be used to reflect the nutritional and systemic inflammatory status of cancer patients and can be used as a prognostic marker for diverse cancers, such as lung cancer (4), lymphoma (5), renal cell carcinoma (6), breast cancer (7, 8) and gastrointestinal cancers (9). Globulin, as one of the main cortisol-binding proteins, can participate in immune and inflammatory responses (10). Furthermore, the albumin-to-globulin ratio (AGR) has been widely recognized as a prognostic indicator of various cancers. Therefore, we retrospectively studied the clinical significance of the AGR in predicting the overall survival (OS) and progression-free survival (PFS) of patients with stage IV non-small-cell lung cancer (NSCLC).

METHODS

Study Design

After approval by the Hubei Provincial Ethics Committee, this study retrospectively analyzed patients with stage IV lung cancer who were pathologically diagnosed in our hospital from June 2012 to December 2013. Fluorodeoxyglucose (FDG) PET/CT, contrast-enhanced MRI, contrast-enhanced CT and exfoliative cytology were used to identify the tumor stage according to the eighth edition of the TNM staging standard for non-small cell lung cancer. A total of 399 patients who met the inclusion requirements were initially identified. After applying the exclusion criteria, 91 patients were excluded. Patients with obvious infection within 2 weeks ($n = 3$); patients with other chronic infectious diseases, including tuberculosis ($n = 25$), chronic obstructive pulmonary disease ($n = 23$), chronic liver disease and/or severe liver insufficiency ($n = 21$), patients with chronic kidney disease and/or severe renal insufficiency ($n = 11$), autoimmune diseases ($n = 2$); and patients with other primary malignant tumors ($n = 6$) were excluded.

Demographic and Clinical Variables

The clinicopathological data of patients, including age, sex, smoking, and drinking status, tumor location, family history of cancer, histology, local or distant metastases distant metastatic sites. Patients with one or more metastatic sites in the contralateral lobe, malignant tumor nodules in the pericardium or pleura, and malignant pericardial effusion or pleural effusion are considered stage M1a. M1b is used to describe patients with a single extrathoracic metastasis of a single organ. M1c is used to describe patients with multiple extrathoracic metastatic lesions. Therapeutic data were collected through medical records. Treatment options include chemotherapy, radiotherapy, anti-VEGF-therapy and EGFR-TKI therapy. The chemotherapy regimen mainly includes platin-vinorelbine, platin-gemcitabine, platin-pemetrexed and others. Other relevant laboratory indicators, such as alkaline phosphatase (ALP), lactate dehydrogenase (LDH), triglycerides (TG), AGR, prognostic nutritional index (PNI), lymphocyte-to-mononuclear cell ratio (LMR), neutrophil-to-lymphocyte ratio (NLR) and platelet-to-lymphocyte ratio (PLR), were measured at baseline before treatment and recorded in the patient information system. The calculation formula for the AGR was serum albumin (g/l)/(total protein–serum albumin), and that for PNI was $10 \times$ serum albumin (g/dl) $+ 0.005 \times$ lymphocyte count (per mm^3).

Follow-Up

The follow-up period was from the time of diagnosis in Hubei Cancer Hospital to December 2013 or last contact. The average follow up duration is 39.53 months (38.70–40.37). During this period, the patient underwent routine reexamination, such as blood tests and imaging examinations.

Statistical Analysis

The optimal cutoff values of relevant laboratory indicators were determined through X-tile and converted into two categorical variables. The chi-square test and Fisher's exact test were used to analyze the relationship between categorical variables expressed as frequencies and percentages. The Kaplan-Meier method was used to analyze OS and PFS rates, and the R language was used to draw survival curves including 95% confidence intervals (95% CIs). Univariate and multivariate Cox regression models were used to analyze the hazard ratio (HR) and 95% CI. All tests were bilateral, and the differences were only considered statistically significant when $P < 0.05$. Statistical analysis was performed using SPSS Statistics 25.0 software.

RESULTS

Patient Characteristics

The clinical and demographic characteristics of the patients pathologically diagnosed with stage IV NSCLC are summarized in **Table 1**. The majority of them ($n = 216$) were younger than 65 years old. Overall, 64.0% ($n = 197$) of the patients were male, while 36% ($n = 111$) were female. Of the 308 patients, 159

TABLE 1 | Clinical parameters in 308 patients with metastatic NSCLC.

Variable	*N* (%)	Variable	*N* (%) or Median [IQR]
Age		**Chemotherapy regimen**	
<65	216 (70.1)	Platin-Vinorelbine	100 (32.5)
≥65	92 (29.9)	Platin-Gemcitabine	147 (47.7)
Gender		Platin-Pemetrexed	111 (36.0)
Male	197 (64.0)	Others	68 (22.1)
Female	111 (36.0)	**Chemotherapy**	
Smoking Status		No chemotherapy	72 (23.4)
Never	159 (51.6)	First-line treatment	228 (74.0)
Current or ever	149(48.4)	Second-line treatment	8 (2.6)
Drinking Status		**EGFR-TKI**	
Never	232 (75.3)	No	222 (72.1)
Current or ever	76 (24.7)	Yes	86 (27.9)
Location		**AGR**	0.87 (0.77–1.00)
Left	188 (61.0)		
Right	120 (39.0)		
family history of cancer		**ALP**	75.6 (63.7–98.0)
No	244 (79.2)		
Yes	64 (20.8)		
Histology		**LDH**	199.6 (167.9–256.7)
Adenocarcinoma	186 (60.4)		
Squamous cell carcinomas	74 (24.0)		
Others	48 (15.6)		
Local or distant metastases		**TG**	1.17 (0.91–1.62)
M1a	76 (24.7)		
M1b	65 (21.1)		
M1c	167 (54.2)		
Distant metastatic site		**PNI**	48.2 (43.2–52.5)
Lung contralateral	121 (39.3)		
Pleural	106 (34.4)		
Cerebral	82 (26.6)	**LMR**	2.55 (1.92–3.63)
Bones	125 (40.6)		
Adrenal	15 (4.9)		
Liver	32 (10.4)	**PLR**	156.1 (115.6–198.5)
Others	28 (9.1)		
Radiotherapy		**NLR**	3.12 (2.12–4.47)
No	199 (64.6)		
Yes	109 (35.4)		
Anti-VEGF-therapy			
No	290 (94.2)		
Yes	18 (5.8)		

(51.6%) and 149 (48.4%) were never and current/ever smokers, respectively; 60.4% (n = 186) of patients were pathologically diagnosed with lung adenocarcinoma. 76 patients were M1a (24.7%), 65 patients were M1b (21.1%), 167 patients were M1c (54.2%). Treatment options include chemotherapy (n = 236, 76.6%), radiotherapy (n = 109, 35.4%), anti-VEGF-therapy (n = 18, 5.8%) and EGFR-TKI therapy (n = 86, 27.9%). The chemotherapy regimen mainly includes platin-vinorelbine (n = 100, 32.5%), platin-gemcitabine (n = 147, 47.7%), platin-pemetrexed (n = 111, 36.0%) and others (n = 68, 22.1%). Some of these patients received more than one chemotherapy regimen. 228 patients received chemotherapy as first-line treatment. The median number of first-line chemotherapy cycles was 4 [interquartile range (IQR): [2, 5] (not shown in the table)]. The median AGR was 0.87 (IQR: [0.77, 1.00]), and the median ALP was 75.6 (IQR: [63.7, 98.0]).

Cutoff Values for the Parameters

The median of the AGR is 0.87 (0.77–1.00). For OS analysis, X-tile determined the significant cutoff value of the AGR to be 1.12. Then, the patients were divided into two groups (AGR < 1.12, AGR ≥ 1.12). Through this method, the optimal cutoff values for ALP, LDH, TG, PNI, LMR, NLR and PLR for OS analysis were determined, as shown in **Table 2**. We compared the AGR values based on clinical and demographic characteristics such as age, sex, smoking and drinking status, tumor location, family history of cancer, histology, local or distant metastases, distant metastatic sites and therapy regimens. The AGR was only significantly related to gender. The AGR was significantly related to certain laboratory indicators (such as the ALP, PNI, LMR, PLR, and NLR). For the PFS analysis, the cutoff value of the AGR was set to 1.09, and patients were divided into low AGR and high AGR groups. Similarly, the cutoff values of ALP (70.3), LDH (179.8), TG (0.87), PNI (53.2), LMR (1.92), NLR (2.1), and PLR (145.6) were identified for the PFS analysis.

Univariate Survival Analysis and Survival Curve Analysis

In the univariate analysis, age, sex, smoking and drinking status, tumor location, family history of cancer and histology were not associated with OS or PFS (**Table 3**). Local or distant metastases and some distant metastasis sites are related to prognosis. Compared with M1a category disease, patients with M1b category had poorer OS (HR = 1.83, P = 0.01) and PFS (HR = 2.05, P = 0.001) (**Figure 1A**). Compared with M1a category, M1c category disease had poorer OS (HR = 2.20, P < 0.001) and PFS (HR = 2.76, P < 0.001) (**Figure 1B**). Cerebral metastasis was associated with poor OS (HR = 1.76, P<0.001) and PFS (HR = 1.91, P < 0.001) in univariate analysis. Bone metastasis was associated with poor OS (HR = 1.38, P = 0.03) and PFS (HR = 1.55, P = 0.001). Adrenal metastasis was only associated with poor PFS (HR = 1.69, P = 0.05). Patients who received chemotherapy as a first-line treatment seemed to have a longer OS (HR = 0.62, P = 0.04). However, specific chemotherapy regimens, epidermal-growth-factor receptor tyrosine-kinase inhibitors (EGFR-TKI) and anti-vascular endothelial growth factor (anti-VEGF) were not significantly associated with OS in patients with stage IV lung cancer (**Table 3**). EGFR-TKI was associated with PFS (HR = 1.37, P = 0.03) in univariate analysis. A low AGR was significantly

TABLE 2 | Statistical cutoff values for demographic and clinical variables.

Variable	AGR		X2	P
	AGR<1.12 N = 258 (%)	AGR≥1.12 N = 50 (%)		
Age			0.49	0.49
<65	183 (70.9)	33 (66.0)		
≥65	75 (29.1)	17 (34.0)		
Gender			3.75	0.05
Male	159 (61.6)	38 (76.0)		
Female	99 (38.4)	12 (24.0)		
Smoking Status			1.39	0.24
Never	137 (53.1)	22 (44)		
Current or ever	121 (46.9)	28 (56)		
Drinking Status			1.72	0.19
Never	198 (76.7)	34 (68)		
Current or ever	60 (23.3)	16 (32)		
Location			0.22	0.64
Left	156 (60.5)	32 (64.0)		
Right	102 (39.5)	18 (34.0)		
Family history of cancer			1.67	0.20
No	201 (77.9)	43 (86.0)		
Yes	57 (22.1)	7 (14.0)		
Histology			1.39	0.50
Adenocarcinoma	168 (65.1)	18 (36.0)		
Squamous cell carcinomas	54 (20.9)	20 (40.0)		
Others	36 (14.0)	12 (24.0)		
Local or distant metastases			0.91	0.64
M1a	65 (25.2)	11 (22.0)		
M1b	52 (20.2)	13 (26.0)		
M1c	141 (54.7)	26 (52.0)		
Distant metastatic site				
Lung contralateral	101 (39.1)	20 (40.0)	0.01	1.91
Pleural	91 (35.3)	15 (30.0)	0.51	0.47
Cerebral	69 (26.7)	13 (26.0)	0.01	1.91
Bones	108 (41.9)	17 (34.0)	0.07	0.30
Adrenal	13 (5.0)	2 (4.0)	0.10	0.76
Liver	29 (11.2)	3 (6.0)	1.24	0.27
Others	23 (8.9)	5 (10.0)	0.06	0.81
Radiotherapy			0.18	0.67
No	168 (65.1)	31 (62.0)		
Yes	90 (34.9)	19 (38.0)		
Chemotherapy			0.76	0.68
No chemotherapy	58 (22.5)	14 (28.0)		
First-line treatment	193 (74.8)	35 (70.0)		
Second-line treatment	7 (2.7)	1 (2.0)		
Chemotherapy regimen				
Platin-Vinorelbine	83 (32.2)	17 (34.0)	0.06	0.8
Platin-Gemcitabine	123 (47.7)	24 (48.0)	0.002	0.97
Platin-Pemetrexed	92 (35.7)	19 (38.0)	0.1	0.75
Others	59 (22.9)	9 (18.0)	0.58	0.45
Anti-VEGF-therapy			0.003	0.96
No	243 (94.2)	47 (94.0)		
Yes	15 (5.8)	3 (6.0)		
EGFR-TKI			2.92	0.08
No	181 (70.2)	41 (82.0)		
Yes	77 (29.8)	9 (18.0)		
ALP			4.12	0.04
<70.3	149 (41.6)	15 (36.6)		
≥70.3	209 (58.4)	26 (63.4)		
LDH			1.37	0.24
<269.6	281 (78.5)	28 (68.3)		
≥269.6	77 (21.5)	13 (31.7)		
TG			1.02	0.31
<1.05	117 (32.7)	17 (41.4)		
≥1.05	241 (67.3)	24 (58.6)		
PNI			13.31	<0.001
<51.2	275 (76.8)	41 (100)		
≥51.2	83 (23.2)	0 (0)		
LMR			6.04	0.01
<1.9	85 (23.7)	16 (39)		
≥1.9	273 (76.3)	25 (61)		
PLR			4.62	0.03
<122.5	110 (30.7)	5 (12.2)		
≥122.5	248 (69.3)	36 (87.8)		
NLR			7.32	0.007
<2.77	325 (90.8)	29 (70.7)		
≥2.77	33 (9.2)	12 (29.3)		

associated with poor OS and PFS (**Figure 2**). The difference in survival rate between patients with different AGR levels was statistically significant ($p = 0.04$). The OS of patients with a high AGR (≥1.12) was longer than that of patients with a low AGR (<1.12). The PFS of patients with a high AGR (≥1.09) was longer than that of patients with a low AGR (<1.09) (16.9 vs. 32.07 months, respectively). In addition, LDH ($P = 0.04$) has also been shown to be associated with the prognosis of patients. TG ($P = 0.03$), PNI ($P = 0.02$) and LMR ($P = 0.05$) were predictive of OS but not PFS (**Table 4**, **Figure 3**).

Multivariate Cox Regression Model

The influence of variables on OS and PFS was analyzed by a multivariate Cox proportional hazard model. Local or distant metastases, cerebral metastasis, bone metastasis, radiotherapy and chemotherapy, as well as laboratory indicators that were statistically significant in the univariate analysis model, were included in the multivariate Cox regression model (**Table 5**). Local or distant metastases (M1b, HR: 1.66; 95% CI: 1.00–2.75; $P = 0.05$. M1c, HR: 1.84; 95% CI: 1.10–3.08; $P = 0.02$),

TABLE 3 | Univariate survival analysis of baseline characteristics for OS and PFS.

Variable	OS		PFS		Variable	OS		PFS	
	HR	*P*	HR	*P*		HR	*P*	HR	*P*
Age					Adrenal				
< 65	1.00				No	1.00			
≥ 65	0.88	0.43	0.92	0.59	Yes	1.36	0.31	1.69	0.05
Gender					Liver				
Male	1.00				No	1.00			
Female	1.08	0.60	1.05	0.74	Yes	1.20	0.41	1.22	0.34
Smoking Status					Others				
Never	1.00				No	1.00			
Current or ever	0.84	0.25	0.97	0.80	Yes	0.83	0.49	0.70	1.17
Drinking Status					**Radiotherapy**				
Never	1.00				No	1.00			
Current or ever	0.97	0.86	1.19	0.26	Yes	1.36	0.04	1.48	0.005
Location					**Chemotherapy**				
Left	1.00				No chemotherapy	1.00			
Right	1.25	0.13	1.17	0.27	First-line treatment	0.62	0.04	0.82	0.22
Family history of cancer					Second-line treatment	1.28	0.54	1.78	0.13
No	1.00				**Anti-VEGF**				
Yes	0.93	0.69	1.00	0.98	No	1.00			
Histology					Yes	1.11	0.72	1.27	0.37
Adenocarcinoma	1.00				**EGFR-TKI**				
SCC	1.09	0.63	0.87	0.43	No	1.00			
Others	1.18	0.42	1.00	0.99	Yes	1.20	0.24	1.37	0.03
Local or distant metastases					**Chemotherapy regimen**				
M1a	1.00				Platin-Vinorelbine				
M1b	1.83	0.01	2.05	0.001	No	1.00			
M1c	2.20	<0.001	2.76	<0.001	Yes	0.74	0.07	0.92	0.58
Metastatic site					Platin-Gemcitabine				
Lung contralateral					No	1.00			
No	1.00				Yes	0.99	0.93	1.10	0.52
Yes	1.23	0.37	1.19	0.78	Platin-Pemetrexed				
Pleural					No	1.00			
No	1.00				Yes	0.95	0.76	1.06	0.69
Yes	1.31	0.07	1.21	0.17	Others				
Cerebral					No	1.00			
No	1.00				Yes	0.72	0.08	0.72	0.08
Yes	1.76	<0.001	1.91	<0.001					
Bones									
No	1.00								
Yes	1.38	0.03	1.55	0.001					

first-line chemotherapy treatment (HR: 0.60; 95% CI: 0.43–0.84; $P = 0.003$), AGR (HR: 0.55; 95% CI: 0.35–0.86; $P = 0.009$), TG (HR: 1.40; 95% CI: 1.02–1.94; $P = 0.04$) and PNI (HR: 0.56; 95% CI: 0.39–0.80; $P = 0.02$) were independent prognostic factors for OS. Furthermore, local or distant metastases (M1b, HR: 1.87; 95% CI: 1.18–2.97; $P = 0.08$. M1c, HR: 2.36; 95% CI: 1.50–3.71; $P < 0.001$), and the AGR was an independent prognostic factor for PFS (HR: 0.55; 95% CI: 0.37–0.83; $P = 0.004$).

DISCUSSION

Inflammation plays an important role in lung cancer and contributes to its occurrence and development (11–13). The AGR, which accounts for the values of both albumin and globulin, can be used as one of the inflammatory parameters to evaluate the systemic inflammatory status of the host (14). In addition to reflecting the nutritional status of the host, serum albumin can also be affected by inflammatory factors, which in

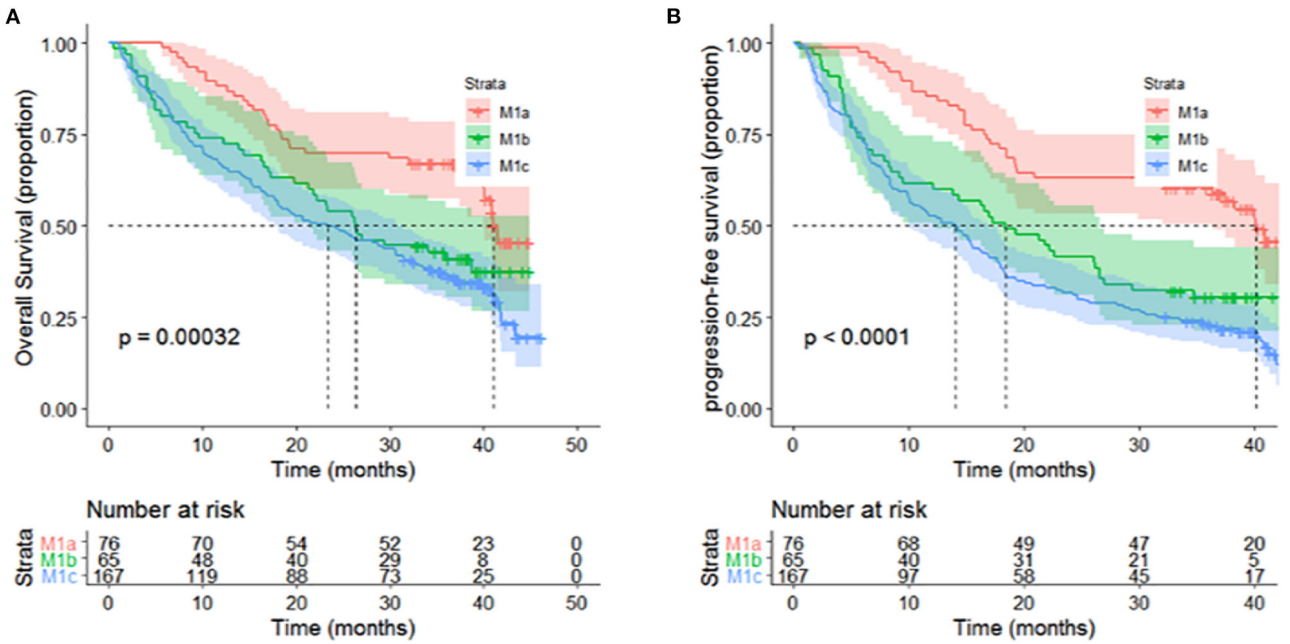

FIGURE 1 | Different distant metastasis stages presented significant associations with **(A)** OS ($P < 0.001$) and **(B)** PFS ($P < 0.0001$) of patients with metastatic non-small-cell lung cancer in univariate analyses.

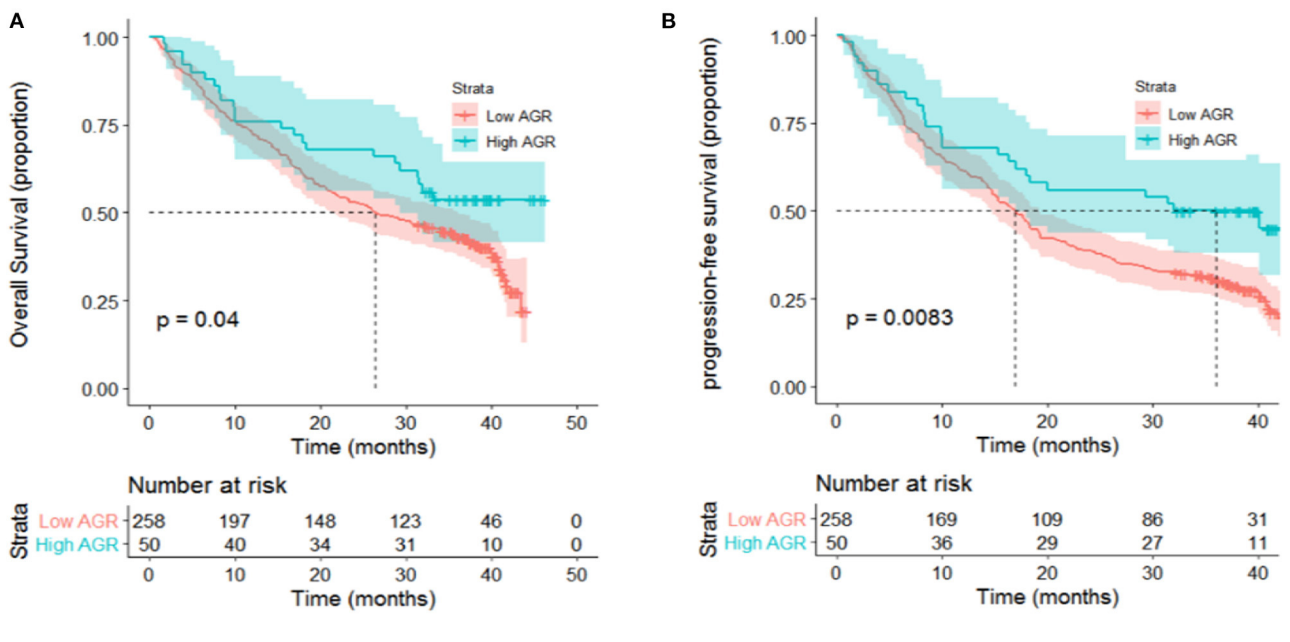

FIGURE 2 | High levels of AGR presented significant associations with **(A)** OS ($P = 0.04$) and **(B)** PFS ($P = 0.008$) of patients with metastatic non-small-cell lung cancer in univariate analyses.

turn reflects the level of inflammation in the body (15). Albumin production can be regulated by proinflammatory cytokines such as tumor necrosis factor (TNF) and interleukin-6 (IL-6). For example, TNF can inhibit the transcription of the albumin gene, leading to a low level of albumin in the host, which is conducive to tumor progression (16). Globulin levels may increase with the accumulation of acute phase proteins, including C-reactive protein and serum amyloid A. Some studies have found that the common variants of TNF receptor superfamily member 13B and other genes are strongly correlated with the increase in

immunoglobulin, which suggests that globulin may be related to apoptosis and cancer progression (17). As mentioned above, both albumin and globulin could be involved in cancer progression in a variety of ways and play important roles. Based on this, it is reasonable to suggest that AGR, an index derived from albumin and globulin, can be used as one of the prognostic factors for cancer. A low AGR can reflect low albumin and/or high globulin levels in the host. In fact, the prognostic value of the AGR has been confirmed in many cancers, including NSCLC.

In this study, we investigated the prognostic value of the AGR, an index based on inflammation, in 308 patients with advanced metastatic NSCLC. In our study, we found that the AGR was not significantly associated with demographic characteristics but was significantly correlated with some laboratory indicators, such as the PNI, LMR, PLR and NLR. The patients were divided into two groups based on the best AGR cutoff value determined by X-Tile. In both the univariate and multivariate analysis models, the AGR was found to be significantly associated with the prognosis of patients with IV stage NSCLC. A low AGR predicted poor OS and PFS (HR: 0.55; 95% CI: 0.35–0.86; $P = 0.009$; HR: 0.55; 95% CI: 0.37–0.83; $P = 0.004$, respectively). Our results suggest that the AGR can be used as an index to predict the OS and PFS of patients with advanced metastatic NSCLC. In the future, more studies, especially prospective randomized studies, are needed to confirm the importance of the AGR in NSCLC.

For the specific clinical implementation of this inflammatory biomarker, the appropriate method for determining the optimal cutoff value will need to be considered. However, there is no consensus method for determining the cutoff value of the AGR. Different studies have used different methods to calculate the cutoff value of the AGR. Some studies used the median as the cutoff value; some studies used receiver operating characteristic (ROC) curve analysis to find the best cutoff value; and some studies even selected the appropriate cutoff value according

TABLE 4 | Univariate survival analysis of inflammatory biomarkers for OS and PFS.

Variable	OS		PFS		Variable	OS		PFS	
	HR	*P*	HR	*P*		HR	*P*	HR	*P*
AGR					**PNI**				
Low	1.00				Low	1.00			
High	0.63	0.04	0.58	0.007	High	0.67	0.02	0.79	0.17
ALP					**LMR**				
Low	1.00				Low	1.00			
High	1.31	0.07	1.19	0.20	High	0.72	0.05	0.79	0.13
LDH					**PLR**				
Low	1.00				Low	1.00			
High	1.41	0.04	1.33	0.05	High	0.79	0.13	0.80	0.10
TG					**NLR**				
Low	1.00				Low	1.00			
High	1.41	0.03	0.81	0.18	High	1.28	0.11	1.29	0.12

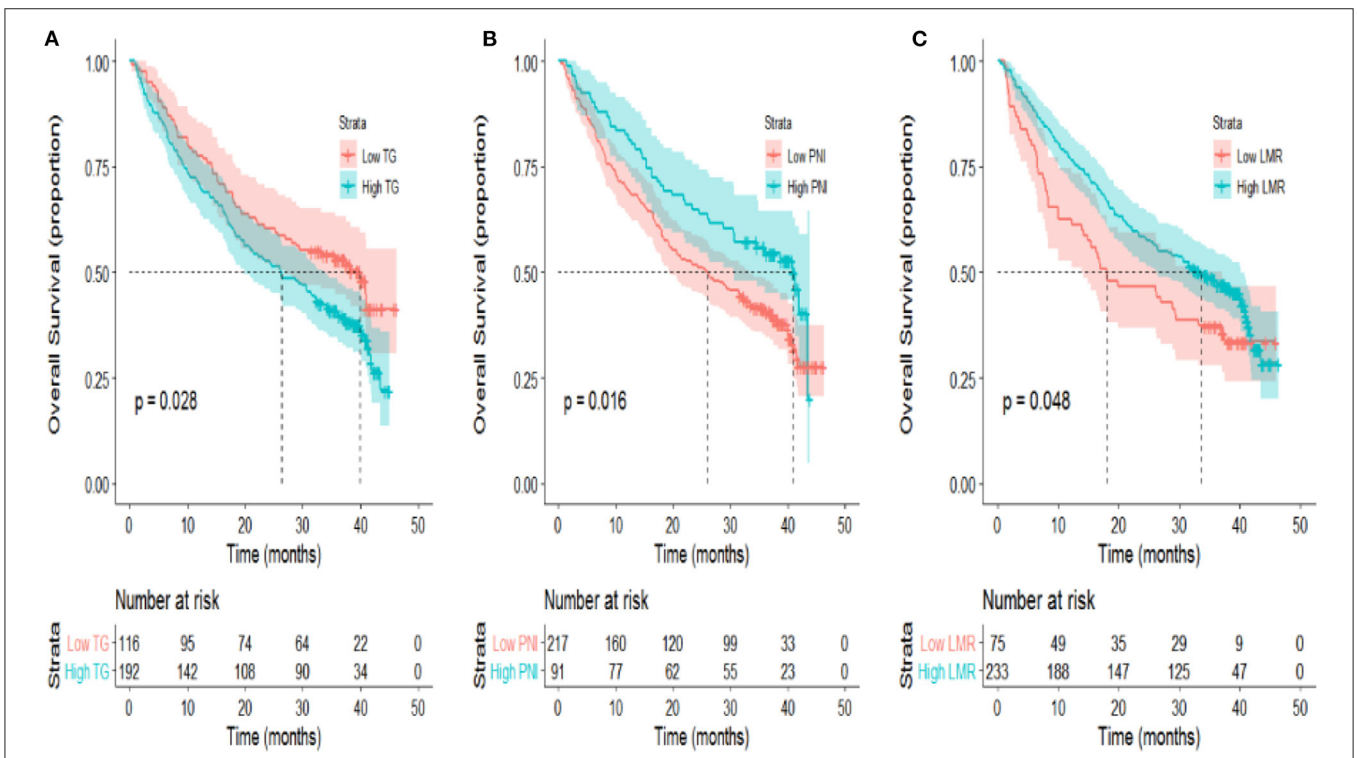

FIGURE 3 | (A) TG ($P = 0.028$), **(B)** PNI ($P = 0.016$), **(C)** LMR ($P = 0.048$) presented significant associations with OS of patients with metastatic non-small-cell lung cancer in univariate analyses.

TABLE 5 | Multivariate analysis of baseline characteristics and inflammatory biomarkers for the prediction of OS and PFS.

Variables	OS		Variables	PFS	
	HR (95% CI)	*P*		HR (95% CI)	*P*
Metastasis			**Local or distant metastases**		
M1a			M1a		
M1b	1.66 (1.00–2.75)	0.05	M1b	1.87 (1.18–2.97)	0.08
M1c	1.84 (1.10–3.08)	0.02	M1c	2.36 (1.50–3.71)	<0.001
Cerebral			**Cerebral**		
No			No		
Yes	1.40 (0.98–2.00)	0.07	Yes	1.32 (0.95–1.82)	0.10
Bones			**Bones**		
No			No		
Yes	0.97 (0.67–1.39)	0.86	Yes	0.96 (0.70–1.32)	0.82
Chemotherapy			**Adrenal**		
No chemotherapy			No		
First-line treatment	0.60 (0.43–0.84)	0.003	Yes	1.39 (0.81–2.40)	0.23
Second-line treatment	1.22 (0.53–2.81)	0.65	**Radiotherapy**		
Radiotherapy			No		
No			Yes	1.17 (0.87–1.58)	0.29
Yes	1.22 (0.87–1.70)	0.25	**EGFR-TKI**		
AGR			No		
Low			Yes	1.09 (0.81–1.47)	0.57
High	0.55 (0.35–0.86)	0.009	**AGR**		
LDH			Low		
Low			High	0.55 (0.37–0.83)	0.004
High	1.12 (0.78–1.60)	0.55	**LDH**		
TG			Low		
Low			High	1.16 (0.87–1.55)	0.32
High	1.40 (1.02–1.94)	0.04			
PNI					
Low					
High	0.56 (0.39–0.80)	0.02			
LMR					
Low					
High	0.83 (0.59–1.18)	0.31			

to the quartiles. The cutoff value of the AGR ranges from 1.01 to 1.71 (18–20). In this study, using X-tile software, we determined the best cutoff value of the AGR to be 1.13. In the future, more verification cohorts are needed to determine whether these thresholds can be applied to other independent cohorts to further confirm the clinical prognostic value of the AGR.

CONCLUSION

We report that a low AGR independently predicts poor OS and PFS in patients with IV NSCLC. The OS and PFS rates of patients with a low AGR are worse than those of patients with a high AGR. Therefore, the AGR is an important index for predicting the survival outcome of NSCLC and could assist in the selection of different treatment strategies.

DATA AVAILABILITY STATEMENT

The raw data supporting the conclusions of this article will be made available by the authors, without undue reservation.

ETHICS STATEMENT

The studies involving human participants were reviewed and approved by Ethics Committee of Hubei Cancer Hospital. The patients/participants provided their written informed consent to participate in this study.

AUTHOR CONTRIBUTIONS

XL and SW: study design and final approval. PL and YM: performed study and literature search. PL: data collection,

analysis of data, and drafting the work. All authors contributed to the article and approved the submitted version.

FUNDING

This work was financially supported by the National Natural Sciences Foundation of China (Grant Numbers: 81572287 and 81772499), the Chinese Society of Clinical Oncology (Grant Numbers: CSCO: Y-HS2019–39), the Natural Science Foundation of Hubei Province (Grant Number: 2017CFB555), and the Health and Family Planning Commission of Hubei Province (Grant Number: WJ2017 M142). The funders had no role in the design and conduct of the study; the collection, management, analysis, and interpretation of the data; the preparation, review, or approval of the manuscript; or the decision to submit the manuscript for publication. The content is solely the responsibility of the authors.

REFERENCES

1. Miller KD, Nogueira L, Mariotto AB, Rowland JH, Yabroff KR, Alfano CM, et al. Cancer treatment and survivorship statistics, 2019. *CA Cancer J Clin*. (2019) 69:363–85. doi: 10.3322/caac.21565
2. Siegel RL, Miller KD, Jemal A. Cancer statistics, 2019. *CA Cancer J Clin*. (2019) 69:7–34. doi: 10.3322/caac.21551
3. Liu Y, Li X, Yin Z, Lu P, Ma Y, Kai J, et al. Prognostic prediction models based on clinicopathological indices in patients with resectable lung cancer. *Front Oncol*. (2020) 10:571169. doi: 10.3389/fonc.2020.571169
4. Zhang H, Zhang B, Zhu K, Wu C, Gao L, Sun X, et al. Preoperative albumin-to-globulin ratio predicts survival in patients with non-small-cell lung cancer after surgery. *J Cell Physiol*. (2019) 234:2471–9. doi: 10.1002/jcp.26766
5. Gupta N, Sharma A, Sharma A. Emerging biomarkers in multiple myeloma: a review. *Clin Chim Acta*. (2020) 503:45–53. doi: 10.1016/j.cca.2019.12.026
6. Teishima J, Inoue S, Hayashi T, Matsubara A. Current status of prognostic factors in patients with metastatic renal cell carcinoma. *Int J Urol*. (2019) 26:608–17. doi: 10.1111/iju.13956
7. Mantzorou M, Koutelidakis A, Theocharis S, Giaginis C. Clinical value of nutritional status in cancer: what is its impact and how it affects disease progression and prognosis? *Nutr Cancer*. (2017) 69:1151–76. doi: 10.1080/01635581.2017.1367947
8. Liu X, Meng QH, Ye Y, Hildebrandt MA, Gu J, Wu X. Prognostic significance of pretreatment serum levels of albumin, LDH and total bilirubin in patients with non-metastatic breast cancer. *Carcinogenesis*. (2015) 36:243–8. doi: 10.1093/carcin/bgu247
9. Tuomisto AE, Mäkinen MJ, Väyrynen JP. Systemic inflammation in colorectal cancer: underlying factors, effects, and prognostic significance. *World J Gastroenterol*. (2019) 25:4383–404. doi: 10.3748/wjg.v25.i31.4383
10. Meyer EJ, Nenke MA, Rankin W, Lewis JG, Torpy DJ. Corticosteroid-binding globulin: a review of basic and clinical advances. *Horm Metab Res*. (2016) 48:359–71. doi: 10.1055/s-0042-108071
11. Liu Y, Yin Z, Lu P, Ma Y, Luo B, Xiang L, et al. Lung carcinoma cells secrete exosomal MALAT1 to inhibit dendritic cell phagocytosis, inflammatory response, costimulatory molecule expression and promote dendritic cell autophagy via AKT/mTOR pathway. *Onco Targets Ther*. (2020) 13:10693–705. doi: 10.2147/OTT.S256669
12. Weiss G, Ganz T, Goodnough LT. Anemia of inflammation. *Blood*. (2019) 133:40–50. doi: 10.1182/blood-2018-06-856500
13. Ritter B, Greten FR. Modulating inflammation for cancer therapy. *J Exp Med*. (2019) 216:1234–43. doi: 10.1084/jem.20181739
14. Yuk HD, Ku JH. Role of systemic inflammatory response markers in urothelial carcinoma. *Front Oncol*. (2020) 10:1473. doi: 10.3389/fonc.2020.01473
15. Chi J, Xie Q, Jia J, Liu X, Sun J, Chen J, et al. Prognostic value of albumin/globulin ratio in survival and lymph node metastasis in patients with cancer: a systematic review and meta-analysis. *J Cancer*. (2018) 9:2341–8. doi: 10.7150/jca.24889
16. Suh B, Park S, Shin DW, Yun JM, Keam B, Yang HK, et al. Low albumin-to-globulin ratio associated with cancer incidence and mortality in generally healthy adults. *Ann Oncol*. (2014) 25:2260–6. doi: 10.1093/annonc/mdu274
17. Osman W, Okada Y, Kamatani Y, Kubo M, Matsuda K, Nakamura Y. Association of common variants in TNFRSF13B, TNFSF13, and ANXA3 with serum levels of non-albumin protein and immunoglobulin isotypes in Japanese. *PLoS ONE*. (2012) 7:e32683. doi: 10.1371/journal.pone.0032683
18. Oki S, Toiyama Y, Okugawa Y, Shimura T, Okigami M, Yasuda H, et al. Clinical burden of preoperative albumin-globulin ratio in esophageal cancer patients. *Am J Surg*. (2017) 214:891–8. doi: 10.1016/j.amjsurg.2017.04.007
19. Park S, Park S, Lee SH, Suh B, Ock CY, Keam B, et al. Pretreatment albumin-to-globulin ratio as a predictive marker for tyrosine kinase inhibitor in non-small cell lung cancer. *Cancer Biomark*. (2016) 16:425–33. doi: 10.3233/CBM-160581
20. Shibutani M, Maeda K, Nagahara H, Ohtani H, Iseki Y, Ikeya T, et al. The pretreatment albumin to globulin ratio predicts chemotherapeutic outcomes in patients with unresectable metastatic colorectal cancer. *BMC Cancer*. (2015) 15:347. doi: 10.1186/s12885-015-1375-x

Conflict of Interest: The authors declare that the research was conducted in the absence of any commercial or financial relationships that could be construed as a potential conflict of interest.

Copyright © 2021 Lu, Ma, Wei and Liang. This is an open-access article distributed under the terms of the Creative Commons Attribution License (CC BY). The use, distribution or reproduction in other forums is permitted, provided the original author(s) and the copyright owner(s) are credited and that the original publication in this journal is cited, in accordance with accepted academic practice. No use, distribution or reproduction is permitted which does not comply with these terms.

frontiers in Medicine

ORIGINAL RESEARCH
published: 12 March 2021
doi: 10.3389/fmed.2021.612933

A Novel Normalized Cross-Correlation Speckle-Tracking Ultrasound Algorithm for the Evaluation of Diaphragm Deformation

Xiong Ye[1,2], *Zhi Liu*[3], *Ying Ma*[4], *Ye Song*[4], *Lihua Hu*[4], *Jianwen Luo*[3] *and Hui Xiao*[5]*

[1] School of Clinical Medicine, Shanghai University of Medicine & Health Sciences, Shanghai, China, [2] National Medical Products Administration (NMPA) Key Laboratory for Respiratory and Anaesthetic Equipment, Shanghai, China, [3] Department of Biomedical Engineering, School of Medicine, Tsinghua University, Beijing, China, [4] Department of Ultrasound, Shanghai University of Medicine and Health Sciences Affiliated Zhoupu Hospital, Shanghai, China, [5] Department of Respiratory and Critical Care Medicine, Shanghai General Hospital, Shanghai Jiaotong University, Shanghai, China

OPEN ACCESS

Edited by:
Hauke Busch,
University of Lübeck, Germany

Reviewed by:
Sairam Parthasarathy,
University of Arizona, United States
Ming Chen,
Tongji University, China

***Correspondence:**
Hui Xiao
xiaohui771210@163.com

Specialty section:
This article was submitted to Pulmonary Medicine, a section of the journal Frontiers in Medicine

Received: 01 October 2020
Accepted: 22 February 2021
Published: 12 March 2021

Citation:
Ye X, Liu Z, Ma Y, Song Y, Hu L, Luo J and Xiao H (2021) A Novel Normalized Cross-Correlation Speckle-Tracking Ultrasound Algorithm for the Evaluation of Diaphragm Deformation. Front. Med. 8:612933. doi: 10.3389/fmed.2021.612933

Objectives: To develop a two-dimensional normalized cross-correlation (NCC)-based ultrasonic speckle-tracking algorithm for right diaphragm deformation analysis.

Methods: Six healthy and eight mechanical ventilation patients were enrolled in this study. Images were acquired by a portable ultrasound system in three sections. DICOM data were processed with NCC to obtain the interframe/cumulative vertical and horizontal displacements, as well as the global strain of the right diaphragm, with continuous tracking and drift correction.

Results: The NCC algorithm can track the contraction and relaxation of the right diaphragm by following the respiratory movement continuously. For all three sections, the interframe and accumulated horizontal displacements were both significantly larger than the corresponding vertical displacements (interframe p values: 0.031, 0.004, and 0.000; cumulative p values: 0.039, 0.001, and <0.0001). For the global strain of the right diaphragm, there was no significant difference between each pair of sections (all $p > 0.05$), regardless of whether the horizontal interval of the initial diaphragm point was 1, 3, 5, or 10 times in the sampling interval.

Conclusions: This study developed a novel diaphragm deformation ultrasound imaging method. This method can be used to estimate the diaphragm interframe/accumulated displacement in the horizontal and vertical directions and the global strain on three different imaging planes, and it was found that the strain was not sensitive to the imaging plane.

Keywords: diaphragm, deformation, ultrasound, speckle tracking, strain

KEYPOINTS

- We developed a two-dimensional normalized cross-correlation-based ultrasound speckle-tracking algorithm as a novel method for diaphragm deformation analysis.
- The interpolation of both the radiofrequency signals and cross-correlation function algorithm can be used to track the contraction and relaxation of the right diaphragm with respiratory movement continuously in the horizontal and vertical directions.

INTRODUCTION

The diaphragm is a thin (2–4 mm), movable, dome-shaped, muscular-fibrous structure with a central tendon that separates the thorax from the abdomen and maintains the pressure gradient between those two cavities (1). It is also a vital organ that plays a major role in maintaining ventilation for mammals, as it provides ∼80% of the volume capacity for respiration (2). Diaphragm contractility and relaxation occur throughout an individual's life span without resting, not even during sleep; its importance is almost equal to that of the heart, if without normal movement of the diaphragm, life as it is currently known would not be possible (2). The phrenic nerve (PhN), which emerges mainly from the fourth cervical nerve root and partly from the third and fifth nerve roots, maintains the function of the human diaphragm (3). Unilateral PhN injury in most young people without lung pathology is well-tolerated, but in patients with chronic obstructive pulmonary disease, emphysema, or other lung disease may produce symptoms even with mild exertion. Bilateral diaphragmatic paralysis is usually always symptomatic, and the patient may be symptomatic even at rest (4), due to accessory muscles for respiration can compensate only in the short term (5, 6). Protecting the PhN is important because ipsilateral PhN damage significantly reduces the expiratory lung volume, gas exchange, and exercise capacity (7–9). There are various causes of PhN injury, such as cardiac or neck surgery, trauma, pneumonectomy, lung tumors, lung or liver transplantation, metabolic disorders, chronic lung diseases, as well as many systemic diseases, such as multiple sclerosis, that can lead to diaphragm paralysis and ultimately respiratory failure. The use of ice slush is an independent risk factor for PhN dysfunction in patients undergoing cardiac surgery with hypothermic cardiopulmonary bypass (10). Among intensive care unit (ICU) patients, 70% of those with sepsis and multiple organ failure will develop diaphragm dysfunction, which can lead to difficulty in weaning from mechanical ventilation and a prolonged ICU stay (11, 12). Although there are many clinical situations in which the diaphragm can be damaged, the assessment of diaphragm function is often fairly under-recognized (13, 14). The main reason is that there has never been a convenient and accurate method to evaluate the deformation and elastic characteristics of the diaphragm, and there is still a lack of real-time and non-invasive tools for monitoring diaphragm activity at the bedside (15), although such monitoring is sometimes necessary. Currently, Twitch transdiaphragm pressure following magnetic stimulation of the PhN is the gold standard for the non-volitional assessment of diaphragm function (16). Other methods to assess diaphragm function often have little diagnostic value, such as chest X-rays (17), or involve radiation exposure and are difficult to perform at the bedside, as is the case for computed tomography (CT) and magnetic resonance imaging (MRI). Ultrasound is the only non-invasive, radiation-free, portable, and safe diagnostic method with which to directly assess diaphragm motor function in various clinical departments (18–20). Accordingly, many related studies have been published in recent years based on M- and B-mode ultrasound, but the results of each study are quite different. Moreover, M-mode ultrasound provides a one-dimensional measurement of moving tissue along the ultrasound propagation beam. When tissue concurrently moves laterally, this vector cannot be captured (21); consequently, M-mode cannot reflect the true motion of locomotive organs. B-mode ultrasound can only reflect structural information and cannot provide details regarding the elastic characteristics of tissues. Furthermore, both B- and M-mode ultrasound depends on the angle of incidence of the ultrasound beam and requires the operator to have experience.

The ultrasound speckle-tracking imaging technique can provide tissue deformation and more dimensional motion information, such as radial, longitudinal, and circular vectors, which has been successfully used to assess myocardial strain. In 2013, we proposed the concept of diaphragm deformation analysis and used commercial myocardial speckle-tracking software to evaluate diaphragm strain in healthy volunteers (22). Hatam et al. (23) and Orde et al. (24) also used myocardial strain analysis software to evaluate diaphragm strain. All of the above studies were performed using the algorithm designed specifically for myocardium. Currently, in commercial myocardial strain analysis software, analysis of the region of interest is triggered by the R wave of the electrocardiogram, and the analytical process lasts until aortic valve closure. The entire duration of myocardial strain analysis is ∼0.02 s, which is much shorter than the duration of inspiration in one respiratory cycle. It is obvious that for the direct analysis of diaphragm deformation using myocardial strain software, the mode of triggering and the duration of the analysis are not consistent with the physiological characteristics of respiration. One potential solution for this limitation is to develop a new specialized algorithm that makes the analytical process cover the entire breathing process or the inspiration phase to fully evaluate the dynamics of the diaphragm (22).

In this study, according to respiratory physiology, we developed a novel speckle-tracking algorithm [i.e., normalized cross-correlation (NCC) algorithm (25)] to evaluate the kinetic characteristics (i.e., displacement and strain) of the right diaphragm first and then carried out a preliminary clinical study in 14 volunteers.

Abbreviations: BMI, Body mass index; C T, Computed tomography; DICOM, Digital imaging and communications in medicine; GS, Global strain; MRI, Magnetic resonance imaging; MV, Mechanical ventilation; NCC, Normalized cross-correlation; PhN, Phrenic nerve; ICU, Intensive care unit; Interp_Both, Interpolation of both the radiofrequency signals and cross-correlation function; ROI, Region of interest; SIMV, Synchronized intermittent mandatory ventilation.

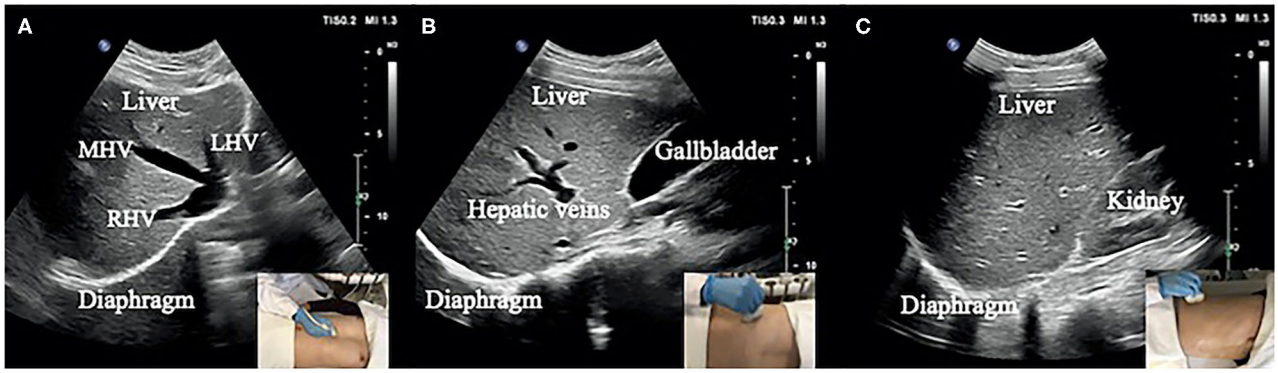

FIGURE 1 | (A) Section I: Oblique section of the lower right costal arch through the second hepatic portal with the left hepatic vein (LHV), middle hepatic vein (MHV), and right hepatic vein (RHV) as anatomical markers. **(B)** Section II: Oblique section of the right intercostal passage through the first hepatic portal with the inferior vena cava, hepatic vein, and gallbladder as anatomical markers. **(C)** Section III: Sagittal section of the liver and right kidney with the right kidney and hepatorenal space as anatomical markers.

METHODS

Participants

Six healthy subjects and eight mechanical ventilation patients (a total of 14 participants) were prospectively enrolled in this study. The healthy subjects were examined in the supine position during normal quiet breathing, and the invasive mechanical ventilation patients were lying in bed at a 35-degree angle. The tidal volume of mechanical ventilation was measured with a spirometer for healthy subjects and was obtained from machine settings for mechanical ventilation patients. All of our mechanical ventilation patients were kept in an intubated state using a synchronized intermittent mandatory ventilation model. The ethics committee of the Shanghai University of Medicine & Health Sciences approved this study, and written consent was obtained from all participants.

Design of Diaphragm Ultrasound Scanning Sections

Movement of the diaphragm in three sections (**Figure 1**) was assessed by ultrasound using a 3–5-MHz convex-array probe and a LOGIQ V2 ultrasound machine (General Electric Healthcare, Horton, Norway). Twenty-second dynamic digital imaging and communications in medicine (DICOM) images were saved for subsequent ultrasound speckle-tracking imaging analysis. To achieve the desired high-quality boundary of the right diaphragm (26), the dynamic range (e.g., 45–65 dB) was selected based on the clinical application and the patient's condition.

1) Section I: Oblique section of the right costal arch through the second hepatic portal (**Figure 1A**).
2) Section II: Oblique section of the right intercostal passage through the first hepatic portal (**Figure 1B**).
3) Section III: Sagittal section of the liver and right kidney (**Figure 1C**).

Basic Process of Tracking Diaphragm Deformation

The specific process of diaphragm deformation can be found in **Figure 2A**. For the normalized cross-correlation-based speckle-tracking method (i.e., lateral interpolation of both the radiofrequency signals and cross-correlation function (Interp_Both), please kindly refer to the study by Liu Z and his colleagues (27).

Establishment of the Region of Interest (ROI) on Diaphragm Ultrasound

The ROI was set up with four initial points on the diaphragm with 1-, 3-, 5-, and 10-fold (a, b, c, and d) horizontal sampling spacing, as shown in **Figure 2B**.

Definition of Diaphragm Displacement and Strain

Diaphragm Displacement

The peak-to-peak value of the overall interframe/cumulative vertical and horizontal displacement was extracted as the displacement of the right diaphragm in one breathing cycle by taking the mean and median displacement of all points in the diaphragm ROI (**Figure 3A**).

Global Diaphragm Strain

The Euclidean distance between each two adjacent points in the ROI was calculated, which can be considered to be approximately equal to the initial length of the diaphragm (i.e., the length of the green segment shown in **Figure 3**), and it is marked as L0. Continuous tracking of these initial points and calculation of the sum of their distances can yield the length of the diaphragm at a certain time, which is recorded as Lt (**Figure 3B**). The global strain (GS) of the diaphragm can then be calculated by the following formula (1).

$$GS = \frac{Lt - L0}{L0} * 100\% \quad (1)$$

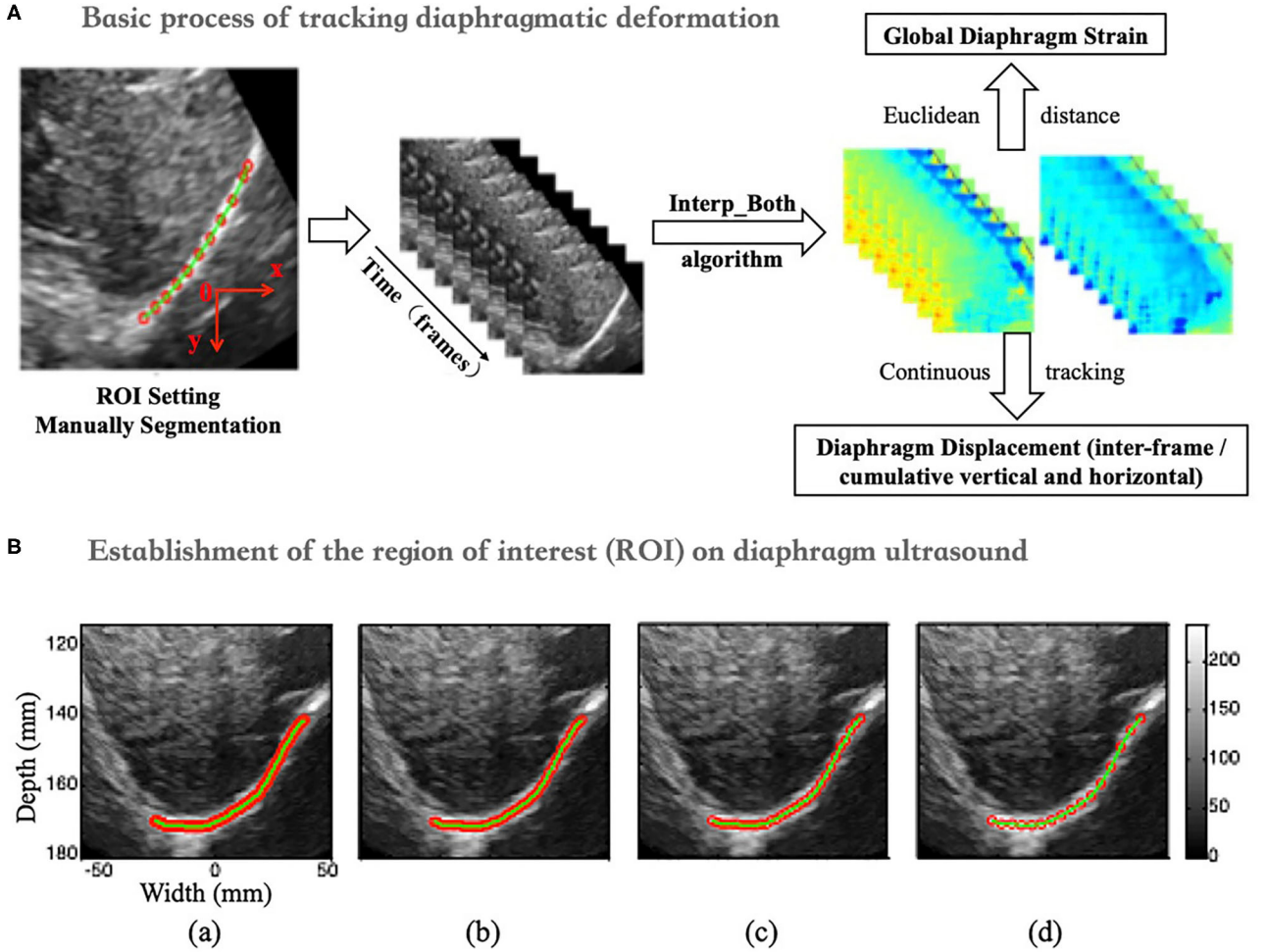

FIGURE 2 | (A) Flow chart of diaphragm speckle tracking. **(B)** ROI (initial point) of the diaphragm based on 1- (a), 3- (b), 5- (c), and 10-fold (d) horizontal sampling spacing.

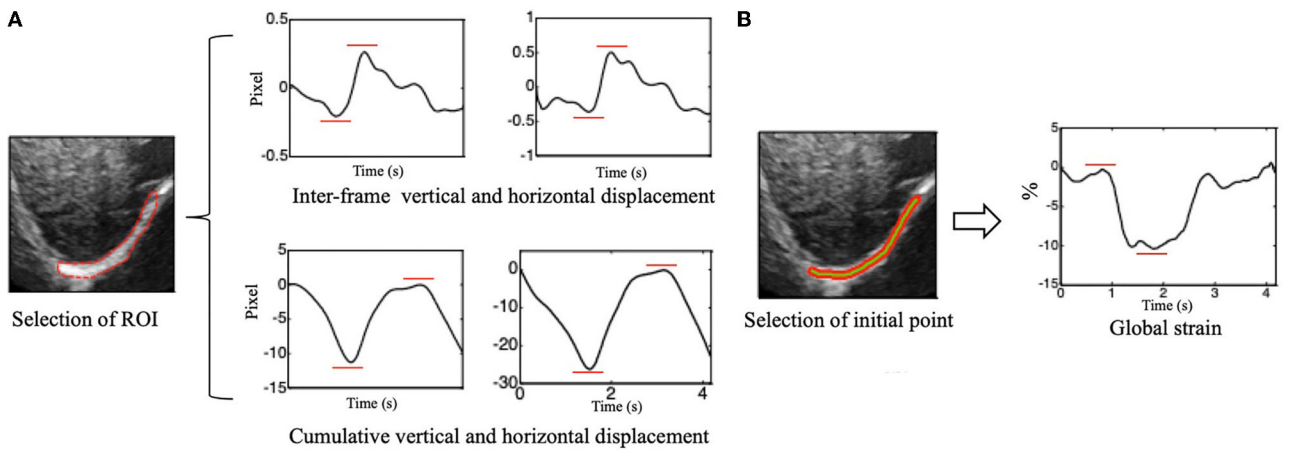

FIGURE 3 | (A) Vertical (left side) and horizontal (right side) of inter-frame and cumulative displacement of the right diaphragm in one breathing cycle and schematics of peak-to-peak value extraction. **(B)** Time-dependent global strain curves of the right diaphragm and schematic of peak-to-peak value extraction.

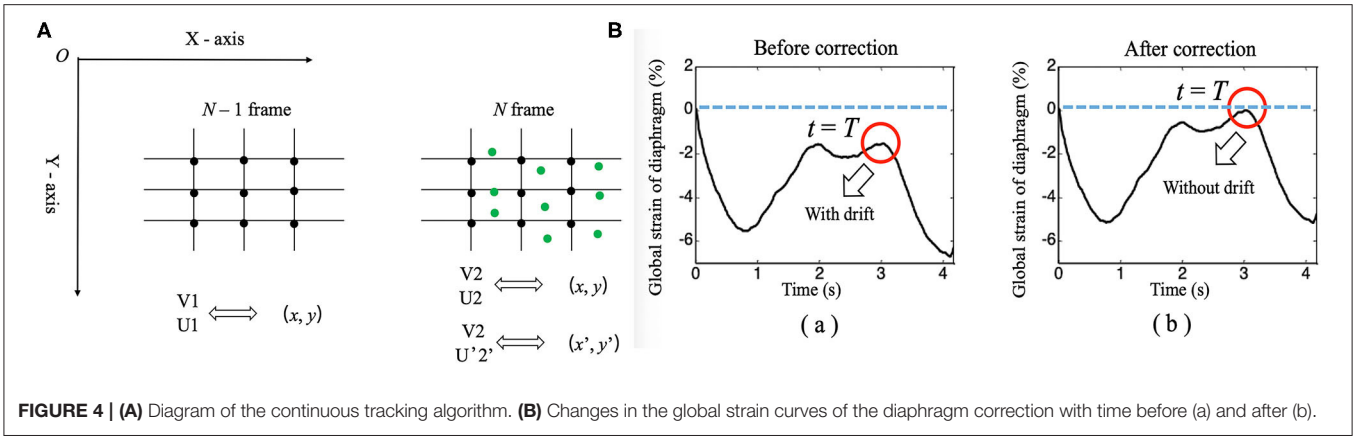

FIGURE 4 | (A) Diagram of the continuous tracking algorithm. **(B)** Changes in the global strain curves of the diaphragm correction with time before (a) and after (b).

Normalization of Interframe Displacement

To eliminate the influence of the frame rate on the estimation of the interframe displacement, the interframe displacement was normalized with the following formula (2).

$$D\_norm = \frac{FR}{FR\ max} * D \tag{2}$$

D_norm and D denote the interframe displacement after and before normalization, respectively. FR is the acquisition frame rate of the data used to calculate the interframe displacement D, while FRmax refers to the maximum of all data acquisition frame rates.

Continuous Diaphragm Deformation Tracking Algorithm (Figure 4A)

1) When calculating the interframe displacement, the selected grid points are represented by black dots. The coordinates of the black dots are assumed to be (x, y), while the vertical and horizontal displacements are represented by V1 (U1) and V2 (U2), respectively, which are obtained from the N-1 and N frames and the N and N+1 frames, respectively.
2) Because the diaphragm is moving at all times during breathing, the selected grid point (i.e., black dot) in frame N-1 has moved to a new position (i.e., green dot) in frame N when calculating the displacement, and its coordinates are assumed to be (x', y'); here, x'= x + U1 and y'= y + V1.
3) We can interpolate linearly the vertical and horizontal displacements of the green dots based on the displacements of the black dots in frame N and express them as V2' and U2'.
4) Finally, when frame N-1 changes to frame N, the interframe vertical displacement of the diaphragm changes from V1 to V2' (instead of V2), the interframe horizontal displacement of the diaphragm changes from U1 to U2' (instead of U2), the cumulative vertical displacement of the diaphragm changes from V1 to V1 + V2', and the cumulative horizontal displacement of the diaphragm changes from U1 to U1 + U2'. Similarly, the GS of the diaphragm can be obtained by applying the above process to continuously track the position of the initial points of the diaphragm, followed by calculating the Euclidean distances between the adjacent points, summing the distances, and applying formula (1).

Drift Correction Algorithm

An unavoidable problem in continuous tracking is that the displacement or strain curve will drift with the increase in frame number (time), which occurs due to estimation error accumulation in the tracking process (28). Therefore, a drift correction algorithm is used to compensate for the drift in the displacement or strain curve. The process of drift correction is described as follows. First, the movement cycle of the diaphragm with respiration was determined by M-mode ultrasonography, which was assumed to be T. Then, the distribution of the displacement or strain of the diaphragm with time was assumed to be S (t). Displacement or strain begins to accumulate at $t = 0$, and S (T) should return to the original position when $t = T$ [i.e., S (T) = 0]. However, due to error accumulation, S (T) is usually not zero. Therefore, to correct the drift of displacement or strain, we adopted formula (3), as follows.

$$S\_corr\ (t) = \begin{cases} S\ (t) - \frac{S(T)}{T} * t,\ 0 \le t \le T \\ S\ (t) - S\ (T),\ t \ge T \end{cases} \tag{3}$$

In formula (3), S_corr(t), and S(t) represent the displacement or strain after and before correction, respectively. **Figure 4B** shows the drift correction effect of this algorithm for the GS of the diaphragm.

Data Analysis

After correcting the drift, the peak-to-peak values of displacement and strain were extracted to evaluate diaphragm function, and statistical analyses were performed using SPSS 19.0 software (SPSS, Inc., Chicago, IL, USA). All values are shown as the mean ± standard deviation. Descriptive analyses were performed for all investigated variables, and the D'Agostino-Pearson test was used to test for normality. The unpaired *t*-test and non-parametric tests were used to analyze the results of differences in the displacement or strain of the right diaphragm between the two groups, and one-way ANOVA was used for comparing three groups according to data characteristics.

Bartlett's test was used to analyze statistical significance, which was defined as $P < 0.05$.

RESULTS

Baseline Characteristics of the Subjects

Diaphragm ultrasound images were acquired from six healthy subjects during quiet spontaneous breathing and eight ICU patients under mechanical ventilation, all of whom were males. The baseline characteristics of all subjects are described in **Table 1**.

Continual Tracking of Diaphragm Movement

Figure 5 shows the results of continuous tracking of the diaphragm ROI during one breathing cycle based on lateral interpolation of both the radiofrequency signals and the cross-correlation function (Interp_Both) algorithm. The ROI of the diaphragm was obtained by manual segmentation at $t = 0$ s. In addition, the ROI of the diaphragm at $t = 1.31$ s was significantly shorter than that at $t = 0$ s, which indicates that the diaphragm was contracting during the inspiratory phase. Then, the diaphragm ROI began to stretch slowly from $t = 1.31$ s to $t = 2.60$ s, which indicated passive relaxation of the diaphragm during the expiratory phase. Most importantly, at the end of the expiratory phase ($t = 3.03$ s), the ROI of the diaphragm essentially returned to the initial position and shape ($t = 0$ s).

TABLE 1 | Baseline characteristics of 14 subjects (mean ± SD).

Variable	Healthy subjects ($N = 6$)	MV patents ($N = 8$)	P
Age (years)	56 ± 8.2	51 ± 3.6	0.061
BMI (kg/m^2)	21 ± 5.3	23 ± 2.8	0.084
Tidal volume (ml)	520 ± 17.3	450 ± 38.2	0.102
Ventilation mode	-	SIMV	-

BMI, body mass index; MV, mechanical ventilation; SIMV, synchronized intermittent mandatory ventilation.

Displacement of the Diaphragm

On ultrasound imaging of the three different sections, there were no significant differences in the peak-to-peak values of the vertical or horizontal displacement and strain of the diaphragm based on the median and mean in the same section, and the P values were all >0.05. Therefore, the following results of this study were compared according to the median values.

Figure 6 depicts the horizontal and vertical interframe (**Figure 6A**) and cumulative (**Figure 6B**) displacements of the right diaphragm for the same sections. The red and blue boxes represent the horizontal and vertical displacements of sections I, II, and III, respectively. The interframe and cumulative horizontal displacements of sections I, II, and III were significantly greater than the vertical displacements. In terms of significant differences, the P values for the differences between the interframe horizontal and vertical displacements of sections I, II, and III were 0.031, 0.004, and 0.000, respectively, while those for the cumulative horizontal and vertical displacements of sections I, II, and III were 0.039, 0.001, and <0.0001, respectively.

GS of the Diaphragm

Table 2 is based on the differential distribution of the GS of the right diaphragm for the three imaging sections estimated by selecting the initial point of the diaphragm at different sampling intervals. **Table 2** shows that when different horizontal intervals were selected to estimate the GS of the diaphragm, the

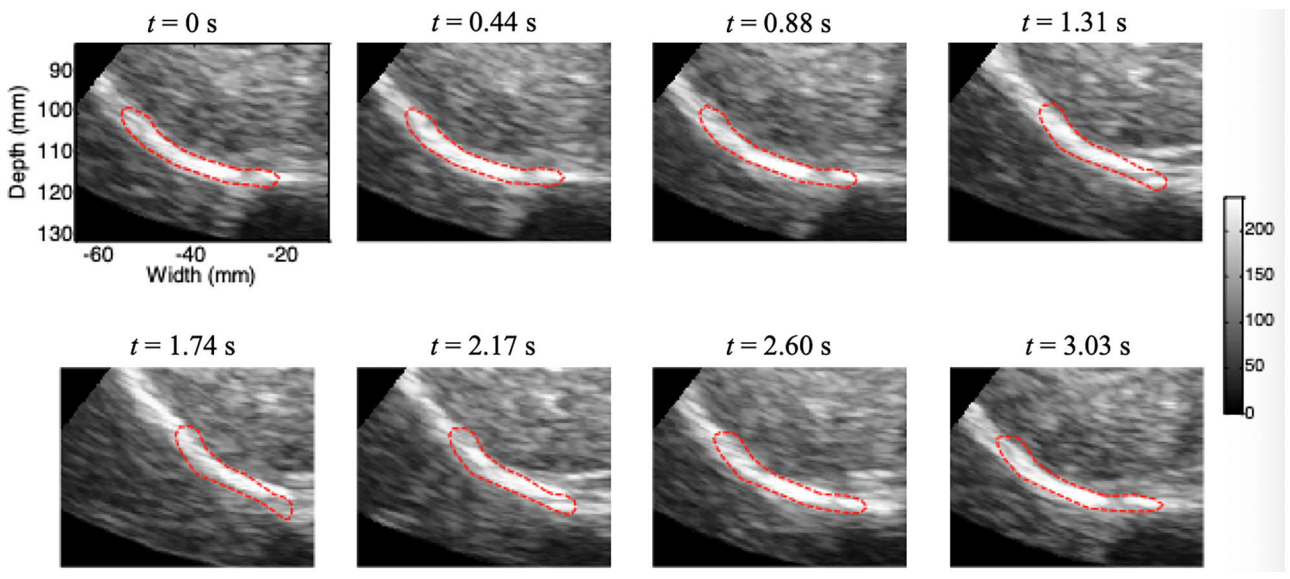

FIGURE 5 | Movement of the diaphragm tracked during one breathing cycle based on the Interp_Both algorithm (red circle, ROI).

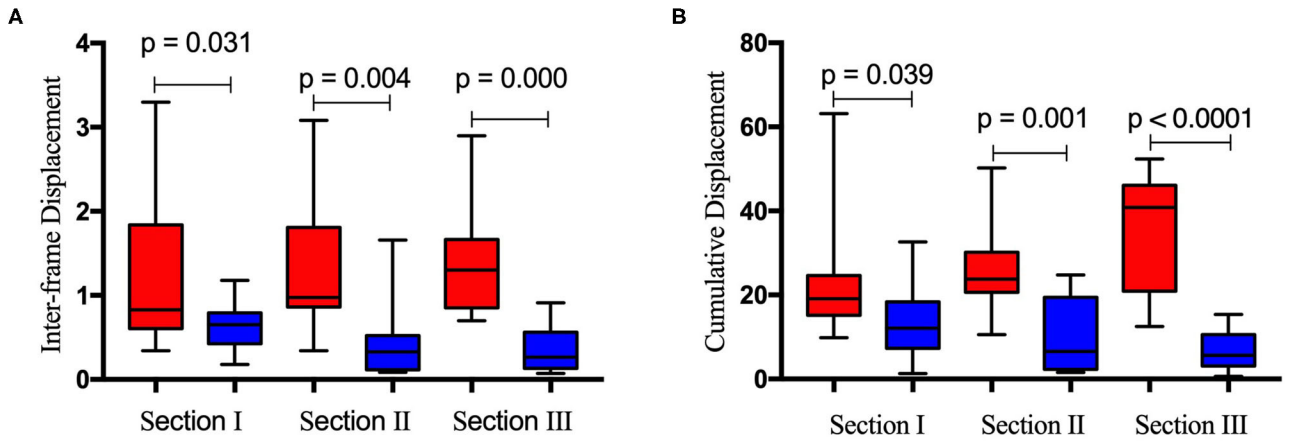

FIGURE 6 | Difference between inter-frame horizontal (red bar) and vertical (blue bar) displacement **(A)** and cumulative horizontal (red bar) and vertical (blue bar) displacement **(B)** of the right diaphragm for the same ultrasound imaging sections.

strain values were slightly different. However, after testing the difference in the strain between each pair of sections by one-way ANOVA, it was found that the GS of the diaphragm did not differ significantly by section ($P > 0.05$), regardless of whether the horizontal sampling interval of the initial diaphragm point was 1, 3, 5, or 10 (**Table 3**).

DISCUSSION

The diaphragm is widely distributed between the thoracic and abdominal regions as the main respiratory muscle pump, including the crural, dorsocostal, midcostal, and ventrocostal regions and the zone of apposition (29). The diaphragm has important physiological functions; thus, evaluating and monitoring changes in its function in the clinic is necessary (30, 31). In ultrasound strain imaging, the displacement and deformation of tissue are estimated using pre- and post-compression imaging data (32). The mechanics of the interaction between the diaphragm and the load are well-understood, but the force-length properties of the diaphragm are non-linear, and algebraic analysis of the interaction is ineffective (33). Ultrasound speckle is granular and textured in appearance due to the backscattered echoes of either randomly or coherently distributed scatterers in tissue. The statistical properties of the received echo speckle signals have been shown to depend on the density and spatial distribution of scatters.

In this study, we developed a new Interp_Both algorithm for ultrasound speckle-tracking imaging of the right diaphragm, and the deformation characteristics of the diaphragm were analyzed successfully by this method. Our previous research showed that Interp_Both with a small interpolation factor (e.g., 3–5) yields the best tradeoff between the estimation accuracy and the time required for computation, thus suggesting such a factor for lateral motion estimation in the case of a low line density (i.e., <2.8 lines/mm) (27). All of the ultrasound data of the right diaphragm that we collected had a low line density. The entire process of active contraction in the inspiratory phase and passive relaxation in the expiratory phase of the right diaphragm could be observed, as shown in **Figure 5**. The vertical and horizontal movements of the right diaphragm during one respiratory cycle could successfully be tracked continuously. The drift phenomenon could be completely removed from the corrected strain curve by applying the drift correction algorithm. To our knowledge, this is the first study in which a newly designed Interp_Both algorithm based on diaphragm anatomy and respiratory physiology was used to analyze diaphragm deformation. Referencing the standard sections used in liver ultrasonography, we defined three sections

TABLE 2 | GS of the right diaphragm determined by selecting the initial point of the ROI based on the horizontal sampling spacing of 1, 3, 5, and 10 for three sections ($N = 14$).

Horizontal sampling spacing	ANOVA summary		Bartlett's test	
	F (dfn, dfd)	*P*	Bartlett's statistic	*P*
1	0.309 (2, 32)	0.737	10.54	0.005
3	0.793 (2, 32)	0.641	10.81	0.005
5	1.664 (2, 32)	0.205	23.7	<0.0001
10	1.441 (2, 32)	0.252	16.24	0.000

TABLE 3 | GS of the right diaphragm determined by selecting the initial point of the ROI based on the horizontal sampling spacing of 5 for the three sections ($N = 14$).

Section	GS (%) (Mean ± SD)	95% CI	*F* (dfn, dfd)	*P*
I	7.89 ± 2.46	6.40 - 9.38		0.218
II	12.9 ± 10.94	5.95 – 19.85	1.602 (2, 31)	
III	10.07 ± 4.00	7.00 – 13.14		

of the right diaphragm, which were marked by the three hepatic veins (section I), the inferior vena cava and gallbladder (section II), and the right kidney (section III). According to our newly developed algorithm, the deformation information of these three diaphragm sections was analyzed in 6 normal persons and 8 patients under mechanical ventilation. We used the peak-to-peak values of the instantaneous and cumulative horizontal and vertical displacements and the GS of the right diaphragm as indexes of diaphragm kinetics. The dynamic index of strain reflects the internal characteristics and provides insight into the elastic properties of tissues in either active or passive contraction processes.

This work yielded several interesting findings. First, the instantaneous horizontal displacement was larger than the vertical displacement at both the interframe and cumulative level for the same section, as shown in **Figure 6**, which indicates that the diaphragm moves horizontally more than vertically in the inspiratory period. Understanding regional diaphragm mechanics and kinematics is very important; however, no studies have shown how the diaphragm moves in different directions during the breathing cycle. Brooke Greybeck and his team studied four dogs and showed that the volume displacement of the diaphragm was heterogeneous and dependent on regional muscle shortening, posture and level of muscle activation (34). Another finding was that the GS of the diaphragm obtained for the three sections did not differ significantly ($P > 0.05$), regardless of whether the horizontal sampling interval of the initial diaphragm point was 1, 3, 5, or 10. This shows that for the diaphragm strain, the section selected has little effect. Furthermore, the initial points of the diaphragm ROI determined with different sampling spacings at different levels have little influence on the final results, which indicates that the selection of imaging sections may not be so strict when calculating the GS of the diaphragm. Although the concept of diaphragm strain in this study is consistent with previous studies (22–24), the results are not comparable due to the completely different algorithm used.

There are some limitations to this study. First, although we have established a new method for diaphragm deformation analysis, the number of samples used for verification was small. Second, the good contrast of the right diaphragm ultrasound images makes it possible to set the ROI, but ultrasound images are probably the most difficult medical images to use for segmentation during image recognition and tracking. Before the ROI set up, we manually segmented the diaphragm images according to the dynamic B- and M-mode ultrasound images, which led to a reduction in the tracking quality. In further research on diaphragm deformation, sensors could be added to display the respiratory waveform on the ultrasound equipment and allow automatic segmentation of the image with the starting point of the inspiratory phase curve as the trigger point for analysis. Because the left diaphragm does not have as nice an acoustic window as the right diaphragm (due to the liver), it is difficult to obtain an ideal image of the left diaphragm. We have not yet attempted to conduct a deformation tracking analysis on the left diaphragm but will in future studies.

CONCLUSIONS

In summary, a novel ultrasound algorithm for deformation (displacement and strain) imaging of the diaphragm based on cross-correlation was developed in our study, and the peak-to-peak values of instantaneous and cumulative displacement and GS were proposed as kinetic indexes of diaphragm function. Differences in the interframe and cumulative vertical and horizontal displacements of the right diaphragm and the GS among three different sections were analyzed. The results show greater horizontal than vertical movement of the diaphragm in each section, and the GS of the diaphragm was not sensitive to the imaging section, which will help reduce the difficulty of choosing the section when performing strain imaging of the diaphragm in the future. In subsequent studies, more clinical data need to be collected to further explore the value and significance of this new technology.

DATA AVAILABILITY STATEMENT

The original contributions presented in the study are included in the article/supplementary material, further inquiries can be directed to the corresponding authors.

ETHICS STATEMENT

The studies involving human participants were reviewed and approved by Ethics approval was granted by the Human Research Ethics Committee of the Shanghai University of Medicine & Health Sciences, research protocol number 2017/175. The patients/participants provided their written informed consent to participate in this study.

AUTHOR CONTRIBUTIONS

XY, HX, ZL, and JL contributed to the design of the study, analysis of the data, and drafting of the manuscript. XY, YM, YS, and LH contributed to obtaining the ultrasound images. All authors critically revised the paper and agreed to be accountable for all aspects of the work.

FUNDING

This work was supported by grants from the Shanghai Municipal Health Commission (no. 201740227).

ACKNOWLEDGMENTS

The authors would like to thank our patients, who willingly gave their time to participate in this research.

REFERENCES

1. Downey R. Anatomy of the normal diaphragm. *Thorac Surg Clin.* (2011) 21:273–9. doi: 10.1016/j.thorsurg.2011.01.001
2. Maish MS. The diaphragm. *Surg Clin North Am.* (2010) 90:955–68. doi: 10.1016/j.suc.2010.07.005
3. Fell SC. Surgical anatomy of the diaphragm and the phrenic nerve. *Chest Surg Clin N Am.* (1998) 8:281–94.
4. Shahid Z, Burns B. *Anatomy, Abdomen and Pelvis, Diaphragm.* Treasure Island, FL: StatPearls (2020).
5. Kokatnur L, Rudrappa M. Diaphragmatic Palsy. *Diseases.* (2018) 6:E16. doi: 10.3390/diseases6010016
6. Mandoorah S, Mead T. Phrenic nerve injury. Treasure Island, FL: StatPearls (2019).
7. Burns J, Dunning J. Is the preservation of the phrenic nerve important after pneumonectomy? *Interact Cardiovasc Thorac Surg.* (2011) 12:47–50. doi: 10.1510/icvts.2010.248583
8. Kocher GJ, Mauss K, Carboni GL, Hoksch B, Kuster R, Ott SR, et al. Effect of phrenic nerve palsy on early postoperative lung function after pneumonectomy: a prospective study. *Ann Thorac Surg.* (2013) 96:2015–20. doi: 10.1016/j.athoracsur.2013.07.006
9. Ugalde P, Miro S, Provencher S, Quevillon M, Chau L, Deslauriers DR, et al. Ipsilateral diaphragmatic motion and lung function in long-term pneumonectomy patients. *Ann Thorac Surg.* (2008) 86:1745–51. discussion 1751–42. doi: 10.1016/j.athoracsur.2008.05.081
10. Dimopoulou I, Daganou M, Dafni U, Karakatsani A, Khoury M, Geroulanos S, et al. Phrenic nerve dysfunction after cardiac operations: electrophysiologic evaluation of risk factors. *Chest.* (1998) 113:8–14. doi: 10.1378/chest.113.1.8
11. Watson AC, Hughes PD, Louise Harris M, Hart N, Ware RJ, Wendon J, et al. Measurement of twitch transdiaphragmatic, esophageal, and endotracheal tube pressure with bilateral anterolateral magnetic phrenic nerve stimulation in patients in the intensive care unit. *Crit Care Med.* (2001) 29:1325–31. doi: 10.1097/00003246-200107000-00005
12. Doorduin J, van Hees HW, van der Hoeven JG, Heunks LM. Monitoring of the respiratory muscles in the critically ill. *Am J Respir Crit Care Med.* (2013) 187:20–7. doi: 10.1164/rccm.201206-1117CP
13. McCool FD, Tzelepis GE. Dysfunction of the diaphragm. *N Engl J Med.* (2012) 366:932–42. doi: 10.1056/NEJMra1007236
14. Nason LK, Walker CM, McNeeley MF, Burivong W, Fligner CL, Godwin JD. Imaging of the diaphragm: anatomy and function. *Radiographics.* (2012) 32:E51–70. doi: 10.1148/rg.322115127
15. Zambon M, Greco M, Bocchino S, Cabrini L, Beccaria PF, Zangrillo A. Assessment of diaphragmatic dysfunction in the critically ill patient with ultrasound: a systematic review. *Intensive Care Med.* (2017) 43:29–38. doi: 10.1007/s00134-016-4524-z
16. Spiesshoefer J, Henke C, Herkenrath SD, Randerath W, Brix T, Görlich D, et al. Noninvasive prediction of twitch transdiaphragmatic pressure: insights from spirometry, diaphragm ultrasound, and phrenic nerve stimulation studies. *Respiration.* (2019) 98:301–11. doi: 10.1159/000501171
17. Chetta A, Rehman AK, Moxham J, Carr DH, Polkey MI. Chest radiography cannot predict diaphragm function. *Respir Med.* (2005) 99:39–44. doi: 10.1016/j.rmed.2004.04.016
18. Nekludova GV, Avdeev SN. Possibilities of ultrasound research of the diaphragm. *Ter Arkh.* (2019) 91:86–92. doi: 10.26442/00403660.2019.03.000129
19. Sferrazza Papa GF, Pellegrino GM, Di Marco F, Imeri G, Brochard L, Goligher E, et al. A review of the ultrasound assessment of diaphragmatic function in clinical practice. *Respiration.* (2016) 91:403–11. doi: 10.1159/000446518
20. Vetrugno L, Guadagnin GM, Barbariol F, Langiano N, Zangrillo A, Bove T. Ultrasound imaging for diaphragm dysfunction: a narrative literature review. *J Cardiothorac Vasc Anesth.* (2019) 33:2525–36. doi: 10.1053/j.jvca.2019.01.003
21. Goutman SA, Hamilton JD, Swihart B, Foerster B, Feldman EL, Rubin JM. Speckle tracking as a method to measure hemidiaphragm excursion. *Muscle Nerve.* (2017) 55:125–7. doi: 10.1002/mus.25380
22. Ye X, Xiao H, Bai W, Liang Y, Chen M, Zhang S. Two-dimensional strain ultrasound speckle tracking as a novel approach for the evaluation of right hemidiaphragmatic longitudinal deformation. *Exp Ther Med.* (2013) 6:368–72. doi: 10.3892/etm.2013.1133
23. Hatam N, Goetzenich A, Rossaint R, et al. A novel application for assessing diaphragmatic function by ultrasonic deformation analysis in noninvasively ventilated healthy young adults. *Ultraschall Med.* (2014) 35:540–6. doi: 10.1055/s-0034-1366090
24. Orde SR, Boon AJ, Firth DG, Villarraga HR, Sekiguchi H. Diaphragm assessment by two dimensional speckle tracking imaging in normal subjects. *BMC Anesthesiol.* (2016) 16:43. doi: 10.1186/s12871-016-0201-6
25. Luo J, Konofagou E. A fast normalized cross-correlation calculation method for motion estimation. *IEEE Trans Ultrason Ferroelectr Freq Control.* (2010) 57:1347–57. doi: 10.1109/TUFFC.2010.1554
26. Lee Y, Kang J, Yoo Y. Automatic dynamic range adjustment for ultrasound B-mode imaging. *Ultrasonics.* (2015) 56:435–43. doi: 10.1016/j.ultras.2014.09.012
27. Liu Z, Huang C, Luo J. A systematic investigation of lateral estimation using various interpolation approaches in conventional ultrasound imaging. *IEEE Trans Ultrason Ferroelectr Freq Control.* (2017) 64:1149–60. doi: 10.1109/TUFFC.2017.2705186
28. Rivaz H, Boctor EM, Choti MA, Hager GD. Ultrasound elastography using multiple images. *Med Image Anal.* (2014) 18:314–29. doi: 10.1016/j.media.2013.11.002
29. De Troyer A, Boriek AM. Mechanics of the respiratory muscles. *Compr Physiol.* (2011) 1:1273–300. doi: 10.1002/cphy.c100009
30. Bertoni M, Spadaro S, Goligher EC. Monitoring patient respiratory effort during mechanical ventilation: lung and diaphragm-protective ventilation. *Crit Care.* (2020) 24:106. doi: 10.1186/s13054-020-2777-y
31. Schepens T, Fard S, Goligher EC. Assessing diaphragmatic function. *Respir Care.* (2020) 65:807–19. doi: 10.4187/respcare.07410
32. Lopata RG, Nillesen MM, Hansen HH, Gerrits IH, Thijssen JM, de Korte CL. Performance evaluation of methods for two-dimensional displacement and strain estimation using ultrasound radio frequency data. *Ultrasound Med Biol.* (2009) 35:796–812. doi: 10.1016/j.ultrasmedbio.2008.11.002
33. Wilson TA, De Troyer A. Diagrammatic analysis of the respiratory action of the diaphragm. *J Appl Physiol.* (2010) 108:251–5. doi: 10.1152/japplphysiol.00960.2009
34. Greybeck B, Lu R, Ramanujam A, Adeyeye M, Wettergreen M, Wynd S, et al. Regional diaphragm volume displacement is heterogeneous in dogs. *Am J Physiol Regul Integr Comp Physiol.* (2017) 312:R443–50. doi: 10.1152/ajpregu.00270.2016

Conflict of Interest: The authors declare that the research was conducted in the absence of any commercial or financial relationships that could be construed as a potential conflict of interest.

Copyright © 2021 Ye, Liu, Ma, Song, Hu, Luo and Xiao. This is an open-access article distributed under the terms of the Creative Commons Attribution License (CC BY). The use, distribution or reproduction in other forums is permitted, provided the original author(s) and the copyright owner(s) are credited and that the original publication in this journal is cited, in accordance with accepted academic practice. No use, distribution or reproduction is permitted which does not comply with these terms.

frontiers in Medicine

BRIEF RESEARCH REPORT
published: 12 April 2021
doi: 10.3389/fmed.2021.665057

Relationship of Soluble Interleukin-6 Receptors With Asthma: A Mendelian Randomization Study

Yoshihiko Raita[1], Zhaozhong Zhu[1], Carlos A. Camargo Jr.[1], Robert J. Freishtat[2,3,4], Debby Ngo[5], Liming Liang[6,7] and Kohei Hasegawa[1]*

[1] Department of Emergency Medicine, Massachusetts General Hospital and Harvard Medical School, Boston, MA, United States, [2] Division of Emergency Medicine, Children's National Hospital, Washington, DC, United States, [3] Department of Pediatrics, George Washington University School of Medicine and Health Sciences, Washington, DC, United States, [4] Department of Genomics and Precision Medicine, George Washington University School of Medicine and Health Sciences, Washington, DC, United States, [5] Pulmonary, Critical Care and Sleep Medicine, Beth Israel Deaconess Medical Center, Boston, MA, United States, [6] Program in Genetic Epidemiology and Statistical Genetics, Department of Epidemiology, Harvard T.H. Chan School of Public Health, Boston, MA, United States, [7] Department of Biostatistics, Harvard T.H. Chan School of Public Health, Boston, MA, United States

Purpose: Emerging evidence suggests a potential role of interleukin-6 pathways—trans-signaling with soluble interleukin-6 receptors—in the asthma pathobiology. Despite the evidence for their associations with asthma, the causal role of soluble interleukin-6 receptors remains uncertain. We investigated the relations of soluble interleukin-6 receptors with asthma and its major phenotypes.

Methods: We conducted a two-sample Mendelian randomization study. As genetic instruments, we selected 33 independent *cis*-acting variants strongly associated with the level of plasma soluble interleukin-6 receptor in the INTERVAL study. To investigate the association of variants with asthma and its phenotypes, we used genome-wide association study data from the UK Biobank. We combined variant-specific causal estimates by the inverse-variance weighted method for each outcome.

Results: Genetically-instrumented soluble interleukin-6 receptor level was associated with a significantly higher risk of overall asthma (OR per one standard deviation increment in inverse-rank normalized soluble interleukin-6 receptor level, 1.02; 95%CI, 1.01–1.03; $P = 0.004$). Sensitivity analyses demonstrated consistent results and indicated no directional pleiotropy—e.g., MR-Egger (OR, 1.03; 95%CI, 1.01–1.05; $P = 0.002$; $P_{\text{intercept}} = 0.37$). In the stratified analysis, the significant association persisted across asthma phenotypes—e.g., childhood asthma (OR, 1.05; 95%CI, 1.02–1.08; $P < 0.001$) and obese asthma (OR, 1.02; 95%CI 1.01–1.03; $P = 0.007$). Sensitivity analysis using 16 variants selected with different thresholds also demonstrated significant associations with overall asthma and its phenotypes.

Conclusion: Genetically-instrumented soluble interleukin-6 receptor level was causally associated with modestly but significantly higher risks of asthma and its phenotypes. Our observations support further investigations into identifying specific endotypes in which interleukin-6 pathways may play major roles.

Keywords: interleukin-6, soluble interleukin-6 receptor, trans-signaling pathway, asthma, Mendelian randomization, GWAS, UK Biobank

OPEN ACCESS

Edited by:
Mahmood Yaseen Hachim, Mohammed Bin Rashid University of Medicine and Health Sciences, United Arab Emirates

Reviewed by:
Cynthia Koziol-White, Rutgers, The State University of New Jersey, United States
Khuloud Bajbouj, University of Sharjah, United Arab Emirates

****Correspondence:***
Yoshihiko Raita
yraita1@mgh.harvard.edu

Specialty section:
This article was submitted to Pulmonary Medicine, a section of the journal Frontiers in Medicine

Received: *07 February 2021*
Accepted: *17 March 2021*
Published: *12 April 2021*

Citation:
Raita Y, Zhu Z, Camargo CA Jr, Freishtat RJ, Ngo D, Liang L and Hasegawa K (2021) Relationship of Soluble Interleukin-6 Receptors With Asthma: A Mendelian Randomization Study. Front. Med. 8:665057. doi: 10.3389/fmed.2021.665057

INTRODUCTION

Among many immune components involved in the pathobiology of asthma, recent research has suggested a potential role of interleukin-6 (IL-6) signaling—the classic and trans-signaling pathways (1). The trans-signaling pathway starts with coupling with IL-6 and soluble IL-6 receptor (sIL-6R), and formation of a complex with the ubiquitously expressed membrane-bound glycoprotein 130, thereby activating downstream pro-inflammatory cascades—e.g., Janus kinase-signal transducer and activator of transcription (JAK-STAT) pathway (1). This IL-6 trans-signaling pathway plays major roles in a range of inflammatory conditions (e.g., rheumatic diseases, inflammatory bowel diseases, obesity), and is the target of anti-IL-6 therapies (e.g., tocilizumab) (1).

Epidemiologic studies have found associations of an increased IL-6 level in the serum, sputum, and bronchoalveolar lavage fluid with asthma prevalence and its severity (2–4). Genome-wide association studies (GWAS) have also reported that the single nucleotide polymorphism (SNP) rs2228145 ($Asp^{358}Ala$)—a variant in *IL6R* that increases IL-6R shedding and promotes IL-6 trans-signaling—is associated with asthma prevalence, asthma severity, and lower pulmonary function (5, 6). Moreover, rs4129267—which has a perfect linkage disequilibrium with rs2228145 above in European subjects—is also known as an asthma susceptibility locus (7). Despite the evidence on these *associations* which may suffer from unmeasured confounding, the *causal* role of sIL-6R in asthma (and hence the potential role of anti-IL-6R therapies) remains uncertain. To address the knowledge gap in the literature, we performed an instrumental variable analysis with genetic instruments (i.e., Mendelian randomization) to examine the effect of sIL-6R on asthma and its major phenotypes.

METHODS

This is a two-sample Mendelian randomization study using GWAS summary statistics from two large cohort studies—the INTERVAL study (8) and UK Biobank (9–12). Detailed Methods can be found in the **Supplementary Material**. In brief, Mendelian randomization can provide unbiased causal estimates in an observation study because the genetic polymorphisms associated with the exposure (sIL-6R levels) are allocated randomly at conception and its causal inference is less susceptible to confounding and reverse causation (13).

DATA SUMMARY

The Interval Study

The INTERVAL study is a prospective cohort study that recruited approximately 50,000 blood donors aged ≥18 years. For the proteomic profiling, randomly selected two non-overlapping sub-cohorts of 2,731 and 831 participants of European ancestry were enrolled. The levels of 2,994 plasma proteins were measured by the use of SomaLogic assays. A genome-wide protein quantitative trait loci (pQTL) analysis of 2,994 plasma proteins in 3,301 healthy adults of European ancestry was conducted (8). Overall, 1,927 significant ($P_{GWAS} < 1.5 \times 10^{-11}$) associations between 764 genomic regions and 1,478 proteins were identified. The summary statistics data are publicly available at http://www.phpc.cam.ac.uk/ceu/proteins/.

The UK Biobank

The UK Biobank is a prospective cohort study that enrolled approximately 500,000 adults (aged 40–69 years at enrollment in 2006–2010), and collected comprehensive phenotypic data and performed genome-wide genotyping (9). The current analysis restricted the sample to 394,256 subjects of European ancestry to minimize population stratification (46,799 cases with asthma and 347,457 controls). In the current study, the primary outcome was (overall) asthma (n = 46,799). The secondary outcomes were six major asthma phenotypes: (1) childhood asthma (defined as age of onset ≤12 years; n = 9,676) (12), (2) adult-onset asthma (defined as age of onset ≥26 years; n = 22,294) (12), (3) allergic asthma (defined as asthma with an allergic disease—eczema, food allergy, and/or allergy rhinitis [identified by data fields 6152, 20002, 41202, 41204]; n = 23,183) (10, 11), (4) non-allergic asthma (defined as asthma without any allergic disease; n = 23,616), (5) obese asthma (defined as BMI of ≥30 kg/m^2; n = 13,550), and (6) non-obese asthma (defined as BMI of <30 kg/m^2; n = 33,095). We also identified shared controls (n = 347,457) with high-quality genotyping and complete phenotype and covariate data for GWAS association analysis. All participants from this study provided UK Biobank-acquired informed consent and provided data according to the UK Biobank protocol. The institutional review board of Harvard University and Massachusetts General Hospital approved the study.

Statistical Analysis

As the genetic instruments, we identified 33 independent *cis*-acting variants strongly associated with plasma sIL-6R levels ($P_{GWAS} < 5 \times 10^{-6}$, r^2 <0.1, 250kb from *IL6R*; **Supplementary Table 1**) in the INTERVAL study (mean age, 44 years; female, 49%) (8). All variants had an *F*-statistic of >10, without a significant association with major confounders (such as education status, smoking, and physical activity; **Supplementary Table 1**) nor a known pleiotropy in Ensembl, GWAS catalog, and PhenoScanner. Separately, using the UK Biobank data, we computed the GWAS statistics for asthma and six major asthma phenotypes, as previously described (10–12).

To investigate the association of variants with outcomes, we used GWAS summary statistics of the UK Biobank. We weighted the magnitude of association of each variant with outcomes by that with sIL-6R, and combined causal estimates of sIL-6R on each outcome by the inverse-variance weighted meta-analysis method with a random-effects model (14, 15) by using *MendelianRandomization* package (16).

In the sensitivity analyses, we first applied MR-Egger regression (17), MR Pleiotropy RESidual Sum and Outlier (MR-PRESSO) test (18), and MR weighted median method (19). MR-Egger regression detects pleiotropy based on the assumption that the pleiotropic associations are independent from the genetic associations with the exposure (i.e., the instrument strength

independent of direct effect [InSIDE] assumption) and provides corrected estimates. MR-PRESSO test (18) detects violation of the restriction exclusion criterion assumption and provides corrected estimates by removing variants which exhibit pleiotropy. MR weighted median method provides consistent estimates even when 50% of the information comes from invalid variants. We conducted MR-Egger regression and weighted median method using *MendelianRandomization* package (16) and MR-PRESSO using *MRPRESSO* package (18). Second, we also used more-stringent P_{GWAS} ($P_{GWAS} < 5\times10^{-8}$) and linkage disequilibrium (r^2 <0.02) thresholds to select genetic instruments in order to examine the robustness of the inferences. We analyzed the data using R version 3.6.3 (R foundation for Statistical Computing, Vienna, Austria).

RESULTS

Higher genetically-instrumented sIL-6R levels were associated with a modestly but significantly increased risk of overall asthma (OR per one standard deviation increment in inverse-rank normalized sIL-6R level, 1.02; 95%CI, 1.01–1.03; $P = 0.004$; **Figure 1**) with the use of inverse-variance weighted meta-analysis method. Of the 33 genetic instruments, rs4129267—an asthma susceptibility locus[7] with a linkage disequilibrium of r^2 =1 with rs2228145 (Asp^{358}Ala) (6)—had the largest weight on the Mendelian randomization estimate. The sensitivity analysis (**Table 1**) not only demonstrated consistent results—MR-Egger (OR, 1.03; 95%CI, 1.01–1.05; $P = 0.002$), MR-$PRESSO_{corrected}$ (OR, 1.03; 95%CI, 1.02–1.04; $P < 0.001$), and MR weighted median (OR, 1.03; 95%CI, 1.02–1.04; $P < 0.001$), but also indicated no directional pleiotropy in MR-Egger test ($P_{intercept}$ =0.37). Although the sensitivity analyses using MR-PRESSO suggested potential pleiotropy (P_{global} =0.02), the corrected MR-PRESSO yielded an estimate that is consistent with the primary analysis (OR, 1.03; 95%CI, 1.02–1.04; $P < 0.001$) after removing variants with potential pleiotropy.

In the stratified analysis, the significant association persisted across the asthma phenotypes (**Figure 2**)—e.g., childhood asthma (OR, 1.05; 95%CI, 1.02–1.08; $P < 0.001$) and obese asthma (OR, 1.02; 95%CI, 1.01–1.03; $P = 0.007$). Likewise, the sensitivity analysis also demonstrated consistent results (**Table 1**)—e.g., MR-Egger for childhood asthma (OR, 1.04; 95%CI, 1.00–1.08; $P = 0.04$), MR-PRESSO for obese asthma (OR, 1.02; 95%CI, 1.00–1.03; $P = 0.001$), and MR weighted median for childhood asthma (OR, 1.04; 95%CI, 1.02–1.07; $P < 0.001$). Although the sensitivity analyses using MR-PRESSO suggested potential pleiotropy for allergic asthma (P_{global} =0.02) and non-obese asthma (P_{global} =0.004), the corrected MR-PRESSO yielded an estimate that is consistent with the primary analysis—allergic asthma (OR, 1.03; 95%CI, 1.02–1.05; $P < 0.001$) and non-obese asthma (OR, 1.03; 95%CI, 1.02–1.04; $P < 0.001$)—after removing variants with potential pleiotropy.

Lastly, the sensitivity analysis using 16 variants selected by the use of more stringent thresholds—$P_{GWAS} < 5\times10^{-8}$ and linkage disequilibrium ($r^2 < 0.02$)—also demonstrated significant associations with overall asthma (OR, 1.03; 95%CI, 1.02–1.04; $P < 0.001$; **Supplementary Figure 1**) and its phenotypes—e.g., childhood asthma (OR, 1.05; 1.01–1.09; $P = 0.01$) and obese asthma (OR, 1.03; 95%CI, 1.01–1.05; $P = 0.01$; **Figure 3**).

DISCUSSION

In this two-sample Mendelian randomization study, we demonstrated that higher genetically-instrumented sIL-6R levels were associated with a modestly but significantly increased risk of overall asthma. The sensitivity analyses also showed consistent results. Our results are in line with recent findings that higher circulating IL-6 levels are associated with a greater

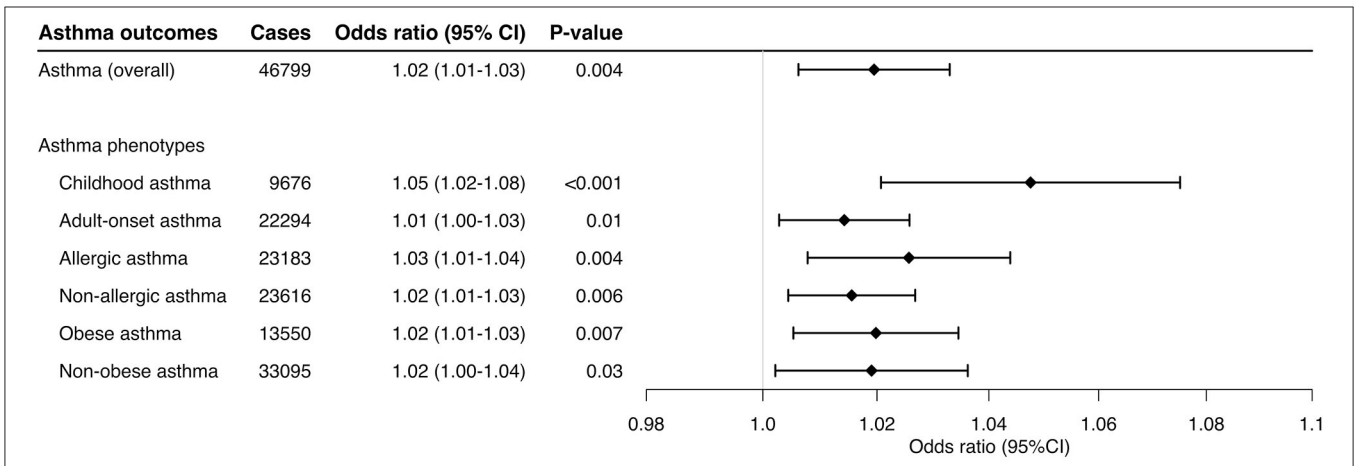

FIGURE 1 | Mendelian randomization estimates for the effect of soluble interleukin-6 receptors on overall asthma outcome. The size of the squares is proportional to the weight of the Mendelian randomization estimate for each variant, with the horizontal lines indicating their 95% confidence intervals. The center of the diamond represents the combined Mendelian randomization point estimate with the lateral tips indicating its 95% confidence interval, estimated by the inverse variance weighted method. The odds ratios were estimated per one standard deviation increment in the inverse-rank normalized sIL-6R level. CI, confidence interval; IVW, inverse variance weighted.

TABLE 1 | Sensitivity analysis using MR Egger, MR-PRESSO, and MR weighted median methods.

Outcomes	Inverse variance weighted estimate (primary analysis)		MR-Egger			MR-PRESSO (raw)			MR-PRESSO (corrected)		MR weighted median	
	Odds ratio(95% CI)	*P*-value	Odds ratio (95% CI)	*P*-value	$P^{*}_{intercept}$	Odds ratio (95% CI)	*P*-value	P_{global} †	Odds ratio (95% CI)	*P*-value	Odds ratio (95% CI)	*P*-value
Asthma (overall)	1.02 (1.01–1.03)	0.004	1.03 (1.01–1.05)	0.002	0.37	1.02 (1.01–1.03)	<0.001	0.02	1.03 (1.02–1.04)	<0.001	1.03 (1.02–1.04)	<0.001
Childhood asthma	1.05 (1.02–1.08)	<0.001	1.04 (1.00–1.08)	0.04	0.95	1.04 (1.02–1.07)	<0.001	0.05			1.04 (1.02–1.07)	<0.001
Adult-onset asthma	1.01 (1.00–1.03)	0.01	1.02 (0.99–1.04)	0.058	0.46	1.01 (1.00–1.03)	0.02	0.56			1.02 (1.00–1.03)	0.03
Allergic asthma	1.03 (1.01–1.04)	0.004	1.05 (1.02–1.07)	0.001	0.28	1.03 (1.02–1.05)	<0.001	0.02	1.03 (1.02–1.05)	<0.001	1.04 (1.02–1.06)	<0.001
Non-allergic asthma	1.02 (1.00–1.03)	0.006	1.02 (0.99–1.04)	0.096	0.77	1.02 (1.00–1.03)	0.007	0.63			1.02 (1.00–1.03)	0.04
Obese asthma	1.02 (1.01–1.03)	0.007	1.02 (0.99–1.04)	0.26	0.75	1.02 (1.00–1.03)	0.001	0.97			1.02 (0.99–1.04)	0.12
Non-obese asthma	1.02 (1.00–1.04)	0.03	1.04 (1.01–1.06)	0.002	0.25	1.03 (1.01–1.04)	<0.001	0.004	1.03 (1.02–1.04)	<0.001	1.03 (1.02–1.05)	<0.001

CI, confidence interval.

**The non-significant P-values of the MR-Egger intercept test (Pintercept) indicate the absence of directional pleiotropy and the absence of violation for the instrument strength independent of direct effect (InSIDE) assumption, and indicate that the inverse variance weighted estimate is unbiased.*

†Significant Pglobal indicates potential horizontal pleiotropy.

exacerbation risk both in children (20) and adults (21, 22). Additionally, genetic studies showed the associations of *IL6R*-related polymorphisms with asthma prevalence and severity, and lower pulmonary function (5, 6). For example, the Severe Asthma Research Program (SARP) cohorts found that rs2228145 is associated with a higher serum sIL-6R level, greater asthma severity, and lower pulmonary function in patients with severe asthma (6). However, their subsequent study also reported discordant results—e.g., no association of sIL-6R level with severity or exacerbation risk (22). The apparent discrepancies between these reports may be attributable to the differences in study design, setting, sample, analytical assumptions, or any combination of these factors. Regardless, the validity of the current study is buttressed by the use of the Mendelian randomization design. This design can mitigate unmeasured confounding and reverse causation that occur with conventional observational studies (13). The current analysis meets the assumptions of Mendelian randomization design in that we identified the genetic variants that are strongly associated with the sIL-6R level (the relevance assumption) and do not share common causes with asthma (the independence assumption), and in that we ensured no effects of known or unknown pleiotropy (the exclusion restriction assumption) (23). The current analysis using the data of two large cohorts corroborates the earlier reports, and extends them by investigating potential causal effects of sIL-6R on asthma and its phenotypes.

The mechanisms underlying our findings remain to be elucidated. For example, inflammatory signals (e.g., C-reactive protein, chemokine ligand 1, IL-1β, IL-8, tumor necrosis factor, bacterial lipopolysaccharides) promote alternative mRNA splicing and shedding of IL-6R from the cell surface, thereby producing sIL-6R and activating the IL-6 trans-signaling pathway (24–29). An analysis of U-BIOPRED data reported that adult patients characterized by IL-6 trans-signaling-related epithelial gene signature had upregulated innate immune pathways, type 2 inflammation-independent eosinophilia, increased submucosal inflammation and airway remodeling, and higher asthma exacerbation rate (25). In patients with obese asthma, their airway inflammation is characterized by dominance of neutrophils and macrophages—major sources of sIL-6R in both lungs (5) and adipose tissue (30). Experimental asthma models also demonstrated that IL-6R inhibitors attenuate the airway inflammatory response characterized by mixed granulocytic infiltration with elevated IL-6 and IL-6R levels (31). These data collectively present a rationale for targeting the IL-6 trans-signaling pathway in asthma. We acknowledge that, in the current analysis, the observed magnitude of estimates was nominally small. Nevertheless, our findings encourage further investigations into identifying patients with specific asthma endotype(s) in which IL-6 pathways play major roles [e.g., patients with adiposopathy—"sick fat" (30)].

This study has potential limitations. First, misclassification of asthma and its phenotypes is possible, while it is unrelated to the measured sIL-6R levels in the current two-sample design. Therefore, this independent non-differential misclassification would have biased the inferences toward the null. Second, the

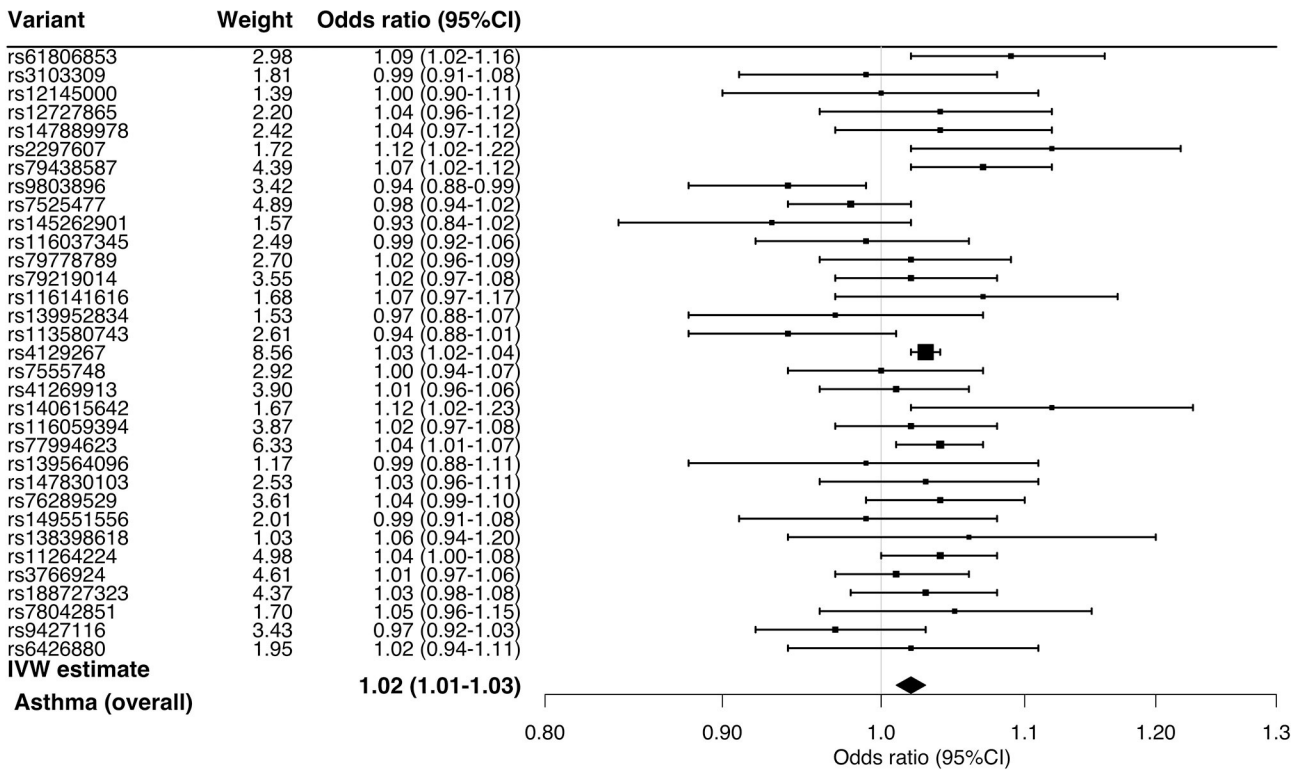

FIGURE 2 | Mendelian randomization estimates for the effect of soluble interleukin-6 receptors on asthma and its phenotypes. By using the inverse variance weighted method, the combined causal effect of sIL-6R on the asthma (overall) outcome and six asthma phenotypes was estimated. The odds ratios were estimated per one standard deviation increment in the inverse-rank normalized sIL-6R level. CI, confidence interval.

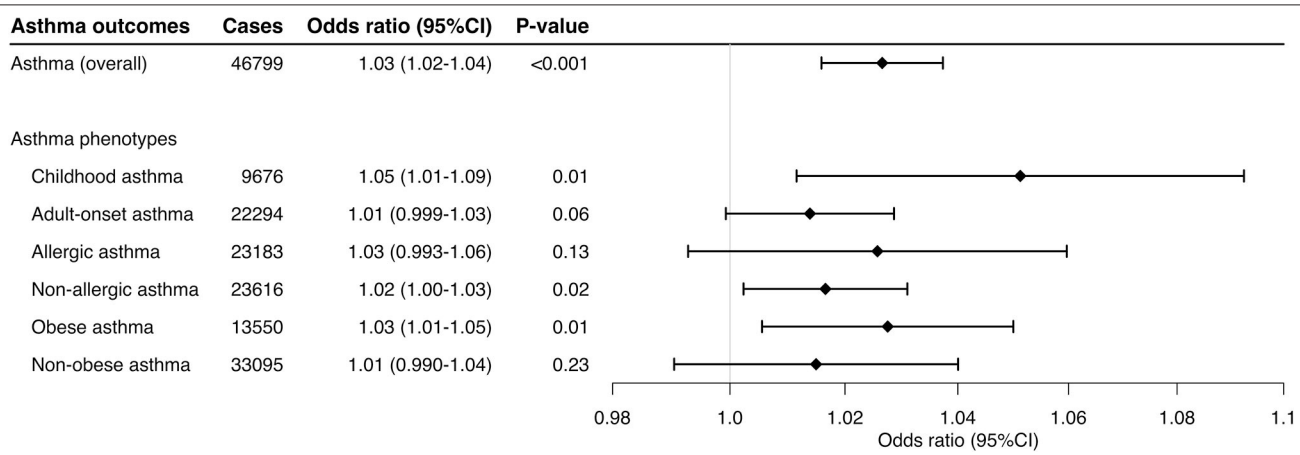

FIGURE 3 | Mendelian randomization estimates for the effect of soluble interleukin-6 receptors on asthma and its phenotypes using different thresholds. This sensitivity analysis used 16 variants selected with the use of more-stringent P_{GWAS} ($P_{GWAS} < 5 \times 10^{-8}$) and linkage disequilibrium ($r^2 < 0.02$) thresholds. By using the inverse variance weighted method, the combined causal effect of sIL-6R on the asthma (overall) outcome and six asthma phenotypes was estimated. The odds ratios were estimated per one standard deviation increment in the inverse-rank normalized sIL-6R level. CI, confidence interval.

small sample size of patients with moderate-to-severe asthma precluded us from robustly examining this specific group that may benefit more from anti-IL-6 therapies. Third, as with any Mendelian randomization study, survivor (selection) bias is possible. However, participants from the INTERVAL study (mean age, 44 years) and UK Biobank (mean age, 57 years) were not in age ranges where survivor bias imposes a substantial impact. Fourth, the current study design

using summary statistics precluded us from evaluating a potential non-linear relationship of sIL-6R with the asthma outcomes. Fourth, the influence of genetic instruments may be abated or buffered by feedback mechanisms or developmental processes. Yet, such mechanisms would have diminished the genetic effects, thereby biasing the inferences toward the null. Lastly, to minimize the population stratification bias, we restricted the study sample to individuals of European ancestry. Therefore, the inferences may not be generalizable to other racial/ethnic populations.

In conclusion, the current Mendelian randomization study using two large cohort data demonstrated that higher genetically-instrumented sIL-6R levels are associated with a significantly but modestly increased risk of overall asthma. The observation was consistent across the asthma phenotypes and different assumptions. Our inferences support further research into delineating the roles of IL-6 pathways in the asthma pathobiology and identifying patients with a distinct endotype who would benefit most from anti-IL-6 therapies.

DATA AVAILABILITY STATEMENT

The raw data supporting the conclusions of this article will be made available by the authors, without undue reservation.

ETHICS STATEMENT

The studies involving human participants were reviewed and approved by all participants from this study provided UK Biobank-acquired informed consent and provided data according to the UK Biobank protocol. The current study has complied with all ethical regulations according to UK Biobank policy. This research was approved and conducted using the UK Biobank under application number 16549 and 45052. The institutional review board of Harvard University and Massachusetts General Hospital approved the study. The patients/participants provided their written informed consent to participate in this study.

AUTHOR CONTRIBUTIONS

YR carried out the main statistical analysis, drafted the initial manuscript, and approved the final manuscript as submitted. ZZ created the summary statistics of UK Biobank, drafted the initial manuscript, and approved the final manuscript as submitted. CC conceptualized and designed the study, supervised the conduct of study, critically reviewed and revised the initial manuscript, and approved the final manuscript as submitted. RF assisted study design, reviewed the manuscript, and approved the final manuscript. LL conceptualized the study, obtained funding and reviewed the manuscript, and approved the final manuscript. DN conceptualized the study, reviewed the manuscript, and approved the final manuscript. KH conceptualized the study, obtained funding, supervised the statistical analysis, reviewed and revised the initial manuscript, and approved the final manuscript as submitted. All authors contributed to the article and approved the submitted version.

FUNDING

This study was supported by grants (R01 AI-134940 and R01 AI-148338) from the National Institutes of Health (Bethesda, MD). The content of this manuscript is solely the responsibility of the authors and does not necessarily represent the official views of the National Institutes of Health. The funding organization was not involved in the collection, management, or analysis of the data; preparation or approval of the manuscript; or decision to submit the manuscript for publication.

ACKNOWLEDGMENTS

This research was conducted using the UK Biobank Resource under Applications #16549 and #45052.

SUPPLEMENTARY MATERIAL

The Supplementary Material for this article can be found online at: https://www.frontiersin.org/articles/10.3389/fmed.2021.665057/full#supplementary-material

REFERENCES

1. Rose-John S. IL-6 Trans-signaling via the soluble IL-6 receptor: importance for the pro-inflammatory activities of IL-6. *Int J Biol Sci.* (2012) 8:1237–47. doi: 10.7150/ijbs.4989
2. Yokoyama A, Kohno N, Fujino S, Hamada H, Inoue Y, Fujioka S, et al. Circulating interleukin-6 levels in patients with bronchial asthma. *Am J Respir Crit Care Med.* (1995) 151:1354–8. doi: 10.1164/ajrccm.151.5.7735584
3. Neveu WA, Allard JL, Raymond DM, Bourassa LM, Burns SM, Bunn JY, et al. Elevation of IL-6 in the allergic asthmatic airway is independent of inflammation but associates with loss of central airway function. *Respir Res.* (2010) 11:28. doi: 10.1186/1465-9921-11-28
4. Zhang J-G, Chen X-J, Liu T, Jiang S-J. FOXP3+ associated with the pro-inflammatory regulatory T and T helper 17 effector cells in asthma patients. *Exp Ther Med.* (2016) 12:2753–8. doi: 10.3892/etm.2016.3662
5. Farahi N, Paige E, Balla J, Prudence E, Ferreira RC, Southwood M, et al. Neutrophil-mediated IL-6 receptor trans-signaling and the risk of chronic obstructive pulmonary disease and asthma. *Hum Mol Genet.* (2017) 26:1584–96. doi: 10.1093/hmg/ddx053
6. Hawkins GA, Robinson MB, Hastie AT, Li X, Li H, Moore WC, et al. The IL6R variation Asp(358)Ala is a potential modifier of lung function in subjects with asthma. *J Allergy Clin Immunol.* (2012) 130:510–5.e1. doi: 10.1016/j.jaci.2012.03.018
7. Ferreira MAR, Matheson MC, Duffy DL, Marks GB, Hui J, Le Souëf P, et al. Identification of IL6R and chromosome 11q13.5 as risk loci for asthma. *Lancet.* (2011) 378:1006–14. doi: 10.1016/S0140-6736(11)60874-X
8. Sun BB, Maranville JC, Peters JE, Stacey D, Staley JR, Blackshaw J, et al. Genomic atlas of the human plasma proteome. *Nature.* (2018) 558:73–9. doi: 10.1038/s41586-018-0175-2
9. Sudlow C, Gallacher J, Allen N, Beral V, Burton P, Danesh J, et al. UK biobank: an open access resource for identifying the causes of a wide range of complex diseases of middle and old age. *PLoS Med.* (2015) 12:e1001779. doi: 10.1371/journal.pmed.1001779

10. Zhu Z, Lee PH, Chaffin MD, Chung W, Loh P-R, Lu Q, et al. A genome-wide cross-trait analysis from UK Biobank highlights the shared genetic architecture of asthma and allergic diseases. *Nat Genet.* (2018) 50:857–64. doi: 10.1038/s41588-018-0121-0
11. Zhu Z, Guo Y, Shi H, Liu C-L, Panganiban RA, Chung W, et al. Shared genetic and experimental links between obesity-related traits and asthma subtypes in UK Biobank. *J Allergy Clin Immunol.* (2020) 145:537–49. doi: 10.1016/j.jaci.2019.09.035
12. Zhu Z, Zhu X, Liu C-L, Shi H, Shen S, Yang Y, et al. Shared genetics of asthma and mental health disorders: a large-scale genome-wide cross-trait analysis. *Eur Respir J.* (2019) 54:1901507. doi: 10.1183/13993003.01507-2019
13. Davies NM, Holmes MV, Davey Smith G. Reading Mendelian randomisation studies: a guide, glossary, and checklist for clinicians. *BMJ.* (2018) 362:k601. doi: 10.1136/bmj.k601
14. Bowden J, Spiller W, Del Greco M F, Sheehan N, Thompson J, Minelli C, et al. Improving the visualization, interpretation and analysis of two-sample summary data Mendelian randomization via the Radial plot and Radial regression. *Int J Epidemiol.* (2018) 47:1264–78. doi: 10.1093/ije/dyy101
15. Burgess S, Dudbridge F, Thompson SG. Combining information on multiple instrumental variables in Mendelian randomization: comparison of allele score and summarized data methods. *Stat Med.* (2016) 35:1880–906. doi: 10.1002/sim.6835
16. Staley OYJ. *MendelianRandomization: Mendelian Randomization Package*. (2020). Available online at: https://CRAN.R-project.org/package=MendelianRandomization (accessed November 2, 2020).
17. Burgess S, Thompson SG. Interpreting findings from Mendelian randomization using the MR-Egger method. *Eur J Epidemiol.* (2017) 32:377–89. doi: 10.1007/s10654-017-0255-x
18. Verbanck M, Chen C-Y, Neale B, Do R. Detection of widespread horizontal pleiotropy in causal relationships inferred from Mendelian randomization between complex traits and diseases. *Nature Genetics.* (2018) 50:693–8. doi: 10.1038/s41588-018-0099-7
19. Bowden J, Davey Smith G, Haycock PC, Burgess S. Consistent estimation in Mendelian randomization with some invalid instruments using a weighted median estimator. *Genet Epidemiol.* (2016) 40:304–14. doi: 10.1002/gepi.21965
20. Jackson DJ, Bacharier LB, Calatroni A, Gill MA, Hu J, Liu AH, et al. Serum IL-6: a biomarker in childhood asthma? *J Allergy Clin Immunol.* (2020) 145:1701–4.e3. doi: 10.1016/j.jaci.2020.01.021
21. Peters MC, McGrath KW, Hawkins GA, Hastie AT, Levy BD, Israel E, et al. Plasma interleukin-6 concentrations, metabolic dysfunction, and asthma severity: a cross-sectional analysis of two cohorts. *Lancet Respir Med.* (2016) 4:574–84. doi: 10.1016/S2213-2600(16)30048-0
22. Li X, Hastie AT, Peters MC, Hawkins GA, Phipatanakul W, Li H, et al. Investigation of the relationship between IL-6 and type 2 biomarkers in patients with severe asthma. *J Allergy Clin Immunol.* (2020) 145:430–3. doi: 10.1016/j.jaci.2019.08.031
23. Zhu Z, Hasegawa K, Camargo CA, Liang L. Investigating asthma heterogeneity through shared and distinct genetics: insights from genome-wide cross-trait analysis. *J Allergy Clin Immunol.* (2020) 147:796–807. doi: 10.1016/j.jaci.2020.07.004
24. Franchimont N, Lambert C, Huynen P, Ribbens C, Relic B, Chariot A, et al. Interleukin-6 receptor shedding is enhanced by interleukin-1beta and tumor necrosis factor alpha and is partially mediated by tumor necrosis factor alpha-converting enzyme in osteoblast-like cells. *Arthritis Rheum.* (2005) 52:84–93. doi: 10.1002/art.20727
25. Jevnikar Z, Östling J, Ax E, Calvén J, Thörn K, Israelsson E, et al. Epithelial IL-6 trans-signaling defines a new asthma phenotype with increased airway inflammation. *J Allergy Clin Immunol.* (2019) 143:577–90. doi: 10.1016/j.jaci.2018.05.026
26. Jones SA, Novick D, Horiuchi S, Yamamoto N, Szalai AJ, Fuller GM. C-reactive protein: a physiological activator of interleukin 6 receptor shedding. *J Exp Med.* (1999) 189:599–604. doi: 10.1084/jem.189.3.599
27. Hurst SM, Wilkinson TS, McLoughlin RM, Jones S, Horiuchi S, Yamamoto N, et al. Il-6 and its soluble receptor orchestrate a temporal switch in the pattern of leukocyte recruitment seen during acute inflammation. *Immunity.* (2001) 14:705–14. doi: 10.1016/S1074-7613(01)00151-0
28. Walev I, Vollmer P, Palmer M, Bhakdi S, Rose-John S. Pore-forming toxins trigger shedding of receptors for interleukin 6 and lipopolysaccharide. *Proc Natl Acad Sci USA.* (1996) 93:7882–7. doi: 10.1073/pnas.93.15.7882
29. Yan I, Schwarz J, Lücke K, Schumacher N, Schumacher V, Schmidt S, et al. ADAM17 controls IL-6 signaling by cleavage of the murine IL-6Rα from the cell surface of leukocytes during inflammatory responses. *J Leukoc Biol.* (2016) 99:749–60. doi: 10.1189/jlb.3A0515-207R
30. Peters U, Dixon AE, Forno E. Obesity and asthma. *J Allergy Clin Immunol.* (2018) 141:1169–79. doi: 10.1016/j.jaci.2018.02.004
31. Ullah MA, Revez JA, Loh Z, Simpson J, Zhang V, Bain L, et al. Allergen-induced IL-6 trans-signaling activates γδ T cells to promote type 2 and type 17 airway inflammation. *J Allergy Clin Immunol.* (2015) 136:1065–73. doi: 10.1016/j.jaci.2015.02.032

Conflict of Interest: CC has participated in scientific advisory boards for AstraZeneca and GSK. KH has received a research grant from Novartis.

The remaining authors declare that the research was conducted in the absence of any commercial or financial relationships that could be construed as a potential conflict of interest.

Copyright © 2021 Raita, Zhu, Camargo, Freishtat, Ngo, Liang and Hasegawa. This is an open-access article distributed under the terms of the Creative Commons Attribution License (CC BY). The use, distribution or reproduction in other forums is permitted, provided the original author(s) and the copyright owner(s) are credited and that the original publication in this journal is cited, in accordance with accepted academic practice. No use, distribution or reproduction is permitted which does not comply with these terms.

frontiers in Medicine

ORIGINAL RESEARCH
published: 14 May 2021
doi: 10.3389/fmed.2021.636869

The Association Between the Baseline and the Change in Neutrophil-to-Lymphocyte Ratio and Short-Term Mortality in Patients With Acute Respiratory Distress Syndrome

Wei Zhang[1]*, *Yadan Wang*[2], *Weijie Li*[1] and *Guizuo Wang*[1]

[1] Department of Respiratory and Critical Care Medicine, Shaanxi Provincial People's Hospital, Xi'an, China, [2] Ruibiao (Wuhan) Biotechnology Co. Ltd., Wuhan, China

OPEN ACCESS

Edited by:
Rifat Hamoudi,
University of Sharjah, United Arab Emirates

Reviewed by:
Wei Li,
The Second Affiliated Hospital of Xi'an Jiaotong University, China
Majid Marjani,
National Research Institute of Tuberculosis and Lung Diseases (NRITLD), Iran

***Correspondence:**
Wei Zhang
zhangwei2384@126.com

Specialty section:
This article was submitted to Pulmonary Medicine, a section of the journal Frontiers in Medicine

Received: 02 December 2020
Accepted: 22 April 2021
Published: 14 May 2021

Citation:
Zhang W, Wang Y, Li W and Wang G (2021) The Association Between the Baseline and the Change in Neutrophil-to-Lymphocyte Ratio and Short-Term Mortality in Patients With Acute Respiratory Distress Syndrome. Front. Med. 8:636869. doi: 10.3389/fmed.2021.636869

Background: Two previous studies have shown that increased neutrophil to lymphocyte ratio (NLR) is associated with short-term prognosis in patients with acute respiratory distress syndrome (ARDS), but it is usually assessed as a single threshold value at baseline. We investigated the relationship between the baseline and the early change in NLR and 30-day mortality in patients with ARDS to evaluate the prognostic value of NLR baseline and NLR changes during the first 7 days after ICU admission.

Methods: This is a retrospective cohort study, with all ARDS patients diagnosed according to the Berlin definition from the Medical Information Mart for Intensive Care III (MIMIC-III) database. We calculated the NLR by dividing the neutrophil count by the lymphocyte count. The multivariable logistic regression analysis was used to investigate the relationship between the baseline NLR and short-term mortality. Then the generalized additive mixed model was used to compare trends in NLR over time among survivors and non-survivors after adjusting for potential confounders.

Results: A total of 1164 patients were enrolled in our study. Multivariable logistic regression analysis showed that after adjusting for confounders, elevated baseline NLR was a significant risk factor predicting 30-day mortality (OR 1.02, 95%CI 1.01, 1.03, $P = 0.0046$) and hospital mortality (OR 1.02, 95%CI 1.01, 1.03, $P = 0.0003$). The result of the generalized additive mixed model showed that the NLR decreased in the survival group and increased in the non-survival group gradually within 7 days after ICU admission. The difference between the two groups showed a trend of increase gradually and the difference increased by an average of 0.67 daily after adjusting for confounders.

Conclusions: We confirmed that there was a positive correlation between baseline NLR and short-term mortality, and we found significant differences in NLR changes over time between the non-survival group and the survival group. The early increase in NLR was associated with short-term mortality in ARDS patients.

Keywords: change, neutrophil to lymphocyte ratio, NLR, ARDS, 30-day mortality, intensive care unit

INTRODUCTION

Acute respiratory distress syndrome (ARDS) is a fatal form of acute respiratory failure requiring mechanical ventilation, which is caused by direct (pneumonia or aspiration) or indirect lung injury (sepsis or trauma) (1). It is a type of acute diffuse inflammatory lung injury that results in damage to the pulmonary endothelium, increased capillary permeability, pulmonary edema formation, and thus leads to decreased effective pulmonary ventilation area (2). Despite the efforts in early diagnosis and treatment, to our knowledge, there is no available treatment which can aim directly at the pathological mechanism of ARDS, and mechanical ventilation and supportive care are still the main approaches (1, 3). Approximately 35–46% of patients died consequently during hospitalization, making it one of the most common causes of death in intensive care units (ICU) (4). Therefore, it is urgent to find specific biological markers to accurately identify high-risk patients and adjust clinical treatment and nursing intervention to ultimately improve the prognosis of patients with ARDS.

Inflammatory response plays an important role in the development of ARDS, and is also an important factor affecting the prognosis of ARDS patients (2, 5). *In vivo* and *in vitro* studies have shown that inflammatory response can cause increased permeability of alveolar endothelium and epithelial cells, leading to the occurrence of pulmonary edema (5, 6). Neutrophil lymphocyte ratio (NLR) as a marker of systemic inflammation has been shown to be associated with the prognosis of a variety of diseases, including sepsis (7), COVID-19 pneumonia (8, 9), chronic obstructive pulmonary disease (COPD) (10), acute coronary syndrome (11), and several solid tumors (12–14). Two previous studies have shown that elevated baseline NLR was associated with short-term prognosis in ARDS patients (15, 16). However, these two studies only revealed the relationship between static NLR at baseline and short-term patient prognosis, which may not reflect the overall dynamics of the patient's condition. In this study, we investigated the relationship between baseline and early changes within the first week after ICU admission in NLR and short-term prognosis among ARDS patients.

PATIENTS AND METHODS

Data Sources

This is a retrospective cohort study of 1164 patients with ARDS according to the Berlin definition. We obtained all the data from the Medical Information Mart for Intensive Care III (MIMIC-III), which is a single-center and freely accessible database and contains more than 60,000 health-related hospitalizations from 2001 to 2012 in the ICU of Beth Israel Deaconess Medical Center in Boston. We have completed the online course and passed the online exams (no. 6182750) to gain access to the database. The establishment of the MIMIC III database was approved by the institutional review board of Beth Israel deacons Medical Center and Massachusetts Institute of Technology. Because hospitalization information is anonymous, the informed consent was not required.

Patients

We screened all the patients in the database. Our inclusion criteria were as follows: at least 16 years, ICU stay more than 72 h, ARDS diagnosis meeting Berlin standard at the time of ICU admission, had lymphocyte and neutrophil count within 24 h after ICU admission. We excluded patients with chronic hematologic disorders, lacked the baseline of lymphocyte and neutrophil records. If a patient was admitted repeatedly during the study period, we used only the record of his first ICU admission.

The Berlin standard included: acute onset, arterial oxygen partial pressure (PaO_2)/fraction of inspired oxygen (FiO_2) <300 mmHg and positive end-expiratory pressure (PEEP) ≥5 cm H_2O on the first day of ICU admission, bilateral infiltrates on chest radiograph, absence of heart failure. According to the Berlin standard, ARDS were classified into mild (>200 mmHg, ≤300 mmHg), moderate (>100 mmHg, ≤ 200 mmHg), and severe (<100 mmHg) based on the PaO_2/FiO_2 ratio.

Data Extraction

We used the Structured Query Language to extract the data. We extracted or calculated the following variables, including the baseline characteristics (age, gender, ethnicity, admission type), the patients' comorbidity, the Elixhauser Comorbidity Index (SID30), the risk factors leading to ARDS, the vital signs within 24 h after ICU admission (heart rate, temperature, mean arterial pressure, Spo2), the severity of organ dysfunction (Simplified Acute Physiology Score, SAPS II; Oxford Acute Severity of Illness Score, OASIS; Sequential Organ Failure Assessment, SOFA), PaO_2/FiO_2 at diagnosis, PEEP at diagnosis and the treatment received (ventilation received; vasopressor therapy; renal replacement therapy; corticosteroids therapy; antibiotic therapy). The serious score of organ dysfunction was estimated for all patients within 24 h of ICU admission.

The baseline of NLR was determined by the absolute neutrophil count divided by the absolute lymphocyte count based on the first laboratory parameters after ICU admission. Repeated measurements of NLR were performed during the first 7 days after ICU admission. The repeated measurements of NLR were irregularly spaced over time.

Statistical Analysis

We processed and analyzed all the data by EmpowerStats software (www.empowerstats.com version R.3.4.3) and statistical software package R. We presented the continuous variables as the mean (SD) and compared them by Student's *t*-test (normal distribution) or Mann-Whitney test (non-normal distribution); we presented the categorical variables as percentages and compared them by chi-square test. A two-tailed $P < 0.05$ was considered statistically significant.

We first analyzed the relationship between the baseline NLR and short-term clinical outcomes in ARDS patients. We divided the patients into three groups according to the tertile of the baseline NLR values. We used multivariable logistic regression analysis and smooth curve fitting to test the independent effects of the baseline NLR and in-hospital and 30-day mortality with crude and full models. The adjusted variables included age,

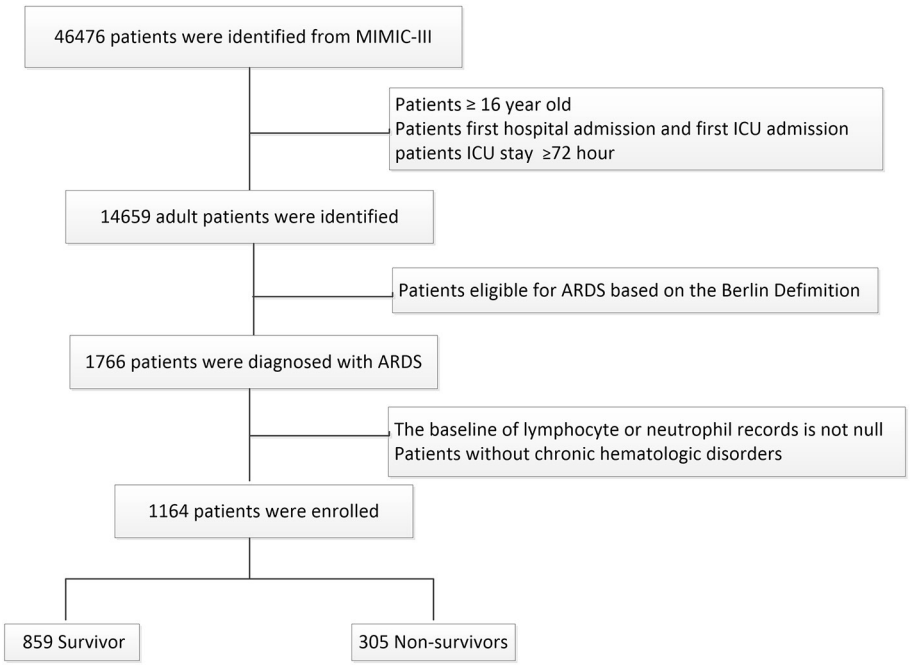

FIGURE 1 | Flow chart of the current study.

gender, ethnicity, smoking, admission type, COPD, hypertension, tumor, diabetes mellitus, renal failure, SID30, pneumonia, sepsis, aspiration, trauma/surgery, other non-pulmonary, PaO_2/FiO_2, SAPS II, OASIS, SOFA, corticosteroids therapy, antibiotic therapy, vasopressor therapy, ventilation received and renal replacement therapy. We selected those confounders based on their associations with the outcomes of interest or a change in effect estimate of more than 10%.

Then we analyzed the relationship between the early change of NLR and 30-day mortality. We showed the difference in NLR between survivors and non-survivors within the first 7 days after ICU admission. We used the generalized additive mixed model (GAMM) to investigate the early changes of NLR over time between survivors and non-survivors, with crude and full models. The GAMM is commonly used to analyze the results of repeated measurements, especially when the interval between repeated measurements is irregular and some data is missing (17, 18).

RESULTS

Characteristics of Patients

A total of 1164 patients with ARDS were included in this study, which contained 859 survivors and 305 non-survivors who were stratified on 30-day mortality. The flowchart of study cohort selection was shown in **Figure 1**. The characteristics of the study participants were displayed in **Table 1**.

The average age of the study participants was 60.27 ± 17.74 years and 40.87% of participants were female. The main risk factors of ARDS were non-pulmonary sepsis ($N = 549$ 47.12%) and pneumonia ($N = 345$ 29.64%). There were 208 (17.87%), 534 (45.88%), and 422 (36.25%) patients with mild, moderate and severe ARDS, respectively, upon ICU admission. The median values of NLR at baseline were 13.14 ± 10.66 in survivors and 16.78 ± 13.38 in non-survivors, respectively. We found that there was a significant difference between the two groups in terms of age, ethnicity, smoking and admission type; The SAPS II, OASIS, and SOFA scores within 24 h of ICU admission were significantly higher in non-survivors than that in survivors. There were also significant differences in vital signs (temperature, mean arterial pressure, Spo2, and PaO_2/FiO_2 at diagnosis) and treatment received (mechanical ventilation and antibiotic therapy).

Association Between Baseline NLR and Mortality

We divided all the patients into three groups according to the tertiles of baseline NLR and **Table 2** displayed the clinical outcomes of the subjects across the tertile of baseline NLR. Patients with high NLR (NLR ≥14.8) had shorter days free of mechanical ventilation, higher in-hospital, and 30-day mortality.

We used the smooth curve fitting to show the association between baseline NLR levels and risk of in-hospital and 30-day mortality which was presented in **Figure 2**. Taking NLR on admission as a continuous variable, there was a significant positive association with the short-term mortality in the adjusted model.

We further evaluated this finding by the multivariable logistic regression analysis, which was shown in **Table 3**. As a continuous variable, after adjusting for the clinical confounders listed, an SD increase in baseline NLR levels was associated with a 2% higher

TABLE 1 | Baseline characteristics of total cohort, 30-day survivors, and 30-day non-survivors.

Variables	Total cohort *N* = 1164	30-day survivor *N* = 859	30-day non-survivors *N* = 305	*P*-value
Age (years)	60.27 ± 17.74	58.23 ± 17.53	66.03 ± 17.06	<0.001
Female	479 (40.87%)	346 (40.28%)	129 (42.30%)	0.538
Ethnicity				<0.001
Caucasian	782 (67.18%)	606 (70.55%)	176 (57.70%)	
Black	64 (5.50%)	48 (5.59%)	16 (5.25%)	
Hispanic	30 (2.58%)	26 (3.03%)	4 (1.31%)	
Others	288 (24.74%)	179 (20.84%)	109 (35.74%)	
Smoking, *n* (%)	595 (51.12%)	452 (52.62%)	143 (46.89%)	<0.001
Admission type				0.033
Emergency	1021 (87.71%)	744 (86.61%)	277 (90.82%)	
Urgent	94 (8.08%)	80 (9.31%)	14 (4.59%)	
Elective	49 (4.21%)	35 (4.07%)	14 (4.59%)	
Risk factor, *n* (%)				
Pneumonia	345 (29.64%)	235 (27.36%)	110 (36.07%)	0.004
Non-pulmonary sepsis	549 (47.12%)	390 (45.40%)	159 (52.13%)	0.043
Aspiration	77 (6.62%)	56 (6.52%)	21 (6.89%)	0.825
Trauma/surgery	293 (25.17%)	250 (29.10%)	43 (14.10%)	<0.001
Other non-pulmonary	328 (28.18%)	236 (27.47%)	92 (30.16%)	0.370
Comorbidity				
COPD	61 (5.24%)	43 (5.01%)	18 (5.90%)	0.546
Tumor	78 (6.70%)	39 (4.54%)	39 (12.79%)	0.001
Renal failure	140 (12.03%)	98 (11.41%)	42 (13.77%)	0.276
Hypertension	121 (10.40%)	92 (10.71%)	29 (9.51%)	0.555
Diabetes mellitus	272 (23.37%)	204 (23.75%)	68 (22.30%)	0.606
SID30	8.51 ± 7.58	7.73 ± 7.40	10.70 ± 7.63	<0.001
Severity scale				
SAPSII	44.36 ± 15.02	41.89 ± 13.79	51.30 ± 16.16	<0.001
OASIS	38.86 ± 8.08	37.92 ± 7.81	41.50 ± 8.25	<0.001
SOFA	7.20 ± 3.65	6.81 ± 3.35	8.30 ± 4.22	<0.001
Baseline vital data				
Temperature, °C	37.12 ± 0.79	37.20 ± 0.76	36.89 ± 0.81	<0.001
HR, beats/min	91.40 ± 17.28	91.66 ± 17.21	90.64 ± 17.49	0.375
MAP mmHg	76.52 ± 9.63	77.42 ± 9.58	73.98 ± 9.33	<0.001
Spo2	96.82 ± 2.95	97.01 ± 2.84	96.30 ± 3.18	<0.001
PaO_2/FiO_2 at diagnosis	136.57 ± 64.37	140.08 ± 63.98	126.69 ± 64.54	<0.001
PEEP at diagnosis	8.33 ± 13.57	7.91 ± 3.96	9.51 ± 25.65	0.076
NLR at diagnosis	14.10 ± 11.54	13.14 ± 10.66	16.78 ± 13.38	<0.001
Berlin classification, *n* (%)				0.007
Mild	208 (17.87%)	162 (18.86%)	46 (15.08%)	
Moderate	534 (45.88%)	408 (47.50%)	126 (41.31%)	
Severe	422 (36.25%)	289 (33.64%)	133 (43.61%)	
Treatment received				
Ventilation received	1032 (88.66%)	776 (90.34%)	256 (83.93%)	0.002
Vasopressor therapy	586 (50.34%)	426 (49.59%)	160 (52.46%)	0.390
Renal replacement therapy	74 (6.36%)	57 (6.64%)	17 (5.57%)	0.514
Corticosteroids therapy	87 (7.47%)	62 (7.22%)	25 (8.20%)	0.576
Antibiotic therapy	549 (47.16%)	444 (51.69%)	105 (34.43%)	<0.001

Data were mean ± SD, n (%). p-values comparing groups were from Student's t-test or Mann-Whitney test for continuous data and chi-squared test for categorical variables. COPD, chronic obstructive pulmonary disease; SID30, elixhauser comorbidity score; MAP, mean arterial pressure; HR, heart rate; PaO_2/FiO_2, arterial oxygen partial pressure/fraction of inspired oxygen; SAPSII, Simplified Acute Physiology Score; OASIS, Oxford Acute Severity of Illness Score; SOFA, Sequential Organ Failure Assessment; PEEP, positive end-expiratory pressure.

TABLE 2 | Outcomes of the patients with ARDS across tertile of the baseline NLR.

Variables	All patients	NLR			*P*-value
		<7.5	≥7.5, <14.8	≥14.8	
n	1,164	388	388	388	
Time in ICU (days)	15.53 ± 13.13	15.13 ± 12.20	15.81 ± 12.80	15.63 ± 14.33	0.757
Time in hospital (days)	22.34 ± 16.68	22.56 ± 17.67	22.25 ± 14.94	22.21 ± 17.34	0.950
Days free of MV at day 30	15.37 ± 11.07	16.39 ± 10.62	16.54 ± 10.69	13.19 ± 11.57	<0.001
In-hospital mortality	336 (28.87%)	91 (23.45%)	103 (26.55%)	142 (36.60%)	<0.001
30-day mortality	305 (26.20%)	82 (21.13%)	91 (23.45%)	132 (34.02%)	<0.001

Data were mean ± SD, n (%). p-values comparing groups were from Student's t-test for continuous data and chi-squared test for categorical variables.

risk of 30-day mortality (OR 1.02, 95% CI, 1.01, 1.03, $P = 0.0046$), and there was a similar trend for in-hospital mortality (OR 1.02, 95% CI, 1.01, 1.03, $P = 0.0004$). When RDW was assessed as tertiles, we found that patients in high baseline NLR (NLR ≥14.8) also had significantly higher risks of in-hospital (OR 1.48, 95% CI 1.03–2.12, $P = 0.0319$) and 30-day (OR 1.48, 95% CI 1.02–2.16, $P = 0.0409$) mortality than patients in low group (NLR <7.5) in the adjusted model.

The subgroup analyses for the relationship between baseline NLR and mortality were presented in **Supplementary Table 1**, which were performed according to age, gender, race, smoking, type of admission, risk factor, comorbidity, Berlin classification, and treatment received. The results showed that in different subgroups the relationship between baseline NLR and the risk of mortality stably existed except for patients of other race.

Association Between Early Change in NLR and Mortality

We compared the difference in NLR between 30-day survivors and 30-day non-survivors on admission, on the 2–3th, the 4–5th, and the 6–7th day. We found that there were significant differences in NLR between the survival and the non-survival at the time points mentioned above. The result was shown in **Table 4**.

We used GAMM to show the changes in NLR over time (the first week after ICU admission) between 30-day survivors and 30-day non-survivors after adjusted for clinical confounders listed. The result was presented in **Figure 3**. We found that, as time went on, NLR increased in the non-survival group. While the trend was reversed and it decreased in the survival group gradually within 1 week after ICU admission. And the difference between the two groups increased over time.

Furthermore, we revealed the association between early changes in NLR and 30-day mortality in ARDS patients which was presented in **Table 5**. The results indicated that NLR in the non-survival group was significantly higher than that in the survival group, and more importantly the difference between the two groups showed an increasing trend within 1 week after ICU admission. This difference increased by an average of 0.69 per day, and the results were consistent in the adjusted model ($\beta = 0.67$, 95% CI 0.23 1.11, $P = 0.0030$). These trends were also observed for in-hospital mortality.

DISCUSSION

In this retrospective cohort study, we confirmed that there was a significant positive correlation between baseline NLR and short-term mortality of patients with ARDS. High NLR at ICU admission was associated with higher 30-day and in-hospital mortality. Moreover, the NLR dynamic during the first 7-days after ICU admission also appears to be a good prognostic factor in patients with ARDS. We found that NLR increased gradually within 7 days after ICU admission in the non-survival group, but decreased gradually in the survival group. Furthermore, this difference between the two groups increased significantly over time. The relationship remained stable after adjusting for clinical confounders. This might suggest that an early increase in NLR is associated with poor short-term prognosis in ARDS patients.

Previous studies have shown that increased NLR was associated with short-term prognosis in a variety of diseases, including tumors, cardiovascular disease, and inflammatory diseases (7, 8, 10–12, 14, 19, 20). To our knowledge, there are only two previous studies on the relationship between baseline NLR and clinical outcomes of ARDS. The results of these two studies both showed that increased NLR on admission was associated with poor outcomes of ARDS patients. Wang et al. suggested that NLR >14 can be used as the cut-off threshold for predicting the 28-day mortality in patients with ARDS (16). Li et al. found that combining NLR could improve the prognostic value of APACHE II score and Berlin classification than using any of them alone (15). Our results for the relationship between baseline NLR and short-term prognosis in ARDS patients were consistent with previous studies. However, there is no study to explore the association between an early change of NLR and mortality in ARDS patients, which may reflect the comprehensive dynamic changes of the patient's condition and the evolution of the disease.

Therefore, we first used the GAMM model to explore the temporal variation of NLR in ARDS patients and its relationship with short-term outcomes. First, our study showed that NLR changed over time in ARDS patients within the first 7 days after ICU admission. Second, we compared the different trends of NLR over time between survival and death groups. Finally, the GAMM model was used to investigate the relationship between early changes in NLR and short-term prognosis in ARDS patients. We found that the difference between the two groups showed an

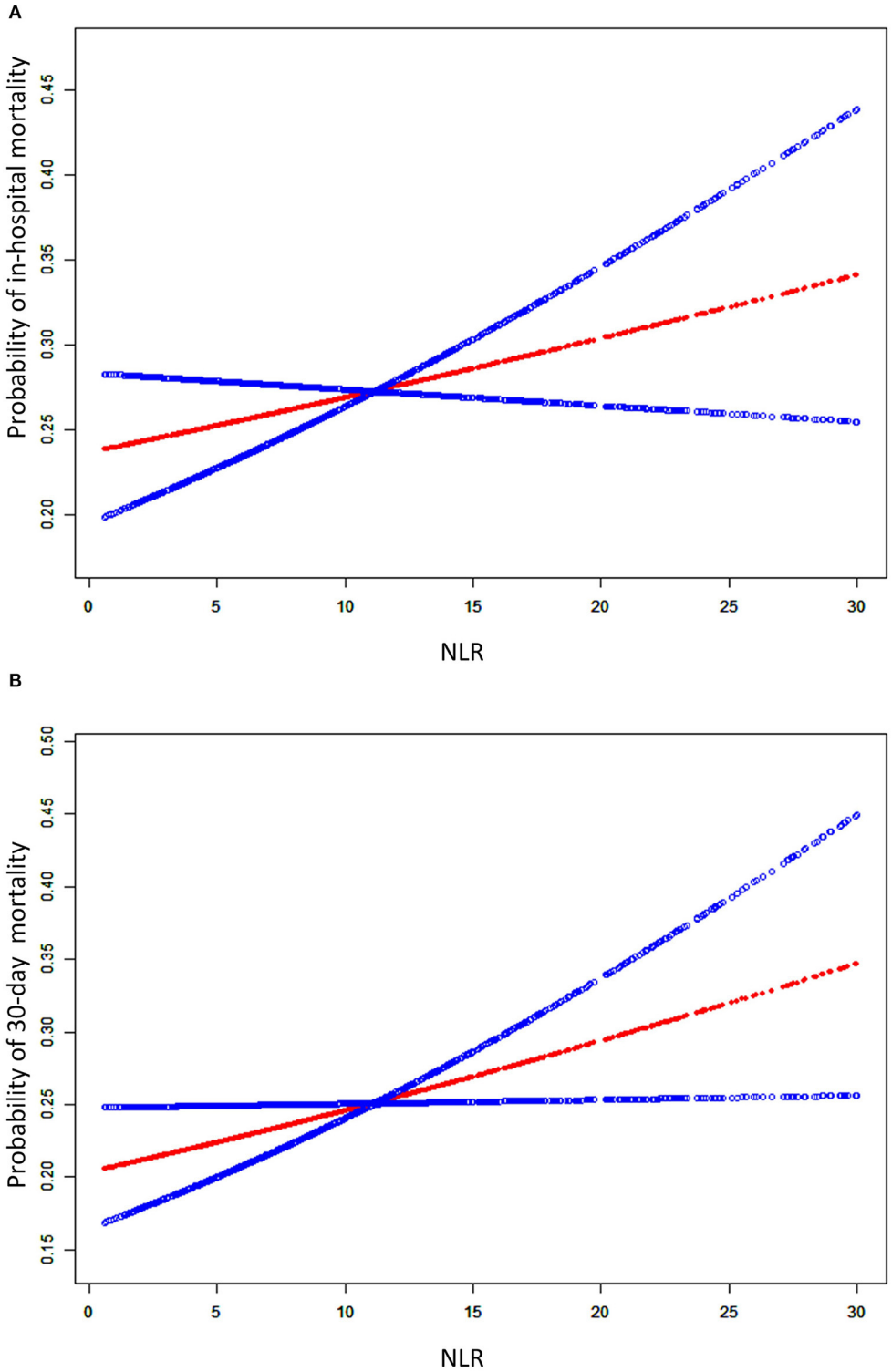

FIGURE 2 | A smooth curve fitting for the relationship between the baseline NLR and the risk of in-hospital mortality **(A)** and 30-day mortality **(B)**. The resulting figures show the risk of mortality in the y-axis and the NLR (continuous variable) in the x-axis. The red line shows the dose-response curve between NLR and probability of short-term mortality, the two blue lines refer to 95% CIs. A positive relationship between NLR and the risk of short-term mortality was observed after adjusting for age, gender, ethnicity, smoking, admission type, COPD, hypertension, tumor, diabetes mellitus, renal failure, SID30, pneumonia, sepsis, aspiration, trauma/surgery, other non-pulmonary, PaO_2/FiO_2, SAPS II, OASIS, SOFA, corticosteroids therapy, antibiotic therapy, vasopressor therapy, ventilation received, and renal replacement therapy by spline smoothing plot.

TABLE 3 | Multivariable logistic regression analysis of baseline NLR for mortality.

Exposure	Non-adjusted			Adjust I			Adjust II		
30-day mortality	**OR**	**95% CI**	***p*-value**	**OR**	**95% CI**	***p*-value**	**OR**	**95% CI**	***p*-value**
NLR Per 1 sd	1.03	(1.01, 1.04)	<0.0001	1.02	(1.01, 1.03)	0.0003	1.02	(1.01, 1.03)	0.0046
NLR tertile									
T1	1.0	(Reference)		1.0	(Reference)		1.0	(Reference)	
T2	1.14	(0.82, 1.60)	0.4378	1.07	(0.75, 1.53)	0.6921	1.09	(0.74, 1.60)	0.6643
T3	1.92	(1.39, 2.65)	<0.0001	1.74	(1.24, 2.45)	0.0015	1.48	(1.02, 2.16)	0.0409
In-hospital mortality	**OR**	**95% CI**	***p*-value**	**OR**	**95% CI**	***p*-value**	**OR**	**95% CI**	***p*-value**
NLR Per 1 sd	1.03	(1.02, 1.04)	<0.0001	1.02	(1.01, 1.04)	<0.0001	1.02	(1.01, 1.03)	0.0004
NLR tertile									
T1	1.0	(Reference)		1.0	(Reference)		1.0	(Reference)	
T2	1.18	(0.85, 1.63)	0.3201	1.11	(0.78, 1.54)	0.5510	1.15	(0.80, 1.66)	0.4544
T3	1.88	(1.38, 2.58)	<0.0001	1.71	(1.23, 2.39)	0.0014	1.48	(1.03, 2.12)	0.0319

OR, odds ratio; CI, confidence interval.

Adjusted I for age, gender, ethnicity, smoking, admission type.

Adjusted II for age, gender, ethnicity, smoking, admission type, COPD, hypertension, tumor, diabetes mellitus, renal failure, SID30, pneumonia, sepsis, aspiration, trauma/surgery, other non-pulmonary, PaO_2/FiO_2, SAPSII, OASIS, SOFA, corticosteroids therapy, antibiotic therapy, vasopressor therapy, ventilation received, and renal replacement therapy.

TABLE 4 | The evolution of NLR after ICU admission between 30-day survivors and 30-day non survivors.

Time	NLR, mean (SD) median (25th–75th percentile)		
	Survivors	**Non-survivors**	***P*-value**
On admission	13.14 (10.66), 9.89 (5.97–16.40)	16.78 (13.38), 12.67 (6.96–22.32)	<0.001
On 2–3th day	11.97 (9.16), 9.08 (6.15–15.48)	17.39 (15.09), 13.33 (6.87–20.74)	<0.001
On 4-5th day	12.52 (9.31), 9.66 (5.86–15.70)	18.68 (19.04), 12.09 (8.06–20.53)	<0.001
On 6–7th day	11.73 (9.89), 9.25 (5.90–14.11)	21.25 (22.87), 13.56 (8.21–21.83)	<0.001

p-value: as for the difference between survivors and non-survivors; Mann-Whitney test was applied for the variables with a skewed distribution.

increasing trend (an average of 0.69 per day) within 1 week after ICU admission.

The systemic inflammatory response is closely related to the occurrence and development of ARDS (2, 5). Elevated levels of inflammatory markers were associated with poor clinical outcomes of ARDS patients (21). Previous studies have shown that increased NLR including neutrophils rising and lymphocytes apoptosis, can be used as a marker of systemic inflammation to reflect the relative degree of inflammation and host immune status (22). In the latest study, the increased NLR can be used as an indicator to predict the development of ARDS in patients with COVID-19 (8). However, the physiologic mechanism behind the association between elevated NLR and poor clinical outcomes in ARDS remains unclear. We can give some possible reasons.

The literature showed that neutrophil counts are positively correlated with the degree of inflammation in ARDS (23). It has been reported that neutrophils and neutrophil-derived particles are significantly increased in bronchoalveolar lavage fluid of ARDS patients (24, 25). Several studies have shown that during the occurrence of acute lung injury (ALI), neutrophils are the first immune cells to be recruited to inflammatory sites, after being stimulated by chemokines released from damaged lung tissue. Activated neutrophils can trigger oxidative stress, release proteases, and form neutrophils extracellular traps (NETs), which induce positive feedback and further enhance the inflammatory response to lung damage (5, 23, 26). Recent studies also showed that increased neutrophils and neutrophil extracellular traps are key pathological drivers of progressive lung injury in COVID-19 patients (27). Targeting neutrophil therapy may improve the clinical outcomes of ARDS caused by SARS-COV-2 infection (19). Previous studies have shown that lymphopenia was associated with high mortality in patients with systemic inflammatory response syndrome and ARDS caused by COVID-19 (28, 29). Lymphocytes play an important role in regulating appropriate inflammatory responses, and lymphopenia may perpetuate harmful inflammation (15). Moreover, *in vitro* experiments, when lymphocytes were cultured with neutrophils, their cytolytic activity was inhibited, and the degree of inhibition increased with the addition of neutrophils (30). NLR reflects the balance between lymphocytes and neutrophils and may reflect the immune status more comprehensively. Therefore, we speculated that the dynamic elevation of NLR may reflect the severity of inflammatory response in ARDS patients, which can be an important indicator for monitoring the clinical prognosis of ARDS.

Although many studies have assessed the prognosis of ARDS patients, none of the biomarkers is perfect (31). NLR is the ratio of neutrophil count to lymphocyte count that can be obtained through routine blood tests without any additional cost, which may make it more convenient for clinical use. Early changes in

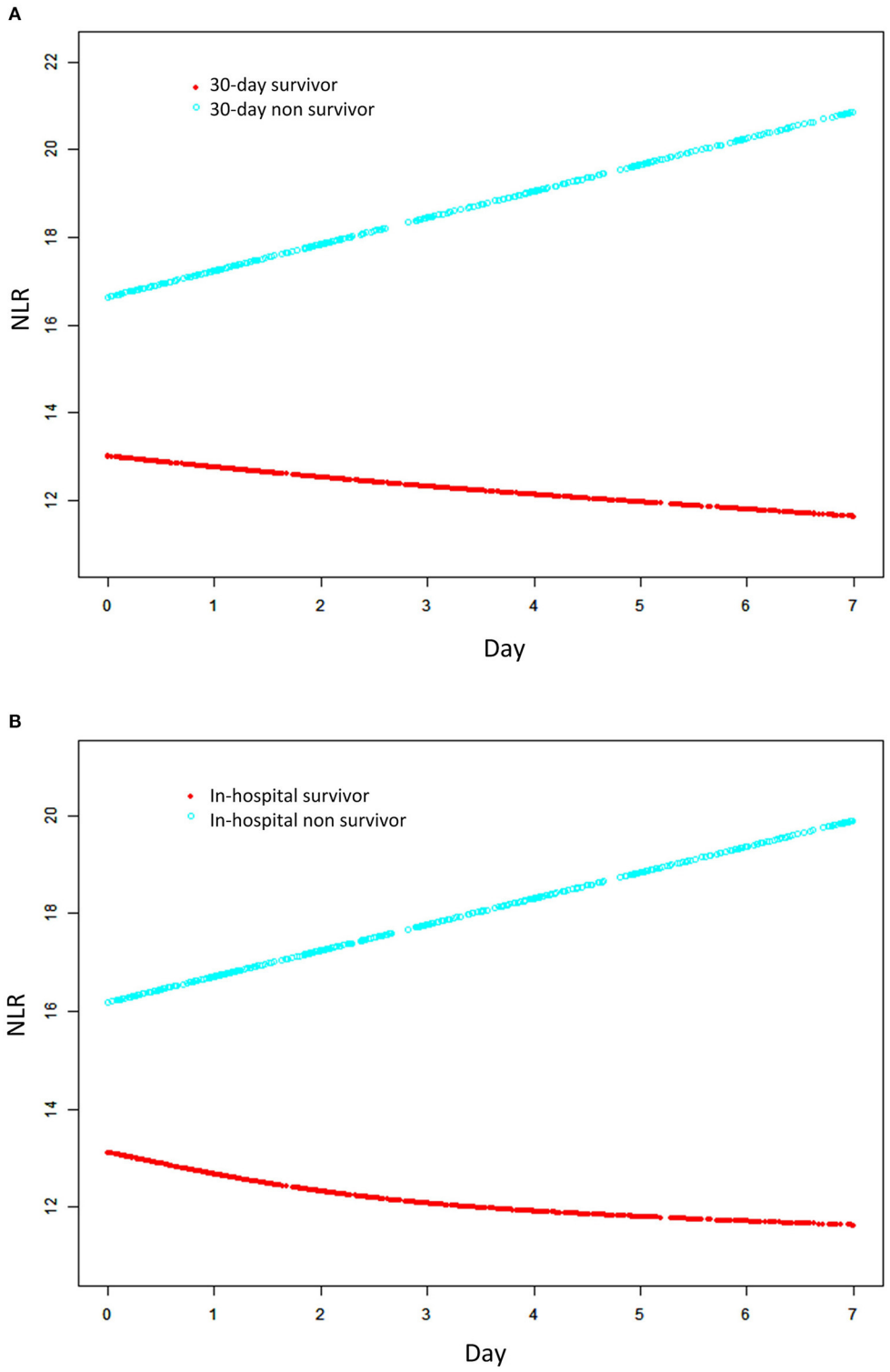

FIGURE 3 | Association between changes in NRL and 30-day mortality **(A)** and in-hospital mortality **(B)**. A linear association between changes in NLR and mortality was found in a generalized additive mix model (GAMM). Smooth curve fitting graph illustrated the NLR in 1164 ARDS patients based on the days after admission to ICU. The red line represented the survivors. The blue line represented the non-survivors. All adjusted for age, gender, ethnicity, smoking, admission type, COPD, hypertension, tumor, diabetes mellitus, renal failure, SID30, pneumonia, sepsis, aspiration, trauma/surgery, other non-pulmonary, PaO_2/FiO_2, SAPS II, OASIS, SOFA, corticosteroids therapy, antibiotic therapy, vasopressor therapy, ventilation received, and renal replacement therapy.

TABLE 5 | Relationship between changes (0–7 days) NLR and short-term mortality in patients with ARDS derived from a generalized additive mixed model (GAMM).

	Unadjusted		Adjusted I		Adjusted II	
30-day mortality	**β (95%CI)**	***P*-value**	**β (95%CI)**	***P*-value**	**β (95%CI)**	***P*-value**
Day	−0.23 (−0.46, −0.001)	0.0496	−0.23 (−0.46, 0.01)	0.0562	−0.25 (−0.48, −0.02)	0.0358
Death	3.86 (2.43, 5.28)	<0.0001	3.43 (1.97, 4.88)	<0.0001	2.64 (1.09, 4.19)	0.0009
Day × death	0.69 (0.25, 1.13)	0.0022	0.68 (0.24, 1.12)	0.0026	0.67 (0.23, 1.11)	0.0030
In-hospital mortality	**β (95%CI)**	***P*-value**	**β (95%CI)**	***P*-value**	**β (95%CI)**	***P*-value**
Day	−0.30 (−0.54, −0.06)	0.0132	−0.29 (−0.53, −0.06)	0.0159	−0.31 (−0.55, −0.07)	0.0103
Death	3.38 (2.00, 4.77)	<0.0001	2.98 (1.56, 4.39)	<0.0001	2.22 (0.76, 3.73)	0.0032
Day × death	0.75 (0.33, 1.18)	0.0005	0.74 (0.32, 1.16)	0.0006	0.73 (0.31, 1.15)	0.0007

CI, confidence interval; Day, the mean of the increasing of NLR at death = 0 over time (daily); Death, the difference of NLR at day = 0 between the group of death = 1 and the group of death = 0; Day × death, the average increasing in NLR daily under the condition of the group of death = 1 compared with the group of death = 0.

Adjusted I for age, gender, ethnicity, smoking, admission type.

Adjusted II for age, gender, ethnicity, smoking, admission type, COPD, hypertension, tumor, diabetes mellitus, renal failure, SID30, pneumonia, sepsis, aspiration, trauma/surgery, other non-pulmonary, PaO_2/FiO_2, SAPSII, OASIS, SOFA, corticosteroids therapy, antibiotic therapy, vasopressor therapy, ventilation received, and renal replacement therapy.

NLR can be a sensitive indicator of disease severity. Therefore, we believe that dynamic monitoring of NLR after ICU admission is helpful for the early detection of patients with poor prognosis and early adoption of different treatments and nursing measures.

There were some limitations in our study. First, this was a single-center retrospective cohort study, so there was the possibility of selection bias; Second, although we have shown that the increased baseline NLR and an increasing trend over time after ICU admission were related to the poor prognosis of patients with ARDS, the causal relationship between baseline elevated NLR, early change in NLR and mortality cannot be established. So further basic research is needed. Third, the accuracy of the results may be affected due to the lack of information on the active infection (bacterial infection or viral infection) and the medication which can alter NLR levels. Fourth, as a single-center study, the results should be interpreted with caution when implicating in other populations and areas.

CONCLUSION

In our study, there was a positive correlation between baseline NLR and short-term prognosis in ARDS patients. Furthermore, we found that there was a significant difference in the changes of NLR over time between non-survival and survival groups. The early increase in NLR was associated with higher short-term mortality in ARDS patients. These results suggest the potential benefit of monitoring early change in NLR for patients with ARDS. However, prospective studies are needed for further validation.

DATA AVAILABILITY STATEMENT

The original contributions presented in the study are included in the article/**Supplementary Material**, further inquiries can be directed to the corresponding author/s.

AUTHOR CONTRIBUTIONS

WZ designed the study, collected and analyzed data, and contributed to writing this manuscript. YW collected and analyzed data. GW and WL designed and supervised the study and drafted the manuscript. All authors have read and approved the final manuscript.

FUNDING

This study was funded by General Projects of Social Development in Shaanxi Province (2019SF-151) and Natural Science Basic Research Program of Shaanxi (Program No. 2021JQ-907).

ACKNOWLEDGMENTS

The authors thank all the researchers who created and managed the MIMIC III database.

SUPPLEMENTARY MATERIAL

The Supplementary Material for this article can be found online at: https://www.frontiersin.org/articles/10.3389/fmed.2021.636869/full#supplementary-material

REFERENCES

1. Fan E, Brodie D, Slutsky AS. Acute respiratory distress syndrome: advances in diagnosis and treatment. *JAMA*. (2018) 319:698–710. doi: 10.1001/jama.2017.21907
2. Huppert LA, Matthay MA, Ware LB. Pathogenesis of acute respiratory distress syndrome. *Semin Resp Crit Care*. (2019) 40:31–9. doi: 10.1055/s-0039-1683996
3. Ben Salem C. Acute respiratory distress syndrome. *N Engl J Med*. (2017) 377:1903–5. doi: 10.1056/NEJMc1711824

4. Bellani G, Laffey JG, Pham T, Fan E, Brochard L, Esteban A, et al. Epidemiology, patterns of care, and mortality for patients with acute respiratory distress syndrome in intensive care units in 50 countries. *JAMA*. (2016) 315:788–800. doi: 10.1001/jama.2016.0291
5. Yang S, Tsai Y, Pan Y, Hwang T. Understanding the role of neutrophils in acute respiratory distress syndrome. *Biomed J.* (2020) 9:10. doi: 10.1016/j.bj.2020.09.001
6. Wang M, Zhang T, Li L, Xie Q, Wang Y, Li Y, et al. Protective effects of HY1702 on lipopolysaccharide-induced mild acute respiratory distress syndrome in mice. *Eur J Pharmacol.* (2020) 887:173563. doi: 10.1016/j.ejphar.2020.173563
7. Ni J, Wang H, Li Y, Shu Y, Liu Y. Neutrophil to lymphocyte ratio (NLR) as a prognostic marker for in-hospital mortality of patients with sepsis: a secondary analysis based on a single-center, retrospective, cohort study. *Medicine.* (2019) 98:e18029. doi: 10.1097/MD.0000000000018029
8. Ma A, Cheng J, Yang J, Dong M, Liao X, Kang Y. Neutrophil-to-lymphocyte ratio as a predictive biomarker for moderate-severe ARDS in severe COVID-19 patients. *Crit Care.* (2020) 24:288. doi: 10.1186/s13054-020-03007-0
9. Liu Y, Li G, He J, Liu Y, Li M, Zhang R, et al. Combined use of the neutrophil-to-lymphocyte ratio and CRP to predict 7-day disease severity in 84 hospitalized patients with COVID-19 pneumonia: a retrospective cohort study. *Ann Transl Med.* (2020) 8:635. doi: 10.21037/atm-20-2372
10. Guo R, Li J, Ma X, Pan L. The predictive value of neutrophil-to-lymphocyte ratio for chronic obstructive pulmonary disease: a systematic review and meta-analysis. *Expert Rev Resp Med.* (2020) 14:929–36. doi: 10.1080/17476348.2020.1776613
11. Dong C, Wang Z, Chen S. Neutrophil to lymphocyte ratio predict mortality and major adverse cardiac events in acute coronary syndrome: a systematic review and meta-analysis. *Clin Biochem.* (2018) 52:131–6. doi: 10.1016/j.clinbiochem.2017.11.008
12. McLellan P, Henriques J, Ksontini F, Doat S, Hammel P, Desrame J, et al. Prognostic value of the early change in neutrophil-to-lymphocyte ratio in metastatic pancreatic adenocarcinoma. *Clin Res Hepatol Gas.* (2020) 11:101541. doi: 10.1016/j.clinre.2020.08.016
13. Li M, Spakowicz D, Burkart J, Patel S, Husain M, He K, et al. Change in neutrophil to lymphocyte ratio during immunotherapy treatment is a non-linear predictor of patient outcomes in advanced cancers. *J Cancer Res Clin.* (2019) 145:2541–6. doi: 10.1007/s00432-019-02982-4
14. Kim HS, Ku JH. Systemic inflammatory response based on neutrophil-to-lymphocyte ratio as a prognostic marker in bladder cancer. *Dis Markers.* (2016) 2016:8345286. doi: 10.1155/2016/8345286
15. Li W, Ai X, Ni Y, Ye Z, Liang Z. The association between the neutrophil-to-lymphocyte ratio and mortality in patients with acute respiratory distress syndrome: a retrospective cohort study. *Shock.* (2019) 51:161–7. doi: 10.1097/SHK.0000000000001136
16. Wang Y, Ju M, Chen C, Yang D, Hou D, Tang X, et al. Neutrophil-to-lymphocyte ratio as a prognostic marker in acute respiratory distress syndrome patients: a retrospective study. *J Thor Dis.* (2018) 10:273–82. doi: 10.21037/jtd.2017.12.131
17. Najjar SS, Scuteri A, Shetty V, Wright JG, Muller DC, Fleg JL, et al. Pulse wave velocity is an independent predictor of the longitudinal increase in systolic blood pressure and of incident hypertension in the Baltimore Longitudinal Study of Aging. *J Am Coll Cardiol.* (2008) 51:1377–83. doi: 10.1016/j.jacc.2007.10.065
18. Zhao X, Wang K, Zuo P, Liu Y, Zhang M, Xie S, et al. Early decrease in blood platelet count is associated with poor prognosis in COVID-19 patients-indications for predictive, preventive, and personalized medical approach. *EPMA J.* (2020) 11:1–7. doi: 10.1007/s13167-020-00208-z
19. Chiang C, Korinek M, Cheng W, Hwang T. Targeting neutrophils to treat acute respiratory distress syndrome in coronavirus disease. *Front Pharmacol.* (2020) 11:572009. doi: 10.3389/fphar.2020.572009
20. Guo Z, Yu S, Xiao L, Chen X, Ye R, Zheng P, et al. Dynamic change of neutrophil to lymphocyte ratio and hemorrhagic transformation after thrombolysis in stroke. *J Neuroinflamm.* (2016) 13:199. doi: 10.1186/s12974-016-0680-x
21. Calfee CS, Delucchi K, Parsons PE, Thompson BT, Ware LB, Matthay MA. Subphenotypes in acute respiratory distress syndrome: latent class analysis of data from two randomised controlled trials. *Lancet Respir Med.* (2014) 2:611–20 doi: 10.1016/S2213-2600(14)70097-9
22. Faria SS, Fernandes PCJ, Silva MJB, Lima VC, Fontes W, Freitas-Junior R, et al. The neutrophil-to-lymphocyte ratio: a narrative review. *Ecancermedicalscience.* (2016) 10:702. doi: 10.3332/ecancer.2016.702
23. Grommes J, Soehnlein O. Contribution of neutrophils to acute lung injury. *Mol Med.* (2011) 17:293–307. doi: 10.2119/molmed.2010.00138
24. Zhao J, Zhang G, Cui W, Tian B. [Progress of neutrophil extracellular traps in airway inflammation of acute lung injury/acute respiratory distress syndrome: Review]. *Xi Bao Yu Fen Zi Mian Yi Xue Za Zhi.* (2020) 36:664–70.
25. Ojima M, Yamamoto N, Hirose T, Hamaguchi S, Tasaki O, Kojima T, et al. Serial change of neutrophil extracellular traps in tracheal aspirate of patients with acute respiratory distress syndrome: report of three cases. *J Intensive Care.* (2020) 8:25. doi: 10.1186/s40560-020-00444-5
26. Vassallo A, Wood AJ, Subburayalu J, Summers C, Chilvers ER. The counter-intuitive role of the neutrophil in the acute respiratory distress syndrome. *Brit. Med Bull.* (2019) 131:43–55. doi: 10.1093/bmb/ldz024
27. Narasaraju T, Tang BM, Herrmann M, Muller S, Chow VTK, Radic M. Neutrophilia and NETopathy as key pathologic drivers of progressive lung impairment in patients with COVID-19. *Front Pharmacol.* (2020) 11:870. doi: 10.3389/fphar.2020.00870
28. Riff R, Cohen Y, Eini-Rider H, Naamani O, Mazar J, Haviv YS, et al. Systemic inflammatory response syndrome-related lymphopenia is associated with adenosine A(1) receptor dysfunction. *J Leukocyte Biol.* (2017) 102:95–103. doi: 10.1189/jlb.3A0816-345RR
29. Wang A, Gao G, Wang S, Chen M, Qian F, Tang W, et al. Clinical characteristics and risk factors of Acute Respiratory Distress Syndrome (ARDS) in COVID-19 patients in Beijing, China: a retrospective study. *Med Sci Monitor.* (2020) 26:e925974. doi: 10.12659/MSM.925974
30. Chen Y, Yan H, Wang Y, Shi Y, Dai G. Significance of baseline and change in neutrophil-to-lymphocyte ratio in predicting prognosis: a retrospective analysis in advanced pancreatic ductal adenocarcinoma. *Sci Rep.* (2017) 7:753. doi: 10.1038/s41598-017-00859-5
31. Bime C, Camp SM, Casanova N, Oita RC, Ndukum J, Lynn H, et al. The acute respiratory distress syndrome biomarker pipeline: crippling gaps between discovery and clinical utility. *Transl Res.* (2020) 226:105–15. doi: 10.1016/j.trsl.2020.06.010

Conflict of Interest: YW was employed by the company Ruibiao (Wuhan) Biotechnology Co.

The remaining authors declare that the research was conducted in the absence of any commercial or financial relationships that could be construed as a potential conflict of interest.

Copyright © 2021 Zhang, Wang, Li and Wang. This is an open-access article distributed under the terms of the Creative Commons Attribution License (CC BY). The use, distribution or reproduction in other forums is permitted, provided the original author(s) and the copyright owner(s) are credited and that the original publication in this journal is cited, in accordance with accepted academic practice. No use, distribution or reproduction is permitted which does not comply with these terms.

frontiers in Medicine

ORIGINAL RESEARCH
published: 14 May 2021
doi: 10.3389/fmed.2021.619077

Metabolic Fingerprinting Uncovers the Distinction Between the Phenotypes of Tuberculosis Associated COPD and Smoking-Induced COPD

Da Jung Kim[1,2†‡], *Jee Youn Oh*[3†], *Chin Kook Rhee*[4], *Seoung Ju Park*[5], *Jae Jeong Shim*[3] *and Joo-Youn Cho*[1,6*]

[1] Department of Clinical Pharmacology and Therapeutics, Seoul National University College of Medicine and Hospital, Seoul, South Korea, [2] Seoul National University Medical Research Center, Seoul National University College of Medicine and Hospital, Seoul, South Korea, [3] Division of Pulmonary, Allergy and Critical Care Medicine, Department of Internal Medicine, Korea University Guro Hospital, Seoul, South Korea, [4] Division of Pulmonary Medicine, Department of Internal Medicine, Catholic University Seoul Hospital, Seoul, South Korea, [5] Division of Pulmonary Medicine, Department of Internal Medicine, Chonbuk National University Hospital, Jeonju, South Korea, [6] Department of Biomedical Sciences, Seoul National University College of Medicine, Seoul, South Korea

Background: Although smoking is considered the main cause of chronic obstructive pulmonary disease (COPD), several other risk factors, including pulmonary tuberculosis (TB), contribute significantly to disease causation, particularly in developing countries. However, the underlying pathogenesis of TB-associated COPD (T-COPD) is unclear. Moreover, the need for prompt diagnosis and treatment of T-COPD to decrease the future burden of inflammation is underestimated. This study aimed to identify distinctive endogenous metabotypes of T-COPD, compared to smoking-associated COPD (S-COPD).

Methods: Cross-sectional metabolomic analyses and clinical examinations of serum samples were performed for three groups of 168 male subjects: T-COPD ($n = 59$), S-COPD ($n = 70$), and healthy normal controls ($n = 39$). To retain a broad spectrum of metabolites, we performed technically distinct analyses (global metabolomic profiling using LC-QTOFMS and targeted analyses using LC-MS/MS).

Results: Higher levels of IL-6 and C-reactive protein and St. George Respiratory Questionnaire scores were seen in the T-COPD group, compared to those in the S-COPD group. Global metabolomic profiling showed elevated metabolites, including arachidonic and eicosanoic acids, in the T-COPD group. Typical changes in tryptophan catabolism were observed through targeted profiling. Additionally, in the T-COPD group, kynurenine was elevated, and serotonin levels were reduced; therefore, indoleamine dioxygenase (IDO)/tryptophan hydroxylase (TPH) activities were dysregulated. Correlation analyses showed that changes in oxylipins were positively correlated with serum levels of IL-6 and C-reactive protein.

OPEN ACCESS

Edited by:
Hauke Busch,
University of Lübeck, Germany

Reviewed by:
Geoffroy Andrieux,
Universität Freiburg, Germany
Chai K. Lim,
Macquarie University, Australia

***Correspondence:**
Joo-Youn Cho
joocho@snu.ac.kr

[†] These authors have contributed equally to this work

[‡] Present address:
Da Jung Kim,
Metabolomics Core Facility, Department of Transdisciplinary Research and Collaboration, Biomedical Research Institute, Seoul National University Hospital, Seoul, South Korea

Specialty section:
This article was submitted to Pulmonary Medicine, a section of the journal Frontiers in Medicine

Received: *19 October 2020*
Accepted: *12 April 2021*
Published: *14 May 2021*

Citation:
Kim DJ, Oh JY, Rhee CK, Park SJ, Shim JJ and Cho J-Y (2021) Metabolic Fingerprinting Uncovers the Distinction Between the Phenotypes of Tuberculosis Associated COPD and Smoking-Induced COPD. Front. Med. 8:619077. doi: 10.3389/fmed.2021.619077

Conclusion: Patients with TB-related COPD have enhanced inflammatory responses that may be linked to fatty acid pathways and tryptophan catabolism, which could be novel therapeutic targets for T-COPD.

Keywords: chronic obstructive pulmonary disease, tuberculosis, metabolomics, biomarker, smoking

INTRODUCTION

Chronic obstructive pulmonary disease (COPD) is a major global health problem that causes airflow limitation and increases patient vulnerability to exacerbations and serious inflammatory responses (1). Apart from smoking, several other risk factors, including biomass fuel smoke exposure, childhood lower respiratory tract infections, outdoor air pollution, and treated cases of pulmonary tuberculosis (TB) play a significant role in disease etiology, particularly in developing countries (2). Approximately 10 million people are infected with TB annually, and pulmonary system injury is the major effect of TB (3). Appropriate treatment can effectively cure TB. However, permanent COPD occurring after eradication of the organism is seen in more than 50% of the infected patients (3, 4). TB-associated COPD (T-COPD) develops at a younger age compared with smoking-associated COPD (S-COPD) (5–7). However, prompt diagnosis and treatment of T-COPD based on an understanding of the pathogenesis to decrease the future burden of chronic airflow obstruction and inflammation are seldom achieved (8).

T-COPD was previously considered a static disease causing only parenchymal destruction, and extensive research on the treatment and control of morbidities in these patients have not been conducted to the same extent as with S-COPD. However, lung remodeling and chronic inflammatory responses have recently been shown to persist in these patients after treatment completion (9, 10). The pathogenesis and inflammatory properties of T-COPD need to be investigated and compared with those of S-COPD, to evaluate the need for the treatment and management of T-COPD.

Global profiling of metabolites in biofluids and tissues has been popularized for identifying the underlying mechanisms, developing disease-specific or grade-specific biomarkers, and assessing therapeutic effects (11–13). The identification of numerous endogenous metabolites has been used to characterize patients with pulmonary diseases, and endogenous metabotyping is a useful technique to differentiate the characteristic features of diseases with very similar phenotypes, such as asthma and chronic airway obstructive disease (11, 14). In this study, we used metabolomics to characterize patients with S-COPD and T-COPD, and we investigated the associations of various metabolites with these disease groups.

METHODS

Study Population

This multi-center cohort study was performed to identify clinically useful biological markers in chronic airway diseases for the diagnosis and assessment of treatment response, conducted at the Korea University Guro Hospital, Seoul St. Mary's Hospital, and Chonbuk National University Hospital. The study protocol was approved by the institutional review boards (Korea University Guro Hospital: KUGH 13246; Seoul St. Mary's Hospital: KC15OIMI0553; and Chonbuk National University Hospital: 2015-01-018-005), and it fulfilled the tenets of the Declaration of Helsinki. The patients provided written informed consent.

The inclusion criteria for patients with T-COPD were: (1) history of TB with no change in the chest images over the past year; (2) at least one finding of destroyed pulmonary parenchyma on chest images (lung volume loss, bronchovascular distortion, fibrosis, or secondary bronciectasis), with the total volume of all lesions being greater than one-third of one lung, confirmed by a radiologist or pulmonologist; (3) airflow limitation (post-bronchodilator spirometry with forced expiratory volume in 1 second [FEV_1]/forced vital capacity [FVC] $< 70\%$) and no history of asthma or COPD before the diagnosis of TB; and (4) no history of respiratory infections within the previous 6 weeks.

S-COPD was diagnosed according to the American Thoracic Society and Global Initiative for Chronic Obstructive Lung Disease guidelines (post-bronchodilator spirometry with $FEV_1/FVC < 70\%$). Patients with a smoking history of > 10 packs per year were enrolled, and patients with bronchiectasis, sequelae from a prior TB infection, interstitial lung disease, or other diseases causing airflow obstruction, were excluded.

Blood samples and data from healthy normal controls (NC) with no history of COPD or respiratory symptoms, who had visited for general health assessments, were provided by the Biobank of Korea University Guro Hospital (KU Guro Gene Bank 2018-026). Data on age, sex, body mass index (BMI), and smoking status were collected. For patients with S-COPD and T-COPD, the variables collected at baseline were smoking amount, BMI, symptom scores, results of pulmonary function tests, rate of decline in FEV_1, acute exacerbation history, and chest imaging data. Detailed protocol of measurements of clinical parameters is available in the **Supplementary Material**.

Global Metabolomics Profiling Using LC-QTOF-MS

The frozen samples of plasma and urine were briefly diluted with an acetonitrile:methanol:water (3:3:4) mixture (HPLC-grade, Millipore, Bedford, MA, USA) and 10% methanol, respectively. Each sample (5 μL) was loaded onto an Acquity UPLC BEH C18 (1.7 μm, 2.1 mm × 100 mm; Waters Corp., Milford, MA, USA) column and analyzed using an Agilent 6530 QTOF mass spectrometer (Agilent Technologies). The experimental procedure is described in detail in our previous studies (12, 15).

All samples were examined simultaneously in a single run to avoid the batch effect and the overall quality of the analysis procedure was monitored using repeat extracts of a pooled plasma sample.

Targeted Metabolomics Using LC-MS/MS

The AbsoluteIDQ® p180 kit with an LC-MS/MS system was used to quantify 188 metabolites, allowing the concurrent high-throughput detection and quantification of metabolites in serum samples. The sample preparation and LC-MS/MS analytical procedure are described in detail in our previous reports (13). The average % coefficient of variance of analytes ranged between 15–30 % CV range and the concentrations of limit of detection are listed in **Supplementary Table 1**.

Statistical Analysis

Clinical data were presented as the median and interquartile range for continuous variables and as a percentage for categorical variables. Data were compared using the Mann–Whitney *U*-test or Kruskal–Wallis test for continuous variables, and Pearson's χ^2 test or Fisher's exact test for categorical variables. ANCOVA was used to compare age, BMI, smoking and underlying diseases for IL-6 and CRP. Statistical significance was defined as $P < 0.05$. All statistics were analyzed using SPSS 20.0 software (IBM, Chicago, Illinois, USA). We performed logistic regression of discrimination of T-COPD and S-COPD for targeted metabolites. Variables with a $P < 0.05$ on univariate analysis and demographic factors including age, BMI, underlying diseases and smoking history were analyzed using multivariate logistic regression analysis. ROC analysis was done for significant metabolites by multivariate logistic regression.

Statistical analyses for the untargeted and targeted metabolic data and network analysis for visualization are available in the **Supplementary Material**.

RESULTS

Patient Demographics

The study included 168 patients (T-COPD, $n = 59$; S-COPD, $n = 70$; NC, $n = 39$). The median age of NCs was 55.0 years (50.0–65.0 years), and the median BMI, 23.7 (22.3–26.1) (**Supplementary Table 2**). **Table 1** shows the baseline characteristics of patients with T-COPD and S-COPD. The patient-reported scores for symptoms and quality of life were similar in both groups, except for the St. George Respiratory Questionnaire (SGRQ) score, which was higher in the T-COPD group than in the S-COPD group. The rate of FEV_1 decline and the percentage of acute exacerbations did not show significant differences among the groups. C-reactive protein (CRP) levels, erythrocyte sedimentation rate (ESR), and IL-6 levels were significantly higher in patients with T-COPD than in those with S-COPD (**Table 1**).

TABLE 1 | Demographics of patients with S-COPD and T-COPD.

	S-COPD ($N = 70$)	T-COPD ($N = 59$)	*P*-value
Age, years	66.0 (59.0–72.5)	68.0 (64.0–73.0)	0.165
Sex, male	70 (100)	59 (100)	–
BMI, kg/m^2	23.1 (21.1–25.9)	22.9 (21.1–25.5)	0.519
Smoking amount (pack-year)	40.0 (30.0–50.0)	0.0 (0.0–30.0)	<0.001
Comorbidities			
Heart disease	27 (38.6)	25 (42.4)	0.661
Cerebrovascular disease	9 (12.9)	5 (8.5)	0.425
Depression	2 (2.9)	1 (1.7)	0.663
Pulmonary function tests			
FEV_1 % predicted	62.5 (45.8–71.0)	54.0 (45.0–73.0)	0.496
FVC % predicted	84.0 (74.0–93.3)	78.0 (66.0–89.0)	0.089
FEV_1/FVC % predicted	54.5 (41.0–62.0)	53.0 (42.0–65.0)	0.465
DL_{CO} %	80.5 (64.8–97.0)	75.0 (62.0–87.0)	0.180
Symptom scores			
mMRC	1.0 (0.0–1.0)	1.0 (0.0–1.0)	0.654
CAT	14.0 (10.0–19.0)	17.0 (11.0–21.0)	0.096
SGRQ	16.9 (9.0–29.2)	22.1 (13.8–34.5)	0.048
FEV_1 decline ml/yr	0.5 (-50.0–170.0)	60.0 (-30.0–170.0)	0.335
Frequent AE *n*, (%)	7 (10.0%)	12 (20.3%)	0.099
Inflammatory markers			
IL-6 (pg/dl)	1.46 (0.43–2.46)	2.67 (1.52–6.80)	<0.001*
ESR (mm/h)	10.00 (6.00–16.25)	15.00 (7.00–21.00)	0.011*
CRP (mg/dl)	1.25 (0.63–2.30)	3.39 (1.49–6.74)	0.044*

Data are presented as median (interquartile range) for continuous variables and number (percentage) for categorical variables.

**This P-value was analyzed by ANCOVA (after adjusting age, BMI, smoking, and underlying diseases).*

AE, acute exacerbation; BMI, body mass index; CAT, chronic obstructive pulmonary disease assessment test; CRP, C-reactive protein; ESR, erythrocyte sedimentation rate; DL_{CO}, diffusing capacity of the lung for carbon monoxide; FEV_1, forced expiratory volume in 1 s; FVC, forced vital capacity; IL-6, interleukin-6; mMRC, modified Medical Research Council; S-COPD, smoking-induced chronic obstructive pulmonary disease; SGRQ, St. George Respiratory Questionnaire; T-COPD, tuberculosis-associated COPD.

Metabotyping of Patients: Global and Targeted Metabolic Profiling

The metabolic profiling workflow is shown in **Figure 1**. We used two different techniques to obtain a broad range of candidate metabolites. We performed global metabolomics profiling, which can screen thousands of unknown features in two conditions. The detected metabolic features were then subjected to statistical analyses. **Supplementary Figure 1** shows the results of the unsupervised pattern recognition analysis. **Supplementary Figures 1A–C** shows the score plots describing variation and account for the varied influences of the NC and S-COPD groups, the NC and T-COPD groups, and the T-COPD and S-COPD groups. In the univariate analysis, FDR-adjusted values <0.05 with a 2.0-fold change were applied for marker selection. Sixty-nine metabolites remained after the univariate analysis compared the NC and S-COPD groups, and 58 metabolites remained after the comparison for the NC and T-COPD groups. Among these, 29 metabolites overlapped and their changes (increase or decrease) showed similar trends (**Figure 2A**). Volcano plots of each analysis are available in **Supplementary Figure 2**.

For further analysis, targeted metabolic profiling was performed, which measures the absolute concentrations of

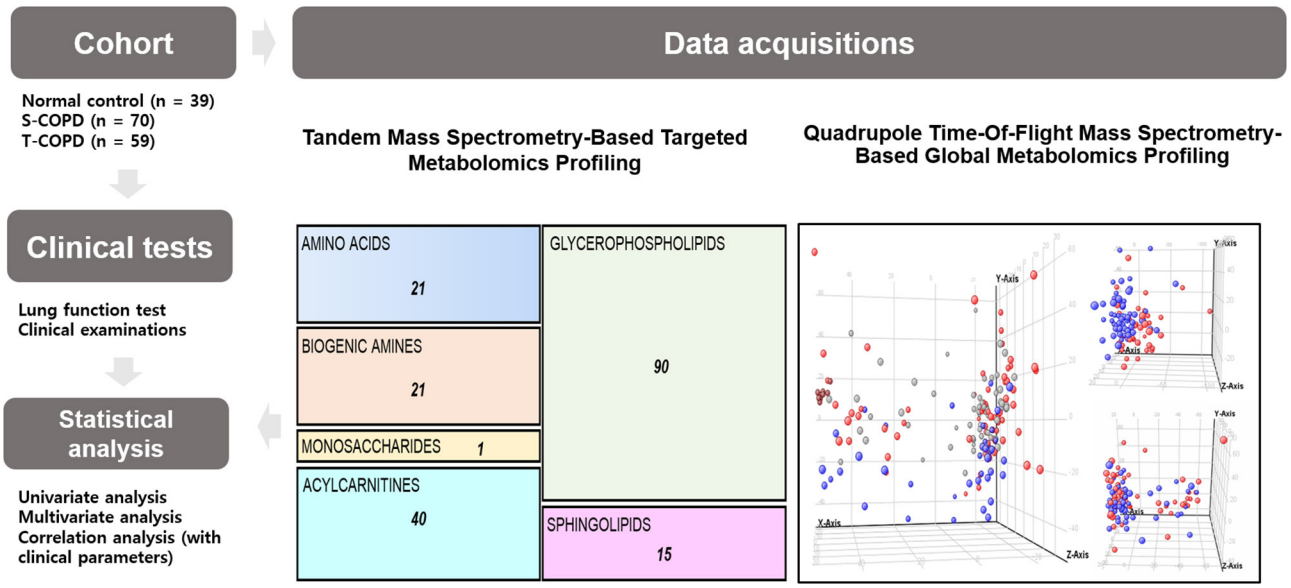

FIGURE 1 | Schematic of the study. This study included 39 healthy subjects, 70 patients with S-COPD, and 59 patients with T-COPD. All patients underwent clinical examinations, including lung function tests and metabolic profiling. For the targeted analysis, a tandem mass spectrometry-based technique was used. The absolute quantification of 188 metabolites, including 21 amino acids, 21 biogenic amines, one monosaccharide, 40 acylcarnitines, 90 glycerophospholipids, and 15 sphingolipids, was performed. For global metabolomic profiling, a QTOF-MS-based technique was chosen. Metabolic biomarkers were selected by performing multivariate and univariate analyses. The correlations of the metabolic biomarkers with clinical parameters were then calculated. NC, normal control; T-COPD, TB-associated COPD; S-COPD, smoking-associated COPD.

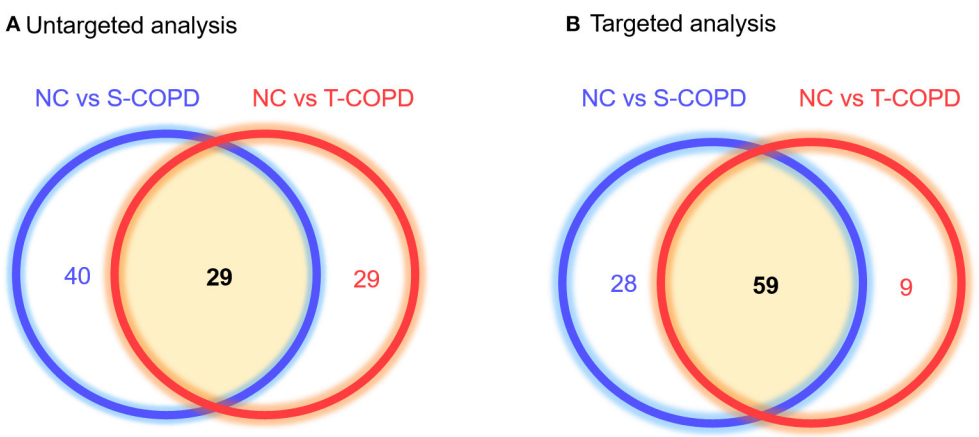

FIGURE 2 | Venn diagram of metabolites identified in patients with T-COPD and S-COPD. **(A)** Comparison of the NC and S-COPD groups revealed that 8,183 ions and 69 metabolites were significantly altered. In the comparison of the NC and T-COPD groups, 5,193 ions were detected, and 58 metabolites were significantly different. Twenty-nine metabolites were shared by the two COPD groups. **(B)** Using the targeted analysis, 188 metabolites were quantified, 87 metabolites were significantly altered between the NC and S-COPD groups, and 68 metabolites were significantly altered between the NC and T-COPD groups. Fifty-nine metabolites overlapped in these two comparisons and their direction of regulation was also similar in the S-COPD and T-COPD groups, compared to the NC group. The blue circle indicates metabolic biomarkers obtained from the comparison of the NC and S-COPD groups, and the red circle represents metabolic biomarkers identified in the comparison of the NC and T-COPD groups. NC, normal control; T-COPD, TB-associated COPD; S-COPD, smoking-associated COPD.

molecules and the conversion rates from one molecule to another. For the targeted analysis, 188 metabolites were quantified based on the LC-MS analyses. This technique provided quantitative data for 40 acylcarnitines, 42 amino acids, biogenic amines, monosaccharides, 15 sphingolipids, and 90 glycerophospholipids in each sample. The absolute

concentration in each sample was then adjusted for statistical analysis, with a *P*-value <0.05, indicating significance. We obtained 87 distinct metabolites that differentiated the NC and S-COPD groups, and 68 metabolites that differentiated the NC and T-COPD groups (**Figure 2B**).

Significantly altered metabolites are displayed in **Figure 3**. All the identified metabolites were mapped and linked to each other based on their biological interactions. In patients with S-COPD, we observed increased levels of long-chain fatty acids (specifically myristoleic acid, palmitic acid, and oleic acid), bile acid-related metabolites, and multiple glycerophospholipids and acylcarnitines (**Figure 3A** and **Supplementary Table 3**). All metabolites identified using global metabolomics are listed in **Supplementary Table 4**. In the T-COPD group, we observed specific changes in the arachidonic and eicosanoic acid metabolic pathways (**Figure 3A** and **Supplementary Table 3**). Similar changes in the levels of myristoleic acid, palmitic acid, oleic acid, ethyl arachidonate, and prostaglandin E, were observed in all the groups. However, there was more than a two-fold increase in the levels of arachidonic acid, eicosanoic acid, docosapentaenoic acid, dihomo-alpha-linolenic acid, dihomo-linoleic acid, hydroxyeicosatrienoic acid (HETrE), and hydroxyeicosapentaenoic acid (HEPE) in the T-COPD patients, compared to the healthy controls, whereas no gradual changes were observed in the S-COPD group.

Changes in Tryptophan Catabolism

Among the 188 targeted metabolites subjected to absolute quantification, 59 were shared among the COPD groups and predominantly comprised acylcarnitines or glycerophospholipids. Notably, biogenic amines (kynurenine and serotonin) and amino acids (aspartate and threonine) were detected in the T-COPD group. Furthermore, the association between tryptophan catabolism and disease status was investigated (**Figure 4**). Although the total serum concentration of tryptophan did not change among the groups, we observed significant alterations in the kynurenine and serotonin levels in T-COPD patients (**Figures 4A,C**). Along with the changes in metabolite levels, the enzymatic activities of indoleamine dioxygenase (IDO) and tryptophan hydroxylase (TPH) were altered in the T-COPD group, which showed increased IDO activity compared with the control group (**Figure 4D**), and decreased TPH activity (**Figure 4E**). These changes were reversed in the S-COPD group. Although the total tryptophan level did not change, tryptophan catabolizing enzyme activities differed according to disease status, particularly in the T-COPD group. A categorical analysis was subsequently performed to determine whether the levels of these metabolites changed with disease severity (**Supplementary Figure 3**). Patients in each group were divided based on a FEV_1 cut-off value of 50%. None of these markers, including tryptophan, kynurenine, serotonin, and IDO/TPH activity, were related to lung function. Thus, these metabolic biomarkers of T-COPD are unique phenotypes in the COPD population; however, they still have a limited ability to identify disease severity. **Figure 5** reveals the distinct metabolic pathways that were specifically altered in patients with T-COPD. After excluding the metabolites that overlapped with those identified in patients with S-COPD, metabolic pathways related to arachidonic and eicosanoic acid, bile acid metabolism, and tryptophan catabolism, were identified in this study.

Discrimination of T-COPD and S-COPD by Targeted Metabolites

We further performed logistic regression of discrimination of T-COPD and S-COPD for targeted metabolites. Aspartate was the important metabolites associated with T-COPD diagnosis and serotonin and asparagine were the important metabolites associated with S-COPD (**Supplementary Table 5**). When we perform ROC analysis with aspartate, asparagine and serotonin, the AUC of T-COPD diagnosis was 0.780 (**Supplementary Figure 4**).

DISCUSSION

This is the first study to comprehensively profile serum samples from patients with COPD caused by smoking or a previous TB infection. The levels of IL-6 and CRP, and the SGRQ scores, were found to be higher in patients with T-COPD than in those with S-COPD. The multi-platform approach further discovered endogenous metabolites that distinguished these two disease groups. The metabolism of fatty acids, especially arachidonic acid and eicosanoic acid, and tryptophan catabolism were correlated, particularly in the T-COPD group. These results are consistent with the findings of our previous study, demonstrating an association between systemic inflammation and the COPD sub-phenotype in this cohort (16).

Overall, the metabolites identified in patients with T-COPD and S-COPD shared some common features, as shown in **Figure 2**. The presence of similar physiological symptoms such as dyspnea, sputum production, and acute exacerbation might result in similar metabolic changes, even though the etiology of S-COPD and T-COPD are different. We observed major changes in the levels of acylcarnitines and phospholipids in both COPD groups, with the levels being higher than that in healthy subjects. The close relationship between acylcarnitines and physiological activities is well-known as the evidence of energy metabolism. Circulating fatty acids are generally conjugated with carnitines to be utilized as an energy source in mitochondria, and their use is decreased in damaged lungs (17). Thus, increased serum acylcarnitine levels can be expected in COPD, and altered phospholipid levels could be another metabolic hallmark of COPD. The imbalance between phospholipids and lysophospholipids in COPD is controversial. However, multiple studies have reported a close association between increased levels of circulating phospholipids and the production of proinflammatory mediators during COPD exacerbations (18).

Changes in fatty acid metabolites indicate notable distinction between T-COPD and S-COPD. Here, the T-COPD group showed higher levels of some lipid metabolites, such as arachidonic acid or eicosanoic acids, than the S-COPD group did. Arachidonic acid, a polyunsaturated fatty acid (PUFA), is a member of the ω-6 fatty acid family and the primary

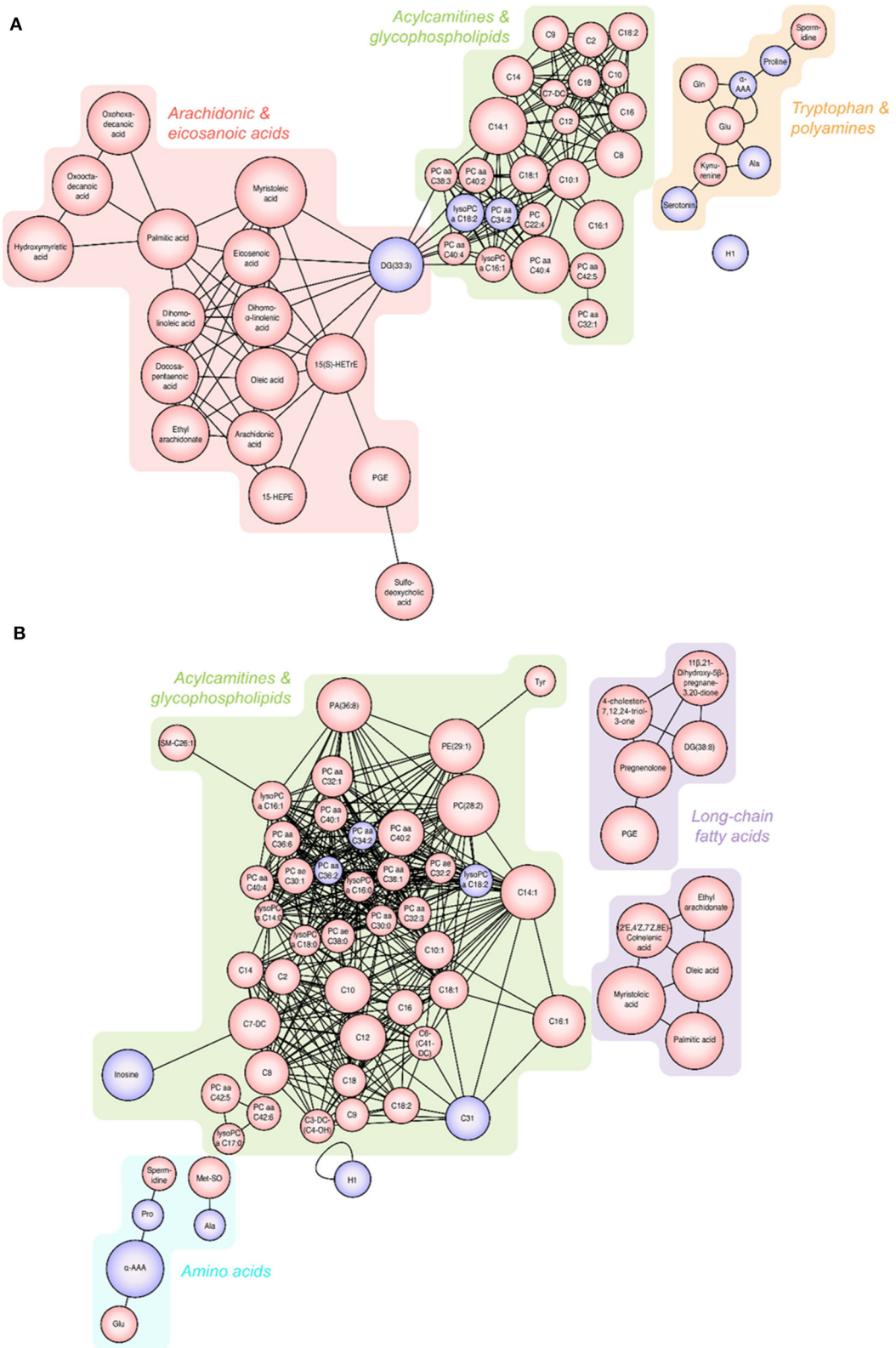

FIGURE 3 | Changes in metabolites seen in patients with T-COPD and S-COPD. **(A)** Significantly altered metabolites were observed between the NC and T-COPD groups. **(B)** Significantly altered metabolites were observed between the NC and S-COPD groups. The size of the circle indicates the relative fold change compared to the NC group. The red circle represents increased levels and the purple circle represents decreased levels of metabolites in patients, compared to healthy controls. NC, normal control; T-COPD, TB-associated COPD; S-COPD, smoking-associated COPD.

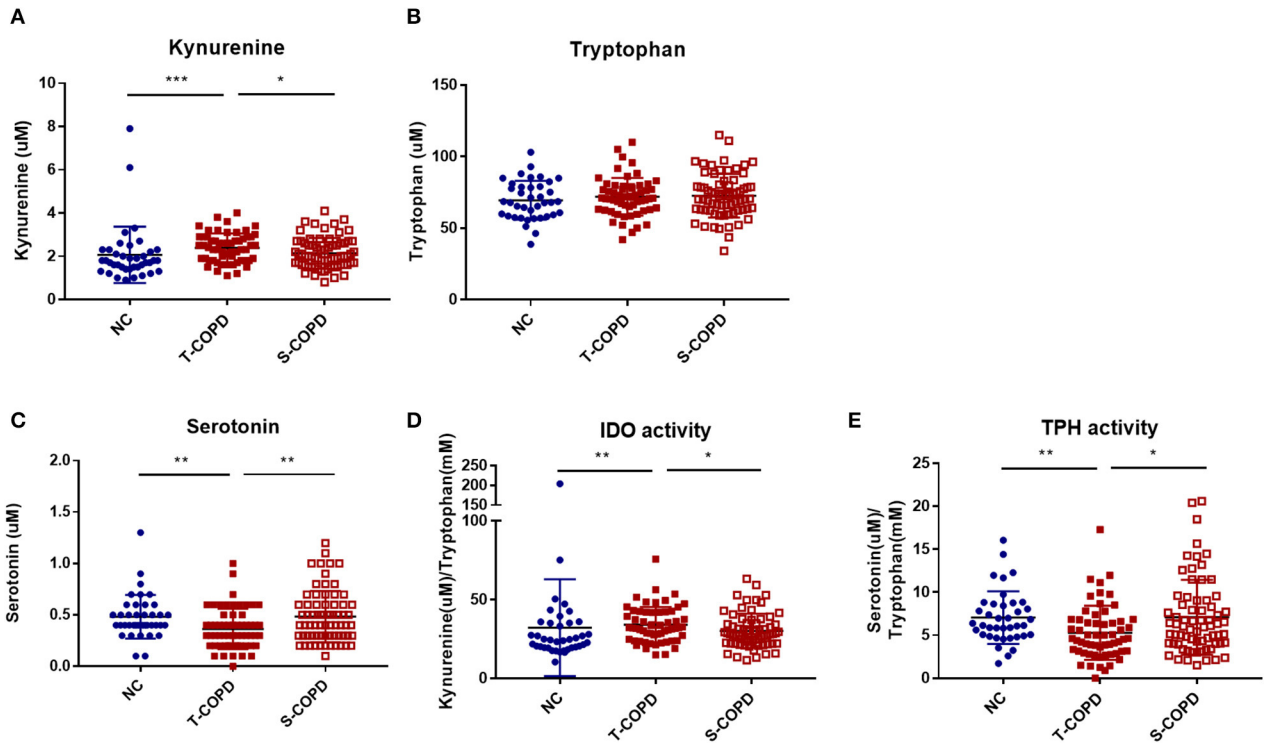

FIGURE 4 | Alternation of tryptophan metabolism in patients with T-COPD. Serum concentrations of **(A)** kynurenine, **(B)** tryptophan, and **(C)** serotonin are shown in scatter plots. **(D)** and **(E)** indicate IDO and TPH activities, respectively. Data are presented as the mean ± standard error of the mean. $^{*}P$-value <0.05, $^{**}P$-value < 0.01, and $^{***}P$-value < 0.001. NC, normal control; T-COPD, TB-associated COPD; S-COPD, smoking-associated COPD; IDO, indoleamine dioxygenase; TPH, tryptophan hydroxylase.

target of cyclooxygenases (COX) and lipoxygenase (LOX). By-products such as prostaglandins and eicosanoids, well-known proinflammatory mediators, are generated following oxidization (17). Lipid metabolism in the lungs is associated with chronic respiratory failure, airway obstruction, bronchoconstriction, IL-6 generation, vascular permeability, airway remodeling, mucus secretion, and inflammation in COPD (19). Interestingly, excess levels of arachidonic acid and eicosanoids were observed in the T-COPD group. Additionally, oxylipins were positively correlated with IL-6 and CRP levels, and docosapentanoic acid, 15-HEPE, and long-chain fatty acids were associated with worsening lung function and acute exacerbation. As lipid metabolite levels were increased in both disease groups compared to the controls, being significantly higher in the T-COPD group than in the S-COPD group, T-COPD can be considered to have similar pathogenesis as S-COPD, but causes more severe local and systemic inflammation.

Moreover, tryptophan catabolism showed greater activation in the T-COPD group than in the S-COPD group. Tryptophan catabolism through the IDO pathway exerts antimicrobial and anti-inflammatory effects in certain infectious or inflammatory conditions (20, 21). Increased levels of inflammatory cytokines such as IL-6 induce IDO expression, and IDO induces regulatory T cells to regulate inflammatory responses (22). The effect of tryptophan catabolism on inflammation is known; several studies have already analyzed IDO and TPH activities in COPD patients. Although a study reported increased IDO activity during acute exacerbations of COPD (21), no apparent alterations in this biological process have been reported to date (23, 24). Similar to the results from previous studies, the levels of the associated metabolites were altered in the T-COPD group, but not in the S-COPD group. Furthermore, higher systemic levels of inflammatory mediators, such as IL-6 and CRP, were observed in the T-COPD group than in the S-COPD group. Based on these findings, coexisting bronchiectasis, destroyed lung parenchyma, and bacterial colonization may cause repeated infections and inflammation (25, 26). Activation of immunological mechanisms may also result in sustained systemic inflammation after TB, and elevated IL-6 levels may subsequently induce activation of the IDO pathway.

The contribution of the gut microbiota cannot be excluded. Tryptophan is a microbiome-derived amino acid catalyzed by three pathways: (1) direct conversion into ligands of the aryl hydrocarbon receptor via the gut microbiota; (2) entry into the IDO-mediated kynurenine pathway in immune and epithelial cells; and (3) serotonin production by tryptophan hydroxylase in enterochromaffin cells (27, 28). Although the role of functional microbiota in the pathophysiology

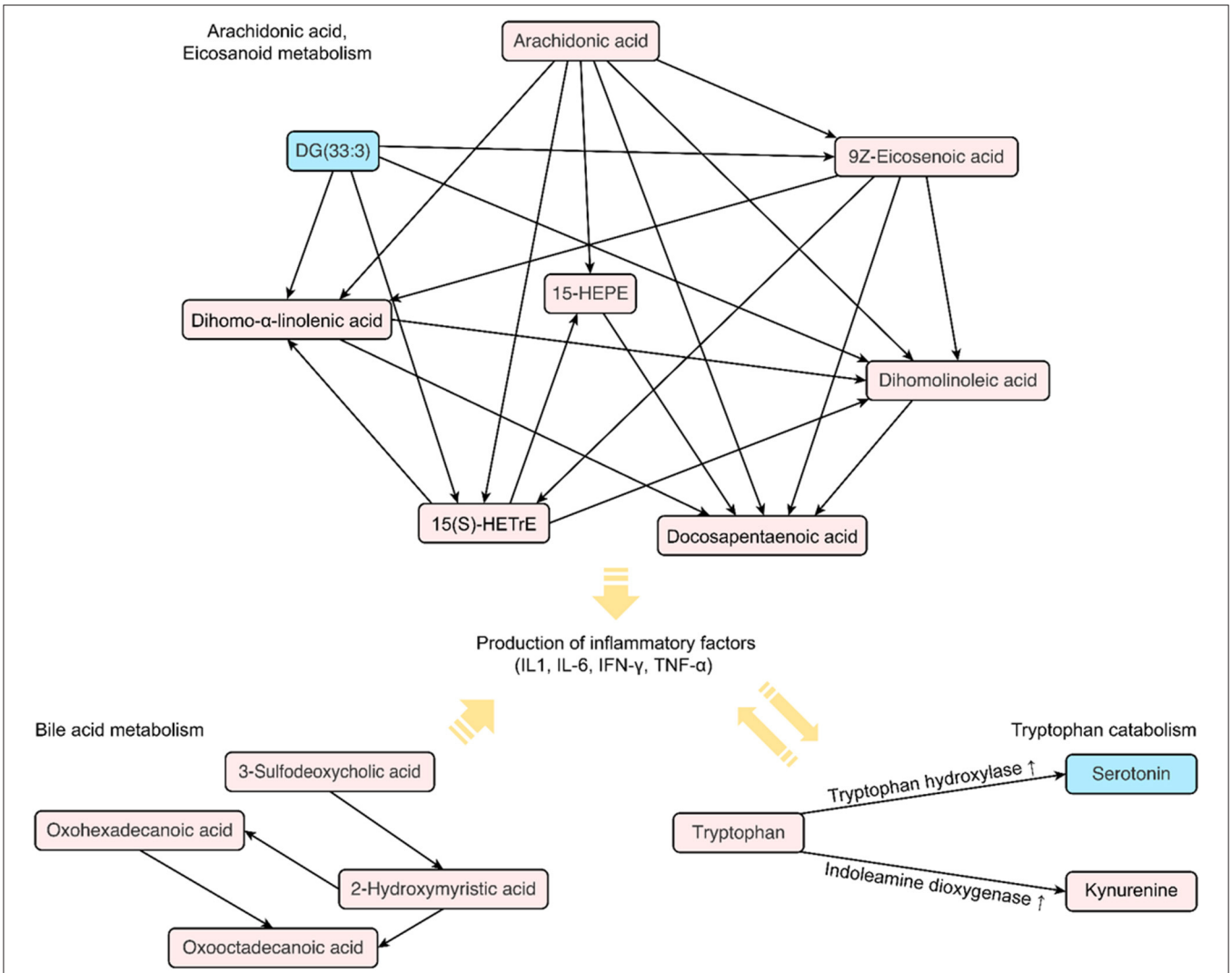

FIGURE 5 | Distinct metabolic pathways identified in patients with COPD following a TB infection. The diagram shows a map of metabolic biomarkers exclusively selected in patients with TB-induced COPD. The red square indicates increased levels of metabolites in the serum of patients with COPD, whereas blue indicates decreased levels. The arrow indicates the possible direction of the metabolic pathway based on the KEGG database.

of COPD is being investigated, alterations in the gut microbiome have been observed; its diversity decreases with increasing disease severity, compared to healthy subjects (29, 30). Nevertheless, the relationship between tryptophan catabolism and COPD is controversial, although the role of TB infection in tryptophan catabolism is well-known. According to previous *in vivo* and *in vitro studies*, TB induces potent activation of IDO, thereby inducing tryptophan catabolism for kynurenine production, which predominantly occurs in lung and immune cells (29, 31). IDO activity suppression has been shown to improve clinical symptoms of lung destruction and immune response in experimental studies (29). Although T-COPD patients were completely cured of TB, there could have been some irreversible continuous pathophysiological changes. Therefore, these patients might experience persistent effects of the resolved TB infection throughout their lifetime.

Smoking increases systemic neutrophil infiltration and sequesters leukocytes in lung capillaries by decreasing their deformability (32). Factors directly modulating the host immune system increase the production of inflammatory mediators such as interleukins, tumor necrosis factor-alpha (TNF-α), and CRP, resulting in tissue damage (33, 34). The irreversible destruction of alveolar walls induces a progressive decline in lung function and increases inflammation (2, 35). Thus, various therapies for S-COPD, including inhaled corticosteroids, bronchodilators (including β2-agonists and anticholinergics), theophyllines, and phosphodiesterase-4 inhibitors, are targeted to reduce airway inflammation (36, 37). Although recent studies have focused on anti-inflammatory treatment for S-COPD (38), the importance of managing the inflammatory features of T-COPD is usually underestimated. Considering that patients with T-COPD exhibited increased inflammatory responses that might be linked with fatty acid pathways and tryptophan

catabolism, further studies should focus on treatment strategies to control the associated inflammatory consequences of TB-induced COPD. Following the treatment for TB, aggressive treatments for controlling inflammation should be considered along with the existing COPD treatment modalities, for patients with T-COPD.

This study has some limitations. First, the strengths of associations between the metabolic biomarkers and demographic parameters in healthy controls were not performed due to the absence of pulmonary function tests and cytokine measurements. Correlation analysis of metabolic biomarkers and clinical parameters was conducted only among COPD patients (**Supplementary Figure 5**). Consequently, we found a positive correlation between oxylipins and IL-6 and CRP levels, while diacylglyceride and colnelenic acid levels were negatively correlated with these parameters. Additionally, positive correlations were identified between lung function scores, such as the rate of FEV_1 decline and acute exacerbation, and the levels of docosapentanoic acid, 15-HEPE, and long-chain fatty acids were identified. However, the absence of healthy control information resulted in a relatively small slope of the correlations. Second, the metabolomics data included only male patients, since the prevalence of S-COPD is remarkably low in Korean women (39). A validation study would require examinations of females to improve the generalizability of our findings. Moreover, we performed metabolic profiling within one batch and selected metabolites based on strict cut-off values, the FDR-adjusted *P*-value, and fold change, to minimize the output size of raw data and to avoid the batch effect. These processes might limit our ability to detect large changes in metabolites in the direct comparison of patients with S-COPD and those with T-COPD. Further examinations using a validation cohort are required to determine the reproducibility of our findings.

In conclusion, this is the first study to demonstrate increased levels of several inflammatory metabolites in patients with T-COPD compared to those with S-COPD. Lipid and tryptophan metabolism could be potential therapeutic targets for COPD, particularly in T-COPD.

DATA AVAILABILITY STATEMENT

The metabolomics data are available in the electronic **Supplementary Material** and at the NIH Common Fund's National Metabolomics Data Repository (NMDR) website (Project ID: PR000943).

ETHICS STATEMENT

The studies involving human participants were reviewed and approved by the institutional review boards (Korea University Guro Hospital: KUGH 13246; Seoul St. Mary's Hospital: KC15OIMI0553; and Chonbuk National University Hospital: 2015-01-018-005), and it fulfilled the tenets of the Declaration of Helsinki. The patients provided written informed consent. The patients/participants provided their written informed consent to participate in this study.

AUTHOR CONTRIBUTIONS

DK, JO, and J-YC conceptualized the study. JO, CR, SP, and JS collected samples. DK performed metabolic profiling. The results were interpreted by DK, JO, and J-YC. The original draft preparation was done by DK and JO. J-YC reviewed the manuscript. Funding acquisition was prepared by JO and J-YC. All authors contributed to the article and approved the submitted version.

FUNDING

This study was supported by the Bio and Medical Technology Development Programme of the National Research Foundation (NRF) funded by the Korean government (MSIT) (Grant Numbers 2019M3E5D3073365 and 2019M3E5D1A01068994).

SUPPLEMENTARY MATERIAL

The Supplementary Material for this article can be found online at: https://www.frontiersin.org/articles/10.3389/fmed.2021.619077/full#supplementary-material

REFERENCES

1. Mathers CD, Loncar D. Projections of global mortality and burden of disease from 2002 to 2030. *PLoS Med.* (2006) 3:e442. doi: 10.1371/journal.pmed.0030442
2. Barnes PJ, Burney PG, Silverman EK, Celli BR, Vestbo J, Wedzicha JA, et al. Chronic obstructive pulmonary disease. *Nat Rev Dis Primers.* (2015) 1:15076. doi: 10.1038/nrdp.2015.76
3. Ravimohan S, Kornfeld H, Weissman D, Bisson GP. Tuberculosis and lung damage: from epidemiology to pathophysiology. *Eur Respir Rev.* (2018) 27:170077. doi: 10.1183/16000617.0077-2017
4. Yakar HI, Gunen H, Pehlivan E, Aydogan S. The role of tuberculosis in COPD. *Int J Chron Obstruct Pulmon Dis.* (2017) 12:323–9. doi: 10.2147/COPD.S116086
5. Allwood BW, Myer L, Bateman ED. A systematic review of the association between pulmonary tuberculosis and the development of chronic airflow obstruction in adults. *Respiration.* (2013) 86:76–85. doi: 10.1159/000350917
6. Byrne AL, Marais BJ, Mitnick CD, Lecca L, Marks GB. Tuberculosis and chronic respiratory disease: a systematic review. *Int J Infect Dis.* (2015) 32:138–46. doi: 10.1016/j.ijid.2014.12.016
7. Lee JH, Chang JH. Lung function in patients with chronic airflow obstruction due to tuberculous destroyed lung. *Respir Med.* (2003) 97:1237–42. doi: 10.1016/S0954-6111(03)00255-5
8. Sarkar M, Srinivasa, Madabhavi I, Kumar K. Tuberculosis associated chronic obstructive pulmonary disease. *Clin Respir J.* (2017) 11:285–95. doi: 10.1111/crj.12621
9. Radovic M, Ristic L, Ciric Z, Dinic-Radovic V, Stankovic I, Pejcic T, et al. Changes in respiratory function impairment following the treatment of severe

pulmonary tuberculosis—limitations for the underlying COPD detection. *Int J Chron Obstruct Pulmon Dis.* (2016) 11:1307–16. doi: 10.2147/COPD.S106875
10. Malherbe ST, Shenai S, Ronacher K, Loxton AG, Dolganov G, Kriel M, et al. Persisting positron emission tomography lesion activity and Mycobacterium tuberculosis mRNA after tuberculosis cure. *Nat Med.* (2016) 22:1094–100. doi: 10.1038/nm.4177
11. Reinke SN, Gallart-Ayala H, Gómez C, Checa A, Fauland A, Naz S, et al. Metabolomics analysis identifies different metabotypes of asthma severity. *Eur Respir J.* (2017) 49:1601740. doi: 10.1183/13993003.01740-2016
12. Kim DJ, Yoon S, Ji SC, Yang J, Kim YK, Lee S, et al. Ursodeoxycholic acid improves liver function via phenylalanine/tyrosine pathway and microbiome remodelling in patients with liver dysfunction. *Sci Rep.* (2018) 8:11874. doi: 10.1038/s41598-018-30349-1
13. Kim DJ, Cho EJ, Yu KS, Jang IJ, Yoon JH, Park T, et al. Comprehensive Metabolomic Search for Biomarkers to Differentiate Early Stage Hepatocellular Carcinoma from Cirrhosis. *Cancers.* (2019) 11:1497. doi: 10.3390/cancers11101497
14. Oh JY, Lee YS, Min KH, Hur GY, Lee SY, Kang KH, et al. Increased urinary l-histidine in patients with asthma-COPD overlap: a pilot study. *Int J Chron Obstruct Pulmon Dis.* (2018) 13:1809–18. doi: 10.2147/COPD.S163189
15. Kim DJ, Chung H, Ji SC, Lee S, Yu KS, Jang IJ, et al. Ursodeoxycholic acid exerts hepatoprotective effects by regulating amino acid, flavonoid, and fatty acid metabolic pathways. *Metabolomics.* (2019) 15:30. doi: 10.1007/s11306-019-1494-5
16. Oh JY, Lee YS, Min KH, Hur GY, Lee SY, Kang KH, et al. Difference in systemic inflammation and predictors of acute exacerbation between smoking-associated COPD and tuberculosis-associated COPD. *Int J Chron Obstruct Pulmon Dis.* (2018) 13:3381–7. doi: 10.2147/COPD.S177371
17. Chen H, Li Z, Dong L, Wu Y, Shen H, Chen Z. Lipid metabolism in chronic obstructive pulmonary disease. *Int J Chron Obstruct Pulmon Dis.* (2019) 14:1009–18. doi: 10.2147/COPD.S196210
18. Bowler RP, Jacobson S, Cruickshank C, Hughes GJ, Siska C, Ory DS, et al. Plasma sphingolipids associated with chronic obstructive pulmonary disease phenotypes. *Am J Respir Crit Care Med.* (2015) 191:275–84. doi: 10.1164/rccm.201410-1771OC
19. Ran N, Pang Z, Gu Y, Pan H, Zuo X, Guan X, et al. An updated overview of metabolomic profile changes in chronic obstructive pulmonary disease. *Metabolites.* (2019) 9:111. doi: 10.3390/metabo9060111
20. Takikawa O. Biochemical and medical aspects of the indoleamine 2, 3-dioxygenase-initiated L-tryptophan metabolism. *Biochem Biophys Res Commun.* (2005) 338:12–9. doi: 10.1016/j.bbrc.2005.09.032
21. Gulcev M, Reilly C, Griffin TJ, Broeckling CD, Sandri BJ, Witthuhn BA, et al. Tryptophan catabolism in acute exacerbations of chronic obstructive pulmonary disease. *Int J Chron Obstruct Pulmon Dis.* (2016) 11:2435–46. doi: 10.2147/COPD.S107844
22. Suzuki Y, Suda T, Yokomura K, Suzuki M, Fujie M, Furuhashi K, et al. Serum activity of indoleamine 2,3-dioxygenase predicts prognosis of community-acquired pneumonia. *J Infect.* (2011) 63:215–22. doi: 10.1016/j.jinf.2011.07.003
23. Labaki WW, Gu T, Murray S, Curtis JL, Yeomans L, Bowler RP, et al. SPIROMICS metabolomics study. *Sci Rep.* (2019) 9:11367. doi: 10.1038/s41598-019-47761-w
24. Naz S, Bhat M, Ståhl S, Forsslund H, Sköld CM, Wheelock ÅM, et al. Dysregulation of the Tryptophan Pathway Evidences Gender Differences in COPD. *Metabolites.* (2019) 9:212. doi: 10.3390/metabo9100212
25. Jordan TS, Spencer EM, Davies P. Tuberculosis, bronchiectasis and chronic airflow obstruction. *Respirology.* (2010) 15:623–8. doi: 10.1111/j.1440-1843.2010.01749.x
26. Mao B, Lu HW, Li MH, Fan LC, Yang JW, Miao XY, et al. The existence of bronchiectasis predicts worse prognosis in patients with COPD. *Sci Rep.* (2015) 5:10961. doi: 10.1038/srep10961
27. Agus A, Planchais J, Sokol H. Gut microbiota regulation of tryptophan metabolism in health and disease. *Cell Host Microbe.* (2018) 23:716–24. doi: 10.1016/j.chom.2018.05.003
28. Zelante T, Iannitti RG, Cunha C, De Luca A, Giovannini G, Pieraccini G, et al. Tryptophan catabolites from microbiota engage aryl hydrocarbon receptor and balance mucosal reactivity via interleukin-22. *Immunity.* (2013) 39:372–85. doi: 10.1016/j.immuni.2013.08.003
29. Huang YJ, Erb-Downward JR, Dickson RP, Curtis JL, Huffnagle GB, Han MK. Understanding the role of the microbiome in chronic obstructive pulmonary disease: principles, challenges, and future directions. *Transl Res.* (2017) 179:71–83. doi: 10.1016/j.trsl.2016.06.007
30. Martinez FJ, Erb-Downward JR, Huffnagle GB. Significance of the microbiome in chronic obstructive pulmonary disease. *Ann Am Thorac Soc.* (2013) 10(Suppl):S170–9. doi: 10.1513/AnnalsATS.201306-204AW
31. Blumenthal A, Nagalingam G, Huch JH, Walker L, Guillemin GJ, Smythe GA, et al. Tuberculosis induces potent activation of IDO-1, but this is not essential for the immunological control of infection. *PLoS ONE.* (2012) 7:e37314. doi: 10.1371/journal.pone.0037314
32. MacNee W, Wiggs B, Belzberg AS, Hogg JC. The effect of cigarette smoking on neutrophil kinetics in human lungs. *N Engl J Med.* (1989) 321:924–8. doi: 10.1056/NEJM198910053211402
33. de Moraes MR, da Costa AC, Correa Kde S, Junqueira-Kipnis AP, Rabahi MF. Interleukin-6 and interleukin-8 blood levels' poor association with the severity and clinical profile of ex-smokers with COPD. *Int J Chron Obstruct Pulmon Dis.* (2014) 9:735–43. doi: 10.2147/COPD.S64135
34. Terashima T, Wiggs B, English D, Hogg JC, van Eeden SF. Phagocytosis of small carbon particles (PM10) by alveolar macrophages stimulates the release of polymorphonuclear leukocytes from bone marrow. *Am J Respir Crit Care Med.* (1997) 155:1441–7. doi: 10.1164/ajrccm.155.4.9105091
35. O'Toole RF, Shukla SD, Walters EH. TB meets COPD: An emerging global co-morbidity in human lung disease. *Tuberculosis.* (2015) 95:659–63. doi: 10.1016/j.tube.2015.08.005
36. Cosio BG, Iglesias A, Rios A, Noguera A, Sala E, Ito K, et al. Low-dose theophylline enhances the anti-inflammatory effects of steroids during exacerbations of COPD. *Thorax.* (2009) 64:424–9. doi: 10.1136/thx.2008.103432
37. Mirza S, Clay RD, Koslow MA, Scanlon PD. COPD Guidelines: a review of the 2018 GOLD report. *May Clin Proc.* (2018) 93:1488–1502. doi: 10.1016/j.mayocp.2018.05.026
38. Barnes PJ. New anti-inflammatory targets for chronic obstructive pulmonary disease. *Nat Rev Drug Discov.* (2013) 12:543–59. doi: 10.1038/nrd4025
39. Lee JY, Chon GR, Rhee CK, Kim DK, Yoon HK, Lee JH, et al. Characteristics of patients with chronic obstructive pulmonary disease at the first visit to a pulmonary medical Center in Korea: The KOrea COpd Subgroup Study Team Cohort. *J Korean Med Sci.* (2016) 31:553–60. doi: 10.3346/jkms.2016.31.4.553

Conflict of Interest: The authors declare that the research was conducted in the absence of any commercial or financial relationships that could be construed as a potential conflict of interest.

Copyright © 2021 Kim, Oh, Rhee, Park, Shim and Cho. This is an open-access article distributed under the terms of the Creative Commons Attribution License (CC BY). The use, distribution or reproduction in other forums is permitted, provided the original author(s) and the copyright owner(s) are credited and that the original publication in this journal is cited, in accordance with accepted academic practice. No use, distribution or reproduction is permitted which does not comply with these terms.

Advantages of publishing in Frontiers

OPEN ACCESS
Articles are free to read for greatest visibility and readership

FAST PUBLICATION
Around 90 days from submission to decision

HIGH QUALITY PEER-REVIEW
Rigorous, collaborative, and constructive peer-review

TRANSPARENT PEER-REVIEW
Editors and reviewers acknowledged by name on published articles

Frontiers
Avenue du Tribunal-Fédéral 34
1005 Lausanne | Switzerland

Visit us: www.frontiersin.org
Contact us: frontiersin.org/about/contact

REPRODUCIBILITY OF RESEARCH
Support open data and methods to enhance research reproducibility

DIGITAL PUBLISHING
Articles designed for optimal readership across devices

FOLLOW US
@frontiersin

IMPACT METRICS
Advanced article metrics track visibility across digital media

EXTENSIVE PROMOTION
Marketing and promotion of impactful research

LOOP RESEARCH NETWORK
Our network increases your article's readership